Mechanical Behavior of Tire Rubber–Reinforced Expansive Soils

By

Amin Soltani MSc, BSc

Thesis submitted in fulfillment of the requirements for the degree of Doctor of Philosophy

The University of Adelaide

Faculty of Engineering, Computer and Mathematical Sciences

School of Civil, Environmental and Mining Engineering

Copyright © October 2018

Summary

Expansive soils are amongst the most significant, widespread, costly, and least publicized geologic hazards. Where exposed to seasonal environments, such soils exhibit significant volume changes as well as desiccation–induced cracking, thereby bringing forth instability concerns to the overlying structures and hence incurring large amounts of maintenance costs. Consequently, expansive soils demand engineering solutions to alleviate the associated socio–economic impacts on human life. Common solutions to counteract the adversities associated with problematic soils include soil replacement and/or soil stabilization. The latter refers to any chemical, mechanical or combined chemical–mechanical practice of altering the soil fabric to meet the intended engineering criteria. Though proven effective, conventional stabilization schemes often suffer from sustainability issues related to high manufacturing and/or transportation costs, and environmental concerns due to greenhouse gas emissions. The transition towards sustainable stabilization necessitates reusing solid wastes and/or industrial by–products as part of the infrastructure system, and more specifically as replacements for conventional stabilization agents such as cement, lime, geogrids and synthetic fibers. Among others, discarded tires constitute for one of the largest volumes of disposals throughout the world, and as such, demand further attention. Given the high–volume generation (and disposal) of waste tire rubbers every year throughout the world, a major concern hitherto has been the space required for storing and transporting such waste materials, and the resulting health hazards and costs. Those characteristics which make waste tire rubbers such a problem while being landfilled, make them one of the most reusable waste materials for engineering applications such as soil stabilization, as the rubber is resilient, lightweight and skin–resistive. Beneficial reuse of recycled tire rubbers for stabilization of expansive soils would not only address the geotechnical–related issue, but would also encourage recycling, mitigate the burden on the environment and assist with waste management.

The present study intends to examine the rubber's capacity of ameliorating the inferior engineering characteristics of expansive soils, thereby solving two widespread hazards with one solution. Two rubber types of fine and coarse categories, i.e. rubber crumbs/powder and rubber buffings, were each examined at various rubber contents (by weight). The experimental program consisted of consistency limits, standard Proctor compaction, oedometer swell–

shrink/consolidation, soil reactivity (or shrink–swell index), cyclic wetting–drying, cracking intensity, unconfined compression (UC), split tensile (ST), direct shear (DS) and scanning electron microscopy (SEM) tests. Improvement in the swell–shrink/consolidation capacity, cracking intensity and shear strength (DS test) were all in favor of both a higher rubber content and a larger rubber size. However, rubber contents greater than 10% (by weight) often raised failure concerns when subjected to compression (UC test) and/or tension (ST test), which was attributed to the clustering of rubber particles under non–confinement testing conditions. Although the rubber of coarser category slightly outperformed the finer rubber, the effect of larger rubber size was mainly translated into higher ductility, lower stiffness and higher energy adsorption capacity rather than peak strength improvements. The volume change properties were cross–checked with the strength–related characteristics to arrive at the optimum rubber content. A rubber inclusion of 10%, preferably the rubber of coarser category, satisfied a notable decrease in the swell–shrink/consolidation capacity as well as improving the strength–related features, and thus was deemed as the optimum choice. Based on the experimental results, along with the SEM findings, the soil–rubber amending mechanisms were discussed in three aspects: **i)** increase in non–expansive fraction; **ii)** frictional resistance generated as a result of soil–rubber contact; and **iii)** mechanical interlocking of rubber particles and soil grains.

A series of empirical models were suggested to quantify the compaction characteristics of soil–rubber mixtures as a function of their consistency limits. Moreover, the dimensional analysis concept was extended to the soil–rubber shear strength problem, thereby leading to the development of a series of practical dimensional models capable of simulating the shear stress–horizontal displacement response as a function of normal stress (or confinement) and the composite's basic index properties, i.e. rubber content, specific surface area and initial placement (or compaction) condition. The predictive capacity of the proposed empirical and dimensional models was examined and further validated by statistical techniques. The proposed empirical and dimensional models contain a limited number of fitting/model parameters, which can be calibrated by minimal experimental effort as well as simple explicit calculations, and thus implemented for preliminary assessments (or predictive purposes).

To justify the use of higher rubber contents in practice, a sustainable polymer agent, namely Polyacrylamide (PAM) of anionic character, was introduced as the binder. A series of additional tests were then carried out to examine the combined capacity of rubber inclusion and PAM treatment in solving the swelling problem of South Australian expansive soils. As a result of PAM treatment, the connection interface between the rubber particles and the clay matrices

were markedly improved, which in turn led to lower swelling/shrinkage properties, higher resistance to cyclic wetting–drying, and reduced tendency for cracking compared to that of the conventional soil–rubber blend. A rubber inclusion of 20%, paired with 0.2 g/l PAM, was suggested to effectively stabilize South Australian expansive soils.

Keywords: Expansive soil; Sustainable stabilization; Waste tire rubber; Rubber content and size; Swell–shrink/consolidation; Cyclic wetting–drying; Cracking intensity; Shear strength; Dimensional analysis; Polyacrylamide.

Statement of Originality

I certify that this work contains no material which has been accepted for the award of any other degree or diploma in my name, in any university or other tertiary institution and, to the best of my knowledge and belief, contains no material previously published or written by another person, except where due reference has been made in the text. In addition, I certify that no part of this work will, in the future, be used in a submission in my name, for any other degree or diploma in any university or other tertiary institution without the prior approval of the University of Adelaide and where applicable, any partner institution responsible for the joint–award of this degree.

I acknowledge that copyright of published works contained within this thesis resides with the copyright holder(s) of those works.

I also give permission for the digital version of my thesis to be made available on the web, via the University's digital research repository, the Library Search and also through web search engines, unless permission has been granted by the University to restrict access for a period of time.

I acknowledge the support I have received for my research through the provision of an Australian Government Research Training Program Scholarship.

Amin Soltani MSc, BSc

Signature: ___ _ **Date:** 08/15/2018

Acknowledgements

This PhD research began in May 2016 and has been carried out on a full–time basis ever since. I owe an enormous debt of gratitude to my supervisors, Dr. An Deng and Dr. Abbas Taheri, of the School of Civil, Environmental and Mining Engineering, for their time, patience, guidance and continual support throughout this research program. In addition, their advice and encouragement have been of great value to me, and this thesis would not have been possible but for their contribution.

Special thanks go to Prof. Asuri Sridharan, of the Indian National Science Academy (INSA), for his generosity, time, patience, guidance and continual support throughout the period of my candidature. I also wish to acknowledge the enormous support given to me by Dr. Mehdi Mirzababaei, of Central Queensland University (CQU), for his friendship and invaluable contribution to this research. I also wish to express my sincere appreciation to Prof. Hamid Nikraz, of Curtin University, for his guidance, kind support and invaluable contribution to my scientific publications.

I am thankful to the School of Civil, Environmental and Mining Engineering, particularly the laboratory staff, Mr. Gary Bowman, Mr. Dale Hodson and Mr. Simon Golding, for their kind assistance with the experimental work. I also wish to thank fellow postgraduate student, Jiahe Zhang, for his friendship, encouragement and kind support throughout the period of my candidature.

I will always be in debt to my family, particularly my wife, Mahdieh, for her constant love, sacrifice and support throughout the period of my candidature, and my lovely parents, Mehdi and Tahereh, for the considerable sacrifices which they have made on my behalf throughout my life.

This PhD research was funded by the Australian Research Council (ARC) by way of project No. **DP140103004**; this support is gratefully acknowledged.

Table of Contents

Summary I

Statement of Originality IV

Acknowledgements V

Table of Contents VI

Chapter 1: Thesis Overview 1

1. Problem Statement 1

2. Research Gaps 4

3. Research Objectives and Thesis Layout 6

4. Additional Publications 9

5. Concluding Remarks 10

References 14

Chaper 2: Consistency Limits and Compaction Characteristics of Clay Soils Containing Rubber Waste 15

Abstract 15

Abbreviations 17

Notation 17

1. Introduction 18

2. Materials 20

2.1. Clay Soils 20

2.2. Ground Rubber (GR) 20

3. Test Program 21

3.1. Consistency Limits 22

3.2. Compaction Studies 23

4. Statistical Analysis 24

5. Results and Discussions 24

5.1. Effect of Ground Rubber (GR) on Consistency Limits 24

5.2. Effect of Ground Rubber (GR) on Compaction Characteristics 26

5.3. Compaction Characteristics as a Function of Consistency Limits 27

6. Conclusions 31

Acknowledgements 32

References 33

List of Tables 38

List of Figures 41

Statement of Authorship 56

Published Copy 57

Chapter 3: Swell–Shrink–Consolidation Behavior of Rubber–Reinforced Expansive Soils 72

Abstract 72

1. Introduction 74

2. Materials and Methods 75

2.1. Expansive Soil 75

2.2. Tire Rubbers 76

2.3. Sample Preparation 76

2.4. Test Procedure 77

2.4.1. Swell–Shrink–Consolidation Test 77

2.4.2. Unconfined Compression Test 78

3. Results and Discussion 79

3.1. Effect of Rubbers on the Swelling Potential 79

3.2. Effect of Rubbers on the Consolidation Behavior 80

3.3. Effect of Rubbers on the Shrinkage Potential 82

3.4. Effect of Rubbers on the Strength Properties 84

3.5. Amending Mechanisms 85

4. Optimum Rubber Content and Cost Analysis 87

5. Conclusions 88

Acknowledgements 89

References 90

List of Tables 97

List of Figures 104

Statement of Authorship 119

Published Copy 120

Chapter 4: Tire Rubber–Reinforced Expansive Soils: Two Hazards, One Solution? 149

Abstract 149

Abbreviations 151

Notation 151

1. Introduction 152

2. Materials 154

2.1. Soil 154

2.2. Recycled Tire Rubbers 155

3. Experimental Work 155

3.1. Unconfined Compression Test 156

3.2. Split Tensile Test 156

3.3. Direct Shear Test 157

3.4. Desiccation–Induced Crack Test 157

4. Results and Discussions 158

4.1. Effect of Rubbers on Unconfined Compression Strength 158

4.2. Effect of Rubbers on Split Tensile Strength 159

4.3. Effect of Rubbers on Shear Strength Properties 160

4.3.1. Test Results 160

4.3.2. Multiple Linear Regression Model 163

4.4. Soil–Rubber Amending Mechanisms 165

4.5. Effect of Rubbers on Cracking Intensity 166

4.6. Swelling Characteristics and Optimum Rubber Content 167

5. Conclusions 169

Acknowledgements 170

References 171

List of Tables 178

List of Figures 182

Statement of Authorship 200

Chapter 5: Interfacial Shear Strength of Rubber–Reinforced Clays: A Dimensional Analysis Perspective 201

Abstract 201

Abbreviations 203

Notation 203

1. Introduction 205

2. Experimental Work 207

2.1. Materials 207

2.1.1. Clay Soil 207

2.1.2. Tire Rubbers 207

2.2. Compaction Studies and Sample Preparation 208

2.3. Direct Shear Test 209

3. Experimental Results and Discussion 210

3.1. Shear Stress–Horizontal Displacement Response 210

3.2. Shear Strength Parameters 211

3.3. Soil–Rubber Interactions 211

4. Dimensional Analysis 213

4.1. Model Development 213

4.1.1. Method A 216

4.1.2. Method B 217

4.2. Model Validation 217

4.3. Proposed Dimensional Models 218

4.3.1. Model M_1 218

4.3.2. Model M_2 220

4.3.3. Model M_3 221

4.4. Modelling the Shear Stress–Horizonal Displacement Locus 223

5. Conclusions 224

Acknowledgements 225

References 226

List of Tables 234

List of Figures 241

Appendix A 261

Appendix B 262

Statement of Authorship 264

Chapter 6: California Bearing Ratio of Tire Crumbles–Fly Ash Mixed with Clay: A Dimensional Analysis Perspective 266

1. Introduction 266

2. Dimensional Analysis 269

2.1. Model Development 269

2.2. Model Performance 272

3. Summary and Conclusions 273

Acknowledgements 274

References 275

List of Tables 277

List of Figures 279

Statement of Authorship 282

Chapter 7: Swell–Shrink Behavior of Rubberized Expansive Clays During Alternate Wetting and Drying 283

Abstract 283

1. Introduction 285

2. Materials 287

2.1. Expansive Clay Soil 287

2.2. Recycled Tire Rubbers 287

3. Experimental Methodologies 288

3.1. Compaction Studies and Sample Preparations 288

3.2. Cyclic Wetting–Drying Test 289

3.3. Micro–Structure Analysis 290

4. Results and Discussion 290

4.1. Swelling Characteristics 290

4.2. Shrinkage Characteristics 292

4.3. Swell–Shrink Patterns 294

4.4. Amending Mechanisms and Fabric Evolution 295

5. Conclusions 297

Acknowledgments 298

References 299

List of Tables 305

List of Figures 309

Statement of Authorship 321

Chapter 8: Rubber Powder–Polymer Combined Stabilization of South Australian Expansive Soils 323

Abstract 323

Abbreviations 325

Notation 325

1. Introduction 327

2. Materials 329

2.1. Soil 329

2.2. Tire Rubber Powder 329

2.3. Polymer 330

3. Experimental Work 330

3.1. Compaction Studies and Sample Preparation 331

3.2. Oedometer Swell–Compression Test 332

3.3. Soil Reactivity Test and the Shrink–Swell Index 333

3.4. Cyclic Wetting and Drying Test 334

3.5. Desiccation–Induced Crack Studies 335

3.6. Scanning Electron Microscopy (SEM) 336

4. Results and Discussion 336

4.1. Consistency Limits and the Free Swell Ratio 336

4.2. Compaction Characteristics 338

4.3. Swelling Characteristics 338

4.3.1. Swelling Potential and Swelling Pressure 338

4.3.2. Shrink–Swell Index 340

4.3.3. Amending Mechanisms 341

4.3.4. Cyclic Wetting and Drying 342
4.4. Crack Intensity 343
4.5. Micro–Structure (SEM) Analysis 344
5. Conclusions 345
Acknowledgements 346
References 347
List of Tables 355
List of Figures 364
Statement of Authorship 380
Published Copy 381

Chapter 1

Thesis Overview

1. Problem Statement

Expansive soils are amongst the most significant, widespread, costly, and least publicized geologic hazards. Such soils are characterized as poor–quality construction materials, owing to their inferior engineering characteristics including high moisture susceptibility (and plasticity), low strength (and bearing capacity) and high compressibility. A notable fraction of the expansive soil is constituted of active smectite minerals, such as montmorillonite, which exhibits significant swell–shrink volume changes (as well as desiccation–induced cracking) upon the addition or removal of water. Such actions bring forth major instability concerns to the overlying structures, thereby resulting in large amounts of maintenance costs. In a typical year, expansive soils can cause a greater financial loss to property owners than earthquakes, floods, hurricanes and tornadoes combined (Nelson and Miller 1992). Over the past decade, the adverse effects of expansive soils have cost the UK's economy an estimated £3 billion, thus making it the most damaging geohazard in the UK today (Jones and Jefferson 2012). In the USA, for instance, the estimated damage to structures founded on expansive soils has been reported to exceed $13 billion per annum (Dunham-Friel and Carraro 2011). Similar trends have also been reported in Australia where a notable fraction of surface soils, particularly in South Australia and Victoria, are of high expansive nature. Consequently, expansive soils demand engineering solutions to alleviate the adverse socio–economic impacts on human life.

Common solutions to counteract the adversities associated with expansive soils include soil replacement and/or attempting to improve the low–graded expansive soil by means of stabilization techniques. The former involves substituting a portion of the expansive soil with desired quarried materials (or aggregates) possessing minimal swell–shrink tendency. The latter refers to any chemical, mechanical or combined chemical–mechanical practice of altering the expansive soil fabric to meet the intended engineering criteria. In general, soil stabilization is preferred, since the soil replacement technique is often impractical due to haul distances and

economic considerations. The chemical stabilization scheme makes use of chemical binders, e.g. cement, lime, fly ash, polymers and sulfonated oils, which initiate a series of short– and long–term chemical reactions in the soil–binder medium, thereby amending the soil fabric into a coherent matrix of improved mechanical performance. Conventional cementitious agents such as cement and lime, though proven effective, encounter a series of concerning disadvantages: **i)** reduction in material workability (or ductility); **ii)** low durability against local environmental conditions (e.g. organic matter, sulfates, cyclic wetting–drying and acidic/alkaline flows); **iii)** high transportation costs; and **iv)** environmental concerns due to greenhouse gas emissions. Mechanical stabilization often involves the placement of random or systematically–engineered reinforcements in the soil regime, e.g. synthetic/natural fibers and geogrids, thereby engendering a spatial three–dimensional reinforcement network in favor of weaving/interlocking the soil grains into a unitary mass of restricted swell–shrink movements. Such products, while prevailing the environmental concerns raised with chemical techniques, suffer from other disadvantages: **i)** the lack of standardized laboratory test methods for effective prediction of field performance; **ii)** high manufacturing costs associated with synthetic fibers and geogrids; **iii)** biodegradability of natural fibers; and **iv)** availability issues (or limited stock) in some sites. Quite clearly, conventional chemical and mechanical stabilization practices suffer from a sustainability point of view. A sustainable stabilization scheme can be characterized as one that maintains a perfect balance between infrastructure performance and the social, economic and ecological processes required to maintain human equity, diversity, and the functionality of natural systems. Therefore, alternate stabilization techniques capable of replacing or minimizing the need for such conventional practices have been highly encouraged.

Solid waste materials are bulky in nature, owing to their low weight–to–volume ratio, and thus consume valuable landfill space upon disposal. To minimize the need for landfilling, local communities and governmental agencies have been increasingly encouraged to recycle and hence reuse such materials as part of the infrastructure system. As of late, many developed and developing countries have initiated the transition towards ‘sustainable infrastructure’, a concept which encourages the replacement of conventional quarried/stabilization materials with solid wastes and/or industrial by–products (e.g. waste tire rubbers, waste textiles/fibers, demolition wastes, kiln dusts and silicate/calcium chloride geopolymers), thereby conserving natural resources as well as reducing the level of greenhouse gas emissions. In this context, a number of research works have suggested innovative and environmentally sound solutions targeting the application of such materials in various civil engineering projects such as pavement

construction, soil stabilization, concrete manufacturing and thermal insulations. Beneficial reuse of waste resources not only intends to enhance infrastructure performance, but also encourages recycling, mitigates the burden (or hazard) on the environment and assists waste management by preventing the accumulation of bulky waste materials which are normally stored or landfilled without proper utilization. As such, any attempt to assimilate waste resources as part of the infrastructure system is at the forefront of many researchers and governmental authorities.

Among others, discarded tires constitute for one of the largest volumes of disposals throughout the world, and as such, demand further attention. Such materials are amongst the most problematic sources of solid waste, owing to extensive production and their durability over time. In Australia, for instance, it has been estimated that 0.5 million tons of waste tires are generated per annum (Li et al. 2018). A major challenge has therefore been the space required for storing and transporting such waste materials, and the resulting health hazards and costs. Quite clearly, discarded tires are not desired at landfills, due to their low weight–to–volume ratio, durability and resilient behavior, which prevents them from being 'flat–packed'. Those characteristics which make waste tires such a problem while being landfilled, make them one of the most reusable waste materials for soil stabilization and the construction of sustainable earth backfills, thereby serving a variety of infrastructure needs, e.g. embankments, retaining walls and bridge abutments. Similar to fiber–reinforced soils, the rubber assemblage randomly distributes in the soil regime, and due to its rough surface texture, elastic character and low water adsorption capacity, could engender a spatial three–dimensional reinforcement network in favor of weaving/interlocking the soil grains into a coherent matrix of induced strength, improved ductility and deduced heave/settlement, thereby enhancing the integrity and stability of the infrastructure.

The advantages of soil–rubber composites in engineering performance, which conventional soil earth fills rarely exhibit, could favorably promote sustainability of the infrastructure system. However, before the technology can be deployed more research is urgently required. To complement a further step towards sustainability, the present study intends to examine the rubber's capacity of ameliorating the inferior engineering characteristics of expansive soils, thereby attempting to solve two widespread hazards (i.e. the expansive soil problem and the tire rubber disposal problem) with one solution.

2. Research Gaps

The use of recycled tire rubbers in geotechnical practice dates back to the early 1990s, where theoretical concepts governing the performance of soil–rubber blends were put into perspective. It was noted that similar to fiber–reinforced soils, the rubber assemblage randomly distributes in the soil regime, and when optimized in content and geometry, alters the soil fabric by amending the bonding along the interface (or contact) between the soil and the reinforcement, thereby enhancing the integrity and stability of the low–graded host soil. The literature from this era, however, was mainly focused on coarse–grained soils, and as such, the rubber's potential in amending the inferior engineering characteristics of expansive soils remained rather vague. To this date, the available research on rubberized expansive soils remains rather limited, as the majority of literature sources have mainly emphasized on coarse–grained soils and in some cases low plasticity clays. Based on the comprehensive literature review, which will be presented as part of the introductory sections of the subsequent chapters, the following research gaps were identified (and hence addressed) in the present study:

1) A review of the literature indicates a rather common emphasis on the application of coarse–grained tire rubber material in the form of fibers, shreds and aggregates. Such materials, however, would be associated with implementation difficulties when dealing with cohesive clay soils (e.g. mixing difficulties and hence non–uniform distribution of rubber particles in the soil regime). As such, less regarded types of recycled tires, such as rubber crumbs/powder and rubber buffings, take the advantage of better workability, and thus demand further investigation. Quite clearly, a vital step towards the production and placement of suitable soil–rubber earth fills is compaction. In this context, the maximum dry unit weight has been reported to decrease with increase in rubber content, while the reported trends for optimum water content still remain rather inconsistent. In comparison, limited studies have been conducted on the consistency limits, the results of which have yet been systematically correlated with other geotechnical properties such as the compaction characteristics. With the soil–rubber blend gaining ground as a viable geomaterial in practice, the need for an efficient and simple tool to adequately predict its performance, in terms of compaction, arises as an inevitable necessity. If developed, such a predictive toolbox would aid the practicing engineer to arrive at reliable soil–rubber design choices without the hurdles of conducting time–consuming laboratory compaction tests. Though numerous attempts have been made to correlate the compaction

characteristics with the consistency limits for natural fine–grained soils, such correlative models have yet been developed for rubber mixed soils.

2) The mechanical response of rubber–reinforced soils is primarily a function of rubber content, i.e. rubber–to–dry soil weight ratio. However, the rubber's geometrical properties, mainly defined in terms of the rubber's mean particle size, may also portray an equally important role in yielding an effective stabilization scheme. The latter is expected to be somewhat similar to that of aspect ratio (or fiber length) in fiber–reinforced soils, which has been well documented in the fiber reinforcement literature. With rubbers, however, this aspect has not yet been adequately addressed in the literature, in what can describe the rubber reinforcement technique as an ad hoc stabilization solution demanding further examination. It is therefore essential to systematically investigate the effect of rubber size/shape on common geotechnical properties relevant to expansive clay soils, e.g. swell–shrink/consolidation properties, cracking intensity, strength–related features and micro–structure (or fabric) evolution.

3) With the soil–rubber composite gaining ground as a viable geomaterial in practice, the need for an efficient and simple tool to adequately predict its short–term performance under field conditions, in terms of shear strength, arises as an inevitable necessity. Such a predictive toolbox, if developed, would aid the geotechnical engineer to arrive at reliable soil–rubber design choices without the hurdles of conducting time–consuming experimental tests. In this context, a limited number of discrete element models have been proposed, which adequately simulate the interfacial shear strength of rubber–reinforced sands. These studies gained insight into the inter–particle interactions, and demonstrated the role of rubber particles in changing the material fabrics and the material stiffness. Moreover, the use of artificial intelligence, e.g. neural networks, fuzzy logic systems and combined neuro–fuzzy approaches, has also shown great promise in describing/simulating the sand–rubber interactions. To the author's knowledge, there have been no attempts to extend the current numerical or constitutive literature to the clay–rubber shear strength problem. Nonetheless, such models, even if developed for the clay–rubber interface, would most certainly suffer from long–lasting and sophisticated calibration procedures, thus leading to impractical frameworks which are not trivial to implement for practicing engineers. It has been the author's experience that the dimensional analysis concept well provides a feasible path towards the development of physically meaningful models capable of efficiently estimating strength–related parameters of stabilized soil mixtures as

a function of the mixture's index properties. Given the absence of such models for the soil–rubber composite, any attempt in this context would be highly welcome.

4) Seasonal fluctuations, defined as alternate periods of rainfall and drought (or cyclic wetting–drying), lead to the reconstruction of the soil micro–structure, which in turn alters the volume change behavior of the expansive soil. Consequently, arriving at reliable solutions capable of counteracting the adversities associated with expansive soils demands a further examination of the introduced stabilization scheme under the cyclic wetting–drying action. The cyclic wetting–drying behavior of natural expansive soils has been well documented in the literature. In comparison, the number of documented studies addressing the cyclic wetting–drying behavior of stabilized expansive soils are limited, most of which have been carried out in the context of chemical stabilization by means of cementitious and polymeric agents. To the author's knowledge, however, the cyclic wetting–drying behavior of rubber mixed expansive soils remains undetermined.

5) Previous testing conducted in South Australia indicates that the majority of soils in the state are expansive clays. The predominant soils are Hindmarsh and Keswick clays, which are abundantly found in high–population commercial and residential areas. When exposed to South Australia's Mediterranean climate, such soils are prone to significant volume changes, i.e. heave and settlements, which bring forth instability concerns to the overlying structures. These concerns have incurred significant maintenance costs, and thus demand engineering solutions to alleviate the associated socio–economic impacts. As the South Australian government shifts towards a more sustainable mindset, stabilization by means of recycled tire rubbers would be a highly welcome approach in this context. To the author's knowledge, however, no systematic study has been carried out to investigate the rubber's potential in mitigating the swelling problem of South Australian expansive soils. Moreover, the use of recycled tire rubbers alongside other emerging sustainable/green stabilization materials, such as polymeric agents, has yet been investigated with reference to real–life geotechnical problems (e.g. South Australia's expansive soil problem), and thus demands further examination.

3. Research Objectives and Thesis Layout

The present thesis consists of eight chapters and is in the format of a **thesis by publication**. The current chapter, **Chapter 1**, provides an introductory grounding to this research, and

includes topics such as problem statement, research gaps, research objectives, thesis layout and concluding remarks. **Chapters 2** to **8** include seven published, accepted or submitted journal papers, which intend to address the five research gaps outlined in the previous section. A brief description of **Chapters 2** to **8** is provided in the following:

- **Chapter 2** includes a published journal paper entitled "Consistency Limits and Compaction Characteristics of Clay Soils Containing Rubber Waste", which intends to address **Research Gap #1** (see **Section 2**). The details of this publication are as follows:

> **Soltani A**, Deng A, Taheri A and Sridharan A **(2018)** Consistency Limits and Compaction Characteristics of Clay Soils Containing Rubber Waste. ***Proceedings of the Institution of Civil Engineers–Geotechnical Engineering*** **x(x): x–x**, https://doi.org/10.1680/jgeen.18.00042.

- **Chapter 3** includes a published journal paper entitled "Swell–Shrink–Consolidation Behavior of Rubber–Reinforced Expansive Soils", which intends to address **Research Gap #2** (see **Section 2**). The details of this publication are as follows:

> **Soltani A**, Deng A, Taheri A and Sridharan A **(2019)** Swell–Shrink–Consolidation Behavior of Rubber–Reinforced Expansive Soils. ***Geotechnical Testing Journal*** **42(3): x–x**, https://doi.org/10.1520/gtj20170313.

- **Chapter 4** includes a submitted journal paper entitled "Tire Rubber–Reinforced Expansive Soils: Two Hazards, One Solution?", which intends to address those aspects of **Research Gap #2** (see **Section 2**) which were not discussed in **Chapter 3**. The details of this publication are as follows:

> **Soltani A**, Taheri A, Deng A and Nikraz H **(2018)** Tire Rubber–Reinforced Expansive Soils: Two Hazards, One Solution?. ***Proceedings of the Institution of Civil Engineers–Construction Materials*** **x(x): x–x**, http://doi.org/x.[1]

[1]**Under Review** [submitted on **29 September 2018**].

- **Chapter 5** includes a submitted journal paper entitled "Interfacial Shear Strength of Rubber–Reinforced Clays: A Dimensional Analysis Perspective", which intends to address **Research Gap #3** (see **Section 2**). The details of this publication are as follows:

> **Soltani A**, Deng A, Taheri A, Mirzababaei M and Nikraz H **(2018)** Interfacial Shear Strength of Rubber–Reinforced Clays: A Dimensional Analysis Perspective. ***Geosynthetics International*** **x(x): x–x**, http://doi.org/x.[2]

- **Chapter 6** entitled "California Bearing Ratio of Tire Crumbles–Fly Ash Mixed with Clay: A Dimensional Analysis Perspective" includes an accepted discussion paper, which intends to provide further verification for the novel dimensional analysis technique introduced in **Chapter 5**. The details of this publication are as follows:

> **Soltani A** and Mirzababaei M **(2018)** Comment on "Compaction and Strength Behavior of Tire Crumbles–Fly Ash Mixed with Clay" by A. Priyadarshee, A. Kumar, D. Gupta, and P. Pushkarna. ***Journal of Materials in Civil Engineering*** **x(x): x–x**, https://doi.org/x.[3]

- **Chapter 7** includes an unsubmitted journal paper entitled "Swell–Shrink Behavior of Rubberized Expansive Soils During Alternate Wetting and Drying", which intends to address **Research Gap #4** (see **Section 2**). The details of this publication are as follows:

> **Soltani A**, Deng A, Taheri A, Mirzababaei M and Vanapalli SK **(2018)** Swell–Shrink Behavior of Rubberized Expansive Clays During Alternate Wetting and Drying. ***x*** **x(x): x–x**, https://doi.org/x.[4]

- **Chapter 8** includes a published journal paper entitled "Rubber Powder–Polymer Combined Stabilization of South Australian Expansive Soils", which intends to address **Research Gap #5** (see **Section 2**). The details of this publication are as follows:

[2]**Under Review** [submitted in revised form on **13 July 2018**].
[3]**In Press** [accepted on **11 May 2018**].
[4]**Target Journals:** *Journal of Geotechnical and Geoenvironmental Engineering* [Link], *Geotechnical Testing Journal* [Link], *Geotextiles and Geomembranes* [Link], *Geosynthetics International* [Link], *Proceedings of the Institution of Civil Engineers–Ground Improvement* [Link]

Soltani A, Deng A, Taheri A and Mirzababaei M **(2018)** Rubber Powder–Polymer Combined Stabilization of South Australian Expansive Soils. ***Geosynthetics International*** **25(3): 304–321**, http://doi.org/10.1680/jgein.18.00009.

4. Additional Publications

The following is a list of **additional** published and/or submitted journal papers compiled during the author's candidature at the University of Adelaide, most of which address topics **closely related** to that of the present PhD thesis:

Soltani A, Taheri A, Deng A and Azimi M **(2019)** A Note on Determination of the Preconsolidation Pressure. ***Journal of Testing and Evaluation*** **47(6): x–x**, http://doi.org/10.1520/jte20170689.

Soltani A, Deng A and Taheri A **(2018)** Swell–Compression Characteristics of a Fiber–Reinforced Expansive Soil. ***Geotextiles and Geomembranes*** **46(2): 183–189**, http://doi.org/10.1016/j.geotexmem.2017.11.009.

Soltani A, Deng A, Taheri A, Sridharan A and Estabragh AR **(2018)** A Framework for Interpretation of the Compressibility Behavior of Soils. ***Geotechnical Testing Journal*** **41(1): 1–16**, http://doi.org/10.1520/gtj20170088.

Soltani A, Estabragh AR, Taheri A, Deng A and Meegoda JN **(2018)** Experiments and Dimensional Analysis of Contaminated Clay Soils. ***Environmental Geotechnics*** **x(x): x–x**, http://doi.org/10.1680/jenge.18.00018.

Soltani A and Mirzababaei M **(2018)** Comment on "Effects of Lime Addition on Geotechnical Properties of Sedimentary Soil in Curitiba, Brazil" [J Rock Mech Geotech Eng 10 (2018) 188–194]. ***Journal of Rock Mechanics and Geotechnical Engineering*** **x(x): x–x**, http://doi.org/x.[5]

Mirzababaei M, Arulrajah A, Horpibulsuk S, **Soltani A** and Khayat N **(2018)** Stabilization of Soft Clay Using Short Fibers and Poly Vinyl Alcohol. ***Geotextiles and Geomembranes*** **46(5): 646–655**, http://doi.org/10.1016/j.geotexmem.2018.05.001.

Estabragh AR, **Soltani A** and Javadi AA **(2018)** Effect of Pore Water Chemistry on the Behaviour of a Kaolin–Bentonite Mixture During Drying and Wetting Cycles. ***European Journal of Environmental and Civil Engineering*** **x(x): x–x**, http://doi.org/10.1080/19648189.2018.1428691.

[5]**In Press** [accepted on **13 August 2018**].

Zhang J, Deng A, Jaksa MB and **Soltani A (2018)** Mechanical Behavior of Micaceous Clays. ***Journal of Rock Mechanics and Geotechnical Engineering*** **x(x): x–x**, http://doi.org/x.[6]

Soltani A, Taheri A, Khatibi M and Estabragh AR **(2017)** Swelling Potential of a Stabilized Expansive Soil: A Comparative Experimental Study. ***Geotechnical and Geological Engineering*** **35(4): 1717–1744**, http://doi.org/10.1007/s10706-017-0204-1.

Soltani A, Deng A, Taheri A and Mirzababaei M **(2017)** A Sulphonated Oil for Stabilisation of Expansive Soils. ***International Journal of Pavement Engineering*** **x(x): x–x**, http://doi.org/10.1080/10298436.2017.1408270.

Soltani A, Azimi M, Deng A and Taheri A **(2017)** A Simplified Method for Determination of the Soil–Water Characteristic Curve Variables. ***International Journal of Geotechnical Engineering*** **x(x): x–x**, http://doi.org/10.1080/19386362.2017.1344450.

Soltani A (2017) Discussion of "Optimization of Carpet Waste Fibers and Steel Slag Particles to Reinforce Expansive Soil Using Response Surface Methodology" by M. Shahbazi, M. Rowshanzamir, S.M. Abtahi, S.M. Hejazi [Appl. Clay Sci., doi:10.1016/j.clay.2016.11.027]. ***Applied Clay Science*** **x(x): x–x**, http://doi.org/10.1016/j.clay.2017.07.020.

Soltani A (2016) Discussion of "Compressibility Behavior of Soils: A Statistical Approach" by Syed Iftekhar Ahmed and Sumi Siddiqua [Geotechnical and Geological Engineering, doi: 10.1007/s10706-016-9996-7]. ***Geotechnical and Geological Engineering*** **34(5): 1687–1692**, http://doi.org/10.1007/s10706-016-0062-2.

5. Concluding Remarks

The following conclusions can be drawn from this study:

- As a result of rubber inclusion, the consistency limits, i.e. liquid limit w_L, plastic limit w_P, flow index I_F and plasticity index I_P, exhibited a linear monotonic decreasing trend with increase in rubber content. The rate of decrease, however, was dependent on the type of soil, with the CH soils (high–plasticity clays) exhibiting a greater tendency for reduction compared to that of the CI soils (intermediate–plasticity clays). [see **Chapter 2**]

- As a result of rubber inclusion, the compaction characteristics, i.e. optimum water content w_{opt} and maximum dry unit weight γ_{dmax}, exhibited a linear monotonic decreasing trend with increase in rubber content. Similar to the consistency limits, the rate of decrease in w_{opt} was dependent on the type of soil, with the CH soils exhibiting a greater tendency for reduction.

[6]**Under Review** [submitted on **06 October 2018**].

The rate of decrease in γ_{dmax}, however, was less influenced by the type of soil. Such results foster the use of soil–rubber blends as a viable lightweight material for the construction of sustainable earth fills, thus serving a variety of infrastructure needs, e.g. road/railway embankments, retaining walls and bridge abutments. [see **Chapter 2**]

- The compaction characteristics were strongly correlated with the plastic limit. In this case, simple correlative models in the form of $w_{opt}=0.941w_P$ and $\gamma_{dmax}=0.932\gamma_{dP}$ (γ_{dP}=dry unit weight at plastic limit water content with a presumptive saturation degree of 100%) were obtained for the optimum water content and the maximum dry unit weight, respectively. The predictive capacity of the proposed models was examined and further validated by statistical techniques. The proposed correlative models offer a practical procedure towards predicting the compaction characteristics of soil–rubber blends without the hurdles of conducting the conventional compaction test, and hence can be implemented in practice for preliminary assessments. [see **Chapter 2**]

- As a result of rubber inclusion (and/or cyclic wetting–drying), the swelling strain–time locus experienced a major downward shift over the semi–log space, signifying a capacity to counteract the heave in both magnitude and time. Improvement in the rate and potential of swelling was dependent on both the rubber content and the rubber size/shape, with the former taking on a more pronounced role. A similar dependency was also observed for the shrinkage potential. In this case, however, the effect of rubber size/shape was observed to be rather marginal. [see **Chapters 3** and **7**]

- The rubber inclusions altered the void ratio–effective stress consolidation locus, leading to a significant reduction in the swelling pressure. The variations of swelling pressure suggested a trend similar to that of swelling potential. In addition, the rubber inclusions led to a notable reduction in the compression and swell indices, indicating a capacity to counteract material collapse when stressed. The compression index was observed to be rubber size/shape–dependent; however, for the swell index, the performance of both rubber types were found to be on par with each other. [see **Chapter 3**]

- The secondary consolidation rate also exhibited a rubber content and rubber size dependency, indicating a capacity to counteract the settlement in both magnitude and time. The higher the rubber content the lower the secondary consolidation rate, with the finer rubber maintaining a slight advantage over the coarser rubber. The resulted trends for the

secondary swelling and secondary consolidation rates were observed to be consistent and comparable. [see **Chapter 3**]

- The rubber inclusions were able to amend desiccation–induced cracking. The cracking intensity was dependent on both the rubber content and the rubber size/shape, with the former portraying a more significant role. In this case, the higher the rubber content the greater the magnitude of improvement, with the coarser rubber holding a notable advantage over similar samples reinforced with the finer rubber. [see **Chapters 4** and **8**]

- For both fine and coarse rubber types, the peak unconfined compression and peak split tensile strength values were dependent on the rubber content, peaking at R_c=5–10% (by weight of dry soil) then decreasing at higher rubber inclusions. Rubber–clustering effects were vigorously evident for rubber contents greater than 10%, which led to some adverse results. The effect of rubber size and shape was mainly translated to higher ductility, lower stiffness and higher energy adsorption capacity rather than peak strength improvements. [see **Chapters 3** and **4**]

- The peak and critical shear strength values were dependent on both the rubber content and the rubber size, with the former portraying a more significant role. For rubber contents equal to or less than 10%, the rubber of coarser category slightly outperformed the finer rubber in terms of higher peak shear strength properties, while an opposite effect was evident at higher rubber inclusions. In this case, R_c=20% served as a transition point by manifesting a similar performance with marginal differences for the two rubber types. The strain–softening character was less apparent at high inclusions of the coarser rubber, thus resulting in induced strength performance at critical state condition. As a result, the critical shear strength was in favor of both a higher rubber content and a larger rubber size. [see **Chapters 4** and **5**]

- The results of the unconfined compression, split tensile and direct shear tests were cross–checked with the swell–shrink/consolidation properties to arrive at the optimum rubber content. A rubber inclusion of 10% (preferably the rubber of coarser category) satisfied a notable decrease in the swell–shrink/consolidation capacity as well as improving (or maintaining) the strength–related features, and thus was deemed as the optimum choice. Where context changes and the compressive/tensile strength and stiffness of the material are not a primary concern, higher rubber inclusions up to 20% may also be considered as acceptable choices. [see **Chapters 3** and **4**]

- The dimensional analysis concept was extended to the soil–rubber shear strength problem, thereby leading to the development of a series of simple and practical dimensional models capable of simulating the shear stress–horizontal displacement response as a function of the composite's basic index properties. The predictive capacity of the proposed dimensional models was examined and validated by statistical techniques. The proposed dimensional models contain a limited number of fitting/model parameters, which can be calibrated by minimal experimental effort (as well as simple explicit calculations) and hence implemented for predictive purposes. [see **Chapters** 5 and 6]

- To justify the use of higher rubber contents in practice, a sustainable polymer agent, namely Polyacrylamide (PAM) of anionic character, was introduced as the binder, and a case study was carried out with respect to South Australian expansive soils. As a result of PAM treatment, the connection interface between the rubber particles and the clay matrices were markedly improved, which in turn led to lower swelling/shrinkage properties, higher resistance to cyclic wetting–drying, and reduced tendency for cracking compared to that of the conventional soil–rubber blend. A rubber inclusion of 20%, paired with 0.2 g/l PAM, was suggested to effectively stabilize South Australian expansive soils. [see **Chapter** 8]

- The cost efficiency of the rubber reinforcement technique was compared to conventional poly– (ester, ethylene or propylene) fibers. Significant cost reduction can be achieved where rubbers are used as a replacement for conventional fibers. More importantly, beneficial reuse of recycled tires provides a sound environmental alternative to the safe disposal concern associated with such waste materials. [see **Chapter** 3]

References

Dunham-Friel J and Carraro JAH **(2011)** Shear Strength and Stiffness of Expansive Soil and Rubber (ESR) Mixtures in Undrained Axisymmetric Compression. In *Geo–Frontiers 2011 (GSP 211): Advances in Geotechnical Engineering* (Han J and Alzamora DE (eds)). ASCE, Dallas, Texas, USA, pp. 1111–1120, http://doi.org/10.1061/41165(397)114.

Jones LD and Jefferson I **(2012)** Expansive Soils. In *ICE Manual of Geotechnical Engineering: Volume I* (Burland J, Chapman T, Brown M and Skinner H (eds)). ICE Publishing, London, UK, pp. 413–441, http://doi.org/10.1680/moge.57074.0413.

Li J, Saberian M and Nguyen BT **(2018)** Effect of Crumb Rubber on the Mechanical Properties of Crushed Recycled Pavement Materials. *Journal of Environmental Management* **218**: 291–299, http://doi.org/10.1016/j.jenvman.2018.04.062.

Nelson JD and Miller DJ **(1992)** *Expansive Soils: Problems and Practice in Foundation and Pavement Engineering (1st ed)*. John Wiley & Sons, New York, New York, USA, ISBN:0471511862.

Chapter 2

Consistency Limits and Compaction Characteristics of Clay Soils Containing Rubber Waste

Amin Soltani [a,†], An Deng [b], Abbas Taheri [c] and Asuri Sridharan [d,e]

[a] **PhD Student** − School of Civil, Environmental and Mining Engineering, The University of Adelaide, Adelaide, SA 5005, Australia (**Email:** Amin.Soltani@adelaide.edu.au; **ORCID:** 0000-0002-0483-7487)

[b] **Senior Lecturer** − School of Civil, Environmental and Mining Engineering, The University of Adelaide, Adelaide, SA 5005, Australia (**Email:** An.Deng@adelaide.edu.au)

[c] **Senior Lecturer** − School of Civil, Environmental and Mining Engineering, The University of Adelaide, Adelaide, SA 5005, Australia (**Email:** Abbas.Taheri@adelaide.edu.au)

[d] **Professor Emeritus** – Department of Civil Engineering, Indian Institute of Science, Bangalore 560012, India; [e] **Honorary Research Scientist** – Indian National Science Academy, New Delhi 110002, India (**Email:** SridharanAsuri@yahoo.com)

[†] **Correspondence:** Amin Soltani (**Email:** Amin.Soltani@adelaide.edu.au; **ORCID:** 0000-0002-0483-7487)

Publication Details: **Soltani A**, Deng A, Taheri A and Sridharan A **(2018)** Consistency Limits and Compaction Characteristics of Clay Soils Containing Rubber Waste. ***Proceedings of the Institution of Civil Engineers–Geotechnical Engineering*** **x(x): x–x**, https://doi.org/10.1680/jgeen.18.00042.

Abstract

The present study aims at the development of practical correlative models capable of predicting the compaction characteristics of ground rubber–clay (GRC) blends. Four different clay soils, ranging from *intermediate* to *high plasticity*, were adopted for the test program. Each of the four soil choices was blended with four different rubber contents (by weight), i.e. 5%, 10%, 20% and 30%. The test program consisted of cone penetration (consistency limits) and standard Proctor compaction tests. As a result of ground rubber (GR) inclusion, the consistency limits, i.e. liquid limit w_L, plastic limit w_P ($w_P=w_L–0.715I_F$, where I_F=flow index) and plasticity index

I_P (I_P=0.715I_F), and the compaction characteristics, i.e. optimum water content w_{opt} and maximum dry unit weight γ_{dmax}, all exhibited a linear decreasing trend with increase in rubber content. The rate of decrease, however, was greater for the *high plasticity clays*. Simple correlative models in the form of w_{opt}=0.941w_P and γ_{dmax}=0.932γ_{dP} (γ_{dP}=dry unit weight at plastic limit) were suggested and validated by statistical techniques. The proposed models provide a practical procedure towards predicting the compaction characteristics of GRC blends without the hurdles of conducting laboratory compaction tests, and thus can be implemented in practice for preliminary assessments.

Keywords: Clay soil; Ground rubber; Cone Penetration; Flow index; Plastic limit; Optimum water content; Maximum dry unit weight.

Abbreviations

CH	clay with high plasticity
CI	clay with intermediate plasticity
CL	clay with low plasticity
GR	ground rubber
GRC	ground rubber–clay mix
USCS	unified soil classification system
ZAV	zero–air voids

Notation

G_{sm}	average specific gravity of GRC
G_{sr}	specific gravity of GR
G_{ss}	specific gravity of soil solids
I_F	flow index
I_P	plasticity index
MAPE	mean absolute percentage error
NRMSE	normalized root mean squares error
R^2	coefficient of determination
R_c	rubber content (by weight)
R_c^M	median rubber content
w	water content
w_L	liquid limit
w_{opt}	optimum water content
w_P	plastic limit
w_P^M	plastic limit corresponding to R_c^M
w_{Po}	plastic limit for the virgin clay
γ_d	dry unit weight
γ_{dmax}	maximum dry unit weight
γ_{dP}	dry unit weight at plastic limit
γ_w	unit weight of water
δ	cone penetration
η	coefficient of plastic limit reduction
χ	average ratio of I_P to I_F

1. Introduction

The design and construction of geostructures often necessitate incorporating low–graded clay soils, with high moisture susceptibility (and plasticity) and low bearing capacity, into the construction. Common solutions to counteract the adversities associated with such soils include soil–replacement (i.e. replacing the poor–quality clay soil with desired quarried materials) or attempting to improve the problematic soil by means of stabilization techniques. Currently, two stabilization schemes are in vogue for clay soils, i.e. chemical and mechanical stabilization (Soltani et al. 2017[a]). The chemical scheme makes use of chemical binders, which initiate a series of short– and long–term chemical reactions in the clay–binder medium, thereby amending the soil fabric into a coherent matrix of improved mechanical performance. Common binders include agents of traditional (e.g. cement, lime and fly ash) or non–traditional (e.g. polymers, resins and sulfonated oils) categories, both of which have been well documented in the literature (e.g. Mirzababaei et al. 2009; Estabragh et al. 2013, 2014; Georgees et al. 2015; Jha and Sivapullaiah 2016; Soltani et al. 2017[b]). The mechanical technique often involves the placement of randomly or specifically–engineered reinforcements (e.g. natural and synthetic fibers) in the soil regime, thereby engendering a spatial three–dimensional reinforcement network in favor of weaving (or interlocking) the soil grains into a unitary mass of improved mechanical performance (e.g. Tang et al. 2010; Estabragh et al. 2016; Mirzababaei et al. 2017; Wang et al. 2017; Mirzababaei et al. 2018; Soltani et al. 2018[a]). As of late, many developed and developing countries have initiated the transition towards 'sustainable infrastructure', a concept which fosters the beneficial reuse of solid wastes and/or industrial by–products as a replacement for conventional quarried materials (such as sand) and/or stabilization agents, thereby conserving natural resources as well as reducing the level of greenhouse gas emissions. Promising replacements, based on recent studies, include recycled tire rubbers, waste textiles, recycled crushed glass, demolition wastes, mine tailings, spent coffee grounds, kiln and quarry dusts, and silicate/calcium geopolymers (e.g. Soosan et al. 2005; Mirzababaei et al. 2013[a], 2013[b]; Alazigha et al. 2016; Al-Amoudi et al. 2017; Arulrajah et al. 2017; Kua et al. 2017).

Waste tire rubbers are being generated at an increasing rate throughout the world. Such materials are bulky in nature, owing to their low weight to volume ratio, and thus consume valuable landfill space upon disposal. As such, local communities and governmental agencies have been increasingly encouraged to recycle and hence reuse waste tires as part of the infrastructure system. The rubber–soil blend is showing great promise in several aspects, e.g. reduced unit weight, enhanced strength and ductility, increased permeability, and reduced

moisture susceptibility (i.e. swell–shrink capacity), which can facilitate the production and placement of sustainable earth fills such as road and railway embankments (e.g. Cetin et al. 2006; Özkul and Baykal 2007; Trouzine et al. 2012; Cabalar et al. 2014; Srivastava et al. 2014; Signes et al. 2016; Perez et al. 2017; Yadav and Tiwari 2017[a], 2017[b]; Soltani et al. 2018[b], 2018[c]; Wang et al. 2018). When placed in a flowable condition, the rubber–soil blend outperforms conventional soil backfills by enabling the placement of particles into any irregular or inaccessible space without significant compaction efforts (ACI R229 2013). The advantages of rubber mixed soils in engineering performance, which natural soils rarely exhibit, suggests a promising path towards sustainability without compromising performance. Though promising, the leaching of heavy metals from rubber particles (into the soil mass and/or water bodies) could raise some environmental concerns. In this case, most documented studies have reported that the degree of soil and water contamination both remain within the allowable limits provided by various health and environmental agencies. When paired with coarse–grained soils, however, the rubber–soil blend should be stabilized by means of chemical binders to meet the required environmental standards (see Yadav and Tiwari (2017[c]) for more details).

A review of the literature indicates a rather common emphasis on the application of coarse–grained tire rubber material in the form of fibers, shreds and aggregates. Such materials, however, would be associated with implementation difficulties when dealing with cohesive clay soils (e.g. mixing difficulties and hence non–uniform distribution of rubber particles in the soil regime). As such, less regarded types of recycled tires such as fine ground rubber (GR) take the advantage of better workability, and thus demand further investigation. Quite clearly, a vital step towards the production and placement of suitable rubber–clay earth fills is compaction. In this context, the maximum dry unit weight has been reported to decrease with increase in rubber content, while the reported trends for optimum water content still remain rather inconsistent (e.g. Al-Tabbaa et al. 1997; Cetin et al. 2006; Seda et al. 2007; Kalkan 2013; Priyadarshee et al. 2018). In comparison, limited studies (e.g. Cetin et al. 2006; Trouzine et al. 2012; Srivastava et al. 2014) have been conducted on the consistency limits, the results of which have yet been systematically correlated with other geotechnical properties such as the compaction characteristics. With rubber–soil blends gaining ground as a viable geomaterial in practice, the need for an efficient and simple tool to adequately predict its performance, in terms of compaction, poses as an inevitable necessity. If developed, such a predictive toolbox would aid the practicing engineer to arrive at reliable rubber–soil design choices without the hurdles of conducting time–consuming laboratory compaction tests. Though numerous attempts have

been made to correlate the compaction characteristics with the consistency limits for natural fine–grained soils (e.g. Pandian et al. 1997; Blotz et al. 1998; Gurtug and Sridharan 2002, 2004; Sridharan and Nagaraj 2005; Sivrikaya et al. 2008; Di Matteo et al. 2009; Nagaraj et al. 2015; Pillai and Vinod 2016; Gurtug et al. 2018), such correlative models have yet been developed for rubber mixed soils.

In this study, a series of cone penetration (consistency limits) and standard Proctor compaction tests were carried out on various ground rubber–clay (GRC) blends (prepared with four different clay soils) to generate a reliable database allowing for the development of simple correlative models capable of predicting the compaction characteristics of GRC blends as a function of the composite's consistency limits. The models proposed in the present study provide a practical procedure towards predicting the compaction characteristics of GRC blends without the need of conducting time–consuming compaction tests.

2. Materials

2.1. Clay Soils

Four different soils consisting of both natural and commercial soils, covering a wide range of plasticity characteristics, were adopted for the experimental program. The natural soils, hereafter denoted as soils RC1 and RC2, consisted of reddish–brown clays sourced from a landfill site located at Adelaide, South Australia. The commercial soils were supplied by a local manufacturer, and included kaolinite (hereafter soil K) and a mixture of 85% kaolinite and 15% sodium–activated bentonite (hereafter soil KB). Physical and mechanical properties of the soils, determined as per relevant ASTM and Australian standards, are summarized in **Table 1**. The liquid limit w_L and plasticity index I_P were measured as w_L=44% and I_P=22% for soil K, and w_L=47% and I_P=29% for soil RC1, from which both soils were characterized as *clay with intermediate plasticity* (CI) in accordance with the Unified Soil Classification System (USCS). The soils KB and RC2, however, were graded as *clay with high plasticity* (CH), respectively, exhibiting w_L and I_P values of 59% and 31% for soil KB, and 78% and 57% for soil RC2.

2.2. Ground Rubber (GR)

Commercially available ground rubber (hereafter denoted as GR), supplied by a local distributor, was used as the reinforcing agent. The conventional grain–size (or sieve) analysis, carried out in accordance with the ASTM D422–07 standard, indicated that GR is similar in

size to medium–fine sand, with particles ranging between 1.18 mm and 75 μm. The particle diameters corresponding to 10%, 30% and 60% finer were measured as D_{10}=0.182 mm, D_{30}=0.334 mm and D_{60}=0.513 mm. The uniformity (i.e. $C_u=D_{60}/D_{10}$) and curvature (i.e. $C_c=D_{30}^2/D_{10}D_{60}$) coefficients were therefore obtained as C_u=2.81 and C_c=1.20, from which GR was classified as *poorly–graded* in accordance with the USCS criteria. **Figure 1** illustrates microscopic micrographs of the rubber particles at three different magnification ratios (**Figure 1a**: 1x magnification; **Figure 1b**: 50x magnification; and **Figure 1c**: 200x magnification). As depicted in **Figure 1b**, the rubber particles are non–spherical and highly–irregular in shape. Moreover, a series of cavity–like micro–cracks are distributed along the rubber's surface (see **Figure 1c**), thus making for a rough surface texture. Such surface features may potentially promote adhesion and/or induce interfacial friction between the rubber particles and the soil grains, thereby altering the soil fabric into a coherent matrix of enhanced mechanical performance (Soltani et al. 2018[b]). Physical properties and chemical composition of GR, as supplied by the manufacturer, are provided in **Table 2**. The specific gravity of GR was found to be G_{sr}=1.09, which is approximately two–fold lower than the standard value of G_{ss}=2.65 reported for most soils.

3. Test Program

Each of the four soil choices, i.e. soils K, RC1, KB and RC2, was blended with GR at four varying rubber contents (defined as GR to dry soil weight ratio), i.e. R_c=5%, 10%, 20% and 30%, and further tested for consistency limits and compaction characteristics. Hereafter, a simple coding system, defined as KRx, RC1Rx, KBRx and RC2Rx (where Rx=x% GR), will be adopted to designate the various mix designs. As a consequence of rubber particles floating in water, standard procedures outlined in ASTM D854–14 for measuring the specific gravity of solids were not applicable. Therefore, the specific gravity for various ground rubber–clay (GRC) blends was estimated by the following theoretical relationship (Soltani et al. 2018[b]):

$$G_{sm}=\frac{G_{ss}G_{sr}(W_s+W_r)}{W_sG_{sr}+W_rG_{ss}} \quad (1)$$

where G_{sm}=average specific gravity of GRC blends; W_s=weight of dry soil; W_r=weight of GR; G_{ss}=specific gravity of soil solids (see **Table 1**); and G_{sr}=specific gravity of GR particles (=1.09).

3.1. Consistency Limits

The virgin clays and various GRC blends were tested for consistency limits, i.e. liquid limit w_L, plastic limit w_P and plasticity index I_P ($=w_L-w_P$), following the Australian code of practice (see relevant standard designations in **Table 1**). The liquid limit was obtained by means of the cone penetration method. The weight and conical angle of the cone were 80 g and 30°, respectively. The required amount of material (either virgin or GR–blended clay) was divided into six equal portions, each portion paired with a predetermined amount of water, and thoroughly mixed by mechanical effort to obtain slurries of uniform consistency. The resultant slurries where then remolded into rigid cups, measuring 53 mm in diameter and 40 mm in height, and placed in contact with the cone penetrometer for testing. The cone was allowed to freely penetrate into each sample for approximately 5 s. The depth of penetration was measured by means of a digital dial gauge to the nearest of 0.1 mm. As a result of the test, a linear change in water content w against the corresponding cone penetration δ, commonly referred to as the flow curve, can be observed. Test results are plotted over the w:$\log_{10}\delta$ space, the slope of which is defined as the flow index, i.e. $I_F=\Delta w/\Delta\log_{10}\delta$ (Sridharan et al. 1999). Furthermore, the water content at which the cone penetration reaches δ=20 mm is taken as the liquid limit.

The rolling thread method is currently in vogue for direct measurement of the plastic limit. The water content at which a mass of soil (or material) initiates to crumble when manually rolled into a thread of approximately 3.2 mm (in diameter) is taken as the plastic limit. Quite clearly, the rolling thread method is highly–subjective and therefore inevitably biased by personal judgments, which leads to inconsistent and often non–reproducible results amongst different operators. Moreover, it has been the authors' experience that this particular methodology would not be suitable for geomaterials containing notable non–plastic hydrophobic (i.e. low water adsorption capacity) fractions (despite the geomaterial's plastic response in the presence of water). The rubber's elastic character and hydrophobic nature make for a rather difficult, though possible, implementation of the conventional rolling thread technique. Though the rubber inclusion would most certainly lead to a reduced plastic limit, one cannot arrive at a certain/unique value with confidence following the current methodology. Such difficulties are essentially similar to those encountered for natural soils containing notable fractions of sand and silt, which have been well documented in the literature (e.g. Prakash and Sridharan 2006, 2012). Amongst the available experimental alternatives for indirect measurement of the plastic limit, the flow index method suggests a rather practical and objective scheme, which is also supported by robust empirical observations as well as solid fundamental evidence (see

Sridharan et al. (1999) for details). The flow index method states that the plasticity index is proportional to the flow index (obtained from the cone penetration test), i.e. $I_P \propto I_F$, and thus can be estimated by:

$$I_P = \chi I_F \tag{2}$$

where χ =empirical coefficient.

Therefore, the plastic limit can be estimated with a known liquid limit (obtained from the cone penetration test) by:

$$w_P = w_L - \chi I_F \tag{3}$$

The empirical coefficient χ falls between 0.71 and 0.74, which was calibrated based on conventional rolling thread tests conducted on 121 soil samples of widely varying plasticity characteristics and geological origin (Sridharan et al. 1999). As a typical example, and to provide further verification of χ =0.71–0.74, **Figure 2** illustrates the variations of the plasticity index I_P (I_P=w_L–w_P, where w_P=plastic limit obtained by the rolling thread method) against the flow index I_F for the virgin clays used in the present study. As demonstrated in the figure, a perfect correlation in the form of I_P=0.715I_F (with R^2=0.997) can be obtained between the plasticity and flow indices, which well complies with that suggested by Sridharan et al. (1999). Therefore, to avoid the difficulties associated with implementing the conventional rolling thread technique to various GRC blends, the plastic limit for both the virgin clays and various GRC blends was estimated by means of **Equation 3** (with χ =0.715). Hereafter, the term plastic limit will refer to that obtained by means of the flow index method.

3.2. Compaction Studies

Standard Proctor compaction tests were carried out on the virgin clays and various GRC blends in accordance with the ASTM D698–12 standard. The soil (or material) is compacted in three layers, giving each layer 25 blows by a metal hammer weighing 2.5 kg (5.5 lbs) falling through a height of 30.5 cm (12 in), thus making for a compactive effort of 593.7 kJ/m^3. The required amount of material (either virgin or GR–blended clay) was divided into six equal portions, each portion paired with a predetermined amount of water, and thoroughly mixed by hand. Extensive care was dedicated to pulverize the lumped particles, targeting homogeneity of mixtures. The

moist mixtures were sealed in plastic bags and allowed to cure for a period of 24 hours, ensuring even distribution of moisture throughout the composite mass. The cured mixtures were then subjected to the conventional standard Proctor compaction test to arrive at the dry unit weight–water content relationship, and thus quantify the optimum water content and the maximum dry unit weight.

4. Statistical Analysis

The consistency limits, obtained as per **Section 3.1**, were each independently plotted against the corresponding optimum water contents, and further examined for single–coefficient linear correlations, i.e. $w_{opt}=\beta x$ (w_{opt}=optimum water content; $x=w_L$, w_P or I_P; and β=regression coefficient or fitting parameter). The most appropriate consistency parameter (capable of adequately estimating the optimum water content for various GRC blends) was then selected and coupled with basic volume–mass relations to arrive at a semi–empirical relationship for the maximum dry unit weight. The accuracy of the proposed correlative models for both the optimum water content and the maximum dry unit weight was then examined by means of statistical fit–measure indices.

5. Results and Discussions

5.1. Effect of Ground Rubber (GR) on Consistency Limits

The flow curves for the virgin clays and various GRC blends prepared with soils K, RC1, KB and RC2 are provided in **Figures 3a–3d**, respectively. As a result of GR inclusion, the flow curve exhibited a major downward shift over the w:$\log_{10}\delta$ space (w=water content; and δ=cone penetration), indicating a significant reduction in the liquid limit (compare the water contents at δ=20 mm). Meanwhile, the slope of the flow curve was also observed to decrease with increase in rubber content, leading to a notable reduction in the flow index I_F and hence the plasticity index I_P ($I_P=0.715I_F$). As a typical case, the virgin clay KB resulted in I_F=45.12%, while the inclusion of 5%, 10%, 20% and 30% GR resulted in I_F=43.23%, 42.00%, 40.67% and 37.74%, respectively (see **Figure 3c**).

Figures 4a–4d illustrate the variations of the consistency limits, i.e. liquid limit w_L, plastic limit w_P ($w_P=w_L-0.715I_F$) and plasticity index I_P ($I_P=0.715I_F$), against rubber content R_c for the virgin clays and various GRC blends prepared with soils K, RC1, KB and RC2, respectively. The

higher the rubber content the lower the consistency limits, following a linear monotonic decreasing trend. As a typical case, the virgin clay KB resulted in w_L=59%, while the inclusion of 5%, 10%, 20% and 30% GR resulted in w_L=57%, 53%, 51% and 46%, respectively (see **Figure 4c**). The rate of decrease in w_L, w_P and I_P with respect to R_c — represented by the slope of a typical linear trendline fitted through the desired dataset (i.e. $\Delta y/\Delta R_c$, where y=w_L, w_P or I_P) — was observed to be dependent on the type of soil, with the CH soils (i.e. soils KB and RC2) exhibiting a greater tendency for reduction compared with that of the CI soils (i.e. soils K and RC1). In terms of the liquid limit, for instance, the soils KB and RC2 resulted in $\Delta w_L/\Delta R_c$= –0.425 and –0.456, respectively. For the soils K and RC1, however, these values dropped to –0.347 and –0.401, respectively.

Figure 5 illustrates the location of the tested mix designs on Casagrande's plasticity chart (**Figure 5a**: soils K and KB; and **Figure 5b**: soils RC1 and RC2). For a given type of soil, the variations of I_P against w_L followed a linear path (see the arrowed lines '1' and '2' in **Figure 5**), with relatively lower slopes (i.e. $\Delta I_P/\Delta w_L$) compared with that of the 'A' and 'U' lines of the plasticity chart. Furthermore, the value of $\Delta I_P/\Delta w_L$ was dependent on the type of soil, with the CH soils (i.e. soils KB and RC2) exhibiting greater slopes compared with that of the CI soils (i.e. soils K and RC1). The soils KB and RC2 resulted in $\Delta I_P/\Delta w_L$=0.383 and 0.517, respectively. For the soils K and RC1, however, these values changed to 0.329 and 0.395, respectively. For a given type of soil, an increase in rubber content relocated the soil towards lower plasticity regions (follow the arrowed lines '1' and '2' in **Figure 5**), while mainly maintaining the original USCS classification observed for the virgin soil. Two exceptions, however, included the soils K and KB at R_c=30%, which transitioned from the CI and CH categories to CL (*clay with low plasticity*) and CI, respectively (see KR30 and KBR30 in **Figure 5a**).

The consistency limits, the liquid limit in particular, can be employed to infer the development of soil fabric (Wroth and Wood 1978; Kim and Palomino 2009; Soltani et al. 2018[b]). A decrease in the liquid limit, as the case with GRC blends (see **Figure 4**), implies that a face–to–face aggregated (or dispersed) fabric dominates the GRC matrix (Mitchell and Soga 2005). As opposed to the edge–to–face flocculated fabric, a face–to–face aggregated fabric offers less resistance to shear (or cone penetration), which in turn leads to lower liquid limits (i.e. the 20 mm cone penetration is achieved at lower water contents). Moreover, reduction in the consistency limits as a result of GR inclusion can be attributed to the lower specific surface area and water adsorption capacity of the rubber particles compared with the soil grains (Cetin et al.

2006; Trouzine et al. 2012; Srivastava et al. 2014). The consistency limits are primarily a function of the soil's clay (or fines) content, with higher clay contents exhibiting higher liquid and plastic limits. Quite clearly, an increase in rubber content substitutes a larger portion of the clay content with non–plastic hydrophobic rubber particles, thus leading to a further decrease of the consistency limits.

5.2. Effect of Ground Rubber (GR) on Compaction Characteristics

Standard Proctor compaction curves, along with corresponding specific gravities (obtained as per **Equation 1**) and zero–air voids (ZAV) saturation lines, for the virgin clays and various GRC blends prepared with soils K, RC1, KB and RC2 are provided in **Figures 6a–6d**, respectively. For a given type of soil, the higher the rubber content the lower the average specific gravity G_{sm}, following a monotonic decreasing trend. As a result of GR inclusion, the compaction locus exhibited a major downward–leftward translation over the γ_d:w space (γ_d=dry unit weight; and w=water content), indicating a significant reduction in both the optimum water content w_{opt} and the maximum dry unit weight γ_{dmax}. Such results foster the use of GR as a viable lightweight alternative for common quarry materials such as sand. For a given type of soil, the peak (or optimum) points followed a linear decreasing trend with increase in rubber content R_c (follow the arrowed lines in **Figure 6**), thereby signifying the existence of a linear relationship for both w_{opt} and γ_{dmax} with R_c. The linear tendency for reduction is in compliance with that reported in most of the existing literature sources (e.g. Cabalar et al. 2014; Signes et al. 2016; Yadav and Tiwari 2017[a]).

Figures 7a and **7b** illustrate the variations of the compaction characteristics, i.e. w_{opt} and γ_{dmax}, against R_c for the tested mix designs, respectively. The higher the rubber content the lower the compaction characteristics, following a linear monotonic decreasing trend. The virgin clay KB, for instance, resulted in w_{opt}=25% (γ_{dmax}=14.61 kN/m^3), while the inclusion of 5%, 10%, 20% and 30% GR resulted in w_{opt}=24% (γ_{dmax}=14.27 kN/m^3), 22% (γ_{dmax}=14.16 kN/m^3), 21% (γ_{dmax}=13.71 kN/m^3) and 18% (γ_{dmax}=13.17 kN/m^3), respectively. Similar to the consistency limits (see **Figure 4**), the rate of decrease in w_{opt} with respect to R_c — represented by the slope of a typical linear trendline fitted through a desired w_{opt}–R_c dataset, i.e. $\Delta w_{opt}/\Delta R_c$ — was observed to be dependent on the type of soil, with the CH soils (i.e. soils KB and RC2) exhibiting a greater tendency for reduction compared with that of the CI soils (i.e. soils K and RC1). As demonstrated in **Figure 7a**, the soils KB and RC2 resulted in $\Delta w_{opt}/\Delta R_c$= –0.224 and –0.196, respectively. For the soils K and RC1, however, these values dropped to –0.160 and –

0.114, respectively. On the contrary, as depicted in **Figure 7b**, an opposite effect can be concluded for γ_{dmax}, as $\Delta\gamma_{dmax}/\Delta R_c$ was observed to be slightly higher for the CI soils compared with that of the CH soils (i.e. $\Delta\gamma_{dmax}/\Delta R_c$= –0.052, –0.059, –0.046 and –0.043 for soils K, RC1, KB and RC2, respectively).

Reduction in the compaction characteristics as a result of GR inclusion can be attributed to the lower specific gravity and hydrophobic nature of the rubber particles compared with the soil grains (Özkul and Baykal 2007; Cabalar et al. 2014; Signes et al. 2016). Similar to the consistency limits, the optimum water content is primarily a function of the soil's clay/fines content, with higher clay contents exhibiting a higher optimum water content. Consequently, an increase in rubber content substitutes a larger portion of the clay content with hydrophobic rubber particles, which in turn leads to a further decrease of the optimum water content. The maximum dry unit weight is proportional to the composite's specific gravity, with higher specific gravities yielding a higher maximum dry unit weight. As such, an increase in rubber content substitutes a larger portion of the soil (with a high specific gravity) with low–specific gravity rubber particles, which leads to a further decrease of the composite's average specific gravity (see G_{sm} values in **Figure 6**) and hence its maximum dry unit weight. Moreover, the elastic (or rebound) response of GR to dynamic energy during compaction may potentially reduce the compaction efficiency, and thus contribute to a lower maximum dry unit weight (Yadav and Tiwari 2017[b]).

5.3. Compaction Characteristics as a Function of Consistency Limits

The conventional compaction test, though simple in terms of procedure, has been widely regarded as a laborious and time–consuming task (Sridharan and Sivapullaiah 2005). Though numerous attempts have been made in the past to correlate the compaction characteristics with the consistency limits, such correlative models have yet been extended to GRC blends (or other similar geomaterials). As such, the present section will be devoted to the development of practical models capable of predicting the compaction characteristics of GRC blends as a function of the consistency limits.

Figure 8 illustrates the variations of the optimum water content w_{opt} (data presented in **Figure 7a**) against the consistency limits, i.e. liquid limit w_L, plastic limit w_P and plasticity index I_P (data presented in **Figures 4a–4d**), for the tested mix designs (**Figure 8a**: w_{opt}–w_L; **Figure 8b**: w_{opt}–w_P; and **Figure 8c**: w_{opt}–I_P). As depicted in **Figures 8a** and **8c**, w_L and I_P both exhibit weak

correlations with w_{opt}, and thus are deemed as unsuitable for model development. The ineptness of the liquid limit in predicting the compaction characteristics of natural fine–grained soils was first recognized by Sridharan and Nagaraj (2005), and was attributed to the fact that soils having the same liquid limit (but different plasticity characteristics) often exhibit different compaction behavior. On the contrary, w_P exhibits a rather strong correlation (with R^2=0.950) in the form of a single–coefficient linear function with w_{opt} (see **Figure 8b**), which can be given as:

$$w_{opt} = 0.941 w_P \tag{4}$$

Though some scatter can be observed with respect to **Equation 4**, all data points lie between the upper and lower 95% prediction bands, thus indicating no particular outliers associated with the predictions (see **Figure 8b**). Interestingly, the proposed model given in **Equation 4** well complies with those suggested in the literature for natural soils (but with a slightly different coefficient compared to 0.941), e.g. w_{opt}=0.92w_P (Sridharan and Nagaraj 2005), and w_{opt}=0.84w_P (Nagaraj et al. 2015).

It is well accepted that the maximum dry unit weight γ_{dmax} is proportional to the dry unit weight at the plastic limit water content with a presumptive saturation degree of 100% (Gurtug and Sridharan 2002, 2004; Pillai and Vinod 2016; Gurtug et al. 2018). Making use of basic volume–mass relations, the dry unit weight at plastic limit γ_{dP} can be expressed as:

$$\gamma_{dP} = \frac{G_{sm}\gamma_w}{1 + G_{sm} w_P} \tag{5}$$

where G_{sm}=average specific gravity of GRC blends (values presented in **Figure 6**); and γ_w=unit weight of water (=9.81 kN/m^3).

The variations of γ_{dmax} (data presented in **Figure 7b**) were plotted against γ_{dP} (obtained as per **Equation 5**) for the various mix designs, and the results are provided in **Figure 9**. A similar correlation to that observed between w_{opt} and w_P also exists between γ_{dmax} and γ_{dP} (with R^2=0.942), which can be expressed as:

$$\gamma_{dmax} = 0.932\gamma_{dP} = \frac{0.932 G_{sm}\gamma_w}{1 + G_{sm} w_P} \tag{6}$$

As depicted in **Figure 9**, all data points with respect to **Equation 6** position themselves between the upper and lower 95% prediction bands, thereby suggesting no particular outliers associated

with the predictions. Previous studies such as Gurtug and Sridharan (2002) have suggested a different coefficient of 0.98 for natural fine–grained soils, i.e. $\gamma_{dmax}=0.98\gamma_{dP}$, which is slightly higher compared to 0.932 obtained in the present study. This may be attributed to the lower average specific gravity of GRC blends compared with that of the virgin clays, which in turn gives rise to lower γ_{dP} values.

Figures 10a and **10b** illustrate the variations of both the actual and predicted w_{opt} and γ_{dmax} data against rubber content R_c for the tested mix designs, respectively. The proposed models, i.e. **Equation 4** for w_{opt} and **Equation 6** for γ_{dmax}, well comply with experimental observations, as evident with the clustering of actual and predicted data in the figures. Most of the predicted values perfectly overlap with their actual counterparts, thus signifying an excellent capacity to simulate the compaction characteristics of GRC blends by means of the plastic limit. In general, a reliable empirical model can be characterized as one that maintains a perfect balance between the apparent correlation and the exhibited error (or accuracy). The former is taken into consideration by means of the coefficient of determination R^2, with values closer to unity implying a stronger correlation. The latter is commonly examined by means of the normalized root mean squares error NRMSE (in %) and the mean absolute percentage error MAPE (in %), with values closer to zero representing a higher degree of accuracy (Soltani et al. 2018[d]). The NRMSE and MAPE indices can be obtained by the following:

$$\text{NRMSE} = \frac{\sqrt{\frac{1}{N}\sum_{i=1}^{N}(y_{mi}-y_{ai})^2}}{y_{a\,max}-y_{a\,min}}\times 100 \tag{7}$$

$$\text{MAPE} = \frac{1}{N}\sum_{i=1}^{N}\left|\frac{y_{mi}-y_{ai}}{y_{ai}}\right|\times 100 \tag{8}$$

where y_m=predicted value of the dependent variable y (=w_{opt} or γ_{dmax}); y_a=actual value of the dependent variable y (data presented in **Figures 7**); y_{amax}=maximum value of y_a data; y_{amin}=minimum value of y_a data; i=index of summation; and N=number of data points used for model development (=20, consisting of 4 virgin clays and 16 GRC blends).

The suggested models for w_{opt} (**Equation 4**) and γ_{dmax} (**Equation 6**), respectively, resulted in R^2 values of 0.950 and 0.942, thus implying that approximately 95% of the variations in experimental observations are captured and further explained by the proposed correlative models. The NRMSE and MAPE indices were, respectively, found to be 6.73% and 4.09% for

w_{opt}, and 6.05% and 1.18% for γ_{dmax}, thereby indicating an average offset of approximately 5% associated with the predictive capacity of the proposed models.

As demonstrated in **Figures 4a–4d**, the plastic limit w_P exhibited a linear relationship with rubber content R_c. For a given type of soil, one can therefore write the following:

$$w_P = w_{Po} - \eta R_c \tag{9}$$

where w_{Po}=plastic limit for the virgin clay (in %); and η=coefficient of plastic limit reduction (dimensionless).

The coefficient of plastic limit reduction η can be estimated by one plastic limit measurement for an arbitrary GRC blend. The choice of rubber content for the GRC blend would be arbitrary. From a statistical perspective, however, a median rubber content, taken as half the predefined maximum rubber content, is expected to provide a more reliable estimate of η (Mirzababaei et al. 2018; Soltani and Mirzababaei 2018). For the present study where $R_c \leq 30\%$, a median rubber content would be 15%. Consider the following designations:

- $\boldsymbol{R_c^M}$ =an arbitrary median rubber content.
- $\boldsymbol{w_P^M}$ =plastic limit corresponding to an arbitrary median rubber content R_c^M (obtained in accordance with the flow index method, as outlined in **Section 3.1**).

Therefore, the following can be derived for η:

$$\eta = \frac{w_{Po} - w_P^M}{R_c^M} \tag{10}$$

By substituting the recent **Equation 9** into **Equation 4**, one can derive the following for w_{opt}:

$$w_{opt} = 0.941(w_{Po} - \eta R_c) \tag{11}$$

Similarly, by substituting **Equation 9** into **Equation 6**, γ_{dmax} can expressed as:

$$\gamma_{dmax} = 0.932\gamma_{dP} = \frac{0.932 G_{sm}\gamma_w}{1 + G_{sm}(w_{Po} - \eta R_c)} \tag{12}$$

Though the original models given in **Equations 4** and **6** offer a fairly practical procedure towards predicting the compaction characteristics of GRC blends without the hurdles of conducting the conventional compaction test, the procedure may still be somewhat time–consuming, since a separate plastic limit measurement is to be carried out for each desired rubber content. The newly developed models given in **Equations 11** and **12**, however, suggest a more practical approach, one that requires only two plastic limit measurements (i.e. w_{Po}=plastic limit for the virgin clay; and w_P^M =plastic limit corresponding to an arbitrary median rubber content R_c^M) to arrive at an estimate of the compaction characteristics over a wide range of desired rubber contents. Similar correlative models may also be developed for different compaction energy levels, and thus arrive at a unified framework capable of predicting the compaction characteristics of GRC blends for any desired rubber content and/or rational compaction energy level.

6. Conclusions

The following conclusions can be drawn from this study:

- As a result of GR inclusion, the consistency limits, i.e. liquid limit w_L, plastic limit w_P (w_P=w_L–0.715I_F, where I_F=flow index) and plasticity index I_P (I_P=0.715I_F), exhibited a linear monotonic decreasing trend with increase in rubber content. The rate of decrease in w_L, w_P, I_F and I_P was dependent on the type of soil, with the CH soils (*high plasticity clays*) exhibiting a greater tendency for reduction compared with that of the CI soils (*intermediate plasticity clays*).

- As a result of GR inclusion, the compaction characteristics, i.e. optimum water content w_{opt} and maximum dry unit weight γ_{dmax}, exhibited a linear monotonic decreasing trend with increase in rubber content. Similar to the consistency limits, the rate of decrease in w_{opt} was dependent on the type of soil, with the CH soils exhibiting a greater tendency for reduction. The rate of decrease in γ_{dmax}, however, was less influenced by the type of soil. Such results foster the use of GRC blends as a viable lightweight material for the construction of sustainable earth fills, thus serving a variety of infrastructure needs, e.g. road/railway embankments, retaining walls and bridge abutments.

- The compaction characteristics were strongly correlated with the plastic limit. In this case, simple correlative models in the form of w_{opt}=0.941w_P and γ_{dmax}=0.932γ_{dP} (γ_{dP}=dry unit

weight at plastic limit water content with a presumptive saturation degree of 100%) were obtained for the optimum water content and the maximum dry unit weight, respectively. The predictive capacity of the proposed models was examined and further validated by statistical techniques. The proposed correlative models offer a practical procedure towards predicting the compaction characteristics of GRC blends without the hurdles of conducting the conventional compaction test, and hence can be implemented in practice for preliminary assessments.

Acknowledgements

This research was funded by the Australian Research Council (ARC) via project No. **DP140103004**, and their support is gratefully acknowledged.

References

ACI Committee 229 (**2013**) *Report on Controlled Low–Strength Materials*. American Concrete Institute, Farmington Hills, Michigan, USA, ISBN:9780870318160.

Al-Amoudi OSB, Al-Homidy AA, Maslehuddin M and Saleh TA (**2016**) Method and mechanisms of soil stabilization using electric arc furnace dust. *Scientific Reports* **7**(**46676**): 1–10, http://doi.org/10.1038/srep46676.

Alazigha DP, Indraratna B, Vinod JS and Ezeajugh LE (**2016**) The swelling behaviour of lignosulfonate–treated expansive soil. *Proceedings of the Institution of Civil Engineers – Ground Improvement* **169**(**3**): 182–193, http://doi.org/10.1680/jgrim.15.00002.

Al-Tabbaa A, Blackwell O and Porter SA (**1997**) An investigation into the geotechnical properties of soil–tyre mixtures. *Environmental Technology* **18**(**8**): 855–860, http://doi.org/10.1080/09593331808616605.

Arulrajah A, Mohammadinia A, D'Amico A and Horpibulsuk S (**2017**) Effect of lime kiln dust as an alternative binder in the stabilization of construction and demolition materials. *Construction and Building Materials* **152**: 999–1007, http://doi.org/10.1016/j.conbuildmat.2017.07.070.

Blotz LR, Benson CH and Boutwell GP (**1998**) Estimating optimum water content and maximum dry unit weight for compacted clays. *Journal of Geotechnical and Geoenvironmental Engineering* **124**(**9**): 907–912, http://doi.org/10.1061/(asce)1090-0241(1998)124:9(907).

Cabalar AF, Karabash Z and Mustafa WS (**2014**) Stabilising a clay using tyre buffings and lime. *Road Materials and Pavement Design* **15**(**4**): 872–891, http://doi.org/10.1080/14680629.2014.939697.

Cetin H, Fener M and Gunaydin O (**2006**) Geotechnical properties of tire–cohesive clayey soil mixtures as a fill material. *Engineering Geology* **88**(**1**–**2**): 110–120, http://doi.org/10.1016/j.enggeo.2006.09.002.

Di Matteo L, Bigotti F and Ricco R (**2009**) Best–fit models to estimate modified Proctor properties of compacted soil. *Journal of Geotechnical and Geoenvironmental Engineering* **135**(**7**): 992–996, http://doi.org/10.1061/(asce)gt.1943-5606.0000022.

Estabragh AR, Naseh M, Beytolahpour I and Javadi AA (**2013**) Strength of a clay soil and soil–cement mixture with resin. *Proceedings of the Institution of Civil Engineers – Ground Improvement* **166**(**2**): 108–114, http://doi.org/10.1680/grim.12.00014.

Estabragh AR, Rafatjo H and Javadi AA (**2014**) Treatment of an expansive soil by mechanical and chemical techniques. *Geosynthetics International* **21**(**3**): 233–243, http://doi.org/10.1680/gein.14.00011.

Estabragh AR, Soltani A and Javadi AA (**2016**) Models for predicting the seepage velocity and seepage force in a fiber reinforced silty soil. *Computers and Geotechnics* **75**: 174–181, http://doi.org/10.1016/j.compgeo.2016.02.002.

Georgees RN, Hassan RA, Evans RP and Jegatheesan P (**2015**) Effect of the use of a polymeric stabilizing additive on unconfined compressive strength of soils. *Transportation Research Record: Journal of the Transportation Research Board* **2473**: 200–208, http://doi.org/10.3141/2473-23.

Gurtug Y and Sridharan A (**2002**) Prediction of compaction characteristics of fine–grained soils. *Géotechnique* **52**(**10**): 761–763, http://doi.org/10.1680/geot.2002.52.10.761.

Gurtug Y and Sridharan A (**2004**) Compaction behaviour and prediction of its characteristics of fine grained soils with particular reference to compaction energy. *Soils and Foundations* **44**(**5**): 27–36, http://doi.org/10.3208/sandf.44.5_27.

Gurtug Y, Sridharan A and İkizler SB (**2018**) Simplified method to predict compaction curves and characteristics of soils. *Iranian Journal of Science and Technology, Transactions of Civil Engineering* **in press**, http://doi.org/10.1007/s40996-018-0098-z.

Jha AK and Sivapullaiah P V. (**2016**) Gypsum–induced volume change behavior of stabilized expansive soil with fly ash–lime. *Geotechnical Testing Journal* **39**(**3**): 391–406, http://doi.org/10.1520/gtj20150017.

Kalkan E (**2013**) Preparation of scrap tire rubber fiber–silica fume mixtures for modification of clayey soils. *Applied Clay Science* **80–81**: 117–125, http://doi.org/10.1016/j.clay.2013.06.014.

Kim S and Palomino AM (**2009**) Polyacrylamide–treated kaolin: A fabric study. *Applied Clay Science* **45**(**4**): 270–279, http://doi.org/10.1016/j.clay.2009.06.009.

Kua TA, Arulrajah A, Mohammadinia A, Horpibulsuk S and Mirzababaei M (**2017**) Stiffness and deformation properties of spent coffee grounds based geopolymers. *Construction and Building Materials* **138**: 79–87, http://doi.org/10.1016/j.conbuildmat.2017.01.082.

Mirzababaei M, Arulrajah A, Horpibulsuk S and Aldavad M (**2017**) Shear strength of a fibre–reinforced clay at large shear displacement when subjected to different stress histories. *Geotextiles and Geomembranes* **45**(**5**): 422–429, http://doi.org/10.1016/j.geotexmem.2017.06.002.

Mirzababaei M, Miraftab M, Mohamed M and McMahon P (**2013**[a]) Unconfined compression strength of reinforced clays with carpet waste fibers. *Journal of Geotechnical and Geoenvironmental Engineering* **139**(**3**): 483–493, http://doi.org/10.1061/(asce)gt.1943-5606.0000792.

Mirzababaei M, Miraftab M, Mohamed M and McMahon P (**2013**[b]) Impact of carpet waste fibre addition on swelling properties of compacted clays. *Geotechnical and Geological Engineering* **31**(**1**): 173–182, http://doi.org/10.1007/s10706-012-9578-2.

Mirzababaei M, Mohamed M, Arulrajah A, Horpibulsuk S and Anggraini V (**2018**) Practical approach to predict the shear strength of fibre–reinforced clay. *Geosynthetics International*, http://doi.org/10.1680/jgein.17.00033.

Mirzababaei M, Yasrobi SS and Al-Rawas AA (**2009**) Effect of polymers on swelling potential of expansive soils. *Proceedings of the Institution of Civil Engineers – Ground Improvement* **162**(**3**): 111–119, http://doi.org/10.1680/grim.2009.162.3.111.

Mitchell JK and Soga K (**2005**) *Fundamentals of Soil Behavior* (3rd ed). John Wiley & Sons, Hoboken, New Jersey, USA, ISBN:9780471463023.

Nagaraj HB, Reesha B, Sravan MV and Suresh MR (**2015**) Correlation of compaction characteristics of natural soils with modified plastic limit. *Transportation Geotechnics* **2**: 65–77, http://doi.org/10.1016/j.trgeo.2014.09.002.

Özkul ZH and Baykal G (**2007**) Shear behavior of compacted rubber fiber–clay composite in drained and undrained loading. *Journal of Geotechnical and Geoenvironmental Engineering* **133**(**7**): 767–781, http://doi.org/10.1061/(asce)1090-0241(2007)133:7(767).

Pandian NS, Nagaraj TS and Manoj M (**1997**) Re–examination of compaction characteristics of fine–grained soils. *Géotechnique* **47**(**2**): 363–366, http://doi.org/10.1680/geot.1997.47.2.363.

Perez JL, Kwok CY and Senetakis K (**2017**) Investigation of the micromechanics of sand–rubber mixtures at very small strains. *Geosynthetics International* **24**(**1**): 30–44, http://doi.org/10.1680/jgein.16.00013.

Pillai GAS and Vinod PP (**2016**) Re–examination of compaction parameters of fine–grained soils. *Proceedings of the Institution of Civil Engineers – Ground Improvement* **169**(**3**): 157–166, http://doi.org/10.1680/jgrim.15.00005.

Prakash K and Sridharan A (**2006**) Critical appraisal of the cone penetration method of determining soil plasticity. *Canadian Geotechnical Journal* **43**(**8**): 884–888, http://doi.org/10.1139/t06-043.

Prakash K and Sridharan A (**2012**) Classification of non–plastic soils. *Indian Geotechnical Journal* **42**(**2**): 118–123, http://doi.org/10.1007/s40098-012-0007-5.

Priyadarshee A, Kumar A, Gupta D and Pushkarna P (**2018**) Compaction and strength behavior of tire crumbles–fly ash mixed with clay. *Journal of Materials in Civil Engineering* **30**(**4**): 04018033:1–9, http://doi.org/10.1061/(asce)mt.1943-5533.0002171.

Seda JH, Lee JC and Carraro JAH (**2007**) Beneficial use of waste tire rubber for swelling potential mitigation in expansive soils. In *Geo–Denver 2007: Soil Improvement (GSP 172)* (Schaefer VR, Filz GM, Gallagher PM, Sehn AL and Wissmann KJ (eds)). ASCE, Denver, Colorado, USA, pp. 1–9, http://doi.org/10.1061/40916(235)5.

Signes CH, Garzón-Roca J, Fernández PM, Torre MEG and Franco RI (**2016**) Swelling potential reduction of Spanish argillaceous marlstone Facies Tap soil through the addition of crumb rubber particles from scrap tyres. *Applied Clay Science* **132**–**133**: 768–773, http://doi.org/10.1016/j.clay.2016.07.027.

Sivrikaya O, Togrol E and Kayadelena C (**2008**) Estimating compaction behavior of fine–grained soils based on compaction energy. *Canadian Geotechnical Journal* **45**(**6**): 877–887, http://doi.org/10.1139/t08-022.

Soltani A and Mirzababaei M (**2018**) Comment on "Compaction and strength behavior of tire crumbles–fly ash mixed with clay" by A. Priyadarshee, A. Kumar, D. Gupta, and P. Pushkarna. *Journal of Materials in Civil Engineering* **in press**.

Soltani A, Deng A and Taheri A (**2018**[a]) Swell–compression characteristics of a fiber–reinforced expansive soil. *Geotextiles and Geomembranes* **46**(**2**): 183–189, http://doi.org/10.1016/j.geotexmem.2017.11.009.

Soltani A, Deng A, Taheri A and Mirzababaei M (**2017**[b]) A sulphonated oil for stabilisation of expansive soils. *International Journal of Pavement Engineering* **in press**, http://doi.org/10.1080/10298436.2017.1408270.

Soltani A, Deng A, Taheri A and Mirzababaei M (**2018**[b]) Rubber powder–polymer combined stabilization of South Australian expansive soils. *Geosynthetics International* **in press**, http://doi.org/10.1680/jgein.18.00009.

Soltani A, Deng A, Taheri A and Sridharan A (**2018**[c]) Swell–shrink–consolidation behavior of rubber–reinforced expansive soils. *Geotechnical Testing Journal* **in press**.

Soltani A, Deng A, Taheri A, Sridharan A and Estabragh AR (**2018**[d]) A framework for interpretation of the compressibility behavior of soils. *Geotechnical Testing Journal* **41(1)**: 1–16, http://doi.org/10.1520/gtj20170088.

Soltani A, Taheri A, Khatibi M and Estabragh AR (**2017**[a]) Swelling potential of a stabilized expansive soil: A comparative experimental study. *Geotechnical and Geological Engineering* **35**(**4**): 1717–1744, http://doi.org/10.1007/s10706-017-0204-1.

Soosan TG, Sridharan A, Jose BT and Abraham BM (**2005**) Utilization of quarry dust to improve the geotechnical properties of soils in highway construction. *Geotechnical Testing Journal* **28**(**4**): 391–400, http://doi.org/10.1520/gtj11768.

Sridharan A and Nagaraj HB (**2005**) Plastic limit and compaction characteristics of fine–grained soils. *Proceedings of the Institution of Civil Engineers – Ground Improvement* **9**(**1**): 17–22, http://doi.org/10.1680/grim.2005.9.1.17.

Sridharan A and Sivapullaiah P V. (**2005**) Mini compaction test apparatus for fine grained soils. *Geotechnical Testing Journal* **28**(**3**): 240–246, http://doi.org/10.1520/gtj12542.

Sridharan A, Nagaraj HB and Prakash K (**1999**) Determination of the plasticity index from flow index. *Geotechnical Testing Journal* **22**(**2**): 175–181, http://doi.org/10.1520/gtj11276j.

Srivastava A, Pandey S and Rana J (**2014**) Use of shredded tyre waste in improving the geotechnical properties of expansive black cotton soil. *Geomechanics and Geoengineering* **9**(**4**): 303–311, http://doi.org/10.1080/17486025.2014.902121.

Tang CS, Shi B and Zhao LZ (**2010**) Interfacial shear strength of fiber reinforced soil. *Geotextiles and Geomembranes* **28**(**1**): 54–62, http://doi.org/10.1016/j.geotexmem.2009.10.001.

Trouzine H, Bekhiti M and Asroun A (**2012**) Effects of scrap tyre rubber fibre on swelling behaviour of two clayey soils in Algeria. *Geosynthetics International* **19**(**2**): 124–132, http://doi.org/10.1680/gein.2012.19.2.124.

Wang C, Deng A and Taheri A (**2018**) Three–dimensional discrete element modeling of direct shear test for granular rubber–sand. *Computers and Geotechnics* **97**: 204–216, http://doi.org/10.1016/j.compgeo.2018.01.014.

Wang YX, Guo PP, Ren WX, Yuan BX, Yuan HP, Zhao YL, Shan SB and Cao P (**2017**) Laboratory investigation on strength characteristics of expansive soil treated with jute fiber reinforcement. *International Journal of Geomechanics* **17**(**11**): 04017101:1–12, http://doi.org/10.1061/(asce)gm.1943-5622.0000998.

Wroth CP and Wood DM (**1978**) The correlation of index properties with some basic engineering properties of soils. *Canadian Geotechnical Journal* **15**(**2**): 137–145, http://doi.org/10.1139/t78-014.

Yadav JS and Tiwari SK (**2017**[a]) A study on the potential utilization of crumb rubber in cement treated soft clay. *Journal of Building Engineering* **9**: 177–191, http://doi.org/10.1016/j.jobe.2017.01.001.

Yadav JS and Tiwari SK (**2017**[b]) Effect of waste rubber fibres on the geotechnical properties of clay stabilized with cement. *Applied Clay Science* **149**: 97–110, http://doi.org/10.1016/j.clay.2017.07.037.

Yadav JS and Tiwari SK (**2017**[c]) The impact of end–of–life tires on the mechanical properties of fine–grained soil: A Review. *Environment, Development and Sustainability* **in press**, http://doi.org/10.1007/s10668-017-0054-2.

List of Tables

Table 1. Physical and mechanical properties of the clay soils.

Table 2. Physical properties and chemical composition of ground rubber (GR).

Table 1. Physical and mechanical properties of the clay soils.

Properties	Soil K	Soil RC1	Soil KB	Soil RC2	Standard designation
Specific gravity, G_{ss}	2.69	2.67	2.71	2.72	ASTM D854–14
Grain–size distribution					
Clay (< 2 μm) (%)	49	37	53	44	ASTM D422–07
Silt (2–75 μm) (%)	50	32	46	36	
Fine sand (0.075–0.425 mm) (%)	1	19	1	14	
Medium sand (0.425–2 mm) (%)	0	8	0	5	
Coarse sand (2–4.75 mm) (%)	0	5	0	1	
Consistency limits and classification					
Liquid limit, w_L (%)	44	47	59	78	AS 1289.3.9.1–15[†]
Plastic limit, w_P (%)	22	18	28	21	AS 1289.3.2.1–09[‡]
Plasticity index, I_P (=w_L–w_P) (%)	22	29	31	57	AS 1289.3.3.1–09
USCS classification	CI[*]	CI	CH[#]	CH	ASTM D2487–11
Compaction characteristics					
Optimum water content, w_{opt} (%)	21	16	25	19	ASTM D698–12
Maximum dry unit weight, γ_{dmax} (kN/m^3)	15.45	16.41	14.61	15.84	

Note:
[†]cone penetration method (see **Section 3.1** for details); [‡]conventional rolling thread method (see **Section 3.1** for details); [*]*clay with intermediate plasticity*; and [#]*clay with high plasticity*.

Table 2. Physical properties and chemical composition of ground rubber (GR).

Properties	Value/Description
Physical properties	
Solubility in water	Insoluble
Water adsorption	Negligible (< 4%)
Resistance to acid/alkaline	Excellent
Softening point (^{o}C)	170
Specific gravity, G_{sr}	1.09
Grain–size distribution and classification[†]	
D_{10} (mm)[‡]	0.182
D_{30} (mm)	0.334
D_{50} (mm)	0.478
D_{60} (mm)	0.513
Coefficient of uniformity, C_u[*]	2.81
Coefficient of curvature, C_c[#]	1.20
USCS classification	Poorly–graded sand (SP)
Chemical composition	
Styrene–Butadiene copolymer (%)	55
Acetone extract (%)	5–20
Carbon black (%)	25–35
Zinc oxide (%)	2–3
Sulphur (%)	1–3

Note:
[†]ASTM D422–07 method; [‡]particle dimeter corresponding to 10% finer; [*]$C_u=D_{60}/D_{10}$; and [#]$C_c=D_{30}^2/D_{10}D_{60}$.

List of Figures

Figure 1. Ground rubber (GR) particles at different magnification ratios (modified from Soltani et al. (2018[b])): **(a)** 1x magnification; **(b)** 50x magnification; and **(c)** 200x magnification.

Figure 2. Variations of the conventional plasticity index against the flow index for the virgin clays.

Figure 3. Flow curves for the virgin clays and various GRC blends: **(a)** soil K; **(b)** soil RC1; **(c)** soil KB; and **(d)** soil RC2.

Figure 4. Variations of the consistency limits against rubber content for the virgin clays and various GRC blends: **(a)** soil K; **(b)** soil RC1; **(c)** soil KB; and **(d)** soil RC2.

Figure 5. Location of the tested mix designs on Casagrande's plasticity chart: **(a)** soils K and KB; and **(b)** soils RC1 and RC2.

Figure 6. Standard Proctor compaction curves for the virgin clays and various GRC blends: **(a)** soil K; **(b)** soil RC1; **(c)** soil KB; and **(d)** soil RC2.

Figure 7. Variations of the compaction characteristics against rubber content for the tested mix designs: **(a)** optimum water content; and **(b)** maximum dry unit weight.

Figure 8. Variations of the optimum water content against the consistency limits for the tested mix designs: **(a)** liquid limit; **(b)** plastic limit; and **(c)** plasticity index.

Figure 9. Variations of the maximum dry unit weight against the dry unit weight at plastic limit for the tested mix designs.

Figure 10. Variations of both the actual and predicted compaction data against rubber content for the tested mix designs: **(a)** optimum water content (predicted by **Equation 4**); and **(b)** maximum dry unit weight (predicted by **Equation 6**).

Figure 1. Ground rubber (GR) particles at different magnification ratios (modified from Soltani et al. (2018[b])): **(a)** 1x magnification; **(b)** 50x magnification; and **(c)** 200x magnification.

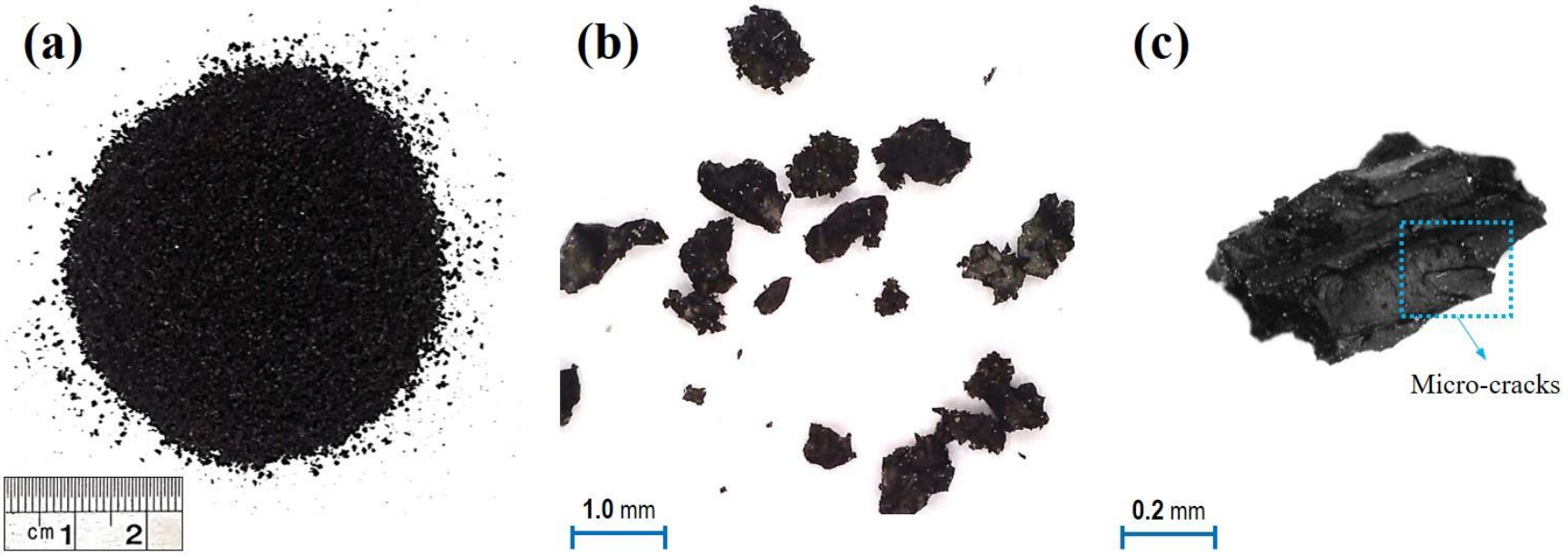

Figure 2. Variations of the conventional plasticity index against the flow index for the virgin clays.

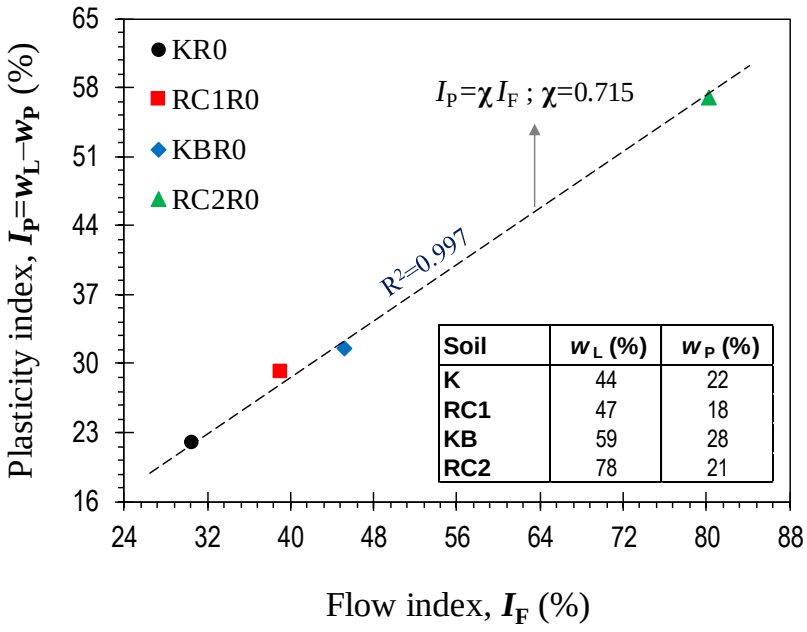

Figure 3. Flow curves for the virgin clays and various GRC blends: **(a)** soil K; **(b)** soil RC1; **(c)** soil KB; and **(d)** soil RC2.

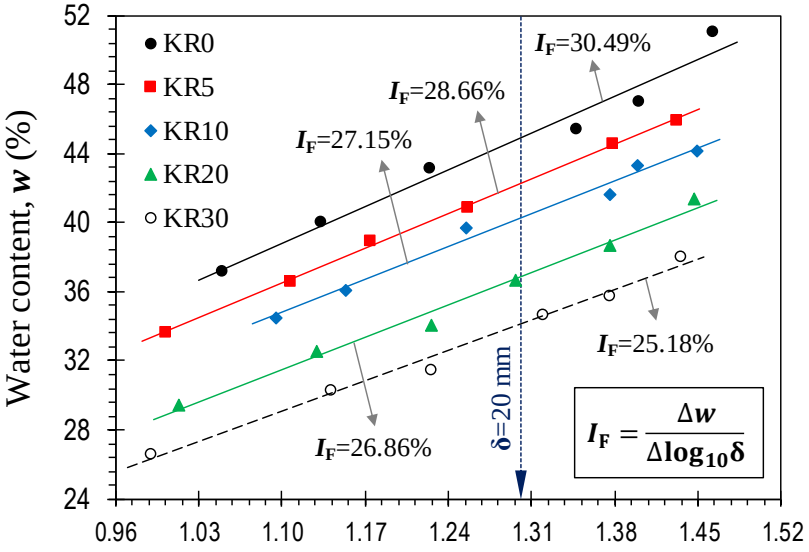

(a) Logarithm of cone penetration, $\log_{10}\delta$ (mm)

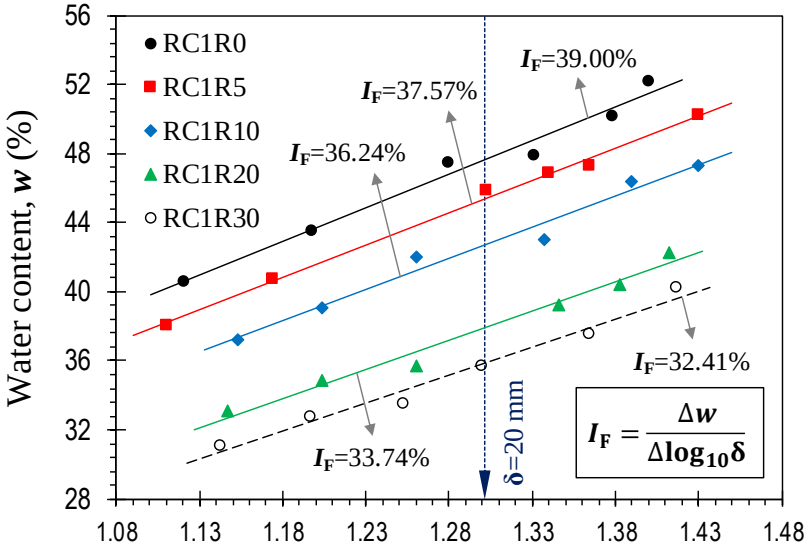

(b) Logarithm of cone penetration, $\log_{10}\delta$ (mm)

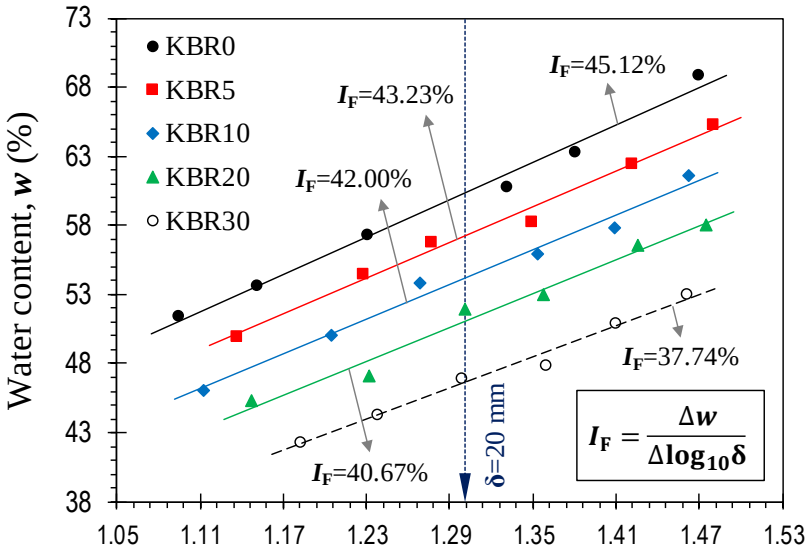

(c) Logarithm of cone penetration, $\log_{10}\delta$ (mm)

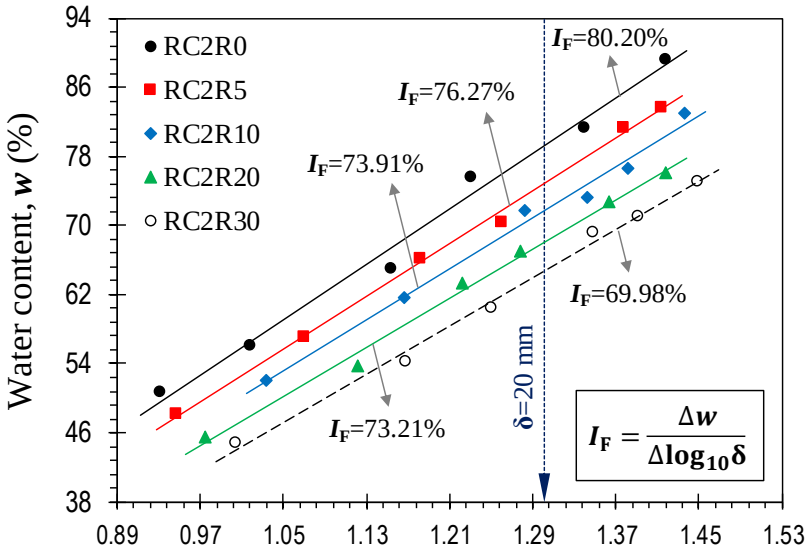

(d) Logarithm of cone penetration, $\log_{10}\delta$ (mm)

Figure 4. Variations of the consistency limits against rubber content for the virgin clays and various GRC blends: **(a)** soil K; **(b)** soil RC1; **(c)** soil KB; and **(d)** soil RC2.

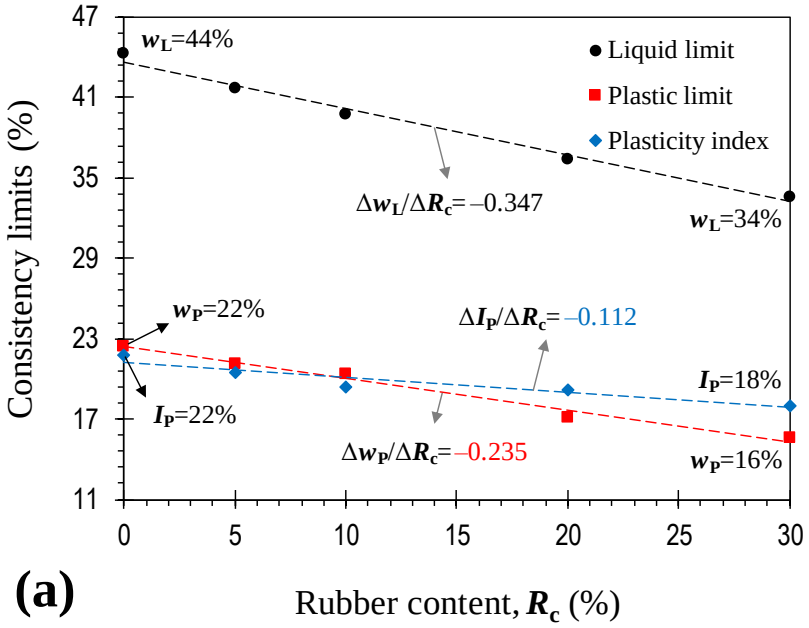

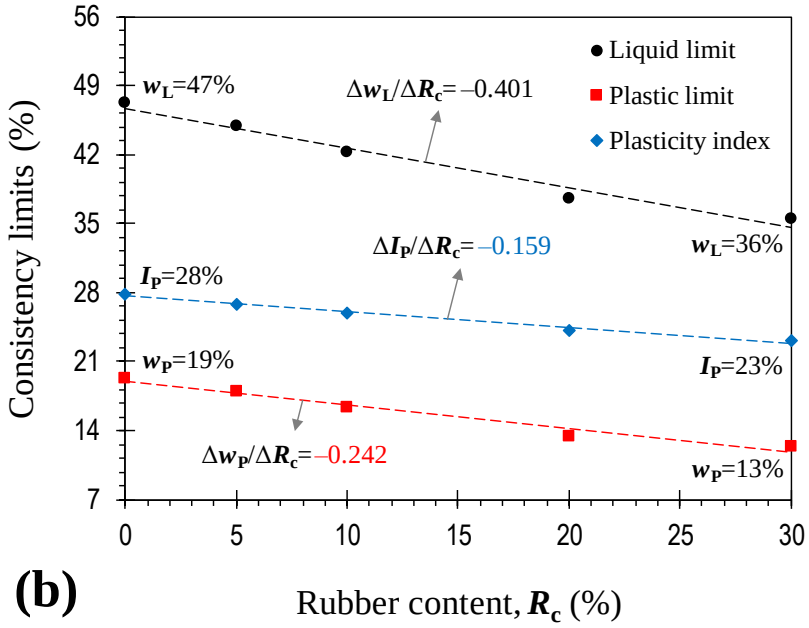

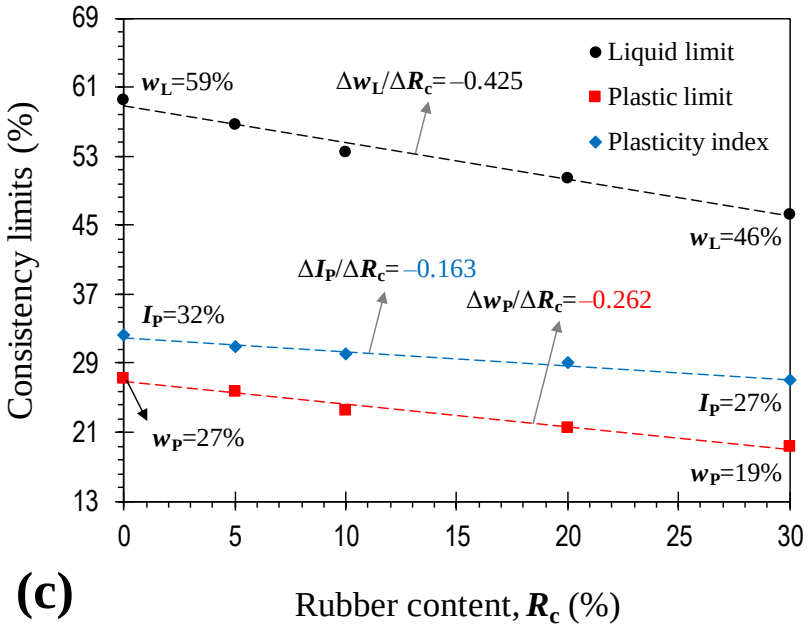
Consistency limits (%)
Liquid limit
Plastic limit
Plasticity index
w_L=59%
$\Delta w_L/\Delta R_c$=–0.425
w_L=46%
$\Delta I_P/\Delta R_c$=–0.163
$\Delta w_P/\Delta R_c$=–0.262
I_P=32%
I_P=27%
w_P=27%
w_P=19%
Rubber content, R_c (%)

(c)

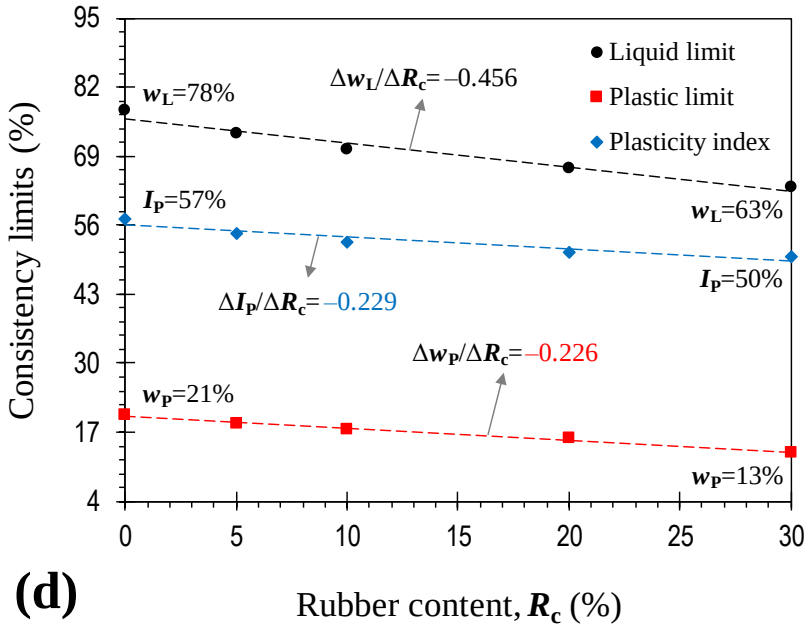
Consistency limits (%)
Liquid limit
Plastic limit
Plasticity index
w_L=78%
$\Delta w_L/\Delta R_c$=–0.456
w_L=63%
I_P=57%
$\Delta I_P/\Delta R_c$=–0.229
I_P=50%
$\Delta w_P/\Delta R_c$=–0.226
w_P=21%
w_P=13%
Rubber content, R_c (%)

(d)

Figure 5. Location of the tested mix designs on Casagrande's plasticity chart: **(a)** soils K and KB; and **(b)** soils RC1 and RC2.

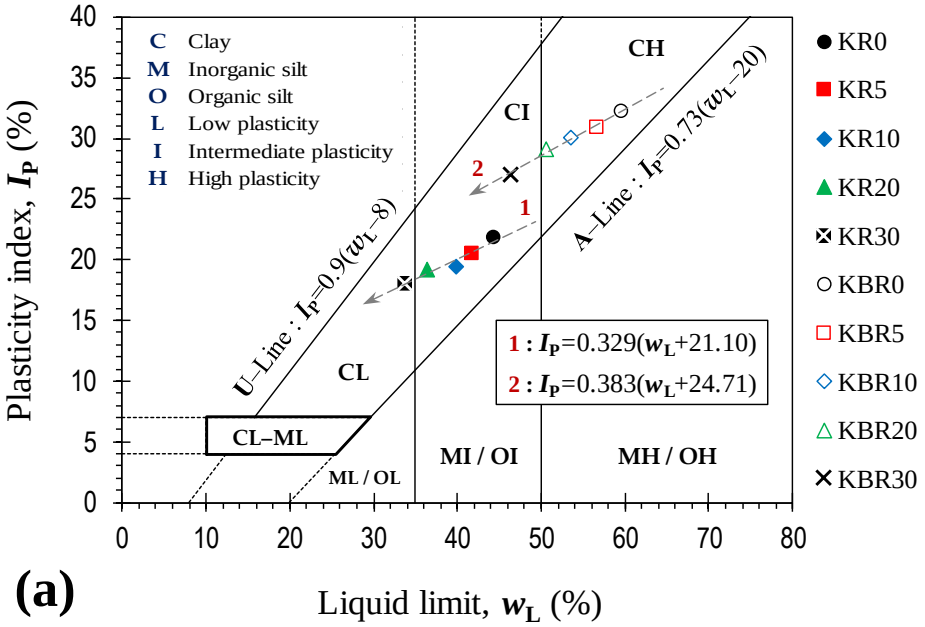

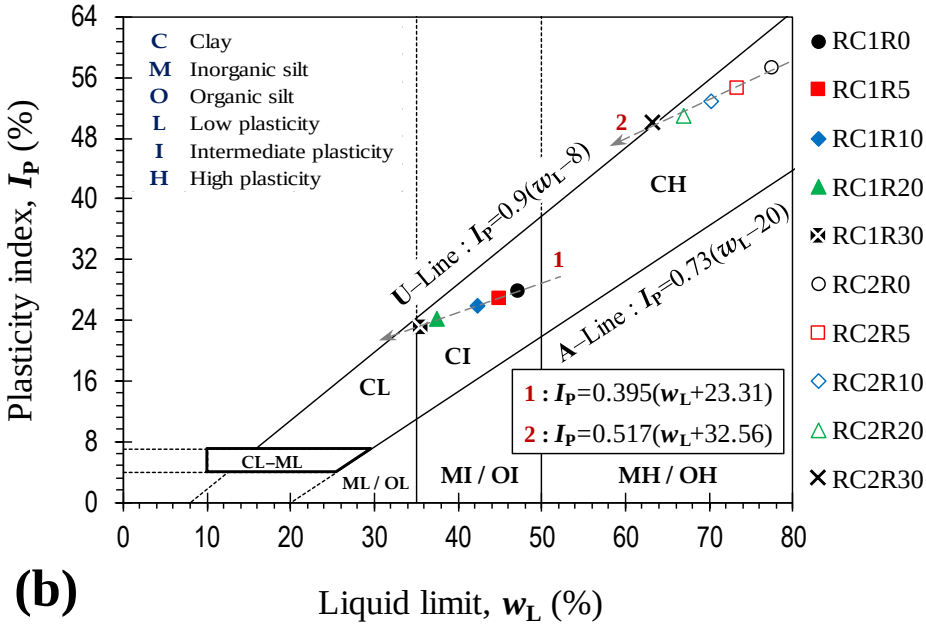

Figure 6. Standard Proctor compaction curves for the virgin clays and various GRC blends: **(a)** soil K; **(b)** soil RC1; **(c)** soil KB; and **(d)** soil RC2.

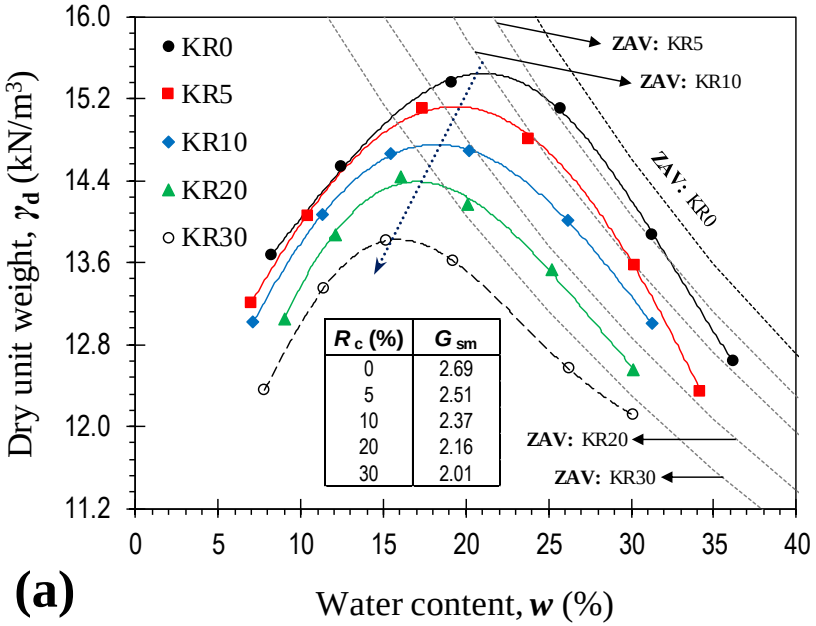

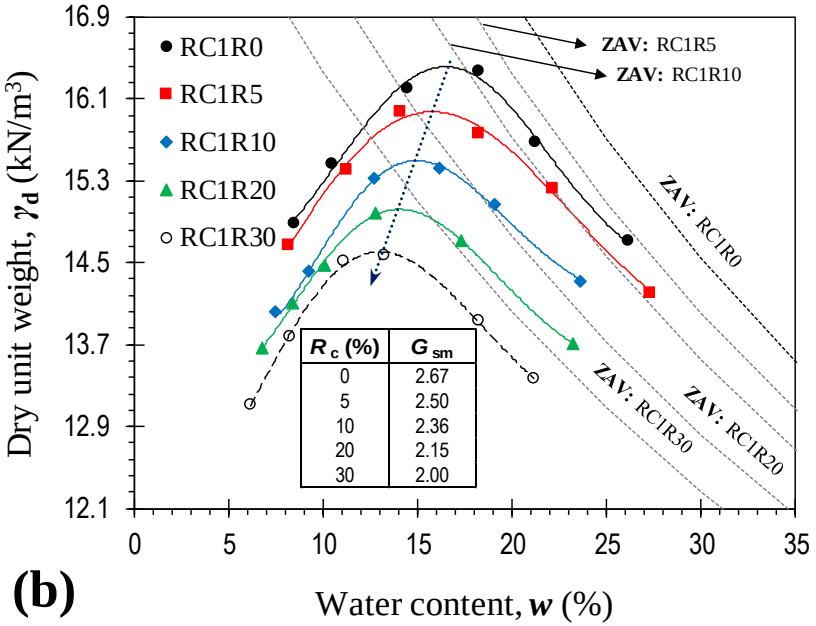

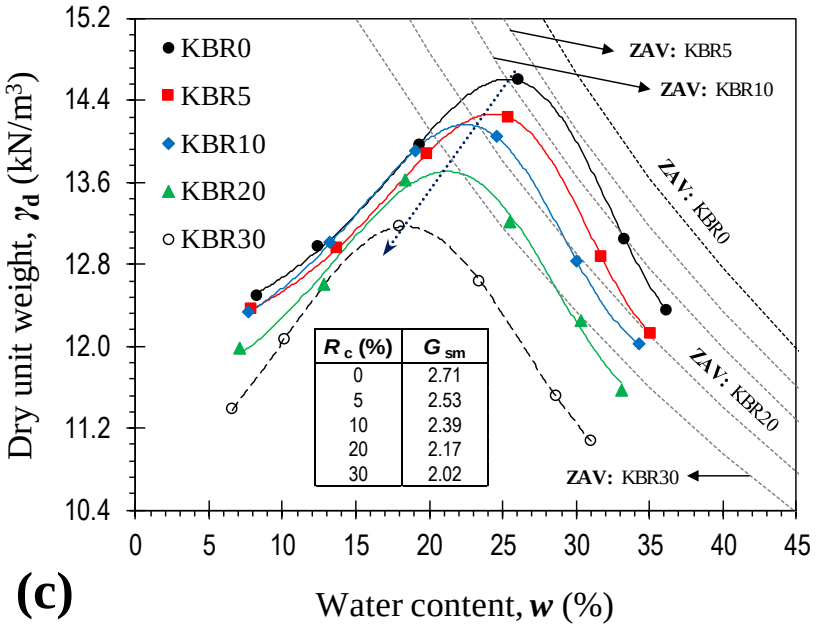
KBR0
KBR5
KBR10
KBR20
KBR30
ZAV: KBR5
ZAV: KBR10
ZAV: KBR0
ZAV: KBR20
ZAV: KBR30
R_c (%) | G_{sm}
0 | 2.71
5 | 2.53
10 | 2.39
20 | 2.17
30 | 2.02
Dry unit weight, γ_d (kN/m^3)
Water content, w (%)

(c)

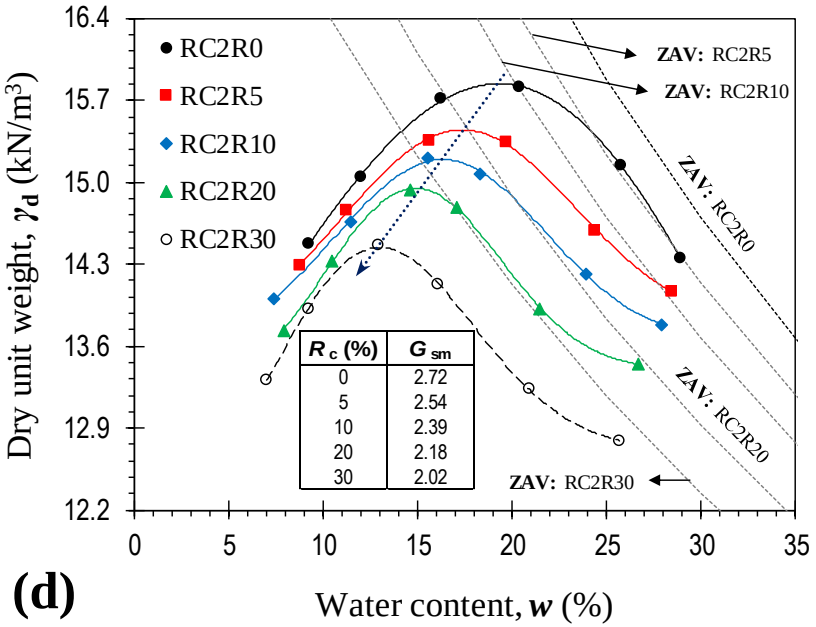
RC2R0
RC2R5
RC2R10
RC2R20
RC2R30
ZAV: RC2R5
ZAV: RC2R10
ZAV: RC2R0
ZAV: RC2R20
ZAV: RC2R30
R_c (%) | G_{sm}
0 | 2.72
5 | 2.54
10 | 2.39
20 | 2.18
30 | 2.02
Dry unit weight, γ_d (kN/m^3)
Water content, w (%)

(d)

Figure 7. Variations of the compaction characteristics against rubber content for the tested mix designs: **(a)** optimum water content; and **(b)** maximum dry unit weight.

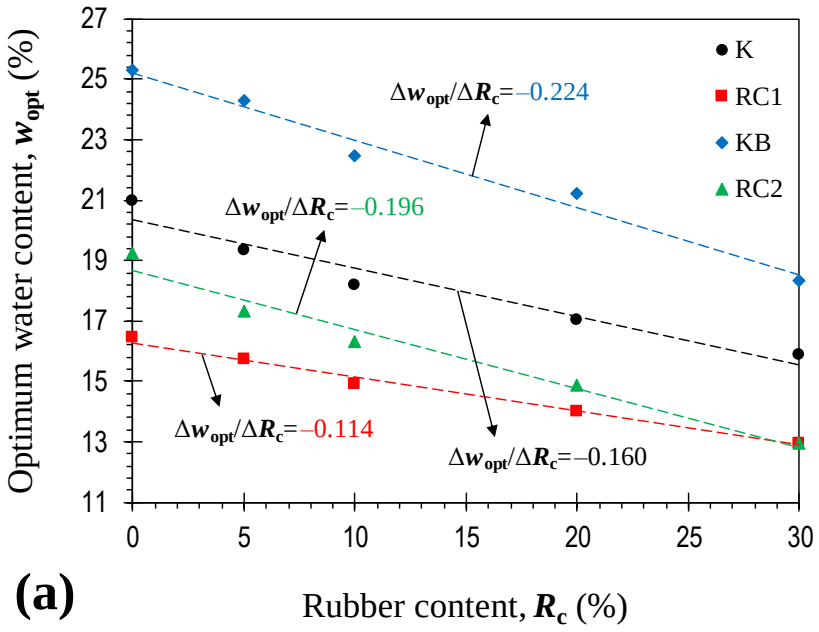

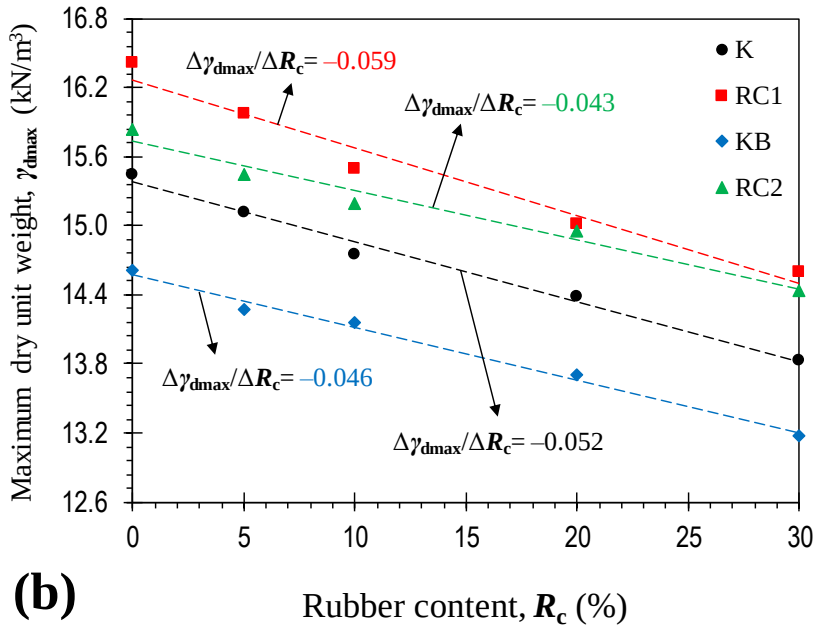

Figure 8. Variations of the optimum water content against the consistency limits for the tested mix designs: **(a)** liquid limit; **(b)** plastic limit; and **(c)** plasticity index.

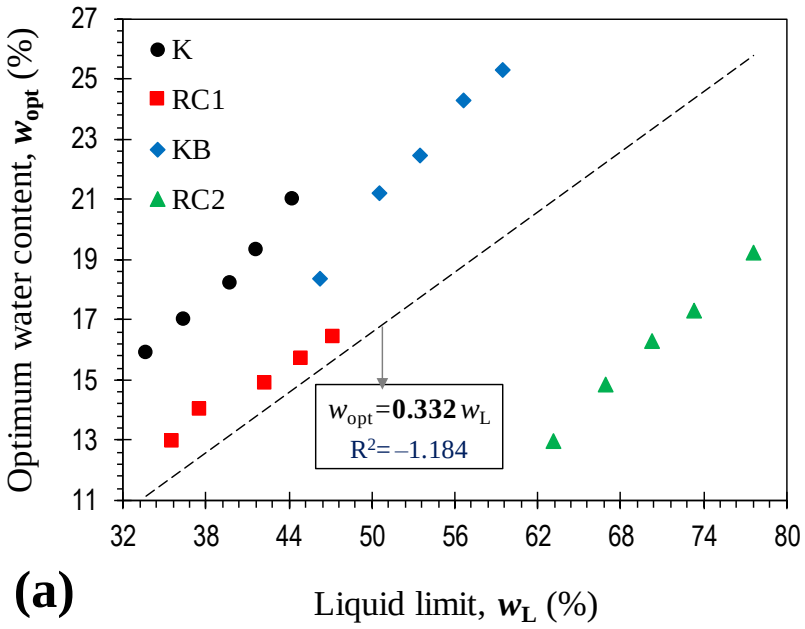

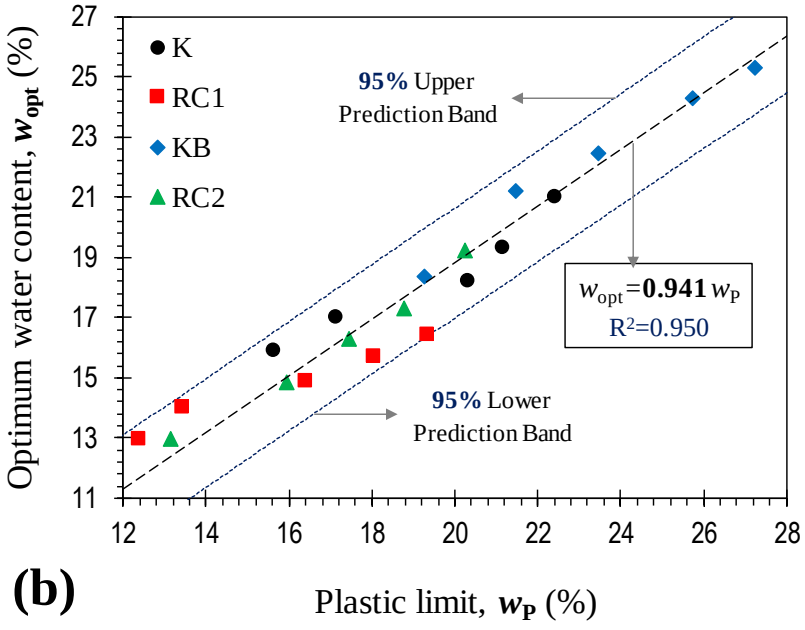

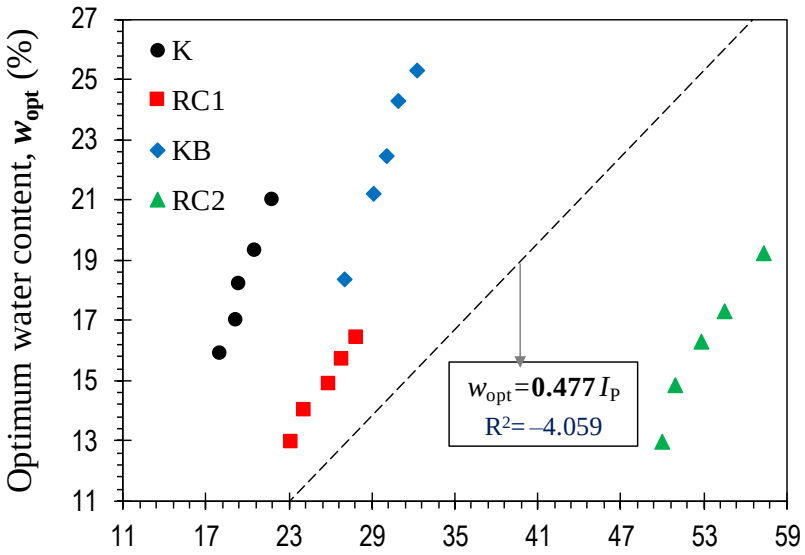
Optimum water content, w_{opt} (%)
27
25
23
21
19
17
15
13
11
K
RC1
KB
RC2
w_{opt}=**0.477** I_P
R^2= –4.059
11
17
23
29
35
41
47
53
59
Plasticity index, I_P (%)

(c)

Figure 9. Variations of the maximum dry unit weight against the dry unit weight at plastic limit for the tested mix designs.

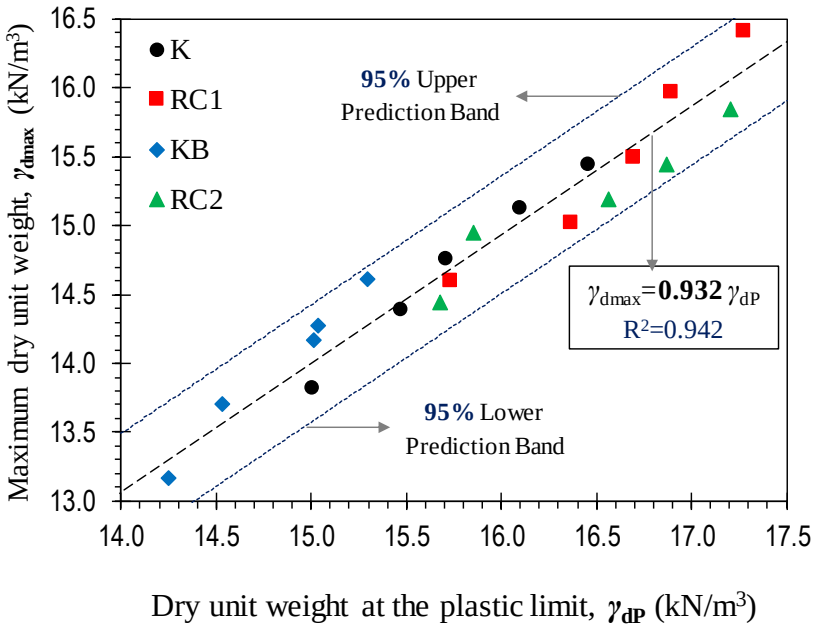

Figure 10. Variations of both the actual and predicted compaction data against rubber content for the tested mix designs: **(a)** optimum water content (predicted by **Equation 4**); and **(b)** maximum dry unit weight (predicted by **Equation 6**).

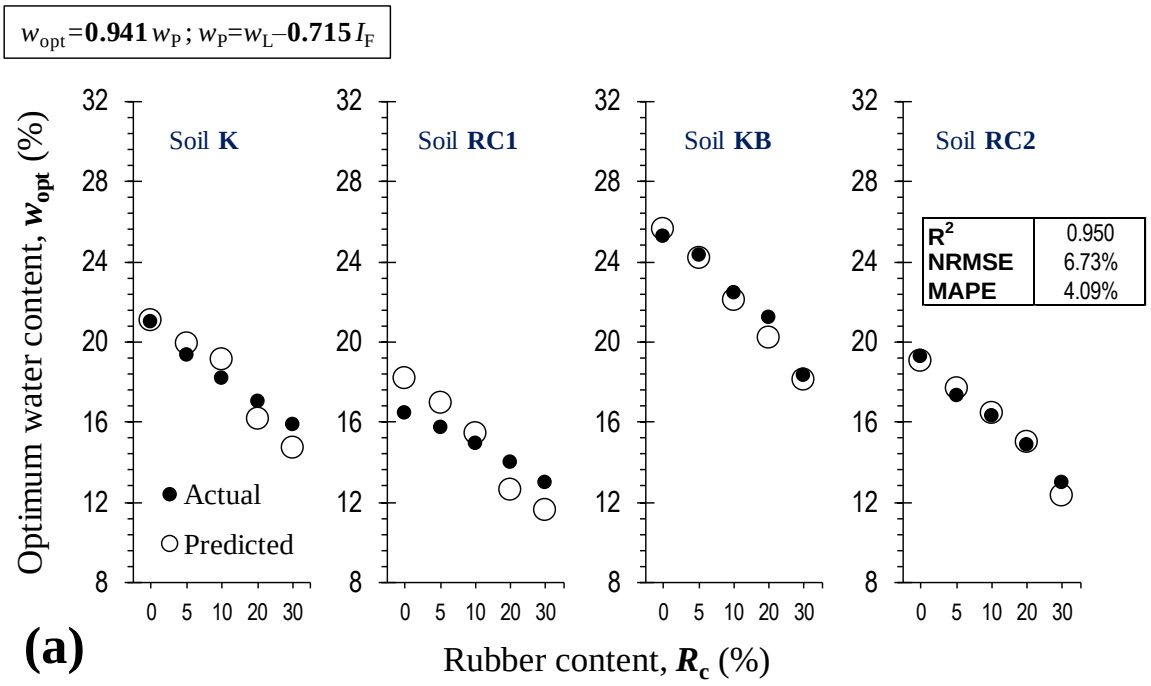

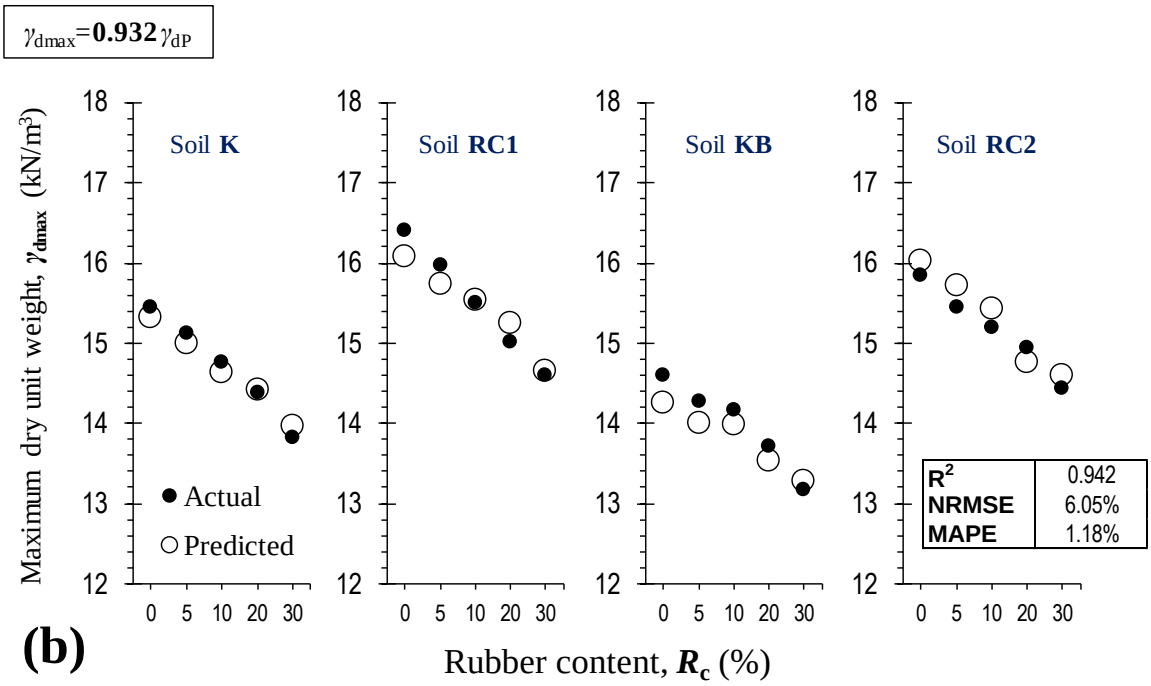

Statement of Authorship

Statement of Authorship

Title of Paper	Consistency Limits and Compaction Characteristics of Clay Soils Containing Rubber Waste
Publication Status	■ Published ☐ Accepted for Publication ☐ Submitted for Publication ☐ Unpublished and Unsubmitted work written in manuscript style
Publication Details	**Soltani A**, Deng A, Taheri A and Sridharan A **(2018)** Consistency Limits and Compaction Characteristics of Clay Soils Containing Rubber Waste. ***Proceedings of the Institution of Civil Engineers–Geotechnical Engineering* x(x): x–x**, https://doi.org/10.1680/jgeen.18.00042.

Principal Author

Name of Principal Author (Candidate)	Amin Soltani (**Email:** Amin.Soltani@adelaide.edu.au)		
Contribution to the Paper	Overall paper preparation		
Overall percentage (%)	85%		
Certification:	This paper reports on original research I conducted during the period of my Higher Degree by Research candidature and is not subject to any obligations or contractual agreements with a third party that would constrain its inclusion in this thesis. I am the primary author of this paper.		
Signature		Date	06/29/2018

Co-Author Contributions

By signing the Statement of Authorship, each author certifies that:

i. the candidate's stated contribution to the publication is accurate (as detailed above);
ii. permission is granted for the candidate in include the publication in the thesis; and
iii. the sum of all co-author contributions is equal to 100% less the candidate's stated contribution.

Name of Co-Author	An Deng **Senior Lecturer**, School of Civil, Environmental and Mining Engineering, The University of Adelaide, Adelaide, SA 5005, Australia (**Email:** An.Deng@adelaide.edu.au)		
Contribution to the Paper	Paper review and revision		
Signature		Date	07/23/2018

Name of Co-Author	Abbas Taheri **Senior Lecturer**, School of Civil, Environmental and Mining Engineering, The University of Adelaide, Adelaide, SA 5005, Australia (**Email:** Abbas.Taheri@adelaide.edu.au)		
Contribution to the Paper	Paper review and revision		
Signature		Date	07/16/2018

Name of Co-Author	Asuri Sridharan **Professor Emeritus**, Department of Civil Engineering, Indian Institute of Science, Bangalore 560012, India; **Honorary Research Scientist**, Indian National Science Academy (INSA), New Delhi 110002, India (**Email:** SridharanAsuri@yahoo.com)		
Contribution to the Paper	Paper review and revision		
Signature	**Note:** Sign–off by Principal Supervisor in place of this co–author who is based overseas. Co–author agreement in email is retained by Candidate.	Date	07/23/2018

1

Published Copy [Link]

Cite this article
Soltani A, Deng A, Taheri A and Sridharan A
Consistency limits and compaction characteristics of clay soils containing rubber waste.
Proceedings of the Institution of Civil Engineers – Geotechnical Engineering,
https://doi.org/10.1680/jgeen.18.00042

Research Article
Paper 1800042
Received 06/03/2018;
Accepted 08/06/2018

ICE Publishing: All rights reserved

Keywords: recycling & reuse of materials/soil-geosynthetic interaction/statistical analysis

Geotechnical Engineering

ice publishing

Consistency limits and compaction characteristics of clay soils containing rubber waste

Amin Soltani
PhD Student, School of Civil, Environmental and Mining Engineering, The University of Adelaide, Adelaide, SA, Australia (corresponding author: amin.soltani@adelaide.edu.au) (Orcid:0000-0002-0483-7487)

An Deng
Senior Lecturer, School of Civil, Environmental and Mining Engineering, The University of Adelaide, Adelaide, SA, Australia

Abbas Taheri
Senior Lecturer, School of Civil, Environmental and Mining Engineering, The University of Adelaide, Adelaide, SA, Australia

Asuri Sridharan
Professor Emeritus, Department of Civil Engineering, Indian Institute of Science, Bangalore, India; Honorary Research Scientist, Indian National Science Academy, New Delhi, India

The aim of the study reported in this paper was to develop practical correlative models capable of predicting the compaction characteristics of clay soils blended with rubber from waste vehicle tyres. Four different clay soils, ranging from intermediate to high plasticity, were adopted for the test programme and each was blended with four different percentages of ground rubber waste. The test programme consisted of cone penetration (consistency limits) and standard Proctor compaction tests. As a result of ground rubber inclusion, the consistency limits and compaction characteristics all exhibited a linear decreasing trend with increase in rubber content. The rate of decrease, however, was greater for the high-plasticity clays. Simple correlative models, linking the compaction characteristics to the consistency limits, were suggested and validated by statistical techniques. The proposed models provide a practical procedure towards predicting the compaction characteristics of ground rubber–clay blends without the hurdles of conducting laboratory compaction tests, and thus can be implemented in practice for preliminary assessments.

Notation

G_{sm}	average specific gravity of ground rubber–clay mix
G_{sr}	specific gravity of ground rubber
G_{ss}	specific gravity of soil solids
I_F	flow index
I_P	plasticity index
R^2	coefficient of determination
R_c	rubber content (by weight)
R_c^M	median rubber content
w	water content
w_L	liquid limit
w_{opt}	optimum water content
w_P	plastic limit
w_P^M	plastic limit corresponding to R_c^M
w_{Po}	plastic limit for the virgin clay
γ_d	dry unit weight
γ_{dmax}	maximum dry unit weight
γ_{dP}	dry unit weight at plastic limit
γ_w	unit weight of water
δ	cone penetration
η	coefficient of plastic limit reduction
χ	average ratio of I_P to I_F

1. Introduction

The design and construction of geostructures often necessitate incorporating low-graded clay soils, with high moisture susceptibility (and plasticity) and low bearing capacity, in the construction. Common solutions to counteract the adversities associated with such soils include soil replacement (i.e. replacing the poor-quality clay soil with desired quarried materials) or attempting to improve the problematic soil by means of stabilisation techniques. Currently, two stabilisation schemes are in vogue for clay soils – namely, chemical and mechanical stabilisation (Soltani *et al.*, 2017a). The chemical scheme makes use of chemical binders, which initiate a series of short- and long-term chemical reactions in the clay–binder medium, thereby amending the soil fabric into a coherent matrix of improved mechanical performance. Common binders include agents of traditional (e.g. cement, lime and fly ash) or non-traditional (e.g. polymers, resins and sulfonated oils) categories, both of which have been well documented in the literature (e.g. Estabragh *et al.*, 2013, 2014; Georgees *et al.*, 2015; Jha and Sivapullaiah, 2016; Mirzababaei *et al.*, 2009; Soltani *et al.*, 2017b). The mechanical technique often involves the placement of randomly or specifically engineered reinforcements (e.g. natural and synthetic fibres) in the soil regime, thereby engendering a spatial three-dimensional reinforcement network in favour of weaving (or interlocking) the soil grains into a unitary mass of improved mechanical performance (e.g. Estabragh *et al.*, 2016; Mirzababaei *et al.*, 2017, 2018; Soltani *et al.*, 2018a; Tang *et al.*, 2010; Wang *et al.*, 2017). Lately, many developed and developing countries have initiated the transition towards 'sustainable infrastructure', a concept which fosters the beneficial reuse of solid wastes and/or industrial by-products as a replacement for conventional quarried materials (such as sand) and/or stabilisation agents, thereby conserving natural resources as well as reducing the level of greenhouse gas emissions. Promising replacements, based on recent studies, include recycled tyre rubbers, waste textiles,

Offprint provided courtesy of www.icevirtuallibrary.com
Author copy for personal use, not for distribution

demolition wastes, kiln and quarry dusts, and silicate/calcium geopolymers (e.g. Al-Amoudi *et al.*, 2017; Alazigha *et al.*, 2016; Arulrajah *et al.*, 2017; Kua *et al.*, 2017; Mirzababaei *et al.*, 2013a, 2013b; Soosan *et al.*, 2005).

Waste tyre rubbers are being generated at an increasing rate throughout the world. Such materials are bulky in nature, owing to their low weight-to-volume ratio, and thus consume valuable landfill space upon disposal. As such, local communities and governmental agencies have been increasingly encouraged to recycle and hence reuse waste tyres as part of the infrastructure system. The rubber–soil blend is showing great promise in several respects – for example, reduced unit weight, enhanced strength and ductility, increased permeability and reduced moisture susceptibility (i.e. swell–shrink capacity), which can facilitate the production and placement of sustainable earth fills such as road and railway embankments (e.g. Cabalar *et al.*, 2014; Cetin *et al.*, 2006; Özkul and Baykal, 2007; Perez *et al.*, 2017; Signes *et al.*, 2016; Soltani *et al.*, 2018b, 2018c; Srivastava *et al.*, 2014; Trouzine *et al.*, 2012; Wang *et al.*, 2018; Yadav and Tiwari, 2017a, 2017b). When placed in a flowable condition, the rubber–soil blend outperforms conventional soil backfills by enabling the placement of particles into any irregular or inaccessible space without significant compaction efforts (ACI R229 (ACI, 2013)). The advantages of rubber-mixed soils in engineering performance, which natural soils rarely exhibit, suggest a promising path towards sustainability without compromising performance. Although these materials are promising, the leaching of heavy metals from rubber particles (into the soil mass and/or water bodies) could raise some environmental concerns. In such cases, most documented studies have reported that the degree of soil and water contamination both remain within the allowable limits provided by various health and environmental agencies. When paired with coarse-grained soils, however, the rubber–soil blend should be stabilised by means of chemical binders to meet the required environmental standards (see Yadav and Tiwari (2017c) for more details).

A review of the literature indicates a rather common emphasis on the application of coarse-grained tyre rubber material in the form of fibres, shreds and aggregates. Such materials, however, would be associated with implementation difficulties when dealing with cohesive clay soils (e.g. mixing difficulties and hence non-uniform distribution of rubber particles in the soil regime). As such, types of recycled tyres less often considered for this purpose, such as fine ground rubber (GR), offer the advantage of better workability, and thus demand further investigation. Quite clearly, a vital step towards the production and placement of suitable rubber–clay earth fills is compaction. In this context, the maximum dry unit weight has been reported to decrease with increase in rubber content, while the reported trends for optimum water content still remain rather inconsistent (e.g. Al-Tabbaa *et al.*, 1997; Cetin *et al.*, 2006; Kalkan, 2013; Priyadarshee *et al.*, 2018; Seda *et al.*, 2007). In comparison, limited studies (e.g. Cetin *et al.*, 2006; Srivastava *et al.*, 2014; Trouzine *et al.*, 2012) have been conducted on the consistency limits, the results of which have yet been systematically correlated with other geotechnical properties such as the compaction characteristics. With rubber–soil blends gaining ground as a viable geomaterial in practice, the need for an efficient and simple tool to adequately predict its performance, in terms of compaction, arises as an inevitable necessity. If developed, such a predictive toolbox would help the practising engineer to arrive at reliable rubber–soil design choices without the hurdles of conducting time-consuming laboratory compaction tests. Although numerous attempts have been made to correlate the compaction characteristics with the consistency limits for natural fine-grained soils (e.g. Blotz *et al.*, 1998; Di Matteo *et al.*, 2009; Gurtug and Sridharan, 2002, 2004; Gurtug *et al.*, 2018; Nagaraj *et al.*, 2015; Pandian *et al.*, 1997; Pillai and Vinod, 2016; Sivrikaya *et al.*, 2008; Sridharan and Nagaraj, 2005), such correlative models have yet to be developed for rubber-mixed soils.

In this study, a series of cone penetration (consistency limits) and standard Proctor compaction tests were carried out on various ground rubber–clay (GRC) blends (prepared with four different clay soils) to generate a reliable database allowing for the development of simple correlative models capable of predicting the compaction characteristics of GRC blends as a function of the composite's consistency limits. The models proposed in the present study provide a practical procedure towards predicting the compaction characteristics of GRC blends without the need for conducting time-consuming compaction tests.

2. Materials

2.1 Clay soils

Four different soils consisting of both natural and commercial soils, covering a wide range of plasticity characteristics, were adopted for the experimental programme. The natural soils, hereafter denoted as soils RC1 and RC2, consisted of reddish-brown clays sourced from a landfill site located at Adelaide, South Australia. The commercial soils were supplied by a local manufacturer, and included kaolinite (hereafter termed soil K) and a mixture of 85% kaolinite and 15% sodium-activated bentonite (hereafter termed soil KB). The physical and mechanical properties of the soils, determined as per relevant ASTM and Australian standards, are summarised in Table 1. The liquid limit w_L and plasticity index I_P were measured as $w_L = 44\%$ and $I_P = 22\%$ for soil K, and $w_L = 47\%$ and $I_P = 29\%$ for soil RC1, from which both soils were characterised as 'clay with intermediate plasticity' (CI) in accordance with the Unified Soil Classification System (USCS). The soils KB and RC2, however, were graded as 'clay with high plasticity' (CH), exhibiting w_L and I_P values of 59% and 31% for soil KB, and 78% and 57% for soil RC2, respectively.

Offprint provided courtesy of www.icevirtuallibrary.com
Author copy for personal use, not for distribution

Table 1. Physical and mechanical properties of the clay soils

Properties	Soil K	Soil RC1	Soil KB	Soil RC2	Standard designation
Specific gravity, G_{ss}	2·69	2·67	2·71	2·72	ASTM D854-14 (ASTM, 2014)
Grain-size distribution					
Clay (< 2 μm): %	49	37	53	44	ASTM D422-07 (ASTM, 2007)
Silt (2–75 μm): %	50	32	46	36	
Fine sand (0·075–0·425 mm): %	1	19	1	14	
Medium sand (0·425–2 mm): %	0	8	0	5	
Coarse sand (2–4·75 mm): %	0	5	0	1	
Consistency limits and classification					
Liquid limit, w_L: %	44	47	59	78	AS 1289·3·9·1-15[a] (SA, 2015)
Plastic limit, w_P: %	22	18	28	21	AS 1289·3·2·1-09[b] (SA, 2009)
Plasticity index, I_P (= $w_L - w_P$): %	22	29	31	57	AS 1289·3·3·1-09 (SA, 2009)
USCS classification	CI[c]	CI	CH[d]	CH	ASTM D2487-11 (ASTM, 2011)
Compaction characteristics					
Optimum water content, w_{opt}: %	21	16	25	19	ASTM D698-12 (ASTM, 2012)
Maximum dry unit weight, γ_{dmax}: kN/m^3	15·45	16·41	14·61	15·84	

[a]Cone penetration method (see Section 3.1 for details)
[b]Conventional rolling thread method (see Section 3.1 for details)
[c]Clay with intermediate plasticity
[d]Clay with high plasticity

2.2 Ground rubber

Commercially available GR, supplied by a local distributor, was used as the reinforcing agent. The conventional grain-size (or sieve) analysis, carried out in accordance with the ASTM D422-07 (ASTM, 2007) standard, indicated that GR is similar in size to medium-fine sand, with particles ranging between 1·18 mm and 75 μm. The particle diameters corresponding to 10, 30 and 60% finer were measured as $D_{10} = 0{\cdot}182$ mm, $D_{30} = 0{\cdot}334$ mm and $D_{60} = 0{\cdot}513$ mm. The uniformity (i.e. $C_u = D_{60}/D_{10}$) and curvature (i.e. $C_c = D_{30}^2/D_{10}D_{60}$) coefficients were therefore obtained as $C_u = 2{\cdot}81$ and $C_c = 1{\cdot}20$, from which GR was classified as 'poorly graded' in accordance with the USCS criteria. Figure 1 depicts microscopic micrographs of the rubber particles at three different magnification ratios (Figure 1(a): 1× magnification; Figure 1(b): 50× magnification; and Figure 1(c): 200× magnification). As shown in Figure 1(b), the rubber particles are non-spherical and highly irregular in shape. Moreover, a series of cavity-like micro-cracks are distributed along the rubber's surface (see Figure 1(c)), thus making for a rough surface texture. Such surface features may potentially promote adhesion and/or induce interfacial friction between the rubber particles and the soil grains, thereby altering the soil fabric into a coherent matrix of enhanced mechanical performance (Soltani *et al.*, 2018b). The physical properties and chemical composition of GR, as supplied by the manufacturer, are provided in Table 2. The specific gravity of GR was found to be $G_{sr} = 1{\cdot}09$, which is lower by two-fold approximately than the standard value of $G_{ss} = 2{\cdot}65$ reported for most soils.

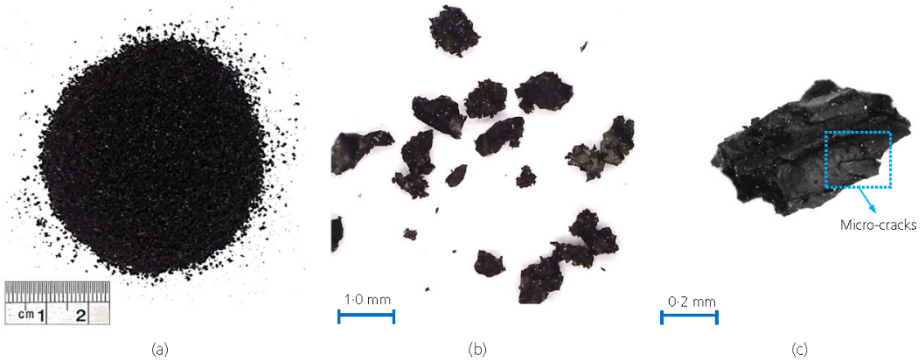

Figure 1. Ground rubber (GR) particles at different magnification ratios (modified from Soltani *et al.*, 2018b): (a) 1× magnification; (b) 50× magnification; (c) 200× magnification

Offprint provided courtesy of www.icevirtuallibrary.com
Author copy for personal use, not for distribution

Table 2. Physical properties and chemical composition of GR

Properties	Value/description
Physical properties	
Solubility in water	Insoluble
Water adsorption	Negligible (< 4%)
Resistance to acid/alkaline	Excellent
Softening point: °C	170
Specific gravity, G_{sr}	1·09
Grain-size distribution and classification[a]	
D_{10}: mm[b]	0·182
D_{30}: mm	0·334
D_{50}: mm	0·478
D_{60}: mm	0·513
Coefficient of uniformity, C_u[c]	2·81
Coefficient of curvature, C_c[d]	1·20
USCS classification	Poorly graded sand (SP)
Chemical composition	
Styrene–butadiene copolymer: %	55
Acetone extract: %	5–20
Carbon black: %	25–35
Zinc oxide: %	2–3
Sulfur: %	1–3

[a]ASTM D422-07 (ASTM, 2007) method
[b]Particle diameter corresponding to 10% finer
[c]$C_u = D_{60}/D_{10}$
[d]$C_c = D_{30}^2/D_{10}D_{60}$

3. Test programme

Each of the four soil choices – namely, soils K, RC1, KB and RC2 – was blended with GR at four varying rubber contents (defined as GR to dry soil weight ratio) – that is, $R_c = 5$, 10, 20 and 30% – and further tested for consistency limits and compaction characteristics. Hereafter, a simple coding system, defined as KRx, RC1Rx, KBRx and RC2Rx (where R$x = x$% GR), will be adopted to designate the various mix designs. As a consequence of rubber particles floating in water, standard procedures outlined in ASTM D854-14 (ASTM, 2014) for measuring the specific gravity of solids were not applicable. Therefore, the specific gravity for various GRC blends was estimated by the following theoretical relationship (Soltani *et al.*, 2018b)

$$1. \quad G_{sm} = \frac{G_{ss}G_{sr}(W_s + W_r)}{W_s G_{sr} + W_r G_{ss}}$$

where G_{sm} is the average specific gravity of GRC blends; W_s is the weight of dry soil; W_r is the weight of GR; G_{ss} is the specific gravity of soil solids (see Table 1); and G_{sr} is the specific gravity of GR particles (= 1·09).

3.1 Consistency limits

The virgin clays and various GRC blends were tested for consistency limits – namely, the liquid limit w_L, plastic limit w_P and plasticity index I_P (= $w_L - w_P$), following the Australian code of practice (see relevant standard designations in Table 1). The liquid limit was obtained by means of the cone penetration method. The weight and conical angle of the cone were 80 g and 30°, respectively. The required amount of material (either virgin or GR-blended clay) was divided into six equal portions, each portion paired with a predetermined amount of water, and thoroughly mixed by mechanical effort to obtain slurries of uniform consistency. The resulting slurries where then remoulded into rigid cups, measuring 53 mm in diameter and 40 mm height, and placed in contact with the cone penetrometer for testing. The cone was allowed to freely penetrate into each sample for approximately 5 s. The depth of penetration was measured by means of a digital dial gauge to the nearest 0·1 mm. As a result of the test, a linear change in water content w against the corresponding cone penetration δ, commonly referred to as the flow curve, can be observed. Test results are plotted over the w–$\log_{10}\delta$ space, the slope of which is defined as the flow index – that is, $I_F = \Delta w/\Delta\log_{10}\delta$ (Sridharan *et al.*, 1999). Furthermore, the water content at which the cone penetration reaches $\delta = 20$ mm is taken as the liquid limit.

The rolling thread method is currently in vogue for direct measurement of the plastic limit. The water content at which a mass of soil (or material) begins to crumble when manually rolled into a thread of approximately 3·2 mm (dia.) is taken as the plastic limit. Quite clearly, the rolling thread method is highly subjective and therefore inevitably biased by personal judgements, which leads to inconsistent and often non-reproducible results among different operators. Moreover, it has been the authors' experience that this particular methodology would not be suitable for geomaterials containing notable non-plastic hydrophobic (i.e. low water adsorption capacity) fractions (despite the geomaterial's plastic response in the presence of water). The rubber's elastic character and hydrophobic nature make for a rather difficult, although possible, implementation of the conventional rolling thread technique. Although the rubber inclusion would most certainly lead to a reduced plastic limit, it is not possible to arrive at a certain/unique value with confidence following the current methodology. Such difficulties are essentially similar to those encountered for natural soils containing notable fractions of sand and silt, which have been well documented in the literature (e.g. Prakash and Sridharan, 2006, 2012). Among the available experimental alternatives for indirect measurement of the plastic limit, the flow index method suggests a rather practical and objective scheme, which is also supported by robust empirical observations as well as solid fundamental evidence (see Sridharan *et al.* (1999) for details). The flow index method states that the plasticity index is proportional to the flow index (obtained from the cone penetration test) – that is, $I_P \propto I_F$, and thus can be estimated by

$$2. \quad I_P = \chi I_F$$

where χ = empirical coefficient.

Offprint provided courtesy of www.icevirtuallibrary.com
Author copy for personal use, not for distribution

Therefore, the plastic limit can be estimated with a known liquid limit (obtained from the cone penetration test) by

3. $$w_P = w_L - \chi I_F$$

The empirical coefficient χ falls between 0·71 and 0·74, which was calibrated based on conventional rolling thread tests conducted on 121 soil samples of widely varying plasticity characteristics and geological origin (Sridharan *et al.*, 1999). As a typical example, and to provide further verification of $\chi = 0{\cdot}71$–$0{\cdot}74$, Figure 2 illustrates the variations of the plasticity index I_P ($I_P = w_L - w_P$ where w_P = plastic limit obtained by the rolling thread method) against the flow index I_F for the virgin clays used in the present study. As demonstrated in the figure, a perfect correlation in the form of $I_P = 0{\cdot}715 I_F$ (with $R^2 = 0{\cdot}997$) can be obtained between the plasticity and flow indices, which complies well with that suggested by Sridharan *et al.* (1999). Therefore, to avoid the difficulties associated with implementing the conventional rolling thread technique to various GRC blends, the plastic limit for both the virgin clays and various GRC blends was estimated by means of Equation 3 (with $\chi = 0{\cdot}715$). Hereafter, the term plastic limit will refer to that obtained by means of the flow index method.

3.2 Compaction studies

Standard Proctor compaction tests were carried out on the virgin clays and various GRC blends in accordance with the ASTM D698-12 (ASTM, 2012) standard. The required amount of material (either virgin or GR-blended clay) was divided into six equal portions, each portion paired with a predetermined amount of water, and thoroughly mixed by hand. Extensive care was taken to pulverise the lumped particles, aiming for homogeneity of the mixtures. The moist mixtures were sealed in plastic bags and allowed to cure for a period of 24 h, ensuring even distribution of moisture throughout the composite mass. The cured mixtures were then subjected to the conventional standard Proctor compaction test to arrive at the dry unit weight–water content relationship, and thus quantify the optimum water content and the maximum dry unit weight.

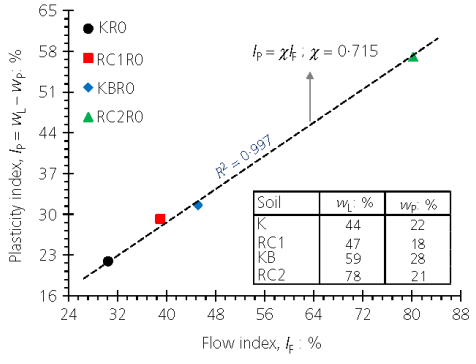

Figure 2. Variations of the conventional plasticity index plotted against the flow index for the virgin clays

4. Statistical analysis

The consistency limits, obtained as per Section 3.1, were each independently plotted against the corresponding optimum water contents, and further examined for single-coefficient linear correlations – that is, $w_{opt} = \beta x$ (w_{opt} is the optimum water content; $x = w_L$, w_P or I_P; and β is the regression coefficient or fitting parameter). The most appropriate consistency parameter (capable of adequately estimating the optimum water content for various GRC blends) was then selected and coupled with basic volume–mass relations to arrive at a semi-empirical relationship for the maximum dry unit weight. The accuracy of the proposed correlative models for both the optimum water content and the maximum dry unit weight was then examined by means of statistical fit-measure indices.

5. Results and discussion

5.1 Effect of GR on consistency limits

The flow curves for the virgin clays and various GRC blends prepared with soils K, RC1, KB and RC2 are provided in Figures 3(a), 3(b), 3(c) and 3(d), respectively. As a result of GR inclusion, the flow curve exhibited a major downward shift over the w–$\log_{10}\delta$ space (w is the water content and δ is the cone penetration), indicating a significant reduction in the liquid limit (compare the water contents at $\delta = 20$ mm). Meanwhile, the slope of the flow curve was also observed to decrease with increase in rubber content, leading to a notable reduction in the flow index I_F and hence the plasticity index I_P ($I_P = 0{\cdot}715 I_F$). As a typical case, the virgin clay KB resulted in $I_F = 45{\cdot}12\%$, while the inclusion of 5, 10, 20 and 30% GR resulted in $I_F = 43{\cdot}23\%$, $42{\cdot}00\%$, $40{\cdot}67\%$ and $37{\cdot}74\%$, respectively (see Figure 3(c)).

Figures 4(a), 4(b), 4(c) and 4(d) illustrate the variations of the consistency limits – namely, the liquid limit w_L, plastic limit w_P ($w_P = w_L - 0{\cdot}715 I_F$) and plasticity index I_P ($I_P = 0{\cdot}715 I_F$), against rubber content R_c for the virgin clays and various GRC blends prepared with soils K, RC1, KB and RC2, respectively. The higher the rubber content the lower the consistency limits, following a linear monotonic decreasing trend. As a typical case, the virgin clay KB resulted in $w_L = 59\%$, while the inclusion of 5, 10, 20 and 30% GR resulted in $w_L = 57$, 53, 51 and 46%, respectively (see Figure 4(c)). The rate of decrease in w_L, w_P and I_P with respect to R_c – represented by the slope of a typical linear trend line fitted through the desired dataset (i.e. $\Delta y/\Delta R_c$, where $y = w_L$, w_P or I_P) – was observed to be dependent on the type of soil, with

Offprint provided courtesy of www.icevirtuallibrary.com
Author copy for personal use, not for distribution

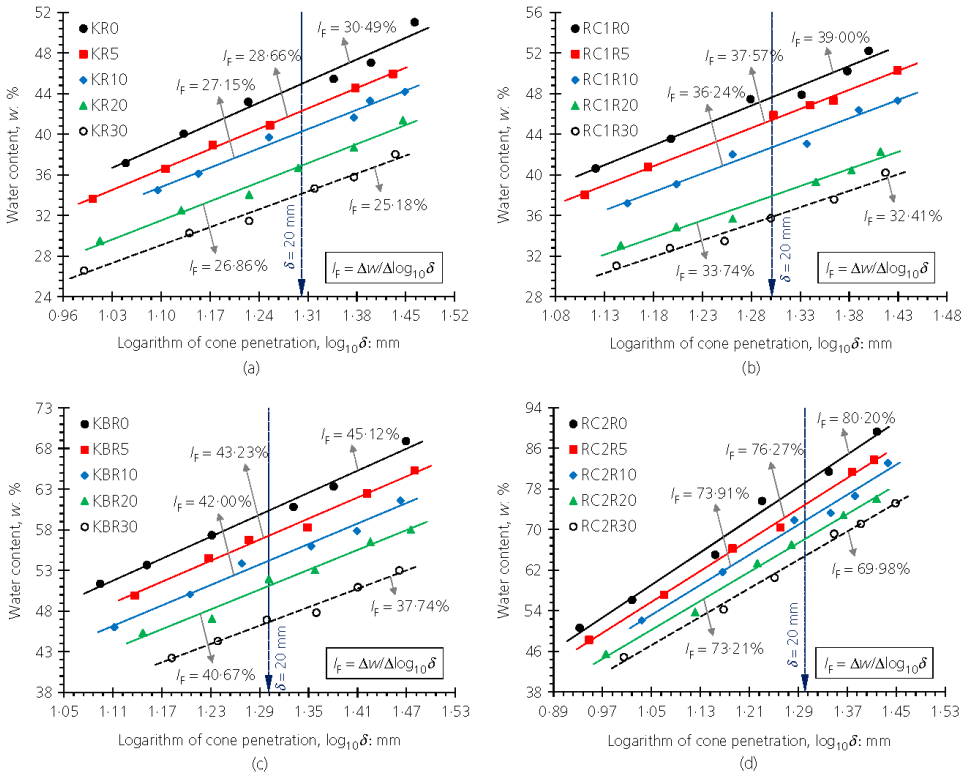

Figure 3. Flow curves for the virgin clays and various GRC blends: (a) soil K; (b) soil RC1; (c) soil KB; (d) soil RC2

the CH soils (i.e. soils KB and RC2) exhibiting a greater tendency for reduction compared with the CI soils (i.e. soils K and RC1). In terms of the liquid limit, for instance, the soils KB and RC2 resulted in $\Delta w_L/\Delta R_c = -0{\cdot}425$ and $-0{\cdot}456$, respectively. For the soils K and RC1, however, these values dropped to $-0{\cdot}347$ and $-0{\cdot}401$, respectively.

Figure 5 illustrates the location of the tested mix designs on Casagrande's plasticity chart (Figure 5(a): soils K and KB; Figure 5(b): soils RC1 and RC2). For a given type of soil, the variations of I_P against w_L followed a linear path (see the arrowed lines labelled '1' and '2' in Figure 5), with relatively lower slopes (i.e. $\Delta I_P/\Delta w_L$) compared with that of the 'A' and 'U' lines of the plasticity chart. Furthermore, the value of $\Delta I_P/\Delta w_L$ was dependent on the type of soil, with the CH soils (i.e. soils KB and RC2) exhibiting greater slopes compared with that of the CI soils (i.e. soils K and RC1). The soils KB and RC2 resulted in $\Delta I_P/\Delta w_L = 0{\cdot}383$ and $0{\cdot}517$, respectively. For the soils K and RC1, however, these values changed to $0{\cdot}329$ and $0{\cdot}395$, respectively. For a given type of soil, an increase in rubber content relocated the soil towards lower plasticity regions (follow the arrowed lines '1' and '2' in Figure 5), while mainly maintaining the original USCS classification observed for the virgin soil. Two exceptions, however, were the soils K and KB at $R_c = 30\%$, which transitioned from the CI and CH categories to CL ('clay with low plasticity') and CI categories, respectively (see KR30 and KBR30 in Figure 5(a)).

The consistency limits, the liquid limit in particular, can be employed to infer the development of soil fabric (Kim and Palomino, 2009; Soltani *et al.*, 2018b; Wroth and Wood, 1978). A decrease in the liquid limit, as is the case with GRC blends (see Figure 4), implies that a face-to-face aggregated (or dispersed) fabric dominates the GRC matrix (Mitchell and Soga, 2005). As opposed to the edge-to-face flocculated fabric, a face-to-face aggregated fabric offers less resistance to shear (or cone penetration), which in turn leads to lower liquid limits

Offprint provided courtesy of www.icevirtuallibrary.com
Author copy for personal use, not for distribution

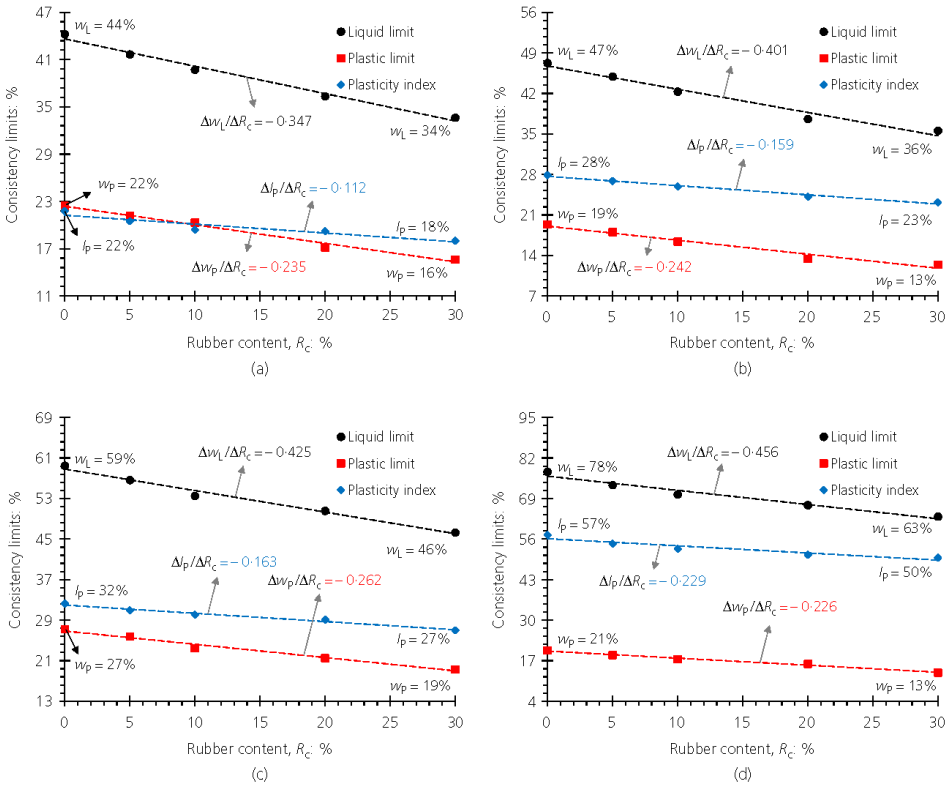

Figure 4. Variations of the consistency limits against rubber content for the virgin clays and various GRC blends: (a) soil K; (b) soil RC1; (c) soil KB; (d) soil RC2

(i.e. the 20 mm cone penetration is achieved at lower water contents). Moreover, reduction in the consistency limits as a result of GR inclusion can be attributed to the lower specific surface area and water adsorption capacity of the rubber particles compared with the soil grains (Cetin *et al.*, 2006; Srivastava *et al.*, 2014; Trouzine *et al.*, 2012). The consistency limits are primarily a function of the soil's clay (or fines) content, with higher clay contents exhibiting higher liquid and plastic limits. Quite clearly, an increase in rubber content substitutes a larger portion of the clay content with non-plastic hydrophobic rubber particles, thus leading to a further decrease of the consistency limits.

5.2 Effect of GR on compaction characteristics

Standard Proctor compaction curves, along with corresponding specific gravities (obtained as per Equation 1) and zero-air voids (ZAV) saturation lines, for the virgin clays and various GRC blends prepared with soils K, RC1, KB and RC2 are provided in Figures 6(a), 6(b), 6(c) and 6(d), respectively. For a given type of soil, the higher the rubber content the lower the average specific gravity G_{sm}, following a monotonic decreasing trend. As a result of GR inclusion, the compaction locus exhibited a major downward–leftward translation over the γ_d–w space (γ_d is the dry unit weight and w is the water content), indicating a significant reduction in both the optimum water content w_{opt} and the maximum dry unit weight γ_{dmax}. Such results foster the use of GR as a viable lightweight alternative for common quarry materials such as sand. For a given type of soil, the peak (or optimum) points followed a linear decreasing trend with increase in rubber content R_c (follow the arrowed lines in Figure 6), thereby signifying the existence of a linear relationship for both w_{opt} and γ_{dmax} with R_c. The linear tendency for reduction is in compliance with that reported in most of the existing literature sources (e.g. Cabalar *et al.*, 2014; Signes *et al.*, 2016; Yadav and Tiwari, 2017a).

Offprint provided courtesy of www.icevirtuallibrary.com
Author copy for personal use, not for distribution

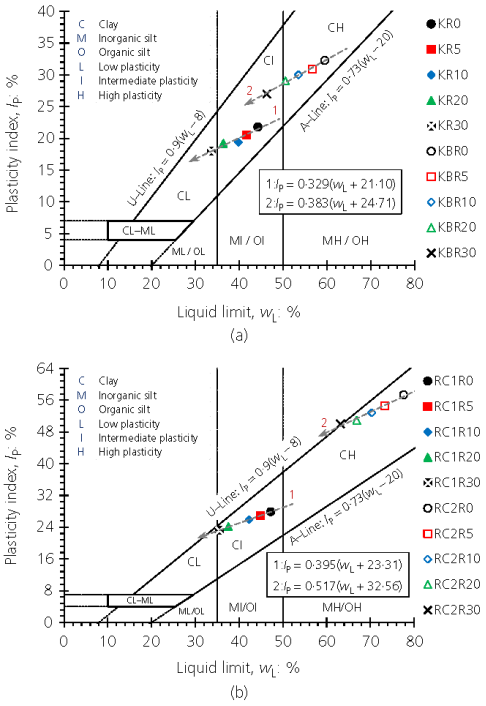

Figure 5. Location of the tested mix designs on Casagrande's plasticity chart: (a) soils K and KB; (b) soils RC1 and RC2

Figures 7(a) and 7(b) illustrate the variations of the compaction characteristics – namely, w_{opt} and γ_{dmax} – against R_c for the tested mix designs, respectively. The higher the rubber content the lower the compaction characteristics, following a linear monotonic decreasing trend. The virgin clay KB, for instance, resulted in $w_{opt} = 25\%$ ($\gamma_{dmax} = 14{\cdot}61$ kN/m^3), while the inclusion of 5, 10, 20 and 30% GR resulted in $w_{opt} = 24\%$ ($\gamma_{dmax} = 14{\cdot}27$ kN/m^3), 22% ($\gamma_{dmax} = 14{\cdot}16$ kN/m^3), 21% ($\gamma_{dmax} = 13{\cdot}71$ kN/m^3) and 18% ($\gamma_{dmax} = 13{\cdot}17$ kN/m^3), respectively. Similarly to the consistency limits (see Figure 4), the rate of decrease in w_{opt} with respect to R_c – represented by the slope of a typical linear trend line fitted through a desired w_{opt}–R_c dataset (i.e. $\Delta w_{opt}/\Delta R_c$) – was observed to be dependent on the type of soil, with the CH soils (i.e. soils KB and RC2) exhibiting a greater tendency for reduction compared with the CI soils (i.e. soils K and RC1). As demonstrated in Figure 7(a), the soils KB and RC2 resulted in $\Delta w_{opt}/\Delta R_c = -0{\cdot}224$ and $-0{\cdot}196$, respectively. For the soils K and RC1, however, these values dropped to $-0{\cdot}160$ and $-0{\cdot}114$, respectively. On the contrary, as depicted in Figure 7(b), an opposite effect can be concluded for γ_{dmax}, as $\Delta\gamma_{dmax}/\Delta R_c$ was observed to be slightly higher for the CI soils compared with that of the CH soils (i.e. $\Delta\gamma_{dmax}/\Delta R_c = -0{\cdot}052$, $-0{\cdot}059$, $-0{\cdot}046$ and $-0{\cdot}043$ for soils K, RC1, KB and RC2, respectively).

Reduction in the compaction characteristics as a result of GR inclusion can be attributed to the lower specific gravity and hydrophobic nature of the rubber particles compared with the soil grains (Cabalar *et al.*, 2014; Özkul and Baykal, 2007; Signes *et al.*, 2016). Similarly to the consistency limits, the optimum water content is primarily a function of the soil's clay/fines content, with higher clay contents exhibiting a higher optimum water content. Consequently, an increase in rubber content substitutes a larger portion of the clay content with hydrophobic rubber particles, which in turn leads to a further decrease of the optimum water content. The maximum dry unit weight is proportional to the composite's specific gravity, with higher specific gravities yielding a higher maximum dry unit weight. As such, an increase in rubber content substitutes a larger portion of the soil (with a high specific gravity) with low-specific-gravity rubber particles, which leads to a further decrease of the composite's average specific gravity (see G_{sm} values in Figure 6) and hence its maximum dry unit weight. Moreover, the elastic (or rebound) response of GR to dynamic energy during compaction may potentially reduce the compaction efficiency, and thus contribute to a lower maximum dry unit weight (Yadav and Tiwari, 2017b).

5.3 Compaction characteristics as a function of consistency limits

The conventional compaction test, although simple in terms of procedure, has been widely regarded as a laborious and time-consuming task (Sridharan and Sivapullaiah, 2005). Although numerous attempts have been made in the past to correlate the compaction characteristics with the consistency limits, such correlative models have not yet been extended to GRC blends (or other similar geomaterials). As such, the present section will be devoted to the development of practical models capable of predicting the compaction characteristics of GRC blends as a function of the consistency limits.

Figure 8 illustrates the variations of the optimum water content w_{opt} (data presented in Figure 7(a)) against the consistency limits – namely, the liquid limit w_L, plastic limit w_P and plasticity index I_P (data presented in Figures 4(a)–4(d)), for the tested mix designs (Figure 8(a): w_{opt}–w_L; Figure 8(b): w_{opt}–w_P; and Figure 8(c): w_{opt}–I_P). As depicted in Figures 8(a) and 8(c), w_L and I_P both exhibit weak correlations with w_{opt}, and thus are deemed as unsuitable for model development. The ineptness of the liquid limit in predicting the compaction characteristics of natural fine-grained soils was first recognised by Sridharan and Nagaraj (2005), and was attributed to the fact that soils having the same liquid limit (but different plasticity characteristics) often exhibit different compaction behaviour. On the contrary, w_P exhibits a rather strong correlation

Offprint provided courtesy of www.icevirtuallibrary.com
Author copy for personal use, not for distribution

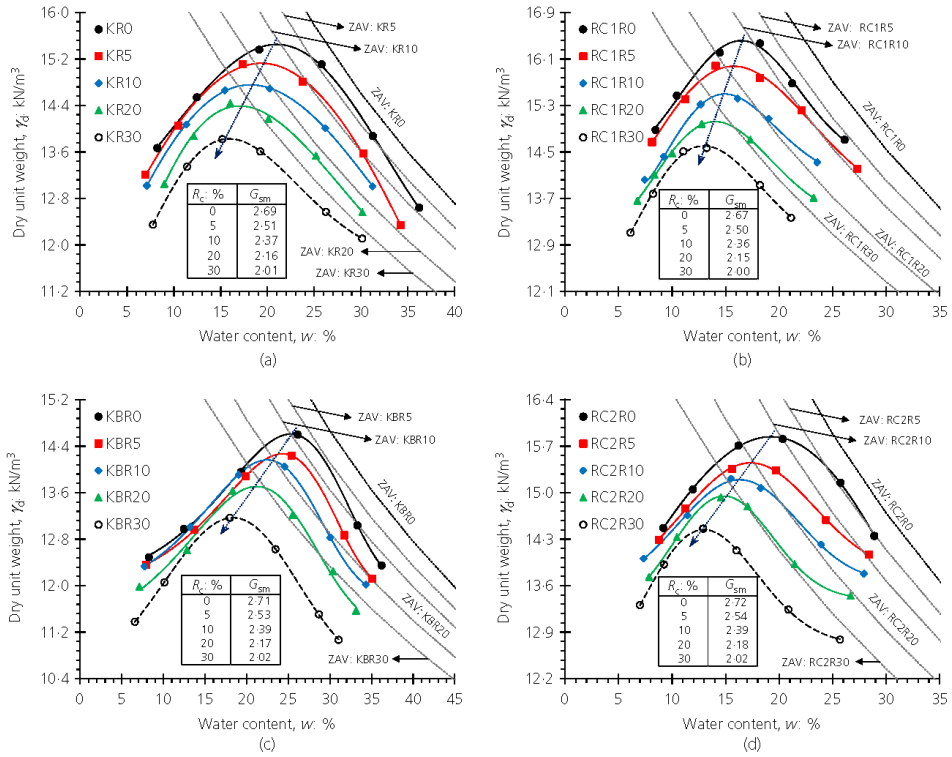

Figure 6. Standard Proctor compaction curves for the virgin clays and various GRC blends: (a) soil K; (b) soil RC1; (c) soil KB; (d) soil RC2

(with $R^2 = 0{\cdot}950$) in the form of a single-coefficient linear function with w_{opt} (see Figure 8(b)), which can be given as

4. $$w_{opt} = 0{\cdot}941 w_P$$

Although some scatter can be observed with respect to Equation 4, all data points lie between the upper and lower 95% prediction bands, thus indicating no particular outliers associated with the predictions (see Figure 8(b)). Interestingly, the proposed model given in Equation 4 complies well with those suggested in the literature for natural soils (but with a slightly different coefficient compared to 0·941) – for example, $w_{opt} = 0{\cdot}92 w_P$ (Sridharan and Nagaraj, 2005) and $w_{opt} = 0{\cdot}84 w_P$ (Nagaraj *et al.*, 2015).

It is well accepted that the maximum dry unit weight γ_{dmax} is proportional to the dry unit weight at the plastic limit water content with a presumptive saturation degree of 100% (Gurtug and Sridharan, 2002, 2004; Gurtug *et al.*, 2018; Pillai and Vinod, 2016). Making use of basic volume–mass relations, the dry unit weight at plastic limit γ_{dP} can be expressed as

5. $$\gamma_{dP} = \frac{G_{sm}\gamma_w}{1 + G_{sm} w_P}$$

where G_{sm} is the average specific gravity of GRC blends (values presented in Figure 6); and γ_w is the unit weight of water (= 9·81 kN/m^3).

The variations of γ_{dmax} (data presented in Figure 7(b)) were plotted against γ_{dP} (obtained as per Equation 5) for the various mix designs, and the results are provided in Figure 9. A similar correlation to that observed between w_{opt} and w_P also exists between γ_{dmax} and γ_{dP} (with $R^2 = 0{\cdot}942$), which can be expressed as

6. $$\gamma_{dmax} = 0{\cdot}932\gamma_{dP} = \frac{0{\cdot}932 G_{sm}\gamma_w}{1 + G_{sm} w_P}$$

Offprint provided courtesy of www.icevirtuallibrary.com
Author copy for personal use, not for distribution

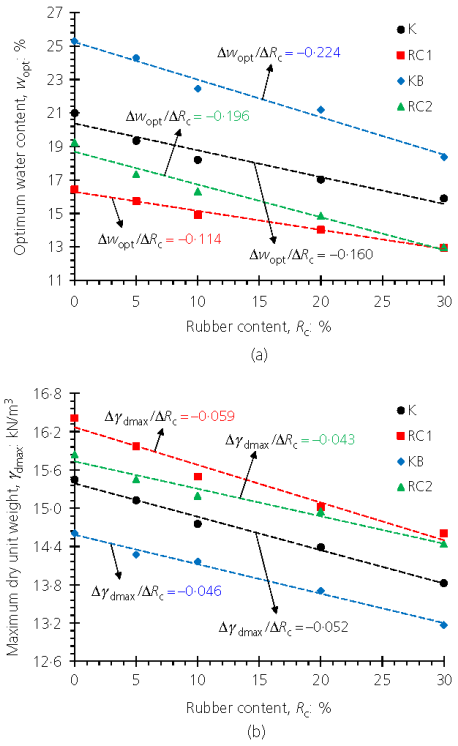

Figure 7. Variations of the compaction characteristics plotted against rubber content for the tested mix designs: (a) optimum water content; (b) maximum dry unit weight

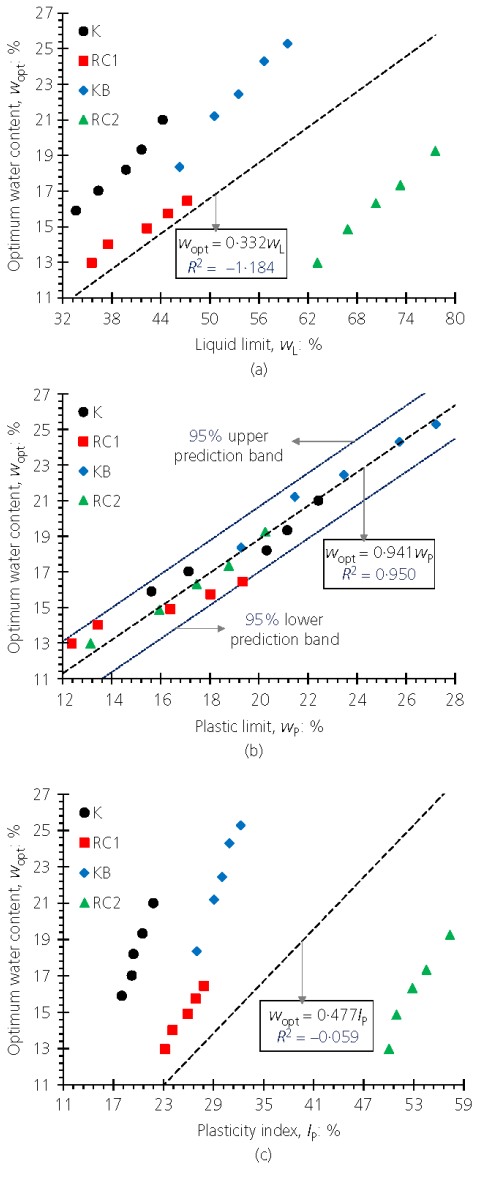

Figure 8. Variations of the optimum water content plotted against the consistency limits for the tested mix designs: (a) liquid limit; (b) plastic limit; (c) plasticity index

As depicted in Figure 9, all data points with respect to Equation 6 position themselves between the upper and lower 95% prediction bands, thereby suggesting no particular outliers associated with the predictions. Previous studies such as Gurtug and Sridharan (2002) have suggested a different coefficient of 0·98 for natural fine-grained soils – that is, $\gamma_{dmax} = 0{\cdot}98\gamma_{dP}$, which is slightly higher compared to the 0·932 obtained in the present study. This may be attributed to the lower average specific gravity of GRC blends compared with that of the virgin clays, which in turn gives rise to lower γ_{dP} values.

Figures 10(a) and 10(b) illustrate the variations of both the actual and predicted w_{opt} and γ_{dmax} data against rubber content R_c for the tested mix designs, respectively. The proposed models – that is, Equation 4 for w_{opt} and Equation 6 for γ_{dmax}, comply well with experimental observations, as evident with the clustering of actual and predicted data in the figures.

Offprint provided courtesy of www.icevirtuallibrary.com
Author copy for personal use, not for distribution

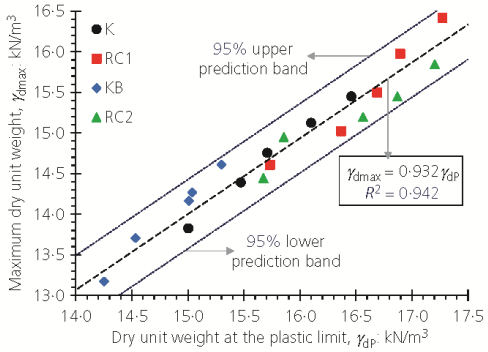

Figure 9. Variations of the maximum dry unit weight plotted against the dry unit weight at the plastic limit for the tested mix designs

Most of the predicted values perfectly overlap with their actual counterparts, thus signifying an excellent capacity to simulate the compaction characteristics of GRC blends by means of the plastic limit. In general, a reliable empirical model can be characterised as one that maintains a perfect balance between the apparent correlation and the exhibited error (or accuracy). The former is taken into consideration by means of the coefficient of determination R^2, with values closer to unity implying a stronger correlation. The latter is commonly examined by means of the normalised root-mean-square error (NRMSE) (in %) and the mean absolute percentage error (MAPE) (in %), with values closer to zero representing a higher degree of accuracy (Soltani *et al.*, 2018d). The NRMSE and MAPE indices can be obtained by the following

$$7.\quad \mathrm{NRMSE} = \frac{\sqrt{(1/N)\sum_{i=1}^{N}(y_{mi} - y_{ai})^2}}{y_{a\,max} - y_{a\,min}} \times 100$$

$$8.\quad \mathrm{MAPE} = \frac{1}{N}\sum_{i=1}^{N}\left|\frac{y_{mi} - y_{ai}}{y_{ai}}\right| \times 100$$

where y_m is the predicted value of the dependent variable y (= w_{opt} or γ_{dmax}); y_a is the actual value of the dependent variable y (data presented in Figure 7); $y_{a\,max}$ is the maximum value of y_a data; $y_{a\,min}$ is the minimum value of y_a data; i is the index of summation; and N is the number of data points used for model development (= 20, consisting of four virgin clays and 16 GRC blends).

The suggested models for w_{opt} (Equation 4) and γ_{dmax} (Equation 6), respectively, resulted in R^2 values of 0·950 and 0·942, thus implying that approximately 95% of the variations in experimental observations are captured and further explained by the proposed correlative models. The NRMSE and MAPE indices were, respectively, found to be 6·73% and 4·09% for w_{opt}, and 6·05% and 1·18% for γ_{dmax}, thereby indicating an average offset of approximately 5% associated with the predictive capacity of the proposed models.

As demonstrated in Figures 4(a)–4(d), the plastic limit w_P exhibited a linear relationship with rubber content R_c. For a given type of soil, it is therefore possible to write the following

$$9.\quad w_P = w_{Po} - \eta R_c$$

where w_{Po} is the plastic limit for the virgin clay (%) and η is the coefficient of plastic limit reduction (dimensionless).

The coefficient of plastic limit reduction η can be estimated by one plastic limit measurement for an arbitrary GRC blend. The choice of rubber content for the GRC blend would be arbitrary. From a statistical perspective, however, a median rubber content, taken as half the predefined maximum rubber content, is expected to provide a more reliable estimate of η (Mirzababaei *et al.*, 2018). For the present study where $R_c \leq 30\%$, a median rubber content would be 15%. Consider the following designations

- R_c^M = an arbitrary median rubber content
- w_P^M = plastic limit corresponding to an arbitrary median rubber content R_c^M (obtained in accordance with the flow index method, as outlined in Section 3.1).

Therefore, the following can be derived for η

$$10.\quad \eta = \frac{w_{Po} - w_P^M}{R_c^M}$$

By substituting the recent Equation 9 into Equation 4, it is possible to derive the following for w_{opt}

$$11.\quad w_{opt} = 0{\cdot}941(w_{Po} - \eta R_c)$$

Similarly, by substituting Equation 9 into Equation 6, γ_{dmax} can expressed as

$$12.\quad \gamma_{dmax} = 0{\cdot}932\gamma_{dP} = \frac{0{\cdot}932 G_{sm}\gamma_w}{1 + G_{sm}(w_{Po} - \eta R_c)}$$

Although the original models given in Equations 4 and 6 offer a fairly practical procedure towards predicting the compaction characteristics of GRC blends without the hurdles of

Offprint provided courtesy of www.icevirtuallibrary.com
Author copy for personal use, not for distribution

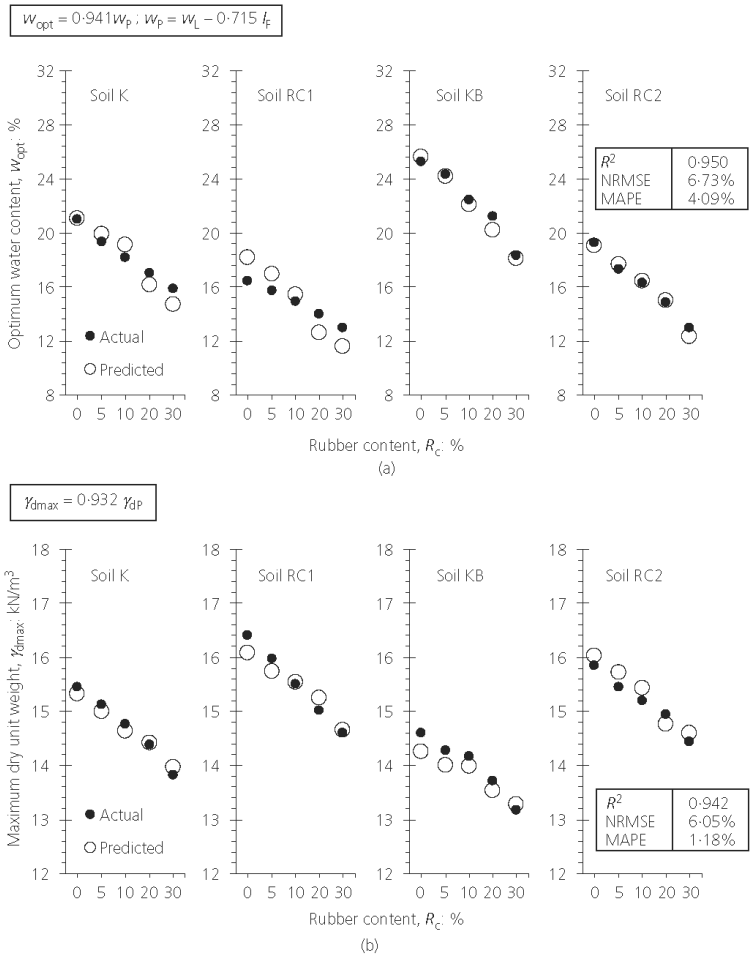

Figure 10. Variations of both the actual and predicted compaction data plotted against rubber content for the tested mix designs: (a) optimum water content (predicted by Equation 4); (b) maximum dry unit weight (predicted by Equation 6)

conducting the conventional compaction test, the procedure may still be somewhat time-consuming, since a separate plastic limit measurement is to be carried out for each desired rubber content. The newly developed models given in Equations 11 and 12, however, suggest a more practical approach, one that requires only two plastic limit measurements (i.e. w_{Po}, which is the plastic limit for the virgin clay; and w_P^M, which is the plastic limit corresponding to an arbitrary median rubber content R_c^M) to arrive at an estimate of the compaction characteristics over a wide range of desired rubber contents. Similar correlative models may also be developed for different compaction energy levels, and thus to arrive at a unified framework capable of predicting the compaction characteristics of GRC blends for any desired rubber content and/or rational compaction energy level.

6. Conclusions

The following conclusions can be drawn from this study.

- As a result of GR inclusion, the consistency limits – namely, the liquid limit w_L, plastic limit w_P ($w_P = w_L - 0{\cdot}715 I_F$, where I_F = flow index) and plasticity

Offprint provided courtesy of www.icevirtuallibrary.com
Author copy for personal use, not for distribution

index I_P ($I_P = 0{\cdot}715I_F$), exhibited a linear monotonic decreasing trend with increase in rubber content. The rate of decrease in w_L, w_R I_F and I_P was dependent on the type of soil, with the CH soils (high-plasticity clays) exhibiting a greater tendency for reduction compared with that of the CI soils (intermediate-plasticity clays).

- As a result of GR inclusion, the compaction characteristics – that is, the optimum water content w_{opt} and the maximum dry unit weight γ_{dmax} – exhibited a linear monotonic decreasing trend with increase in rubber content. Similarly to the consistency limits, the rate of decrease in w_{opt} was dependent on the type of soil, with the CH soils exhibiting a greater tendency for reduction. The rate of decrease in γ_{dmax}, however, was less influenced by the type of soil. Such results foster the use of GRC blends as a viable lightweight material for the construction of sustainable earth fills, thus serving a variety of infrastructure needs – for example, road/railway embankments, retaining walls and bridge abutments.
- The compaction characteristics were strongly correlated with the plastic limit. In this case, simple correlative models in the form of $w_{opt} = 0{\cdot}941w_P$ and $\gamma_{dmax} = 0{\cdot}932\gamma_{dP}$ (γ_{dP} is the dry unit weight at plastic limit water content with a presumptive saturation degree of 100%) were obtained for the optimum water content and the maximum dry unit weight, respectively. The predictive capacity of the proposed models was examined and further validated by statistical techniques. The proposed correlative models offer a practical procedure towards predicting the compaction characteristics of GRC blends without the hurdles of conducting the conventional compaction test, and hence can be implemented in practice for preliminary assessments.

Acknowledgement

This research was funded by the Australian Research Council (ARC) by way of project no. DP140103004; this support is gratefully acknowledged.

REFERENCES

ACI (American Concrete Institute) (2013) ACI 229: Report on controlled low-strength materials. American Concrete Institute, Farmington Hills, MI, USA.

Al-Amoudi OSB, Al-Homidy AA, Maslehuddin M and Saleh TA (2017) Method and mechanisms of soil stabilisation using electric arc furnace dust. *Scientific Reports* **7**: 46676, https://doi.org/10.1038/srep46676.

Alazigha DP, Indraratna B, Vinod JS and Ezeajugh LE (2016) The swelling behaviour of lignosulfonate-treated expansive soil. *Proceedings of the Institution of Civil Engineers Ground Improvement* **169(3)**: 182 193, https://doi.org/10.1680/jgrim.15.00002.

Al-Tabbaa A, Blackwell O and Porter SA (1997) An investigation into the geotechnical properties of soil tyre mixtures. *Environmental Technology* **18(8)**: 855 860, https://doi.org/10.1080/09593331808616605.

Arulrajah A, Mohammadinia A, D'Amico A and Horpibulsuk S (2017) Effect of lime kiln dust as an alternative binder in the stabilisation of construction and demolition materials. *Construction and Building Materials* **152**: 999 1007, https://doi.org/10.1016/j.conbuildmat.2017.07.070.

ASTM (2007) D422-63(2007)e2: Standard test method for particle-size analysis of soils. ASTM International, West Conshohocken, PA, USA.

ASTM (2011) D2487-11: Standard practice for classification of soils for engineering purposes (Unified Soil Classification System). ASTM International, West Conshohocken, PA, USA.

ASTM (2012) D698-12e2: Standard test methods for laboratory compaction characteristics of soil using standard effort (12,400 ft lbf/ft^3 (600 kN m/m^3)). ASTM International, West Conshohocken, PA, USA.

ASTM (2014) D854-14: Standard test methods for specific gravity of soil solids by water pycnometer. ASTM International, West Conshohocken, PA, USA.

Blotz LR, Benson CH and Boutwell GP (1998) Estimating optimum water content and maximum dry unit weight for compacted clays. *Journal of Geotechnical and Geoenvironmental Engineering* **124(9)**: 907 912, https://doi.org/10.1061/(asce)1090-0241(1998)124:9(907).

Cabalar AF, Karabash Z and Mustafa WS (2014) Stabilising a clay using tyre buffings and lime. *Road Materials and Pavement Design* **15(4)**: 872 891, https://doi.org/10.1080/14680629.2014.939697.

Cetin H, Fener M and Gunaydin O (2006) Geotechnical properties of tire cohesive clayey soil mixtures as a fill material. *Engineering Geology* **88(1–2)**: 110 120, https://doi.org/10.1016/j.enggeo.2006.09.002.

Di Matteo L, Bigotti F and Ricco R (2009) Best-fit models to estimate modified Proctor properties of compacted soil. *Journal of Geotechnical and Geoenvironmental Engineering* **135(7)**: 992 996, https://doi.org/10.1061/(asce)gt.1943-5606.0000022.

Estabragh AR, Naseh M, Beytolahpour I and Javadi AA (2013) Strength of a clay soil and soil cement mixture with resin. *Proceedings of the Institution of Civil Engineers Ground Improvement* **166(2)**: 108 114, https://doi.org/10.1680/grim.12.00014.

Estabragh AR, Rafatjo H and Javadi AA (2014) Treatment of an expansive soil by mechanical and chemical techniques. *Geosynthetics International* **21(3)**: 233 243, https://doi.org/10.1680/gein.14.00011.

Estabragh AR, Soltani A and Javadi AA (2016) Models for predicting the seepage velocity and seepage force in a fiber reinforced silty soil. *Computers and Geotechnics* **75**: 174 181, https://doi.org/10.1016/j.compgeo.2016.02.002.

Georgees RN, Hassan RA, Evans RP and Jegatheesan P (2015) Effect of the use of a polymeric stabilising additive on unconfined compressive strength of soils. *Transportation Research Record* **2473**: 200 208, https://doi.org/10.3141/2473-23.

Gurtug Y and Sridharan A (2002) Prediction of compaction characteristics of fine-grained soils. *Géotechnique* **52(10)**: 761 763, https://doi.org/10.1680/geot.2002.52.10.761.

Gurtug Y and Sridharan A (2004) Compaction behaviour and prediction of its characteristics of fine grained soils with particular reference to compaction energy. *Soils and Foundations* **44(5)**: 27 36, https://doi.org/10.3208/sandf.44.5_27.

Gurtug Y, Sridharan A and İkizler SB (2018) Simplified method to predict compaction curves and characteristics of soils. *Iranian Journal of Science and Technology, Transactions of Civil Engineering*, in press, https://doi.org/10.1007/s40996-018-0098-z.

Jha AK and Sivapullaiah PV (2016) Gypsum-induced volume change behavior of stabilised expansive soil with fly ash lime. *Geotechnical Testing Journal* **39(3)**: 391 406, https://doi.org/10.1520/gtj20150017.

Offprint provided courtesy of www.icevirtuallibrary.com
Author copy for personal use, not for distribution

Kalkan E (2013) Preparation of scrap tire rubber fiber silica fume mixtures for modification of clayey soils. *Applied Clay Science* **80–81**: 117 125, https://doi.org/10.1016/j.clay.2013.06.014.

Kim S and Palomino AM (2009) Polyacrylamide-treated kaolin: a fabric study. *Applied Clay Science* **45(4)**: 270 279, https://doi.org/10.1016/j.clay.2009.06.009.

Kua TA, Arulrajah A, Mohammadinia A, Horpibulsuk S and Mirzababaei M (2017) Stiffness and deformation properties of spent coffee grounds based geopolymers. *Construction and Building Materials* **138**: 79 87, https://doi.org/10.1016/j.conbuildmat.2017.01.082.

Mirzababaei M, Yasrobi SS and Al-Rawas AA (2009) Effect of polymers on swelling potential of expansive soils. *Proceedings of the Institution of Civil Engineers Ground Improvement* **162(3)**: 111 119, https://doi.org/10.1680/grim.2009.162.3.111.

Mirzababaei M, Miraftab M, Mohamed M and McMahon P (2013a) Unconfined compression strength of reinforced clays with carpet waste fibers. *Journal of Geotechnical and Geoenvironmental Engineering* **139(3)**: 483 493, https://doi.org/10.1061/(asce)gt.1943-5606.0000792.

Mirzababaei M, Miraftab M, Mohamed M and McMahon P (2013b) Impact of carpet waste fibre addition on swelling properties of compacted clays. *Geotechnical and Geological Engineering* **31(1)**: 173 182, https://doi.org/10.1007/s10706-012-9578-2.

Mirzababaei M, Arulrajah A, Horpibulsuk S and Aldavad M (2017) Shear strength of a fibre-reinforced clay at large shear displacement when subjected to different stress histories. *Geotextiles and Geomembranes* **45(5)**: 422 429, https://doi.org/10.1016/j.geotexmem.2017.06.002.

Mirzababaei M, Mohamed M, Arulrajah A, Horpibulsuk S and Anggraini V (2018) Practical approach to predict the shear strength of fibre-reinforced clay. *Geosynthetics International* **25(1)**: 50 66, https://doi.org/10.1680/jgein.17.00033.

Mitchell JK and Soga K (2005) *Fundamentals of Soil Behavior*, 3rd edn. John Wiley & Sons, Hoboken, NJ, USA.

Nagaraj HB, Reesha B, Sravan MV and Suresh MR (2015) Correlation of compaction characteristics of natural soils with modified plastic limit. *Transportation Geotechnics* **2**: 65 77, https://doi.org/10.1016/j.trgeo.2014.09.002.

Özkul ZH and Baykal G (2007) Shear behavior of compacted rubber fiber clay composite in drained and undrained loading. *Journal of Geotechnical and Geoenvironmental Engineering* **133(7)**: 767 781, https://doi.org/10.1061/(asce)1090-0241(2007)133:7(767).

Pandian NS, Nagaraj TS and Manoj M (1997) Re-examination of compaction characteristics of fine-grained soils. *Géotechnique* **47(2)**: 363 366, https://doi.org/10.1680/geot.1997.47.2.363.

Perez JL, Kwok CY and Senetakis K (2017) Investigation of the micromechanics of sand rubber mixtures at very small strains. *Geosynthetics International* **24(1)**: 30 44, https://doi.org/10.1680/jgein.16.00013.

Pillai GAS and Vinod PP (2016) Re-examination of compaction parameters of fine-grained soils. *Proceedings of the Institution of Civil Engineers Ground Improvement* **169(3)**: 157 166, https://doi.org/10.1680/jgrim.15.00005.

Prakash K and Sridharan A (2006) Critical appraisal of the cone penetration method of determining soil plasticity. *Canadian Geotechnical Journal* **43(8)**: 884 888, https://doi.org/10.1139/t06-043.

Prakash K and Sridharan A (2012) Classification of non-plastic soils. *Indian Geotechnical Journal* **42(2)**: 118 123, https://doi.org/10.1007/s40098-012-0007-5.

Priyadarshee A, Kumar A, Gupta D and Pushkarna P (2018) Compaction and strength behavior of tire crumbles fly ash mixed with clay. *Journal of Materials in Civil Engineering* **30(4)**: 04018033, https://doi.org/10.1061/(asce)mt.1943-5533.0002171.

SA (Standards Australia) (2009a) AS 1289.3.2.1-09: Methods of testing soils for engineering purposes: soil classification tests determination of the plastic limit of a soil. Standards Australia, Sydney, NSW, Australia.

SA (2009b) AS 1289.3.3.1-09: Methods of testing soils for engineering purposes: soil classification tests calculation of the plasticity index of a soil. Standards Australia, Sydney, NSW, Australia.

SA (2015) AS 1289.3.9.1-15: Methods of testing soils for engineering purposes: soil classification tests determination of the cone liquid limit of a soil. Standards Australia, Sydney, NSW, Australia.

Seda JH, Lee JC and Carraro JAH (2007) Beneficial use of waste tire rubber for swelling potential mitigation in expansive soils. In *Geo-Denver 2007: Soil Improvement* (Schaefer VR, Filz GM, Gallagher PM, Sehn AL and Wissmann KJ (eds)). American Society of Civil Engineers, Reston, VA, USA, GSP 172, pp. 1 9, https://doi.org/10.1061/40916(235)5.

Signes CH, Garzón-Roca J, Fernández PM, Torre MEG and Franco RI (2016) Swelling potential reduction of Spanish argillaceous marlstone Facies Tap soil through the addition of crumb rubber particles from scrap tyres. *Applied Clay Science* **132–133**: 768 773, https://doi.org/10.1016/j.clay.2016.07.027.

Sivrikaya O, Togrol E and Kayadelena C (2008) Estimating compaction behavior of fine-grained soils based on compaction energy. *Canadian Geotechnical Journal* **45(6)**: 877 887, https://doi.org/10.1139/t08-022.

Soltani A, Taheri A, Khatibi M and Estabragh AR (2017a) Swelling potential of a stabilised expansive soil: a comparative experimental study. *Geotechnical and Geological Engineering* **35(4)**: 1717 1744, https://doi.org/10.1007/s10706-017-0204-1.

Soltani A, Deng A, Taheri A and Mirzababaei M (2017b) A sulphonated oil for stabilisation of expansive soils. *International Journal of Pavement Engineering*, in press, https://doi.org/10.1080/10298436.2017.1408270.

Soltani A, Deng A and Taheri A (2018a) Swell compression characteristics of a fiber-reinforced expansive soil. *Geotextiles and Geomembranes* **46(2)**: 183 189, https://doi.org/10.1016/j.geotexmem.2017.11.009.

Soltani A, Deng A, Taheri A and Mirzababaei M (2018b) Rubber powder polymer combined stabilisation of South Australian expansive soils. *Geosynthetics International* **25(3)**: 304 321, https://doi.org/10.1680/jgein.18.00009.

Soltani A, Deng A, Taheri A and Sridharan A (2018c) Swell shrink-consolidation behavior of rubber-reinforced expansive soils. *Geotechnical Testing Journal*, in press, https://doi.org/10.1520/gtj20170313.

Soltani A, Deng A, Taheri A, Sridharan A and Estabragh AR (2018d) A framework for interpretation of the compressibility behavior of soils. *Geotechnical Testing Journal* **41(1)**: 1 16, https://doi.org/10.1520/gtj20170088.

Soosan TG, Sridharan A, Jose BT and Abraham BM (2005) Utilisation of quarry dust to improve the geotechnical properties of soils in highway construction. *Geotechnical Testing Journal* **28(4)**: 391 400, https://doi.org/10.1520/gtj11768.

Sridharan A and Nagaraj HB (2005) Plastic limit and compaction characteristics of fine-grained soils. *Proceedings of the Institution of Civil Engineers Ground Improvement* **9(1)**: 17 22, https://doi.org/10.1680/grim.2005.9.1.17.

Sridharan A and Sivapullaiah PV (2005) Mini compaction test apparatus for fine grained soils. *Geotechnical Testing Journal* **28(3)**: 240 246, https://doi.org/10.1520/gtj12542.

Sridharan A, Nagaraj HB and Prakash K (1999) Determination of the plasticity index from flow index. *Geotechnical Testing Journal* **22(2)**: 175 181, https://doi.org/10.1520/gtj11276j.

Srivastava A, Pandey S and Rana J (2014) Use of shredded tyre waste in improving the geotechnical properties of expansive black cotton

Offprint provided courtesy of www.icevirtuallibrary.com
Author copy for personal use, not for distribution

soil. *Geomechanics and Geoengineering* **9(4)**: 303–311, https://doi.org/10.1080/17486025.2014.902121.

Tang CS, Shi B and Zhao LZ (2010) Interfacial shear strength of fiber reinforced soil. *Geotextiles and Geomembranes* **28(1)**: 54–62, https://doi.org/10.1016/j.geotexmem.2009.10.001.

Trouzine H, Bekhiti M and Asroun A (2012) Effects of scrap tyre rubber fibre on swelling behaviour of two clayey soils in Algeria. *Geosynthetics International* **19(2)**: 124–132, https://doi.org/10.1680/gein.2012.19.2.124.

Wang YX, Guo PP, Ren WX *et al.* (2017) Laboratory investigation on strength characteristics of expansive soil treated with jute fiber reinforcement. *International Journal of Geomechanics* **17(11)**: 04017101, https://doi.org/10.1061/(asce)gm.1943-5622.0000998.

Wang C, Deng A and Taheri A (2018) Three-dimensional discrete element modeling of direct shear test for granular rubber–sand. *Computers and Geotechnics* **97**: 204–216, https://doi.org/10.1016/j.compgeo.2018.01.014.

Wroth CP and Wood DM (1978) The correlation of index properties with some basic engineering properties of soils. *Canadian Geotechnical Journal* **15(2)**: 137–145, https://doi.org/10.1139/t78-014.

Yadav JS and Tiwari SK (2017a) A study on the potential utilisation of crumb rubber in cement treated soft clay. *Journal of Building Engineering* **9**: 177–191, https://doi.org/10.1016/j.jobe.2017.01.001.

Yadav JS and Tiwari SK (2017b) Effect of waste rubber fibres on the geotechnical properties of clay stabilised with cement. *Applied Clay Science* **149**: 97–110, https://doi.org/10.1016/j.clay.2017.07.037.

Yadav JS and Tiwari SK (2017c) The impact of end-of-life tires on the mechanical properties of fine-grained soil: a review. *Environment, Development and Sustainability*, in press, https://doi.org/10.1007/s10668-017-0054-2.

How can you contribute?

To discuss this paper, please email up to 500 words to the editor at journals@ice.org.uk. Your contribution will be forwarded to the author(s) for a reply and, if considered appropriate by the editorial board, it will be published as discussion in a future issue of the journal.

Proceedings journals rely entirely on contributions from the civil engineering profession (and allied disciplines). Information about how to submit your paper online is available at www.icevirtuallibrary.com/page/authors, where you will also find detailed author guidelines.

Chapter 3

Swell–Shrink–Consolidation Behavior of Rubber–Reinforced Expansive Soils

Amin Soltani [a,†], An Deng [b], Abbas Taheri [c] and Asuri Sridharan [d,e]

[a] **PhD Student** − School of Civil, Environmental and Mining Engineering, The University of Adelaide, Adelaide, SA 5005, Australia (**Email:** Amin.Soltani@adelaide.edu.au; **ORCID:** 0000-0002-0483-7487)

[b] **Senior Lecturer** − School of Civil, Environmental and Mining Engineering, The University of Adelaide, Adelaide, SA 5005, Australia (**Email:** An.Deng@adelaide.edu.au)

[c] **Senior Lecturer** − School of Civil, Environmental and Mining Engineering, The University of Adelaide, Adelaide, SA 5005, Australia (**Email:** Abbas.Taheri@adelaide.edu.au)

[d] **Professor Emeritus** – Department of Civil Engineering, Indian Institute of Science, Bangalore 560012, India; [e] **Honorary Research Scientist** – Indian National Science Academy, New Delhi 110002, India (**Email:** SridharanAsuri@yahoo.com)

[†] **Correspondence:** Amin Soltani (**Email:** Amin.Soltani@adelaide.edu.au; **ORCID:** 0000-0002-0483-7487)

Publication Details: **Soltani A**, Deng A, Taheri A and Sridharan A **(2019)** Swell–Shrink–Consolidation Behavior of Rubber–Reinforced Expansive Soils. ***Geotechnical Testing Journal*** **42(3): x–x**, https://doi.org/10.1520/gtj20170313.

Abstract

This study examines the effect of two types of recycled tire rubber of fine (1.18–0.075 mm) and coarse (4.75–1.18 mm) category on the swell–shrink–consolidation behavior of a highly expansive soil mixture. Each of the two rubber choices were incorporated into the soil at four different contents (i.e. rubber to dry soil mass ratio) of 5%, 10%, 20% and 30%. The experimental program consisted of consistency limits, compaction, swell–consolidation, swell–shrink and unconfined compression tests. Improvement in the swell–shrink–consolidation capacity was in favor of higher rubber contents; however, when excessively included raised

strength concerns. The swell–shrink–consolidation properties were also rubber size–dependent, meaning that the rubber of coarser size often outperformed the finer rubber. In terms of strength, however, the two rubber types promoted similar results with marginal differences. The results of the unconfined compression tests were cross checked with the swell–shrink–consolidation properties to arrive at the optimum stabilization scenarios. A maximum rubber inclusion of 10%, preferably the rubber of coarser category, proved to satisfy the stabilization objectives (i.e. decrease in the swell–shrink–consolidation capacity as well as maintaining or improving the strength), and thus was deemed as the optimum choice. Where context changes and the strength and stiffness is not a primary concern, higher rubber inclusions up to 20% may also be considered acceptable.

Keywords: Expansive soils; Recycled tire rubbers; Rubber content and size; Swell–shrink–consolidation; Unconfined compression.

1. Introduction

Expansive soils are low–graded due to their inferior engineering characteristics (e.g. low strength, high compressibility, and a high potential for swelling and shrinkage), and thus are characterized as unsuitable construction materials for the majority of engineering applications (Dif and Bluemel 1991; Nalbantoglu 2006; Estabragh et al. 2013[a]). Where exposed to seasonal environments, such soils are prone to significant volume changes, i.e. heave and settlements, thereby causing instability concerns to the overlying structures. Such concerns have incurred a large amount of maintenance costs, and therefore demand engineering solutions to alleviate the associated socio–economic impacts on human's life (Jones and Jefferson 2012). Stabilization of expansive soils is often achieved through two approaches, i.e. chemical and mechanical techniques (Winterkorn and Pamukcu 1991). Chemical techniques mainly involve the addition of chemical binders, i.e. traditional (e.g. cement, lime and fly–ash) or non–traditional (e.g. polymers, sulfonated oils, resins and enzymes), to the soil mass, thereby amending the soil fabric into a coherent matrix of restricted heave/settlement and induced strength (e.g. Al-Rawas et al. 2005; Mirzababaei et al. 2009; Thyagaraj and Zodinsanga 2014; Onyejekwe and Ghataora 2015; Alazigha et al. 2016; Jha and Sivapullaiah 2016; Soltani et al. 2017[a]). The mechanical approach makes use of compaction with the aid of reinforcements. Conventional reinforcements include fibers of synthetic (e.g. polypropylene, steel and nylon) or natural (e.g. coir and palm) origin (e.g. Cai et al. 2006; Al-Akhras et al. 2008; Viswanadham et al. 2009[a], 2009[b]; Mirzababaei et al. 2013[a]; Olgun 2013; Estabragh et al. 2014, 2016; Phanikumar and Singla 2016; Shahbazi et al. 2017; Mirzababaei et al. 2017[a], 2017[b]; Soltani et al. 2017[b]). As the global community is shifting towards a more sustainable mindset, alternate stabilization techniques capable of replacing or minimizing the use of such conventional agents have been highly encouraged. Beneficial reuse of solid waste materials and industrial by–products may be regarded amongst the most well–received propositions in this context. The proposition not only addresses the expansive soil problem, but also offers a sound solution to minimizing the environmental impacts associated with waste materials.

Discarded tires have become an ongoing environmental crisis, particularly in industrialized countries where tire stockpiles have reached alarming volumes. In Australia, for instance, it is estimated that 48 million tires are disposed each year, signifying a relative abundance of waste tires available for beneficial reuse (Hannam 2014). Waste tires have excellent mechanical properties (e.g. durability, resiliency and frictional resistance), promoting them as an attractive material for geotechnical applications such as soil stabilization (Zornberg et al. 2004). Similar

to fiber–reinforced soils, the rubber assemblage randomly distributes in the soil regime, and where optimized in dosage and geometry, could potentially ameliorate the expansive soil with respect to moisture insensitivity (i.e. swell–shrink related volume changes), compressibility, strength and ductility (e.g. Edil and Bosscher 1994; Cetin et al. 2006; Akbulut et al. 2007; Seda et al. 2007; Özkul and Baykal 2007; Dunham-Friel and Carraro 2011; Garcia et al. 2011; Patil et al. 2011; Trouzine et al. 2012; Kalkan 2013; Srivastava et al. 2014; Signes et al. 2016; Yadav and Tiwari 2017). As such, the rubber–reinforcement mechanism is expected to be primarily a function of rubber content. However, the rubber's geometrical properties, hereafter referred to as rubber size, could also portray an equally important role in yielding an effective stabilization scheme. The latter should be somewhat similar to the aspect ratio (i.e. fiber length to diameter ratio) in fiber–reinforced soils, which has been well documented in the aforementioned fiber–reinforcement literature (e.g. Estabragh et al. 2014; Phanikumar and Singla 2016; Soltani et al. 2017[b]). With rubbers, however, this aspect has not yet been adequately addressed in the literature (e.g. Cetin et al. 2006; Srivastava et al. 2014), in what can describe the rubber–reinforcement technique as an ad hoc stabilization solution demanding further examination.

To address the uncertainties associated with selecting effective soil–rubber proportions, this study intends to evaluate the effect of two types of recycled tire rubber of fine and coarse category on the swell–shrink–consolidation behavior of a highly expansive soil mixture. A series of unconfined compression tests were also carried out, and the results where cross checked with the swell–shrink–consolidation properties to arrive the optimum stabilization scenarios.

2. Materials and Methods

2.1. Expansive Soil

Commercially available kaolinite and bentonite were used for this study. A mixture of 85% kaolinite and 15% bentonite was selected as the expansive soil for further experimental work. This mixture, hereafter simply referred to as soil, was characterized as *clay with high plasticity* (CH) in accordance with the Unified Soil Classification System (USCS). Mechanical properties of kaolinite, bentonite and the kaolinite–bentonite mixture, determined as per relevant ASTM or Australian standards, are summarized in **Table 1**. Chemical composition of the kaolinite and bentonite, as supplied by the manufacturer, are provided in **Table 2**. The free swell ratio for kaolinite, bentonite and the kaolinite–bentonite mixture was 1.19, 7.53 and 2.91, from which

these soils were graded into *lowly expansive*, *very highly expansive* and *highly expansive* with respect to the classification criteria proposed by Prakash and Sridharan (2004), respectively.

2.2. Tire Rubbers

Two types of commercially available recycled tire rubber, commonly traded as rubber crumbs and rubber buffings (a by–product of the tire retreading process), were used as the reinforcements. Hereafter, these rubber types will be referred to as rubbers A and B, respectively. The grain–size distribution curves for kaolinite, bentonite, and rubbers A and B, determined as per the ASTM D422 (2007) standard, are shown in **Figure 1**. Rubber A can be assumed similar in size to fine sand, having an average particle size ranging between 1.18 mm and 75 μm (d_{50}=0.478 mm). Rubber B, however, falls into the coarse sand category, having an average particle size ranging between 4.75 mm and 1.18 mm (d_{50}=1.582 mm). Both rubber types can be classified as poorly–graded sand or SP (in accordance with USCS) corresponding to uniformity and curvature coefficients of C_u=2.81 and C_c=1.20 for rubber A, and C_u=1.56 and C_c=1.04 for rubber B. Each of the two rubber choices were incorporated into the soil at four different contents (defined as rubber to dry soil mass ratio), i.e. R_c=5%, 10%, 20% and 30%. Physical and chemical properties, as supplied by the manufacturer, along with a photograph (to scale) of the rubber particles are provided in **Table 3** and **Figure 2**, respectively.

2.3. Sample Preparation

A series of standard Proctor compaction tests were carried out on the natural soil and various soil–rubber mixtures in accordance with the ASTM D698 (2012) standard, and the results are provided in **Figures 3a** and **3b** for rubbers A and B, respectively. The specific gravity of soil–rubber mixtures, as shown in **Figure 3**, was estimated by the theoretical relationship proposed by Trouzine et al. (2012). Rubber–reinforcement led to a noticeable decrease in both the optimum water content ω_{opt} and the maximum dry unit weight γ_{dmax} (see the compaction paths in **Figure 3**). The compaction behavior, however, was observed to be independent from the rubber size. Decrease in ω_{opt} and γ_{dmax} can be attributed to the lower specific gravity, specific surface area and water adsorption capacity of rubber particles compared to soil grains (Özkul and Baykal 2007; Kalkan 2013; Signes et al. 2016).

Samples for the swell–shrink–consolidation test (see **Section 2.4.1**) were prepared by the static compaction technique at dry of optimum condition (i.e. $\omega_0=\omega_{opt}$–5% and its corresponding dry

unit weight γ_{d0}). The required amount of water corresponding to the desired water content (see ω_0 in **Table 4**) was added to each mixture, and thoroughly mixed by hand. Extensive care was dedicated to pulverize the lumped particles, targeting homogeneity of mixtures. Mixtures were then enclosed in plastic bags and stored under room temperature conditions for 24 hours, ensuring even distribution of moisture throughout the soil mass. A special split mold, similar to that described in Soltani et al. (2017[c]), was designed and fabricated from stainless steel to accomplish static compaction. The mold consisted of three sections, i.e. the top collar, the middle oedometer ring and the bottom collar. The oedometer ring measures 50 mm in diameter and 20 mm in height, and accommodates the sample for the swell–shrink–consolidation test. The mixtures were gradually compressed in the mold in three layers to a specific compaction load, each layer having attained the target dry unit weight (see γ_{d0} in **Table 4**). The inner surface of the mold was smeared with a thin layer of silicon grease to avoid friction during compaction. The surface of the first and second compacted layers were scarified to ensure a good bond between adjacent layers of the mixture. Samples for the unconfined compression (UC) test (see **Section 2.4.2**) were prepared in a similar fashion. In this case, however, a different mold, resulting in samples measuring 50 mm in diameter and 100 mm in height, along with five compaction layers was adopted. In addition, the UC samples were prepared at optimum condition (see ω_{opt} and γ_{dmax} in **Table 4**). Mechanical properties of the prepared samples including the consistency limits and the initial placement conditions are summarized in **Table 4**. For natural soils, the optimum water content ω_{opt} can be estimated by means of the plastic limit PL through $\omega_{opt}=0.92PL$ (Gurtug and Sridharan 2002, 2004; Sridharan and Nagaraj 2005). Interestingly, the same holds true for various soil–rubber mixtures (see **Table 4**).

2.4. Test Procedure

2.4.1. Swell–Shrink–Consolidation Test

Samples were subjected to a series of swell–shrink–consolidation tests. A typical illustration of the test scheme is provided in **Figure 4**. The swell–consolidation phase, carried out in accordance with the ASTM D4546 (2014) standard, includes two stages, i.e. swell and consolidation. In the first stage, the desired sample is allowed to freely swell under a low nominal overburden stress of σ'_0=1 kPa. The incurred swelling strain was recorded during various time intervals to a point in which swell–time equilibrium, a state corresponding to the sample's swelling potential (defined as the ultimate swelling strain), could be achieved (see path O→A in **Figure 4a**). During consolidation, the swollen sample, now at state A, is gradually

loaded to counteract the built–up swelling strain. The stress required to retain the sample's initial placement or void ratio is taken as the swelling pressure (Sridharan et al. 1986). Upon completion of the loading scheme, the sample is gradually unloaded back to σ'_0=1 kPa (see path A→B_1 for loading, and path B_1→C for unloading in **Figure 4b**). Test results are presented in the form of swelling strain–time (for the swell stage) and void ratio–effective stress (for the consolidation stage) curves plotted over a semi–log space (see **Figures 4a** and **4b**, respectively).

The swell–shrink phase also consists of two stages, i.e. swell and shrink. The swell component is essentially similar to that described in the swell–consolidation test. During the shrink stage, the swollen sample, now at state A, is allowed to desiccate under a constant temperature of 40 ^{o}C. The volumetric shrinkage strain along with the corresponding water content were directly measured during various time intervals to a point in which shrinkage ceases (see path A→B_2 in **Figure 4c**). The volumetric shrinkage strain was measured by the volume displacement technique outlined in the ASTM D427 (2004) standard, which has also been commonly adopted in the literature (e.g. Sibley and Williams 1989; Hanafy et al. 1991; Subba Rao et al. 2000; Tripathy et al. 2002; Tripathy and Subba Rao 2009). For the shrink stage, test results are presented in the form of void ratio–water content curves plotted over an arithmetic space (see **Figure 4c**).

2.4.2. Unconfined Compression Test

The unconfined compression test was carried out in accordance with the ASTM D2166 (2016) standard. The samples were compressed by a constant displacement rate of 1 %/min, as commonly adopted in the literature (e.g. Ang and Loehr 2003; Fatahi et al. 2012; Signes et al. 2016). To ensure sufficient accuracy, triplicate samples were tested for each scenario. Axial stress and its corresponding axial strain were recorded during various loading stages to a point in which maximum axial stress required for sample failure, denoted as q_u, and its corresponding axial strain, denoted as ε_u, could be achieved. The area under the stress–strain curve up to q_u and ε_u — a measure of the material's toughness defined as strain energy at peak E_p (Maher and Ho 1994; Mirzababaei et al. 2013[b]) — was also obtained for the tested samples.

3. Results and Discussion

3.1. Effect of Rubbers on the Swelling Potential

Swelling strain–time curves, represented by the two–parameter rectangular hyperbola function (e.g. Dakshanamurthy 1978; Sivapullaiah et al. 1996; Sridharan and Gurtug 2004), for the natural soil and various soil–rubber composites are provided in **Figures 5a** and **5b** for rubbers A and B, respectively. As a result of rubber–reinforcement, the swelling strain–time locus experienced a major downward shift over the ε_{sw}:log$t$ space (ε_{sw}=swelling strain; and t=time), indicating a significant reduction in the magnitude of exhibited swelling strain, and thus swelling potential (defined as the ultimate swelling strain) compared to the natural soil. At t=24 hours, for instance, the natural soil displayed a swelling strain of $\varepsilon_{sw}(t)$=15.23%, while the inclusion of 5%, 10%, 20% and 30% rubber A resulted in $\varepsilon_{sw}(t)$=14.99%, 11.82%, 9.01% and 7.67%, respectively (see **Figure 5a**). Similar inclusions of rubber B, however, exhibited a slightly more pronounced decreasing trend where the above given values dropped to $\varepsilon_{sw}(t)$=13.67%, 11.44%, 8.01% and 7.21%, respectively (see **Figure 5b**). The natural soil and soil–rubber A mixtures corresponding to R_c=5%, 10%, 20% and 30% resulted in swelling potential values of S_p=18.35%, 16.02%, 13.01%, 11.17% and 9.56%, respectively. For similar inclusions of rubber B, these values further decreased to S_p=14.74%, 12.18%, 9.02% and 8.11%, respectively.

A typical swell path (see path O→A in **Figure 4a**), plotted over a semi–log space, develops into an *S*–shaped curve, and thus can be divided into three regions, i.e. the initial, primary and secondary swelling, which are defined as phases during which swelling takes place (Dakshanamurthy 1978; Sivapullaiah et al. 1996; Sridharan and Gurtug 2004; Rao et al. 2006; Soltani et al. 2017[c]). The initial swelling phase, also recognized as inter–void or inter–crystalline swelling, rapidly evolves at macro–structural level, and is accompanied by small volume changes (i.e. $\varepsilon_{isw} \leq 0.1S_p$). The primary swelling phase constitutes for up to 80% of the total volume increase (i.e. $\varepsilon_{psw} \approx 0.8S_p$), and is graphically bounded by the initial and primary swelling time margins (see **Figure 4a**). The secondary swelling phase occurs as a result of double–layer repulsion, which results in small time–dependent volume changes. In comparison to initial swelling, both the primary and secondary swelling phases evolve at micro–structural level where the swelling of active minerals takes place. Critical variables obtained from the *S*–shaped swell curve are useful concepts capable of describing the time–dependency nature of the swelling phenomenon under field conditions (Sridharan and Gurtug 2004). These variables,

defined by a conventional graphical construction as depicted in **Figure 4a**, can be categorized as:

- Completion time of the initial and primary swelling phases, i.e. t_{isw} and t_{psw}.
- Initial, primary and secondary swelling strains, i.e. ε_{isw}, ε_{psw} and ε_{ssw}, where $S_p=\varepsilon_{isw}+\varepsilon_{psw}+\varepsilon_{ssw}$.
- Primary and secondary swelling rates, i.e. C_{psw} and C_{ssw}, which are defined as:

$$C_{psw}=\frac{\Delta\varepsilon_{sw}}{\Delta\log t}\Bigg]_{t_{isw}}^{t_{psw}}=\frac{\varepsilon_{psw}}{\log\left(\frac{t_{psw}}{t_{isw}}\right)} \tag{1}$$

$$C_{ssw}=\frac{\Delta\varepsilon_{sw}}{\Delta\log t}\Bigg]_{t_{psw}}^{t_{ssw}}=\frac{\varepsilon_{ssw}}{\log\left(\frac{t_{ssw}}{t_{psw}}\right)} \tag{2}$$

where t_{ssw}=completion time of the secondary swelling phase (≈240 hours).

Figures 6a and **6b** illustrate the variations of C_{psw} and C_{ssw} against rubber content for the tested samples, respectively. The rubber inclusions led to a noticeable reduction in C_{psw} and C_{ssw}, indicating a capacity to counteract the heave in both magnitude and time. The greater the rubber content the greater the decrease in C_{psw}, following a monotonic trend. Rubber contents greater than 5%, however, did not further deviate C_{ssw}. Rubber B consistently outperformed rubber A by exhibiting lower swelling rates for similar rubber inclusions. The natural soil resulted in $C_{psw}=8.38\times10^{-2}$ and $C_{ssw}=2.56\times10^{-2}$. As a typical case, these values, respectively, dropped to 5.89×10^{-2} and 1.54×10^{-2} for rubber A, and 5.58×10^{-2} and 1.19×10^{-2} for rubber B where R_c=10%.

3.2. Effect of Rubbers on the Consolidation Behavior

Void ratio–effective stress consolidation curves for the natural soil and various soil–rubber composites are provided in **Figures 7a** and **7b** for rubbers A and B, respectively. A typical consolidation curve with respect to the loading stage (see path A→B_1 in **Figure 4b**), plotted over a semi–log space, develops into a two segment–curvilinear relationship, and thus can be divided into two regions, i.e. the elastic and elasto–plastic compression, which are defined as phases during which consolidation takes place (Sridharan et al. 1991). The two regions are

separated by the yield stress, which is commonly interpreted by means of conventional graphical constructions implemented to the e–logσ' or log$e$–logσ' curve (e=void ratio; and σ'=effective stress). Recently, the authors have proposed a subjective–free framework for determination of the yield stress with respect to four common graphical constructions, i.e. the maximum curvature method (Casagrande 1936), the Silva method (Pacheco Silva 1970), the RCL–VCL intercept method (RCL=recompression line; and VCL=virgin compression line), and the log–log method (Jose et al. 1989; Sridharan et al. 1991). Adopting the proposed framework in Soltani et al. (2017[d]), the average of the four graphical constructions was calculated for each sample, and the results are provided in the form of yield stress paths in **Figure 7**. Rubber–reinforcement led to a slight increase in the yield stress. Natural soil exhibited a yield stress of σ'_y=17.73 kPa. Maximum increase in σ'_y was observed in the case of 30% rubber inclusion, which resulted in σ'_y=23.42 kPa and 22.10 kPa for rubbers A and B, respectively.

Figures 8a and **8b** illustrate the variations of the compression index C_c (=slope of the VCL in **Figure 4b**) and the swell index C_s (=slope of the unloading path 'B$_1$→C' in **Figure 4b**) against rubber content for the tested samples, respectively. The rubber inclusions led to a noticeable reduction in C_c and C_s, indicating a capacity of counteracting material collapse when stressed. The greater the rubber content the lower the C_c and C_s values, following a monotonic trend. Rubber B often outperformed rubber A in terms of lower C_c values. Regarding C_s, however, the performance of both rubber types seemed to be on par with each other. The natural soil resulted in C_c=0.249 and C_s=0.136. As a typical case, these values, respectively, dropped to 0.191 and 0.087 for rubber A, and 0.187 and 0.078 for rubber B where R_c=20%.

Rubber–reinforcement altered the void ratio–effective stress locus, resulting in a major downward shift over the e:logσ' space. As a result, major variations were observed in the swelling pressure (see the swelling pressure paths in **Figure 7**). **Figure 9** illustrates the variations of swelling pressure and swelling potential against rubber content for the tested samples. The variations of swelling pressure P_s followed a trend quite similar to that of swelling potential S_p, indicating that the greater the rubber content the greater the decrease in S_p and P_s. For P_s, however, R_c=30% promoted similar results to R_c=20% with marginal differences, indicating a maximum rubber inclusion of 20% being sufficient to counteract the swelling properties. Similar to S_p, soil–rubber B mixtures consistently outperformed similar samples reinforced with rubber A. The natural soil and soil–rubber mixtures corresponding to R_c=5%, 10%, 20% and 30% resulted in P_s=120.3 kPa, 99.6 kPa, 70.0 kPa, 54.1 kPa, and 51.4 kPa,

respectively. With rubber B, these values dropped to P_s=73.0 kPa, 51.0 kPa, 32.2 kPa and 33.6 kPa, respectively.

The secondary consolidation characteristics were studied under an effective stress of σ'=50 kPa, and the results are provided in **Figure 10**. The completion time of the primary consolidation stage t_{pc} decreased due to the inclusion of rubber A (see **Figure 10a**). This effect, however, was less apparent for samples reinforced with rubber B, which essentially did not deviate t_{pc} (see **Figure 10b**). The secondary consolidation rate C_{sc} can be defined as:

$$C_{sc} = \frac{\Delta \varepsilon_c}{\Delta \log t}\Bigg]_{t_{pc}}^{t_{sc}} = \frac{\varepsilon_{sc}}{\log\left(\frac{t_{sc}}{t_{pc}}\right)} \tag{3}$$

where $\varepsilon_c(t)$=compression strain with respect to elapsed time t; ε_{sc}=secondary consolidation strain; and t_{sc}=completion time of the secondary consolidation stage (=24 hours).

As a result of rubber–reinforcement, the secondary consolidation rate exhibited a noticeable decreasing trend, indicating a capacity to counteract the settlement in both magnitude and time. The natural soil resulted in C_{sc}=7.28×10^{-3}. Where reinforced with 5%, 10%, 20% and 30% rubber A, C_{sc} dropped to 6.05×10^{-3}, 5.57×10^{-3}, 5.34×10^{-3} and 5.02×10^{-3}, respectively. Similar inclusions of rubber B, however, promoted slightly greater values, while still maintaining a noticeable advantage over the natural soil. In this case, R_c=5%, 10%, 20% and 30% resulted in C_{sc}=6.74×10^{-3}, 6.68×10^{-3}, 5.88×10^{-3} and 4.94×10^{-3}, respectively. It is noteworthy to cross check the resulted trends for C_{sc} with C_{ssw}, which are expected to be somewhat consistent and comparable (Sridharan and Gurtug 2004; Phanikumar and Singla 2016).

3.3. Effect of Rubbers on the Shrinkage Potential

Void ratio–water content shrinkage curves, represented by the four–parameter logistic function (e.g. McGarry and Malafant 1987; Peng and Horn 2005; Thyagaraj et al. 2017), along with corresponding 100% saturation lines, for the natural soil and various soil–rubber composites are provided in **Figures 11a** and **11b** for rubbers A and B, respectively. The four–parameter logistic function can be given as:

$$e(\omega) = e_{rsh} + \frac{e_{ssw} - e_{rsh}}{1 + \left(\frac{\omega}{\alpha}\right)^{-\beta}} \tag{4}$$

where e_{ssw}=void ratio at the swollen state A (i.e. the end of secondary swelling, as shown in **Figure 4c**); e_{rsh}=void ratio at the fully desiccated state B_2 (see **Figure 4c**); and α and β=fitting parameters (α and $\beta > 0$).

Similar to the swell path, a typical shrink path (see path O→B_2 in **Figure 4c**) develops into an *S*–shaped curve, and thus can be divided into three regions, i.e. the structural, primary and residual shrinkage, which are defined as phases during which shrinkage takes place (Haines 1923; Tripathy et al. 2002; Cornelis et al. 2006; Estabragh et al. 2013[b], 2015). In the structural shrinkage phase, the decrease in volume of the soil is less than the volume of water lost from the stable void spaces. This portion of the shrinkage curve constitutes for small volume changes, and is graphically represented by a mild–sloped curvilinear relationship. During primary shrinkage, also commonly referred to as normal shrinkage, the decrease in volume of the soil is essentially equal to the volume of lost water, thereby preventing the entrance of air into the soil pores. This portion of the shrinkage curve is represented by a steep–sloped linear relationship, which is theoretically parallel to the *Sr*=100% saturation line. The primary shrinkage phase extends up to the shrinkage limit, which marks a transitional state where the rate of volume change rapidly decreases, i.e. $\Delta e/\Delta\omega \rightarrow 0$. The majority of volume decrease takes place during the primary shrinkage phase. Completion of the primary shrinkage phase is further accompanied by residual shrinkage, where the entrance of air is allowed into the soil pores, thereby resulting in air–filled porosity. As a consequence of particles coming in contact, the decrease in volume of the soil becomes less than the volume of lost water. The magnitude of structural, primary and residual shrinkage strains, i.e. ε_{ssh}, ε_{psh} and ε_{rsh}, can be obtained by the following relationships (Mishra et al. 2008; Thyagaraj et al. 2017):

$$\varepsilon_{ssh} = \frac{\Delta e}{1 + e_{ssw}} \Bigg|_{e_{ssh}}^{e_{ssw}} = \frac{e_{ssw} - e_{ssh}}{1 + e_{ssw}} \tag{5}$$

$$\varepsilon_{psh} = \frac{\Delta e}{1 + e_{ssh}} \Bigg|_{e_{psh}}^{e_{ssh}} = \frac{e_{ssh} - e_{psh}}{1 + e_{ssh}} \tag{6}$$

$$\varepsilon_{rsh} = \frac{\Delta e}{1+e_{psh}}\Bigg]_{e_{rsh}}^{e_{psh}} = \frac{e_{psh}-e_{rsh}}{1+e_{psh}} \quad (7)$$

where as outlined in **Figure 4c**, e_{ssw}=void ratio at the swollen state A (i.e. the end of secondary swelling); e_{ssh}=void ratio at the end of structural shrinkage; e_{psh}=void ratio at the end of primary shrinkage (or at the shrinkage limit); and e_{rsh}=void ratio at the fully desiccated state B_2.

The total shrinkage strain, denoted as the shrinkage potential, can be defined as $SH_p=\varepsilon_{ssh}+\varepsilon_{psh}+\varepsilon_{rsh}$. The shrinkage strains and the shrinkage limit for the tested samples are presented in **Table 5**. The shrinkage strains demonstrated a rubber content–dependency, meaning that the greater the rubber content the lower the shrinkage strains. The effect of rubber size, however, was observed to be marginal for the majority of cases. The shrinkage potential demonstrated a trend similar to that observed for the swelling potential. The natural soil displayed a shrinkage potential of SH_p=28.60%. Soil–rubber A mixtures corresponding to R_c=5%, 10%, 20% and 30% resulted in SH_p=23.44%, 21.30%, 18.27% and 15.30%, respectively. Similar inclusions of rubber B promoted slightly lower values, and were measured as SH_p=24.61%, 20.44%, 16.01% and 14.04%, respectively. As a result of rubber–reinforcement, the shrinkage limit experienced a minor increase; however, the resulted variations were observed to be less dependent on rubber content and rubber size. The shrinkage limit is primarily a result of the "packing phenomenon" (i.e. optimal packing of soil particles during drying), which in turn is governed by the grain–size distribution of the soil. As the soil's gradation becomes more and more uniform/poor (reduced packing capacity), the shrinkage limit tends to increase (Sridharan and Prakash 1998). The rubber particles used in this study are both classified as poorly–graded sand (see **Figure 1**). As such, the addition of the poorly–graded rubber to the well–graded soil offsets the well–distributed gradation of the host soil, and thus gives rise to higher shrinkage limits. Consequently, this mechanism is expected to be in line with rubber content. The greater the rubber content the more uniform/poor the grain–size distribution, and thus the higher the shrinkage limit.

3.4. Effect of Rubbers on the Strength Properties

Stress–strain curves, obtained from the unconfined compression tests, for the natural soil and various soil–rubber composites are provided in **Figures 12a** and **12b** for rubbers A and B, respectively. The natural soil displayed a peak strength of q_u=113 kPa, while the inclusion of

5% rubbers A and B resulted in q_u=129 kPa and 142 kPa, respectively. With R_c=10%, q_u dropped to 128 kPa (for rubber A) and 127 kPa (for rubber B), which still maintains a noticeable advantage over the natural soil. Higher rubber inclusions, i.e. 20% and 30%, however, gave rise to lower q_u values compared to that observed for the natural soil (i.e. q_u=102kPa and 98 kPa for 20% rubbers A and B; and q_u=72 kPa and 88 kPa for 30% rubbers A and B). It is noteworthy to cross check q_u with S_p, P_s and SH_p, which are in favor of a higher rubber content. This discrepancy implies that even though the rubbers are consistently effective at weaving the soil into a coherent matrix of restricted heave and settlement, when excessively included raise strength concerns.

Figure 13 illustrates the variations of strain energy at peak E_p along with corresponding q_u values against rubber content for the tested samples. The variations of E_p followed a trend quite similar to that observed for q_u. A noticeable improvement in the toughness can be achieved for rubber inclusions equal to or less than 10%, while the higher rubber inclusions of 20% and 30% gave rise to less toughness. Although in terms of q_u, the performance of both rubber types seemed to be on par with each other, soil–rubber B mixtures consistently (an exception was R_c=5%) promoted a higher toughness (i.e. higher E_p) compared to similar samples reinforced with rubber A. As optimum cases, E_p increased from 6.91 kJ/m^3 for the natural soil to 9.04 kJ/m^3 and 10.84 kJ/m^3 for the samples reinforced with 5% rubber A and 10% rubber B, respectively. The elastic stiffness modulus E_{50}, defined as the secant modulus at 50% of the peak strength (Radovic et al. 2004; Iyengar et al. 2013), was also measured for the tested samples. In general, the greater the rubber content the lower the E_{50} value, following a monotonic decreasing trend. Expect for 5% rubber B, all samples exhibited a lower E_{50} compared to the natural soil. The natural soil resulted in E_{50}=3.15 MPa, while the inclusion of 5%, 10%, 20% and 30% rubber A resulted in E_{50}=2.47 MPa, 2.56 MPa, 1.69 MPa and 1.15 MPa, respectively. Similar inclusions of rubber B did not significantly deviate the aforementioned values (an exception was R_c=5%), and resulted in E_{50}=3.27 MPa, 2.19 MPa, 1.45 MPa and 1.59 MPa, respectively.

3.5. Amending Mechanisms

Similar to fiber–reinforced soils, the rubber inclusions are able to amend the soil fabric through improvements achieved in three aspects, i.e. increase in non–expansive fraction or non–wetting attribute (Viswanadham et al. 2009[a]; Patil et al. 2011; Trouzine et al. 2012; Estabragh et al. 2014; Soltani et al. 2017[b]), interlocking of rubber particles and soil grains (Tang et al. 2007,

2010; Kalkan 2013; Phanikumar and Singla 2016; Soltani et al. 2017[b]), and frictional resistive forces generated as a result of soil–rubber contact (Cai et al. 2006; Al-Akhras et al. 2008; Viswanadham et al. 2009[b]; Patil et al. 2011; Trouzine et al. 2012; Phanikumar and Singla 2016). The randomly distributed rubber particles resemble a spatial three–dimensional network in favor of weaving or interlocking the soil grains into a coherent matrix of restricted heave and settlement. The greater the number of included rubber particles, i.e. increase in rubber content, the more effective the interlocking effect. The frictional resistive forces grow as a consequence of rubber particles experiencing tensile/compressive stress in the presence of strong swelling/compression forces. Increase in rubber content leads to an increase in the total surface area, and thus a greater interfacial contact between rubber particles and soil grains. This in turn enhances the frictional effect between rubber particles, thereby mitigating the swell–shrink–consolidation capacity.

The swell–shrink–consolidation dependence on rubber size (or shape) is on par with the aspect ratio (i.e. fiber length to diameter ratio) in fiber–reinforced soils, and thus can be ascribed to the improvement mechanisms ‘interlocking’ and ‘frictional resistive forces’. Increase in rubber size increases the soil–rubber contacts, which in turn generates a greater net frictional resistance between rubbers coupled with an enhanced soil–rubber interlocking effect. This improvement mechanism is also in line with rubber shape. As opposed to the granular form of rubber A, the particles of rubber B are relatively more fiber–shaped (see **Figure 2**); hence, they are more resilient to withstand (or translate) tensile/compressive stress along their axis, which in turn restricts the movement of soil particles interlocked to the rubber.

The amending mechanisms governing the soil–rubber shear strength, i.e. mechanical interlocking and frictional resistance, only hold provided that the rubber particles are well distributed in the soil regime and do not cluster (or adhere to each other) during sample preparation and/or external loading. At high rubber contents and potentially for the rubber of coarser category, the behavior of the composite at some points could be governed by a dominant rubber–to–rubber interaction, which though offers a notable improvement to the composite’s ductility, offsets the desired soil–to–rubber interaction capable of improving the composite’s shear strength (see R_c=20% and 30% in **Figure 12**).

4. Optimum Rubber Content and Cost Analysis

The primary objective of any introduced stabilization scheme dealing with expansive soils should complement a decrease in the swell–shrink–consolidation capacity, while either maintaining or improving the strength–related properties (Soltani 2017). Although both rubber types are consistently effective at weaving the soil into a coherent matrix of restricted heave and settlement (i.e. improvement in the swell–shrink–consolidation capacity is in favor of higher rubber contents), when excessively included raise strength concerns. Based on the results presented in **Sections 3.1** to **3.4**, a maximum rubber inclusion of 10% seems to satisfy both objectives, and thus can be deemed as the optimum choice. Where context changes and the strength and stiffness is not a primary concern, higher rubber inclusions up to 20% may also be considered acceptable. The swell–shrink–consolidation properties were rubber size–dependent, meaning that the rubber of coarser size often outperformed the finer rubber. In terms of strength, however, the two rubber types promoted similar results with marginal differences. Therefore, the choice of rubber size would be dependent on design requirements/project objectives, rubber availability and costs.

Table 6 summarizes a comparative cost analysis performed for the reinforcement of an assumed mass of 1000 kg of soil using recycled tire rubbers and conventional poly– (ester, ethylene or propylene) fibers. The unit price for both rubber types and poly fibers were taken in accordance with common prices found in South Australian markets, which are approximately 0.5 AU$/kg and 14.3 AU$/kg, respectively. Other costs such as transportation, labor and compaction have not been included as they are highly case– and region–dependent. Significant cost reduction can be achieved where rubbers are used as a replacement for conventional fibers. For instance, R_c=10% results in a total cost of 50 AU$, while the use of poly fibers at their so–called optimum contents, i.e. f_c=0.8% and 1.5%, results in 114.4 AU$ and 214.5 AU$, respectively. Unlike fibers, the rubber–reinforcement technique requires a large quantity of rubber material to ameliorate the swell–shrink–consolidation capacity. However, in terms of total cost, it still maintains a significant advantage over conventional fibers. More importantly, beneficial reuse of recycled tires provides a sound environmental alternative to the safe disposal concern associated with such waste materials. The results of the cost analysis are in agreement with Yadav and Tiwari (2017), whom carried out a similar comparative analysis with respect to the Indian market.

5. Conclusions

The following conclusions can be drawn from this study:

- As a result of rubber–reinforcement, the swelling strain–time locus experienced a major downward shift over the semi–log space, signifying a capacity to counteract the heave in both magnitude and time. Improvement in the rate and potential of swelling was dependent on both the rubber content and the rubber size, with the former taking on a more pronounced role. A similar dependency was also observed for the shrinkage potential. In this case, however, the effect of rubber size was observed to be marginal for the majority of cases.

- Rubber–reinforcement altered the void ratio–effective stress consolidation locus, resulting in a significant reduction in the swelling pressure. The variations of swelling pressure suggested a trend similar to that of swelling potential. In addition, the rubber inclusions led to a noticeable reduction in the compression and swell indices, indicating a capacity to counteract material collapse when stressed. The compression index was observed to be rubber size–dependent; however, for the swell index, the performance of both rubber types seemed to be on par with each other.

- The secondary consolidation rate also exhibited a rubber content/size–dependency, indicating a capacity to counteract the settlement in both magnitude and time. The greater the rubber content the lower the secondary consolidation rate, with the finer rubber maintaining a slight advantage over the coarser rubber. The resulted trends for the secondary swelling and secondary consolidation rates were observed to be consistent and comparable.

- The results of the unconfined compression tests were cross checked with the swell–shrink–consolidation properties to arrive the optimum stabilization scenarios. A maximum rubber inclusion of 10%, preferably the rubber of coarser category, proved to satisfy the stabilization objectives, and thus was deemed as the optimum choice. Where context changes and the strength and stiffness is not a primary concern, higher rubber inclusions up to 20% could also be considered acceptable.

- The cost efficiency of the rubber–reinforcement technique was compared to conventional poly– (ester, ethylene or propylene) fibers. Significant cost reduction can be achieved where rubbers are used as a replacement for conventional fibers. More importantly, beneficial

reuse of recycled tires provides a sound environmental alternative to the safe disposal concern associated with such waste materials.

Acknowledgements

This research was funded by the Australian Research Council (ARC) via project No. **DP140103004**, and their support is gratefully acknowledged.

References

Akbulut, S., Arasan, S., and Kalkan, E., 2007, "Modification of Clayey Soils Using Scrap Tire Rubber and Synthetic Fibers," *Appl. Clay Sci.*, Vol. 38, No. 1–2, pp. 23–32. doi:10.1016/J.CLAY.2007.02.001.

Al-Akhras, N. M., Attom, M. F., Al-Akhras, K. M., and Malkawi, A. I. H., 2008, "Influence of Fibers on Swelling Properties of Clayey Soil," *Geosynth. Int.*, Vol. 15, No. 4, pp. 304–309. doi:10.1680/GEIN.2008.15.4.304.

Alazigha, D. P., Indraratna, B., Vinod, J. S., and Ezeajugh, L. E., 2016, "The Swelling Behaviour of Lignosulfonate–Treated Expansive Soil," *Proc. ICE Gr. Improv.*, Vol. 169, No. 3, pp. 182–193. doi:10.1680/JGRIM.15.00002.

Al-Rawas, A. A., Hago, A. W., and Al-Sarmi, H., 2005, "Effect of Lime, Cement and Sarooj (Artificial Pozzolan) on the Swelling Potential of an Expansive Soil from Oman," *Build. Environ.*, Vol. 40, No. 5, pp. 681–687. doi:10.1016/J.BUILDENV.2004.08.028.

Ang, E. C., and Loehr, J. E., 2003, "Specimen Size Effects for Fiber–Reinforced Silty Clay in Unconfined Compression," *Geotech. Test. J.*, Vol. 26, No. 2, pp. 191–200. doi:10.1520/GTJ11320J.

AS 1289.3.2.1:09, 2009, *Methods of Testing Soils for Engineering Purposes: Soil Classification Tests–Determination of the Plastic Limit of a Soil*, Standards Australia, Sydney, NSW.

AS 1289.3.3.1:09, 2009, *Methods of Testing Soils for Engineering Purposes: Soil Classification Tests–Calculation of the Plasticity Index of a Soil*, Standards Australia, Sydney, NSW.

AS 1289.3.9.1:15, 2015, *Methods of Testing Soils for Engineering Purposes: Soil Classification Tests–Determination of the Cone Liquid Limit of a Soil*, Standards Australia, Sydney, NSW.

ASTM D2166/D2166M-16, 2016, *Standard Test Method for Unconfined Compressive Strength of Cohesive Soil*, ASTM International, West Conshohocken, PA. doi:10.1520/D2166_D2166M-16.

ASTM D2487-11, 2011, *Standard Practice for Classification of Soils for Engineering Purposes (Unified Soil Classification System)*, ASTM International, West Conshohocken, PA. doi:10.1520/D2487-11.

ASTM D422-63(2007)e2, 2007, *Standard Test Method for Particle–Size Analysis of Soils*, ASTM International, West Conshohocken, PA. doi:10.1520/D0422-63R07E02.

ASTM D427-04, 2004, *Test Method for Shrinkage Factors of Soils by the Mercury Method*, ASTM International, West Conshohocken, PA. doi:10.1520/D0427-04.

ASTM D4546-14, 2014, *Standard Test Methods for One–Dimensional Swell or Collapse of Soils*, ASTM International, West Conshohocken, PA. doi:10.1520/D4546.

ASTM D698-12e2, 2012, *Standard Test Methods for Laboratory Compaction Characteristics of Soil Using Standard Effort (12,400 ft–lbf/ft^3 (600 kN–m/m^3))*, ASTM International, West Conshohocken, PA. doi:10.1520/D0698-12E02.

ASTM D854-14, 2014, *Standard Test Methods for Specific Gravity of Soil Solids by Water Pycnometer*, ASTM International, West Conshohocken, PA. doi:10.1520/D0854-14.

Cai, Y., Shi, B., Ng, C. W. W., and Tang, C. S., 2006, "Effect of Polypropylene Fibre and Lime Admixture on Engineering Properties of Clayey Soil," *Eng. Geol.*, Vol. 87, No. 3–4, pp. 230–240. doi:10.1016/J.ENGGEO.2006.07.007.

Casagrande, A., 1936, "The Determination of Pre–Consolidation Load and Its Practical Significance," In: Casagrande, A., Rutledge, P. C., and Watson, J. D. (Eds.), *First International Conference on Soil Mechanics and Foundation Engineering*, ASCE, Cambridge, MA, pp. 60–64.

Cetin, H., Fener, M., and Gunaydin, O., 2006, "Geotechnical Properties of Tire–Cohesive Clayey Soil Mixtures as a Fill Material," *Eng. Geol.*, Vol. 88, No. 1–2, pp. 110–120. doi:10.1016/J.ENGGEO.2006.09.002.

Cornelis, W. M., Corluy, J., Medina, H., Díaz, J., Hartmann, R., van Meirvenne, M., and Ruiz, M. E., 2006, "Measuring and Modelling the Soil Shrinkage Characteristic Curve," *Geoderma*, Vol. 137, No. 1–2, pp. 179–191. doi:10.1016/J.GEODERMA.2006.08.022.

Dakshanamurthy, V., 1978, "A New Method to Predict Swelling Using Hyperbola Equation," *Geotech. Eng. J. SEAGS AGSSEA*, Vol. 8, No. 1, pp. 29–38.

Dif, A., and Bluemel, W., 1991, "Expansive Soils under Cyclic Drying and Wetting," *Geotech. Test. J.*, Vol. 14, No. 1, pp. 96–102. doi:10.1520/GTJ10196J.

Dunham-Friel, J., and Carraro, J. A. H., 2011, "Shear Strength and Stiffness of Expansive Soil and Rubber (ESR) Mixtures in Undrained Axisymmetric Compression," In: Han, J., and Alzamora, D. E. (Eds.), *Geo–Frontiers 2011: Advances in Geotechnical Engineering (GSP 211)*, ASCE, Dallas, TX, pp. 1111–1120. doi:10.1061/41165(397)114.

Edil, T., and Bosscher, P., 1994, "Engineering Properties of Tire Chips and Soil Mixtures," *Geotech. Test. J.*, Vol. 17, No. 4, pp. 453–464. doi:10.1520/GTJ10306J.

Estabragh, A. R., Moghadas, M., and Javadi, A. A., 2013[b], "Effect of Different Types of Wetting Fluids on the Behaviour of Expansive Soil during Wetting and Drying," *Soils Found.*, Vol. 53, No. 5, pp. 617–627. doi:10.1016/J.SANDF.2013.08.001.

Estabragh, A. R., Parsaei, B., and Javadi, A. A., 2015, "Laboratory Investigation of the Effect of Cyclic Wetting and Drying on the Behaviour of an Expansive Soil," *Soils Found.*, Vol. 55, No. 2, pp. 304–314. doi:10.1016/J.SANDF.2015.02.007.

Estabragh, A. R., Pereshkafti, M. R. S., Parsaei, B., and Javadi, A. A., 2013[a], "Stabilised Expansive Soil Behaviour during Wetting and Drying," *Int. J. Pavement Eng.*, Vol. 14, No. 4, pp. 418–427. doi:10.1080/10298436.2012.746688.

Estabragh, A. R., Rafatjo, H., and Javadi, A. A., 2014, "Treatment of an Expansive Soil by Mechanical and Chemical Techniques," *Geosynth. Int.*, Vol. 21, No. 3, pp. 233–243. doi:10.1680/GEIN.14.00011.

Estabragh, A. R., Soltani, A., and Javadi, A. A., 2016, "Models for Predicting the Seepage Velocity and Seepage Force in a Fiber Reinforced Silty Soil," *Comput. Geotech.*, Vol. 75, pp. 174–181. doi:10.1016/J.COMPGEO.2016.02.002.

Fatahi, B., Khabbaz, H., and Fatahi, B., 2012, "Mechanical Characteristics of Soft Clay Treated with Fibre and Cement," *Geosynth. Int.*, Vol. 19, No. 3, pp. 252–262. doi:10.1680/GEIN.12.00012.

Garcia, M., Pando, M. A., and Tempest, B., 2011, "Tire Derived Aggregates as a Sustainable Recycled Material for Retaining Wall Backfills," In: W. K. O. Chong & C. Hermreck (Eds.), *ICSDC 2011: Integrating Sustainability Practices in the Construction Industry*, ASCE, Kansas City, MO, pp. 542–552. doi:10.1061/41204(426)67.

Gurtug, Y., and Sridharan, A., 2002, "Prediction of Compaction Characteristics of Fine–Grained Soils," *Géotechnique*, Vol. 52, No. 10, pp. 761–763. doi:10.1680/GEOT.2002.52.10.761.

Gurtug, Y., and Sridharan, A., 2004, "Compaction Behaviour and Prediction of its Characteristics of Fine–Grained Soils with Particular Reference to Compaction Energy," *Soils Found.*, Vol. 44, No. 5, pp. 27–36. doi:10.3208/SANDF.44.5_27.

Haines, W. B., 1923, "The Volume–Changes Associated with Variations of Water Content in Soil," *J. Agric. Sci.*, Vol. 13, No. 3, pp. 296–310. doi:10.1017/S0021859600003580.

Hanafy, E. A. D. E., 1991, "Swelling/Shrinkage Characteristic Curve of Desiccated Expansive Clays," *Geotech. Test. J.*, Vol. 14, No. 2, pp. 206–211. doi:10.1520/GTJ10562J.

Hannam, P., 2014, "Tyre Industry Divided over How to Handle Toxic Waste," *The Sydney Morning Herald*, Sydney, NSW, http://www.smh.com.au/environment/tyre-industry-divided-over-how-to-handle-toxic-waste-20140120-314ic.html. (accessed 8/10/2017)

Iyengar, S. R., Masad, E., Rodriguez, A. K., Bazzi, H. S., Little, D., and Hanley, H. J. M., 2013, "Pavement Subgrade Stabilization Using Polymers: Characterization and Performance," *J. Mater. Civ. Eng.*, Vol. 25, No. 4, pp. 472–483. doi:10.1061/(ASCE)MT.1943-5533.0000612.

Jha, A. K., and Sivapullaiah, P. V., 2016, "Gypsum–Induced Volume Change Behavior of Stabilized Expansive Soil With Fly Ash–Lime," *Geotech. Test. J.*, Vol. 39, No. 3, pp. 391–406. doi:10.1520/GTJ20150017.

Jones, L. D., and Jefferson, I., 2012, "Expansive Soils," In: Burland, J., Chapman, T., Brown, M., and Skinner, H. (Eds.), *ICE Manual of Geotechnical Engineering: Volume I*, ICE Publishing, London, pp. 413–441. doi:10.1680/MOGE.57074.0413.

Jose, B. T., Sridharan, A., and Abraham, B. M., 1989, "Log–Log Method for Determination of Preconsolidation Pressure," *Geotech. Test. J.*, Vol. 12, No. 3, pp. 230–237. doi:10.1520/GTJ10974J.

Kalkan, E., 2013, "Preparation of Scrap Tire Rubber Fiber–Silica Fume Mixtures for Modification of Clayey Soils," *Appl. Clay Sci.*, Vol. 80–81, pp. 117–125. doi:10.1016/J.CLAY.2013.06.014.

Maher, M. H., and Ho, Y. C., 1994, "Mechanical Properties of Kaolinite/Fiber Soil Composite," *J. Geotech. Eng.*, Vol. 120, No. 8, pp. 1381–1393. doi:10.1061/(ASCE)0733-9410(1994)120:8(1381).

McGarry, D., and Malafant, K. W. J., 1987, "The Analysis of Volume Change in Unconfined Units of Soil," *Soil Sci. Soc. Am. J.*, Vol. 51, No. 2, pp. 290–297. doi:10.2136/SSSAJ1987.03615995005100020059X.

Mirzababaei, M., Arulrajah, A., Horpibulsuk, S., and Aldavad, M., 2017[b], "Shear Strength of a Fibre–Reinforced Clay at Large Shear Displacement When Subjected to Different Stress Histories," *Geotext. Geomembranes*, Vol. 45, No. 5, pp. 422–429. doi:10.1016/J.GEOTEXMEM.2017.06.002.

Mirzababaei, M., Miraftab, M., Mohamed, M., and McMahon, P., 2013[a], "Impact of Carpet Waste Fibre Addition on Swelling Properties of Compacted Clays," *Geotech. Geol. Eng.*, Vol. 31, No. 1, pp. 173–182. doi:10.1007/S10706-012-9578-2.

Mirzababaei, M., Miraftab, M., Mohamed, M., and McMahon, P., 2013[b], "Unconfined Compression Strength of Reinforced Clays with Carpet Waste Fibers," *J. Geotech. Geoenvironmental Eng.*, Vol. 139, No. 3, pp. 483–493. doi:10.1061/(ASCE)GT.1943-5606.0000792.

Mirzababaei, M., Mohamed, M., Arulrajah, A., Horpibulsuk, S., and Anggraini, V., 2017[a], "Practical Approach to Predict the Shear Strength of Fibre–Reinforced Clay," *Geosynth. Int.*, in press. doi:10.1680/JGEIN.17.00033.

Mirzababaei, M., Yasrobi, S. S., and Al-Rawas, A. A., 2009, "Effect of Polymers on Swelling Potential of Expansive Soils," *Proc. ICE Gr. Improv.*, Vol. 162, No. 3, pp. 111–119. doi:10.1680/GRIM.2009.162.3.111.

Mishra, A. K., Dhawan, S., and Rao, S. M., 2008, "Analysis of Swelling and Shrinkage Behavior of Compacted Clays," *Geotech. Geol. Eng.*, Vol. 26, No. 3, pp. 289–298. doi:10.1007/S10706-007-9165-0.

Nalbantoglu, Z., 2006, "Lime Stabilization of Expansive Clay," In: Al-Rawas, A. A., and Goosen, M. F. A. (Eds.), *Expansive soils: Recent Advances in Characterization and Treatment*, Taylor & Francis Group, London, pp. 139–148. doi:10.1201/9780203968079.CH23.

Olgun, M., 2013, "The Effects and Optimization of Additives for Expansive Clays under Freeze–Thaw Conditions," *Cold Reg. Sci. Technol.*, Vol. 93, pp. 36–46. doi:10.1016/J.COLDREGIONS.2013.06.001.

Onyejekwe, S., and Ghataora, G. S., 2015, "Soil Stabilization Using Proprietary Liquid Chemical Stabilizers: Sulphonated Oil and a Polymer," *Bull. Eng. Geol. Environ.*, Vol. 74, No. 2, pp. 651–665. doi:10.1007/S10064-014-0667-8.

Özkul, Z. H., and Baykal, G., 2007, "Shear Behavior of Compacted Rubber Fiber–Clay Composite in Drained and Undrained Loading," *J. Geotech. Geoenvironmental Eng.*, Vol. 133, No. 7, pp. 767–781. doi:10.1061/(ASCE)1090-0241(2007)133:7(767).

Pacheco Silva, F., 1970, "A New Graphical Construction for Determination of the Preconsolidation Stress of a Soil Sample," In: *Proceedings of the Fourth Brazilian Conference on Soil Mechanics and Foundation Engineering*, Rio de Janeiro, pp. 225–232.

Patil, U., Valdes, J. R., and Evans, T. M., 2011, "Swell Mitigation with Granulated Tire Rubber," *J. Mater. Civ. Eng.*, Vol. 23, No. 5, pp. 721–727. doi:10.1061/(ASCE)MT.1943-5533.0000229.

Peng, X., and Horn, R., 2005, "Modeling Soil Shrinkage Curve across a Wide Range of Soil Types," *Soil Sci. Soc. Am. J.*, Vol. 69, No. 3, pp. 584–592. doi:10.2136/SSSAJ2004.0146.

Phanikumar, B. R., and Singla, R., 2016, "Swell–Consolidation Characteristics of Fibre–Reinforced Expansive Soils," *Soils Found.*, Vol. 56, No. 1, pp. 138–143. doi:10.1016/J.SANDF.2016.01.011.

Prakash, K., and Sridharan, A., 2004, "Free Swell Ratio and Clay Mineralogy of Fine–Grained Soils," *Geotech. Test. J.*, Vol. 27, No. 2, pp. 220–225. doi:10.1520/GTJ10860.

Radovic, M., Lara-Curzio, E., and Riester, L., 2004, "Comparison of Different Experimental Techniques for Determination of Elastic Properties of Solids," *Mater. Sci. Eng. A*, Vol. 368, No. 1–2, pp. 56–70. doi:10.1016/J.MSEA.2003.09.080.

Rao, S. M., Thyagaraj, T., and Thomas, H. R., 2006, "Swelling of Compacted Clay under Osmotic Gradients," *Géotechnique*, Vol. 56, No. 10, pp. 707–713. doi:10.1680/GEOT.2006.56.10.707.

Seda, J. H., Lee, J. C., and Carraro, J. A. H., 2007, "Beneficial Use of Waste Tire Rubber for Swelling Potential Mitigation in Expansive Soils," In: Schaefer, V. R., Filz, G. M., Gallagher, P. M., Sehn, A. L., and Wissmann, K. J. (Eds.), *Geo–Denver 2007: Soil Improvement (GSP 172)*, ASCE, Denver, CO, pp. 1–9. doi:10.1061/40916(235)5.

Shahbazi, M., Rowshanzamir, M., Abtahi, S. M., and Hejazi, S. M., 2017, "Optimization of Carpet Waste Fibers and Steel Slag Particles to Reinforce Expansive Soil Using Response Surface Methodology," *Appl. Clay Sci.*, Vol. 142, No. 15, pp. 185–192. doi:10.1016/J.CLAY.2016.11.027.

Sibley, J. W., and Williams, D. J., 1989, "A Procedure for Determining Volumetric Shrinkage of an Unsaturated Soil," *Geotech. Test. J.*, Vol. 12, No. 3, pp. 181–187. doi:10.1520/GTJ10966J.

Signes, C. H., Garzón-Roca, J., Fernández, P. M., Torre, M. E. G., and Franco, R. I., 2016, "Swelling Potential Reduction of Spanish Argillaceous Marlstone Facies Tap Soil through the Addition of Crumb Rubber Particles from Scrap Tyres," *Appl. Clay Sci.*, Vol. 132–133, pp. 768–773. doi:10.1016/J.CLAY.2016.07.027.

Sivapullaiah, P. V., Sridharan, A., and Stalin, V. K., 1996, "Swelling Behaviour of Soil–Bentonite Mixtures," *Can. Geotech. J.*, Vol. 33, No. 5, pp. 808–814. doi:10.1139/T96-106-326.

Soltani, A., 2017, "Discussion of 'Optimization of Carpet Waste Fibers and Steel Slag Particles to Reinforce Expansive Soil Using Response Surface Methodology' by M. Shahbazi, M. Rowshanzamir, S.M. Abtahi, S.M. Hejazi [Appl. Clay Sci., doi:10.1016/j.clay.2016.11.027]," *Appl. Clay Sci.*, in press. doi:10.1016/J.CLAY.2017.07.020.

Soltani, A., Deng, A., and Taheri, A., 2017[b], "Swell–Compression Characteristics of a Fiber–Reinforced Expansive Soil," *Geotext. Geomembranes*, in press. doi:10.1016/J.GEOTEXMEM.2017.11.009.

Soltani, A., Deng, A., Taheri, A., and Mirzababaei, M., 2017[a], "A Sulphonated Oil for Stabilisation of Expansive Soils," *Int. J. Pavement Eng.*, in press. doi:10.1080/10298436.2017.1408270.

Soltani, A., Deng, A., Taheri, A., Sridharan, A., and Estabragh, A. R., 2017[d], "A Framework for Interpretation of the Compressibility Behavior of Soils," *Geotech. Test. J.*, in press. doi:10.1520/GTJ20170088.

Soltani, A., Taheri, A., Khatibi, M., and Estabragh, A. R., 2017[c], "Swelling Potential of a Stabilized Expansive Soil: A Comparative Experimental Study," *Geotech. Geol. Eng.*, Vol. 35, No. 4, pp. 1717–1744. doi:10.1007/S10706-017-0204-1.

Sridharan, A., Abraham, B. M., and Jose, B. T., 1991, "Improved Technique for Estimation of Preconsolidation Pressure," *Géotechnique*, Vol. 41, No. 2, pp. 263–268. doi:10.1680/GEOT.1991.41.2.263.

Sridharan, A., and Gurtug, Y., 2004, "Swelling Behaviour of Compacted Fine–Grained Soils," *Eng. Geol.*, Vol. 72, No. 1, pp. 9–18. doi:10.1016/S0013-7952(03)00161-3.

Sridharan, A., and Nagaraj, H. B., 2005, "Plastic Limit and Compaction Characteristics of Fine–Grained Soils," *Proc. ICE Gr. Improv.*, Vol. 9, No. 1, pp. 17–22. doi:10.1680/GRIM.2005.9.1.17.

Sridharan, A., and Prakash, K., 1998, "Mechanism Controlling the Shrinkage Limit of Soils," *Geotech. Test. J.*, Vol. 21, No. 3, pp. 240–250. doi:10.1520/GTJ10897J.

Sridharan, A., Rao, A., and Sivapullaiah, P., 1986, "Swelling Pressure of Clays," *Geotech. Test. J.*, Vol. 9, No. 1, pp. 24–33. doi:10.1520/GTJ10608J.

Srivastava, A., Pandey, S., and Rana, J., 2014, "Use of Shredded Tyre Waste in Improving the Geotechnical Properties of Expansive Black Cotton Soil," *Geomech. Geoengin.*, Vol. 9, No. 4, pp. 303–311. doi:10.1080/17486025.2014.902121.

Subba Rao, K. S., Rao, S. M., and Gangadhara, S., 2000, "Swelling Behavior of a Desiccated Clay," *Geotech. Test. J.*, Vol. 23, No. 2, pp. 193–198. doi:10.1520/GTJ11043J.

Tang, C. S., Shi, B., and Zhao, L. Z., 2010, "Interfacial Shear Strength of Fiber Reinforced Soil," *Geotext. Geomembranes*, Vol. 28, No. 1, pp. 54–62. doi:10.1016/J.GEOTEXMEM.2009.10.001.

Tang, C. S., Shi, B., Gao, W., Chen, F., and Cai, Y., 2007, "Strength and Mechanical Behavior of Short Polypropylene Fiber Reinforced and Cement Stabilized Clayey Soil," *Geotext. Geomembranes*, Vol. 25, No. 3, pp. 194–202. doi:10.1016/J.GEOTEXMEM.2006.11.002.

Thyagaraj, T., and Zodinsanga, S., 2014, "Swell–Shrink Behaviour of Lime Precipitation Treated Soil," *Proc. ICE Gr. Improv.*, Vol. 167, No. 4, pp. 260–273. doi:10.1680/GRIM.12.00028.

Thyagaraj, T., Thomas, S. R., and Das, A. P., 2017, "Physico–Chemical Effects on Shrinkage Behavior of Compacted Expansive Clay," *Int. J. Geomech.*, Vol. 17, No. 2, pp. 06016013-1–06016013-11. doi:10.1061/(ASCE)GM.1943-5622.0000698.

Tripathy, S., and Subba Rao, K. S., 2009, "Cyclic Swell–Shrink Behaviour of a Compacted Expansive Soil," *Geotech. Geol. Eng.*, Vol. 27, No. 1, pp. 89–103. doi:10.1007/S10706-008-9214-3.

Tripathy, S., Subba Rao, K. S., and Fredlund, D. G., 2002, "Water Content–Void Ratio Swell–Shrink Paths of Compacted Expansive Soils," *Can. Geotech. J.*, Vol. 39, No. 4, pp. 938–959. doi:10.1139/T02-022.

Trouzine, H., Bekhiti, M., and Asroun, A., 2012, "Effects of Scrap Tyre Rubber Fibre on Swelling Behaviour of Two Clayey Soils in Algeria," *Geosynth. Int.*, Vol. 19, No. 2, pp. 124–132. doi:10.1680/GEIN.2012.19.2.124.

Viswanadham, B. V. S., Phanikumar, B. R., and Mukherjee, R. V., 2009[b], "Effect of Polypropylene Tape Fibre Reinforcement on Swelling Behaviour of an Expansive Soil," *Geosynth. Int.*, Vol. 16, No. 5, pp. 393–401. doi:10.1680/GEIN.2009.16.5.393.

Viswanadham, B. V. S., Phanikumar, B. R., and Mukherjee, R. V., 2009[a], "Swelling Behaviour of a Geofiber–Reinforced Expansive Soil," *Geotext. Geomembranes*, Vol. 27, No. 1, pp. 73–76. doi:10.1016/J.GEOTEXMEM.2008.06.002.

Winterkorn, H. F., and Pamukcu, S., 1991, "Soil Stabilization and Grouting," In: Fang, H. Y. (Ed.), *Foundation Engineering Handbook*, Springer, New York, NY, pp. 317–378. doi:10.1007/978-1-4615-3928-5_9.

Yadav, J. S., and Tiwari, S. K., 2017, "A Study on the Potential Utilization of Crumb Rubber in Cement Treated Soft Clay," *J. Build. Eng.*, Vol. 9, pp. 177–191. doi:10.1016/J.JOBE.2017.01.001.

Zornberg, J. G., Cabral, A. R., and Viratjandr, C., 2004, "Behaviour of Tire Shred–Sand Mixtures," *Can. Geotech. J.*, Vol. 41, No. 2, pp. 227–241. doi:10.1139/T03-086.

List of Tables

Table 1. Mechanical properties of kaolinite, bentonite and the expansive soil.

Table 2. Chemical composition of kaolinite and bentonite (as supplied by the manufacturer).

Table 3. Physical properties and chemical composition of the tire rubbers (as supplied by the manufacturer).

Table 4. Mechanical properties of the prepared samples.

Table 5. Shrinkage strains and the shrinkage limit for the tested samples.

Table 6. Comparative cost analysis between rubbers and conventional fibers.

Table 1. Mechanical properties of kaolinite, bentonite and the expansive soil.

Properties	Kaolinite	Bentonite	Expansive soil	Standard designation
Specific gravity, G_s	2.68	2.81	2.73	ASTM D854 (2014)
Clay (< 2 μm) (%)	49.78	62.43	N/A[†]	ASTM D422 (2007)
Silt (2–75 μm) (%)	49.43	35.75	N/A	
Sand (0.075–4.75 mm) (%)	0.79	1.82	N/A	
Liquid limit, *LL* (%)	41.04	379.21	59.60	AS 1289.3.9.1 (2015)
Plastic limit, *PL* (%)	23.67	45.18	27.28	AS 1289.3.2.1 (2009)
Plasticity index, *PI* (%)	17.37	334.03	32.32	AS 1289.3.3.1 (2009)
Free swell ratio, *FSR*[‡]	1.19	7.53	2.91	Prakash and Sridharan (2004)
USCS classification	CI	CH	CH	ASTM D2487 (2011)
Optimum water content, ω_{opt} (%)	19.82	36.34	26.00	ASTM D698 (2012)
Maximum dry unit weight, γ_{dmax} (kN/m^3)	15.67	11.74	15.07	

Note:
[†]not measured; and [‡]ratio of equilibrium sediment volume of 10 gr oven–dried soil passing sieve 425 μm in distilled water to that of kerosene.

Table 2. Chemical composition of kaolinite and bentonite (as supplied by the manufacturer).

Properties	**Kaolinite**	**Bentonite**
SiO_2 (%)	64.9	63.2
Al_2O_3 (%)	22.2	13.3
TiO_2 (%)	1.4	0.3
Fe_2O_3 (%)	1.0	2.6
CaO (%)	0.1	0.3
Na_2O (%)	0.2	1.9
MgO (%)	0.6	2.2
K_2O (%)	2.7	0.2
Acidity, pH	7.4	9.5
LOI at 1000 ^oC (%)[†]	6.5	16.0
CEC (meq/100mL)[‡]	N/A[*]	82
SSA (m^2/gr)[#]	11.2	N/A

Note:
[†]loss on ignition; [‡]cation exchange capacity; [*]not available; and [#]specific surface area.

Table 3. Physical properties and chemical composition of the tire rubbers (as supplied by the manufacturer).

Properties	Value/Description
Physical properties	
Solubility in water	Insoluble
Water adsorption	Negligible
Resistance to acid and alkaline	Excellent
Specific gravity at 20°C	1.09
Particle size for rubber A (mm)	1.18–0.075
Particle size for rubber B (mm)	4.75–1.18
Softening point (°C)	170
Chemical composition	
Styrene–butadiene copolymer (%)	55
Acetone extract (%)	5–20
Carbon black (%)	25–35
Zinc oxide (%)	2.5
Sulphur (%)	1–3

Table 4. Mechanical properties of the prepared samples.

Rubber type	R_c **(%)**	G_s	LL **(%)**	PL **(%)**	PI **(%)**	ω_{opt} **(%)**	**0.92**PL **(%)**[†]	γ_{dmax} **(kN/m^3)**	e_{opt}[‡]	ω_0 **(%)**	γ_{d0} **(kN/m^3)**	e_0[*]
—	0	2.73	59.60	27.28	32.32	26.00	25.10	15.07	0.775	21.00	14.52	0.842
Rubber A	5	2.54	57.03	27.02	30.01	24.77	24.86	14.63	0.706	19.77	14.16	0.763
	10	2.40	55.04	25.54	29.50	23.87	23.50	14.35	0.639	18.87	13.90	0.693
	20	2.18	51.51	23.46	28.05	21.85	21.58	13.87	0.541	16.85	13.40	0.596
	30	2.02	49.58	22.70	26.88	20.07	20.88	13.52	0.469	15.07	12.92	0.537
Rubber B	5	2.54	56.88	26.61	30.27	24.47	24.48	14.61	0.709	19.47	14.15	0.764
	10	2.40	55.62	24.77	30.85	23.46	22.79	14.37	0.638	18.46	13.94	0.689
	20	2.18	52.44	23.27	29.17	21.15	21.41	13.86	0.543	16.15	13.43	0.593
	30	2.02	51.21	22.15	29.06	19.94	20.38	13.52	0.469	14.94	12.99	0.528

Note:
[†]predicted optimum water content; [‡]initial placement condition for unconfined compression tests; and [*]initial placement condition for swell–shrink–consolidation tests.

Table 5. Shrinkage strains and the shrinkage limit for the tested samples.

Rubber type	R_c **(%)**	ε_{ssh} **(%)**	ε_{psh} **(%)**	ε_{rsh} **(%)**	SH_p **(%)**	SL **(%)**[†]
—	0	4.15	21.47	2.98	28.60	14.88
Rubber A	5	2.99	17.50	2.95	23.44	17.82
	10	3.07	15.53	2.71	21.30	18.00
	20	2.49	13.62	2.15	18.27	16.25
	30	2.01	11.24	2.06	15.30	17.86
Rubber B	5	3.54	18.16	2.92	24.61	17.67
	10	2.43	15.33	2.68	20.44	16.40
	20	1.83	12.33	1.85	16.01	15.16
	30	1.86	10.43	1.75	14.04	15.18

Note:
[†]shrinkage limit.

Table 6. Comparative cost analysis between rubbers and conventional fibers.

Type of reinforcement	R_c (%)	f_c (%)[†]	Unit price (AU$/kg)	Total cost (AU$)
Rubber (A or B)	5	—	0.5	25.0
	10	—		50.0
	20	—		100.0
Poly– (ester, ethylene or propylene) fiber	—	0.8[‡]	14.3	114.4
	—	1.5[*]		214.5

Note:
[†]fiber content (i.e. fiber to dry soil mass ratio); [‡]suggested by Olgun (2013) and Shahbazi et al. (2017); and [*]suggested by Estabragh et al. (2014) and Soltani et al. (2017[c]).

List of Figures

Figure 1. Grain–size distribution curves for kaolinite, bentonite and the tire rubbers.

Figure 2. Tire rubbers at 50x magnification: **(a)** rubber A; and **(b)** rubber B.

Figure 3. Standard Proctor compaction curves for the natural soil and various soil–rubber mixtures: **(a)** rubber A; and **(b)** rubber B.

Figure 4. A typical illustration of the swell–shrink–consolidation test scheme: **(a)** swell path; **(b)** consolidation path; and **(c)** shrink path.

Figure 5. Swelling strain–time curves for the natural soil and various soil–rubber composites: **(a)** rubber A; and **(b)** rubber B.

Figure 6. Variations of the **(a)** primary and **(b)** secondary swelling rates against rubber content for the tested samples.

Figure 7. Void ratio–effective stress consolidation curves for the natural soil and various soil–rubber composites: **(a)** rubber A; and **(b)** rubber B.

Figure 8. Variations of the **(a)** compression and **(b)** swell indices against rubber content for the tested samples.

Figure 9. Variations of swelling pressure and swelling potential against rubber content for the tested samples.

Figure 10. Secondary consolidation characteristics (under σ'=50 kPa) for the natural soil and various soil–rubber composites: **(a)** rubber A; and **(b)** rubber B.

Figure 11. Void ratio–water content shrinkage curves for the natural soil and various soil–rubber composites: **(a)** rubber A; and **(b)** rubber B.

Figure 12. Stress–strain unconfined compression curves for the natural soil and various soil–rubber composites: **(a)** rubber A; and **(b)** rubber B.

Figure 13. Variations of strain energy at peak and the peak strength against rubber content for the tested samples.

Figure 1. Grain–size distribution curves for kaolinite, bentonite and the tire rubbers.

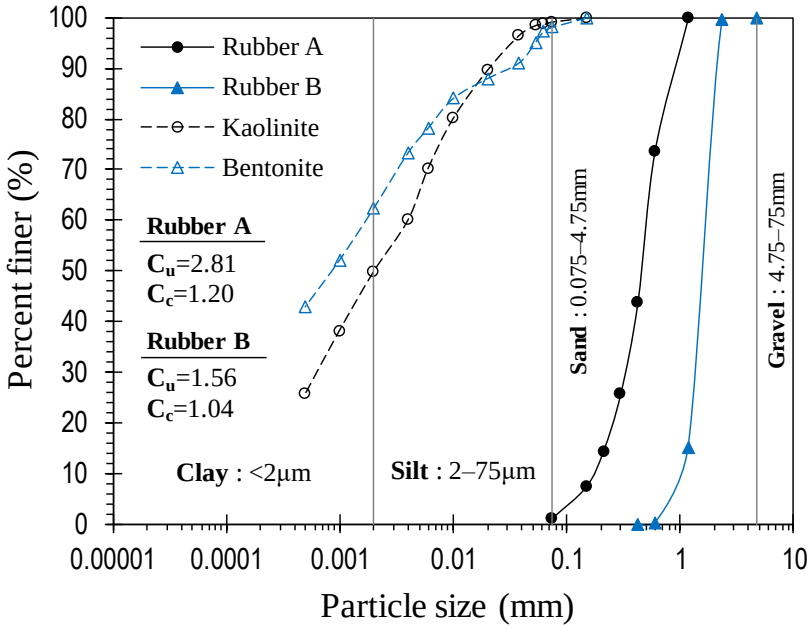

Figure 2. Tire rubbers at 50x magnification: **(a)** rubber A; and **(b)** rubber B.

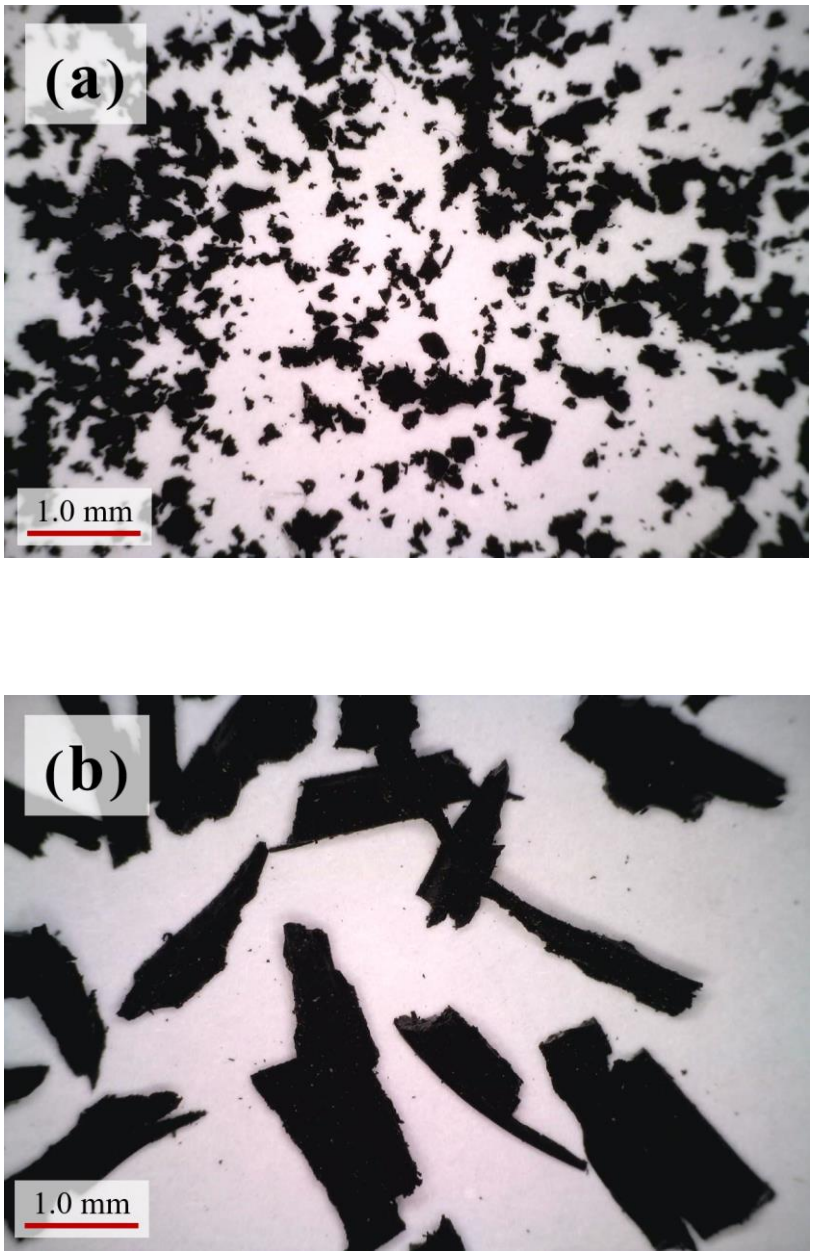

Figure 3. Standard Proctor compaction curves for the natural soil and various soil–rubber mixtures: **(a)** rubber A; and **(b)** rubber B.

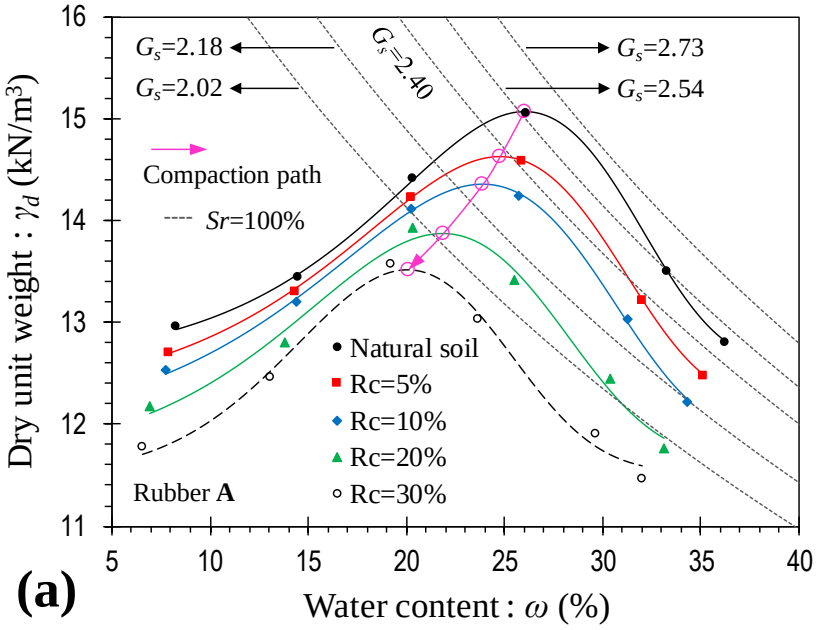

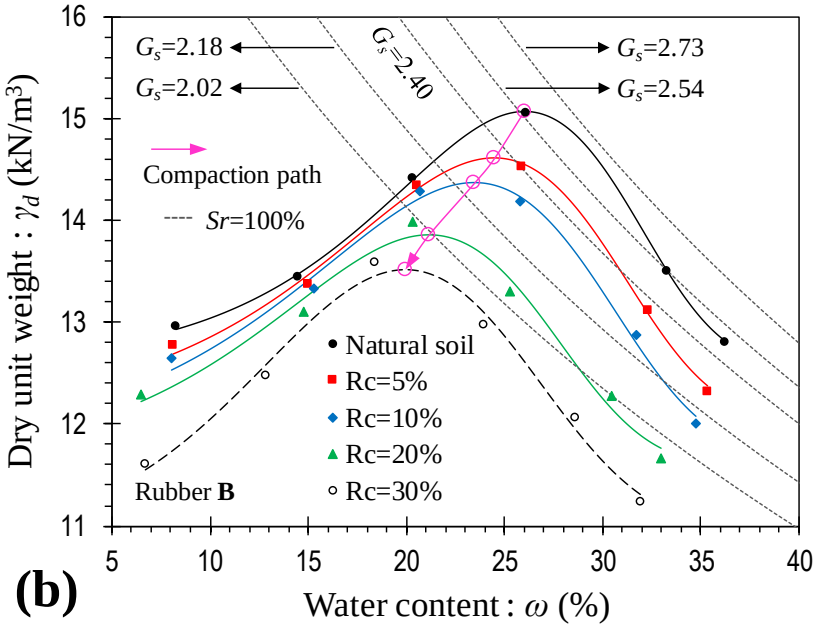

Figure 4. A typical illustration of the swell–shrink–consolidation test scheme: **(a)** swell path; **(b)** consolidation path; and **(c)** shrink path.

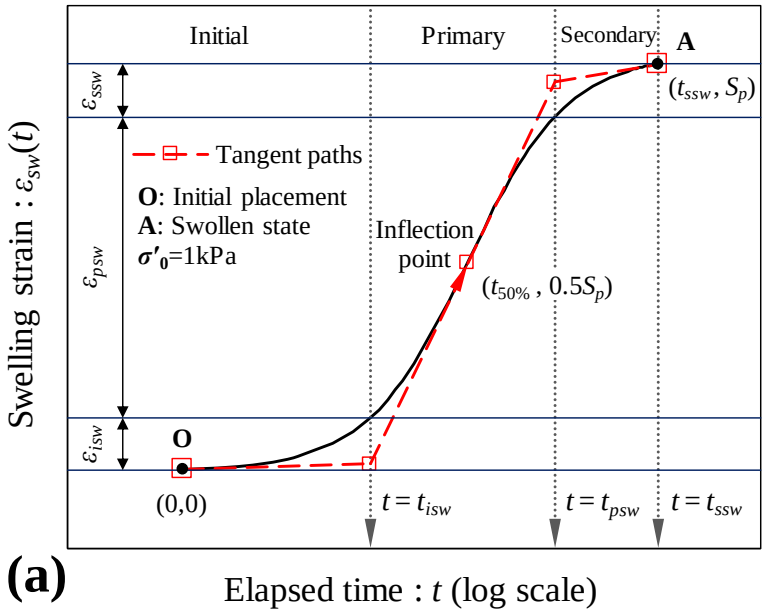

(a)

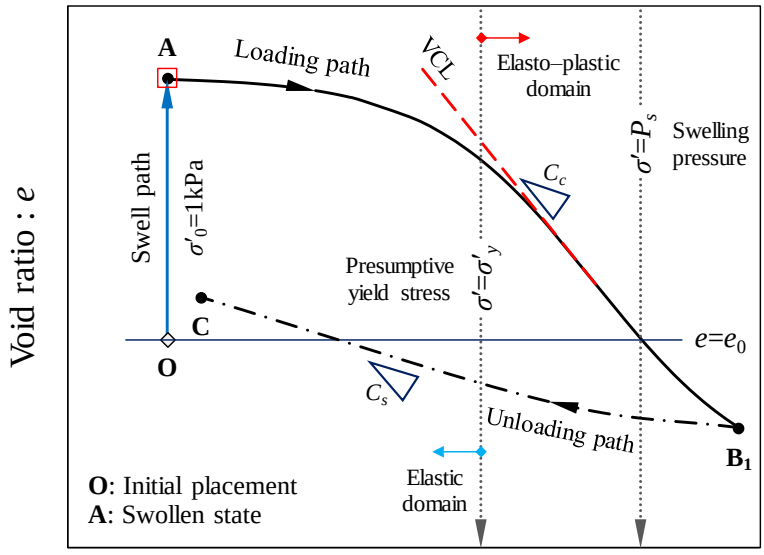

(b)

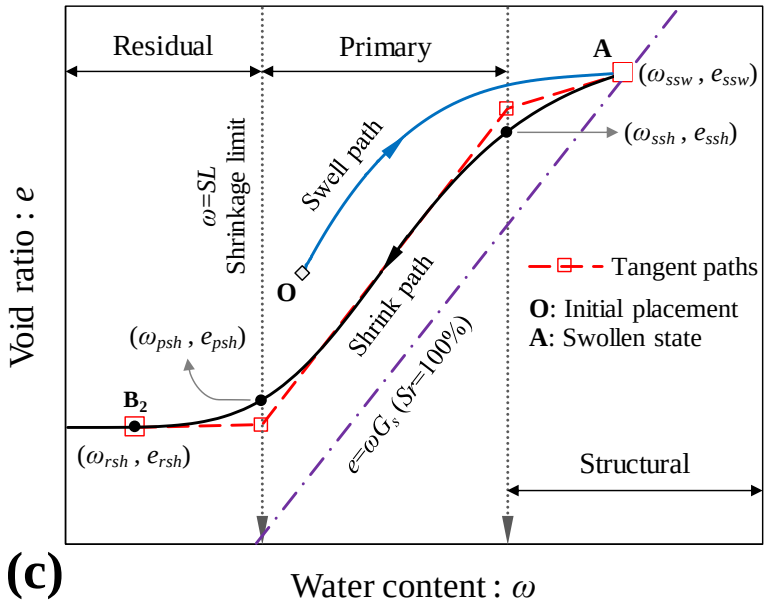
Residual
Primary
A
(ω_{ssw}, e_{ssw})
(ω_{ssh}, e_{ssh})
Swell path
ω=SL
Shrinkage limit
O
Shrink path
Tangent paths
O: Initial placement
A: Swollen state
(ω_{psh}, e_{psh})
B_2
(ω_{rsh}, e_{rsh})
$e=\omega G_s$ (Sr=100%)
Structural
Void ratio : e
Water content : ω

(c)

Figure 5. Swelling strain–time curves for the natural soil and various soil–rubber composites: **(a)** rubber A; and **(b)** rubber B.

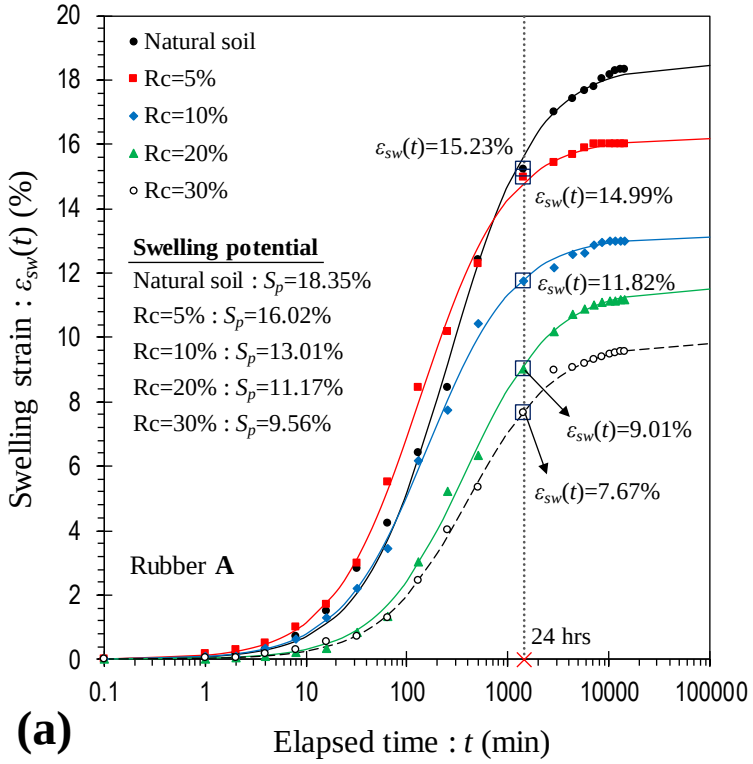

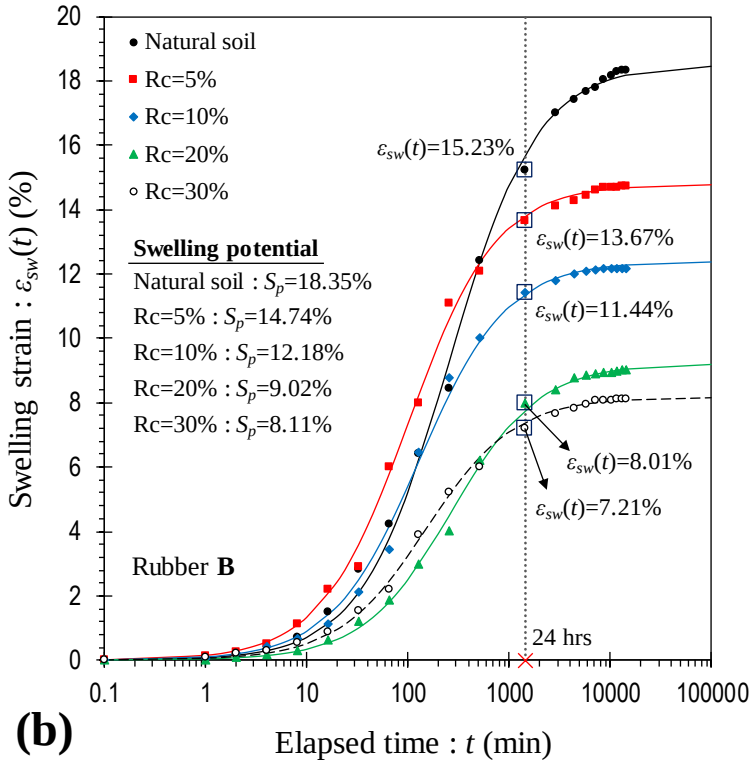

Figure 6. Variations of the **(a)** primary and **(b)** secondary swelling rates against rubber content for the tested samples.

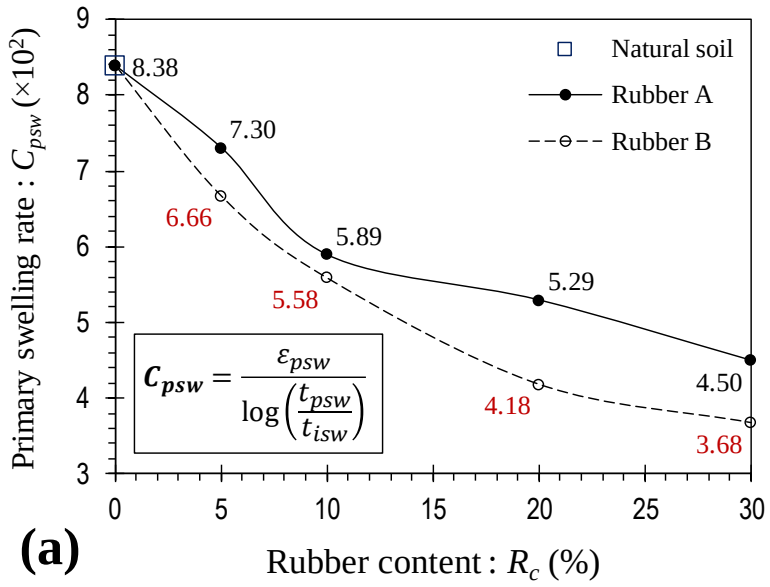

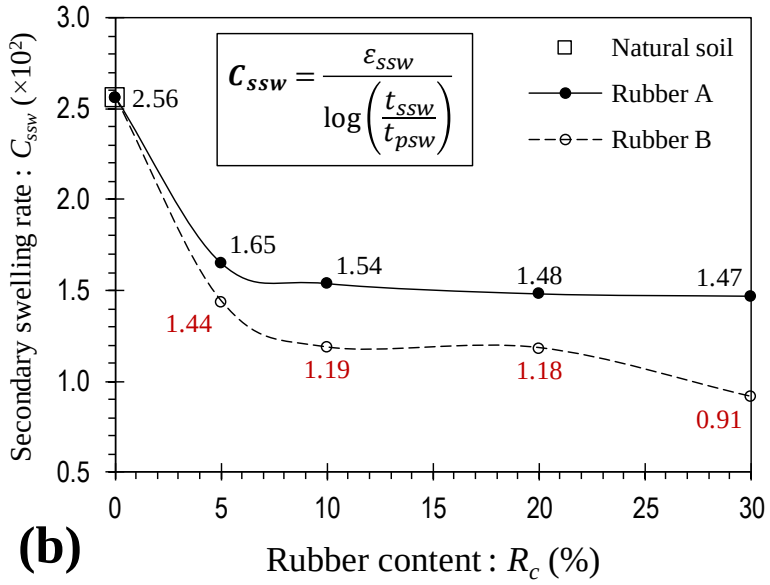

Figure 7. Void ratio–effective stress consolidation curves for the natural soil and various soil–rubber composites: **(a)** rubber A; and **(b)** rubber B.

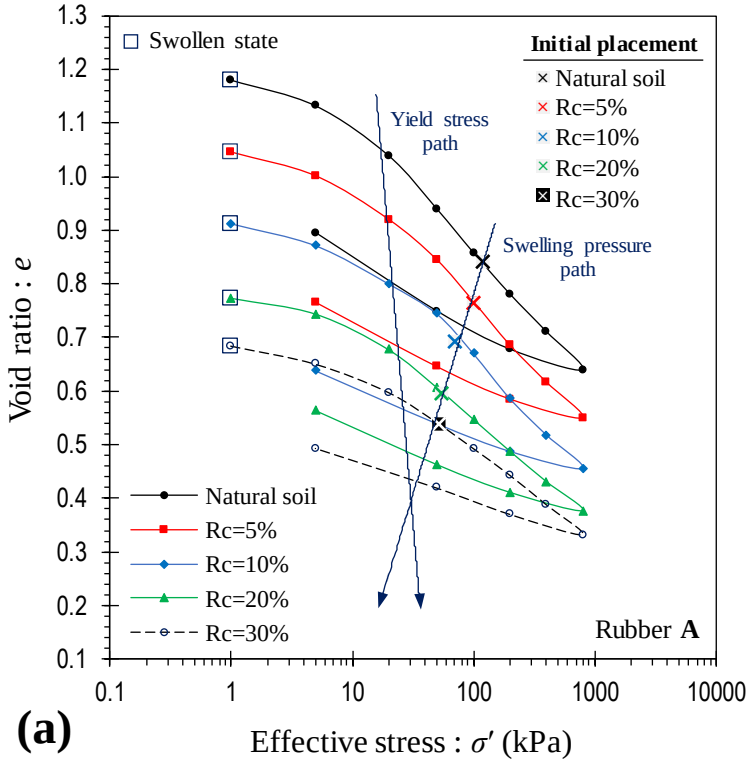

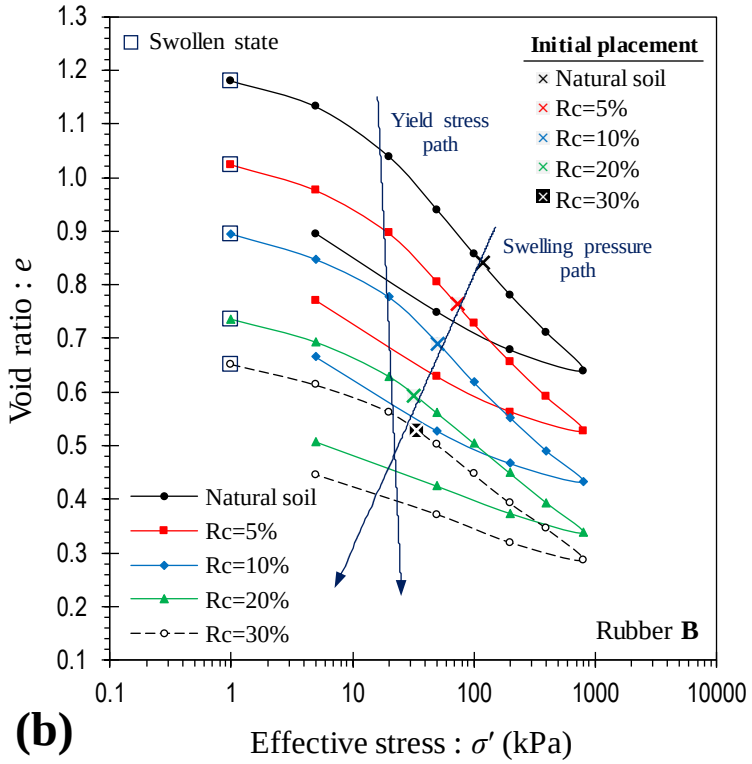

Figure 8. Variations of the **(a)** compression and **(b)** swell indices against rubber content for the tested samples.

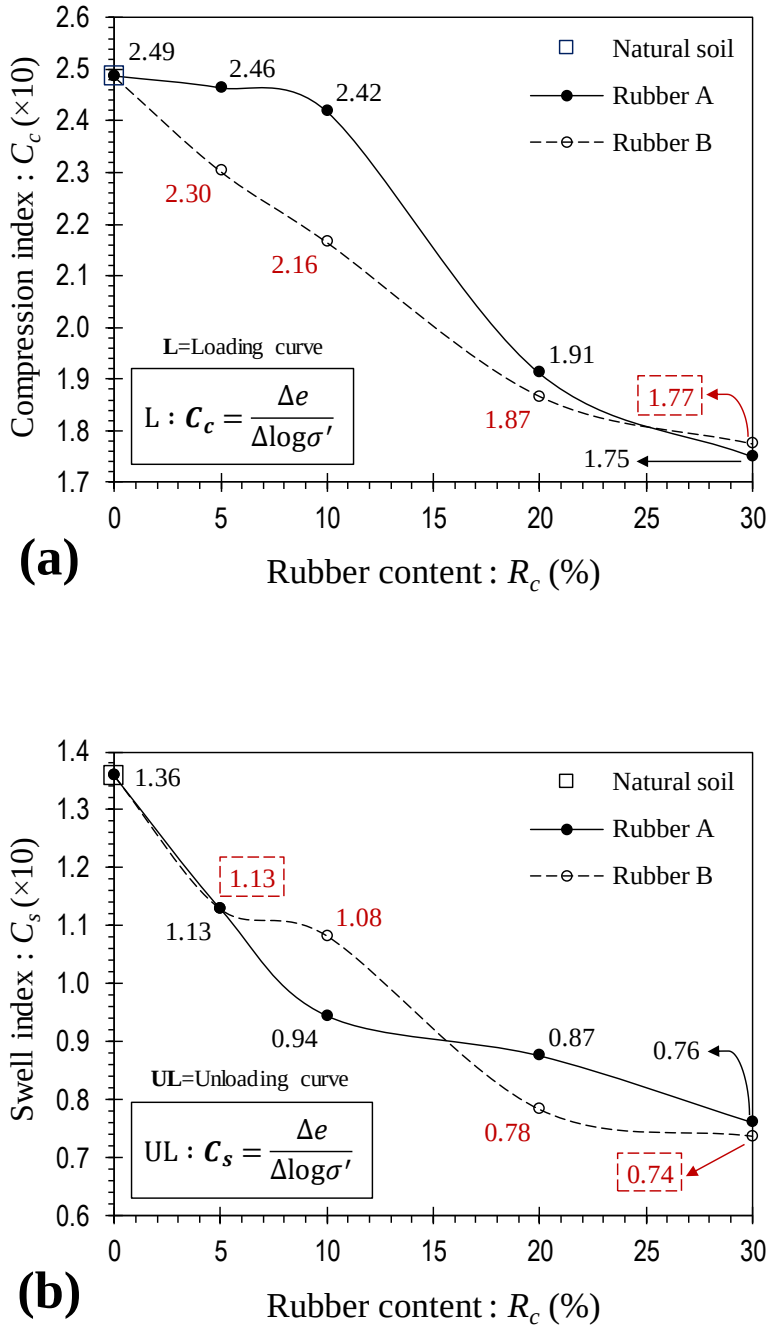

Figure 9. Variations of swelling pressure and swelling potential against rubber content for the tested samples.

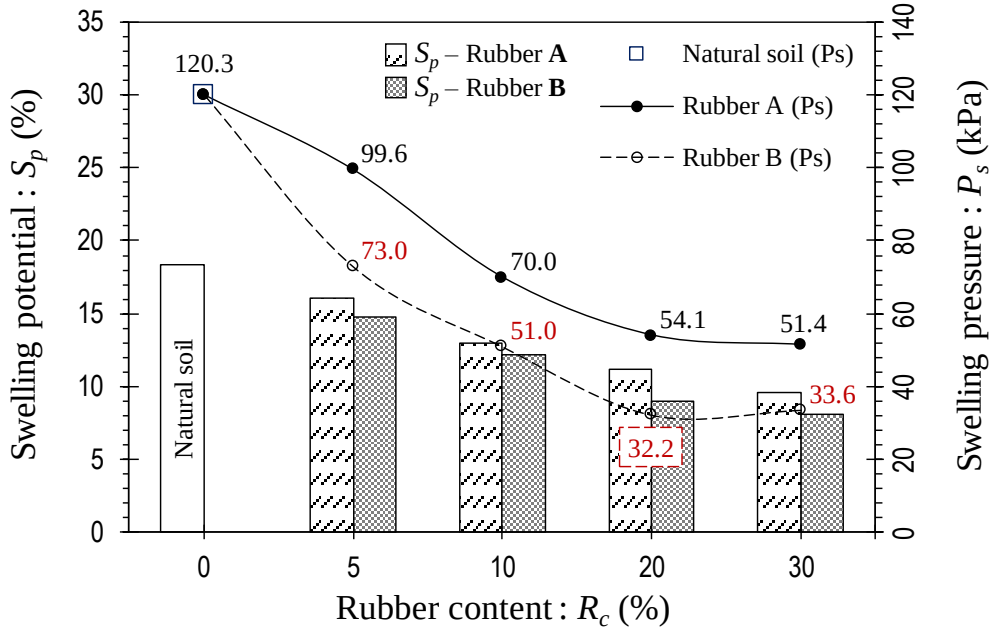

Figure 10. Secondary consolidation characteristics (under σ'=50 kPa) for the natural soil and various soil–rubber composites: **(a)** rubber A; and **(b)** rubber B.

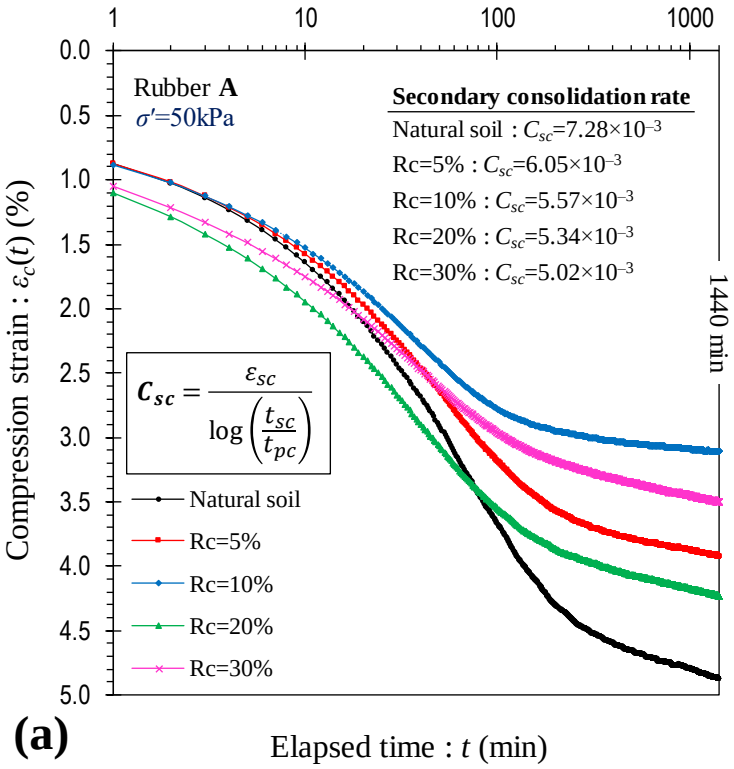

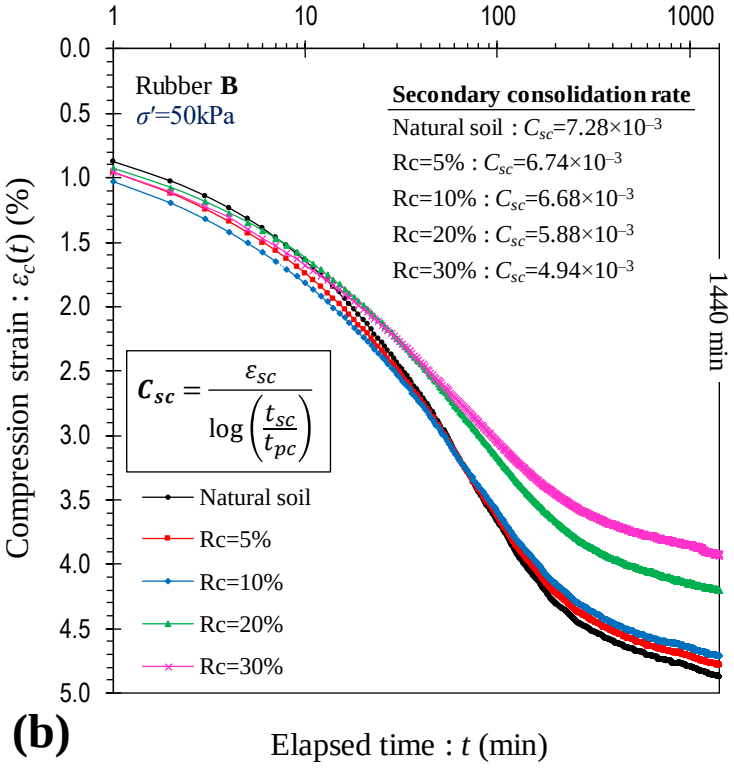

Figure 11. Void ratio–water content shrinkage curves for the natural soil and various soil–rubber composites: **(a)** rubber A; and **(b)** rubber B.

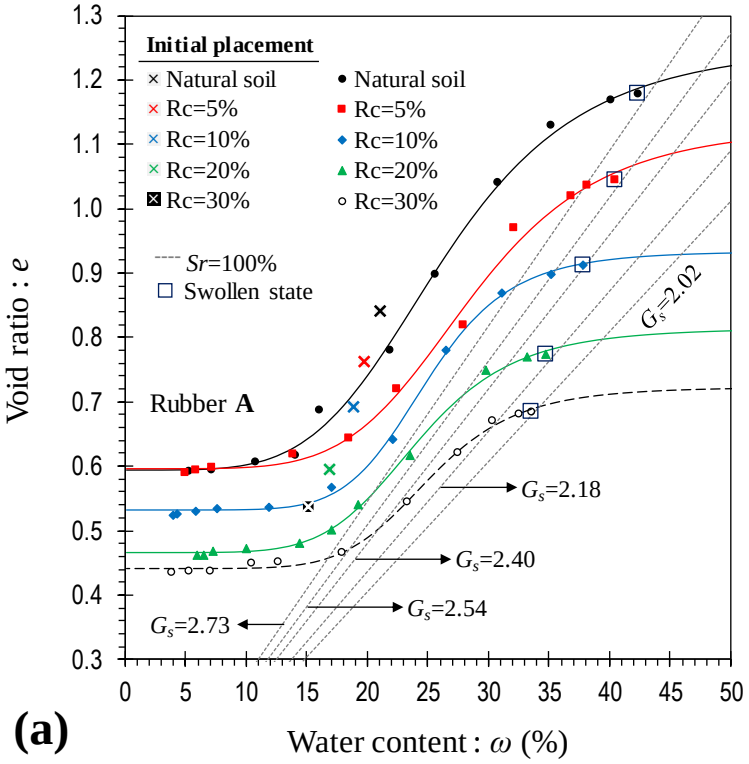

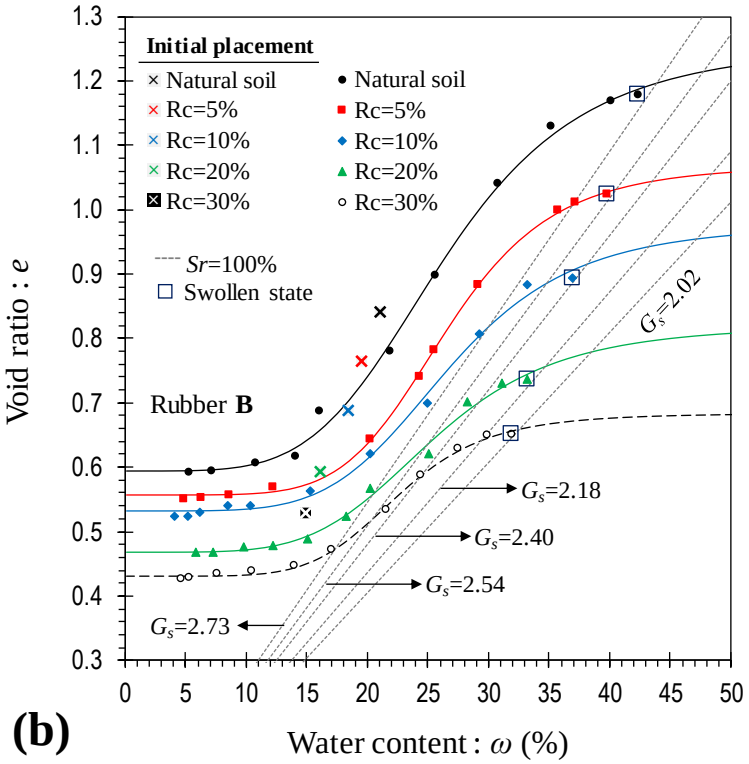

Figure 12. Stress–strain unconfined compression curves for the natural soil and various soil–rubber composites: **(a)** rubber A; and **(b)** rubber B.

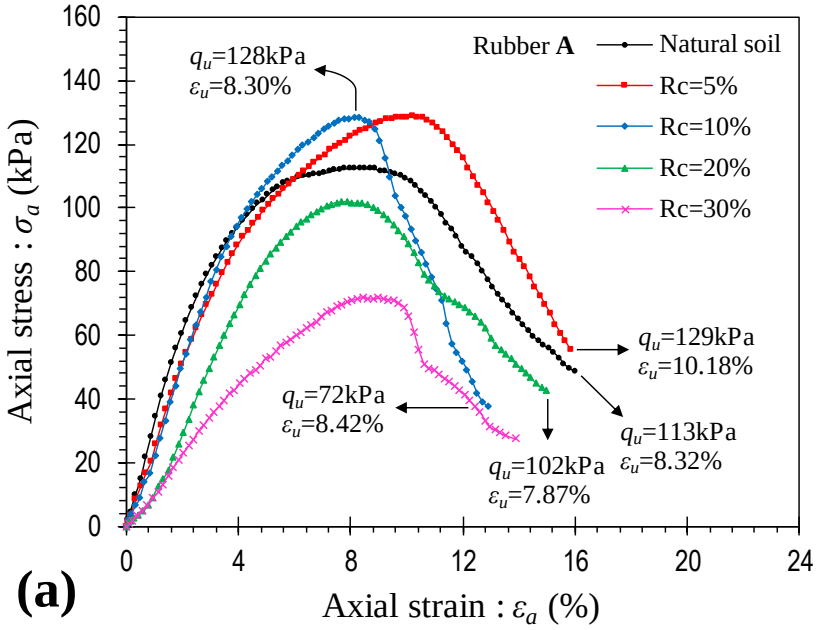

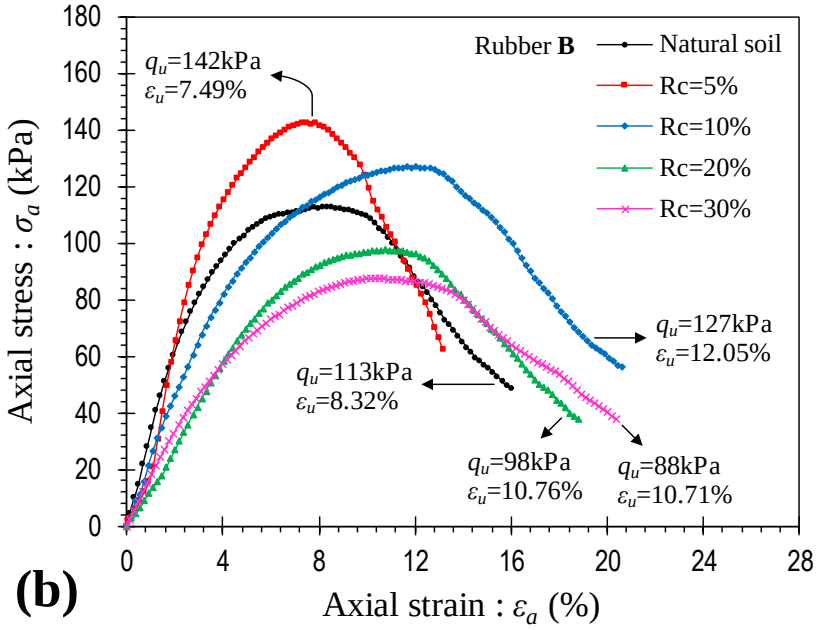

Figure 13. Variations of strain energy at peak and the peak strength against rubber content for the tested samples.

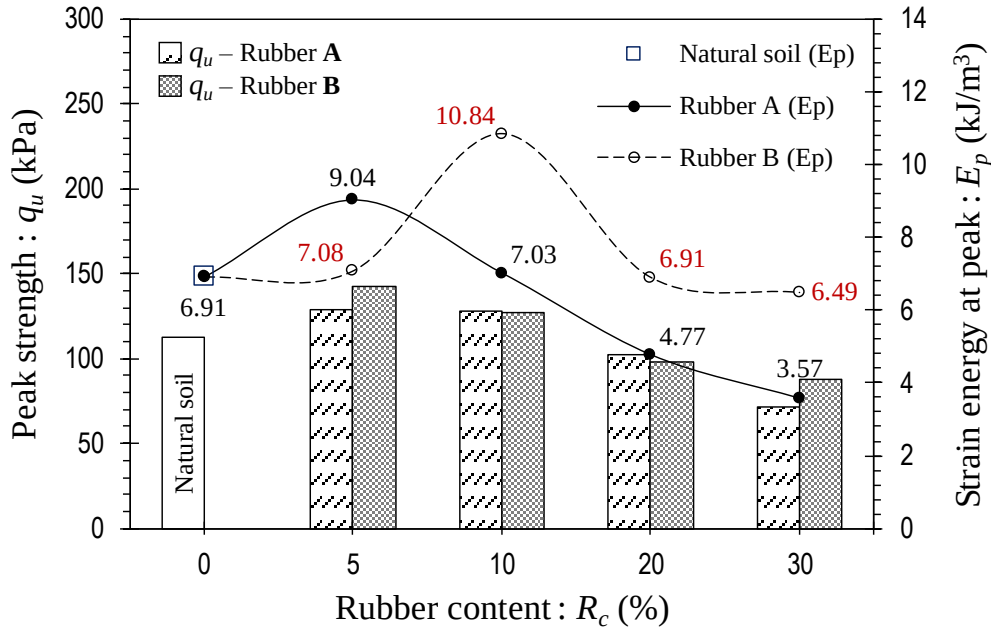

Statement of Authorship

Statement of Authorship

Title of Paper	Swell–Shrink–Consolidation Behavior of Rubber–Reinforced Expansive Soils
Publication Status	■ Published ☐ Accepted for Publication ☐ Submitted for Publication ☐ Unpublished and Unsubmitted work written in manuscript style
Publication Details	**Soltani A**, Deng A, Taheri A and Sridharan A **(2019)** Swell–Shrink–Consolidation Behavior of Rubber–Reinforced Expansive Soils. ***Geotechnical Testing Journal* 42(3): x–x**, https://doi.org/10.1520/gtj20170313.

Principal Author

Name of Principal Author (Candidate)	Amin Soltani (**Email:** Amin.Soltani@adelaide.edu.au)		
Contribution to the Paper	Overall paper preparation		
Overall percentage (%)	85%		
Certification:	This paper reports on original research I conducted during the period of my Higher Degree by Research candidature and is not subject to any obligations or contractual agreements with a third party that would constrain its inclusion in this thesis. I am the primary author of this paper.		
Signature	(	Date	06/29/2018

Co-Author Contributions

By signing the Statement of Authorship, each author certifies that:

i. the candidate's stated contribution to the publication is accurate (as detailed above);
ii. permission is granted for the candidate in include the publication in the thesis; and
iii. the sum of all co-author contributions is equal to 100% less the candidate's stated contribution.

Name of Co-Author	An Deng **Senior Lecturer**, School of Civil, Environmental and Mining Engineering, The University of Adelaide, Adelaide, SA 5005, Australia (**Email:** An.Deng@adelaide.edu.au)		
Contribution to the Paper	Paper review and revision		
Signature		Date	07/23/2018

Name of Co-Author	Abbas Taheri **Senior Lecturer**, School of Civil, Environmental and Mining Engineering, The University of Adelaide, Adelaide, SA 5005, Australia (**Email:** Abbas.Taheri@adelaide.edu.au)		
Contribution to the Paper	Paper review and revision		
Signature		Date	07/16/2018

Name of Co-Author	Asuri Sridharan **Professor Emeritus**, Department of Civil Engineering, Indian Institute of Science, Bangalore 560012, India; **Honorary Research Scientist**, Indian National Science Academy (INSA), New Delhi 110002, India (**Email:** SridharanAsuri@yahoo.com)		
Contribution to the Paper	Paper review and revision		
Signature	. **Note:** Sign–off by Principal Supervisor in place of this co–author who is based overseas. Co–author agreement in email is retained by Candidate.	Date	07/23/2018

1

Published Copy [Link]

ASTM INTERNATIONAL

Geotechnical Testing Journal

Amin Soltani,[1] An Deng,[2] Abbas Taheri,[2] and Asuri Sridharan[3]

DOI: 10.1520/GTJ20170313

Swell-Shrink-Consolidation Behavior of Rubber-Reinforced Expansive Soils

Geotechnical Testing Journal

doi:10.1520/GTJ20170313 available online at www.astm.org

Amin Soltani,[1] An Deng,[2] Abbas Taheri,[2] and Asuri Sridharan[3]

Swell-Shrink-Consolidation Behavior of Rubber-Reinforced Expansive Soils

Reference

Soltani, A., Deng, A., Taheri, A., and Sridharan, A., "Swell-Shrink-Consolidation Behavior of Rubber-Reinforced Expansive Soils," *Geotechnical Testing Journal* https://doi.org/10.1520/GTJ20170313. ISSN 0149-6115

ABSTRACT

This study examines the effects of two types of recycled tire rubber of fine and coarse categories on the swell-shrink-consolidation behavior of a highly expansive soil mixture. Each of the two rubber choices were incorporated into the soil at four different content levels (i.e., rubber to dry soil mass ratio) of 5, 10, 20, and 30 %. The experimental program consisted of consistency limits, compaction, swell-consolidation, swell-shrink, and unconfined compression tests. Improvement in the swell-shrink-consolidation capacity was in favor of higher rubber contents; however, when excessively included, it raised strength concerns. The swell-shrink-consolidation properties were also rubber size–dependent, meaning that the rubber of coarser sizes often outperformed finer rubber. In terms of strength, however, the two rubber types promoted similar results with marginal differences. The results of the unconfined compression tests were cross checked with the swell-shrink-consolidation properties to arrive at the optimum stabilization scenarios. A maximum rubber inclusion of 10 %, preferably the rubber in the coarser category, proved to satisfy the stabilization objectives (i.e., decrease in the swell-shrink-consolidation capacity as well as maintain or improve the strength) and thus was deemed as the optimum choice. Where context changes and the strength and stiffness are not a primary concern, higher rubber inclusions of up to 20 % may also be considered acceptable.

Keywords

expansive soils, recycled tire rubbers, rubber content and size, swell-shrink-consolidation, unconfined compression

Manuscript received September 8, 2017; accepted for publication March 26, 2018; published online xxxx xx, xxxx.

[1] School of Civil, Environmental and Mining Engineering, University of Adelaide, N. Terrace, SA 5005, Australia (Corresponding author), e-mail: Amin.Soltani@adelaide.edu.au, https://orcid.org/0000-0002-0483-7487

[2] School of Civil, Environmental and Mining Engineering, University of Adelaide, N. Terrace, SA 5005, Australia

[3] Indian National Science Academy, New Delhi 110009, India; Department of Civil Engineering, Indian Institute of Science, Bangalore 560012, India (retired)

Copyright © 2018 by ASTM International, 100 Barr Harbor Drive, PO Box C700, West Conshohocken, PA 19428-2959

Introduction

Expansive soils are low graded because of their inferior engineering characteristics (e.g., low strength, high compressibility, and a high potential for swelling and shrinkage), and thus are characterized as unsuitable construction materials for the majority of engineering applications (Dif and Bluemel 1991; Nalbantoglu 2006; Estabragh et al. 2013a). When exposed to seasonal environments, such soils are prone to significant volume changes, i.e., heave and settlements, thereby causing instability concerns to the overlying structures. Such concerns incur a great amount of maintenance costs and therefore demand engineering solutions to alleviate the associated socioeconomic impacts on human life (Jones and Jefferson 2012). Stabilization of expansive soils is often achieved through two approaches, i.e., chemical and mechanical techniques (Winterkorn and Pamukcu 1991). Chemical techniques mainly involve the addition of chemical binders, such as traditional cement, lime, and fly ash or nontraditional polymers, sulfonated oils, resins, and enzymes, to the soil mass, thereby amending the soil fabric into a coherent matrix of restricted heave/settlement and induced strength (e.g., Al-Rawas, Hago, and Al-Sarmi 2005; Mirzababaei, Yasrobi, and Al-Rawas 2009; Thyagaraj and Zodinsanga 2014; Onyejekwe and Ghataora 2015; Alazigha et al. 2016; Jha and Sivapullaiah 2016; Soltani et al. 2017a). The mechanical approach makes use of compaction with the aid of reinforcements. Conventional reinforcements include fibers of synthetic (e.g., polypropylene, steel, and nylon) or natural (e.g., coir and palm) origin (e.g., Cai et al. 2006; Al-Akhras et al. 2008; Viswanadham, Phanikumar, and Mukherjee 2009a, 2009b; Mirzababaei et al. 2013a; Olgun 2013; Estabragh, Rafatjo, and Javadi 2014; Estabragh, Soltani, and Javadi 2016; Phanikumar and Singla 2016; Shahbazi et al. 2017; Mirzababaei et al. 2018, 2017; Soltani, Deng, and Taheri 2018a). As the global community shifts toward a more sustainable mindset, alternate stabilization techniques capable of replacing or minimizing the use of such conventional agents have been highly encouraged. Beneficial reuse of solid waste materials and industrial byproducts may be regarded amongst the most well-received propositions in this context. The proposition not only addresses the expansive soil problem, but also offers a sound solution to minimizing the environmental impacts associated with waste materials.

Discarded tires have become an ongoing environmental crisis, particularly in industrialized countries where tire stockpiles have reached alarming volumes. In Australia, for instance, it is estimated that 48 million tires are disposed of each year, signifying a relative abundance of waste tires available for beneficial reuse (Hannam 2014). Waste tires have excellent mechanical properties (e.g., durability, resiliency, and frictional resistance), which suggests that they are an attractive material for geotechnical applications, such as soil stabilization (Zornberg, Cabral, and Viratjandr 2004). Similar to fiber-reinforced soils, the rubber assemblage randomly distributes in the soil regime, and where optimized in dosage and geometry, could potentially ameliorate the expansive soil with respect to moisture insensitivity (i.e., swell-shrink–related volume changes), compressibility, strength, and ductility (e.g., Edil and Bosscher 1994; Cetin, Fener, and Gunaydin 2006; Akbulut, Arasan, and Kalkan 2007; Seda, Lee, and Carraro 2007; Özkul and Baykal 2007; Dunham-Friel and Carraro 2011; Garcia, Pando, and Tempest 2011; Patil, Valdes, and Evans 2011; Trouzine, Bekhiti, and Asroun 2012; Kalkan 2013; Srivastava, Pandey, and Rana 2014; Signes et al. 2016; Yadav and Tiwari 2017). As such, the rubber-reinforcement mechanism is expected to be primarily a function of rubber content.

However, the rubber's geometrical properties, hereafter referred to as rubber size, could also portray an equally important role in yielding an effective stabilization scheme. The latter should be somewhat similar to the aspect ratio (i.e., fiber length to diameter ratio) in fiber-reinforced soils, which has been well documented in the aforementioned fiber-reinforcement literature (e.g., Estabragh, Rafatjo, and Javadi 2014; Phanikumar and Singla 2016; Soltani, Deng, and Taheri 2018a). With rubbers, however, this aspect has not yet been adequately addressed in the literature (e.g., Cetin, Fener, and Gunaydin 2006; Srivastava, Pandey, and Rana 2014) in what can describe the rubber-reinforcement technique as an ad hoc stabilization solution demanding further examination.

To address the uncertainties associated with selecting effective soil-rubber proportions, this study intends to evaluate the effect of two types of recycled tire rubber of fine and coarse category on the swell-shrink-consolidation behavior of a highly expansive soil mixture. A series of unconfined compression (UC) tests was also carried out, and the results were cross checked with the swell-shrink-consolidation properties to arrive at the optimum stabilization scenarios.

Materials and Methods

EXPANSIVE SOIL

Commercially available kaolinite and bentonite were used for this study. A mixture of 85 % kaolinite and 15 % bentonite was selected as the expansive soil for further experimental work. This mixture, hereafter simply referred to as soil, was characterized as "clay with high plasticity" (CH) in accordance with the Unified Soil Classification System (USCS). The mechanical properties of kaolinite, bentonite, and the kaolinite-bentonite mixture, determined as per relevant ASTM or Australian standards, are summarized in Table 1. The chemical compositions of the kaolinite and bentonite, as supplied by the manufacturer, are provided in Table 2. The free swell ratio for kaolinite, bentonite, and the

TABLE 1

Mechanical properties of kaolinite, bentonite, and the expansive soil.

Properties	Kaolinite	Bentonite	Expansive Soil	Standard Designation
Specific gravity, G_s	2.68	2.81	2.73	ASTM D854 (2014)[a]
Clay (<2 μm) (%)	49.78	62.43	N/A[b]	ASTM D422 (2007)[c]
Silt (2–75 μm) (%)	49.43	35.75	N/A	ASTM D422 (2007)
Sand (0.075–2 mm) (%)	0.79	1.82	N/A	ASTM D422 (2007)
Liquid limit, *LL* (%)	41.04	379.21	59.60	AS 1289.3.9.1 (2015)[d]
Plastic limit, *PL* (%)	23.67	45.18	27.28	AS 1289.3.2.1 (2009)[e]
Plasticity index, *PI* (%)	17.37	334.03	32.32	AS 1289.3.3.1 (2009)[f]
Free swell ratio, *FSR*[g]	1.19	7.53	2.91	Prakash and Sridharan (2004)
USCS classification	CL	CH	CH	ASTM D2487[h] (2011)
Optimum water content, ω_{opt} (%)	19.82	36.34	26.00	ASTM D698[i] (2012)
Maximum dry unit weight, γ_{dmax} (kN/m^3)	15.67	11.74	15.07	ASTM D698 (2012)

Note: [a]ASTM D854, *Standard Test Methods for Specific Gravity of Soil Solids by Water Pycnometer*; [b]not measured; [c]ASTM D422, *Standard Test Method for Particle–Size Analysis of Soils*; [d]AS 1289.3.9.1, *Methods of Testing Soils for Engineering Purposes: Soil Classification Tests–Determination of the Cone Liquid Limit of a Soil*; [e]AS 1289.3.2.1:09, *Methods of Testing Soils for Engineering Purposes: Soil Classification Tests–Determination of the Plastic Limit of a Soil*; [f]AS 1289.3.3.1:09, 2009, *Methods of Testing Soils for Engineering Purposes: Soil Classification Tests–Calculation of the Plasticity Index of a Soil*; [g]ratio of equilibrium sediment volume of 10 gr oven-dried soil passing sieve 425 μm in distilled water to that of kerosene; [h] ASTM D2487, *Standard Practice for Classification of Soils for Engineering Purposes (Unified Soil Classification System)*; [i] ASTM D698, *Standard Test Methods for Laboratory Compaction Characteristics of Soil Using Standard Effort (12,400 ft–lbf/ft^3 (600 kN–m/m^3))*.

TABLE 2
Chemical composition of kaolinite and bentonite (as supplied by the manufacturer).

Properties	Kaolinite	Bentonite
SiO_2 (%)	64.9	63.2
Al_2O_3 (%)	22.2	13.3
TiO_2 (%)	1.4	0.3
Fe_2O_3 (%)	1.0	2.6
CaO (%)	0.1	0.3
Na_2O (%)	0.2	1.9
MgO (%)	0.6	2.2
K_2O (%)	2.7	0.2
Acidity, pH	7.4	9.5
LOI at 1,000°C (%)[a]	6.5	16.0
CEC (meq/100mL)[b]	N/A[c]	82
SSA (m^2/gr)[d]	11.2	N/A

Note: [a]loss on ignition; [b]cation exchange capacity; [c]not available; [d]specific surface area.

kaolinite-bentonite mixture was 1.19, 7.53, and 2.91, from which these soils were graded into "lowly expansive," "very highly expansive," and "highly expansive" with respect to the classification criteria proposed by Prakash and Sridharan (2004), respectively.

TIRE RUBBERS

Two types of commercially available recycled tire rubber, commonly traded as rubber crumbs and rubber buffings (a byproduct of the tire retreading process), were used as reinforcements. Hereafter, these rubber types will be referred to as Rubbers A and B, respectively. The grain size distribution curves for kaolinite, bentonite, and Rubbers A and B, determined as per ASTM D422, *Standard Test Method for Particle–Size Analysis of Soils*, are shown in Fig. 1. Rubber A can be assumed to be similar in size to fine sand, having an average particle size ranging between 1.18 mm and 75 μm ($d_{50} = 0.461$ mm). Rubber B, however, falls into the coarse sand category, having an

FIG. 1
Grain size distribution curves for kaolinite, bentonite, and the tire rubbers.

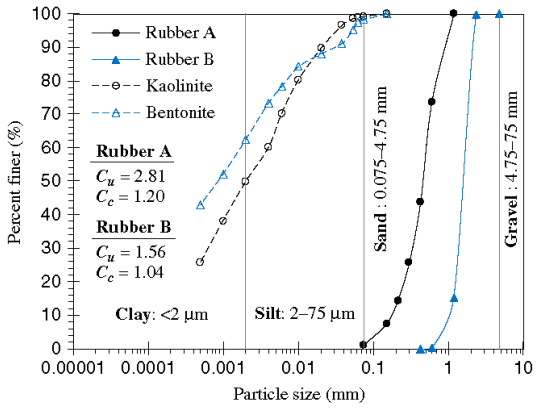

TABLE 3
Physical properties and chemical composition of the tire rubbers (as supplied by the manufacturer).

Properties	Value
Physical Properties	
Solubility in water	Insoluble
Water adsorption	Negligible
Resistance to acid and alkaline	Excellent
Specific gravity at 20°C	1.09
Particle size for Rubber A (mm)	1.18–0.075
Particle size for Rubber B (mm)	4.75–1.18
Softening point (°C)	170
Chemical Composition	
Styrene-butadiene copolymer (%)	55
Acetone extract (%)	5–20
Carbon black (%)	25–35
Zinc oxide (%)	2.5
Sulphur (%)	1–3

average particle size ranging between 4.75 and 1.18 mm ($d_{50} = 1.582$ mm). Both rubber types can be classified as poorly graded sand or SP (in accordance with USCS) corresponding to uniformity and curvature coefficients of $C_u = 2.81$ and $C_c = 1.20$ for Rubber A, and $C_u = 1.56$ and $C_c = 1.04$ for Rubber B. Each of the two rubber choices were incorporated into the soil at four different contents (defined as rubber to dry soil mass ratio), i.e., $R_c = 5$, 10, 20, and 30 %. The physical and chemical properties, as supplied by the manufacturer, along with a photograph (to scale) of the rubber particles are provided in Table 3 and Fig. 2, respectively.

SAMPLE PREPARATION

A series of standard Proctor compaction tests were carried out on the natural soil and various soil-rubber mixtures in accordance with ASTM D698-12e2, *Standard Test Methods for Laboratory Compaction Characteristics of Soil Using Standard Effort (12,400 ft–lbf/ft^3 (600 kN–m/m^3))*, and the results are provided in Fig. 3a and b for Rubbers A and B, respectively. The specific gravity of soil-rubber mixtures, as shown in Fig. 3, was estimated by the theoretical relationship proposed by Trouzine, Bekhiti, and Asroun (2012). Rubber reinforcement led to a noticeable decrease in both the optimum water content ω_{opt} and the maximum dry unit weight γ_{dmax} (see the compaction paths in Fig. 3). The compaction behavior, however, was observed to be independent from the rubber size. Decrease in ω_{opt} and γ_{dmax} can be attributed to the lower specific gravity, specific surface area and water adsorption capacity of rubber particles compared to soil grains (Özkul and Baykal 2007; Kalkan 2013; Signes et al. 2016).

Samples for the swell-shrink-consolidation test (see section under the "Swell-Shrink-Consolidation Test" heading) were prepared by the static compaction technique at dry of optimum condition (i.e., $\omega_0 = \omega_{opt}$–5 % and its corresponding dry unit weight γ_{d0}). The required amount of water corresponding to the desired water content (see ω_0 in Table 4) was added to each mixture and thoroughly mixed by hand. Extensive care was dedicated to pulverizing the lumped particles, targeting homogeneity of mixtures. Mixtures were then enclosed in plastic bags and stored under room temperature conditions for 24 hours, ensuring even distribution of moisture throughout the soil mass.

FIG. 2

Tire rubbers at 50× magnification: (a) Rubber A and (b) Rubber B.

(a)

(b)

A special split mold, similar to that described in Soltani et al. (2017b), was designed and fabricated from stainless steel to accomplish static compaction. The mold consisted of three sections, i.e., the top collar, the middle oedometer ring, and the bottom collar. The oedometer ring measures 50 mm in diameter and 20 mm in height, and it accommodates the sample for the swell-shrink-consolidation test. The mixtures were gradually compressed in the mold in three layers to a specific compaction load, each layer having attained the target dry unit weight (see γ_{d0} in Table 4). The inner surface of the mold was smeared with a thin layer of silicon grease to avoid friction during compaction. The surface of the first and second compacted layers were scarified to ensure a good bond between adjacent layers of the mixture. Samples for the UC test (see the section under the "UC Test" heading) were prepared in a similar fashion. In this case, however, a different mold, resulting in samples measuring 50 mm in diameter and 100 mm in height, along with five compaction layers was adopted. In addition, the UC samples were prepared at optimum condition (see ω_{opt} and γ_{dmax} in Table 4). Mechanical properties of the prepared samples, including the consistency limits and the initial placement conditions, are summarized in Table 4. For natural soils, the optimum water content ω_{opt} can be estimated by means of the plastic limit PL through $\omega_{opt} = 0.92PL$ (Gurtug and Sridharan 2002, 2004; Sridharan and Nagaraj 2005). Interestingly, the same holds true for various soil-rubber mixtures (see Table 4).

FIG. 3

Standard Proctor compaction curves for the natural soil and various soil-rubber mixtures: (a) Rubber A and (b) Rubber B.

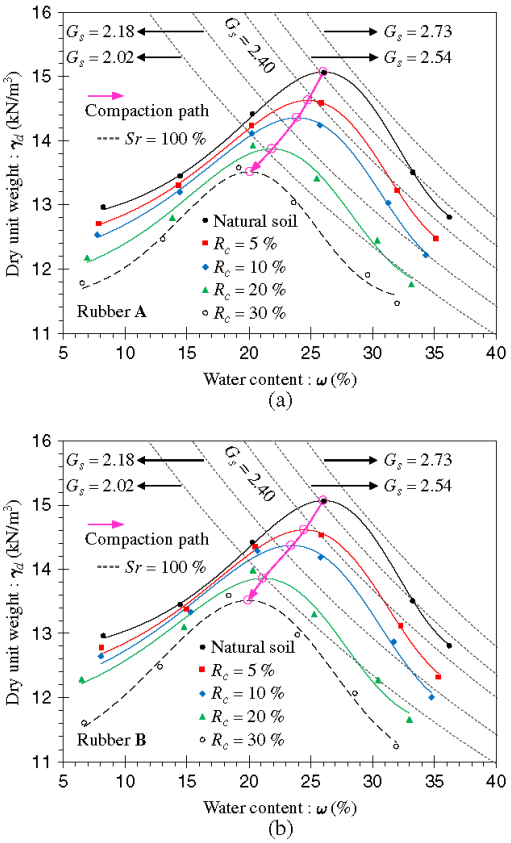

TABLE 4

Mechanical properties of the prepared samples.

Rubber Type	R_c (%)	G_s	LL (%)	PL (%)	PI (%)	ω_{opt} (%)	0.92PL (%)[1]	γ_{dmax} (kN/m^3)	e_{opt}[2]	ω_0 (%)	γ_{d0} (kN/m^3)	e_0[3]
–	0	2.73	59.60	27.28	32.32	26.00	25.10	15.07	0.775	21.00	14.52	21.00
Rubber A	5	2.54	57.03	27.02	30.01	24.77	24.86	14.63	0.706	19.77	14.16	19.77
	10	2.40	55.04	25.54	29.50	23.87	23.50	14.35	0.639	18.87	13.90	18.87
	20	2.18	51.51	23.46	28.05	21.85	21.58	13.87	0.541	16.85	13.40	16.85
	30	2.02	49.58	22.70	26.88	20.07	20.88	13.52	0.469	15.07	12.92	15.07
Rubber B	5	2.54	56.88	26.61	30.27	24.47	24.48	14.61	0.709	19.47	14.15	19.47
	10	2.40	55.62	24.77	30.85	23.46	22.79	14.37	0.638	18.46	13.94	18.46
	20	2.18	52.44	23.27	29.17	21.15	21.41	13.86	0.543	16.15	13.43	16.15
	30	2.02	51.21	22.15	29.06	19.94	20.38	13.52	0.469	14.94	12.99	14.94

Note: [1]predicted optimum water content; [2]initial placement condition for UC tests; [3]initial placement condition for swell-shrink-consolidation tests.

TEST PROCEDURE

Swell-Shrink-Consolidation Test

Samples were subjected to a series of swell-shrink-consolidation tests. A typical illustration of the test scheme is provided in Fig. 4. The swell-consolidation phase, carried out in accordance with ASTM D4546, *Standard Test Methods for One–Dimensional Swell or Collapse of Soils*, includes two stages, i.e., swell and consolidation. In the first stage, the desired sample is allowed to freely swell under a low nominal overburden stress of $\sigma'_0 = 1$ kPa. The incurred swelling strain was recorded during various time intervals to a point in which swell-time equilibrium, a state corresponding to the sample's swelling potential (defined as the ultimate swelling strain), could be achieved (see Path O→A in Fig. 4a). During consolidation, the swollen sample, now at State A, is gradually loaded to counteract the built-up swelling strain. The stress required to retain the sample's initial placement or void ratio is taken as the swelling pressure (Sridharan, Rao, and Sivapullaiah 1986). Upon completion of the loading scheme, the sample is gradually unloaded back to $\sigma'_0 = 1$ kPa (see Path A→B_1 for loading, and Path B_1→C for unloading in Fig. 4b). Test

FIG. 4 A typical illustration of the swell-shrink-consolidation test scheme: (a) swell path, (b) consolidation path, and (c) shrink path.

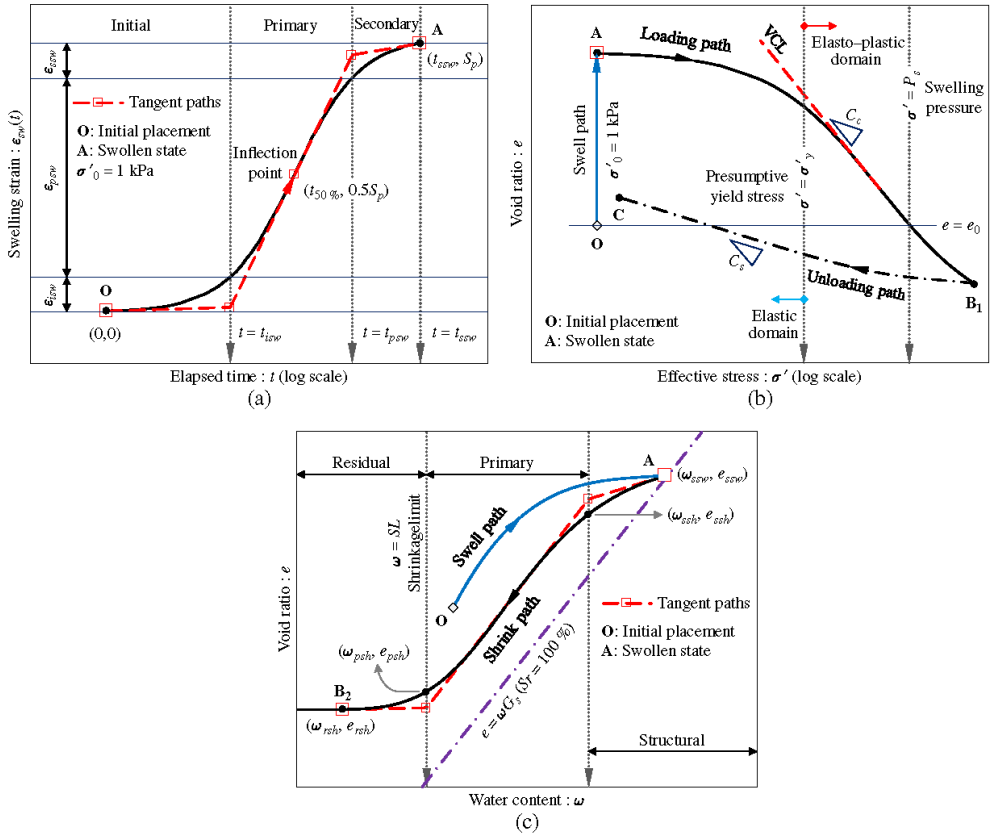

results are presented in the form of swelling strain-time (for the swell stage) and void ratio–effective stress (for the consolidation stage) curves plotted over a semilog space (see Fig. 4a and b, respectively).

The swell-shrink phase also consists of two stages, i.e., swell and shrink. The swell component is essentially similar to that described in the swell-consolidation test. During the shrink stage, the swollen sample, now at State A, is allowed to desiccate under a constant temperature of 40°C. The volumetric shrinkage strain along with the corresponding water content was directly measured during various time intervals to a point in which shrinkage ceases (see Path A→B_2 in Fig. 4c). The volumetric shrinkage strain was measured by the volume displacement technique outlined in ASTM D427, *Test Method for Shrinkage Factors of Soils by the Mercury Method*, which has also been commonly adopted in the literature (e.g., Sibley and Williams 1989; Hanafy 1991; Subba Rao, Rao, and Gangadhara 2000; Tripathy, Subba Rao, and Fredlund 2002; Tripathy and Subba Rao 2009). For the shrink stage, test results are presented in the form of void ratio–water content curves plotted over an arithmetic space (see Fig. 4c).

UC Test

The UC test was carried out in accordance with ASTM D2166, *Standard Test Method for Unconfined Compressive Strength of Cohesive Soil*. The samples were compressed by a constant displacement rate of 1 %/min, as commonly adopted in the literature (e.g., Ang and Loehr 2003; Fatahi, Khabbaz, and Fatahi 2012; Signes et al. 2016). To ensure sufficient accuracy, triplicate samples were tested for each scenario. Axial stress and its corresponding axial strain were recorded during various loading stages to a point in which maximum axial stress required for sample failure, denoted as q_u, and its corresponding axial strain, denoted as ε_u, could be achieved. The area under the stress-strain curve up to q_u and ε_u—a measure of the material's toughness defined as strain energy at peak E_p (Maher and Ho 1994; Mirzababaei et al. 2013b)—was also obtained for the tested samples.

Results and Discussion

EFFECT OF RUBBERS ON THE SWELLING POTENTIAL

Swelling strain-time curves, represented by the two-parameter rectangular hyperbola function (e.g., Dakshanamurthy 1978; Sivapullaiah, Sridharan, and Stalin 1996; Sridharan and Gurtug 2004), for the natural soil and various soil-rubber composites are provided in Fig. 5a and b for Rubbers A and B, respectively. As a result of rubber reinforcement, the swelling strain-time locus experienced a major downward shift over the ε_{sw}:log$t$ space (ε_{sw} = swelling strain, and t = time), indicating a significant reduction in the magnitude of exhibited swelling strain, and thus swelling potential (defined as the ultimate swelling strain) compared to the natural soil. At t = 24 hours, for instance, the natural soil displayed a swelling strain of $\varepsilon_{sw}(t)$ = 15.23 %, while the inclusion of 5, 10, 20, and 30 % Rubber A resulted in $\varepsilon_{sw}(t)$ = 14.99, 11.82, 9.01, and 7.67 %, respectively (see Fig. 5a). Similar inclusions of Rubber B, however, exhibited a slightly more pronounced decreasing trend where the above given values dropped to $\varepsilon_{sw}(t)$ = 13.67, 11.44, 8.01, and 7.21 %, respectively (see Fig. 5b). The natural soil and soil-Rubber A mixtures corresponding to R_c = 5, 10, 20, and 30 % resulted in swelling potential values of S_p = 18.35, 16.02, 13.01, 11.17, and 9.56 %, respectively. For similar inclusions of Rubber B, these values further decreased to S_p = 14.74, 12.18, 9.02, and 8.11 %, respectively.

FIG. 5

Swelling strain-time curves for the natural soil and various soil-rubber composites: (a) Rubber A and (b) Rubber B.

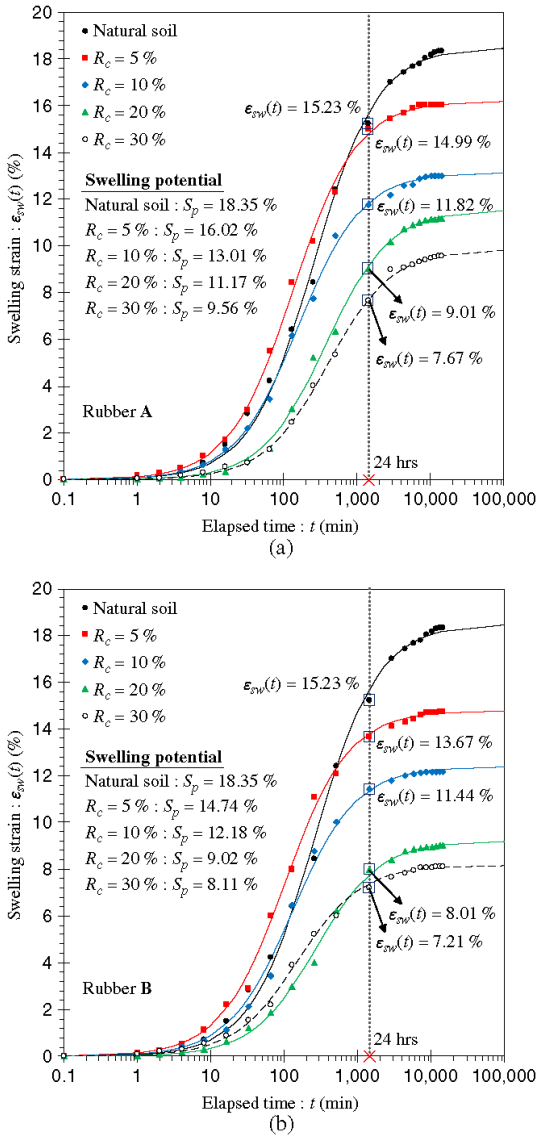

A typical swell path (see Path O→A in Fig. 4a), plotted over a semilog space, develops into an *S*-shaped curve, and thus can be divided into three regions, i.e., the initial, primary, and secondary swelling, which are defined as phases during which swelling takes place (Dakshanamurthy 1978; Sivapullaiah, Sridharan, and Stalin 1996; Sridharan and Gurtug 2004; Rao, Thyagaraj, and Thomas 2006; Soltani et al. 2017b). The initial swelling

phase, also recognized as intervoid or intercrystalline swelling, rapidly evolved at a macrostructural level and is accompanied by small volume changes (i.e., $\varepsilon_{isw} \leq 0.1S_p$). The primary swelling phase constitutes up to 80 % of the total volume increase (i.e., $\varepsilon_{psw} \approx 0.8S_p$) and is graphically bound by the initial and primary swelling time margins (see Fig. 4a). The secondary swelling phase occurs as a result of double-layer repulsion, which results in small time-dependent volume changes. In comparison to initial swelling, both the primary and secondary swelling phases evolve at a microstructural level where the swelling of active minerals takes place. Critical variables obtained from the *S*-shaped swell curve are useful concepts capable of describing the time-dependent nature of the swelling phenomenon under field conditions (Sridharan and Gurtug 2004). These variables, defined by a conventional graphical construction, as depicted in Fig. 4a, can be categorized as follows:

- Completion time of the initial and primary swelling phases, i.e., t_{isw} and t_{psw}.
- Initial, primary, and secondary swelling strains, i.e., ε_{isw}, ε_{psw}, and ε_{ssw}, where $S_p = \varepsilon_{isw} + \varepsilon_{psw} + \varepsilon_{ssw}$.
- Primary and secondary swelling rates, i.e., C_{psw} and C_{ssw}, which are defined as follows:

$$C_{psw} = \frac{\Delta \varepsilon_{sw}}{\Delta \log t}\Bigg]_{t_{isw}}^{t_{psw}} = \frac{\varepsilon_{psw}}{\log\left(\frac{t_{psw}}{t_{isw}}\right)} \tag{1}$$

$$C_{ssw} = \frac{\Delta \varepsilon_{sw}}{\Delta \log t}\Bigg]_{t_{psw}}^{t_{ssw}} = \frac{\varepsilon_{ssw}}{\log\left(\frac{t_{ssw}}{t_{psw}}\right)} \tag{2}$$

where t_{ssw} = completion time of the secondary swelling phase (≈240 hours).

Fig. 6a and b illustrates the variations of C_{psw} and C_{ssw} against rubber content for the tested samples, respectively. The rubber inclusions led to a noticeable reduction in C_{psw} and C_{ssw}, indicating a capacity to counteract the heave in both magnitude and time. The greater the rubber content, the greater the decrease in C_{psw} following a monotonic trend. Rubber contents greater than 5 %, however, did not further deviate C_{ssw}. Rubber B consistently outperformed Rubber A by exhibiting lower swelling rates for similar rubber inclusions. The natural soil resulted in $C_{psw} = 8.38 \times 10^{-2}$ and $C_{ssw} = 2.56 \times 10^{-2}$. As a typical case, these values, respectively, dropped to 5.89×10^{-2} and 1.54×10^{-2} for Rubber A, and 5.58×10^{-2} and 1.19×10^{-2} for Rubber B where $R_c = 10$ %.

EFFECT OF RUBBERS ON THE CONSOLIDATION BEHAVIOR

Void ratio–effective stress consolidation curves for the natural soil and various soil-rubber composites are provided in Fig. 7a and b for Rubbers A and B, respectively. A typical consolidation curve with respect to the loading stage (see Path A→B_1 in Fig. 4b), plotted over a semilog space, develops into a two-segment curvilinear relationship and thus can be divided into two regions, i.e., the elastic and elastoplastic compression, which are defined as phases during which consolidation takes place (Sridharan, Abraham, and Jose 1991). The two regions are separated by the yield stress, which is commonly interpreted by means of conventional graphical constructions implemented to the e–logσ' or log$e$–logσ' curve (e = void ratio and σ' = effective stress). Recently, the authors have proposed a subjective-free framework for determination of the yield stress with respect to four common graphical constructions, i.e., the maximum curvature method (Casagrande 1936), the Silva method (Pacheco Silva 1970), the recompression line–virgin compression line (VCL)

FIG. 6

Variations of the (a) primary and (b) secondary swelling rates against rubber content for the tested samples.

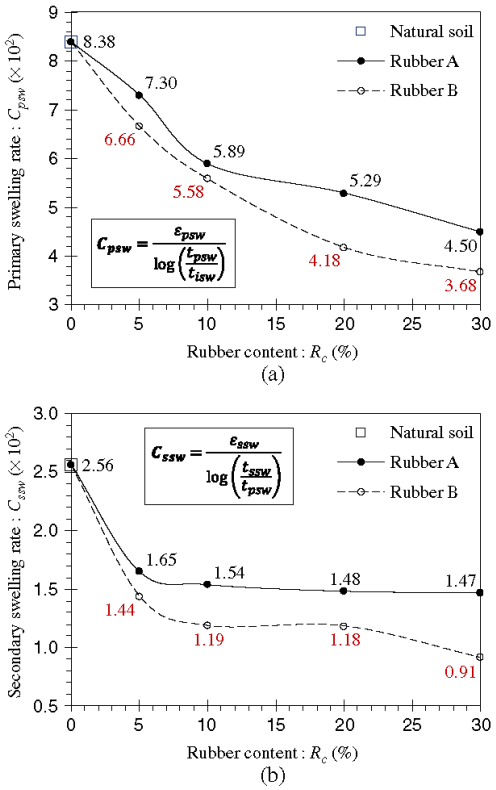

intercept method, and the log-log method (Jose, Sridharan, and Abraham 1989; Sridharan, Abraham, and Jose 1991). Adopting the proposed framework in Soltani et al. (2018b), the average of the four graphical constructions was calculated for each sample, and the results are provided in the form of yield stress paths in Fig. 7. Rubber reinforcement led to a slight increase in the yield stress. Natural soil exhibited a yield stress of $\sigma'_y = 17.73$ kPa. Maximum increase in σ'_y was observed in the case of 30 % rubber inclusion, which resulted in $\sigma'_y = 23.42$ and 22.10 kPa for Rubbers A and B, respectively.

Fig. 8a and b illustrates the variations of the compression index C_c (= slope of the VCL in Fig. 4b) and the swell index C_s (= slope of the unloading Path $B_1 \rightarrow C$ in Fig. 4b) against rubber content for the tested samples, respectively. The rubber inclusions led to a noticeable reduction in C_c and C_s, indicating a capacity of counteracting material collapse when stressed. The greater the rubber content, the lower the C_c and C_s values following a monotonic trend. Rubber B often outperformed Rubber A in terms of lower C_c values. Regarding C_s, however, the performance of both rubber types seemed to be on par with each other. The natural soil resulted in $C_c = 0.249$ and $C_s = 0.136$. As a typical case, these values, respectively, dropped to 0.191 and 0.087 for Rubber A, and 0.187 and 0.078 for Rubber B, where $R_c = 20$ %.

FIG. 7

Void ratio–effective stress consolidation curves for the natural soil and various soil-rubber composites: (a) Rubber A and (b) Rubber B.

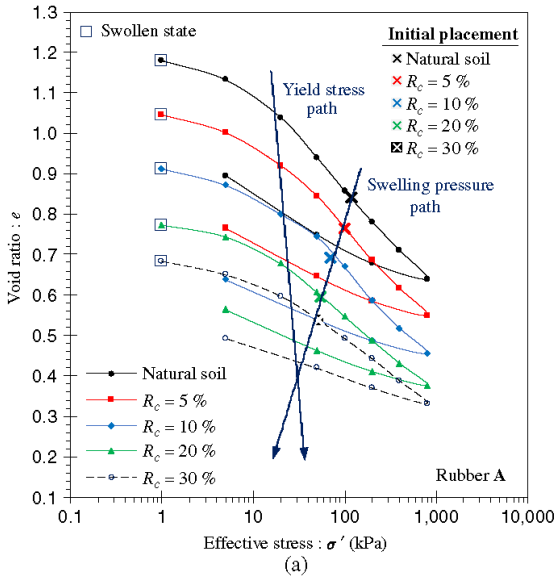

(a)

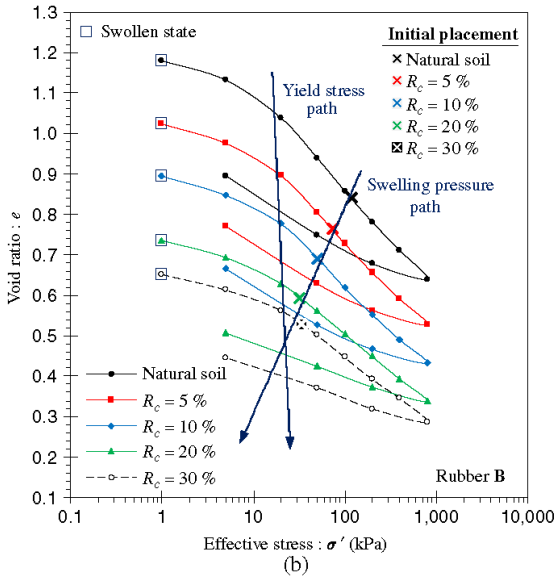

(b)

Rubber reinforcement altered the void ratio–effective stress locus, resulting in a major downward shift over the e:logσ' space. As a result, major variations were observed in the swelling pressure (see the swelling pressure paths in Fig. 7). Fig. 9 illustrates the variations

FIG. 8

Variations of the (a) compression and (b) swell indexes against rubber content for the tested samples.

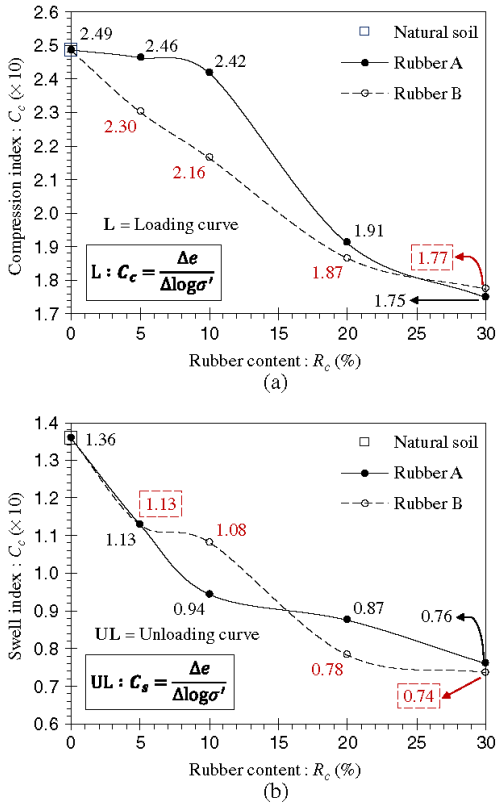

FIG. 9

Variations of swelling pressure and swelling potential against rubber content for the tested samples.

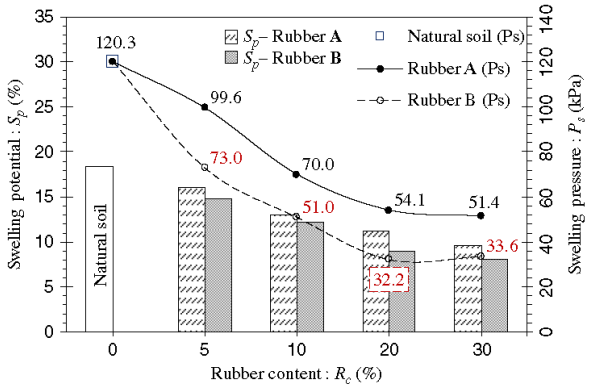

of swelling pressure and swelling potential against rubber content for the tested samples. The variations of swelling pressure P_s followed a trend quite similar to that of swelling potential S_p, indicating that the greater the rubber content, the greater the decrease in S_p and P_s. For P_s, however, $R_c = 30$ % and promoted similar results to $R_c = 20$ % with marginal differences, indicating a maximum rubber inclusion of 20 % that is sufficient to counteract the swelling properties. Similar to S_p, soil-Rubber B mixtures consistently outperformed similar samples reinforced with Rubber A. The natural soil and soil-rubber mixtures corresponding to $R_c = 5$, 10, 20, and 30 % resulted in $P_s = 120.3$, 99.6, 70.0, 54.1, and 51.4 kPa, respectively. With Rubber B, these values dropped to $P_s = 73.0$, 51.0, 32.2, and 33.6 kPa, respectively.

The secondary consolidation characteristics were studied under an effective stress of $\sigma' = 50$ kPa, and the results are provided in Fig. 10. The completion time of the primary consolidation stage t_{pc} decreased because of the inclusion of Rubber A (see Fig. 10a). This effect, however, was less apparent for samples reinforced with Rubber B, which essentially did not deviate t_{pc} (see Fig. 10b). The secondary consolidation rate C_{sc} can be defined as follows:

$$C_{sc} = \frac{\Delta \varepsilon_c}{\Delta \log t}\Bigg]_{t_{pc}}^{t_{sc}} = \frac{\varepsilon_{sc}}{\log\left(\frac{t_{sc}}{t_{pc}}\right)} \tag{3}$$

where $\varepsilon_c(t)$ = compression strain with respect to elapsed time t; ε_{sc} = secondary consolidation strain; and t_{sc} = completion time of the secondary consolidation stage (= 24 hours).

As a result of rubber reinforcement, the secondary consolidation rate exhibited a noticeable decreasing trend, indicating a capacity to counteract the settlement in both magnitude and time. The natural soil resulted in $C_{sc} = 7.28 \times 10^{-3}$. Where reinforced with 5, 10, 20, and 30 % Rubber A, C_{sc} dropped to 6.05×10^{-3}, 5.57×10^{-3}, 5.34×10^{-3}, and 5.02×10^{-3}, respectively. Similar inclusions of Rubber B, however, promoted slightly greater values, while still maintaining a noticeable advantage over the natural soil. In this case, $R_c = 5$, 10, 20, and 30 % resulted in $C_{sc} = 6.74 \times 10^{-3}$, 6.68×10^{-3}, 5.88×10^{-3}, and 4.94×10^{-3}, respectively. It is noteworthy to cross check the resulting trends for C_{sc} with C_{ssw}, which are expected to be somewhat consistent and comparable (Sridharan and Gurtug 2004; Phanikumar and Singla 2016).

EFFECT OF RUBBERS ON THE SHRINKAGE POTENTIAL

Void ratio–water content shrinkage curves, represented by the four-parameter logistic function (e.g., McGarry and Malafant 1987; Peng and Horn 2005; Thyagaraj, Thomas, and Das 2017), along with corresponding 100 % saturation lines, for the natural soil and various soil-rubber composites, are provided in Fig. 11a and b for Rubbers A and B, respectively. The four-parameter logistic function can be given as follows:

$$e(\omega) = e_{rsh} + \frac{e_{ssw} - e_{rsh}}{1 + \left(\frac{\omega}{\alpha}\right)^{-\beta}} \tag{4}$$

where e_{ssw} = void ratio at the swollen state A (i.e., the end of secondary swelling, as shown in Fig. 4c); e_{rsh} = void ratio at the fully desiccated state B_2 (see Fig. 4c); and α and β = fitting parameters (α and $\beta > 0$).

Similar to the swell path, a typical shrink path (see Path O→B_2 in Fig. 4c) develops into an S-shaped curve and thus can be divided into three regions, i.e., the structural,

FIG. 10

Secondary consolidation characteristics (under $\sigma' = 50$ kPa) for the natural soil and various soil-rubber composites: (a) Rubber A and (b) Rubber B.

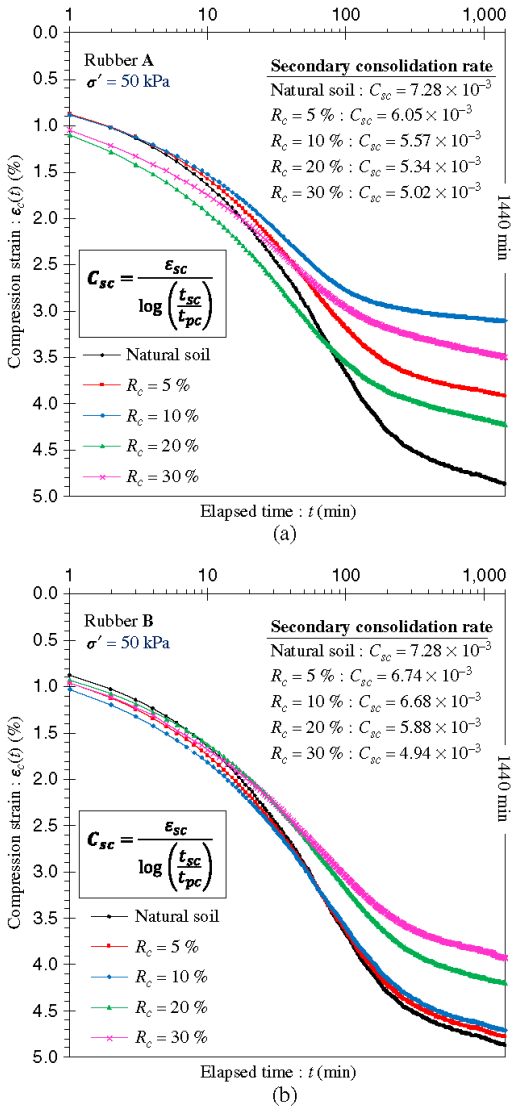

primary, and residual shrinkage, which are defined as phases during which shrinkage takes place (Haines 1923; Tripathy, Subba Rao, and Fredlund 2002; Cornelis et al. 2006; Estabragh, Moghadas, and Javadi 2013; Estabragh, Parsaei, and Javadi 2015). In the structural shrinkage phase, the decrease in volume of the soil is less than the volume of water lost from the stable void spaces. This portion of the shrinkage curve constitutes for small

FIG. 11

Void ratio–water content shrinkage curves for the natural soil and various soil-rubber composites: (a) Rubber A and (b) Rubber B.

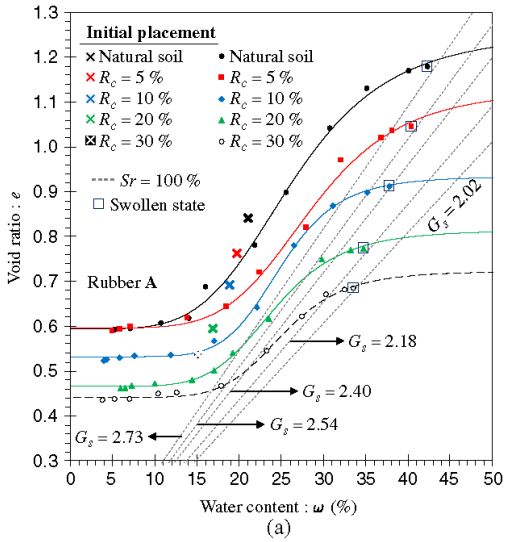

volume changes and is graphically represented by a mildly sloped curvilinear relationship. During primary shrinkage, also commonly referred to as normal shrinkage, the decrease in volume of the soil is essentially equal to the volume of lost water, thereby preventing the entrance of air into the soil pores. This portion of the shrinkage curve is represented by a steep sloped linear relationship, which is theoretically parallel to the $Sr = 100$ % saturation line. The primary shrinkage phase extends up to the shrinkage limit, which marks a

transitional state where the rate of volume change rapidly decreases, i.e., $\Delta e/\Delta\omega \rightarrow 0$. The majority of volume decrease takes place during the primary shrinkage phase. Completion of the primary shrinkage phase is further accompanied by residual shrinkage, where the entrance of air is allowed into the soil pores, thereby resulting in air-filled porosity. As a consequence of particles coming in contact, the decrease in volume of the soil becomes less than the volume of lost water. The magnitude of structural, primary, and residual shrinkage strains, i.e., ε_{ssh}, ε_{psh}, and ε_{rsh}, can be obtained by the following relationships (Mishra, Dhawan, and Rao 2008; Thyagaraj, Thomas, and Das 2017):

$$\varepsilon_{ssh} = \frac{\Delta e}{1 + e_{ssw}}\Bigg]_{e_{ssh}}^{e_{ssw}} = \frac{e_{ssw} - e_{ssh}}{1 + e_{ssw}} \tag{5}$$

$$\varepsilon_{psh} = \frac{\Delta e}{1 + e_{ssh}}\Bigg]_{e_{psh}}^{e_{ssh}} = \frac{e_{ssh} - e_{psh}}{1 + e_{ssh}} \tag{6}$$

$$\varepsilon_{rsh} = \frac{\Delta e}{1 + e_{psh}}\Bigg]_{e_{rsh}}^{e_{psh}} = \frac{e_{psh} - e_{rsh}}{1 + e_{psh}} \tag{7}$$

where, as outlined in Fig. 4c, e_{ssw} = void ratio at the swollen state A (i.e., the end of secondary swelling); e_{ssh} = void ratio at the end of structural shrinkage; e_{psh} = void ratio at the end of primary shrinkage (or at the shrinkage limit); and e_{rsh} = void ratio at the fully desiccated state B_2.

The total shrinkage strain, denoted as the shrinkage potential, can be defined as $SH_p = \varepsilon_{ssh} + \varepsilon_{psh} + \varepsilon_{rsh}$. The shrinkage strains and the shrinkage limit for the tested samples are presented in Table 5. The shrinkage strains demonstrated a rubber content dependency, meaning that the greater the rubber content, the lower the shrinkage strains. The effect of rubber size, however, was observed to be marginal for the majority of cases. The shrinkage potential demonstrated a trend similar to that observed for the swelling potential. The natural soil displayed a shrinkage potential of $SH_p = 28.60$ %. Soil-Rubber A mixtures corresponding to $R_c = 5$, 10, 20, and 30 % resulted in $SH_p = 23.44$, 21.30, 18.27, and 15.30 %, respectively. Similar inclusions of Rubber B promoted slightly lower values and were measured as $SH_p = 24.61$, 20.44, 16.01, and 14.04 %, respectively. As a result of rubber reinforcement, the shrinkage limit experienced a minor increase; however, the resulting variations were observed to be less dependent on rubber content and

TABLE 5

Shrinkage strains and the shrinkage limit for the tested samples.

Rubber Type	R_c (%)	ε_{ssh} (%)	ε_{psh} (%)	ε_{rsh} (%)	SH_p (%)	SL (%) [1]
–	–	4.15	21.47	2.98	28.60	14.88
Rubber A	5	2.99	17.50	2.95	23.44	17.82
	10	3.07	15.53	2.71	21.30	18.00
	20	2.49	13.62	2.15	18.27	16.25
	30	2.01	11.24	2.06	15.30	17.86
Rubber B	5	3.54	18.16	2.92	24.61	17.67
	10	2.43	15.33	2.68	20.44	16.40
	20	1.83	12.33	1.85	16.01	15.16
	30	1.86	10.43	1.75	14.04	15.18

Note: [1]shrinkage limit.

rubber size. The shrinkage limit is primarily a result of the "packing phenomenon" (i.e., optimal packing of soil particles during drying), which in turn is governed by the grain size distribution of the soil. As the soil's gradation becomes more and more uniform/poor (reduced packing capacity), the shrinkage limit tends to increase (Sridharan and Prakash 1998). The rubber particles used in this study are both classified as SP sand (see Fig. 1). As such, the addition of the poorly graded rubber to the well-graded soil offsets the well-distributed gradation of the host soil and thus gives rise to higher shrinkage limits. Consequently, this mechanism is expected to be in line with rubber content. The greater the rubber content, the more uniform/poor the grain size distribution, and thus the higher the shrinkage limit.

EFFECT OF RUBBERS ON THE STRENGTH PROPERTIES

Stress-strain curves obtained from the UC tests for the natural soil and various soil-rubber composites are provided in Fig. 12a and b for Rubbers A and B, respectively. The natural soil displayed a peak strength of $q_u = 113$ kPa, while the inclusion of 5 % Rubbers A and B resulted in $q_u = 129$ and 142 kPa, respectively. With $R_c = 10$ %, q_u dropped to 128 kPa

FIG. 12

Stress-strain UC curves for the natural soil and various soil-rubber composites: (a) Rubber A and (b) Rubber B.

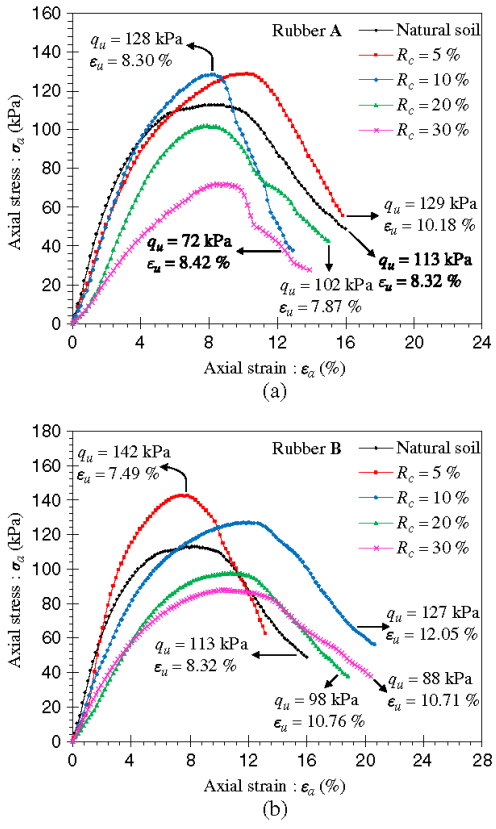

FIG. 13

Variations of strain energy at peak, and the peak strength against rubber content for the tested samples.

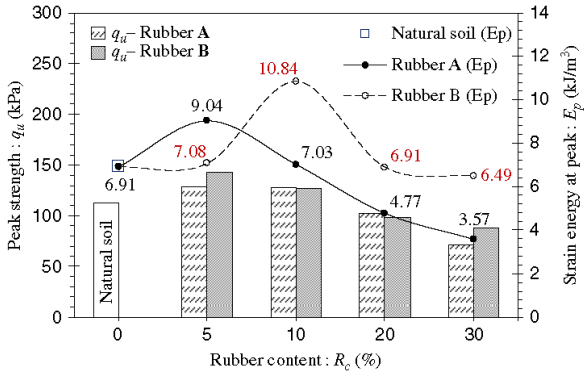

(for Rubber A) and 127 kPa (for Rubber B), which still maintains a noticeable advantage over the natural soil. Higher rubber inclusions, i.e., 20 and 30 %, however, gave rise to lower q_u values compared to that observed for the natural soil (i.e., $q_u = 102$ and 98 kPa for 20 % Rubbers A and B; and $q_u = 72$ and 88 kPa for 30 % Rubbers A and B). It is noteworthy to cross check q_u with S_p, P_s, and SH_p, which are in favor of a higher rubber content. This discrepancy implies that even though the rubbers are consistently effective at weaving the soil into a coherent matrix of restricted heave and settlement, when excessively included, they raise strength concerns.

Fig. 13 illustrates the variations of strain energy at peak E_p along with corresponding q_u values against rubber content for the tested samples. The variations of E_p followed a trend quite similar to that observed for q_u. A noticeable improvement in the toughness can be achieved for rubber inclusions equal to or less than 10 %, while the higher rubber inclusions of 20 and 30 % gave rise to less toughness. Although in terms of q_u, the performance of both rubber types seemed to be on par with each other, soil-Rubber B mixtures consistently (with the exception of $R_c = 5$ %) promoted a higher toughness (i.e., higher E_p) compared to similar samples reinforced with Rubber A. As optimum cases, E_p increased from 6.91 kJ/m^3 for the natural soil to 9.04 and 10.84 kJ/m^3 for the samples reinforced with 5 % Rubber A and 10 % Rubber B, respectively. The elastic stiffness modulus E_{50}, defined as the secant modulus at 50 % of the peak strength (Radovic, Lara-Curzio, and Riester 2004; Iyengar et al. 2013), was also measured for the tested samples. In general, the greater the rubber content, the lower the E_{50} value following a monotonic decreasing trend. Except for 5 % Rubber B, all samples exhibited a lower E_{50} compared to the natural soil. The natural soil resulted in $E_{50} = 3.15$ MPa, while the inclusion of 5, 10, 20, and 30 % Rubber A resulted in $E_{50} = 2.47$, 2.56, 1.69, and 1.15 MPa, respectively. Similar inclusions of Rubber B did not significantly deviate from the aforementioned values (an exception was $R_c = 5$ %) and resulted in $E_{50} = 3.27$, 2.19, 1.45, and 1.59 MPa2, respectively.

AMENDING MECHANISMS

Similar to fiber-reinforced soils, the rubber inclusions are able to amend the soil fabric through improvements achieved in three aspects, i.e., increase in nonexpansive fraction

or nonwetting attribute (Viswanadham, Phanikumar, and Mukherjee 2009a; Patil, Valdes, and Evans 2011; Trouzine, Bekhiti, and Asroun 2012; Estabragh, Rafatjo, and Javadi 2014; Soltani, Deng, and Taheri 2018a), interlocking of rubber particles and soil grains (Tang et al. 2007, Tang, Shi, and Zhao 2010; Kalkan 2013; Phanikumar and Singla 2016; Soltani, Deng, and Taheri 2018a), and frictional resistive forces were generated as a result of soil-rubber contact (Cai et al. 2006; Al-Akhras et al. 2008; Viswanadham, Phanikumar, and Mukherjee 2009b; Patil, Valdes, and Evans 2011; Trouzine, Bekhiti, and Asroun 2012; Phanikumar and Singla 2016). The randomly distributed rubber particles resemble a spatial three-dimensional network in favor of weaving or interlocking the soil grains into a coherent matrix of restricted heave and settlement. The greater the number of included rubber particles, i.e., increase in rubber content, the more effective the interlocking effect. The frictional resistive forces grow as a consequence of rubber particles experiencing tensile/compressive stress in the presence of strong swelling/compression forces. Increases in rubber content leads to an increase in the total surface area, and thus a greater interfacial contact between rubber particles and soil grains. This in turn enhances the frictional effect between rubber particles, thereby mitigating the swell-shrink-consolidation capacity.

The swell-shrink-consolidation dependence on rubber size (or shape) is on par with the aspect ratio (i.e., fiber length-to-diameter ratio) in fiber-reinforced soils, and thus can be ascribed to the improvement mechanisms' interlocking and frictional resistive forces. Increase in rubber size increases the soil-rubber contact, which in turn generates a greater net frictional resistance between rubbers coupled with an enhanced soil-rubber interlocking effect. This improvement mechanism is also in line with rubber shape. As opposed to the granular form of Rubber A, the particles of Rubber B are relatively more fiber shaped (see **Fig. 2**); hence, they are more resilient to withstand (or translate) tensile/compressive stress along their axis, which, in turn, restricts the movement of soil particles interlocked to the rubber.

Optimum Rubber Content and Cost Analysis

The primary objective of any introduced stabilization scheme dealing with expansive soils should complement a decrease in the swell-shrink-consolidation capacity while either maintaining or improving the strength-related properties (Soltani 2017). Although both rubber types are consistently effective at weaving the soil into a coherent matrix of restricted heave and settlement (i.e., improvement in the swell-shrink-consolidation capacity is in favor of higher rubber contents), when excessively included they raise strength concerns. Based on the results presented in the first four sections under the "Results and Discussion" heading, a maximum rubber inclusion of 10 % seems to satisfy both objectives and thus can be deemed as the optimum choice. Where context changes and the strength and stiffness are not the primary concerns, higher rubber inclusions up to 20 % may also be considered acceptable. The swell-shrink-consolidation properties were rubber-size dependent, meaning that the rubber with a coarser size often outperformed the finer rubber. In terms of strength, however, the two rubber types promoted similar results with marginal differences. Therefore, the choice of rubber size would be dependent on design requirements/project objectives, rubber availability, and costs.

Table 6 summarizes a comparative cost analysis performed for the reinforcement of an assumed mass of 1,000 kg of soil using recycled tire rubbers and conventional polyester, polyethylene, or polypropylene fibers. The unit price for both rubber types and poly fibers

TABLE 6
Comparative cost analysis between rubbers and conventional fibers.

Type of Reinforcement	R_c (%)	f_c (%)[a]	Unit Price (AU$/kg)	Total Cost (AU$)
Rubber (A or B)	5	–	0.5	25.0
	10	–		50.0
	20	–		100.0
Poly- (ester, ethylene or propylene) fiber	–	0.8[b]	14.3	114.4
	–	1.5[c]		214.5

Note: [a]fiber content (i.e., fiber to dry soil mass ratio); [b]suggested by Olgun (2013) and Shahbazi et al. (2017); [c]suggested by Estabragh, Rafatjo, and Javadi (2014) and Soltani et al. (2017b).

were taken in accordance with common prices found in South Australian markets, which are approximately 0.5 and 14.3 AU$/kg, respectively. Other costs, such as transportation, labor, and compaction, have not been included as they are highly case and region dependent. Significant cost reduction can be achieved when rubbers are used as a replacement for conventional fibers. For instance, $R_c = 10$ % results in a total cost of 50 AU$, while the use of poly fibers at their so-called optimum contents, i.e., $f_c = 0.8$ and 1.5, results in 114.4 and 214.5 AU$, respectively. Unlike fibers, the rubber-reinforcement technique requires a large quantity of rubber material to ameliorate the swell-shrink-consolidation capacity. However, in terms of total cost, it still maintains a significant advantage over conventional fibers. More importantly, beneficial reuse of recycled tires provides a sound environmental alternative to the safe disposal concern that is associated with such waste materials. The results of the cost analysis are in agreement with Yadav and Tiwari (2017), who carried out a similar comparative analysis with respect to the Indian market.

Conclusions

The following conclusions can be drawn from this study:

- As a result of rubber reinforcement, the swelling strain-time locus experienced a major downward shift over the semilog space, signifying a capacity to counteract the heave in both magnitude and time. Improvement in the rate and potential of swelling was dependent on both the rubber content and the rubber size, with the former taking on a more pronounced role. A similar dependency was also observed for the shrinkage potential. In this case, however, the effect of rubber size was observed to be marginal for the majority of cases.
- Rubber reinforcement altered the void ratio–effective stress consolidation locus, resulting in a significant reduction in the swelling pressure. The variations of swelling pressure suggested a trend similar to that of swelling potential. In addition, the rubber inclusions led to a noticeable reduction in the compression and swell indexes, indicating a capacity to counteract material collapse when stressed. The compression index was observed to be rubber-size dependent; however, for the swell index, the performance of both rubber types seemed to be on par with each other.
- The secondary consolidation rate also exhibited a rubber content/size dependency, indicating a capacity to counteract the settlement in both magnitude and time. The greater the rubber content, the lower the secondary consolidation rate, with the finer rubber maintaining a slight advantage over the coarser rubber. The resulting trends for the secondary swelling and secondary consolidation rates were observed to be consistent and comparable.

- The results of the UC tests were cross checked with the swell-shrink-consolidation properties to arrive at the optimum stabilization scenarios. A maximum rubber inclusion of 10 %, preferably the rubber of coarser category, proved to satisfy the stabilization objectives, and thus was deemed as the optimum choice. Where context changes and the strength and stiffness are not primary concerns, higher rubber inclusions up to 20 % could also be considered acceptable.
- The cost efficiency of the rubber-reinforcement technique was compared to conventional polyester, polyethylene, and polypropylene fibers. Significant cost reduction can be achieved when rubbers are used as a replacement for conventional fibers. More importantly, beneficial reuse of recycled tires provides a sound environmental alternative to the safe disposal concern associated with such waste materials.

ACKNOWLEDGMENTS

This research was funded by the Australian Research Council via project No. DP140103004, and their support is gratefully acknowledged.

References

Akbulut, S., Arasan, S., and Kalkan, E., 2007, "Modification of Clayey Soils Using Scrap Tire Rubber and Synthetic Fibers," *Appl. Clay Sci.*, Vol. 38, Nos. 1–2, pp. 23–32, https://doi.org/10.1016/J.CLAY.2007.02.001

Al-Akhras, N. M., Attom, M. F., Al-Akhras, K. M., and Malkawi, A. I. H., 2008, "Influence of Fibers on Swelling Properties of Clayey Soil," *Geosynth. Int.*, Vol. 15, No. 4, pp. 304–309, https://doi.org/10.1680/GEIN.2008.15.4.304

Alazigha, D. P., Indraratna, B., Vinod, J. S., and Ezeajugh, L. E., 2016, "The Swelling Behaviour of Lignosulfonate–Treated Expansive Soil," *Proc. ICE—Ground Improv.*, Vol. 169, No. 3, pp. 182–193, https://doi.org/10.1680/JGRIM.15.00002

Al-Rawas, A. A., Hago, A. W., and Al-Sarmi, H., 2005, "Effect of Lime, Cement and Sarooj (Artificial Pozzolan) on the Swelling Potential of an Expansive Soil from Oman," *Build. Environ.*, Vol. 40, No. 5, pp. 681–687, https://doi.org/10.1016/J.BUILDENV.2004.08.028

Ang, E. C. and Loehr, J. E., 2003, "Specimen Size Effects for Fiber–Reinforced Silty Clay in Unconfined Compression," *Geotech. Test. J.*, Vol. 26, No. 2, pp. 191–200, https://doi.org/10.1520/GTJ11320J

AS 1289.3.2.1:09, 2009, *Methods of Testing Soils for Engineering Purposes: Soil Classification Tests–Determination of the Plastic Limit of a Soil*, Standards Australia, Sydney, Australia, www.standards.org

AS 1289.3.3.1:09, 2009, *Methods of Testing Soils for Engineering Purposes: Soil Classification Tests–Calculation of the Plasticity Index of a Soil*, Standards Australia, Sydney, Australia, www.standards.org

AS 1289.3.9.1:15, 2015, *Methods of Testing Soils for Engineering Purposes: Soil Classification Tests–Determination of the Cone Liquid Limit of a Soil*, Standards Australia, Sydney, Australia, www.standards.org

ASTM D2166/D2166M-16, 2016, *Standard Test Method for Unconfined Compressive Strength of Cohesive Soil*, ASTM International, West Conshohocken, PA, www.astm.org

ASTM D2487-11, 2011, *Standard Practice for Classification of Soils for Engineering Purposes (Unified Soil Classification System)*, ASTM International, West Conshohocken, PA, www.astm.org

ASTM D422-63(2007)e2, 2007, *Standard Test Method for Particle–Size Analysis of Soils*, ASTM International, West Conshohocken, PA, www.astm.org

ASTM D427-04, 2004, *Test Method for Shrinkage Factors of Soils by the Mercury Method*, ASTM International, West Conshohocken, PA, www.astm.org

ASTM D4546-14, 2014, *Standard Test Methods for One–Dimensional Swell or Collapse of Soils*, ASTM International, West Conshohocken, PA, www.astm.org

ASTM D698-12e2, 2012, *Standard Test Methods for Laboratory Compaction Characteristics of Soil Using Standard Effort (12,400 ft–lbf/ft^3 (600 kN–m/m^3))*, ASTM International, West Conshohocken, PA, www.astm.org

ASTM D854-14, 2014, *Standard Test Methods for Specific Gravity of Soil Solids by Water Pycnometer*, ASTM International, West Conshohocken, PA, www.astm.org

Cai, Y., Shi, B., Ng, C. W. W., and Tang, C. S., 2006, "Effect of Polypropylene Fibre and Lime Admixture on Engineering Properties of Clayey Soil," *Eng. Geol.*, Vol. 87, Nos. 3–4, pp. 230–240, https://doi.org/10.1016/J.ENGGEO.2006.07.007

Casagrande, A., 1936, "The Determination of Pre–Consolidation Load and Its Practical Significance," *First International Conference on Soil Mechanics and Foundation Engineering*, A. Casagrande, P. C. Rutledge, and J. D. Watson, Eds., Harvard Printing Office, Cambridge, MA, pp. 60–64.

Cetin, H., Fener, M., and Gunaydin, O., 2006, "Geotechnical Properties of Tire–Cohesive Clayey Soil Mixtures as a Fill Material," *Eng. Geol.*, Vol. 88, Nos. 1–2, pp. 110–120, https://doi.org/10.1016/J.ENGGEO.2006.09.002

Cornelis, W. M., Corluy, J., Medina, H., Díaz, J., Hartmann, R., van Meirvenne, M., and Ruiz, M. E., 2006, "Measuring and Modelling the Soil Shrinkage Characteristic Curve," *Geoderma*, Vol. 137, Nos. 1–2, pp. 179–191, https://doi.org/10.1016/J.GEODERMA.2006.08.022

Dakshanamurthy, V., 1978, "A New Method to Predict Swelling Using Hyperbola Equation," *Geotech. Eng.*, Vol. 9, No. 1, pp. 29–38.

Dif, A. and Bluemel, W., 1991, "Expansive Soils under Cyclic Drying and Wetting," *Geotech. Test. J.*, Vol. 14, No. 1, pp. 96–102, https://doi.org/10.1520/GTJ10196J

Dunham-Friel, J. and Carraro, J. A. H., 2011, "Shear Strength and Stiffness of Expansive Soil and Rubber (ESR) Mixtures in Undrained Axisymmetric Compression," presented at the *Geo–Frontiers 2011: Advances in Geotechnical Engineering (GSP 211)*, Dallas, TX, American Society of Civil Engineers, Reston, VA, pp. 1111–1120.

Edil, T. and Bosscher, P., 1994, "Engineering Properties of Tire Chips and Soil Mixtures," *Geotech. Test. J.*, Vol. 17, No. 4, pp. 453–464, https://doi.org/10.1520/GTJ10306J

Estabragh, A. R., Moghadas, M., and Javadi, A. A., 2013, "Effect of Different Types of Wetting Fluids on the Behaviour of Expansive Soil during Wetting and Drying," *Soils Found.*, Vol. 53, No. 5, pp. 617–627, https://doi.org/10.1016/J.SANDF.2013.08.001

Estabragh, A. R., Parsaei, B., and Javadi, A. A., 2015, "Laboratory Investigation of the Effect of Cyclic Wetting and Drying on the Behaviour of an Expansive Soil," *Soils Found.*, Vol. 55, No. 2, pp. 304–314, https://doi.org/10.1016/J.SANDF.2015.02.007

Estabragh, A. R., Pereshkafti, M. R. S., Parsaei, B., and Javadi, A. A., 2013, "Stabilised Expansive Soil Behaviour during Wetting and Drying," *Int. J. Pavement Eng.*, Vol. 14, No. 4, pp. 418–427, https://doi.org/10.1080/10298436.2012.746688

Estabragh, A. R., Rafatjo, H., and Javadi, A. A., 2014, "Treatment of an Expansive Soil by Mechanical and Chemical Techniques," *Geosynth. Int.*, Vol. 21, No. 3, pp. 233–243, https://doi.org/10.1680/GEIN.14.00011

Estabragh, A. R., Soltani, A., and Javadi, A. A., 2016, "Models for Predicting the Seepage Velocity and Seepage Force in a Fiber Reinforced Silty Soil," *Comput. Geotech.*, Vol. 75, pp. 174–181, https://doi.org/10.1016/J.COMPGEO.2016.02.002

Fatahi, B., Khabbaz, H., and Fatahi, B., 2012, "Mechanical Characteristics of Soft Clay Treated with Fibre and Cement," *Geosynth. Int.*, Vol. 19, No. 3, pp. 252–262, https://doi.org/10.1680/GEIN.12.00012

Garcia, M., Pando, M. A., and Tempest, B., 2011, "Tire Derived Aggregates as a Sustainable Recycled Material for Retaining Wall Backfills," presented at the *International Conference on Sustainable Design and Construction* (ICSDC), Kansas City, MO, American Society of Civil Engineers, Reston, VA, pp. 542–552.

Gurtug, Y. and Sridharan, A., 2002, "Prediction of Compaction Characteristics of Fine–Grained Soils," *Géotechnique*, Vol. 52, No. 10, pp. 761–763, https://doi.org/10.1680/GEOT.2002.52.10.761

Gurtug, Y. and Sridharan, A., 2004, "Compaction Behaviour and Prediction of its Characteristics of Fine–Grained Soils with Particular Reference to Compaction Energy," *Soils Found.*, Vol. 44, No. 5, pp. 27–36, https://doi.org/10.3208/SANDF.44.5_27

Haines, W. B., 1923, "The Volume–Changes Associated with Variations of Water Content in Soil," *J. Agric. Sci.*, Vol. 13, No. 3, pp. 296–310, https://doi.org/10.1017/S0021859600003580

Hanafy, E. A. D. E., 1991, "Swelling/Shrinkage Characteristic Curve of Desiccated Expansive Clays," *Geotech. Test. J.*, Vol. 14, No. 2, pp. 206–211, https://doi.org/10.1520/GTJ10562J

Hannam, P., 2014, "Tyre Industry Divided over How to Handle Toxic Waste," The Sydney Morning Herald, Sydney, Australia, https://www.smh.com.au/environment/tyre-industry-divided-over-how-to-handle-toxic-waste-20140120-314ic.html (accessed 10 Aug. 2017)

Iyengar, S. R., Masad, E., Rodriguez, A. K., Bazzi, H. S., Little, D., and Hanley, H. J. M., 2013, "Pavement Subgrade Stabilization Using Polymers: Characterization and Performance," *J. Mater. Civ. Eng.*, Vol. 25, No. 4, pp. 472–483, https://doi.org/10.1061/(ASCE)MT.1943-5533.0000612

Jha, A. K. and Sivapullaiah, P. V., 2016, "Gypsum-Induced Volume Change Behavior of Stabilized Expansive Soil with Fly Ash-Lime," *Geotech. Test. J.*, Vol. 39, No. 3, pp. 391–406, https://doi.org/10.1520/GTJ20150017

Jones, L. D. and Jefferson, I., 2012, "Expansive Soils," *ICE Manual of Geotechnical Engineering: Volume I*, J. Burland, T. Chapman, M. Brown, and H. Skinner, Eds., Institution of Civil Engineers Publishing, London, United Kingdom, pp. 413–441.

Jose, B. T., Sridharan, A., and Abraham, B. M., 1989, "Log–Log Method for Determination of Preconsolidation Pressure," *Geotech. Test. J.*, Vol. 12, No. 3, pp. 230–237, https://doi.org/10.1520/GTJ10974J

Kalkan, E., 2013, "Preparation of Scrap Tire Rubber Fiber–Silica Fume Mixtures for Modification of Clayey Soils," *Appl. Clay Sci.*, Vols. 80–81, pp. 117–125, https://doi.org/10.1016/J.CLAY.2013.06.014

Maher, M. H. and Ho, Y. C., 1994, "Mechanical Properties of Kaolinite/Fiber Soil Composite," *J. Geotech. Eng.*, Vol. 120, No. 8, pp. 1381–1393, https://doi.org/10.1061/(ASCE)0733-9410(1994)120:8(1381)

McGarry, D. and Malafant, K. W. J., 1987, "The Analysis of Volume Change in Unconfined Units of Soil," *Soil Sci. Soc. Am. J.*, Vol. 51, No. 2, pp. 290–297, https://doi.org/10.2136/SSSAJ1987.03615995005100020059X

Mirzababaei, M., Arulrajah, A., Horpibulsuk, S., and Aldava, M., 2017, "Shear Strength of a Fibre-Reinforced Clay at Large Shear Displacement When Subjected to Different Stress Histories," *Geotext. Geomembr.*, Vol. 45, No. 5, pp. 422–429, https://doi.org/10.1016/J.GEOTEXMEM.2017.06.002

Mirzababaei, M., Miraftab, M., Mohamed, M., and McMahon, P., 2013a, "Impact of Carpet Waste Fibre Addition on Swelling Properties of Compacted Clays," *Geotech. Geol. Eng.*, Vol. 31, No. 1, pp. 173–182, https://doi.org/10.1007/S10706-012-9578-2

Mirzababaei, M., Miraftab, M., Mohamed, M., and McMahon, P., 2013b, "Unconfined Compression Strength of Reinforced Clays with Carpet Waste Fibers," *J. Geotech. Geoenviron. Eng.*, Vol. 139, No. 3, pp. 483–493, https://doi.org/10.1061/(ASCE)GT.1943-5606.0000792

Mirzababaei, M., Mohamed, M., Arulrajah, A., Horpibulsuk, S., and Anggraini, V., 2018, "Practical Approach to Predict the Shear Strength of Fibre–Reinforced Clay," *Geosynth. Int.*, Vol. 25, No. 1, https://doi.org/10.1680/JGEIN.17.00033

Mirzababaei, M., Yasrobi, S. S., and Al-Rawas, A. A., 2009, "Effect of Polymers on Swelling Potential of Expansive Soils," *Proc. ICE—Ground Improv.*, Vol. 162, No. 3, pp. 111–119, https://doi.org/10.1680/GRIM.2009.162.3.111

Mishra, A. K., Dhawan, S., and Rao, S. M., 2008, "Analysis of Swelling and Shrinkage Behavior of Compacted Clays," *Geotech. Geol. Eng.*, Vol. 26, No. 3, pp. 289–298, https://doi.org/10.1007/S10706-007-9165-0

Nalbantoglu, Z., 2006, "Lime Stabilization of Expansive Clay," *Expansive Soils: Recent Advances in Characterization and Treatment*, A. A. Al-Rawas and M. F. A. Goosen, Eds., Taylor & Francis Group, London, United Kingdom, pp. 139–148.

Olgun, M., 2013, "The Effects and Optimization of Additives for Expansive Clays under Freeze–Thaw Conditions," *Cold Reg. Sci. Technol.*, Vol. 93, pp. 36–46, https://doi.org/10.1016/J.COLDREGIONS.2013.06.001

Onyejekwe, S. and Ghataora, G. S., 2015, "Soil Stabilization Using Proprietary Liquid Chemical Stabilizers: Sulphonated Oil and a Polymer," *Bull. Eng. Geol. Environ.*, Vol. 74, No. 2, pp. 651–665, https://doi.org/10.1007/S10064-014-0667-8

Özkul, Z. and Baykal, G., 2007, "Shear Behavior of Compacted Rubber Fiber–Clay Composite in Drained and Undrained Loading," *J. Geotech. Geoenviron. Eng.*, Vol. 133, No. 7, pp. 767–781, https://doi.org/10.1061/(ASCE)1090-0241(2007)133:7(767)

Pacheco Silva, F., 1970, "A New Graphical Construction for Determination of the Preconsolidation Stress of a Soil Sample," presented at the *Fourth Brazilian Conference on Soil Mechanics and Foundation Engineering*, Rio de Janeiro, Brazil, pp. 225–232.

Patil, U., Valdes, J. R., and Evans, T. M., 2011, "Swell Mitigation with Granulated Tire Rubber," *J. Mater. Civ. Eng.*, Vol. 23, No. 5, pp. 721–727, https://doi.org/10.1061/(ASCE)MT.1943-5533.0000229

Peng, X. and Horn, R., 2005, "Modeling Soil Shrinkage Curve across a Wide Range of Soil Types," *Soil Sci. Soc. Am. J.*, Vol. 69, No. 3, pp. 584–592, https://doi.org/10.2136/SSSAJ2004.0146

Phanikumar, B. R. and Singla, R., 2016, "Swell–Consolidation Characteristics of Fibre-Reinforced Expansive Soils," *Soils Found.*, Vol. 56, No. 1, pp. 138–143, https://doi.org/10.1016/J.SANDF.2016.01.011

Prakash, K. and Sridharan, A., 2004, "Free Swell Ratio and Clay Mineralogy of Fine–Grained Soils," *Geotech. Test. J.*, Vol. 27, No. 2, pp. 220–225, https://doi.org/10.1520/GTJ10860

Radovic, M., Lara-Curzio, E., and Riester, L., 2004, "Comparison of Different Experimental Techniques for Determination of Elastic Properties of Solids," *Mater. Sci. Eng. A*, Vol. 368, Nos. 1–2, pp. 56–70, https://doi.org/10.1016/J.MSEA.2003.09.080

Rao, S. M., Thyagaraj, T., and Thomas, H. R., 2006, "Swelling of Compacted Clay under Osmotic Gradients," *Géotechnique*, Vol. 56, No. 10, pp. 707–713, https://doi.org/10.1680/GEOT.2006.56.10.707

Seda, J. H., Lee, J. C., and Carraro, J. A. H., 2007, "Beneficial Use of Waste Tire Rubber for Swelling Potential Mitigation in Expansive Soils," *Geo–Denver 2007: Soil Improvement (GSP 172)*, V. R. Schaefer, G. M. Filz, P. M. Gallagher, A. L. Sehn, and K. J. Wissmann, Eds., American Society of Civil Engineers, Reston, VA, pp. 1–9.

Shahbazi, M., Rowshanzamir, M., Abtahi, S. M., and Hejazi, S. M., 2017, "Optimization of Carpet Waste Fibers and Steel Slag Particles to Reinforce Expansive Soil Using Response Surface Methodology," *Appl. Clay Sci.*, Vol. 142, No. 15, pp. 185–192, https://doi.org/10.1016/J.CLAY.2016.11.027

Sibley, J. W. and Williams, D. J., 1989, "A Procedure for Determining Volumetric Shrinkage of an Unsaturated Soil," *Geotech. Test. J.*, Vol. 12, No. 3, pp. 181–187, https://doi.org/10.1520/GTJ10966J

Signes, C. H., Garzón-Roca, J., Fernández, P. M., Torre, M. E. G., and Franco, R. I., 2016, "Swelling Potential Reduction of Spanish Argillaceous Marlstone Facies Tap Soil through the Addition of Crumb Rubber Particles from Scrap Tyres," *Appl. Clay Sci.*, Vols. 132-133, pp. 768–773, https://doi.org/10.1016/J.CLAY.2016.07.027

Sivapullaiah, P. V., Sridharan, A., and Stalin, V. K., 1996, "Swelling Behaviour of Soil–Bentonite Mixtures," *Can. Geotech. J.*, Vol. 33, No. 5, pp. 808–814, https://doi.org/10.1139/T96-106-326

Soltani, A., 2017, "Discussion of 'Optimization of Carpet Waste Fibers and Steel Slag Particles to Reinforce Expansive Soil Using Response Surface Methodology' by M. Shahbazi, M. Rowshanzamir, S.M. Abtahi, S.M. Hejazi [Appl. Clay Sci., doi:10.1016/j.clay.2016.11.027]," *Appl. Clay Sci.*, https://doi.org/10.1016/J.CLAY.2017.07.020 (in press).

Soltani, A., Deng, A., and Taheri, A., 2018a, "Swell–Compression Characteristics of a Fiber–Reinforced Expansive Soil," *Geotext. Geomembr.*, Vol. 46, No. 2, https://doi.org/10.1016/J.GEOTEXMEM.2017.11.009

Soltani, A., Deng, A., Taheri, A., and Mirzababaei, M., 2017a, "A Sulphonated Oil for Stabilisation of Expansive Soils," *Int. J. Pavement Eng.*, https://doi.org/10.1080/10298436.2017.1408270

Soltani, A., Deng, A., Taheri, A., Sridharan, A., and Estabragh, A. R., 2018b, "A Framework for Interpretation of the Compressibility Behavior of Soils," *Geotech. Test. J.*, Vol. 41, No. 1, https://doi.org/10.1520/GTJ20170088

Soltani, A., Taheri, A., Khatibi, M., and Estabragh, A. R., 2017b, "Swelling Potential of a Stabilized Expansive Soil: A Comparative Experimental Study," *Geotech. Geol. Eng.*, Vol. 35, No. 4, pp. 1717–1744, https://doi.org/10.1007/S10706-017-0204-1

Sridharan, A., Abraham, B. M., and Jose, B. T., 1991, "Improved Technique for Estimation of Preconsolidation Pressure," *Géotechnique*, Vol. 41, No. 2, pp. 263–268, https://doi.org/10.1680/GEOT.1991.41.2.263

Sridharan, A. and Gurtug, Y., 2004, "Swelling Behaviour of Compacted Fine–Grained Soils," *Eng. Geol.*, Vol. 72, Nos. 1–2, pp. 9–18, https://doi.org/10.1016/S0013-7952(03)00161-3

Sridharan, A. and Nagaraj, H. B., 2005, "Plastic Limit and Compaction Characteristics of Fine–Grained Soils," *Proc. ICE—Ground Improv.*, Vol. 9, No. 1, pp. 17–22, https://doi.org/10.1680/GRIM.2005.9.1.17

Sridharan, A. and Prakash, K., 1998, "Mechanism Controlling the Shrinkage Limit of Soils," *Geotech. Test. J.*, Vol. 21, No. 3, pp. 240–250, https://doi.org/10.1520/GTJ10897J

Sridharan, A., Rao, A., and Sivapullaiah, P., 1986, "Swelling Pressure of Clays," *Geotech. Test. J.*, Vol. 9, No. 1, pp. 24–33, https://doi.org/10.1520/GTJ10608J

Srivastava, A., Pandey, S., and Rana, J., 2014, "Use of Shredded Tyre Waste in Improving the Geotechnical Properties of Expansive Black Cotton Soil," *Geomech. Geoeng.*, Vol. 9, No. 4, pp. 303–311, https://doi.org/10.1080/17486025.2014.902121

Subba Rao, K. S., Rao, S. M., and Gangadhara, S., 2000, "Swelling Behavior of a Desiccated Clay," *Geotech. Test. J.*, Vol. 23, No. 2, pp. 193–198, https://doi.org/10.1520/GTJ11043J

Tang, C. S., Shi, B., and Zhao, L. Z., 2010, "Interfacial Shear Strength of Fiber Reinforced Soil," *Geotext. Geomembr.*, Vol. 28, No. 1, pp. 54–62, https://doi.org/10.1016/J.GEOTEXMEM.2009.10.001

Tang, C. S., Shi, B., Gao, W., Chen, F., and Cai, Y., 2007, "Strength and Mechanical Behavior of Short Polypropylene Fiber Reinforced and Cement Stabilized Clayey Soil," *Geotext. Geomembr.*, Vol. 25, No. 3, pp. 194–202, https://doi.org/10.1016/J.GEOTEXMEM.2006.11.002

Thyagaraj, T. and Zodinsanga, S., 2014, "Swell–Shrink Behaviour of Lime Precipitation Treated Soil," *Proc. ICE—Ground Improv.*, Vol. 167, No. 4, pp. 260–273, https://doi.org/10.1680/GRIM.12.00028

Thyagaraj, T., Thomas, S. R., and Das, A. P., 2017, "Physico–Chemical Effects on Shrinkage Behavior of Compacted Expansive Clay," *Int. J. Geomech.*, Vol. 17, No. 2, 06016013, https://doi.org/10.1061/(ASCE)GM.1943-5622.0000698

Tripathy, S. and Subba Rao, K. S., 2009, "Cyclic Swell–Shrink Behaviour of a Compacted Expansive Soil," *Geotech. Geol. Eng.*, Vol. 27, No. 1, pp. 89–103, https://doi.org/10.1007/S10706-008-9214-3

Tripathy, S., Subba Rao, K. S., and Fredlund, D. G., 2002, "Water Content–Void Ratio Swell–Shrink Paths of Compacted Expansive Soils," *Can. Geotech. J.*, Vol. 39, No. 4, pp. 938–959, https://doi.org/10.1139/T02-022

Trouzine, H., Bekhiti, M., and Asroun, A., 2012, "Effects of Scrap Tyre Rubber Fibre on Swelling Behaviour of Two Clayey Soils in Algeria," *Geosynth. Int.*, Vol. 19, No. 2, pp. 124–132, https://doi.org/10.1680/GEIN.2012.19.2.124

Viswanadham, B. V. S., Phanikumar, B. R., and Mukherjee, R. V., 2009a, "Swelling Behaviour of a Geofiber–Reinforced Expansive Soil," *Geotext. Geomembr.*, Vol. 27, No. 1, pp. 73–76, https://doi.org/10.1016/J.GEOTEXMEM.2008.06.002

Viswanadham, B. V. S., Phanikumar, B. R., and Mukherjee, R. V., 2009b, "Effect of Polypropylene Tape Fibre Reinforcement on Swelling Behaviour of an Expansive Soil," *Geosynth. Int.*, Vol. 16, No. 5, pp. 393–401, https://doi.org/10.1680/GEIN.2009.16.5.393

Winterkorn, H. F. and Pamukcu, S., 1991, "Soil Stabilization and Grouting," *Foundation Engineering Handbook*, H. Y. Fang, Ed., Springer, New York, NY, pp. 317–378.

Yadav, J. S. and Tiwari, S. K., 2017, "A Study on the Potential Utilization of Crumb Rubber in Cement Treated Soft Clay," *J. Build. Eng.*, Vol. 9, pp. 177–191, https://doi.org/10.1016/J.JOBE.2017.01.001

Zornberg, J. G., Cabral, A. R., and Viratjandr, C., 2004, "Behaviour of Tire Shred–Sand Mixtures," *Can. Geotech. J.*, Vol. 41, No. 2, pp. 227–241, https://doi.org/10.1139/T03-086

Chapter 4

Tire Rubber–Reinforced Expansive Soils: Two Hazards, One Solution?

Amin Soltani [a,†], Abbas Taheri [b], An Deng [c] and Hamid Nikraz [d]

[a] **PhD Student** − School of Civil, Environmental and Mining Engineering, The University of Adelaide, Adelaide, SA 5005, Australia (**Email:** Amin.Soltani@adelaide.edu.au; **ORCID:** 0000-0002-0483-7487)

[b] **Senior Lecturer** − School of Civil, Environmental and Mining Engineering, The University of Adelaide, Adelaide, SA 5005, Australia (**Email:** Abbas.Taheri@adelaide.edu.au)

[c] **Senior Lecturer** − School of Civil, Environmental and Mining Engineering, The University of Adelaide, Adelaide, SA 5005, Australia (**Email:** An.Deng@adelaide.edu.au)

[d] **Professor** − School of Civil and Mechanical Engineering, Curtin University, Perth, WA 6102, Australia (**Email:** H.Nikraz@curtin.edu.au)

[†] **Correspondence:** Amin Soltani (**Email:** Amin.Soltani@adelaide.edu.au; **ORCID:** 0000-0002-0483-7487)

Publication Details: **Soltani A**, Taheri A, Deng A and Nikraz H **(2018)** Tire Rubber–Reinforced Expansive Soils: Two Hazards, One Solution?. ***Proceedings of the Institution of Civil Engineers–Construction Materials*** **x(x): x–x**, http://doi.org/x.[7]

Abstract

This study presents results of an experimental program with respect to the rubber's capacity of ameliorating the inferior characteristics of expansive soils. Two rubber types of fine and coarse categories were each examined at four different contents (by weight), i.e. R_C=5%, 10%, 20% and 30%. The experimental program consisted of unconfined compression, split tensile, direct shear and desiccation–induced crack tests. Improvement in cracking intensity and shear strength were in favor of higher rubber contents. However, rubber contents greater than 10%

[7]**Under Review** [submitted on **29 September 2018**].

raised failure concerns during compression and/or tension, attributed to the clustering of rubber particles under non–confinement testing conditions. Although the rubber of coarser category slightly outperformed the finer rubber, the effect of larger rubber size was mainly translated to higher ductility, lower stiffness and higher energy adsorption capacity rather than peak strength improvements. A multiple linear regression model was suggested to quantify the shear strength as a function of the composite's index properties. The swelling properties (previously investigated by the authors) were revisited and cross–checked with the strength properties to arrive at the optimum rubber content. In this case, R_C=10% satisfied a notable decrease in the swell–shrink capacity as well as improving the strength–related properties.

Keywords: Expansive soil; Rubber content and size; Unconfined compression; Split tensile; Direct shear; Rubber–clustering; Cracking intensity; Swelling; Multiple linear regression.

Abbreviations

DS	direct shear
MLR	multiple linear regression
ST	split tensile
UC	unconfined compression
USCS	unified soil classification system

Notation

CIF	crack intensity factor
c_p	peak cohesion intercept
CRF	crack reduction factor
E_{50}	elastic stiffness modulus
E_s	peak strain energy (ST test)
E_u	peak strain energy (UC test)
MAPE	mean absolute percentage error
NRMSE	normalized root mean squares error
q_s	peak ST strength
q_u	peak UC strength
R^2	coefficient of determination
R_c	rubber content
RMSE	root mean squares error
SSA	specific surface area
w_0	initial water content
w_{opt}	optimum water content
β_0 **to** β_5	MLR fitting parameters
γ_{d0}	initial dry unit weight
γ_{dmax}	maximum dry unit weight
γ_p	failure shear strain (DS test)
ε_s	failure diametrical strain (ST test)
ε_{sw}	swelling potential
ε_u	failure axial strain (UC test)
σ_n	normal stress
σ_{sw}	swelling pressure
τ_{cr}	critical shear strength
τ_p	peak shear strength
φ_p	peak friction angle

1. Introduction

Expansive soils are amongst the most significant, widespread, costly and least publicized geologic hazards. Such soils are characterized as poor–quality construction materials, owing to their inferior engineering characteristics including low strength (and bearing capacity), high compressibility, and high potential for swelling/shrinkage (Nalbantoglu 2006; Estabragh et al. 2013[a]). Where exposed to seasonal environments, the expansive soil exhibits significant volume changes as well as desiccation–induced cracking, thereby bringing forth instability concerns to the overlaying structures and hence incurring large amounts of maintenance costs (Gourley et al. 1994; Estabragh et al. 2018). In a typical year, expansive soils can cause a greater financial loss to property owners than earthquakes, floods, hurricanes and tornadoes combined (Nelson and Miller 1992). Over the past decade, the adverse effects of expansive soils have cost the UK's economy an estimated £3 billion, thus making it the most damaging geohazard in the UK today (Jones and Jefferson 2012). In the USA, for instance, the estimated damage to structures founded on expansive soils exceeds $13 billion per annum (Dunham-Friel and Carraro 2011). Consequently, expansive soils demand engineering solutions to alleviate the adverse socio–economic impacts on human's life.

Common solutions to counteract the adversities associated with expansive soils include soil replacement or attempting to improve the low–graded expansive soil by means of stabilization techniques. The latter is often preferred, since the former is often impractical due to haul distances and economic considerations (Estabragh et al. 2013[b]). Soil stabilization techniques are often categorized as chemical, mechanical or combined chemical–mechanical approaches (Soltani et al. 2017[a]). Chemical techniques involve the addition of chemical agents to the soil mass, e.g. cement, lime, fly ash and polymers, which act as potential binders by entwining within the soil grains, thereby amending the soil fabric into a coherent matrix of restricted heave/settlement and induced strength (e.g. Sezer et al. 2006; Mirzababaei et al. 2009; Estabragh et al. 2013[a], 2013[b]; Calik and Sadoglu 2014; Thyagaraj and Zodinsanga 2014; Soltani et al. 2017[b]; Alazigha et al. 2018). Conventional cementitious agents, though proven effective, encounter a series of concerning disadvantages: **i)** reduction in material workability (or ductility); **ii)** low durability against local environmental conditions (e.g. organic matter, sulfates, alternate wetting–dying and acidic/alkaline flows); **iii)** high transportation costs; and **iv)** environmental concerns due to greenhouse gas emissions (Sivapullaiah et al. 2000; Puppala et al. 2004; Khattak and Alrashidi 2006; Guney et al. 2007; Estabragh et al. 2014). The mechanical stabilization scheme makes use of compaction with the aid of reinforcements such

as natural and synthetic fibers (e.g. Mirzababaei et al. 2013[a], 2013[b]; Estabragh et al. 2016; Qu and Zhao 2016; Mirzababaei et al. 2017, 2018; Soltani et al. 2018[a]). Such products, while prevailing the environmental concerns raised with chemical techniques, suffer from other disadvantages: **i)** the lack of standardized laboratory test methods for effective prediction of field performance; **ii)** high manufacturing costs associated with synthetic fibers; **iii)** biodegradability of natural fibers; and **iv)** availability issues (limited stock) in some sites. Environmentally sustainable and cost–effective stabilization alternatives capable of minimizing (or replacing) the need for conventional construction materials have recently gained increased attention. Beneficial reuse of solid waste materials and industrial by–products (such as waste tire rubbers) are amongst the most well–received propositions in this context. The proposal not only intends to address the geotechnical–related issue associated with problematic soils, but also encourages recycling, mitigates the burden on the environment and assists waste management (Jayasree et al. 2015; Alazigha et al. 2016; Kua et al. 2017).

Discarded tires are amongst the largest and most problematic sources of solid waste, owing to the large volumes produced and their durability. Given the high–volume generation and disposal of waste tire rubbers every year throughout the world, a major concern hitherto has been the space required for storing and transporting such waste materials, and the resulting health hazards and costs (Thomas et al. 2016; Yadav and Tiwari 2017[a]). Those characteristics which make waste tire rubbers such a problem while being landfilled, make them one of the most reusable waste materials for engineering applications, as the rubber is resilient, lightweight and skin–resistive (Edil and Bosscher 1994; Zornberg et al. 2004). Highly elastic and strong–friction polymer materials such as recycled tire rubbers not only alter the fabric and structure of the soil, but also amend the bonding along the interface (or contact) between the soil and the reinforcement, thereby increasing the integrity and stability of the infrastructure in terms of moisture sensitivity (i.e. swell–shrink volume changes), strength and ductility (e.g. Cetin et al. 2006; Özkul and Baykal 2006, 2007; Seda et al. 2007; Dunham-Friel and Carraro 2011; Patil et al. 2011; Trouzine et al. 2012; Kalkan 2013; Kim and Kang 2013; Cabalar et al. 2014; Dunham-Friel and Carraro 2014; Srivastava et al. 2014; Cabalar and Karabash 2015; Signes et al. 2016; Mashiri et al. 2017; Yadav and Tiwari 2017[b], 2017[c]; Soltani et al. 2018[b]). The mechanical response of rubber–reinforced soils is primarily a function of rubber content, i.e. rubber to dry soil weight ratio. However, the rubber's geometrical properties, defined in terms of the rubber's mean particle size, may also portray an equally important role. The latter is expected to be somewhat similar to that of aspect ratio (or fiber length) in fiber–reinforced soils,

which has been well documented in the fiber–reinforcement literature (see Hejazi et al. (2012) for details). With rubbers, however, this aspect has not yet been adequately addressed in the literature, and thus demands further examination. The available research on soil–rubber composites are still limited, and the reported results are not consistent. In addition, fewer documented studies can be found with regard to expansive soils, as the majority of literature sources have mainly emphasized on coarse–grained soils and in some cases low plasticity clays.

The present study intends to examine the rubber's capacity (both of fine and coarse categories) of ameliorating the inferior/hazardous engineering characteristics of expansive soils, thereby solving two widespread hazards (i.e. the expansive soil problem and the tire rubber disposal problem) with one solution. The experimental program was carried out in two phases consisting of preliminary and main tests. The preliminary testing phase included consistency limits and standard Proctor compaction tests. The main test program included unconfined compression (UC), split tensile (ST), direct shear (DS) and desiccation–induced crack tests. A multiple linear regression (MLR) model was also suggested and validated to quantify the peak and critical state shear strengths. Finally, the swelling properties (i.e. swelling potential and swelling pressure) — previously investigated by the authors in Soltani et al. (2018[c]) — were revisited and cross–checked with the results obtained in the present study to arrive at the optimum rubber content suitable for stabilization of expansive soils.

2. Materials

2.1. Soil

The soil used in this study was a mixture of 85% kaolinite and 15% bentonite. It was characterized as *clay with high plasticity* (CH) in accordance with the Unified Soil Classification System (USCS). The free swell ratio (FSR) for kaolinite, bentonite and the kaolinite–bentonite mixture was measured as 1.19, 7.53 and 2.91, from which these soils were graded into *lowly expansive*, *very highly expansive* and *highly expansive* with respect to the classification criterion suggested by Prakash and Sridharan (2004), respectively. Physical and mechanical properties of kaolinite, bentonite and the kaolinite–bentonite mixture (hereafter simply referred to as soil) were determined as per relevant ASTM and Australian standards, and the results are provided in **Table 1**. Other soil properties, as supplied by the manufacturer, included a pH of 7.4 and 9.5, cation exchange capacity (CEC) of 14 meq/100ml and 82

meq/100ml, and specific surface area (SSA) of 11.2 m^2/g and 85.4 m^2/g for kaolinite and bentonite, respectively.

2.2. Recycled Tire Rubbers

Two types of commercially available recycled tire rubbers, i.e. rubber crumbs (hereafter rubber C) and rubber buffings (hereafter rubber B), were used as the reinforcements (see **Figure 1**). **Figure 2** illustrates the grain–size distribution curves for both rubber types, along with kaolinite and bentonite (determined as per ASTM D422–07). Rubber B can be considered similar in size to coarse sand, with particles ranging between 4.75 mm and 1.18 mm. Rubber C, on the other hand, falls into the fine sand category, with particles ranging between 1.18 mm and 75 μm. The uniformity (C_u) and curvature (C_c) coefficients were, respectively, measured as 1.56 and 1.04 for rubber B, and 2.81 and 1.20 for rubber C (see **Figure 2**), from which both rubber types were characterized as *poorly–graded sand* (SP) in accordance with the USCS criterion. Chemical composition of the rubbers, as supplied by the manufacturer, consisted of 55% styrene–butadiene copolymer, 5–20% acetone extract, 25–35% carbon black, 2.5% zinc oxide and 1–3% sulfur. Other physical properties included a specific gravity (at 20 ^oC) of 1.09, and a softening point of 170 ^oC.

3. Experimental Work

Each of the two rubber choices was incorporated into the soil at four different rubber contents (defined as rubber to dry soil weight ratio), i.e. R_c=5%, 10%, 20% and 30%. The experimental program was carried out in two phases consisting of preliminary and main tests. The preliminary testing phase included consistency limits (AS 1289.3.9.1–15, AS 1289.3.2.1–09, AS 1289.3.3.1–09 and AS 1289.3.4.1–08) and standard Proctor compaction (ASTM D698–12) tests, the results of which are summarized in **Table 2**. The higher the rubber content the lower the consistency limits and the compaction characteristics, following a monotonic decreasing trend. For a given rubber content, however, the effect of rubber size was observed to be insignificant. Such trends can be attributed to the lower specific gravity, specific surface area and water adsorption capacity of the rubber particles compared to the soil grains (Özkul and Baykal 2007; Trouzine et al. 2012; Signes et al. 2016; Yadav and Tiwari 2017[b]; Soltani et al. 2018[b]).

The main test program included unconfined compression (UC), split tensile (ST), direct shear (DS) and desiccation–induced crack tests. Samples for the UC, ST and DS tests were prepared by the static compaction technique, as described in Soltani et al. (2017[b] and 2018[a]), at the corresponding optimum condition of each mixture (i.e. w_{opt} and γ_{dmax} in **Table 2**). For desiccation–induced crack tests, however, samples were prepared by the slurry technique — as commonly adopted in the literature (e.g. Tang et al. 2012; Costa et al. 2013; Chaduvula et al. 2017) — at the respective liquid limit of each mixture (i.e. *LL* in **Table 2**). The methodology associated with each component of the main test program will be further presented in detail.

3.1. Unconfined Compression Test

Unconfined compression (UC) tests were carried out in accordance with the ASTM D2166–16 standard. The natural soil and various soil–rubber mixtures were statically compacted in a cylindrical mold (measuring 50 mm in diameter and 100 mm in in height) at their respective optimum water content and maximum dry unit weight (see w_{opt} and γ_{dmax} in **Table 2**). The prepared samples were axially compressed by a constant displacement rate of 1 mm/min (equivalent to 1 %/min), as suggested in the literature (e.g. Estabragh et al. 2012; Signes et al. 2016; Yadav and Tiwari 2017[b]). Axial stress and its corresponding axial strain were recorded at various time intervals to a point in which maximum (or peak) axial stress required for sample failure could be achieved. To ensure sufficient accuracy, triplicate samples were tested for each scenario.

3.2. Split Tensile Test

Split tensile (ST) tests were carried out in accordance with the ASTM C496–17 standard. The prepared samples were similar to those used for the UC tests, and thus measured 50 mm in diameter and 100 mm in height. Two curved steel strips (measuring 10 mm in width and 100 mm in length) were placed on the upper and lower bearing elements of the samples to ensure uniform load distribution. The samples, along with the upper and lower steel strips, were placed horizontally between the bearing blocks of the compression apparatus, and further subjected to the same displacement rate of 1 mm/min adopted in the UC tests (e.g. Kumar et al. 2007; Estabragh et al. 2017; Yadav and Tiwari 2017[c]). Tensile stress and its corresponding diametrical strain (i.e. $\varepsilon_d=\Delta d/d_0$, where Δd=diametrical displacement; and d_0=initial diameter of the sample) were recorded during various stages to a point in which maximum/peak tensile stress required

for sample failure could be achieved. To ensure sufficient accuracy, triplicate samples were tested for each scenario.

3.3. Direct Shear Test

Unconsolidated undrained (UU) direct shear (DS) tests were carried out in accordance with the GB 50007–11 standard, as commonly adopted in the literature (e.g. Qu et al. 2013; Calik and Sadoglu 2014; Wang et al. 2017). The natural soil and various soil–rubber mixtures were statically compacted in the shear box (measuring 60 mm×60 mm in plane and 20 mm in height) at their respective optimum water content and maximum dry unit weight (see w_{opt} and γ_{dmax} in **Table 2**), and further tested for shear strength at varying normal stresses, i.e. σ_n=100 kPa, 200 kPa, 300 kPa and 400 kPa. A high shear rate of 1 mm/min (equivalent to 1.67 %/min) was adopted for the shearing phase to minimize both drainage and excess pore–water pressure effects (Cetin et al. 2006; Sezer et al. 2006; Qu and Zhao 2016). Shear stress was recorded as a function of horizontal displacement up to a total displacement of 10 mm to quantify the stress–strain response at both peak and post–peak (or critical state) conditions. Moreover, the conventional Mohr–Coulomb failure criterion (using a total stress approach) was implemented to arrive at the apparent shear strength parameters at peak condition (Bai and Liu 2012; Al-Aqtash and Bandini 2015). On account of the four normal stresses, a total of 36 tests, i.e. 4 for the natural soil, 16 for rubber C and 16 for rubber B, were conducted to address the nine different mix designs outlined in **Table 2**.

3.4. Desiccation–Induced Crack Test

Desiccation–induced crack tests were carried out on the natural soil and various soil–rubber mixtures prepared at their respective liquid limit (see *LL* in **Table 2**). The required amount of water corresponding to the desired liquid limit was added to each mixture, and thoroughly mixed to obtain slurries of uniform consistency. The resultant slurries were poured into Petri dishes, measuring 100 mm in diameter and 15 mm in height, and were allowed to desiccate at a constant temperature of 40 ^{o}C. Drying of the samples was carried out to a point in which moisture equalization was attained. Still photographs were then taken using a high–resolution digital camera fixed at a vertical angle 50 cm above the desiccated samples. Image processing techniques (e.g. see Chaduvula et al. (2017) for details) were implemented to quantify the crack features consisting of the crack intensity factor (CIF) and the crack reduction factor (CRF), which are defined as (Yesiller et al. 2000; Miller and Rifai 2004):

$$(\%)\ \mathrm{CIF} = \frac{A_c}{A_o} \times 100 \tag{1}$$

$$(\%)\ \mathrm{CRF} = \frac{\mathrm{CIF_N} - \mathrm{CIF_R}}{\mathrm{CIF_N}} \tag{2}$$

where A_c=area of cracks; A_o=initial area of the tested sample; $\mathrm{CIF_N}$=crack intensity factor for the natural soil (or unreinforced sample); and $\mathrm{CIF_R}$=crack intensity factor for the reinforced sample.

4. Results and Discussions

4.1. Effect of Rubbers on Unconfined Compression Strength

Stress–strain curves, obtained from the UC tests, for the natural soil and various soil–rubber composites are provided in **Figures 3a** and **3b** for rubbers C and B, respectively. For both rubber types, the peak UC strength was dependent on the rubber content and demonstrated a rise–fall behavior, peaking at R_c=5% then decreasing at higher rubber inclusions. The natural soil exhibited a peak UC strength of q_u=113 kPa. Where reinforced with 5% rubber, q_u was measured as 129 kPa and 142 kPa for rubbers C and B, respectively. With the inclusion of 10% rubber, these values dropped to 128 kPa for rubber C and 127 kPa for rubber B, which still hold a notable advantage over the natural soil. For the higher rubber inclusions of 20% and 30%, however, q_u dropped below the natural soil margin (i.e. $q_u < 113$ kPa), and thus raises strength concerns (e.g. q_u=72 kPa and 88 kPa for 30% rubbers C and B). The failure axial strain (denoted as ε_u in **Figure 3**) is an indication of the material's ductility, with higher values manifesting a more ductile character (Estabragh et al. 2012, 2017; Soltani et al. 2017[a]). The failure axial strain for samples reinforced with rubber C demonstrated a rise–fall–plateau behavior, peaking at R_c=5% then reverting back to the initial value observed for the natural soil at higher rubber inclusions (see **Figure 3a**). In comparison, the failure axial strain for samples reinforced with rubber B was in favor of higher rubber contents, with R_c=10% suggesting an optimal case amongst the tested mix designs (see **Figure 3b**).

The area under a typical stress–strain curve (i.e. $\int \sigma d\varepsilon$, where σ=stress; and ε=strain) up to the failure point, defined as peak strain energy (or energy adsorption capacity), serves as a measure of the material's toughness (Maher and Ho 1994). **Figure 4a** illustrates the variations of peak strain energy against rubber content with respect to the UC stress–strain data sets. For both

rubber types, the variations of peak strain energy E_u followed a trend similar to that observed for the peak UC strength q_u. Although in terms of q_u the performance of both rubber types was observed to be on par with each other, soil–rubber B composites consistently outperformed similar samples reinforced with rubber C in terms of higher E_u values, with an exception occurring only at R_c=5%. Higher peak strain energy values manifest an increase in either the failure axial strain ε_u or the peak UC strength q_u (or both), thus signifying a balance between ε_u and q_u (Mirzababaei et al. 2013[a]). As depicted in **Figure 4a**, both rubber types result in nearly similar q_u values for a given rubber content, while rubber B often promotes higher ε_u values (higher ductility), which in turn leads to higher energy adsorption capacities compared to that of rubber C. As optimal cases, E_u increased from 6.91 kJ/m^3 for the natural soil to 9.04 kJ/m^3 and 10.84 kJ/m^3 for the samples reinforced with 5% rubber C and 10% rubber B, respectively.

The elastic stiffness modulus E_{50}, defined as the secant modulus at 50% of the peak UC strength (i.e. $E_{50}=0.5q_u/\varepsilon_a^{50\%}$, where $\varepsilon_a^{50\%}$=axial strain corresponding to $0.5q_u$) (Radovic et al. 2004; Iyengar et al. 2013), was also measured for the tested samples, and the results are provided in **Figure 4b**. For both rubber types, the higher the rubber content the lower the E_{50} value, following a monotonic decreasing trend. All reinforced samples exhibited lower E_{50} values compared to the natural soil (an exception was R_c=5% of rubber B), indicating a reduced material stiffness as a result of rubber–reinforcement. The natural soil resulted in E_{50}=3.15 MPa, while the inclusion of 5%, 10%, 20% and 30% rubber C resulted in E_{50}=2.47 MPa, 2.56 MPa, 1.69 MPa and 1.15 MPa, respectively. Similar inclusions of rubber B did not significantly deviate the aforementioned values, and resulted in E_{50}=3.27 MPa, 2.19 MPa, 1.45 MPa and 1.59 MPa, respectively.

4.2. Effect of Rubbers on Split Tensile Strength

Stress–strain curves, obtained from the ST tests, for the natural soil and various soil–rubber composites are provided in **Figures 5a** and **5b** for rubbers C and B, respectively. For both rubber types, the peak ST strength was dependent on the rubber content and followed a trend similar to that observed for the peak UC strength. The effect of rubber size, however, was observed to be marginal in this regard. The natural soil exhibited a peak ST strength of q_s=14 kPa. Where reinforced with 5% rubber, q_s was measured as 20 kPa for both rubber types. With the inclusion of 10% rubber, q_s changed to 18 kPa and 21 kPa for rubbers C and B, respectively. The higher rubber inclusions of 20% and 30% further decreased q_s, while still holding some advantage over the natural soil (e.g. q_s=16 kPa and 17 kPa for 30% rubbers C and B). As

opposed to q_s, the failure diametrical strain ε_s was evidently rubber size–dependent, with soil–rubber B composites yielding at higher strain values (higher ductility) compared to similar samples reinforced with rubber C (e.g. ε_s=2.09%, 2.46% and 3.67% for the natural soil and 20% rubbers C and B).

The peak strain energy with respect to the ST stress–strain data sets were also measured for the tested samples, and the results are provided in **Figure 6**. For both rubber types, the peak strain energy (in this case denoted as E_s) was dependent on the rubber content and demonstrated a rise–fall–plateau behavior, peaking at R_c=10% then slightly decreasing at higher rubber inclusions. All reinforced samples, however, surpassed the natural soil margin, attributed to the improved ductility (higher ε_s values) as a result of rubber–reinforcement. Although the effect of rubber size was observed to be insignificant in terms of q_s, the more ductile character of soil–rubber B composites (higher ε_s values, as shown in **Figure 5**) gave rise to higher energy adsorption capacities compared to similar samples reinforced with rubber C. As optimal cases, E_s increased from 0.19 kJ/m^3 for the natural soil to 0.33 kJ/m^3 and 0.47 kJ/m^3 for the samples reinforced with 10% rubbers C and B, respectively.

4.3. Effect of Rubbers on Shear Strength Properties

4.3.1. Test Results

Typical stress–strain curves, obtained from the DS tests at varying normal stresses, for the natural soil and samples reinforced with 10% rubbers C and B are provided in **Figures 7a**, **7b** and **7c**, respectively. The stress–strain response demonstrated a rise–fall–plateau behavior with visually detectable peak points, thus indicating a strain–softening character for the tested samples. This effect, however, was less pronounced for samples reinforced with rubber B, particularly at higher normal stresses (e.g. see σ_n=400 kPa in **Figure 7c**) as well as higher rubber inclusions (e.g. see R_c=30% in **Figure 8b** in the subsequent section), which is in agreement with the results reported by Özkul and Baykal (2006) and Dunham-Friel and Carraro (2014). For both rubber types, the stress–strain response for a given rubber content was dependent on the applied normal stress, with higher normal stresses exhibiting higher peak and critical shear strength values. The critical shear strength τ_{cr} was defined as the minimum exhibited shear stress within the 10%–15% shear strain region (i.e. shear strain $\gamma=\Delta\delta/\delta_0$, where $\Delta\delta$=horizontal displacement; and δ_0=initial length of the sample), while the peak shear strength τ_p was visually quantified for the majority of cases (Cetin et al. 2006; Liu and Evett 2009). On the contrary, the

failure shear strain γ_p was less influenced by the applied normal stress. At a normal stress of σ_n=200 kPa, for instance, the natural soil and samples reinforced with 10% rubbers C and B resulted in τ_p=94.65 kPa (γ_p=3.74%), 107.01 kPa (γ_p=5.57%) and 116.08 kPa (γ_p=5.24%), respectively. Where σ_n=400 kPa, these values increased to 126.45 kPa (γ_p=3.57%), 159.71 kPa (γ_p=5.90%) and 164.35 kPa (γ_p=5.02%), respectively.

Typical DS stress–strain curves for the natural soil and various soil–rubber composites at σ_n=300 kPa are provided in **Figures 8a** and **8b** for rubbers C and B, respectively. The stress–strain response at a given normal stress was dependent on both the rubber content and the rubber size, with the former portraying a more pronounced role. For both rubber types, the higher the rubber content the higher the exhibited peak and critical shear strength values. For rubber inclusions equal to or less than 10%, the rubber of coarser category outperformed the finer rubber in terms of higher peak shear strength values, while an opposite effect was evident at higher rubber inclusions. In this case, R_c=20% served as a transition point by manifesting a similar performance with marginal differences for the two rubber types (e.g. at σ_n=300 kPa, τ_p=156.45 kPa and 154.32 kPa for 20% rubbers C and B). The strain–softening character was less apparent at high inclusions of rubber B, thus promoting an induced strength performance at critical state condition compared to similar samples reinforced with rubber C (e.g. see R_c=30% in **Figure 8b**). The failure shear strain was also dependent on the rubber content, and to a lesser degree the rubber size. In general, the higher the rubber content (and/or the larger the rubber size) the larger the failure shear strain, signifying an improvement in the material's ductility when subjected to shearing. At σ_n=300 kPa, for instance, the natural soil resulted in τ_p=107.80 kPa (γ_p=4.40%), while the inclusion of 5%, 10%, 20% and 30% rubber C resulted in τ_p=116.19 kPa (γ_p=4.40%), 129.72 kPa (γ_p=4.68%), 156.45 kPa (γ_p=5.29%) and 193.08 kPa (γ_p=7.35%), respectively. For similar inclusions of rubber B, these values were measured as 121.99 kPa (γ_p=4.40%), 146.26 kPa (γ_p=5.02%), 154.32 kPa (γ_p=6.52%) and 171.26 kPa (γ_p=8.18%), respectively.

The peak shear strength values were plotted against the corresponding normal stresses to construct the peak failure envelopes, and the results are provided in **Figures 9a** and **9b** for rubbers C and B, respectively. The conventional Mohr–Coulomb failure criterion (using a total stress approach), i.e. $\tau_p=c_p+\sigma_n\tan\varphi_p$, was implemented to quantify the apparent peak shear strength parameters (i.e. c_p=peak cohesion; and φ_p=peak friction angle), and the results are summarized in **Figure 9**. As a result of rubber–reinforcement, the peak failure envelope experienced a major upward shift over the τ_p:σ_n space, signifying an increase in the material's

apparent cohesion (see c_p values in **Figure 9**). Meanwhile, the slope of the envelope was also observed to increase with an increase in rubber content, thus promoting a notable improvement in the apparent friction angle (see φ_p values in **Figure 9**). The peak shear strength parameters were dependent on both the rubber content and the rubber size, with the latter portraying a less pronounced role. For rubber inclusions equal to or less than 10%, rubber B consistently outperformed rubber C in terms of higher c_p (and to a lesser degree φ_p) values. The performance of both rubber types was observed to be on par with each other at R_c=20% (e.g. c_p=75.89 kPa and 76.06 kPa for rubbers C and B), while the higher rubber inclusion of 30% gave rise to higher c_p and φ_p values for rubber C (e.g. c_p=98.47 kPa and 86.19 kPa for rubbers C and B).

For both rubber types, an increase in rubber content at a given normal stress led to a major improvement in the peak shear strength. The magnitude of improvement, however, was slightly greater at higher normal stresses, thus implying a confinement–dependent amending mechanism. A similar dependency was also observed for the critical shear strength, the results of which are provided in **Figures 10a** and **10b** for rubber C and B, respectively. As typical cases shown in **Figures 9a** and **10b**, 20% rubber C promoted a 38% improvement in the peak shear strength at σ_n=100 kPa (i.e. τ_p increased from 74.25 kPa 'point A_1' to 102.61 kPa 'point A_2' in **Figure 9a**), while a greater improvement of 50% was achieved for the same rubber inclusion at σ_n=400 kPa (i.e. τ_p increased from 126.45 kPa 'point B_1' to 189.67 kPa 'point B_2' in **Figure 9a**). Similarly, 20% rubber B led to a 53% improvement in the critical shear strength at σ_n=100 kPa (i.e. τ_{cr} increased from 49.19 kPa 'point A_1' to 75.22 kPa 'point A_2' in **Figure 10b**), while a 67% improvement was observed for the same rubber inclusion at σ_n=400 kPa (i.e. τ_{cr} increased from 89.36 kPa 'point B_1' to 149.22 kPa 'point B2' in **Figure 10b**).

Figure 11 illustrates the variations of critical shear strength against peak shear strength for the tested samples. As depicted in the figure, a strong correlation in the form of $\tau_{cr}=\alpha\tau_p^{\beta}$ (with $R^2 >$ 0.97) can be obtained for both rubber types, indicating the existence of a unique relationship between the shear strength at peak and critical state conditions. The resulted trendline for rubber B falls above that of rubber C, which predicates the greater capacity of rubber B in improving the soil's shear strength at critical state condition. In this case, the magnitude of improvement was dependent on both the applied normal stress and the rubber content, with more pronounced improvements occurring at higher normal stresses and/or higher rubber contents. This behavior can be attributed to the appearance of strain–hardening effects for soil–rubber B composites at higher normal stresses and/or higher rubber contents (e.g. see σ_n=400 kPa in **Figure 7c**, and R_c=30% in **Figure 8b**), which in turn promotes an induced strength performance at critical state

condition compared to similar samples reinforced with rubber C. The arrived conclusions in this section essentially complement the discussions previously outlined with respect to **Figures 9** and **10**.

4.3.2. Multiple Linear Regression Model

For a given type of fine–grained soil reinforced with a particular type of rubber, the variables governing the peak or critical shear strength can be categorized as: **i)** normal stress σ_n (in kPa); **ii)** rubber content R_c (in %); **iii)** specific surface area SSA (in m^2/g); **iv)** initial water content w_0 (in %); and **v)** initial dry unit weight γ_{d0} (in kN/m^3). Therefore, a multiple linear regression (MLR) model to represent $\tau_p \vee \tau_{cr}$ (in kPa) can be written as:

$$\tau_p \vee \tau_{cr} = \beta_0 + \beta_1\sigma_n + \beta_2 R_c + \beta_3 \mathrm{SSA} + \beta_4 w_0 + \beta_5 \gamma_{d0} \tag{3}$$

where β_0 to β_5=regression coefficients or fitting parameters.

As outlined in **Section 3**, samples for the DS tests were prepared at the corresponding optimum condition of each mixture, meaning that $w_0 = w_{opt}$ and $\gamma_{d0} = \gamma_{dmax}$ (see **Table 2**). Provided that the specific surface area for both the natural soil and the used rubber are at hand, the specific surface area for various soil–rubber mixtures can be calculated by means of the weighted averaging technique (Williamson and Cortes 2014; Zhao et al. 2016; Soltani and Mirzababei 2018). Alternatively, as done in the present study, the specific surface area for both the natural soil and various soil–rubber mixtures can estimated by the following empirical relationship (Locat et al. 1984; Williamson and Cortes 2014):

$$\mathrm{SSA} = \tfrac{10}{7} PI + 5 \tag{4}$$

where SSA=specific surface are (in m^2/g); and PI=plasticity index (in %), as provided in **Table 2**.

For each rubber type, the MLR model given in **Equation 3** was fitted to the experimental τ_p and τ_{cr} data sets by means of the conventional linear least squares optimization technique (Estabragh et al. 2016). Statistical fit–measure indices, i.e. coefficient of determination (R^2), root mean squares error (RMSE), normalized root mean squares error (NRMSE) and mean absolute percentage error (MAPE), were then obtained for model validation by the following relationships (Soltani et al. 2017[c], 2018[d]):

$$\text{RMSE} = \sqrt{\frac{1}{N}\sum_{i=1}^{N}(y_{ai} - y_{mi})^2} \tag{5}$$

$$(\%)\ \text{NRMSE} = \frac{\text{RMSE}}{y_{a\max} - y_{a\min}} \times 100 \tag{6}$$

$$(\%)\ \text{MAPE} = \frac{1}{N}\sum_{i=1}^{N}\left|\frac{y_{ai} - y_{mi}}{y_{ai}}\right| \times 100 \tag{7}$$

where y_a=actual value of the dependent variable y (=$\tau_p \vee \tau_{cr}$); y_m=predicted value of the dependent variable y; y_{amax}=maximum value of y_a data; y_{amin}=minimum value of y_a data; i=index of summation; and N=number of data points used for model development (i.e. 20 for each rubber type consisting of 4 unreinforced and 16 reinforced samples).

The regression analysis outputs with respect to the proposed MLR model for τ_p and τ_{cr} are summarized in **Table 3**. The MLR model well correlates with experimental observations. The high R^2 and low RMSE, NRMSE or MAPE values imply a strong agreement between actual and predicted data, both in terms of correlation and error. The R^2 values were mainly above the 0.97 margin, indicating that approximately 97% of the variations in experimental observations are captured and further explained by the MLR model. In addition, the NRMSE and MAPE values were found to be less than the 5% for the majority of cases, signifying an average offset of only 5% associated with the predictive capacity of the MLR model.

Figures 12a and **12b** illustrate predicted (by **Equation 3**) versus actual data, along with the corresponding 95% confidence bands/intervals, for the peak and critical shear strengths, respectively. All data points lie between the upper and lower 95% confidence bands, thus indicating no particular outliers associated with the predictions. The coefficient of determination was also obtained for these combined data sets, which resulted in a net R^2 of 0.9758 and 0.9705 for τ_p and τ_{cr}, respectively. The proposed MLR model contains a limited number of fitting parameters which can be calibrated by little experimental effort, and hence implemented for predictive purposes. The fitting parameters, i.e. β_0 to β_5, can be adequately estimated by a total of six DS tests. Two scenarios consisting of the natural soil and a desired soil–rubber mixture, each at three different normal stresses, is recommended for the calibration phase. The choice of rubber content for the soil–rubber mixture is arbitrary. However, from a statistical perspective, a median rubber content such as R_c=15% is expected to yield a more reliable estimate of the fitting parameters (Mirzababaei et al. 2018).

4.4. Soil–Rubber Amending Mechanisms

Scanning electron microscopy (SEM) studies conducted by several researchers indicate that rubber particles are non–spherical and highly irregular in shape, with some cavities and micro–cracks propagated along the rubber's surface, thus predicating a rough surface texture (e.g. Yadav and Tiwari 2017[a]; Soltani et al. 2018[b]). Such surface features could potentially promote adhesion and/or induce frictional resistance between the rubber particles and the soil grains, and hence alter the soil fabric into a unitary mass of restricted heave/settlement and improved strength performance. As such, the soil–rubber amending mechanisms can be discussed in two aspects: **i)** interfacial frictional resistance generated as a result of soil–rubber contact; and **ii)** mechanical interlocking of rubber particles and soil grains (Racana et al. 2003; Dove et al. 2006; Tang et al. 2007, 2010; Trouzine et al. 2012; Kalkan 2013; Yadav and Tiwari 2017[b]; Soltani et al. 2018[b]).

The first aspect, the interfacial frictional resistance, is a function of soil–rubber contact area, with greater contact levels offering a higher resistance to bear external loads. Consequently, this amending mechanism is in line with the rubber content and to a lesser degree the rubber size. For a given rubber type (or constant rubber size), the greater the number of included rubber particles (or increase in rubber content) the greater the contact level achieved between the rubber particles and the soil grains, which in turn promotes an induced frictional resistance and hence improved strength performance. Similarly, for a given rubber content, an increase in rubber size would potentially favor a more effective soil–rubber contact level (owing to the rubber's larger size or lower specific surface area), and thus an induced frictional resistance coupled with improved strength properties. This amending mechanism, however, only holds provided that the rubber particles are well distributed in the soil regime and do not cluster (or adhere to each other) during sample preparation (or compaction) and/or external loading (Kim and Kang 2013; Cabalar et al. 2014; Cabalar and Karabash 2015; Zhang et al. 2018). At high rubber contents and potentially for the rubber of coarser category, the behavior of the composite at some points could be governed by a dominant rubber–to–rubber interaction, which though offers a notable improvement to the composite's ductility (as evident with the stress–strain curves obtained from the UC, ST and DS tests shown in **Figures 3**, **5**, **7** and **8**), offsets the desired soil–to–rubber interaction capable of improving the composite's peak strength. Such adverse effects were evident for both rubber types with contents greater than 10%, where the previously improved peak UC and peak ST strength values began to drop with increase in rubber content, thus signifying a rubber–clustering capacity at high rubber inclusions during

compressive (UC) and tensile (ST) loading conditions (see **Figures 4** and **6**). Rubber–clustering effects were not apparent under DS testing conditions. This can be attributed to the role portrayed by confinement (or normal stress) in inducing frictional resistance at the shearing interface, thereby offsetting the adverse effects associated with the clustering of rubber particles. Quite clearly, the greater the magnitude of confinement the less apparent the rubber–clustering effects, and hence the greater the magnitude of improvement in peak strength (e.g. compare the stress paths '$A_1 \rightarrow A_2$' with '$B_1 \rightarrow B_2$' in **Figure 9**). As opposed to the DS test, both the UC and ST tests are characterized as non–confinement tests, which in turn justifies the discrepancy observed between the peak UC (or peak ST) and peak DS strength values at rubber inclusions greater than 10%.

The second aspect, the mechanical interlocking, is achieved during compaction and induces composite adhesion by restricting the movement of soil grains interlocked to the rubber undergoing external loading. In this case, the more effective the achieved mechanical interlocking the higher the resistance to external loads. As such, this amending mechanism is dependent on the rubber content, and more importantly the rubber size/shape. For a given rubber type (or constant rubber size/shape), the greater the number of included rubber particles (or increase in rubber content) the greater the number of interlocked or enwrapped soil grains, and hence the greater the improvement in strength properties. As opposed to the granular form factor of the finer rubber C (see **Figure 2a**), the particles of rubber B are more fiber–shaped (see **Figure 2b**), and thus favor a more pronounced mechanical interlocking by entwining within the matrix and immobilizing the soil grains against external loads with much more efficiency. Although in most cases the rubber of coarser category slightly outperformed the finer rubber, the effect of larger rubber size for UC, ST and DS testing conditions was mainly translated to higher ductility, lower stiffness, higher energy adsorption capacity and higher post–peak (or critical) shear strength (see **Figure 10**) rather than peak strength improvements.

4.5. Effect of Rubbers on Cracking Intensity

Figure 13 illustrates the variations of the crack intensity factor (CIF), along with corresponding crack reduction factors (CRF), against rubber content for the tested samples. The cracking intensity was dependent on both the rubber content and the rubber size, with the former portraying a more significant role. The natural soil exhibited a crack intensity factor of CIF=15.02%, while the inclusion of 5%, 10%, 20% and 30% rubber C resulted in CIF=13.85%, 11.21%, 8.41% and 6.01% (i.e. CRF=8%, 25%, 44% and 60%), respectively. Similar inclusions

of rubber B resulted in lower CIF and higher CRF values, thus indicating a rubber size–dependent amending mechanism. In this case, the aforementioned values dropped to CIF=12.37%, 9.55%, 5.98% and 4.57% (i.e. CRF=18%, 36%, 60% and 70%), respectively.

Typical crack patterns overserved for the natural soil and samples reinforced with 30% rubbers C and B are provided in **Figure 14**. A hierarchical cracking pattern can be observed for the natural soil, which divides the soil mass into a series of rather small cells with wide crack openings (see **Figure 14b**). Reinforced samples, however, manifested larger cells with relatively smaller crack openings (see **Figures 14d** and **14g**). As a consequence of internal (e.g. non–uniform drying) and/or external (e.g. boundary friction/adhesion) restrains acting on the soil during drying, tensile stresses developed within the soil can exceed the soil's tensile strength, which in turn leads to the development and propagation of cracks (Kodikara and Chakrabarti 2005; Tang et al. 2012; Costa et al. 2013). The development and propagation of cracks is primarily a function of clay content, meaning that the higher the clay content the greater the intensity of cracking (Mitchell and Soga 2005; Soltani et al. 2018[b]). As such, the rubber inclusions are able to amend desiccation–induced cracking through rubber–clay substitution. Consequently, this amending mechanism is a function of rubber content, with higher rubber inclusions substituting a larger portion of the clay content and hence ameliorating the effect of cracking with increased efficiency. Moreover, the rubber inclusions complement a notable improvement in the soil's tensile strength, as evident with the ST test results (see **Section 4.2**), which in turn reduces the cracking intensity. As discussed in **Section 4.4**, improvement in the soil's tensile strength can also be achieved through interlocking of rubber particles and soil grains. The interlocking effect is enhanced in the presence of rubber B, owing to its fiber–shaped form factor, which acts as bridges between the desiccated soil cells, thereby immobilizing desiccation–induced movements and hence restricting the development of wide crack openings (see **Figure 14f**).

4.6. Swelling Characteristics and Optimum Rubber Content

Arriving at reliable stabilization schemes with respect to expansive soils often requires solving a two–objective optimization problem, i.e. minimizing the swell–shrink capacity, while either maintaining or improving the strength–related properties (Olgun 2013; Shahbazi et al. 2017; Soltani 2017). The present study deals with the latter objective, while the former was previously investigated (for the same mix designs outlined in **Table 2**) by the authors in Soltani et al. (2018[c]). In this section, typical results outlined in Soltani et al. (2018[c]) will be first revisited,

and then cross–checked with the results obtained in the present study to arrive at the optimum rubber content suitable for stabilization of expansive soils. Samples for the swell tests were prepared by the static compaction technique at the corresponding dry of optimum condition of each mix design (i.e. 5% less than optimum water content and its corresponding dry unit weight). The prepared samples, measuring 50 mm in diameter and 20 mm in height, were subjected to the swell–load oedometer test scheme (ASTM D4546–14). The samples were first allowed to freely swell under a low nominal overburden stress of 1 kPa to a point in which the ultimate swelling strain, denoted as swelling potential (i.e. $\varepsilon_{sw}=\Delta H_u/H_0$, where ΔH_u=ultimate heave; and H_0=initial height of the sample), could be achieved. Upon completion of the swell stage, the samples were gradually loaded to counteract the built–up swelling strain. The stress required to retain the sample's initial placement was defined as the swelling pressure.

Figure 15 illustrates the variations of swelling potential and swelling pressure against rubber content for the natural soil and various soil–rubber composites. The swelling properties were dependent on both the rubber content and the rubber size, with the former portraying a more significant role. The higher the rubber content the lower the swelling properties, following a monotonic decreasing trend. For a given rubber content, however, the rubber of coarser category consistently outperformed the finer rubber by exhibiting lower swelling behavior. The natural soil and samples reinforced with 5%, 10%, 20% and 30% rubber C resulted in swelling potential (and pressure) values of ε_{sw}=18.35% (σ_{sw}=120 kPa), 16.02% (σ_{sw}=100 kPa), 13.01% (σ_{sw}=70 kPa), 11.17% (σ_{sw}=54 kPa) and 9.56% (σ_{sw}=51 kPa), respectively. For similar inclusions of rubber B, these values further decreased to ε_{sw}=14.74% (σ_{sw}=73 kPa), 12.18% (σ_{sw}=51 kPa), 9.02% (σ_{sw}=32 kPa) and 8.11% (σ_{sw}=34 kPa), respectively. As a typical case, the swelling potential and swelling pressure, respectively, experienced notable improvements of 29% and 42% when reinforced with 10% rubber C. For the same inclusion of rubber B, these improvements further increased to 34% and 58%, respectively. For both rubber types, R_c=20% and 30% exhibited similar results with marginal differences, thus indicating a maximum rubber content of 20% as optimal/sufficient to counteract swelling. In addition to the amending mechanisms **'**interfacial frictional resistance**'** and **'**mechanical interlocking**'** described in **Section 4.4**, the reduction in swelling properties can also be ascribed to rubber–expansive clay substitution (Soltani et al. 2018[c]). Similar to desiccation–induced cracking, the swelling properties are primarily a function of the soil's expansive clay content. For a given rubber type, an increase in rubber content substitutes a larger portion of the expansive clay content with non–expansive hydrophobic rubber particles, thereby leading to a further decrease of the

swelling properties (complementary results and discussions on the swell–shrink–consolidation characteristics of rubber–reinforced expansive soils can be found in Soltani et al. (2018[c])).

The swelling and shrinkage properties (i.e. the shrinkage properties refer to that outlined in **Section 4.5**) are in favor of higher rubber contents. Meanwhile, high rubber inclusions, as shown in **Sections 4.1** and **4.2**, could raise strength concerns when subjected to compressive and/or tensile loading. Consequently, a rubber inclusion of 10% (preferably the rubber of coarser category) can satisfy the two–objective design requirement (i.e. minimizing the swell–shrink capacity, while either maintaining or improving the strength–related properties). Where context changes and the strength and stiffness of the material (subjected to compression and/or tension) are not a primary concern, higher rubber inclusions up to 20% may also be considered as acceptable choices.

5. Conclusions

The following conclusions can be drawn from this study:

- For both rubber types, the peak UC and peak ST strength values were dependent on the rubber content, peaking at R_C=5%–10% then decreasing at higher rubber inclusions. Rubber–clustering effects were evident for rubber contents greater than 10%, which led to some adverse results. The effect of rubber size/shape was mainly translated to higher ductility, lower stiffness and higher energy adsorption capacity rather than peak strength improvements.

- The peak and critical shear strengths were dependent on both the rubber content and the rubber size, with the former portraying a more significant role. For rubber contents equal to or less than 10%, the rubber of coarser category slightly outperformed the finer rubber in terms of higher peak shear strength properties, while an opposite effect was evident at higher rubber inclusions. In this case, R_C=20% served as a transition point by manifesting a similar performance with marginal differences for the two rubber types. The strain–softening character was less apparent at high inclusions of the coarser rubber, thus resulting in induced strength performance at critical state condition. As a result, the critical shear strength was in favor of both a higher rubber content and a larger rubber size.

- A multiple linear regression (MLR) model was suggested to quantify the peak and critical shear strengths as a function of the composite's index properties, i.e. normal stress, rubber

content, specific surface area (or plasticity index) and the initial placement/compaction condition. The predictive capacity of the proposed MLR model was examined and validated by statistical techniques. The suggested MLR model contains a limited number of fitting parameters which can be calibrated by little experimental effort, and hence implemented for predictive purposes.

- The rubber inclusions were able to amend desiccation–induced cracking. The cracking intensity was dependent on both the rubber content and the rubber size, with the former portraying a more significant role. In this case, the higher the rubber content the greater the magnitude of improvement, with the coarser rubber holding a notable advantage over similar samples reinforced with the finer rubber.

- The results of the UC, ST and DS tests were cross–checked with the swelling and cracking properties to arrive at the optimum rubber content. A rubber inclusion of 10% (preferably the rubber of coarser category) satisfied a decrease in the swell–shrink capacity as well as improving the strength–related properties, and thus was deemed as the optimum choice. Where context changes and the compressive/tensile strength and stiffness of the material are not a primary concern, higher rubber inclusions up to 20% may also be considered as acceptable choices.

Acknowledgements

This research was funded by the Australian Research Council (ARC) via project No. **DP140103004**, and their support is gratefully acknowledged.

References

Al-Aqtash U and Bandini P (**2015**) Prediction of unsaturated shear strength of an adobe soil from the soil–water characteristic curve. *Construction and Building Materials* **98**: 892–899, http://doi.org/10.1016/j.conbuildmat.2015.07.188.

Alazigha DP, Indraratna B, Vinod JS and Ezeajugh LE (**2016**) The swelling behaviour of lignosulfonate–treated expansive soil. *Proceedings of the Institution of Civil Engineers: Ground Improvement* **169**(**3**): 182–193, http://doi.org/10.1680/jgrim.15.00002.

Alazigha DP, Vinod JS, Indraratna B and Heitor A (**2018**) Potential use of lignosulfonate for expansive soil stabilisation. *Environmental Geotechnics* **in press**, http://doi.org/10.1680/jenge.17.00051.

Bai FQ and Liu SH (**2012**) Measurement of the shear strength of an expansive soil by combining a filter paper method and direct shear tests. *Geotechnical Testing Journal* **35**(**3**): 451–459, http://doi.org/10.1520/gtj103342.

Cabalar AF and Karabash Z (**2015**) California bearing ratio of a sub–base material modified with tire buffings and cement addition. *Journal of Testing and Evaluation* **43**(**6**): 1279–1287, http://doi.org/10.1520/jte20130070.

Cabalar AF, Karabash Z and Mustafa WS (**2014**) Stabilising a clay using tyre buffings and lime. *Road Materials and Pavement Design* **15**(**4**): 872–891, http://doi.org/10.1080/14680629.2014.939697.

Calik U and Sadoglu E (**2014**) Classification, shear strength, and durability of expansive clayey soil stabilized with lime and perlite. *Natural Hazards* **71**(**3**): 1289–1303, http://doi.org/10.1007/s11069-013-0950-1.

Cetin H, Fener M and Gunaydin O (**2006**) Geotechnical properties of tire–cohesive clayey soil mixtures as a fill material. *Engineering Geology* **88**(**1**–**2**): 110–120, http://doi.org/10.1016/j.enggeo.2006.09.002.

Chaduvula U, Viswanadham BVS and Kodikara J (**2017**) A study on desiccation cracking behavior of polyester fiber–reinforced expansive clay. *Applied Clay Science* **142**: 163–172, http://doi.org/10.1016/j.clay.2017.02.008.

Costa S, Kodikara J and Shannon B (**2013**) Salient factors controlling desiccation cracking of clay in laboratory experiments. *Géotechnique* **63**(**1**): 18–29, http://doi.org/10.1680/geot.9.p.105.

Dove JE, Bents DD, Wang J and Gao B (**2006**) Particle–scale surface interactions of non–dilative interface systems. *Geotextiles and Geomembranes* **24**(**3**): 156–168, http://doi.org/10.1016/j.geotexmem.2006.01.002.

Dunham-Friel J and Carraro JAH (**2011**) Shear strength and stiffness of expansive soil and rubber (ESR) mixtures in undrained axisymmetric compression. In *Geo–Frontiers 2011 (GSP 211): Advances in Geotechnical Engineering* (Han J and Alzamora DE (eds)). ASCE, Dallas, Texas, USA, pp. 1111–1120, http://doi.org/10.1061/41165(397)114.

Dunham-Friel J and Carraro JAH (**2014**) Effects of compaction effort, inclusion stiffness, and rubber size on the shear strength and stiffness of expansive soil–rubber (ESR) mixtures. In *Geo–Congress*

2014 Technical Papers: Geo–Characterization and Modeling for Sustainability (GSP 234) (Abu-Farsakh M, Yu X, and Hoyos LR (eds)). ASCE, Atlanta, Georgia, USA, pp. 3635–3644, http://doi.org/10.1061/9780784413272.352.

Edil T and Bosscher P (**1994**) Engineering properties of tire chips and soil mixtures. *Geotechnical Testing Journal* **17**(**4**): 453–464, http://doi.org/10.1520/gtj10306j.

Estabragh AR, Namdar P and Javadi AA (**2012**) Behavior of cement–stabilized clay reinforced with nylon fiber. *Geosynthetics International* **19**(**1**): 85–92, http://doi.org/10.1680/gein.2012.19.1.85.

Estabragh AR, Naseh M, Beytolahpour I and Javadi AA (**2013[b]**) Strength of a clay soil and soil–cement mixture with resin. *Proceedings of the Institution of Civil Engineers: Ground Improvement* **166**(**2**): 108–114, http://doi.org/10.1680/grim.12.00014.

Estabragh AR, Pereshkafti MRS, Parsaei B and Javadi AA (**2013[a]**) Stabilised expansive soil behaviour during wetting and drying. *International Journal of Pavement Engineering* **14**(**4**): 418–427, http://doi.org/10.1080/10298436.2012.746688.

Estabragh AR, Rafatjo H and Javadi AA (**2014**) Treatment of an expansive soil by mechanical and chemical techniques. *Geosynthetics International* **21**(**3**): 233–243, http://doi.org/10.1680/gein.14.00011.

Estabragh AR, Ranjbari S and Javadi AA (**2017**) Properties of clay soil and soil cement reinforced with polypropylene fibers. *ACI Materials Journal* **114**(**2**): 195–205, http://doi.org/10.14359/51689469.

Estabragh AR, Soltani A and Javadi AA (**2016**) Models for predicting the seepage velocity and seepage force in a fiber reinforced silty soil. *Computers and Geotechnics* **75**: 174–181, http://doi.org/10.1016/j.compgeo.2016.02.002.

Estabragh AR, Soltani A and Javadi AA (**2018**) Effect of pore water chemistry on the behaviour of a kaolin–bentonite mixture during drying and wetting cycles. *European Journal of Environmental and Civil Engineering* **in press**, http://doi.org/10.1080/19648189.2018.1428691.

Gourley CS, Newill D and Schreiner HD (**1994**) Expansive soils: TRL's research strategy. In *Proceedings of the 1st International Symposium on Engineering Characteristics of Arid Soils* (Fookes PG and Parry RHG (eds)). A.A. Balkema, Rotterdam, the Netherlands, pp. 247–260, ISBN: 9054103655.

Guney Y, Sari D, Cetin M and Tuncan M (**2007**) Impact of cyclic wetting–drying on swelling behavior of lime–stabilized soil. *Building and Environment* **42**(**2**): 681–688, http://doi.org/10.1016/j.buildenv.2005.10.035.

Hejazi SM, Sheikhzadeh M, Abtahi SM and Zadhoush A (**2012**) A simple review of soil reinforcement by using natural and synthetic fibers. *Construction and Building Materials* **30**: 100–116, http://doi.org/10.1016/j.conbuildmat.2011.11.045.

Iyengar SR, Masad E, Rodriguez AK, Bazzi HS, Little D and Hanley HJM (**2013**) Pavement subgrade stabilization using polymers: Characterization and performance. *Journal of Materials in Civil Engineering* **25**(**4**): 472–483, http://doi.org/10.1061/(asce)mt.1943-5533.0000612.

Jayasree PK, Balan K, Peter L and Nisha KK (**2015**) Volume change behavior of expansive soil stabilized with coir waste. *Journal of Materials in Civil Engineering* **27**(**6**): 4014195–8, http://doi.org/10.1061/(asce)mt.1943-5533.0001153.

Jones LD and Jefferson I (**2012**) Expansive soils. In *ICE Manual of Geotechnical Engineering: Volume I* (Burland J, Chapman T, Brown M and Skinner H (eds)). ICE Publishing, London, UK, pp. 413–441, http://doi.org/10.1680/moge.57074.0413.

Kalkan E (**2013**) Preparation of scrap tire rubber fiber–silica fume mixtures for modification of clayey soils. *Applied Clay Science* **80**–**81**: 117–125, http://doi.org/10.1016/j.clay.2013.06.014.

Khattak MJ and Alrashidi M (**2006**) Durability and mechanistic characteristics of fiber reinforced soil–cement mixtures. *International Journal of Pavement Engineering* **7**(**1**): 53–62, http://doi.org/10.1080/10298430500489207.

Kim YT and Kang HS (**2013**) Effects of rubber and bottom ash inclusion on geotechnical characteristics of composite geomaterial. *Marine Georesources and Geotechnology* **31**(**1**): 71–85, http://doi.org/10.1080/1064119x.2012.667867.

Kodikara J and Chakrabarti S (**2005**) Modeling of moisture loss in cementitiously stabilized pavement materials. *International Journal of Geomechanics* **5**(**4**): 295–303, http://doi.org/10.1061/(asce)1532-3641(2005)5:4(295).

Kua TA, Arulrajah A, Mohammadinia A, Horpibulsuk S and Mirzababaei M (**2017**) Stiffness and deformation properties of spent coffee grounds based geopolymers. *Construction and Building Materials* **138**: 79–87, http://doi.org/10.1016/j.conbuildmat.2017.01.082.

Kumar A, Walia BS and Bajaj A (**2007**) Influence of fly ash, lime, and polyester fibers on compaction and strength properties of expansive soil. *Journal of Materials in Civil Engineering* **19**(**3**): 242–248, http://doi.org/10.1061/(asce)0899-1561(2007)19:3(242).

Liu C and Evett J (**2009**) *Soil Properties: Testing, Measurement, and Evaluation (6th ed)*. Pearson/Prentice Hall, Upper Saddle River, New Jersey, USA, ISBN: 9780136141235.

Locat J, Lefebvre G and Ballivy G (**1984**) Mineralogy, chemistry, and physical properties interrelationships of some sensitive clays from Eastern Canada. *Canadian Geotechnical Journal* **21**(**3**): 530–540, http://doi.org/10.1139/t84-055.

Maher MH and Ho YC (**1994**) Mechanical properties of kaolinite/fiber soil composite. *Journal of Geotechnical Engineering* **120**(**8**): 1381–1393, http://doi.org/10.1061/(asce)0733-9410(1994)120:8(1381).

Mashiri MS, Vinod JS, Sheikh MN and Carraro JAH (**2017**) Shear modulus of sand–tyre chip mixtures. *Environmental Geotechnics* **in press**, http://doi.org/10.1680/jenge.16.00016.

Miller CJ and Rifai S (**2004**) Fiber reinforcement for waste containment soil liners. *Journal of Environmental Engineering* **130**(**8**): 891–895, http://doi.org/10.1061/(asce)0733-9372(2004)130:8(891).

Mirzababaei M, Arulrajah A, Horpibulsuk S and Aldavad M (**2017**) Shear strength of a fibre–reinforced clay at large shear displacement when subjected to different stress histories. *Geotextiles and Geomembranes* **45**(**5**): 422–429, http://doi.org/10.1016/j.geotexmem.2017.06.002.

Mirzababaei M, Miraftab M, Mohamed M and McMahon P (**2013**[a]) Unconfined compression strength of reinforced clays with carpet waste fibers. *Journal of Geotechnical and Geoenvironmental Engineering* **139**(**3**): 483–493, http://doi.org/10.1061/(asce)gt.1943-5606.0000792.

Mirzababaei M, Miraftab M, Mohamed M and McMahon P (**2013**[b]) Impact of carpet waste fibre addition on swelling properties of compacted clays. *Geotechnical and Geological Engineering* **31**(**1**): 173–182, http://doi.org/10.1007/s10706-012-9578-2.

Mirzababaei M, Mohamed M, Arulrajah A, Horpibulsuk S and Anggraini V (**2018**) Practical approach to predict the shear strength of fibre–reinforced clay. *Geosynthetics International* **25**(**1**): 50–66, http://doi.org/10.1680/jgein.17.00033.

Mirzababaei M, Yasrobi SS and Al-Rawas AA (**2009**) Effect of polymers on swelling potential of expansive soils. *Proceedings of the Institution of Civil Engineers: Ground Improvement* **162**(**3**): 111–119, http://doi.org/10.1680/grim.2009.162.3.111.

Mitchell JK and Soga K (**2005**) Soil–water–chemical interactions. In *Fundamentals of Soil Behavior (3rd ed)*. John Wiley & Sons, Hoboken, New Jersey, USA, pp. 143–172, http://doi.org/10.2136/sssaj1976.03615995004000040003x.

Nalbantoglu Z (**2006**) Lime stabilization of expansive clay. In *Expansive Soils: Recent Advances in Characterization and Treatment* (Al-Rawas AA and Goosen MFA (eds)). Taylor & Francis Group, London, UK, pp. 139–148, http://doi.org/10.1201/9780203968079.ch23.

Nelson JD and Miller DJ (**1992**) *Expansive Soils: Problems and Practice in Foundation and Pavement Engineering (1st ed)*. John Wiley & Sons, New York, New York, USA, ISBN: 0471511862.

Olgun M (**2013**) The effects and optimization of additives for expansive clays under freeze–thaw conditions. *Cold Regions Science and Technology* **93**: 36–46, http://doi.org/10.1016/j.coldregions.2013.06.001.

Özkul ZH and Baykal G (**2006**) Shear strength of clay with rubber fiber inclusions. *Geosynthetics International* **13**(**5**): 173–180, http://doi.org/10.1680/gein.2006.13.5.173.

Özkul ZH and Baykal G (**2007**) Shear behavior of compacted rubber fiber–clay composite in drained and undrained loading. *Journal of Geotechnical and Geoenvironmental Engineering* **133**(**7**): 767–781, http://doi.org/10.1061/(asce)1090-0241(2007)133:7(767).

Patil U, Valdes JR and Evans TM (**2011**) Swell mitigation with granulated tire rubber. *Journal of Materials in Civil Engineering* **23**(**5**): 721–727, http://doi.org/10.1061/(asce)mt.1943-5533.0000229.

Prakash K and Sridharan A (**2004**) Free swell ratio and clay mineralogy of fine–grained soils. *Geotechnical Testing Journal* **27**(**2**): 220–225, http://doi.org/10.1520/gtj10860.

Puppala AJ, Griffin JA, Hoyos LR and Chomtid S (**2004**) Studies on sulfate–resistant cement stabilization methods to address sulfate–induced soil heave. *Journal of Geotechnical and Geoenvironmental Engineering* **130**(**4**): 391–402, http://doi.org/10.1061/(asce)1090-0241(2004)130:4(391).

Qu J and Zhao D (**2016**) Stabilising the cohesive soil with palm fibre sheath strip. *Road Materials and Pavement Design* **17**(**1**): 87–103, http://doi.org/10.1080/14680629.2015.1064010.

Qu J, Li C, Liu B, Chen X, Li M and Yao Z (**2013**) Effect of random inclusion of wheat straw fibers on shear strength characteristics of Shanghai cohesive soil. *Geotechnical and Geological Engineering* **31**(**2**): 511–518, http://doi.org/10.1007/s10706-012-9604-4.

Racana N, Grediac M and Gourves R (**2003**) Pull–out response of corrugated geotextile strips. *Geotextiles and Geomembranes* **21**(**5**): 265–288, http://doi.org/10.1016/s0266-1144(03)00031-1.

Radovic M, Lara-Curzio E and Riester L (**2004**) Comparison of different experimental techniques for determination of elastic properties of solids. *Materials Science and Engineering: A* **368**(**1**–**2**): 56–70, http://doi.org/10.1016/j.msea.2003.09.080.

Seda JH, Lee JC and Carraro JAH (**2007**) Beneficial use of waste tire rubber for swelling potential mitigation in expansive soils. In *Geo–Denver 2007: Soil Improvement (GSP 172)* (Schaefer VR, Filz GM, Gallagher PM, Sehn AL and Wissmann KJ (eds)). ASCE, Denver, Colorado, USA, pp. 1–9, http://doi.org/10.1061/40916(235)5.

Sezer A, İnan G, Recep Yılmaz H and Ramyar K (**2006**) Utilization of a very high lime fly ash for improvement of Izmir clay. *Building and Environment* **41**(**2**): 150–155, http://doi.org/10.1016/j.buildenv.2004.12.009.

Shahbazi M, Rowshanzamir M, Abtahi SM and Hejazi SM (**2017**) Optimization of carpet waste fibers and steel slag particles to reinforce expansive soil using response surface methodology. *Applied Clay Science* **142**: 185–192, http://doi.org/10.1016/j.clay.2016.11.027.

Signes CH, Garzón-Roca J, Fernández PM, Torre MEG and Franco RI (**2016**) Swelling potential reduction of Spanish argillaceous marlstone Facies Tap soil through the addition of crumb rubber particles from scrap tyres. *Applied Clay Science* **132**–**133**: 768–773, http://doi.org/10.1016/j.clay.2016.07.027.

Sivapullaiah P V., Sridharan A and Ramesh HN (**2000**) Strength behaviour of lime–treated soils in the presence of sulphate. *Canadian Geotechnical Journal* **37**(**6**): 1358–1367, http://doi.org/10.1139/t00-052.

Soltani A (**2017**) Discussion of "Optimization of carpet waste fibers and steel slag particles to reinforce expansive soil using response surface methodology" by M. Shahbazi, M. Rowshanzamir, S.M. Abtahi, S.M. Hejazi [Appl. Clay Sci., doi:10.1016/j.clay.2016.11.027]. *Applied Clay Science* **in press**, http://doi.org/10.1016/j.clay.2017.07.020.

Soltani A and Mirzababaei M (**2018**) Comment on "Compaction and strength behavior of tire crumbles–fly ash mixed with clay" by A. Priyadarshee, A. Kumar, D. Gupta, and P. Pushkarna. *Journal of Materials in Civil Engineering* **in press**.

Soltani A, Azimi M, Deng A and Taheri A (**2017**[c]) A simplified method for determination of the soil–water characteristic curve variables. *International Journal of Geotechnical Engineering* **in press**, http://doi.org/10.1080/19386362.2017.1344450.

Soltani A, Deng A and Taheri A (**2018**[a]) Swell–compression characteristics of a fiber–reinforced expansive soil. *Geotextiles and Geomembranes* **46**(**2**): 183–189, http://doi.org/10.1016/j.geotexmem.2017.11.009.

Soltani A, Deng A, Taheri A and Mirzababaei M (**2017**[b]) A sulphonated oil for stabilisation of expansive soils. *International Journal of Pavement Engineering* **in press**, http://doi.org/10.1080/10298436.2017.1408270.

Soltani A, Deng A, Taheri A and Mirzababaei M (**2018**[b]) Rubber powder–polymer combined stabilization of South Australian expansive soils. *Geosynthetics International* **in press**, http://doi.org/10.1680/jgein.18.00009.

Soltani A, Deng A, Taheri A and Sridharan A (**2018**[c]) Swell–shrink–consolidation behavior of rubber–reinforced expansive soils. *Geotechnical Testing Journal* **in press**.

Soltani A, Deng A, Taheri A, Sridharan A and Estabragh AR (**2018**[d]) A framework for interpretation of the compressibility behavior of soils. *Geotechnical Testing Journal* **41**(**1**): 1–16, http://doi.org/10.1520/gtj20170088.

Soltani A, Taheri A, Khatibi M and Estabragh AR (**2017**[a]) Swelling potential of a stabilized expansive soil: A comparative experimental study. *Geotechnical and Geological Engineering* **35**(**4**): 1717–1744, http://doi.org/10.1007/s10706-017-0204-1.

Sridharan A and Nagaraj HB (**2000**) Compressibility behaviour of remoulded, fine–grained soils and correlation with index properties. *Canadian Geotechnical Journal* **37**(**3**): 712–722, http://doi.org/10.1139/t99-128.

Srivastava A, Pandey S and Rana J (**2014**) Use of shredded tyre waste in improving the geotechnical properties of expansive black cotton soil. *Geomechanics and Geoengineering* **9**(**4**): 303–311, http://doi.org/10.1080/17486025.2014.902121.

Tang CS, Shi B and Zhao LZ (**2010**) Interfacial shear strength of fiber reinforced soil. *Geotextiles and Geomembranes* **28**(**1**): 54–62, http://doi.org/10.1016/j.geotexmem.2009.10.001.

Tang CS, Shi B, Cui YJ, Liu C and Gua K (**2012**) Desiccation cracking behavior of polypropylene fiber–reinforced clayey soil. *Canadian Geotechnical Journal* **49**(**9**): 1088–1101, http://doi.org/10.1139/t2012-067.

Tang CS, Shi B, Gao W, Chen F and Cai Y (**2007**) Strength and mechanical behavior of short polypropylene fiber reinforced and cement stabilized clayey soil. *Geotextiles and Geomembranes* **25**(**3**): 194–202, http://doi.org/10.1016/j.geotexmem.2006.11.002.

Thomas BS, Gupta RC and Panicker VJ (**2016**) Recycling of waste tire rubber as aggregate in concrete: Durability–related performance. *Journal of Cleaner Production* **112**(**1**): 504–513, http://doi.org/10.1016/j.jclepro.2015.08.046.

Thyagaraj T and Zodinsanga S (**2014**) Swell–shrink behaviour of lime precipitation treated soil. *Proceedings of the Institution of Civil Engineers: Ground Improvement* **167**(**4**): 260–273, http://doi.org/10.1680/grim.12.00028.

Trouzine H, Bekhiti M and Asroun A (**2012**) Effects of scrap tyre rubber fibre on swelling behaviour of two clayey soils in Algeria. *Geosynthetics International* **19**(**2**): 124–132, http://doi.org/10.1680/gein.2012.19.2.124.

Wang YX, Guo PP, Ren WX, Yuan BX, Yuan HP, Zhao YL, Shan SB and Cao P (**2017**) Laboratory investigation on strength characteristics of expansive soil treated with jute fiber reinforcement. *International Journal of Geomechanics* **17**(**11**): 1–12, http://doi.org/10.1061/(asce)gm.1943-5622.0000998.

Williamson S and Cortes DD (**2014**) Dimensional analysis of soil–cement mixture performance. *Géotechnique Letters* **4**(**1**): 33–38, http://doi.org/10.1680/geolett.13.00082.

Yadav JS and Tiwari SK (**2017[a]**) The impact of end–of–life tires on the mechanical properties of fine–grained soil: A review. *Environment, Development and Sustainability* **in press**, http://doi.org/10.1007/s10668-017-0054-2.

Yadav JS and Tiwari SK (**2017[b]**) Effect of waste rubber fibres on the geotechnical properties of clay stabilized with cement. *Applied Clay Science* **149**: 97–110, http://doi.org/10.1016/j.clay.2017.07.037.

Yadav JS and Tiwari SK (**2017[c]**) A study on the potential utilization of crumb rubber in cement treated soft clay. *Journal of Building Engineering* **9**: 177–191, http://doi.org/10.1016/j.jobe.2017.01.001.

Yesiller N, Miller CJ, Inci G and Yaldo K (**2000**) Desiccation and cracking behavior of three compacted landfill liner soils. *Engineering Geology* **57**(**1**–**2**): 105–121, http://doi.org/10.1016/s0013-7952(00)00022-3.

Zhang T, Cai G and Duan W (**2018**) Strength and microstructure characteristics of the recycled rubber tire–sand mixtures as lightweight backfill. *Environmental Science and Pollution Research* **25**(**4**): 3872–3883, http://doi.org/10.1007/s11356-017-0742-3.

Zhao Y, Gao Y, Zhang Y and Wang Y (**2016**) Effect of fines on the mechanical properties of composite soil stabilizer–stabilized gravel soil. *Construction and Building Materials* **126**: 701–710, http://doi.org/10.1016/j.conbuildmat.2016.09.082.

Zornberg JG, Cabral AR and Viratjandr C (**2004**) Behaviour of tire shred–sand mixtures. *Canadian Geotechnical Journal* **41**(**2**): 227–241, http://doi.org/10.1139/t03-086.

List of Tables

Table 1. Physical and mechanical properties of kaolinite, bentonite and the kaolin–bentonite mixture.

Table 2. Soil–rubber mix designs and their properties.

Table 3. Summary of the regression analysis outputs with respect to the proposed MLR model or **Equation 3** for τ_p and τ_{cr}.

Table 1. Physical and mechanical properties of kaolinite, bentonite and the kaolin–bentonite mixture.

Properties	**Kaolinite**	**Bentonite**	**Mixture**[†]
Specific gravity, G_s	2.68	2.81	2.73
Grain–size distribution			
Clay (< 2 μm) (%)	49.78	62.43	Not measured
Silt (2–75 μm) (%)	49.43	35.75	
Sand (0.075–4.75 mm) (%)	0.79	1.82	
Consistency limits			
Liquid limit, *LL* (%)	41.04	379.21	59.60
Plastic limit, *PL* (%)	23.67	45.18	27.28
Plasticity index, *PI* (=*LL*–*PL*) (%)	17.37	334.03	32.32
Linear shrinkage, *LS* (%)	Not measured	Not measured	8.19
Classifications			
USCS classification	CL	CH	CH
Free swell ratio, FSR[‡]	1.19	7.53	2.91
Degree of expansivity	Low	Very high	High
Compaction characteristics			
Optimum water content, w_{opt} (%)	19.82	36.34	26.00
Maximum dry unit weight, γ_{dmax} (kN/m^3)	15.67	11.74	15.07

Note:
[†]85% kaolinite and 15% bentonite; and [‡]ratio of equilibrium sediment volume of 10 g oven–dried soil passing sieve 425 μm in distilled water to that of kerosene, as defined by Prakash and Sridharan (2004).

Table 2. Soil–rubber mix designs and their properties.

Rubber type	**Soil (%)**	**R_c (%)**[†]	***LL* (%)**[‡]	***PL* (%)**	***PI* (%)**	***LS* (%)**	***SI* (%)**[*]	**w_{opt} (%)**[#]	**γ_{dmax} (kN/m^3)**[#]
—	100	0	59.60	27.28	32.32	8.19	51.40	26.00	15.07
Rubber C	95	5	57.03	27.02	30.01	8.02	49.01	24.77	14.63
	90	10	55.04	25.54	29.50	7.58	47.46	23.87	14.35
	80	20	51.51	23.46	28.05	6.76	44.75	21.85	13.87
	70	30	49.58	22.70	26.88	5.93	43.65	20.07	13.52
Rubber B	95	5	56.88	26.61	30.27	7.94	49.39	24.47	14.61
	90	10	55.62	24.77	30.85	7.71	47.91	23.46	14.37
	80	20	52.44	23.27	29.17	7.02	45.42	21.15	13.86
	70	30	51.21	22.15	29.06	5.68	45.54	19.94	13.52

Note:
[†]$R_c=W_R/W_S\times100$ (W_R=weight of rubber; and W_S=weight of dry soil); [‡]initial placement condition for desiccation–induced crack tests; [*]shrinkage index (=*LL*–*LS*, as defined by Sridharan and Nagaraj (2000)); and [#]initial placement condition for UC, ST and DS tests.

Table 3. Summary of the regression analysis outputs with respect to the proposed MLR model or **Equation 3** for τ_p and τ_{cr}.

Rubber type	**Variable**	β_0	β_1	β_2	β_3	β_4	β_5	R^2	**RMSE (kPa)**	**NRMSE (%)**	**MAPE (%)**
Rubber C	τ_p (kPa)	–1009.57	0.231	10.39	–3.53	41.99	9.33	0.9736	6.18	4.37	4.33
	τ_{cr} (kPa)	–1808.08	0.191	10.33	–13.53	26.59	121.51	0.9714	5.53	3.81	4.54
Rubber B	τ_p (kPa)	970.98	0.227	–1.51	8.01	0.31	–89.25	0.9788	4.72	3.85	3.50
	τ_{cr} (kPa)	949.70	0.219	1.77	4.22	23.85	–117.44	0.9627	6.81	5.40	5.84

List of Figures

Figure 1. Recycled tire rubbers: **(a)** rubber C; and **(b)** rubber B.

Figure 2. Grain–size distribution curves for the used materials.

Figure 3. UC stress–strain curves for the tested samples: **(a)** rubber C; and **(b)** rubber B.

Figure 4. Variations of **(a)** peak strain energy E_u and **(b)** elastic stiffness modulus E_{50}, along with corresponding peak UC strength values, against rubber content for the tested samples.

Figure 5. ST stress–strain curves for the tested samples: **(a)** rubber C; and **(b)** rubber B.

Figure 6. Variations of peak strain energy E_s, along with corresponding peak ST strength values, against rubber content for the tested samples.

Figure 7. Typical DS stress–strain curves at varying normal stresses: **(a)** natural soil; **(b)** 10% rubber C; and **(c)** 10% rubber B.

Figure 8. Typical DS stress–strain curves at σ_n=300 kPa: **(a)** rubber C; and **(b)** rubber B.

Figure 9. Peak failure envelopes for the tested samples: **(a)** rubber C; and **(b)** rubber B.

Figure 10. Variations of critical shear strength against normal stress for the tested samples: **(a)** rubber C; and **(b)** rubber B.

Figure 11. Variations of critical shear strength against peak shear strength for the tested samples.

Figure 12. Predicted versus actual data with respect to the proposed MLR model or **Equation 3**: **(a)** peak shear strength τ_p; and **(b)** critical shear strength τ_{cr}.

Figure 13. Variations of the crack intensity factor (CIF), along with corresponding crack reduction factors (CRF), against rubber content for the tested samples.

Figure 14. Typical crack patterns observed for the tested samples: **(a)** natural soil (greyscale); **(b)** natural soil (binary); **(c)** 30% rubber C (greyscale); **(d)** 30% rubber C (binary); **(e)** 30% rubber B (greyscale); **(f)** 30% rubber B (crack interface); and **(g)** 30% rubber B (binary).

Figure 15. Variations of swelling potential and swelling pressure against rubber content for the tested samples (modified from Soltani et al. (2018[c])).

Figure 1. Recycled tire rubbers: **(a)** rubber C; and **(b)** rubber B.

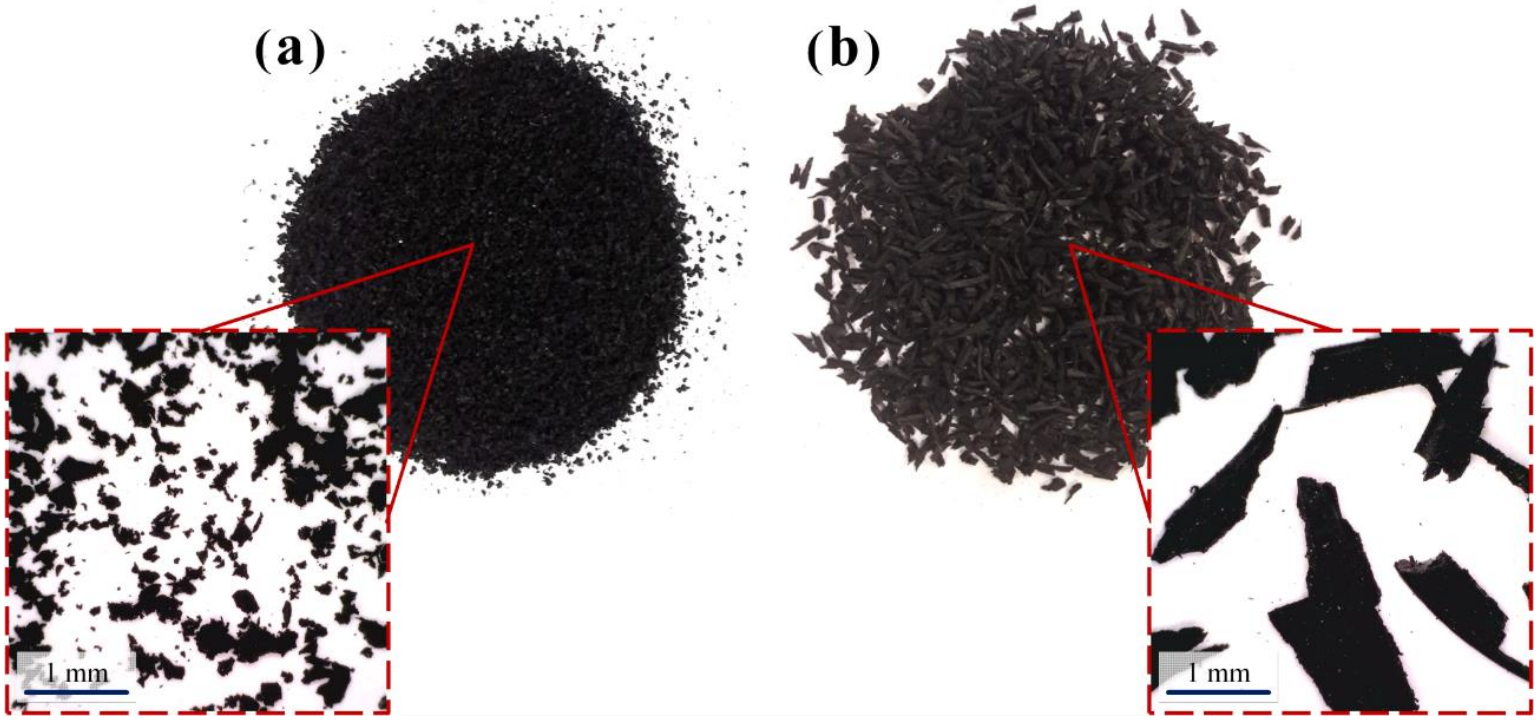

Figure 2. Grain–size distribution curves for the used materials.

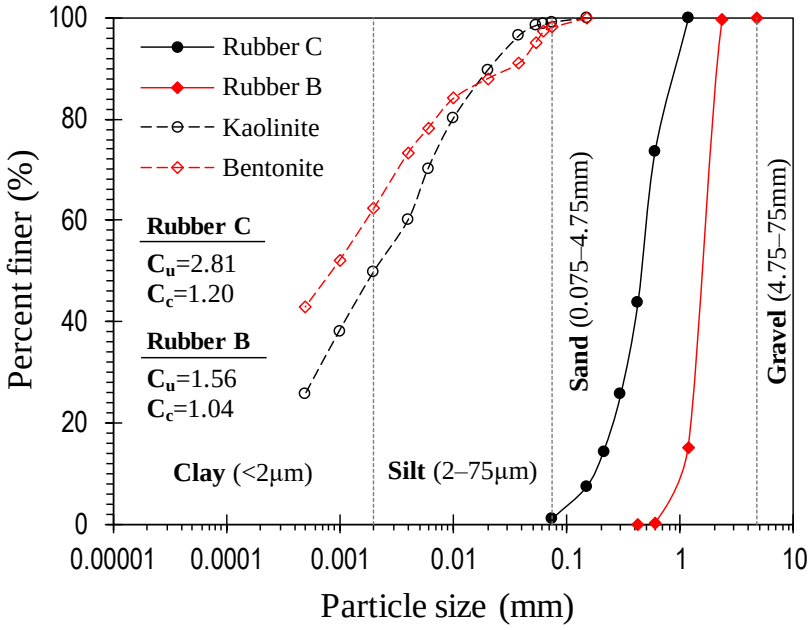

Figure 3. UC stress–strain curves for the tested samples: **(a)** rubber C; and **(b)** rubber B.

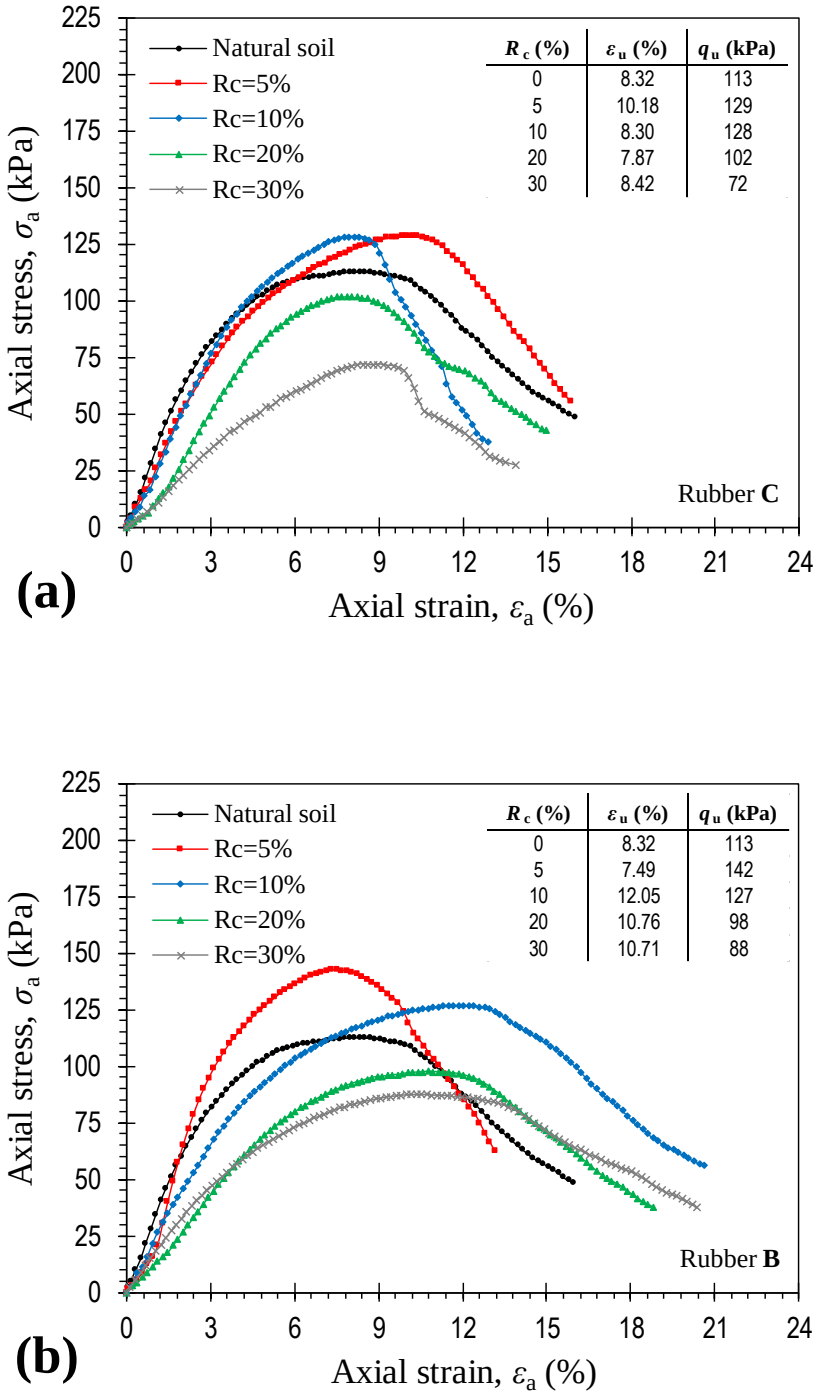

Figure 4. Variations of **(a)** peak strain energy E_u and **(b)** elastic stiffness modulus E_{50}, along with corresponding peak UC strength values, against rubber content for the tested samples.

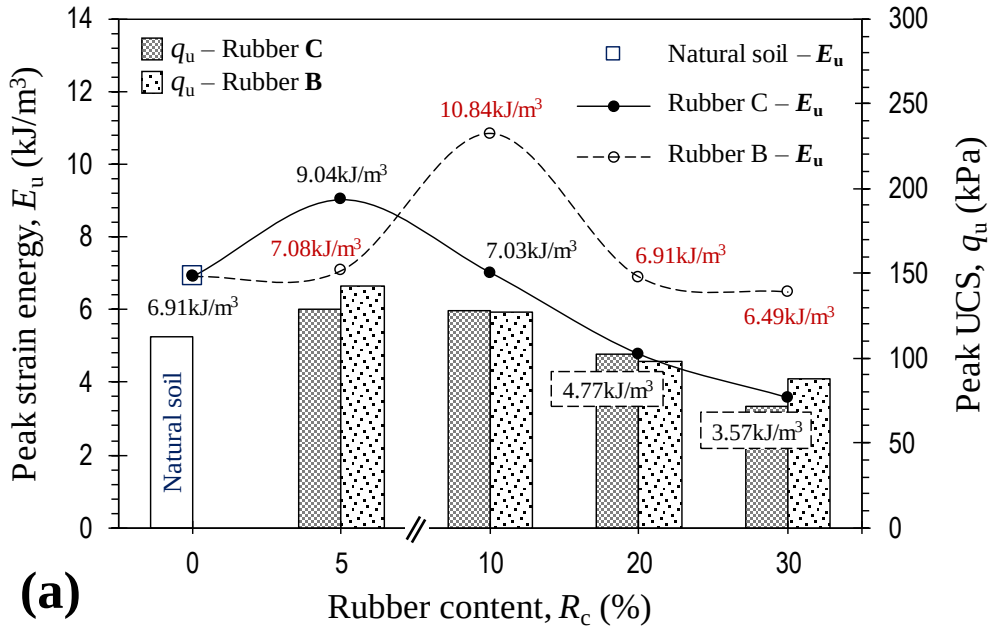

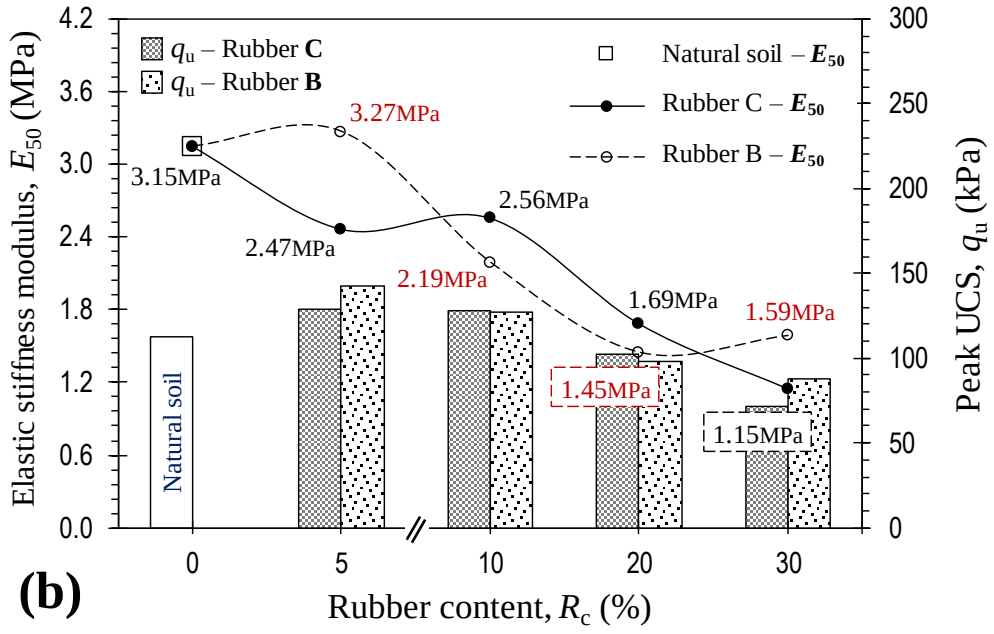

Figure 5. ST stress–strain curves for the tested samples: **(a)** rubber C; and **(b)** rubber B.

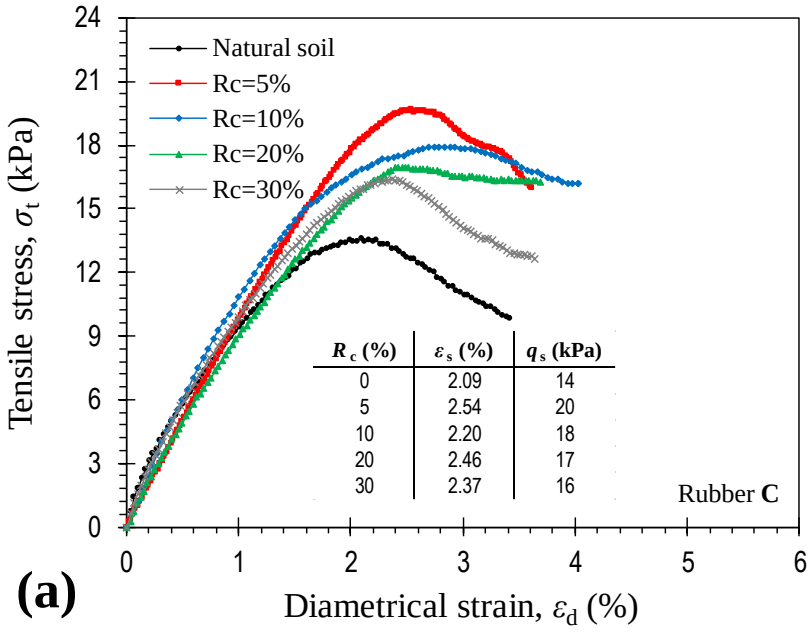

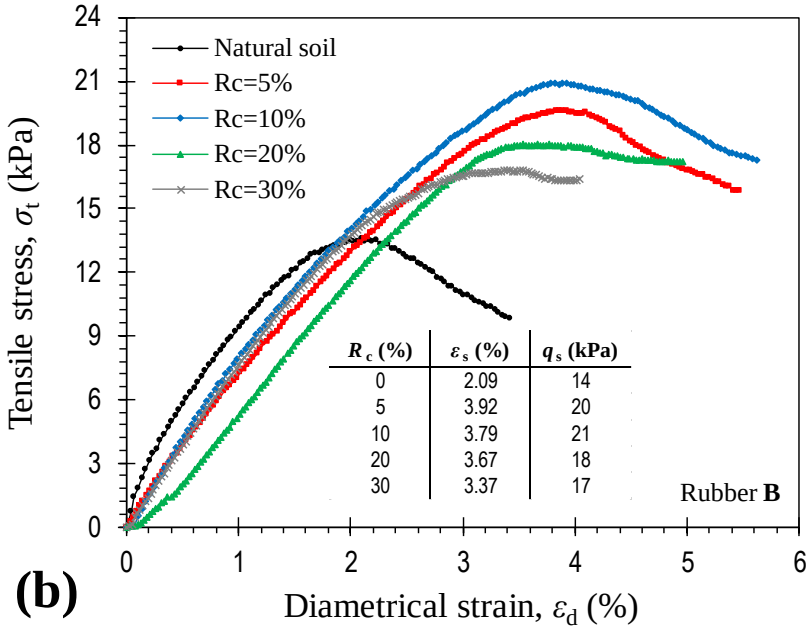

Figure 6. Variations of peak strain energy E_s, along with corresponding peak ST strength values, against rubber content for the tested samples.

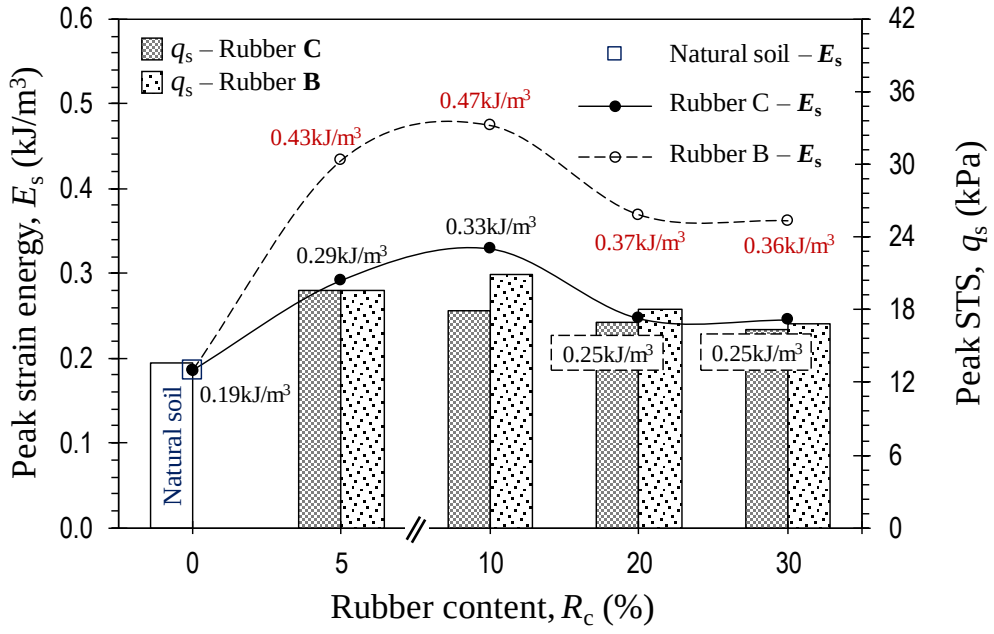

Figure 7. Typical DS stress–strain curves at varying normal stresses: **(a)** natural soil; **(b)** 10% rubber C; and **(c)** 10% rubber B.

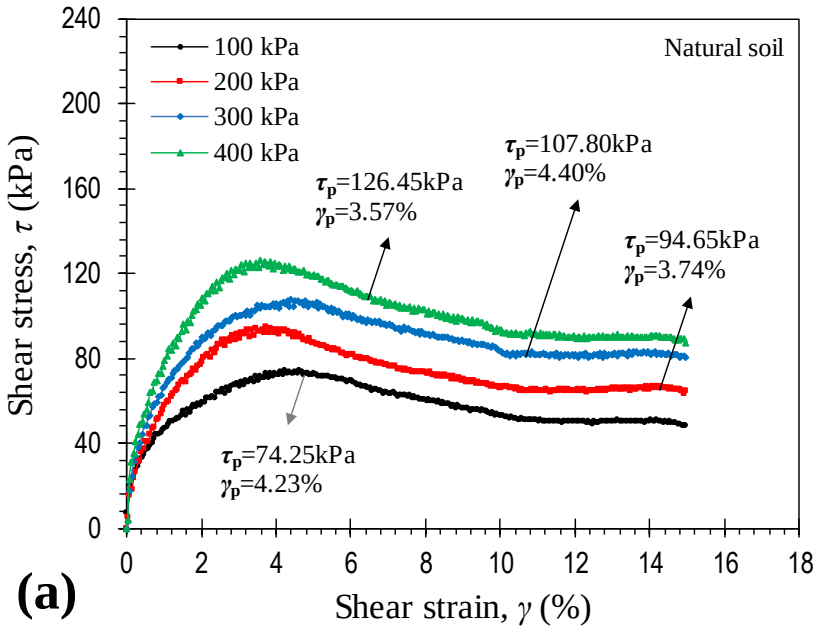

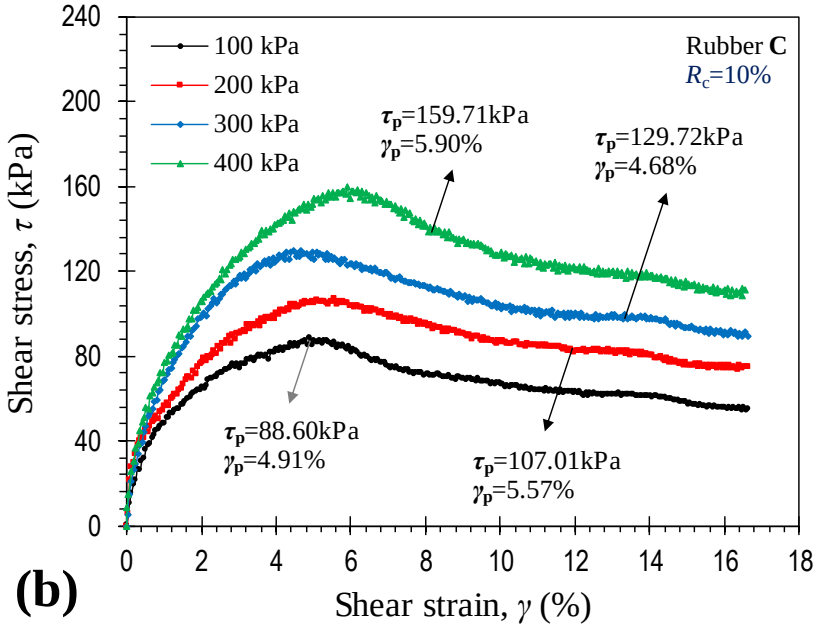

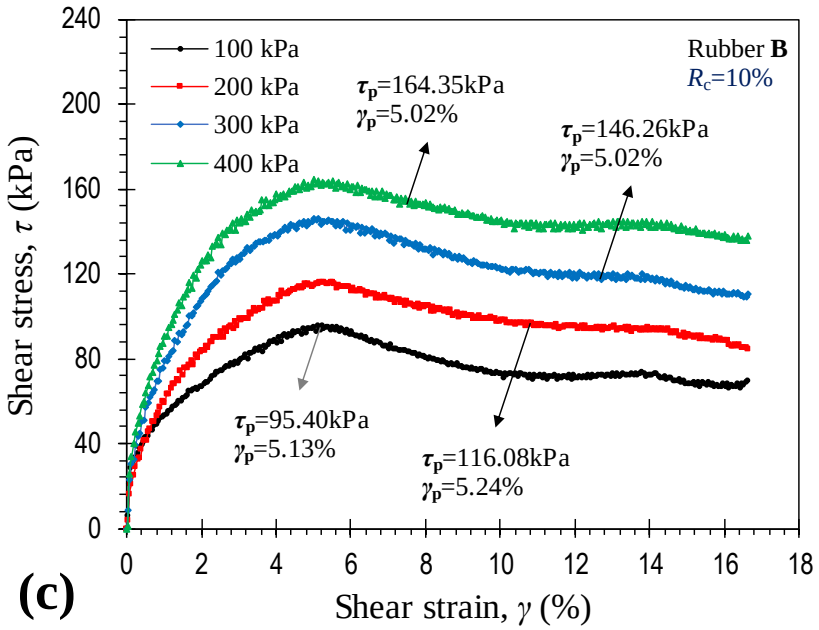
100 kPa
200 kPa
300 kPa
400 kPa
Rubber **B**
R_c=10%
τ_p=164.35kPa
γ_p=5.02%
τ_p=146.26kPa
γ_p=5.02%
τ_p=95.40kPa
γ_p=5.13%
τ_p=116.08kPa
γ_p=5.24%
Shear stress, τ (kPa)
Shear strain, γ (%)
0
40
80
120
160
200
240
0
2
4
6
8
10
12
14
16
18

(c)

Figure 8. Typical DS stress–strain curves at σ_n=300 kPa: **(a)** rubber C; and **(b)** rubber B.

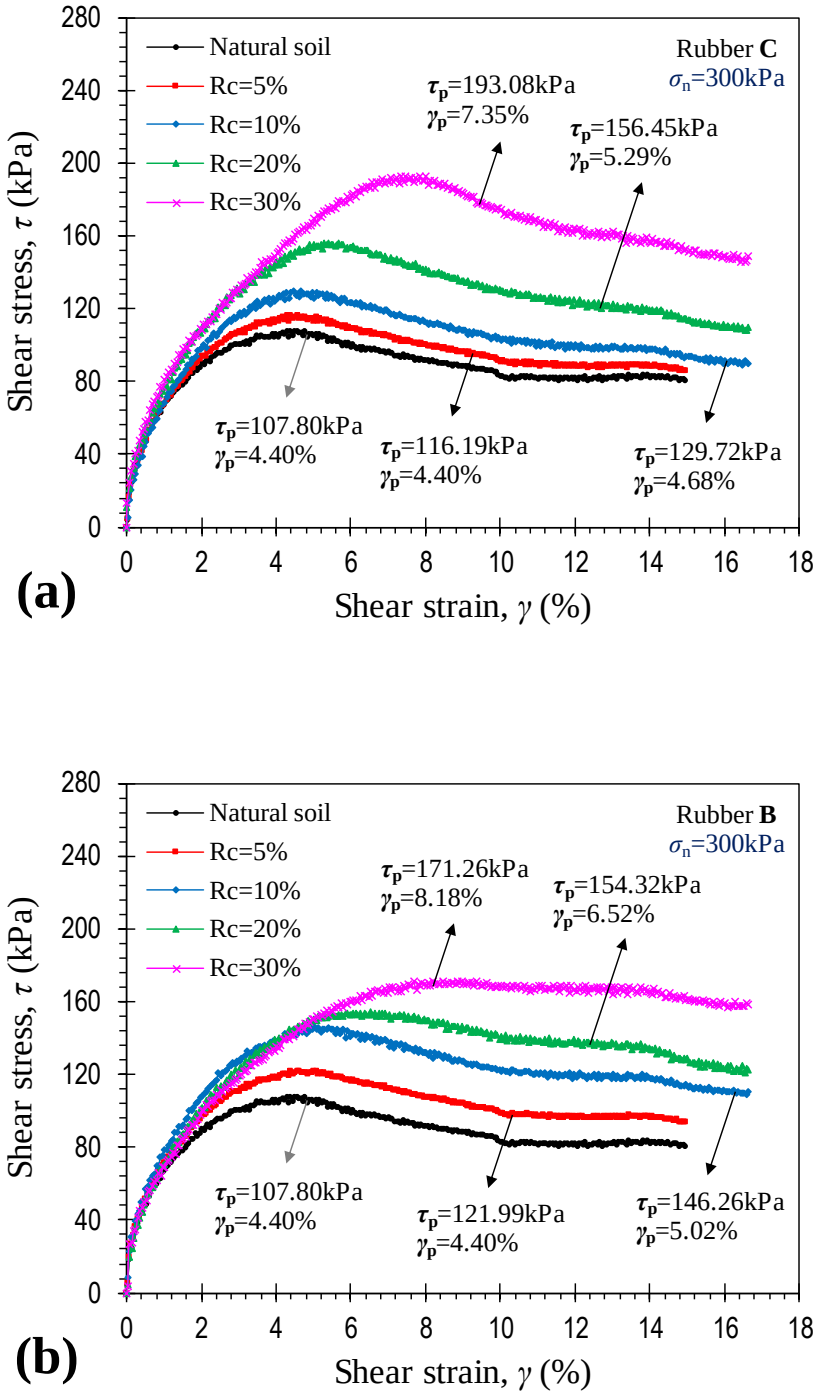

Figure 9. Peak failure envelopes for the tested samples: **(a)** rubber C; and **(b)** rubber B.

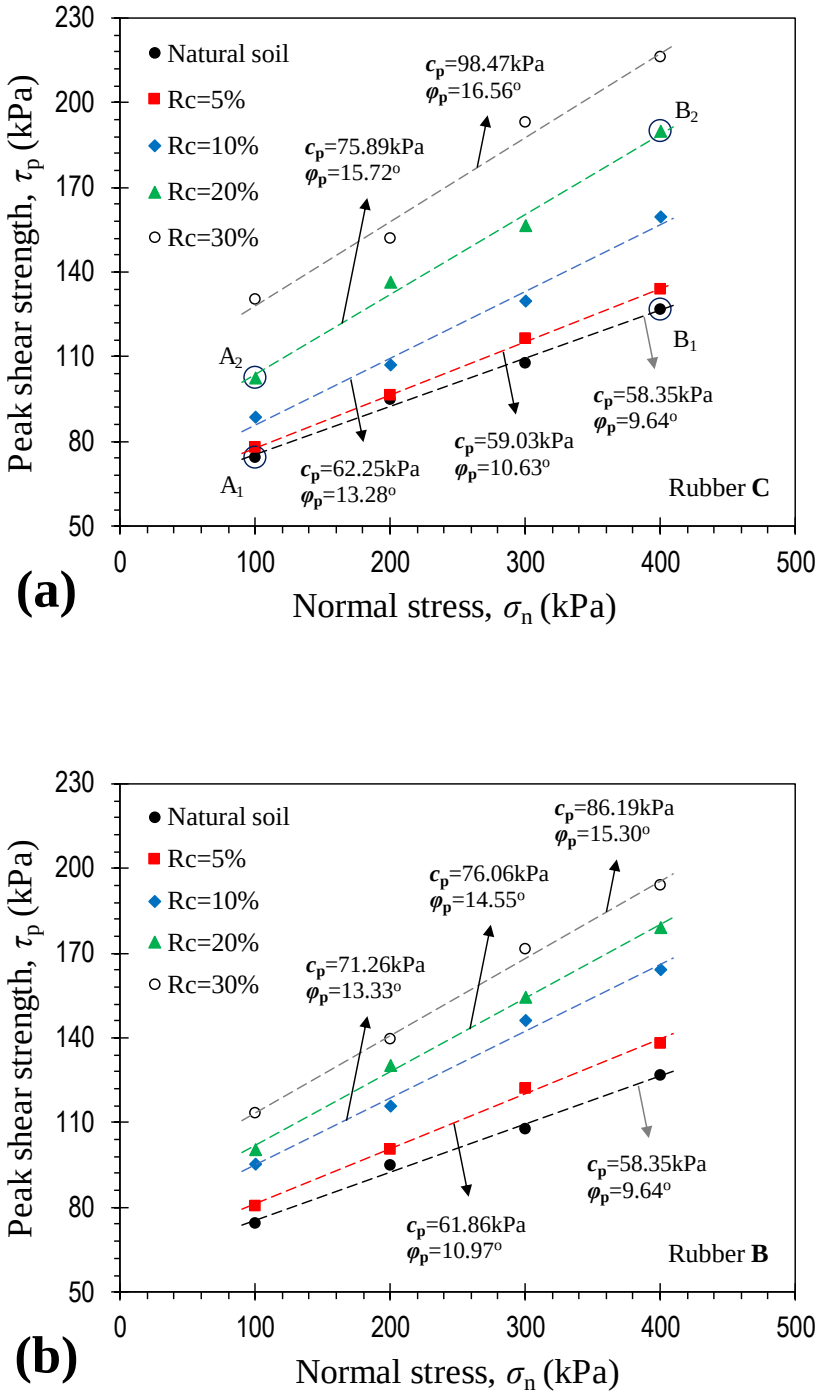

Figure 10. Variations of critical shear strength against normal stress for the tested samples: **(a)** rubber C; and **(b)** rubber B.

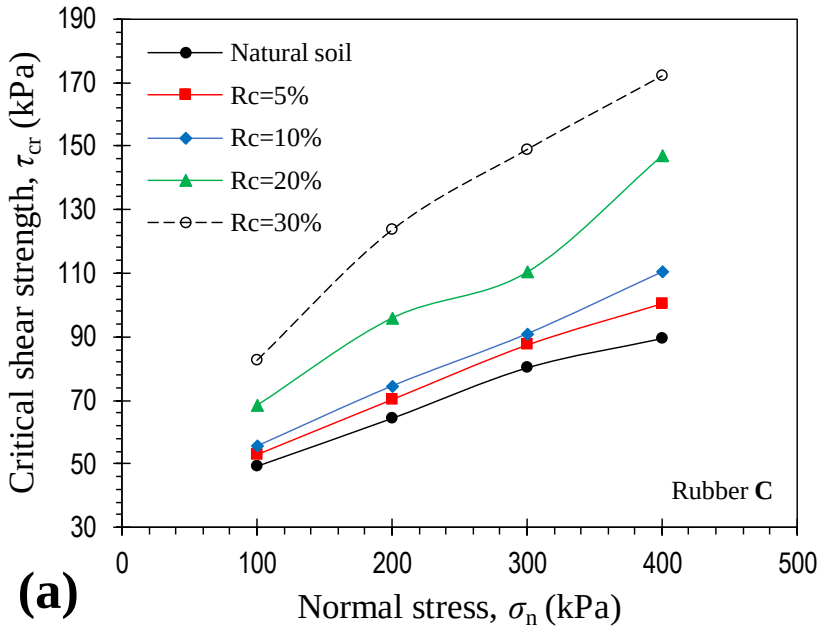

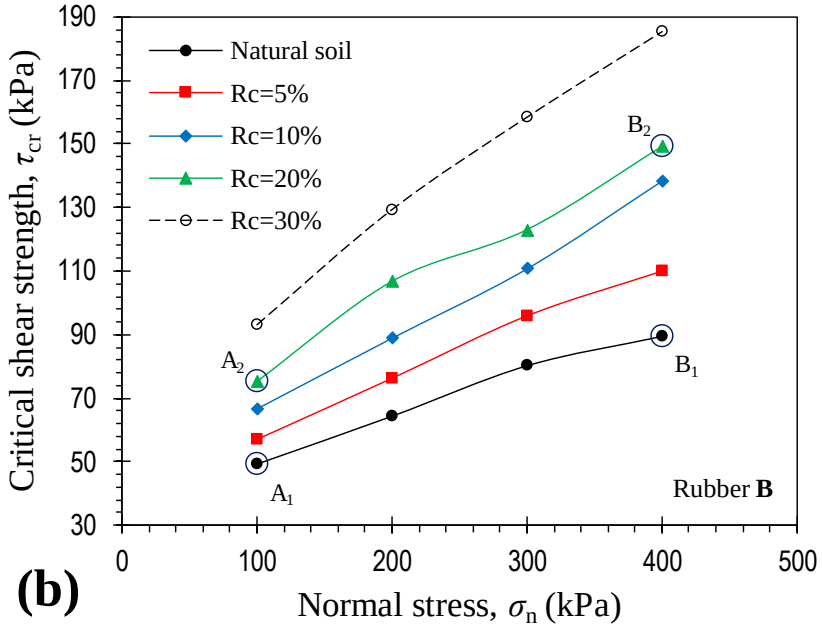

Figure 11. Variations of critical shear strength against peak shear strength for the tested samples.

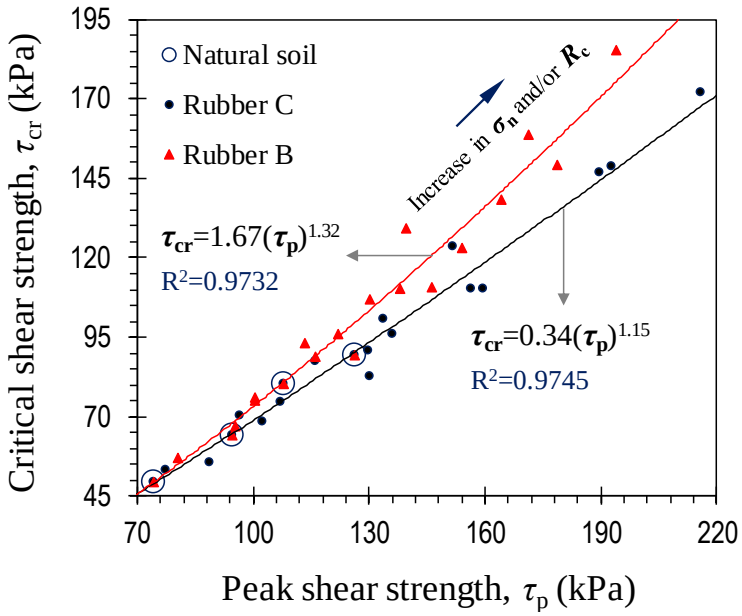

Figure 12. Predicted versus actual data with respect to the proposed MLR model or **Equation 3**: **(a)** peak shear strength τ_p; and **(b)** critical shear strength τ_{cr}.

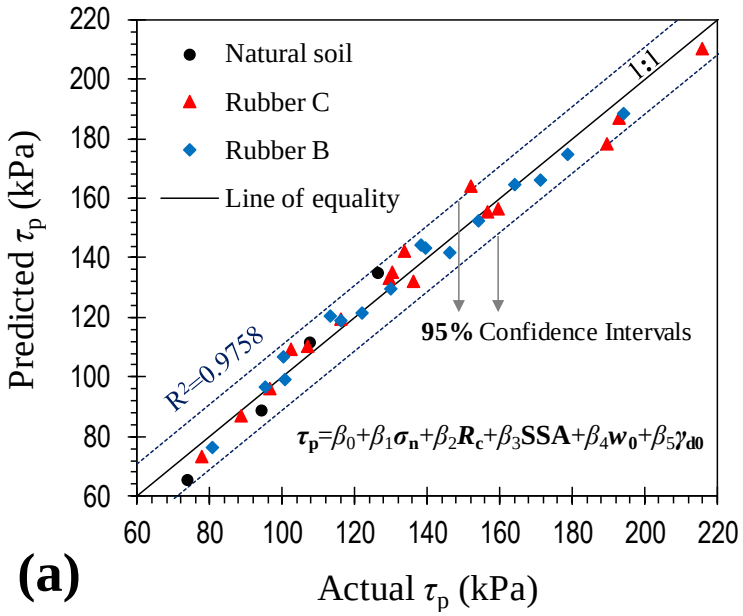

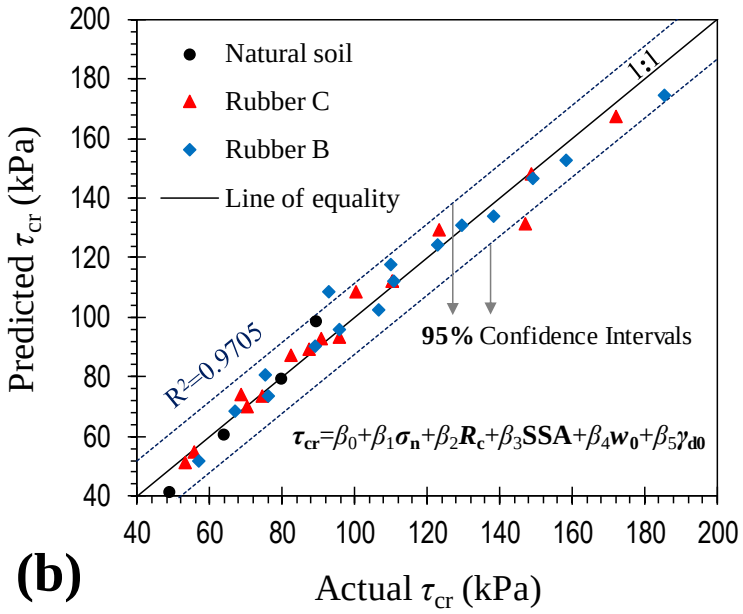

Figure 13. Variations of the crack intensity factor (CIF), along with corresponding crack reduction factors (CRF), against rubber content for the tested samples.

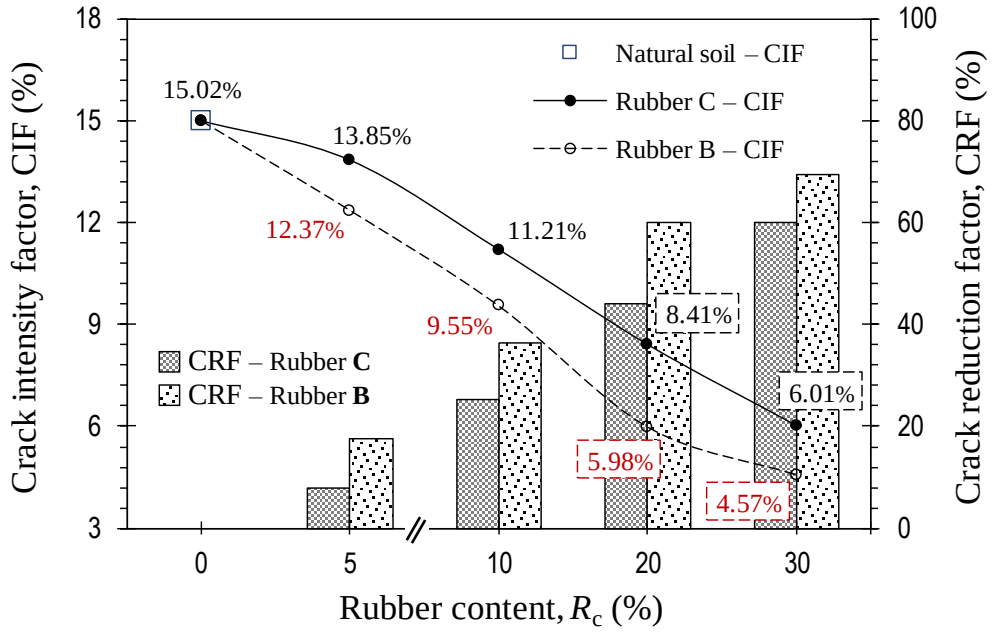

Figure 14. Typical crack patterns observed for the tested samples: **(a)** natural soil (greyscale); **(b)** natural soil (binary); **(c)** 30% rubber C (greyscale); **(d)** 30% rubber C (binary); **(e)** 30% rubber B (greyscale); **(f)** 30% rubber B (crack interface); and **(g)** 30% rubber B (binary).

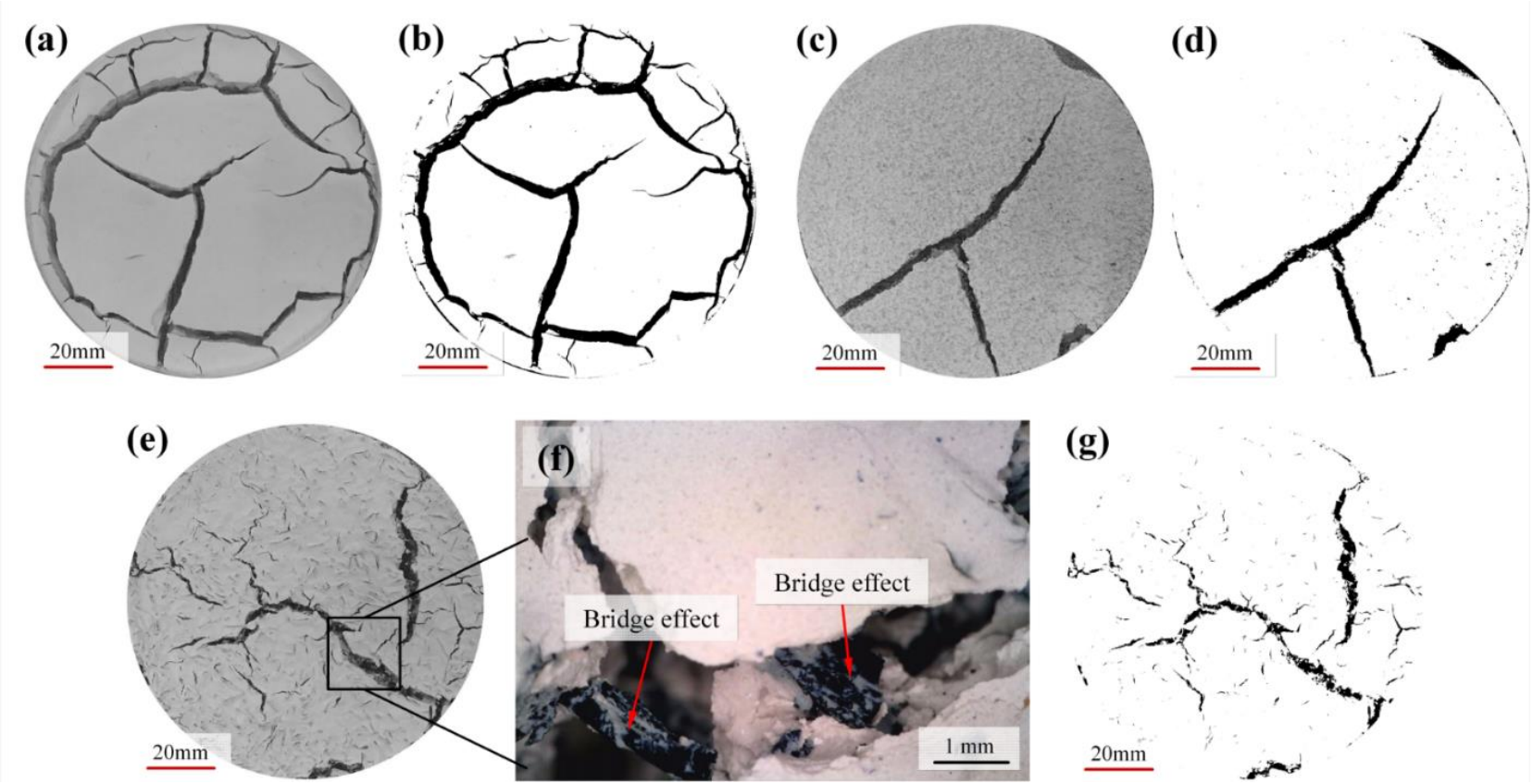

Figure 15. Variations of swelling potential and swelling pressure against rubber content for the tested samples (modified from Soltani et al. (2018[c])).

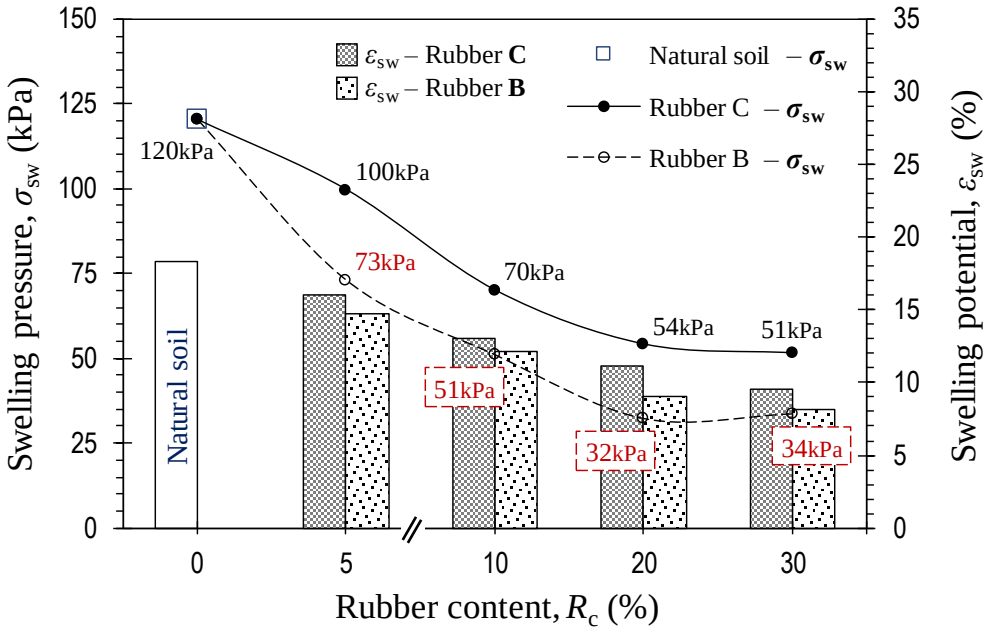

Statement of Authorship

Statement of Authorship

Title of Paper	Tire Rubber–Reinforced Expansive Soils: Two Hazards, One Solution?
Publication Status	☐ Published ☐ Accepted for Publication ■ Submitted for Publication ☐ Unpublished and Unsubmitted work written in manuscript style
Publication Details	**Soltani A**, Taheri A, Deng A and Nikraz H **(2018)** Tire Rubber–Reinforced Expansive Soils: Two Hazards, One Solution?. ***Proceedings of the Institution of Civil Engineers–Construction Materials*** **x(x): x–x**, http://doi.org/x. **Note:** Under Review [submitted on **29 September 2018**].

Principal Author

Name of Principal Author (Candidate)	Amin Soltani (**Email:** Amin.Soltani@adelaide.edu.au)		
Contribution to the Paper	Overall paper preparation		
Overall percentage (%)	85%		
Certification:	This paper reports on original research I conducted during the period of my Higher Degree by Research candidature and is not subject to any obligations or contractual agreements with a third party that would constrain its inclusion in this thesis. I am the primary author of this paper.		
Signature		Date	07/11/2018

Co-Author Contributions

By signing the Statement of Authorship, each author certifies that:

i. the candidate's stated contribution to the publication is accurate (as detailed above);
ii. permission is granted for the candidate in include the publication in the thesis; and
iii. the sum of all co-author contributions is equal to 100% less the candidate's stated contribution.

Name of Co-Author	Abbas Taheri **Senior Lecturer**, School of Civil, Environmental and Mining Engineering, The University of Adelaide, Adelaide, SA 5005, Australia (**Email:** Abbas.Taheri@adelaide.edu.au)		
Contribution to the Paper	Paper review and revision		
Signature		Date	07/16/2018

Name of Co-Author	An Deng **Senior Lecturer**, School of Civil, Environmental and Mining Engineering, The University of Adelaide, Adelaide, SA 5005, Australia (**Email:** An.Deng@adelaide.edu.au)		
Contribution to the Paper	Paper review and revision		
Signature		Date	07/23/2018

Name of Co-Author	Hamid Nikraz **Professor**, School of Civil and Mechanical Engineering, Curtin University, Perth, WA 6102, Australia (**Email:** H.Nikraz@curtin.edu.au)		
Contribution to the Paper	Paper review and revision		
Signature	<	Date	09/02/2018

1

Chapter 5

Interfacial Shear Strength of Rubber–Reinforced Clays: A Dimensional Analysis Perspective

Amin Soltani [a,†], An Deng [b], Abbas Taheri [c], Mehdi Mirzababaei [d] and Hamid Nikraz [e]

[a] **PhD Student** − School of Civil, Environmental and Mining Engineering, The University of Adelaide, Adelaide, SA 5005, Australia (**Email:** Amin.Soltani@adelaide.edu.au; **ORCID:** 0000-0002-0483-7487)

[b] **Senior Lecturer** − School of Civil, Environmental and Mining Engineering, The University of Adelaide, Adelaide, SA 5005, Australia (**Email:** An.Deng@adelaide.edu.au)

[c] **Senior Lecturer** − School of Civil, Environmental and Mining Engineering, The University of Adelaide, Adelaide, SA 5005, Australia (**Email:** Abbas.Taheri@adelaide.edu.au)

[d] **Lecturer** − School of Engineering and Technology, Central Queensland University, Melbourne, VIC 3000, Australia (**Email:** M.Mirzababaei@cqu.edu.au)

[e] **Professor** − School of Civil and Mechanical Engineering, Curtin University, Perth, WA 6102, Australia (**Email:** H.Nikraz@curtin.edu.au)

[†] **Correspondence:** Amin Soltani (**Email:** Amin.Soltani@adelaide.edu.au; **ORCID:** 0000-0002-0483-7487)

Publication Details: **Soltani A**, Deng A, Taheri A, Mirzababaei M and Nikraz H **(2018)** Interfacial Shear Strength of Rubber–Reinforced Clays: A Dimensional Analysis Perspective. ***Geosynthetics International*** **x(x): x–x**, http://doi.org/x.[8]

Abstract

The present study aims towards the development of practical dimensional models capable of simulating the interfacial shear strength of rubber–reinforced clays. Two types of recycled tire rubbers (of fine and coarse categories) were each incorporated into the soil at four different contents (by weight), and statically compacted at their respective Proctor optimum condition

[8] **Under Review** [submitted in revised form on **13 July 2018**].

for direct shear testing. The rubber inclusions amended the soil through improvements achieved in two aspects: **i)** frictional resistance generated as a result of soil–rubber contact; and **ii)** mechanical interlocking of rubber particles and soil grains. In general, both amending mechanisms were in favor of a higher rubber content, and to a lesser degree a larger rubber size. The dimensional analysis concept was extended to the soil–rubber shear strength problem, thereby leading to the development of practical dimensional models capable of simulating the shear stress–horizontal displacement response as a function of the composite's basic index properties. The predictive capacity of the proposed models was examined and validated by statistical techniques. The proposed dimensional models contain a limited number of fitting parameters, which can be calibrated by minimal experimental effort and hence implemented for predictive purposes.

Keywords: Geosynthetics; Rubber–reinforced clay; Interfacial shear strength; Frictional resistance; Mechanical interlocking; Dimensional analysis.

Abbreviations

CH	clay with high plasticity
USCS	unified soil classification system
UU	unconsolidated undrained

Notation[9]

C_c	coefficient of curvature (dimensionless)
c_p	cohesion at peak condition (Pa)
C_u	coefficient of uniformity (dimensionless)
d_{10}	particle diameter corresponding to 10% finer (m)
d_{30}	particle diameter corresponding to 30% finer (m)
d_{50}	particle diameter corresponding to 50% finer (m)
d_{60}	particle diameter corresponding to 60% finer (m)
FSR	free swell ratio (dimensionless)
g	standard gravitational acceleration (m/s^2)
I_p	plasticity index (%)
MAPE	mean absolute percentage error (%)
R^2	coefficient of determination (dimensionless)
R_c	rubber content (%)
RMSE	root mean squares error (Pa)
S_a	specific surface area (m^2/kg)
w_L	liquid limit (%)
w_o	initial water content (%)
w_{opt}	optimum water content (%)
w_P	plastic limit (%)
W_r	weight of rubber particles (kg)
W_s	weight of soil solids (kg)
W_w	weight of water (kg)
β_o, β_1 and β_2	model/fitting parameters of the dimensional models (dimensionless)
γ_{dmax}	maximum dry unit weight (N/m^3)
γ_{do}	initial dry unit weight (N/m^3)
$\Delta\delta_p$	horizontal displacement at failure (m)
η_1	first dimensionless shear number (dimensionless)
η_2	second dimensionless shear number (dimensionless)
π_1, π_2 and π_3	independent Pi terms (dimensionless)

[9]Basic SI units are given in parentheses.

$\boldsymbol{\pi_o}$	dependent Pi term (dimensionless)
$\boldsymbol{\sigma_n}$	normal stress (Pa)
$\boldsymbol{\tau(\Delta\delta)}$	shear stress with respect to horizontal displacement $\Delta\delta$ (Pa)
$\boldsymbol{\tau_{cr}}$	critical shear strength (Pa)
$\boldsymbol{\tau_p}$	peak shear strength (Pa)
$\boldsymbol{\varphi_p}$	friction angle at peak condition (^{o})

1. Introduction

Sustainability in civil engineering is sought as a strategic step towards improving the mechanical performance of construction materials while counteracting the adverse environmental impacts associated with human activities. Solid waste materials are bulky in nature, owing to their low weight–to–volume ratio, and thus consume valuable landfill space upon disposal. To minimize the need for landfilling, local communities and governmental agencies have been increasingly encouraged to recycle and hence reuse such materials as part of the infrastructure system. As of late, many developed and developing countries have initiated the transition towards 'sustainable infrastructure', a concept which encourages the replacement of conventional quarried materials with solid wastes and/or industrial by–products (e.g. waste textiles/fibers, demolition wastes, kiln dusts, silicate/calcium chloride geopolymers and sulfonated oils), thereby conserving natural resources as well as reducing the level of greenhouse gas emissions. In this context, a number of research works have suggested innovative and environmentally sound solutions targeting the application of such materials in various civil engineering projects such as pavement construction, soil stabilization, concrete manufacturing and thermal insulations (e.g. Kim et al. 2008; Yesilata et al. 2009; Puppala et al. 2011; Briga-Sá et al. 2013; Mirzababaei et al. 2013[a], 2013[b]; Parghi and Alam 2016; Arulrajah et al. 2017; Hoy et al. 2017; Kua et al. 2017; Mirzababaei et al. 2018[a]; Soltani et al. 2017[a], 2018[a]). Beneficial reuse of waste resources not only intends to enhance infrastructure performance, but also encourages recycling, mitigates the burden (or hazard) on the environment and assists waste management by preventing the accumulation of bulky waste materials which are normally stored or landfilled without proper utilization. As such, any attempt to assimilate waste resources as part of the infrastructure system is at the forefront of many researchers and governmental authorities.

Discarded tires are amongst the largest and most problematic sources of solid waste, owing to extensive production and their durability over time. Such materials, as an ever–producing consumable element of modern life, constitutes for a large volume of disposals throughout the world. In Australia, for instance, it has been estimated that 48 million waste tires (i.e. equivalent to approximately 381,000 tons) are generated per annum (Hannam 2014). A major challenge has therefore been the space required for storing and transporting such waste materials, and the resulting costs (Thomas et al. 2016; Yadav and Tiwari 2017[a]; Saberian et al. 2018). Quite clearly, discarded tires are not desired at landfills, due to their low weight–to–volume ratio, durability and resilient behavior, which prevents them from being 'flat–packed'. Those

characteristics which make waste tires such a problem while being landfilled, make them one of the most reusable waste materials for the construction of sustainable earth backfills, thereby serving a variety of infrastructure needs, e.g. embankments, retaining walls and bridge abutments (Tweedie et al. 1998; Shalaby and Khan 2002; Yoon et al. 2006; Tanchaisawat et al. 2010; Li et al. 2016). Similar to fiber–reinforced soils, the rubber assemblage randomly distributes in the soil regime, and due to its rough surface texture, elastic character and low water adsorption capacity, engenders a spatial three–dimensional reinforcement network in favor of weaving (or interlocking) the soil grains into a coherent matrix of induced strength, improved ductility and deduced heave/settlement, thereby enhancing the integrity and stability of the infrastructure (e.g. Edil and Bosscher 1994; Zornberg et al. 2004; Cetin et al. 2006; Özkul and Baykal 2007; Tsoi and Lee 2011; Trouzine et al. 2012; Kalkan 2013; Cabalar and Karabash 2015; Signes et al. 2016; Perez et al. 2017; Yadav and Tiwari 2017[b]; Soltani et al. 2018[b], 2018[c]).

The advantages of soil–rubber composites in engineering performance, which conventional soil backfills rarely exhibit, are favorably promoting the sustainability of infrastructure systems. With the soil–rubber composite gaining ground as a viable geomaterial in practice, the need for an efficient and simple tool to adequately predict its short–term performance under field conditions, mainly in terms of shear strength, arises as an inevitable necessity. Such a toolbox, if developed, would aid the geotechnical engineer to arrive at reliable soil–rubber design choices without the hurdles of conducting time–consuming experimental tests. In this context, a limited number of discrete element models have been proposed, which adequately simulate the interfacial shear strength of rubber–reinforced sands (e.g. Youwai and Bergado 2004; Valdes and Evans 2008; Huggins and Ravichandran 2011; Lee et al. 2014; Perez et al. 2016; Wang et al. 2018). These studies gained insight into the inter–particle interactions, and demonstrated the role of rubber particles in changing the material fabrics and the material stiffness. Moreover, the use of artificial intelligence, e.g. neural networks, fuzzy logic systems and combined neuro–fuzzy approaches, has also shown great promise in describing/simulating the sand–rubber interactions (e.g. Edinclilera et al. 2012, 2013). To the authors' knowledge, there have been no attempts to extend the current numerical or constitutive literature to the clay–rubber shear strength problem. Nonetheless, such models, even if developed for the clay–rubber interface, would most certainly suffer from long–lasting and sophisticated calibration procedures, thus leading to impractical frameworks which are not trivial to implement for practicing engineers.

The present study aims towards the development of simple and practical dimensional models, by means of the dimensional analysis concept (Buckingham 1914), capable of simulating the interfacial shear strength of rubber–reinforced clays. Undrained direct shear tests were carried out on various compacted clay–rubber composites (with different consistency limits and initial placement conditions) to generate a reliable database allowing for the validation of the proposed dimensional models. The novel dimensional analysis practiced in this study led to a practical shear strength predicting toolbox by incorporating the composite's basic index properties, thereby avoiding the hurdles of conducting time–consuming experimental tests.

2. Experimental Work

2.1. Materials

2.1.1. Clay Soil

A mixture of 85% kaolinite and 15% sodium–activated bentonite, hereafter simply referred to as soil, was used for the experimental program. Physical and mechanical properties of the soil, determined as per relevant ASTM and Australian (AS) standards, are summarized in **Table 1**. The conventional grain–size analysis, carried out in accordance with ASTM D422 (2007), indicated a clay fraction (< 2 μm) of 52.80%, along with 46.16% silt (2–75 μm) and 1.04% fine sand (0.075–0.425 mm) (see **Figure 1**). The liquid limit and plasticity index were, respectively, measured as w_L=59.60% and I_P=32.32%, from which the soil was characterized as *clay with high plasticity* (CH) in accordance with the Unified Soil Classification System (USCS). The free swell ratio was obtained as FSR=2.91, from which the soil was graded as *highly expansive* with respect to the classification criterion suggested by Prakash and Sridharan (2004).

2.1.2. Tire Rubbers

Two types of commercially available recycled tire rubbers (of fine and coarse categories), commonly traded as rubber crumbs (or ground rubber) and rubber buffings, were used as the reinforcements. Hereafter, these rubber types will be referred to as Rubbers C and B, respectively. The gradation curve for both rubber types was determined as per ASTM D422 (2007), and the results are shown in **Figure 1**. The particles of Rubber C were analogous in size to fine–medium sand (0.075–2 mm), whereas Rubber B was graded into the medium–coarse sand category (0.425–4.75 mm). The particle diameters corresponding to 10%, 30%, 50% and 60% finer (or passing) were measured as d_{10}=0.182 mm and 1.077 mm, d_{30}=0.334 mm and

1.370 mm, d_{50}=0.478 mm and 1.582 mm, and d_{60}=0.513 mm and 1.682 mm for Rubbers C and B, respectively (see **Figure 1**). In addition, the coefficients of uniformity (i.e. $C_u=d_{60}/d_{10}$) and curvature (i.e. $C_c=d_{30}^2/d_{10}d_{60}$) were measured as C_u=2.81 and C_c=1.20 for Rubber C, and C_u=1.56 and C_c=1.04 for Rubber B, from which both rubber types were characterized as *poorly–graded* in accordance with the USCS criterion. **Figure 2** illustrates microscopic micrographs of the rubber particles at different magnification ratios. The rubber particles are non–spherical and irregular in shape (see **Figures 2b** and **2e** at 50x magnification), with some cavities and micro–cracks propagated along the rubber's surface (see **Figures 2c** and **2f** at 200x magnification), thus making for a rough surface texture. Such surface characteristics could potentially promote adhesion and/or induce frictional resistance between the rubber particles and the soil grains, thereby alter the soil fabric into a coherent matrix of induced strength and improved ductility (Yadav and Tiwari 2017[b]; Soltani et al. 2018[b], 2018[d]). Other physical properties, as provided by the manufacturer, included a specific gravity (at 20 °C) of 1.09 and a softening point of 170 °C for both rubber types.

2.2. Compaction Studies and Sample Preparation

Both rubber choices were incorporated into the soil at four different rubber–to–dry soil weight ratios (or rubber contents), i.e. R_c=5%, 10%, 20% and 30%. A series of standard Proctor compaction tests were carried out on the natural soil, i.e. R_c=0%, and various soil–rubber mixtures in accordance with ASTM D698 (2012), and the results are provided in **Table 2**. For a given rubber type, the higher the rubber content the lower the compaction characteristics, following a monotonic decreasing trend. For a given rubber content, however, the effect of rubber size was observed to be marginal. Such trends can be attributed to the lower specific gravity, specific surface area and water adsorption capacity of the rubber particles compared with the soil grains (Özkul and Baykal 2007; Signes et al. 2016; Yadav and Tiwari 2017[b]; Soltani et al. 2018[b], 2018[c]). Moreover, the elastic (or rebound) response of rubber particles to dynamic energy during compaction may potentially reduce the compaction efficiency, and thus contribute to a lower maximum dry unit weight (Yadav and Tiwari 2017[b]; Soltani et al. 2018[d]). It should be noted that rubber–clustering effects were vigorously evident at rubber contents greater than 30%, which led to compactability issues as well as difficulties in achieving homogeneous soil–rubber mixtures. As such, rubber contents greater than 30% were not considered in the present study. Samples for the direct shear tests (see **Section 2.3**) were

prepared by the static compaction technique, as described in Soltani et al. (2017[b]) and Estabragh et al. (2018), at the respective optimum water content and maximum dry unit weight of each mixture (i.e. w_{opt} and γ_{dmax} in **Table 2**). The required amount of water corresponding to the desired optimum water content was added to each mixture, and thoroughly mixed by hand. The mixtures were then enclosed in plastic bags and stored under room temperature conditions for 24 hours, thus ensuring an even distribution of moisture throughout the composite mass. The moist mixtures were statically compressed in the shear box (measuring 60 mm×60 mm in plane and 20 mm in height) at three layers, each layer having attained the desired maximum dry unit weight.

Basic index properties of the prepared samples, including the consistency limits and the compaction characteristics, are summarized in **Table 2**. The natural soil and various soil–rubber mixtures were tested for consistency limits following the Australian code of practice (see relevant standard designations in **Table 1**). The liquid limit was obtained by means of the cone penetration method, while the conventional rolling thread technique was adopted for plastic limit measurements. The water content at which a mass of soil (or material) begins to crumble when manually rolled into a thread of approximately 3.2 mm (in diameter) is conventionally taken as the plastic limit. However, it is well accepted that the effect of thread diameter over a range of 2–6 mm is negligible (Prakash et al. 2009). Therefore, to accommodate the inclusion of rubber particles, which for some particles of Rubber B could measure as high as 3.2 mm in size, the rolling thread technique was implemented to threads of approximately 5 mm (in diameter). The higher the rubber content the lower the consistency limits, following a monotonic decreasing trend. The effect of rubber size, however, was found to be marginal. Similar to the optimum water content, reduction in the consistency limits can be attributed to the lower specific surface area and water adsorption capacity of the rubber particles compared with the soil grains (Cetin et al. 2006; Trouzine et al. 2012; Soltani et al. 2018[d]).

2.3. Direct Shear Test

A series of unconsolidated undrained (UU) direct shear tests, as specified in AS 1289.6.2.2 (1998) and commonly adopted in the literature (e.g. Qu et al. 2013; Calik and Sadoglu 2014; Al-Aqtash and Bandini 2015; Qu and Zhao 2016; Wang et al. 2017), were carried out to investigate the shear strength behavior of the soil–rubber interface. Each of the nine soil–rubber mix designs outlined in **Table 2** was tested for shear strength at four different normal stresses, i.e. σ_n=100 kPa, 200 kPa, 300 kPa and 400 kPa. To minimize both drainage and excess pore–

water pressure effects (thus simulating undrained soil behavior), a high shear rate of 1 mm/min was adopted for the shearing phase (Cetin et al. 2006; Sezer et al. 2006; Bai and Liu 2012). Shear stress was recorded as a function of horizontal displacement up to a total displacement of 10 mm to quantify the stress–displacement response at both peak and post–peak (or critical state) conditions. In addition, the conventional Mohr–Coulomb failure criterion (using a total stress approach) was implemented to arrive at the apparent shear strength parameters at peak condition (Bai and Liu 2012; Al-Aqtash and Bandini 2015).

3. Experimental Results and Discussion

3.1. Shear Stress–Horizontal Displacement Response

Typical shear stress–horizontal displacement curves for the natural soil and various soil–rubber composites at σ_n=200 kPa are shown in **Figures 3a** and **3b** for Rubbers C and B, respectively. The stress–dispalcement response exhibited a rise–fall–plateau behavior with visually detectable peak points, thus signifying a strain–softening character for the tested samples. This effect, however, was less evident for samples reinforced with Rubber B, particularly at higher normal stresses as well as higher rubber inclusions (e.g. compare R_c=30% in **Figures 3a** and **3b**). The critical shear strength τ_{cr} was defined as the minimum shear stress exhibited within the 6–9 mm horizontal displacement region, while the peak shear strength τ_p was visually quantified for the majority of cases (Cetin et al. 2006; Liu and Evett 2009). The stress–displacement relationship at a given normal stress was dependent on both the rubber content and the rubber size, with the former portraying a more pronounced role. For both rubber types, the higher the rubber content the higher the exhibited peak and critical shear strength values. The horizontal displacement at failure $\Delta\delta_p$ was also dependent on the rubber content, and to a lesser degree the rubber size. In general, the higher the rubber content (and/or the larger the rubber size) the higher the horizontal displacement at failure, thus indicating a notable improvement in the composite's ductility. At σ_n=200 kPa, for instance, the natural soil resulted in τ_p=94.65 kPa ($\Delta\delta_p$=2.24 mm), while the inclusion of 5%, 10%, 20% and 30% Rubber C resulted in τ_p=96.48 kPa ($\Delta\delta_p$=2.71 mm), 107.01 kPa ($\Delta\delta_p$=3.34 mm), 136.23 kPa ($\Delta\delta_p$=4.21 mm) and 151.88 kPa ($\Delta\delta_p$=4.80 mm), respectively. For similar inclusions of Rubber B, these values were measured as 100.54 kPa ($\Delta\delta_p$=2.78 mm), 116.08 kPa ($\Delta\delta_p$=3.14 mm), 130.11 kPa ($\Delta\delta_p$=3.74 mm) and 139.48 kPa ($\Delta\delta_p$=7.51 mm), respectively. Similar observations have also been reported by researchers such as Tatlisoz et al. (1997), Özkul and Baykal (2006) and Signes et al. (2016).

Figures 4a and 4b illustrate the variations of the peak and critical shear strength values against normal stress for the tested samples, respectively. For rubber inclusions equal to or less than 10%, the rubber of coarser category, Rubber B, slightly outperformed the finer Rubber C in terms of higher peak shear strength values, while an opposite effect was evident for higher rubber inclusions. In this case, R_c=20% served as a transition point, manifesting a similar performance with marginal differences for the two rubber types (see R_c=20% in **Figure** 4a). The higher rubber inclusion of 30%, however, gave rise to notably higher peak shear strength values for the finer Rubber C (see R_c=30% in **Figure** 4a). These trends are largely consistent with those reported by researchers such as Cetin et al. (2006) and Soltani et al. (2018[c]). A so–called transition was not observed for the critical shear strength, which as previously discussed, can be attributed to the strain–hardening like character exhibited at high inclusions of Rubber B, thus leading to induced strength performance at critical state condition (e.g. compare R_c=30% in **Figures** 3a and 3b). As a result, the critical shear strength was in favor of both a higher rubber content and a larger rubber size (see **Figure** 4b).

3.2. Shear Strength Parameters

The conventional Mohr–Coulomb failure criterion, using a total stress approach expressed as $\tau_p=c_p+\sigma_n\tan\varphi_p$ (c_p=cohesion; and φ_p=friction angle), was implemented to quantify the apparent shear strength parameters at peak condition, and the results are summarized in **Table** 3. The shear strength parameters were dependent on both the rubber content and the rubber size, with the former portraying a more significant role. For rubber inclusions equal to or less than 10%, Rubber B slightly outperformed Rubber C in terms of higher c_p and φ_p values. The performance of both rubber types, particularly in terms of cohesion c_p, were on par with each other at R_c=20% (e.g. c_p=75.89 kPa and 76.06 kPa for 20% Rubbers C and B), while the higher rubber inclusion of 30% gave rise to higher c_p and φ_p values for Rubber C (e.g. c_p=98.47 kPa and 86.19 kPa for 30% Rubbers C and B). These trends are in agreement with the results reported by Cetin et al. (2006).

3.3. Soil–Rubber Interactions

As outlined in **Section** 2.1.2 (see **Figures** 2c and 2f), the rubber's rough surface texture promotes adhesion and/or induces frictional resistance at the soil–rubber interface, and thus alters the soil fabric into a coherent matrix of induced strength and improved ductility. As such, the interfacial shear strength of rubber–reinforced fine–grained soils is governed by the

following amending mechanisms (Tang et al. 2007, 2010; Trouzine et al. 2012; Kalkan 2013; Yadav and Tiwari 2017[b]; Zhang et al. 2017; Mirzababaei et al. 2018[b], 2018[c]; Soltani et al. 2018[b], 2018[c]):

- Frictional resistance generated as a result of soil–rubber contact.
- Mechanical interlocking of rubber particles and soil grains.

The frictional resistance generated at the soil–rubber interface is primarily a function of the soil–rubber contact area, with greater contact levels promoting a more pronounced interfacial frictional resistance, and thus a higher resistance to shearing. This amending mechanism can therefore be ascribed to the rubber content, and to a lesser degree the rubber size. For a given rubber type (constant rubber size), the greater the number of included rubber particles (increase in rubber content) the greater the achieved contact level between the rubber particles and the soil grains, which in turn promotes an induced interfacial frictional resistance followed by an improved shear strength. Similarly, for a given rubber content, the rubber of coarser category is in favor of yielding a greater soil–rubber contact level, and hence a greater interfacial frictional resistance coupled with an improved shear strength. The generated frictional resistance also depends upon the magnitude of confinement (or normal stress) acting on the soil–rubber interface, and increases upon increasing the normal stress. As illustrated in **Figure 4a**, for instance, 20% Rubber C promoted a 38% improvement in the peak shear strength at σ_n=100 kPa (i.e. τ_p increased from 74.25 kPa 'Point A_1' to 102.61 kPa 'Point B_1'), while a greater improvement of 50% was achieved for the same rubber inclusion at σ_n=400 kPa (i.e. τ_p increased from 126.45 kPa 'Point A_2' to 189.67 kPa 'Point B_2'). As another typical case depicted in **Figure 4b**, 20% Rubber B promoted a 53% improvement in the critical shear strength at σ_n=100 kPa (i.e. τ_{cr} increased from 49.19 kPa 'Point A'_1' to 75.22 kPa 'Point B'_1'), whereas a greater improvement of 67% was observed for the same rubber inclusion at σ_n=400 kPa (i.e. τ_{cr} increased from 89.36 kPa 'Point A'_2' to 149.22 kPa 'Point B'_2').

The interlocking of rubber particles and soil grains, achieved during sample preparation (or compaction), induces adhesion at the soil–rubber interface by restricting the movement of soil grains (undergoing shearing) interlocked to the rubber (Mukherjee and Mishra 2017, 2018; Wang et al. 2018). Quite clearly, the more effective the mechanical interlocking the higher the resistance to shearing. Consequently, this amending mechanism is in line with the rubber content, and more importantly the rubber shape. For a given rubber type (constant rubber size

and shape), the greater the number of rubber particles (increase in rubber content) present at the soil–rubber interface the greater the number of interlocked (or enwrapped) soil–rubber lumps, and thus the greater the magnitude of improvement in shear strength. As opposed to the granular form factor of the finer Rubber C (see **Figure 2b**), the particles of Rubber B are more fiber–shaped (see **Figure 2e**), thus making for a more pronounced mechanical interlocking by entwining within the soil matrix and hence immobilizing the soil grains undergoing shearing with increased efficiency.

It should be noted that both amending mechanisms described above only hold provided that the rubber particles do not adhere to each other (or cluster) during sample preparation (or compaction) and shearing (Cabalar et al. 2014; Cabalar and Karabash 2015; Yadav and Tiwari et al. 2017[b]; Zhang et al. 2017). At high rubber contents and potentially for larger rubber sizes, the behavior of the composite at some points of the soil–rubber interface may be governed by a rubber–to–rubber interaction, which though offers a notable improvement to the composite's ductility (e.g. see R_C=30% in **Figure 3b**), offsets the desired soil–to–rubber interaction capable of improving the peak shear strength. For rubber inclusions equal to or less than 10%, the rubber of coarser category, Rubber B, slightly outperformed the finer Rubber C in terms of higher peak shear strength properties, thus indicating an induced interfacial frictional resistance and/or mechanical interlocking owing to the larger size and fibrous form factor of Rubber B. The rubber inclusion of 20% served as a transition point, manifesting a similar performance with marginal differences for the two rubber types, and thus marking the appearance of some rubber–clustering effects for the coarser rubber. For the higher rubber inclusion of 30%, the peak shear strength properties for Rubber B dropped below that of Rubber C, signifying an induced rubber–clustering effect in the presence of the coarser rubber (see **Figure 4a** and **Table 3**). Such a transition was not observed for the critical shear strength (see **Figure 4b**), which can be attributed to the dominant rubber–to–rubber interaction exhibited at high inclusions of Rubber B, thus prompting a strain–hardening like character coupled with induced strength performance at critical state condition compared with that of Rubber C.

4. Dimensional Analysis

4.1. Model Development

The derivation of a dimensional model accounting for all variables governing a physical problem, the shear strength phenomenon in this case, is a formidable but practice–oriented task.

A practical dimensional model can be characterized as one that maintains a perfect balance between simplicity (ease of application) and accuracy, thus involving a limited number of conventional physical parameters capable of arriving at a reliable estimate of the problem in hand (Simon et al. 2017). It is therefore essential avoiding the introduction of any physical parameters which are equally (or more) difficult to measure compared with the physical problem intended to be modeled. For a given fine–grained soil reinforced with a particular type of rubber, governing variables with respect to the soil–rubber shear strength problem, as evident with the experimental results discussed in **Section 3**, can be categorized as: **i)** weight of soil solids W_s (in kg); **ii)** weight of rubber particles W_r (in kg); **iii)** weight of water W_w (in kg); **iv)** initial dry unit weight of the mixture composite γ_{do} (in N/m^3); **v)** specific surface area of the mixture S_a (in m^2/kg); **vi)** the rubber's mean particle size (or diameter) d_{50} (in m); and **vii)** normal stress σ_n (in Pa). The soil–rubber shear strength problem, for peak or critical state condition $\tau_p \vee \tau_{cr}$ (in Pa), can therefore be expressed as:

$$\tau_p \vee \tau_{cr} = f_1(W_s, W_r, W_w, \gamma_{do}, S_a, d_{50}, \sigma_n) \quad (1)$$

where f_1=an unknown multi–variable functional expression.

Although the shear strength of an unsaturated geomaterial, such as the soil–rubber composite in this study, is well known to be related to its matric suction, one may argue that an accurate measurement of suction, for fine–grained soils in particular, is a rather difficult and time–consuming task (Johari et al. 2006; Agus et al. 2010; Malaya and Sreedeep 2011). A typical undrained direct shear test (the problem in hand), however, is deemed as a routine test commonly performed in most laboratories with much less effort. To maintain model simplicity/practicality, it was therefore decided to disregard introducing suction as a governing variable. Interestingly, such a simplification complies with most of the existing literature, where various forms of empirical and dimensional models have been developed and validated for different geomaterials without regarding suction as an input variable (e.g. Rao et al. 2004; Buzzi et al. 2011; Williamson and Cortes 2014; Berrah et al. 2016; Zhao et al. 2016).

The Buckingham Pi concept provides a method for deriving sets of dimensionless variables (commonly referred to as Pi or π terms) from given physical parameters, even if the governing functional expression, e.g. f_1 in **Equation 1**, remains unknown (Buckingham 1914). Despite the concept's successful adoption as a basic principle in fluid mechanics, its application has been less extended to geotechnical–related problems (e.g. Butterfield 1999; Buzzi 2010; Buzzi et al.

2011; Williamson and Cortes 2014; Berrah et al. 2016). The concept states that any physical problem, such as that expressed by **Equation 1**, involving n number of physical parameters with m number of basic physical dimensions (or units) can be further simplified to a new problem involving $k=n–m$ number of dimensionless variables (or Pi terms) capable of adequately describing the original problem in hand. Therefore, the system of $n=7$ physical parameters (γ_{do} is related to W_s and W_r) and $m=3$ basic physical dimensions (i.e. mass [M], length [L] and time [T]) given in **Equation 1** can be simplified to a new system of $k=4$ dimensionless variables given as:

$$\pi_o = \frac{\tau_p \vee \tau_{cr}}{\sigma_n} \tag{2}$$

$$\pi_1 = \frac{W_r}{W_s} = R_c \tag{3}$$

$$\pi_2 = \frac{W_w}{W_s} = w_o(1+R_c) \tag{4}$$

$$\pi_3 = \frac{S_a\sqrt{\sigma_n \gamma_{do} d_{50}}}{g} \tag{5}$$

where π_o=dependent Pi term; π_1, π_2 and π_3=independent Pi terms; w_o=initial water content of the mixture composite ($=W_w/[W_s+W_r]$); and g=standard gravitational acceleration (=9.81 m/s^2).

The soil–rubber shear strength problem, for peak or critical state condition, can therefore be represented by the following simplified expression:

$$\pi_o = \frac{\tau_p \vee \tau_{cr}}{\sigma_n} = f_2(\pi_1, \pi_2, \pi_3) \tag{6}$$

As outlined in **Section 2.2**, samples for the direct shear tests were prepared at the corresponding optimum condition of each mixture, meaning that $w_o=w_{opt}$ and $\gamma_{do}=\gamma_{dmax}$ (see **Table 2**). Furthermore, the specific surface area for both the natural soil and various soil–rubber mixtures was estimated by the following empirical relationship (Locat et al. 1984; Williamson and Cortes 2014; Zhao et al. 2016):

$$I_p = 0.7(S_a - 5) \quad (7)$$

where S_a=specific surface area (in m^2/g); and I_p=plasticity index (in %), as provided in **Table 2**.

In **Equation 6**, f_2 is an unknown multi–variable functional expression, which is to be obtained through trial and error (Simon et al. 2017). To complement the derivation of a practical dimensional model, it is essential that any suggested functional expressions, while arriving at a reliable estimate of τ_p and τ_{cr}, contain a limited number of model (or fitting) parameters, which could be adequately calibrated by minimal experimental effort as well as simple explicit calculations. Although a standard ad hoc solution to f_2 is non–existent, it has been the authors' experience that two inductive approaches, hereafter categorized as Methods A and B, could be employed to complement the trial and error phase, and thus arrive at suitable functional expressions:

4.1.1. Method A

The first approach, the results of which will be presented as Models M_1 and M_2 in **Sections 4.3.1** and **4.3.2**, relies on incorporating the existing independent Pi terms (**Equations 3**, **4** and **5**) into a single dimensionless number, such as η, capable of adequately quantifying the dependent Pi term (**Equation 2**) by means of a conventional single–variable function (e.g. linear, quadratic polynomial and power). The benefit of this particular approach lies within a further simplification of the multi–variable governing problem (expressed by **Equation 6**) to a single–variable governing problem, thereby minimizing the number of expected model parameters as well as the associated experimental effort for their calibration. On the downside, one should consider that unification of the independent Pi terms is highly contingent, and thus depends upon a rigorous trial and error to be carried out which becomes increasingly difficult, if not impossible, when dealing with a large number of independent Pi terms. Provided that the three independent Pi terms given in **Equation 6** could be effectively incorporated into a single dimensionless number, the soil–rubber shear strength problem can be expressed in terms of a single governing variable as:

$$\pi_o = f_2(\pi_1, \pi_2, \pi_3) = f_3(\eta) \quad (8)$$

where f_3=a conventional single–variable function; and η=a dimensionless number yielded by incorporating the independent Pi terms through trial and error.

4.1.2. Method B

The second approach, the results of which will be presented as Model M_3 in **Section 4.3.3**, involves a step–by–step examination of conventional multi–variable functions to arrive at the most simple functional expression capable of quantifying the dependent Pi term with an acceptable degree of accuracy. In essence, such a procedure resembles a typical multiple regression analysis, and thus to some extent prevails the contingent issue associated with Method A. However, as with any multiple regression analysis, the greater the number of input variables (or independent Pi terms) the greater the number of model parameters (or regression coefficients), and thus the more experimental measurements required for model calibration. In this context, two common yet simple solutions include the multi–variable linear and power functions, which for the three independent Pi terms problem given in **Equation 6** can be expressed as:

$$\pi_o = f_2(\pi_1, \pi_2, \pi_3) = \beta_o + \sum_{j=1}^{3} \beta_j \pi_j \tag{9}$$

$$\pi_o = f_2(\pi_1, \pi_2, \pi_3) = \prod_{j=1}^{3} \pi_j^{\beta_{j-1}} \tag{10}$$

where β_o, β_j and β_{j-1}=model parameters (dimensionless); and j=index of summation or multiplication.

4.2. Model Validation

In the present study, a total of three dimensional models, two representing Method A (see Models M_1 and M_2 in **Sections 4.3.1** and **4.3.2**) and one representing Method B (see Model M_3 in **Section 4.3.3**), were proposed. Each model was fitted to the experimental τ_p and τ_{cr} datasets (see **Table A1** in **Appendix A**) by means of the least squares optimization technique (Soltani et al. 2018[e]). Statistical fit–measure indices, namely the coefficient of determination R^2 (dimensionless), the root mean squares error RMSE (in kPa) and the mean absolute percentage error MAPE (in %), were then obtained for model validation (and to compare the performance of the proposed models) by the following relationships (Estabragh et al. 2016):

$$\mathrm{RMSE}=\sqrt{\frac{1}{N}\sum_{i=1}^{N}(y_{mi}-y_{ai})^2} \tag{11}$$

$$\mathrm{MAPE}=\frac{1}{N}\sum_{i=1}^{N}\left|\frac{y_{mi}-y_{ai}}{y_{ai}}\right|\times 100 \tag{12}$$

where y_m=predicted (or modeled) value of the dependent variable y ($=\tau_p \vee \tau_{cr}$); y_a=actual value of the dependent variable y (presented in **Table A1** of **Appendix A**); i=index of summation; and N=number of data points used for model development (=20 for each rubber type consisting of 4 unreinforced and 16 reinforced, as shown in **Table A1** of **Appendix A**).

4.3. Proposed Dimensional Models

4.3.1. Model M_1

Through trial and error, the three independent Pi terms (**Equations 3**, **4** and **5**) were incorporated into a single dimensionless number, hereafter denoted as the first dimensionless shear number η_1, which can be given as:

$$\eta_1=\frac{10^8\pi_2}{(1-\pi_1)\pi_3}=\frac{10^8 g w_o(1+R_c)}{S_a(1-R_c)\sqrt{\sigma_n\gamma_{do}d_{50}}} \tag{13}$$

Figures 5a and **5b** illustrate the variations of π_o (**Equation 2**) against η_1 (**Equation 13**) at both peak and critical state conditions for Rubbers C and B, respectively. As depicted in the figures, a rather strong correlation in the form of a conventional single–variable linear function, i.e. $y=y_o+ax$, can be obtained between π_o and η_1. Let $\pi_o=\beta_o+\beta_1\eta_1$, one can therefore derive the following for $\tau_p \vee \tau_{cr}$:

$$\tau_p \vee \tau_{cr}=\sigma_n(\beta_o+\beta_1\eta_1) \tag{14}$$

where β_o and β_1=model parameters (dimensionless).

The regression analysis outputs with respect to the proposed dimensional model M_1 (**Equation 14**) are summarized in **Table 4** for both rubber types. The high R^2 and low MAPE (and RMSE) values imply a strong agreement between actual and predicted shear strength data, both in terms of correlation and error. The R^2 values mainly surpassed the 0.95 margin, indicating that leastwise 95% of the variations in experimental observations are captured and further explained

by Model M_1. The MAPE values were found to be less than 7% for all cases, signifying a maximum offset of 7% associated with the predictions.

Figures 6a and **6b** illustrate predicted (by Model M_1 or **Equation 14**) versus actual data, along with the corresponding 95% prediction bands/intervals, for various soil–rubber composites at peak and critical state conditions, respectively. Although some scatter can be observed, nearly all data points lie between the upper and lower 95% prediction intervals, thus indicating no major outliers associated with the predictions. The coefficient of determination was also obtained for these combined datasets, which resulted in a net R^2 of 0.950 and 0.979 for τ_p and τ_{cr}, respectively.

The proposed dimensional model M_1 (**Equation 14**) contains two model parameters, i.e. β_0 and β_1, which can be calibrated by minimal experimental effort, and thus further implemented for predictive purposes. The model parameters can be adequately estimated by a total of two direct shear tests. Two test scenarios consisting of the natural soil and a desired soil–rubber mixture, each at a median normal stress, are recommended for the calibration phase. Although the choice of rubber content for the soil–rubber mixture is arbitrary, from a statistical perspective, a median rubber content is expected to yield a more reliable estimate of the model parameters (Mirzababaei et al. 2018[a]). Consider the following designations:

- $\eta_1^{(R_c^o,\sigma_n^m)}$ =first dimensionless shear number (**Equation 13**) for no rubber inclusion, i.e. R_c^o, at a median normal stress, i.e. σ_n^m.

- $\tau_p^{(R_c^o,\sigma_n^m)} \vee \tau_{cr}^{(R_c^o,\sigma_n^m)}$ =actual peak or critical shear strength for no rubber inclusion, i.e. R_c^o, at a median normal stress, i.e. σ_n^m.

- $\eta_1^{(R_c^m,\sigma_n^m)}$ =first dimensionless shear number (**Equation 13**) for a median rubber content, i.e. R_c^m, at a median normal stress, i.e. σ_n^m.

- $\tau_p^{(R_c^m,\sigma_n^m)} \vee \tau_{cr}^{(R_c^m,\sigma_n^m)}$ =actual peak or critical shear strength for a median rubber content, i.e. R_c^m, at a median normal stress, i.e. σ_n^m.

Therefore, the following system of two linear equations should be solved to arrive at an estimate of the M_1 model parameters β_0 and β_1:

$$\mathrm{M}_1:\begin{cases}\dfrac{\tau_{\mathrm{p}}^{(R_{\mathrm{c}}^{\mathrm{o}},\sigma_{\mathrm{n}}^{\mathrm{m}})}\vee\tau_{\mathrm{cr}}^{(R_{\mathrm{c}}^{\mathrm{o}},\sigma_{\mathrm{n}}^{\mathrm{m}})}}{\sigma_{\mathrm{n}}^{\mathrm{m}}}=\beta_{\mathrm{o}}+\beta_1\eta_1^{(R_{\mathrm{c}}^{\mathrm{o}},\sigma_{\mathrm{n}}^{\mathrm{m}})}\\ \dfrac{\tau_{\mathrm{p}}^{(R_{\mathrm{c}}^{\mathrm{m}},\sigma_{\mathrm{n}}^{\mathrm{m}})}\vee\tau_{\mathrm{cr}}^{(R_{\mathrm{c}}^{\mathrm{m}},\sigma_{\mathrm{n}}^{\mathrm{m}})}}{\sigma_{\mathrm{n}}^{\mathrm{m}}}=\beta_{\mathrm{o}}+\beta_1\eta_1^{(R_{\mathrm{c}}^{\mathrm{m}},\sigma_{\mathrm{n}}^{\mathrm{m}})}\end{cases} \tag{15}$$

An explicit solution to **Equation 15** is provided in **Equation B4** of **Appendix B**.

4.3.2. Model M_2

Through trial and error, a second dimensionless shear number, hereafter denoted as η_2, was suggested as:

$$\eta_2=\frac{(1-\pi_1)\pi_2\pi_3}{10^6}=\frac{S_{\mathrm{a}}w_{\mathrm{o}}(1-R_{\mathrm{c}}^2)\sqrt{\sigma_{\mathrm{n}}\gamma_{\mathrm{do}}d_{50}}}{10^6\,\mathrm{g}} \tag{16}$$

The variations of π_{o} (**Equation 2**) were plotted against the second dimensionless shear number η_2 (**Equation 16**), and the results are provided in **Figures 7a** and **7b** at both peak and critical state conditions for Rubbers C and B, respectively. In this case, a rather strong correlation in the form of a conventional single–variable power function, i.e. $y=ax^b$, was observed between π_{o} and η_2. Let $\pi_{\mathrm{o}}=\beta_{\mathrm{o}}\eta_2^{\beta_1}$, the following can therefore be written for $\tau_{\mathrm{p}}\vee\tau_{\mathrm{cr}}$:

$$\tau_{\mathrm{p}}\vee\tau_{\mathrm{cr}}=\sigma_{\mathrm{n}}\beta_{\mathrm{o}}\eta_2^{\beta_1} \tag{17}$$

where β_{o} and β_1=model parameters (dimensionless).

The regression analysis outputs with respect to the proposed dimensional model M_2 (**Equation 17**) are summarized in **Table 5** for both rubber types. Model M_2 mainly exhibited similar R^2, RMSE and MAPE values compared with that of Model M_1 (**Equation 14**), thus indicating a similar performance for both models. Similar to Model M_1, the R^2 values were mainly greater than 0.95, while the MAPE values were found to be less than 7% for all cases.

Figures 8a and **8b** illustrate predicted (by Model M_2 or **Equation 17**) versus actual data, along with the corresponding 95% prediction bands/intervals, for various soil–rubber composites at peak and critical state conditions, respectively. Similar to Model M_1, some scatter can still be observed; however, nearly all data points position themselves between the upper and lower 95% prediction intervals, thus indicating no particular outliers associated with the predictions. The

coefficient of determination for these combined datasets were obtained as 0.955 for τ_p and 0.976 for τ_{cr}, which are similar to those obtained for Model M_1.

The calibration procedure for Model M_2 (**Equation 17**), as a two parameter model, would essentially be similar to that described for Model M_1. In this case, however, the non–linear character of Model M_2, represented by the power component β_1, should first be linearized by means of a logarithmic transformation. Upon linearization, the following system of two semi–linear equations should be solved to arrive at an estimate of the M_2 model parameters β_o and β_1:

$$\mathrm{M}_2:\begin{cases}\mathrm{Ln}\left\langle\dfrac{\tau_p^{(R_c^o,\sigma_n^m)}\vee\tau_{cr}^{(R_c^o,\sigma_n^m)}}{\sigma_n^m}\right\rangle=\mathrm{Ln}\left\langle\beta_o\right\rangle+\beta_1\mathrm{Ln}\left\langle\eta_2^{(R_c^o,\sigma_n^m)}\right\rangle\\ \mathrm{Ln}\left\langle\dfrac{\tau_p^{(R_c^m,\sigma_n^m)}\vee\tau_{cr}^{(R_c^m,\sigma_n^m)}}{\sigma_n^m}\right\rangle=\mathrm{Ln}\left\langle\beta_o\right\rangle+\beta_1\mathrm{Ln}\left\langle\eta_2^{(R_c^m,\sigma_n^m)}\right\rangle\end{cases} \tag{18}$$

An explicit solution to **Equation 18** is provided in **Equation B5** of **Appendix B**. The explicit solution to the M_2 model parameters is of slightly greater complexity compared with that of Model M_1 (compare **Equations B4** and **B5** in **Appendix B**). As it stands, Model M_1 offers a more practical calibration procedure, while maintaining the same performance offered by the more complex Model M_2.

4.3.3. Model M_3

Upon examining various forms of conventional multi–variable functions, a modified form of the three–variable power function, similar to that given in **Equation 10**, was selected as the governing functional expression to link the three independent Pi terms (**Equations 3**, **4** and **5**) to the dependent Pi term (**Equation 2**), which can be given as:

$$\pi_o=(1-\pi_1)^{\beta_o}\pi_2^{\beta_1}\left(\frac{\pi_3}{10^6}\right)^{\beta_2}=(1-R_c)^{\beta_o}\left[w_o(1+R_c)\right]^{\beta_1}\left(\frac{S_a\sqrt{\sigma_n\gamma_{do}d_{50}}}{10^6\,\mathrm{g}}\right)^{\beta_2} \tag{19}$$

Provided that **Equation 19** holds, equating **Equations 2** and **19** yields the following for $\tau_p\vee\tau_{cr}$:

$$\tau_p\vee\tau_{cr}=\sigma_n(1-R_c)^{\beta_o}\left[w_o(1+R_c)\right]^{\beta_1}\left(\frac{S_a\sqrt{\sigma_n\gamma_{do}d_{50}}}{10^6\,\mathrm{g}}\right)^{\beta_2} \tag{20}$$

where β_o, β_1 and β_2=model parameters (dimensionless).

Figures 9a and **9b** illustrate the variations of both predicted (by Model M_3 or **Equation 20**) and actual τ_p and τ_{cr} data against normal stress for Rubbers C and B, respectively. The proposed dimensional model M_3 well correlates with the experimental observations, as evident with the clustering of predicted and actual data in the figures. Most of the predicted values perfectly overlap with their actual counterparts, thus indicating an excellent capacity to simulate the shear strength response at both peak and critical state conditions.

The regression analysis outputs with respect to the proposed dimensional model M_3 (**Equation 20**) are summarized in **Table 6** for both rubber types. Model M_3 outperformed both Models M_1 (**Equation 14**) and M_2 (**Equation 17**), as evident with the higher R^2 and lower RMSE and MAPE values. The R^2 values were unanimously above the 0.98 margin, indicating an excellent goodness of fit. The MAPE values were less the 5% for all cases, thus manifesting a 2% improvement compared with that observed for Models M_1 and M_2.

Figures 10a and **10b** illustrate predicted (by Model M_3 or **Equation 20**) versus actual data, along with the corresponding 95% prediction bands/intervals, for various soil–rubber composites at peak and critical state conditions, respectively. In comparison to Models M_1 and M_2, the data points lie closer to the line of equality, i.e. $y=x$, thus manifesting minimal scatter and no particular outliers associated with the predictions. The coefficient of determination for these combined datasets were obtained as 0.961 and 0.978 for τ_p and τ_{cr}, respectively.

The proposed dimensional model M_3 (**Equation 20**) is a three parameter model, thus a total of three direct shear tests would be required for its calibration. The suggested test scenarios can be given as:

- The natural soil (or no rubber inclusion), i.e. R_c^o, at a low normal stress, i.e. σ_n^o.
- The natural soil (or no rubber inclusion), i.e. R_c^o, at a high normal stress, i.e. σ_n^∞.
- A desired soil–rubber mixture (preferably with a median rubber content, i.e. R_c^m) at a median normal stress, i.e. σ_n^m.

Similar to that described for Model M_2 (**Equation 17**), the non–linear character of Model M_3, represented by the power components β_o, β_1 and β_2, should first be linearized by means of a

logarithmic transformation. Upon linearization, the following system of three semi–linear equations should be solved to arrive at an estimate of the M_3 model parameters β_o, β_1 and β_2:

$$\mathrm{M}_3:\begin{cases}\mathrm{Ln}\left\langle\dfrac{\tau_{\mathrm{p}}^{(R_{\mathrm{c}}^{\mathrm{o}},\sigma_{\mathrm{n}}^{\mathrm{o}})}\vee\tau_{\mathrm{cr}}^{(R_{\mathrm{c}}^{\mathrm{o}},\sigma_{\mathrm{n}}^{\mathrm{o}})}}{\sigma_{\mathrm{n}}^{\mathrm{o}}}\right\rangle=\beta_{\mathrm{o}}\mathrm{Ln}\left\langle 1-\pi_1^{(R_{\mathrm{c}}^{\mathrm{o}},\sigma_{\mathrm{n}}^{\mathrm{o}})}\right\rangle+\beta_1\mathrm{Ln}\left\langle\pi_2^{(R_{\mathrm{c}}^{\mathrm{o}},\sigma_{\mathrm{n}}^{\mathrm{o}})}\right\rangle+\beta_2\mathrm{Ln}\left\langle\dfrac{\pi_3^{(R_{\mathrm{c}}^{\mathrm{o}},\sigma_{\mathrm{n}}^{\mathrm{o}})}}{10^6}\right\rangle\\ \mathrm{Ln}\left\langle\dfrac{\tau_{\mathrm{p}}^{(R_{\mathrm{c}}^{\mathrm{o}},\sigma_{\mathrm{n}}^{\infty})}\vee\tau_{\mathrm{cr}}^{(R_{\mathrm{c}}^{\mathrm{o}},\sigma_{\mathrm{n}}^{\infty})}}{\sigma_{\mathrm{n}}^{\infty}}\right\rangle=\beta_{\mathrm{o}}\mathrm{Ln}\left\langle 1-\pi_1^{(R_{\mathrm{c}}^{\mathrm{o}},\sigma_{\mathrm{n}}^{\infty})}\right\rangle+\beta_1\mathrm{Ln}\left\langle\pi_2^{(R_{\mathrm{c}}^{\mathrm{o}},\sigma_{\mathrm{n}}^{\infty})}\right\rangle+\beta_2\mathrm{Ln}\left\langle\dfrac{\pi_3^{(R_{\mathrm{c}}^{\mathrm{o}},\sigma_{\mathrm{n}}^{\infty})}}{10^6}\right\rangle\\ \mathrm{Ln}\left\langle\dfrac{\tau_{\mathrm{p}}^{(R_{\mathrm{c}}^{\mathrm{m}},\sigma_{\mathrm{n}}^{\mathrm{m}})}\vee\tau_{\mathrm{cr}}^{(R_{\mathrm{c}}^{\mathrm{m}},\sigma_{\mathrm{n}}^{\mathrm{m}})}}{\sigma_{\mathrm{n}}^{\mathrm{m}}}\right\rangle=\beta_{\mathrm{o}}\mathrm{Ln}\left\langle 1-\pi_1^{(R_{\mathrm{c}}^{\mathrm{m}},\sigma_{\mathrm{n}}^{\mathrm{m}})}\right\rangle+\beta_1\mathrm{Ln}\left\langle\pi_2^{(R_{\mathrm{c}}^{\mathrm{m}},\sigma_{\mathrm{n}}^{\mathrm{m}})}\right\rangle+\beta_2\mathrm{Ln}\left\langle\dfrac{\pi_3^{(R_{\mathrm{c}}^{\mathrm{m}},\sigma_{\mathrm{n}}^{\mathrm{m}})}}{10^6}\right\rangle\end{cases}\tag{21}$$

An explicit solution to **Equation 21** is provided in **Equation B6** of **Appendix B**. Quite clearly, the explicit solution to the M_3 model parameters is of significant complexity compared with that of Models M_1 and M_2 (compare **Equation B6** with **Equations B4** and **B5** in **Appendix B**). In essence, Model M_3 sacrifices simplicity/practicality in favor of a higher accuracy.

4.4. Modelling the Shear Stress–Horizonal Displacement Locus

As evident with the results presented in the previous section, the proposed dimensional models, Model M_3 in particular, well predict the shear strength response of the soil–rubber composite at both peak and critical state conditions. It was therefore perceived that the same models, if rewritten in terms of shear stress as a function of horizontal displacement, could potentially provide a basis for simulating the shear stress–horizontal displacement locus during shear evolvement. Let Model M_3 (**Equation 20**), the most superior dimensional model as evident with the results outlined in **Section 4.3.3**, be rewritten in terms of horizontal displacement as:

$$\tau(\Delta\delta)=\sigma_{\mathrm{n}}(1-R_{\mathrm{c}})^{\beta_{\mathrm{o}}(\Delta\delta)}\left[w_{\mathrm{o}}(1+R_{\mathrm{c}})\right]^{\beta_1(\Delta\delta)}\left(\frac{S_{\mathrm{a}}\sqrt{\sigma_{\mathrm{n}}\gamma_{\mathrm{do}}d_{50}}}{10^6\,\mathrm{g}}\right)^{\beta_2(\Delta\delta)}\tag{22}$$

where $\tau(\Delta\delta)$=shear stress with respect to horizontal displacement $\Delta\delta$ (in Pa); and $\beta_o(\Delta\delta)$, $\beta_1(\Delta\delta)$ and $\beta_2(\Delta\delta)$=model parameters (dimensionless), which are a function of horizontal displacement $\Delta\delta$.

Provided that **Equation 22** holds, one can therefore arrive at an estimate of the shear stress for any given horizontal displacement, and thus construct the corresponding shear stress–horizontal

displacement curve. As opposed to continuous mathematical functions, such as hyperbolic–based functions (e.g. Kondner 1963; Duncan and Chang 1970; Stark et al. 1994; Horpibulsuk and Miura 2001; Horpibulsuk and Rachan 2004), which simulate the shear stress–horizontal displacement response by enforcing a predefined form factor over a continues horizontal displacement domain, the dimensional model given in **Equation 22** is a discrete function in nature, and thus simulates each shear stress–horizontal displacement curve point independently. As such, a predefined form factor is not enforced to the problem in hand, thereby allowing for indigenous material properties such as strain–softening to be simply quantified with more accuracy. It has been the authors' experience that a total of six arbitrary horizontal displacement values would satisfy the construction of a desired shear stress–horizontal displacement curve. Quite clearly, the greater the number of adopted horizontal displacement values the more realistic the constructed curve. To test the proposed hypothesis, the performance of the proposed dimensional model given in **Equation 22** was examined at six different low to high horizontal displacements, i.e. $\Delta\delta$=0.5 mm, 1 mm, 2 mm, 4 mm, 6 mm and 8 mm, and the results are provided in **Figure 11** for both rubber types. An obvious clustering of predicted and actual data can be observed, with most of the predicted values perfectly overlapping with their actual counterparts, thus confirming the model's capacity to capture the shear stress response with respect to horizontal displacement.

Figure 12 illustrates typical experimental shear stress–horizontal displacement curves along with their respective simulations by means of the proposed dimensional model given in **Equation 22**. The constructed curves perfectly overlap with their actual counterparts. In particular, the strain–softening character is well simulated by the proposed model, thus resolving an inherent issue associated with common continuous simulative functions. The calibration procedure for **Equation 22** would be identical to that described for Model M_3 (**Equation 20**) in **Section 4.3.3**. In this case, however, for each adopted horizontal displacement $\Delta\delta$, a separate system of three semi–linear equations should to be solved to arrive at an estimate of the corresponding model parameters $\beta_o(\Delta\delta)$, $\beta_1(\Delta\delta)$ and $\beta_2(\Delta\delta)$.

5. Conclusions

The following conclusions can be drawn from this study:

- The rubber inclusions altered the soil fabric into a coherent matrix of induced strength and improved ductility through amendments achieved in two aspects: **i)** frictional resistance

generated as a result of soil–rubber contact; and **ii)** mechanical interlocking of rubber particles and soil grains. Provided that the rubber particles do not cluster during compaction and shearing, both amending mechanisms are expected to be in favor of a higher rubber content, and to a lesser degree a larger rubber size.

- The shear stress–horizontal dispalcement response exhibited a strain–softening character for both the natural soil and various soil–rubber composites. This effect, however, was less evident for samples reinforced with high inclusions (particularly R_C=30%) of the coarser rubber. This behavior was attributed to the dominant rubber–to–rubber interaction (or rubber–clustering) exhibited at high inclusions of the coarser rubber.

- For $R_C \leq 10\%$, the rubber of coarser category, Rubber B, slightly outperformed the finer Rubber C in terms of higher peak shear strength properties. R_C=20% served as a transition point, manifesting a similar performance with marginal differences for the two rubber types. At R_C=30%, the peak shear strength properties for Rubber B dropped below that of Rubber C, signifying an induced rubber–clustering effect in the presence of the coarser rubber. Such a transition was not observed for the critical shear strength values, which was attributed to the strain–hardening like character exhibited at high inclusions of Rubber B.

- The dimensional analysis concept was extended to the soil–rubber shear strength problem, thereby leading to the development of a series of simple and practical dimensional models capable of simulating the shear stress–horizontal displacement response as a function of the composite's basic index properties. The predictive capacity of the proposed models was examined and validated by statistical techniques. The proposed dimensional models contain a limited number of fitting parameters, which can be calibrated by minimal experimental effort and hence implemented for predictive purposes.

Acknowledgements

This research was funded by the Australian Research Council (ARC) by way of project No. **DP140103004**; this support is gratefully acknowledged.

References

Agus, S. S., Schanz, T. & Fredlund, D. G. **(2010)**. Measurements of suction versus water content for bentonite–sand mixtures. *Canadian Geotechnical Journal*, **47**, No. 5, 583–594, http://dx.doi.org/10.1139/t09-120.

Al-Aqtash, U. & Bandini, P. **(2015)**. Prediction of unsaturated shear strength of an adobe soil from the soil–water characteristic curve. *Construction and Building Materials*, **98**, 892–899, http://dx.doi.org/10.1016/j.conbuildmat.2015.07.188.

Arulrajah, A., Mohammadinia, A., D'Amico, A. & Horpibulsuk, S. **(2017)**. Effect of lime kiln dust as an alternative binder in the stabilization of construction and demolition materials. *Construction and Building Materials*, **152**, No. 999–1007, http://dx.doi.org/10.1016/j.conbuildmat.2017.07.070.

AS 1289.3.2.1:09 **(2009)**. Methods of testing soils for engineering purposes: Soil classification tests – Determination of the plastic limit of a soil. *Standards Australia*, Sydney, New South Wales, Australia.

AS 1289.3.3.1:09 **(2009)**. Methods of testing soils for engineering purposes: Soil classification tests – Calculation of the plasticity index of a soil. *Standards Australia*, Sydney, New South Wales, Australia.

AS 1289.3.4.1:08 **(2008)**. Methods of testing soils for engineering purposes: Soil classification tests – Determination of the linear shrinkage of a soil. *Standards Australia*, Sydney, New South Wales, Australia.

AS 1289.3.9.1:15 **(2015)**. Methods of testing soils for engineering purposes: Soil classification tests – Determination of the cone liquid limit of a soil. *Standards Australia*, Sydney, New South Wales, Australia.

AS 1289.6.2.2:98 **(1998)**. Methods of testing soils for engineering purposes: Soil strength and consolidation tests – determination of the shear strength of a soil – direct shear test using a shear box. *Standards Australia*, Sydney, New South Wales, Australia.

ASTM D2487-11 **(2011)**. Standard practice for classification of soils for engineering purposes (Unified Soil Classification System). *ASTM International*, West Conshohocken, Pennsylvania, USA, http://dx.doi.org/10.1520/d2487-11.

ASTM D422-63(2007)e2 **(2007)**. Standard test method for particle–size analysis of soils. *ASTM International*, West Conshohocken, Pennsylvania, USA, http://dx.doi.org/10.1520/d0422-63r07e02.

ASTM D698-12e2 **(2012)**. Standard test methods for laboratory compaction characteristics of soil using standard effort (12,400 ft–lbf/ft^3 (600 kN–m/m^3)). *ASTM International*, West Conshohocken, Pennsylvania, USA, http://dx.doi.org/10.1520/d0698-12e02.

ASTM D854-14 **(2014)**. Standard test methods for specific gravity of soil solids by water pycnometer. *ASTM International*, West Conshohocken, Pennsylvania, USA, http://dx.doi.org/10.1520/d0854-14.

Bai, F. Q. & Liu, S. H. **(2012)**. Measurement of the shear strength of an expansive soil by combining a filter paper method and direct shear tests. *Geotechnical Testing Journal*, **35**, No. 3, 451–459, http://dx.doi.org/10.1520/gtj103342.

Berrah, Y., Boumezbeur, A., Kherici, N. & Charef, N. **(2016)**. Application of dimensional analysis and regression tools to estimate swell pressure of expansive soil in Tebessa (Algeria). *Bulletin of Engineering Geology and the Environment*, **in press**, http://dx.doi.org/10.1007/s10064-016-0973-4.

Briga-Sá, A., Nascimento, D., Teixeira, N., Pinto, J., Caldeira, F., Varum, H. & Paiva, A. **(2013)**. Textile waste as an alternative thermal insulation building material solution. *Construction and Building Materials*, **38**, 155–160, http://dx.doi.org/10.1016/j.conbuildmat.2012.08.037.

Buckingham, E. **(1914)**. On physically similar systems; illustrations of the use of dimensional equations. *Physical Review*, **4**, No. 4, 345–376, http://dx.doi.org/10.1103/physrev.4.345.

Butterfield, R. **(1999)**. Dimensional analysis for geotechnical engineers. *Géotechnique*, **49**, No. 3, 357–366, http://dx.doi.org/10.1680/geot.1999.49.3.357.

Buzzi, O. **(2010)**. On the use of dimensional analysis to predict swelling strain. *Engineering Geology*, **116**, No. 1–2, 149–156, http://dx.doi.org/10.1016/j.enggeo.2010.08.005.

Buzzi, O., Giacomini, A. & Fityus, S. **(2011)**. Towards a dimensionless description of soil swelling behaviour. *Géotechnique*, **61**, No. 3, 271–277, http://dx.doi.org/10.1680/geot.7.00194.

Cabalar, A. F. & Karabash, Z. **(2015)**. California bearing ratio of a sub–base material modified with tire buffings and cement addition. *Journal of Testing and Evaluation*, **43**, No. 6, 1279–1287, http://dx.doi.org/10.1520/jte20130070.

Cabalar, A. F., Karabash, Z. & Mustafa, W. S. **(2014)** Stabilising a clay using tyre buffings and lime. *Road Materials and Pavement Design*, **15**, No. 4, 872–891, http://dx.doi.org/10.1080/14680629.2014.939697.

Calik, U. & Sadoglu, E. **(2014)**. Classification, shear strength, and durability of expansive clayey soil stabilized with lime and perlite. *Natural Hazards*, **71**, No. 3, 1289–1303, http://dx.doi.org/10.1007/s11069-013-0950-1.

Cetin, H., Fener, M. & Gunaydin, O. **(2006)**. Geotechnical properties of tire–cohesive clayey soil mixtures as a fill material. *Engineering Geology*, **88**, No. 1–2, 110–120, http://dx.doi.org/10.1016/j.enggeo.2006.09.002.

Duncan, J. M. & Chang, C. Y. **(1970)**. Nonlinear analysis of stress and strain in soils. *Journal of the Soil Mechanics and Foundations Division*, **96**, No. 5, 1629–1653.

Edil, T. & Bosscher, P. **(1994)**. Engineering properties of tire chips and soil mixtures. *Geotechnical Testing Journal*, **17**, No. 4, 453–464, http://dx.doi.org/10.1520/gtj10306J.

Edincliler, A., Cabalar, A. F. & Cevik, A. **(2013)** Modelling dynamic behaviour of sand–waste tires mixtures using Neural Networks and Neuro–Fuzzy. *European Journal of Environmental and Civil Engineering*, **17**, No. 8, 720–741, http://dx.doi.org/10.1080/19648189.2013.814552.

Edincliler, A., Cabalar, A. F., Cagatay, A. & Cevik, A. **(2012)** Triaxial compression behavior of sand and tire wastes using neural networks. *Neural Computing and Applications*, **21**, No. 3, 441–452, http://dx.doi.org/10.1007/s00521-010-0430-4.

Estabragh, A. R., Soltani, A. & Javadi, A. A. **(2016)**. Models for predicting the seepage velocity and seepage force in a fiber reinforced silty soil. *Computers and Geotechnics*, **75**, 174–181, http://dx.doi.org/10.1016/j.compgeo.2016.02.002.

Estabragh, A. R., Soltani, A. & Javadi, A. A. **(2018)**. Effect of pore water chemistry on the behaviour of a kaolin–bentonite mixture during drying and wetting cycles. *European Journal of Environmental and Civil Engineering*, **in press**, http://dx.doi.org/10.1080/19648189.2018.1428691.

Hannam, P. **(2014)**. Tyre industry divided over how to handle toxic waste. *The Sydney Morning Herald*, Sydney, New South Wales, Australia. See http://www.smh.com.au/environment/tyre-industry-divided-over-how-to-handle-toxic-waste-20140120-314ic.html (accessed 1/29/2018)

Horpibulsuk, S. & Miura, N. **(2001)**. Modified hyperbolic stress–strain response: Uncemented and cement stabilized clays. *Reports of the Faculty of Science and Engineering, Saga University*, **30**, No. 1, 39–47.

Horpibulsuk, S. & Rachan, R. **(2004)**. Modified hyperbolic model for capturing undrained shear behavior. *Lowland Technology International*, **6**, No. 2, 11–20.

Hoy, M., Rachan, R., Horpibulsuk, S., Arulrajah, A. & Mirzababaei, M. **(2017)**. Effect of wetting–drying cycles on compressive strength and microstructure of recycled asphalt pavement–Fly ash geopolymer. *Construction and Building Materials*, **144**, 624–634, http://dx.doi.org/10.1016/j.conbuildmat.2017.03.243.

Huggins, E. & Ravichandran, N. **(2011)**. Numerical study on the dynamic behavior of retaining walls backfilled with shredded tires. In: *GeoRisk 2011: Geotechnical Risk Assessment and Management (GSP 224)*, Juang, C. H., Phoon, K. K., Puppala, A. J., Green, R. A. & Fenton, G. A., Eds., ASCE, Atlanta, Georgia, USA, pp. 955–962, http://dx.doi.org/10.1061/41183(418)103.

Johari, A., Habibagahi, G. & Ghahramani, A. **(2006)**. Prediction of soil–water characteristic curve using genetic programming. *Journal of Geotechnical and Geoenvironmental Engineering*, **132**, No. 5, 661–665, http://dx.doi.org/10.1061/(asce)1090-0241(2006)132:5(661).

Kalkan, E. **(2013)**. Preparation of scrap tire rubber fiber–silica fume mixtures for modification of clayey soils. *Applied Clay Science*, **80**–**81**, 117–125, http://dx.doi.org/10.1016/j.clay.2013.06.014.

Kim, Y. T., Kim, H. J. & Lee, G. H. **(2008)**. Mechanical behavior of lightweight soil reinforced with waste fishing net. *Geotextiles and Geomembranes*, **26**, No. 6, 512–518, http://dx.doi.org/10.1016/j.geotexmem.2008.05.004.

Kondner, R. L. **(1963)**. Hyperbolic stress–strain response: Cohesive soils. *Journal of the Soil Mechanics and Foundations Division*, **89**, No. 1, 115–144.

Kua, T. A., Arulrajah, A., Mohammadinia, A., Horpibulsuk, S. & Mirzababaei, M. **(2017)**. Stiffness and deformation properties of spent coffee grounds based geopolymers. *Construction and Building Materials*, **138**, 79–87, http://dx.doi.org/10.1016/j.conbuildmat.2017.01.082.

Lee, C., Shin, H. & Lee, J. S. **(2014)**. Behavior of sand–rubber particle mixtures: Experimental observations and numerical simulations. *International Journal for Numerical and Analytical Methods in Geomechanics*, **38**, No. 16, 1651–1663, http://dx.doi.org/10.1002/nag.2264.

Li, L., Xiao, H., Ferreira, P. & Cui, X. **(2016)**. Study of a small scale tyre–reinforced embankment. *Geotextiles and Geomembranes*, **44**, No. 2, 201–208, http://dx.doi.org/10.1016/j.geotexmem.2015.08.004.

Liu, C. & Evett, J. **(2009)**. Soil Properties: Testing, Measurement, and Evaluation (6th Ed.). Pearson/Prentice Hall, Upper Saddle River, New Jersey, USA. ISBN: 9780136141235.

Locat, J., Lefebvre, G. & Ballivy, G. **(1984)**. Mineralogy, chemistry, and physical properties interrelationships of some sensitive clays from Eastern Canada. *Canadian Geotechnical Journal*, **21**, No. 3, 530–540, http://dx.doi.org/10.1139/t84-055.

Malaya, C. & Sreedeep, S. **(2011)**. A laboratory procedure for measuring high soil suction. *Geotechnical Testing Journal*, **34**, No. 5, 396–405, http://dx.doi.org/10.1520/gtj103613.

Mirzababaei, M., Arulrajah, A., Haque, A., Nimbalkar, S. & Mohajerani, A. **(2018c)** Effect of fiber reinforcement on shear strength and void ratio of soft clay. *Geosynthetics International*, **in press**, http://dx.doi.org/10.1680/jgein.18.00023.

Mirzababaei, M., Arulrajah, A., Horpibulsuk, S., Soltani, A. & Khayat, N. **(2018b)** Stabilization of soft clay using short fibers and poly vinyl alcohol. *Geotextiles and Geomembranes*, **46**, No. 5, 646–655, http://dx.doi.org/10.1016/j.geotexmem.2018.05.001.

Mirzababaei, M., Miraftab, M., Mohamed, M. & McMahon, P. **(2013a)**. Unconfined compression strength of reinforced clays with carpet waste fibers. *Journal of Geotechnical and Geoenvironmental Engineering*, **139**, No. 3, 483–493, http://dx.doi.org/10.1061/(asce)gt.1943-5606.0000792.

Mirzababaei, M., Miraftab, M., Mohamed, M. & McMahon, P. **(2013b)**. Impact of carpet waste fibre addition on swelling properties of compacted clays. *Geotechnical and Geological Engineering*, **31**, No. 1, 173–182, http://dx.doi.org/10.1007/s10706-012-9578-2.

Mirzababaei, M., Mohamed, M., Arulrajah, A., Horpibulsuk, S. & Anggraini, V. **(2018a)**. Practical approach to predict the shear strength of fibre–reinforced clay. *Geosynthetics International*, **25**, No. 1, 50–66, http://dx.doi.org/10.1680/jgein.17.00033.

Mukherjee, K. & Mishra, A. K. **(2017)** The impact of scrapped tyre chips on the mechanical properties of liner materials. *Environmental Processes*, **4**, No. 1, 219–233, http://dx.doi.org/10.1007/s40710-017-0210-6.

Mukherjee, K. & Mishra, A. K. **(2018)** Hydraulic and mechanical characteristics of compacted sand–bentonite: Tyre chips mix for its landfill application. *Environment, Development and Sustainability*, **in press**, http://dx.doi.org/10.1007/s10668-018-0094-2.

Özkul, Z. H. & Baykal, G. **(2006)** Shear strength of clay with rubber fiber inclusions. *Geosynthetics International*, **13**, No. 5, 173–180, http://dx.doi.org/10.1680/gein.2006.13.5.173.

Özkul, Z. H. & Baykal, G. **(2007)**. Shear behavior of compacted rubber fiber–clay composite in drained and undrained loading. *Journal of Geotechnical and Geoenvironmental Engineering*, **133**, No. 7, 767–781, http://dx.doi.org/10.1061/(asce)1090-0241(2007)133:7(767).

Parghi, A. & Alam, M. S. **(2016)**. Physical and mechanical properties of cementitious composites containing recycled glass powder (RGP) and styrene butadiene rubber (SBR). *Construction and Building Materials*, **104**, 34–43, http://dx.doi.org/10.1016/j.conbuildmat.2015.12.006.

Perez, J. L., Kwok, C. Y. & Senetakis, K. **(2016)**. Effect of rubber size on the behaviour of sand–rubber mixtures: A numerical investigation. *Computers and Geotechnics*, **80**, 199–214, http://dx.doi.org/10.1016/j.compgeo.2016.07.005.

Perez, J. L., Kwok, C. Y. & Senetakis, K. **(2017)**. Investigation of the micromechanics of sand–rubber mixtures at very small strains. *Geosynthetics International*, **24**, No. 1, 30–44, http://dx.doi.org/10.1680/jgein.16.00013.

Prakash, K. & Sridharan, A. **(2004)**. Free swell ratio and clay mineralogy of fine–grained soils. *Geotechnical Testing Journal*, **27**, No. 2, 220–225, http://dx.doi.org/10.1520/gtj10860.

Prakash, K., Sridharan, A. & Prasanna, H. S. **(2009)** A note on the determination of plastic limit of fine–grained soils. *Geotechnical Testing Journal*, **32**, No. 4, 372–374, http://dx.doi.org/10.1520/gtj101960.

Puppala, A. J., Hoyos, L. R. & Potturi, A. K. **(2011)**. Resilient Moduli Response of Moderately Cement-Treated Reclaimed Asphalt Pavement Aggregates. *Journal of Materials in Civil Engineering*, **23**, No. 7, 990–998, http://dx.doi.org/10.1061/(asce)mt.1943-5533.0000268.

Qu, J. & Zhao, D. **(2016)**. Stabilising the cohesive soil with palm fibre sheath strip. *Road Materials and Pavement Design*, **17**, No. 1, 87–103, http://dx.doi.org/10.1080/14680629.2015.1064010.

Qu, J., Li, C., Liu, B., Chen, X., Li, M. & Yao, Z. **(2013)**. Effect of random inclusion of wheat straw fibers on shear strength characteristics of Shanghai cohesive soil. *Geotechnical and Geological Engineering*, **31**, No. 2, 511–518, http://dx.doi.org/10.1007/s10706-012-9604-4.

Rao, A. S., Phanikumar, B. R. & Sharma, R. S. **(2004)**. Prediction of swelling characteristics of remoulded and compacted expansive soils using free swell index. *Quarterly Journal of Engineering Geology and Hydrogeology*, **37**, No. 3, 217–226, http://dx.doi.org/10.1144/1470-9236/03-052.

Saberian, M., Li, J., Nguyen, B. T. & Wang, G. **(2018)** Permanent deformation behaviour of pavement base and subbase containing recycle concrete aggregate, coarse and fine crumb rubber. *Construction and Building Materials*, **178**, 51–58, http://dx.doi.org/10.1016/j.conbuildmat.2018.05.107.

Sezer, A., İnan, G., Recep Yılmaz, H. & Ramyar, K. **(2006)**. Utilization of a very high lime fly ash for improvement of Izmir clay. *Building and Environment*, **41**, No. 2, 150–155, http://dx.doi.org/10.1016/j.buildenv.2004.12.009.

Shalaby, A. & Khan, R. A. **(2002)**. Temperature monitoring and compressibility measurement of a tire shred embankment: Winnipeg, Manitoba, Canada. *Transportation Research Record: Journal of the Transportation Research Board*, **1808**, 67–75, http://dx.doi.org/10.3141/1808-08.

Signes, C. H., Garzón-Roca, J., Fernández, P. M., Torre, M. E. G. & Franco, R. I. **(2016)**. Swelling potential reduction of Spanish argillaceous marlstone Facies Tap soil through the addition of crumb rubber particles from scrap tyres. *Applied Clay Science*, **132**–**133**, 768–773, http://dx.doi.org/10.1016/j.clay.2016.07.027.

Simon, V., Weigand, B. & Gomaa, H. **(2017)**. Dimensional Analysis for Engineers (1st Ed.). Springer International Publishing AG, Gewerbestrasse, Cham, Switzerland, http://dx.doi.org/10.1007/978-3-319-52028-5. ISBN: 9783319520285.

Soltani, A., Deng, A. & Taheri, A. **(2018[a])**. Swell–compression characteristics of a fiber–reinforced expansive soil. *Geotextiles and Geomembranes*, **46**, No. 2, 183–189, http://dx.doi.org/10.1016/j.geotexmem.2017.11.009.

Soltani, A., Deng, A., Taheri, A. & Mirzababaei, M. **(2017[a])**. A sulphonated oil for stabilisation of expansive soils. *International Journal of Pavement Engineering*, **in press**, http://dx.doi.org/10.1080/10298436.2017.1408270.

Soltani, A., Deng, A., Taheri, A. & Mirzababaei, M. **(2018[b])**. Rubber powder–polymer combined stabilization of South Australian expansive soils. *Geosynthetics International*, **25**, No. 3, 304–321, http://doi.org/10.1680/jgein.18.00009.

Soltani, A., Deng, A., Taheri, A. & Sridharan, A. **(2018[c])**. Swell–shrink–consolidation behavior of rubber–reinforced expansive soils. *Geotechnical Testing Journal*, **in press**, http://doi.org/10.1520/gtj20170313.

Soltani, A., Deng, A., Taheri, A. & Sridharan, A. **(2018[d])** Consistency limits and compaction characteristics of clay soils containing rubber waste. *Proceedings of the Institution of Civil Engineers–Geotechnical Engineering*, **in press**, http://dx.doi.org/10.1680/jgeen.18.00042.

Soltani, A., Deng, A., Taheri, A., Sridharan, A. & Estabragh, A. R. **(2018[e])**. A framework for interpretation of the compressibility behavior of soils. *Geotechnical Testing Journal*, **41**, No. 1, 1–16, http://dx.doi.org/10.1520/gtj20170088.

Soltani, A., Taheri, A., Khatibi, M. & Estabragh, A. R. **(2017[b])**. Swelling potential of a stabilized expansive soil: A comparative experimental study. *Geotechnical and Geological Engineering*, **35**, No. 4, 1717–1744, http://dx.doi.org/10.1007/s10706-017-0204-1.

Stark, T. D., Ebeling, R. M. & Vettel, J. J. **(1994)**. Hyperbolic stress–strain parameters for silts. *Journal of Geotechnical Engineering*, **120**, No. 2, 420–441, http://dx.doi.org/10.1061/(asce)0733-9410(1994)120:2(420).

Tanchaisawat, T., Voottipruex, P., Bergado, D. T. & Hayashi, S. **(2008)**. Performance of full scale test embankment with reinforced lightweight geomaterials on soft ground. *Lowland Technology International*, **10**, No. 1, 84–92.

Tang, C. S., Shi, B. & Zhao, L. Z. **(2010)**. Interfacial shear strength of fiber reinforced soil. *Geotextiles and Geomembranes*, **28**, No. 1, 54–62, http://dx.doi.org/10.1016/j.geotexmem.2009.10.001.

Tang, C. S., Shi, B., Gao, W., Chen, F. & Cai, Y. **(2007)**. Strength and mechanical behavior of short polypropylene fiber reinforced and cement stabilized clayey soil. *Geotextiles and Geomembranes*, **25**, No. 3, 194–202, http://dx.doi.org/10.1016/j.geotexmem.2006.11.002.

Tatlisoz, N., Benson, C. H. & Edil, T. B. **(1997)** Effect of fines on mechanical properties of soil–tire chip mixtures. In: *Testing Soil Mixed with Waste or Recycled Materials (ASTM STP1275)*, Wasemiller, M. A. & Hoddinott, K. B., Eds., ASTM International, West Conshohocken, Pennsylvania, USA, http://dx.doi.org/10.1520/stp15645s.

Thomas, B. S., Gupta, R. C. & Panicker, V. J. **(2016)**. Recycling of waste tire rubber as aggregate in concrete: Durability–related performance. *Journal of Cleaner Production*, **112**, No. 1, 504–513, http://dx.doi.org/10.1016/j.jclepro.2015.08.046.

Trouzine, H., Bekhiti, M. & Asroun, A. **(2012)**. Effects of scrap tyre rubber fibre on swelling behaviour of two clayey soils in Algeria. *Geosynthetics International*, **19**, No. 2, 124–132, http://dx.doi.org/10.1680/gein.2012.19.2.124.

Tsoi, W. Y. & Lee, K. M. **(2011)**. Mechanical properties of cemented scrap rubber tyre chips. *Géotechnique*, **61**, No. 2, 133–141, http://dx.doi.org/10.1680/geot.9.p.033.

Tweedie, J. J., Humphrey, D. N. & Sandford, T. C. **(1998)**. Full–scale field trials of tire shreds as lightweight retaining wall backfill under at–rest conditions. *Transportation Research Record: Journal of the Transportation Research Board*, **1619**, 64–71, http://dx.doi.org/10.3141/1619-08.

Valdes, J. R. & Evans, T. M. **(2008)**. Sand–rubber mixtures: Experiments and numerical simulations. *Canadian Geotechnical Journal*, **45**, No. 4, 588–595, http://dx.doi.org/10.1139/t08-002.

Wang, C., Deng, A. & Taheri, A. **(2018)** Three–dimensional discrete element modeling of direct shear test for granular rubber–sand. *Computers and Geotechnics*, **97**, 204–216, http://dx.doi.org/10.1016/j.compgeo.2018.01.014.

Wang, Y. X., Guo, P. P., Ren, W. X., Yuan, B. X., Yuan, H. P., Zhao, Y. L., Shan, S. B. & Cao, P. **(2017)**. Laboratory investigation on strength characteristics of expansive soil treated with jute fiber reinforcement. *International Journal of Geomechanics*, **17**, No. 11, 04017101:1–04017101:12, http://dx.doi.org/10.1061/(asce)gm.1943-5622.0000998.

Williamson, S. & Cortes, D. D. **(2014)**. Dimensional analysis of soil–cement mixture performance. *Géotechnique Letters*, **4**, No. 1, 33–38, http://dx.doi.org/10.1680/geolett.13.00082.

Yadav, J. S. & Tiwari, S. K. **(2017[a])**. The impact of end–of–life tires on the mechanical properties of fine–grained soil: A Review. *Environment, Development and Sustainability*, **in press**, http://dx.doi.org/10.1007/s10668-017-0054-2.

Yadav, J. S. & Tiwari, S. K. **(2017[b])**. Effect of waste rubber fibres on the geotechnical properties of clay stabilized with cement. *Applied Clay Science*, **149**, 97–110, http://dx.doi.org/10.1016/j.clay.2017.07.037.

Yesilata, B., Isıker, Y. & Turgut, P. **(2009)**. Thermal insulation enhancement in concretes by adding waste PET and rubber pieces. *Construction and Building Materials*, **23**, 1878–1882, http://dx.doi.org/10.1016/j.conbuildmat.2008.09.014.

Yoon, S., Prezzi, M., Siddiki, N. Z. & Kim, B. **(2006)**. Construction of a test embankment using a sand–tire shred mixture as fill material. *Waste Management*, **26**, No. 9, 1033–1044, http://dx.doi.org/10.1016/j.wasman.2005.10.009.

Youwai, S. & Bergado, D. T. **(2004)**. Numerical analysis of reinforced wall using rubber tire chips–sand mixtures as backfill material. *Computers and Geotechnics*, **31**, No. 2, 103–114, http://dx.doi.org/10.1016/j.compgeo.2004.01.008.

Zhang, T., Cai, G. & Duan, W. **(2017)**. Strength and microstructure characteristics of the recycled rubber tire–sand mixtures as lightweight backfill. *Environmental Science and Pollution Research*, **in press**, http://dx.doi.org/10.1007/s11356-017-0742-3.

Zhao, Y., Gao, Y., Zhang, Y. & Wang, Y. **(2016)**. Effect of fines on the mechanical properties of composite soil stabilizer–stabilized gravel soil. *Construction and Building Materials*, **126**, 701–710, http://dx.doi.org/10.1016/j.conbuildmat.2016.09.082.

Zornberg, J. G., Cabral, A. R. & Viratjandr, C. **(2004)**. Behaviour of tire shred–sand mixtures. *Canadian Geotechnical Journal*, **41**, No. 2, 227–241, http://dx.doi.org/10.1139/t03-086.

List of Tables

Table 1. Physical and mechanical properties of the soil.

Table 2. Basic index properties of the prepared samples.

Table 3. Shear strength parameters at peak condition for the tested samples.

Table 4. Summary of the regression analysis outputs with respect to the proposed dimensional model M_1 (**Equation 14**) for both rubber types.

Table 5. Summary of the regression analysis outputs with respect to the proposed dimensional model M_2 (**Equation 17**) for both rubber types.

Table 6. Summary of the regression analysis outputs with respect to the proposed dimensional model M_3 (**Equation 20**) for both rubber types.

Table 1. Physical and mechanical properties of the soil.

Properties	Value/Description	Standard designation
Specific gravity, G_s	2.73	ASTM D854 (2014)
Grain–size distribution		
Clay (< 2 μm) (%)	52.80	ASTM D422 (2007)
Silt (2–75 μm) (%)	46.16	
Fine sand (0.075–0.425 mm) (%)	1.04	
Medium sand (0.425–2 mm) (%)	0	
Coarse sand (2–4.75 mm) (%)	0	
Consistency limits		
Liquid limit, w_L (%)	59.60	AS 1289.3.9.1 (2015)†
Plastic limit, w_P (%)	27.28	AS 1289.3.2.1 (2009)‡
Plasticity index, I_P (=w_L–w_P) (%)	32.32	AS 1289.3.3.1 (2009)
Linear shrinkage, w_S (%)	8.19	AS 1289.3.4.1 (2008)
Classifications		
USCS classification	CH	ASTM D2487 (2011)
Free swell ratio, FSR*	2.91	Prakash and Sridharan (2004)
Expansive potential	High	
Compaction characteristics		
Optimum water content, w_{opt} (%)	26.00	ASTM D698 (2012)
Maximum dry unit weight, γ_{dmax} (kN/m^3)	15.07	

Note:
†cone penetration method; ‡rolling thread method; and *ratio of equilibrium sediment volume of 10 g oven–dried soil passing sieve 425 μm in distilled water to that of kerosene.

Table 2. Basic index properties of the prepared samples.

Rubber	R_c **(%)**†	w_L **(%)**	w_P **(%)**	I_P **(%)**	w_{opt} **(%)**‡	γ_{dmax} **(kN/m^3)**‡
—	0	59.60	27.28	32.32	26.00	15.07
Rubber C	5	57.03	27.02	30.01	24.77	14.63
	10	55.04	25.54	29.50	23.87	14.35
	20	51.51	23.46	28.05	21.85	13.87
	30	49.58	22.70	26.88	20.07	13.52
Rubber B	5	56.88	26.61	30.27	24.47	14.61
	10	55.62	24.77	30.85	23.46	14.37
	20	52.44	23.27	29.17	21.15	13.86
	30	51.21	22.15	29.06	19.94	13.52

Note:
†$R_c=W_r/W_s\times100$ (W_r=weight of rubber particles; and W_s=weight of soil solids); and ‡initial placement condition for direct shear tests.

Table 3. Shear strength parameters at peak condition for the tested samples.

Rubber	R_c **(%)**	c_p **(kPa)**	φ_p **(º)**
—	0	58.35	9.64
Rubber C	5	59.03	10.63
	10	62.25	13.28
	20	75.89	15.72
	30	98.47	16.56
Rubber B	5	61.86	10.97
	10	71.26	13.33
	20	76.06	14.55
	30	86.19	15.30

Table 4. Summary of the regression analysis outputs with respect to the proposed dimensional model M_1 (**Equation 14**) for both rubber types.

Rubber	**Variable**	β_0	β_1	R^2	**RMSE (kPa)**	**MAPE (%)**
Rubber C	τ_p (Pa)	–0.099	0.127	0.975	8.59	5.43
	τ_{cr} (Pa)	–0.017	0.080	0.985	4.99	3.75
Rubber B	τ_p (Pa)	–0.063	0.230	0.946	11.29	6.21
	τ_{cr} (Pa)	–0.055	0.183	0.979	7.05	5.21

Table 5. Summary of the regression analysis outputs with respect to the proposed dimensional model M_2 (**Equation 17**) for both rubber types.

Rubber	Variable	β_o	β_1	R^2	RMSE (kPa)	MAPE (%)
Rubber C	τ_p (Pa)	0.759	–1.17	0.978	7.68	4.78
	τ_{cr} (Pa)	0.526	–1.04	0.987	4.88	3.52
Rubber B	τ_p (Pa)	1.489	–1.10	0.946	10.79	6.53
	τ_{cr} (Pa)	1.176	–1.11	0.976	7.49	5.65

Table 6. Summary of the regression analysis outputs with respect to the proposed dimensional model M_3 (**Equation 20**) for both rubber types.

Rubber	Variable	β_0	β_1	β_2	R^2	RMSE (kPa)	MAPE (%)
Rubber C	τ_p (Pa)	–0.90	–1.10	–1.25	0.988	6.56	4.06
	τ_{cr} (Pa)	–1.13	–0.51	–1.00	0.988	4.16	3.37
Rubber B	τ_p (Pa)	–0.64	–1.68	–1.23	0.979	7.02	4.36
	τ_{cr} (Pa)	–1.33	–1.08	–1.04	0.984	5.92	4.10

List of Figures

Figure 1. Gradation curves for the used materials.

Figure 2. Tire rubbers at different magnification ratios: **(a)** Rubber C (no magnification); **(b)** Rubber C (50x magnification); **(c)** Rubber C (200x magnification); **(d)** Rubber B (no magnification); **(e)** Rubber B (50x magnification); and **(f)** Rubber B (200x magnification).

Figure 3. Typical shear stress–horizontal displacement curves at σ_n=200 kPa: **(a)** Rubber C; and **(b)** Rubber B.

Figure 4. Variations of shear strength against normal stress for the tested samples: **(a)** Peak shear strength τ_p; and **(b)** Critical shear strength τ_{cr}.

Figure 5. Variations of the dependent Pi term π_o (**Equation 2**) against the first dimensionless shear number η_1 (**Equation 13**) at both peak and critical state conditions: **(a)** Rubber C; and **(b)** Rubber B.

Figure 6. Predicted (by Model M_1 or **Equation 14**) versus actual data, along with the corresponding 95% prediction bands, for various soil–rubber composites: **(a)** Peak shear strength τ_p; and **(b)** Critical shear strength τ_{cr}.

Figure 7. Variations of the dependent Pi term π_o (**Equation 2**) against the second dimensionless shear number η_2 (**Equation 16**) at both peak and critical state conditions: **(a)** Rubber C; and **(b)** Rubber B.

Figure 8. Predicted (by Model M_2 or **Equation 17**) versus actual data, along with the corresponding 95% prediction bands, for various soil–rubber composites: **(a)** Peak shear strength τ_p; and **(b)** Critical shear strength τ_{cr}.

Figure 9. Variations of both predicted (by Model M_3 or **Equation 20**) and actual τ_p and τ_{cr} data against normal stress: **(a)** Rubber C; and **(b)** Rubber B.

Figure 10. Predicted (by Model M_3 or **Equation 20**) versus actual data, along with the corresponding 95% prediction bands, for various soil–rubber composites: **(a)** Peak shear strength τ_p; and **(b)** Critical shear strength τ_{cr}.

Figure 11. Variations of both predicted (by **Equation 22**) and actual shear stress data against normal stress at various horizontal displacements.

Figure 12. Typical experimental shear stress–horizontal displacement curves along with their respective simulations by means of the proposed dimensional model given in **Equation 22**.

Figure 1. Gradation curves for the used materials.

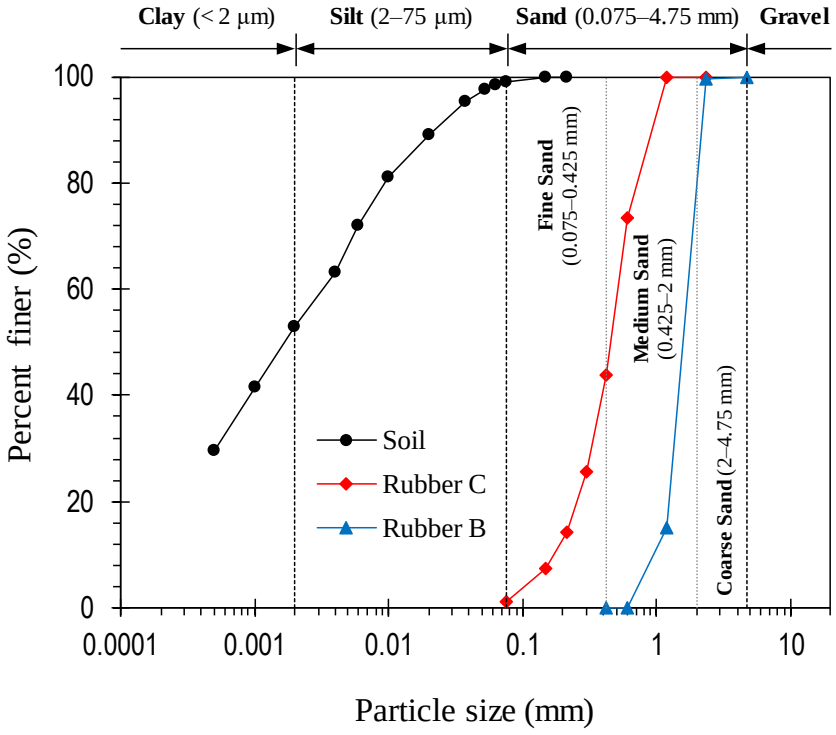

Variable	Rubber C
d_{10} (mm)	0.182
d_{30} (mm)	0.334
d_{50} (mm)	0.478
d_{60} (mm)	0.513
C_c	1.20
C_u	2.81
Variable	**Rubber B**
d_{10} (mm)	1.077
d_{30} (mm)	1.370
d_{50} (mm)	1.582
d_{60} (mm)	1.682
C_c	1.04
C_u	1.56

Figure 2. Tire rubbers at different magnification ratios: **(a)** Rubber C (no magnification); **(b)** Rubber C (50x magnification); **(c)** Rubber C (200x magnification); **(d)** Rubber B (no magnification); **(e)** Rubber B (50x magnification); and **(f)** Rubber B (200x magnification).

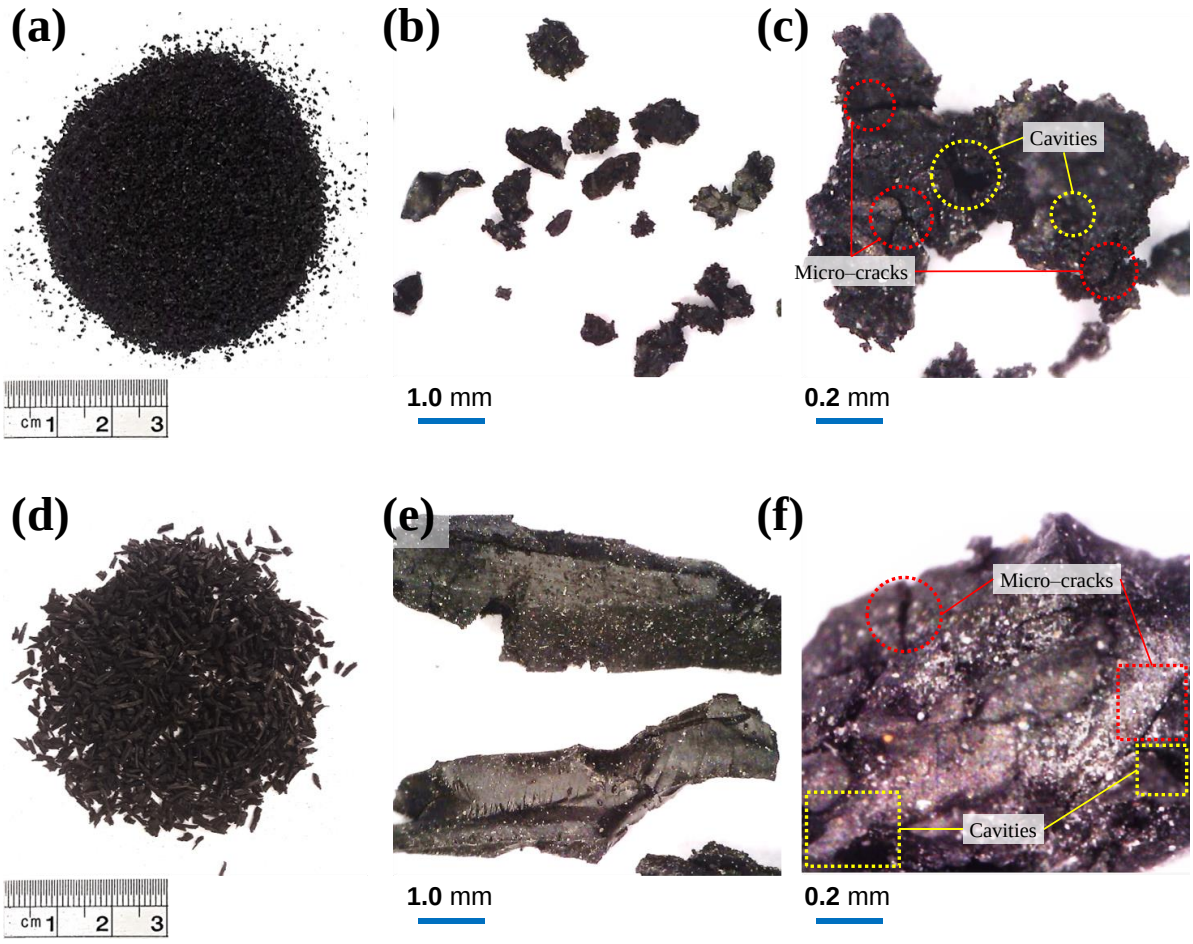

Figure 3. Typical shear stress–horizontal displacement curves at σ_n=200 kPa: **(a)** Rubber C; and **(b)** Rubber B.

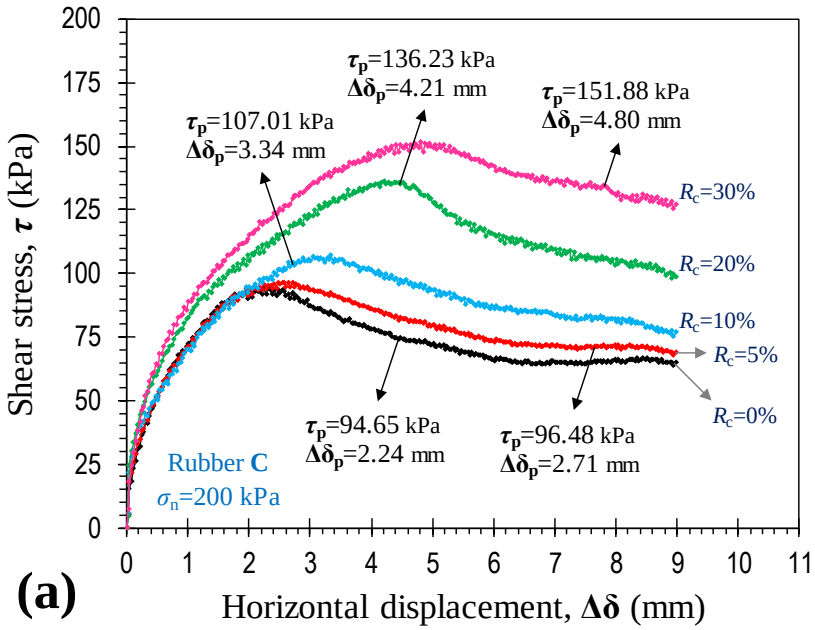

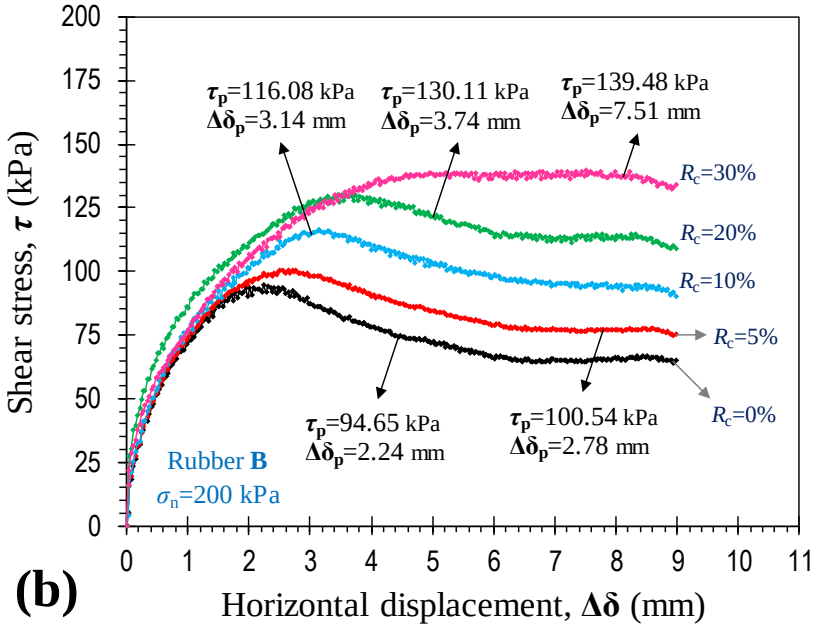

Figure 4. Variations of shear strength against normal stress for the tested samples: **(a)** Peak shear strength τ_p; and **(b)** Critical shear strength τ_{cr}.

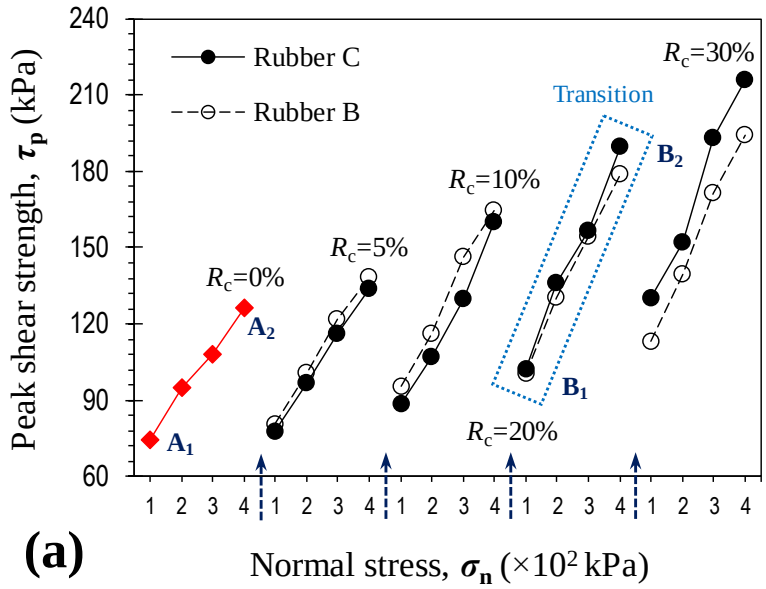

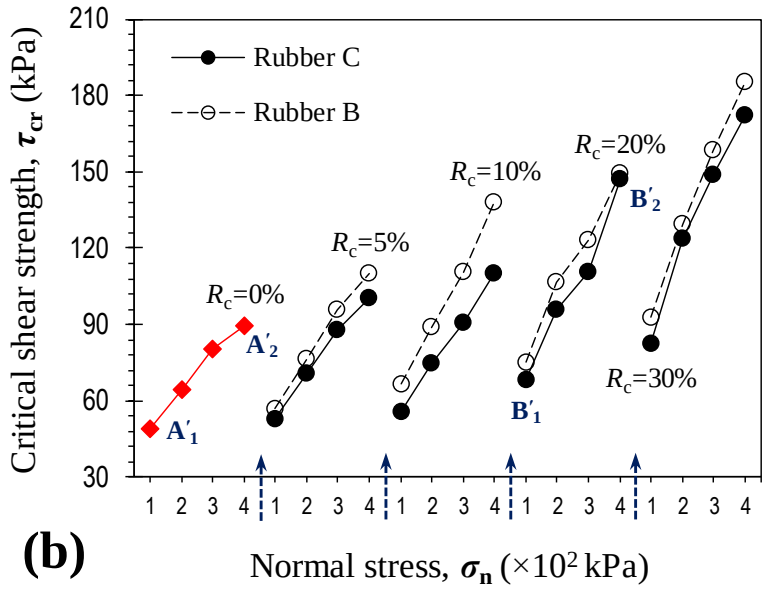

Figure 5. Variations of the dependent Pi term π_o (**Equation 2**) against the first dimensionless shear number η_1 (**Equation 13**) at both peak and critical state conditions: **(a)** Rubber C; and **(b)** Rubber B.

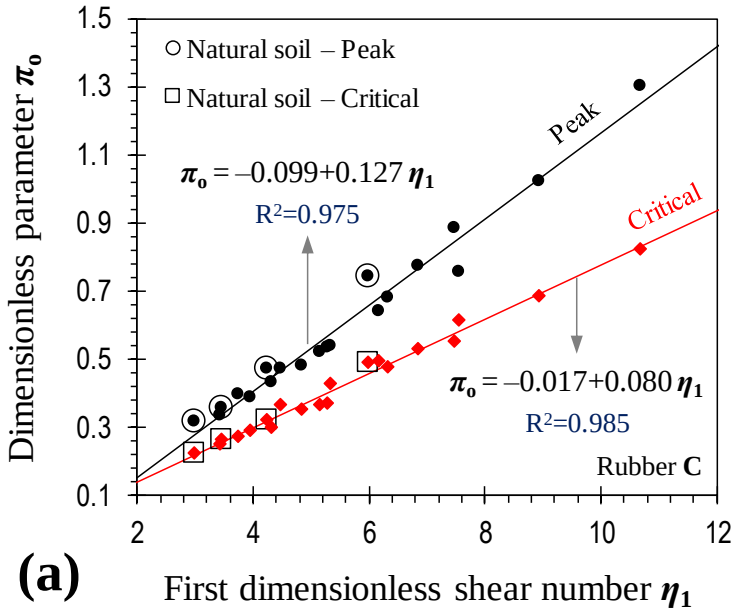

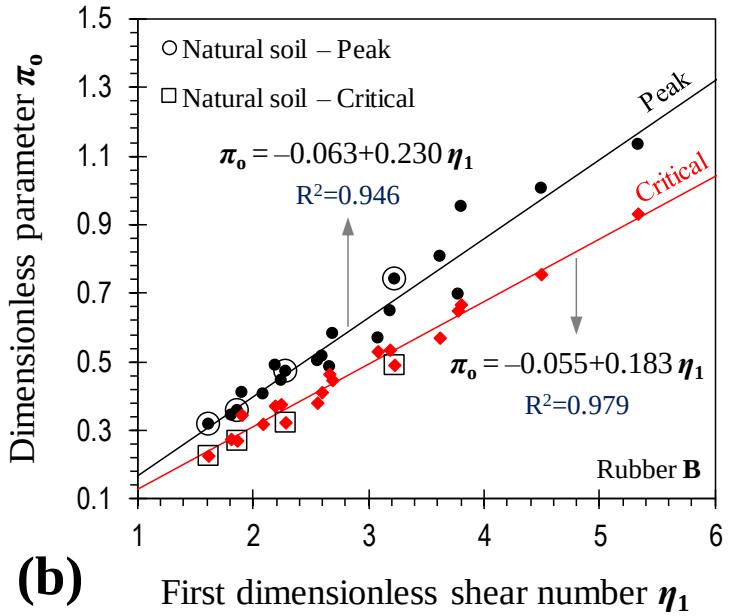

Figure 6. Predicted (by Model M_1 or **Equation 14**) versus actual data, along with the corresponding 95% prediction bands, for various soil–rubber composites: **(a)** Peak shear strength τ_p; and **(b)** Critical shear strength τ_{cr}.

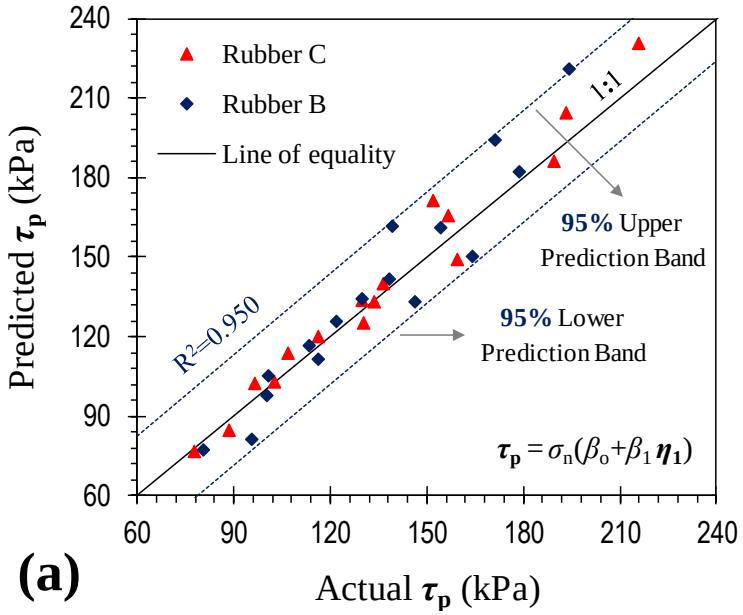

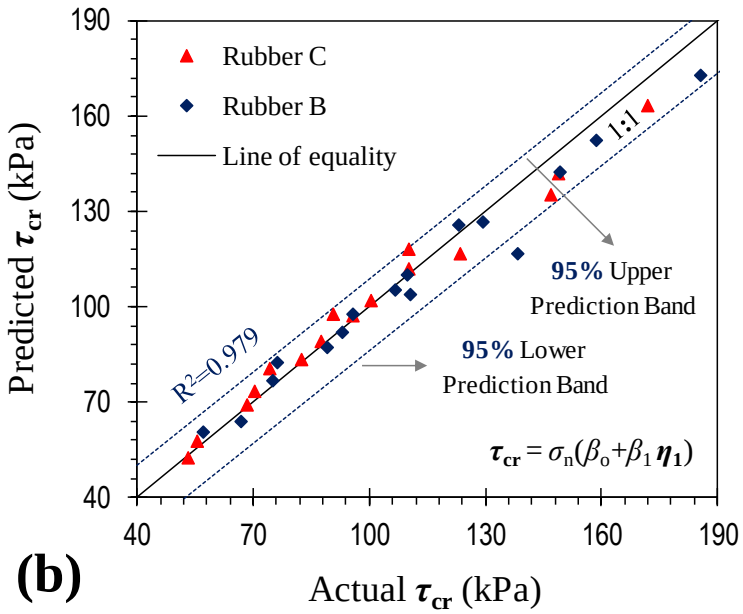

Figure 7. Variations of the dependent Pi term π_o (**Equation 2**) against the second dimensionless shear number η_2 (**Equation 16**) at both peak and critical state conditions: **(a)** Rubber C; and **(b)** Rubber B.

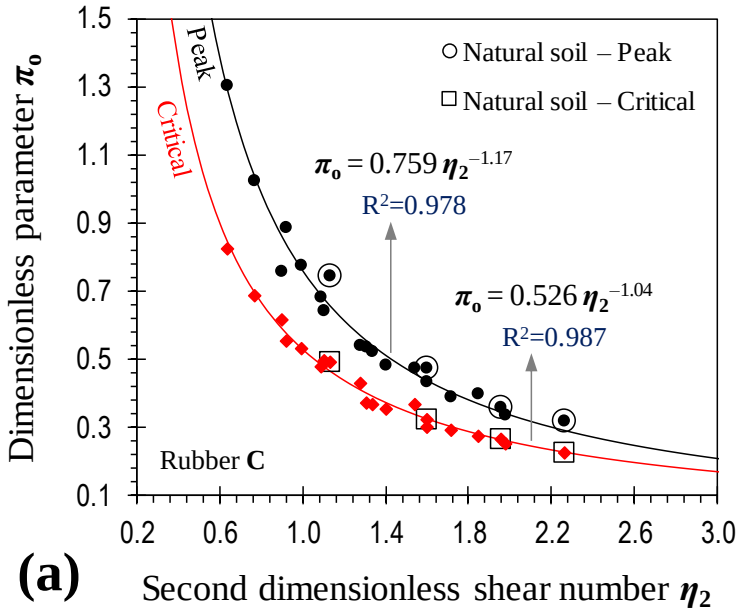

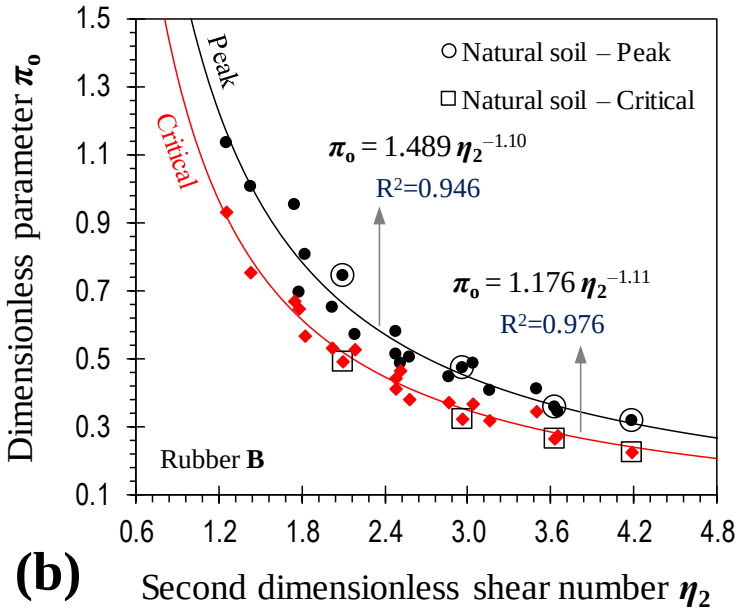

Figure 8. Predicted (by Model M_2 or **Equation 17**) versus actual data, along with the corresponding 95% prediction bands, for various soil–rubber composites: **(a)** Peak shear strength τ_p; and **(b)** Critical shear strength τ_{cr}.

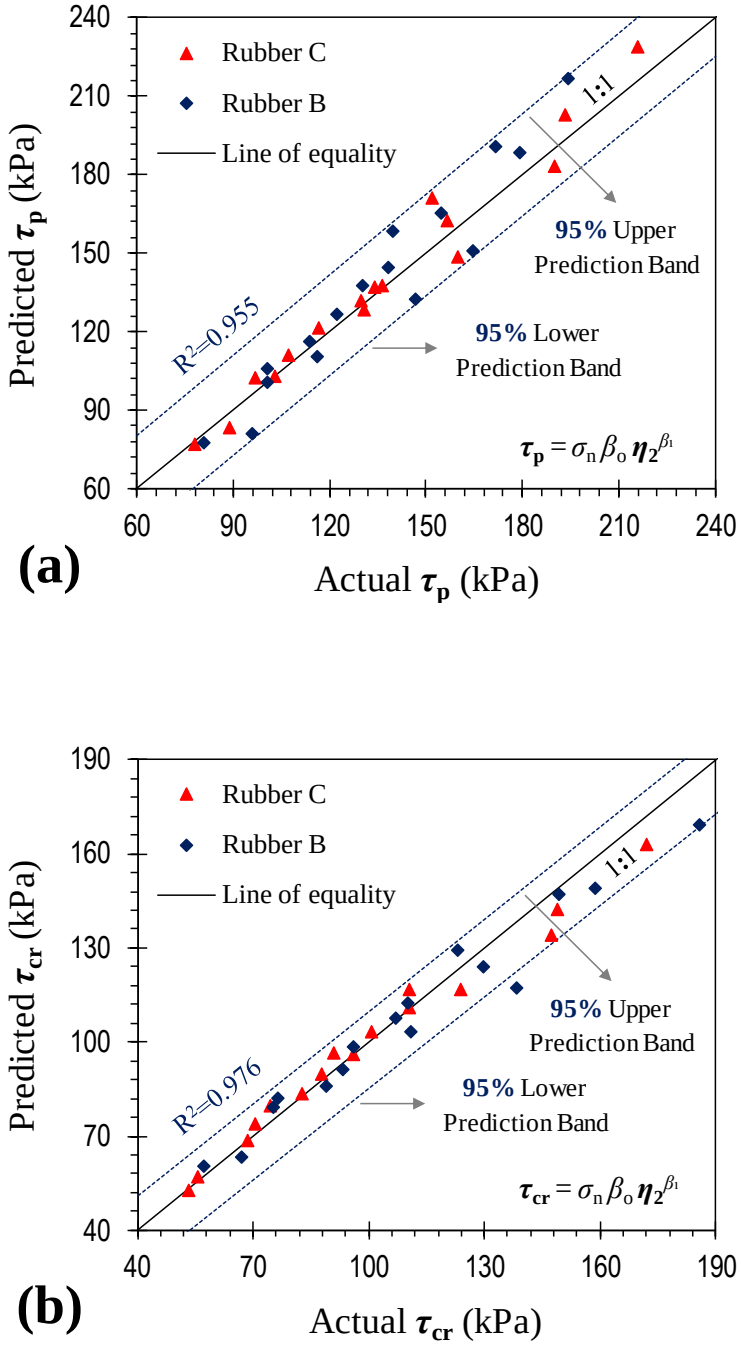

Figure 9. Variations of both predicted (by Model M3 or **Equation 20**) and actual τ_p and τ_{cr} data against normal stress: **(a)** Rubber C; and **(b)** Rubber B.

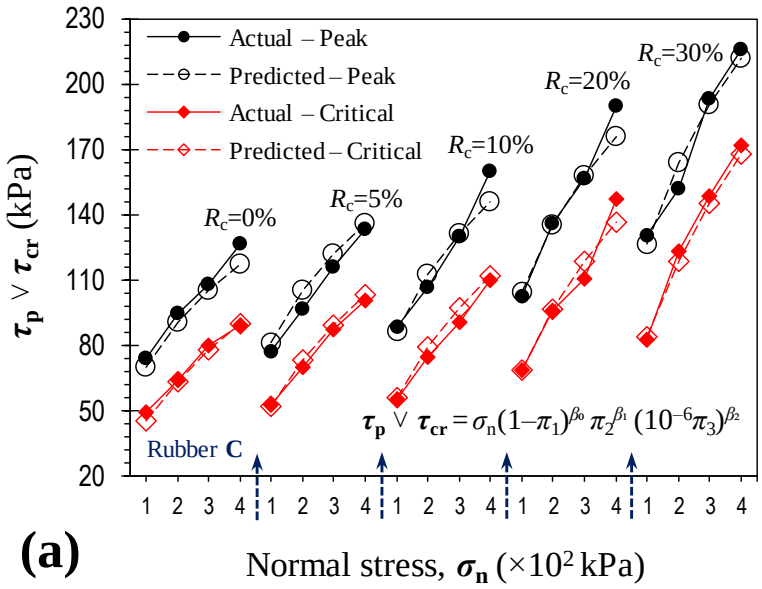

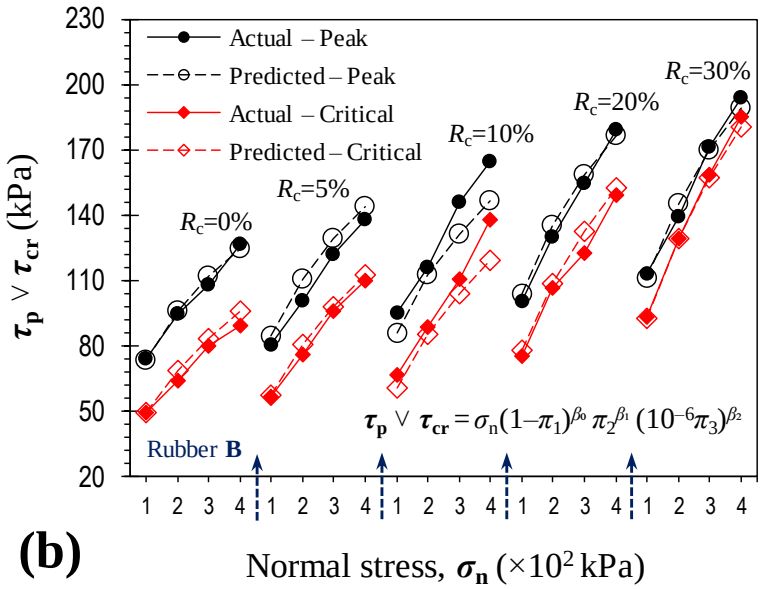

Figure 10. Predicted (by Model M_3 or **Equation 20**) versus actual data, along with the corresponding 95% prediction bands, for various soil–rubber composites: **(a)** Peak shear strength τ_p; and **(b)** Critical shear strength τ_{cr}.

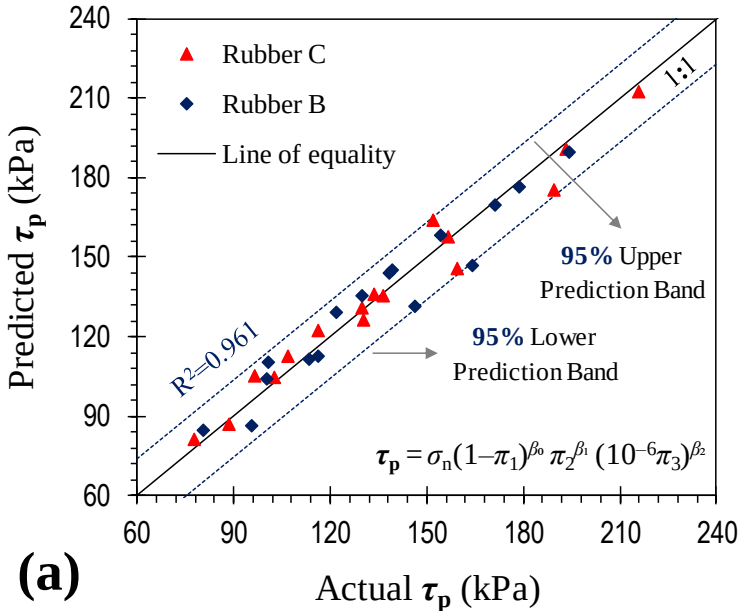

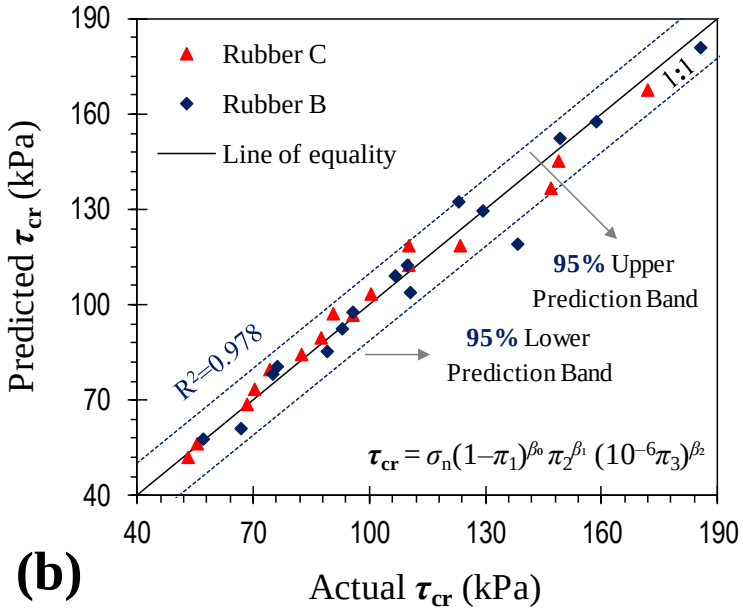

Figure 11. Variations of both predicted (by **Equation 22**) and actual shear stress data against normal stress at various horizontal displacements.

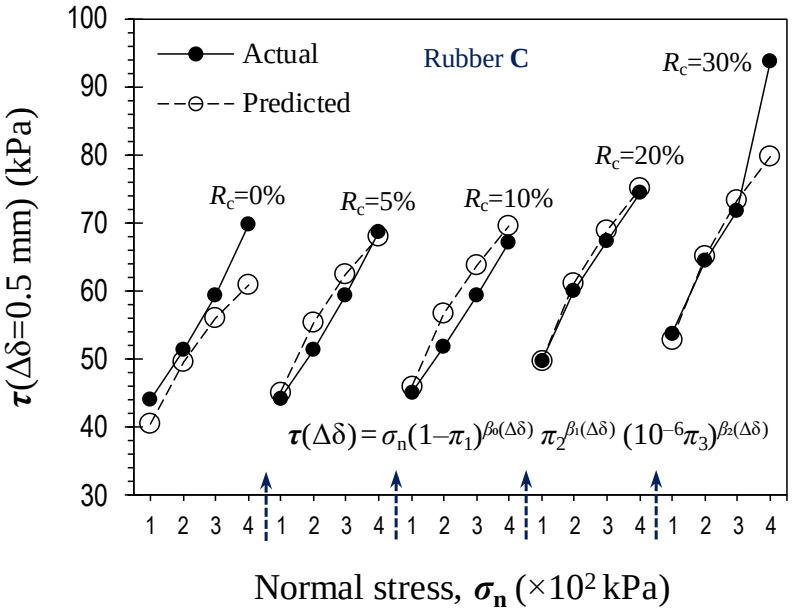

Rubber C: $\Delta\delta$=0.5 mm

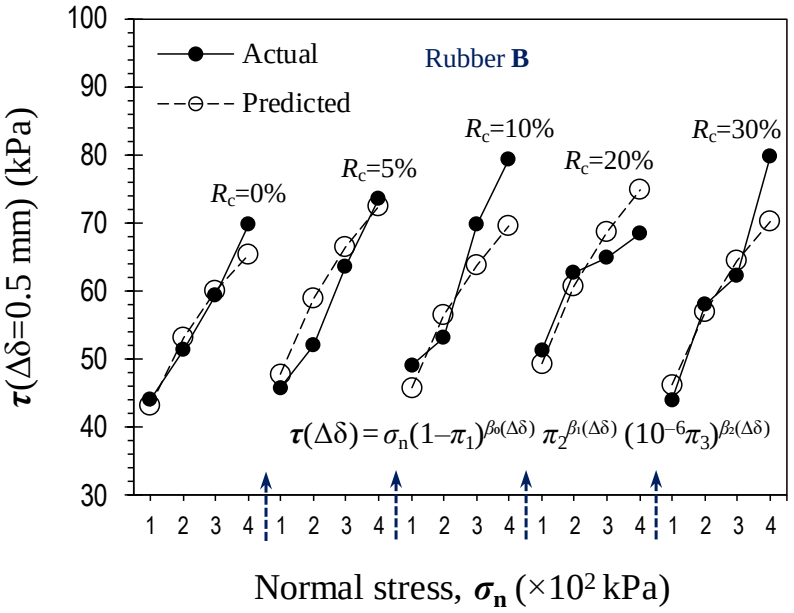

Rubber B: $\Delta\delta$=0.5 mm

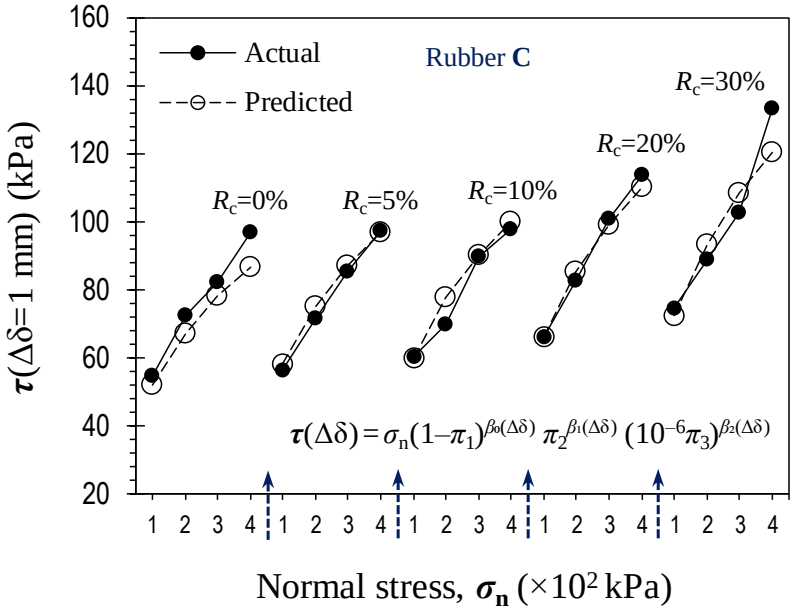

Rubber C: Δδ=1 mm

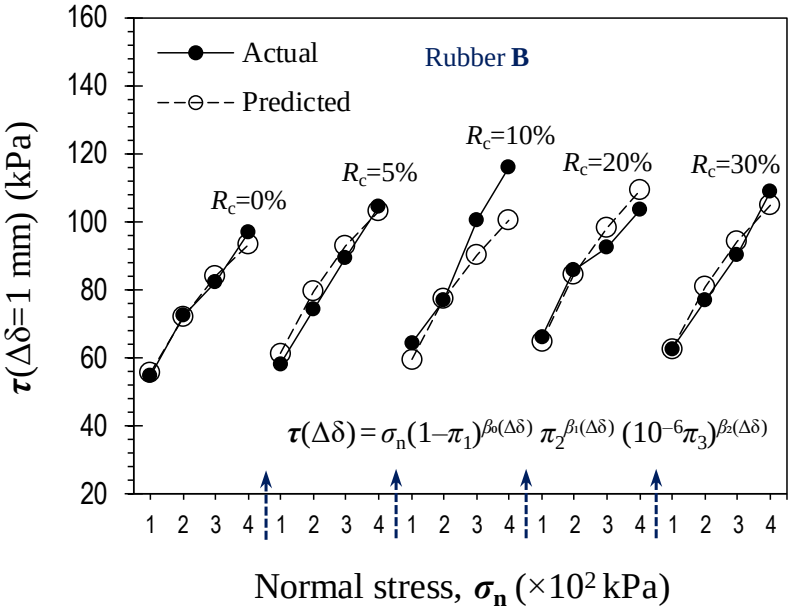

Rubber B: Δδ=1 mm

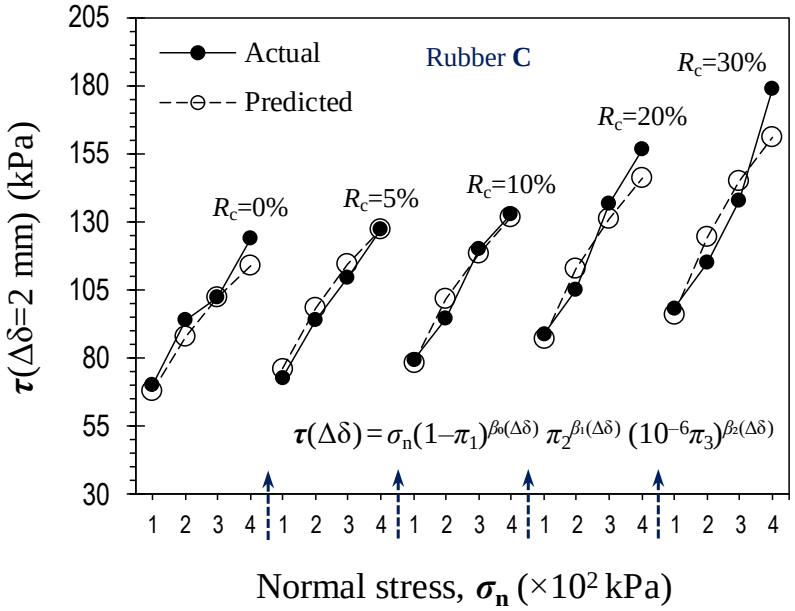

Rubber C: Δδ=2 mm

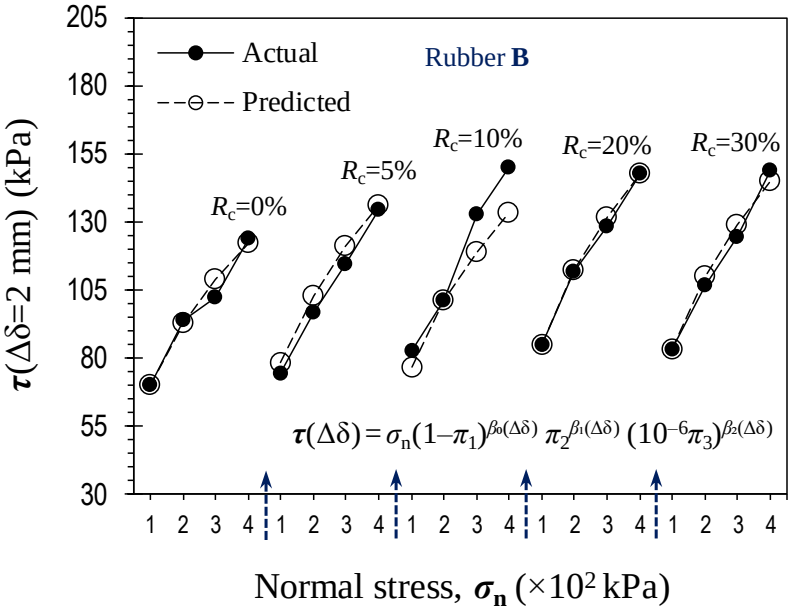

Rubber B: Δδ=2 mm

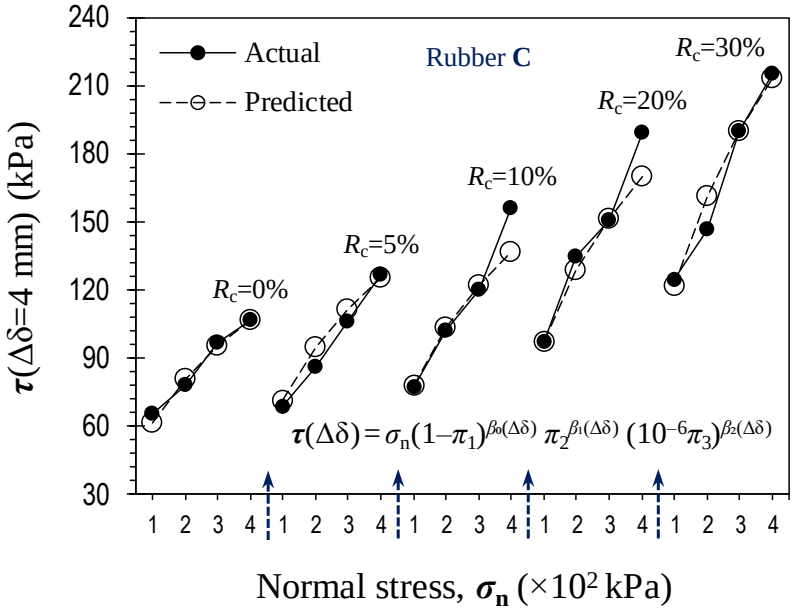

Rubber C: Δδ=4 mm

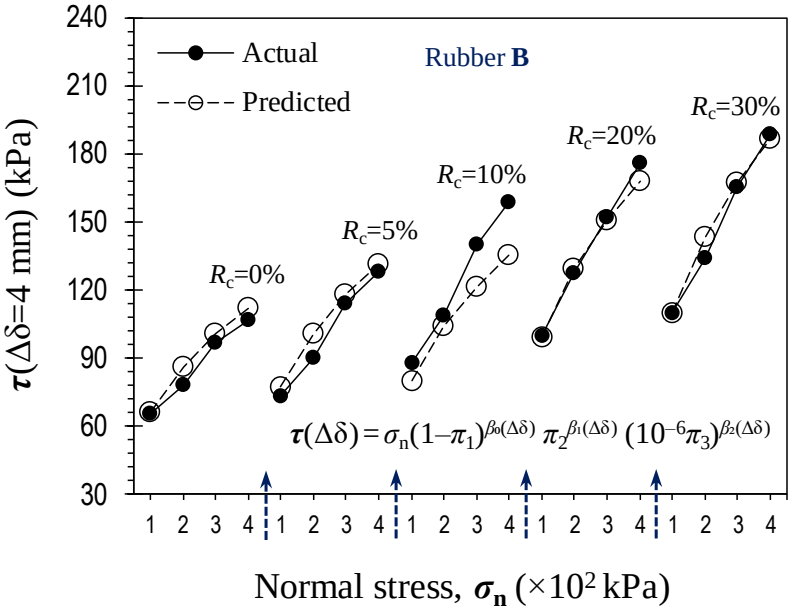

Rubber B: Δδ=4 mm

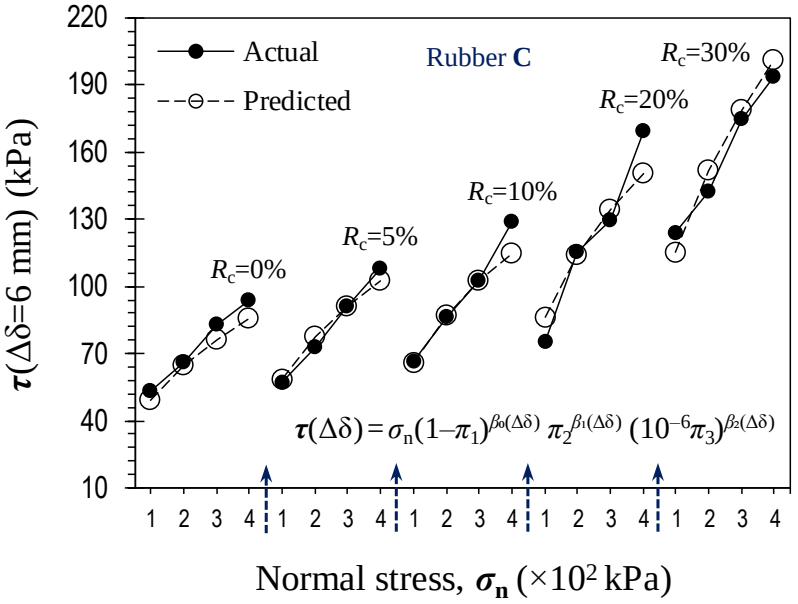

Rubber C: Δδ=6 mm

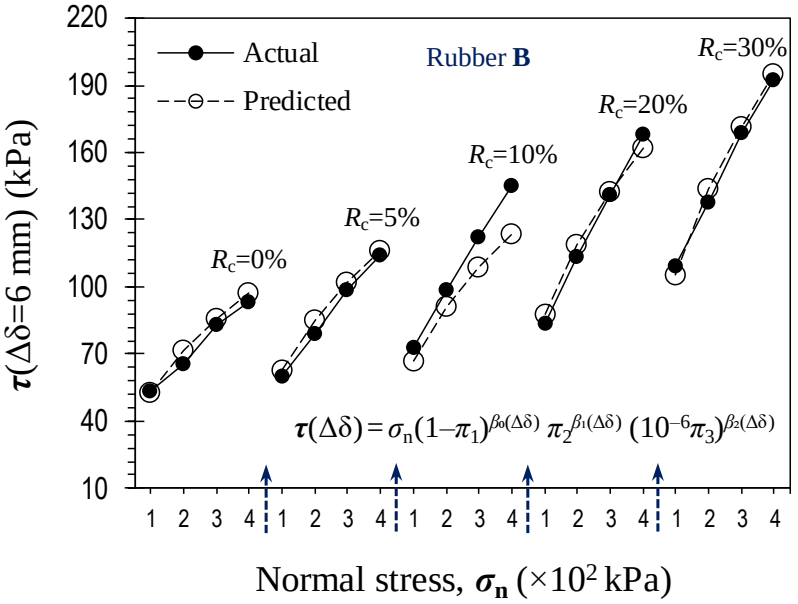

Rubber B: Δδ=6 mm

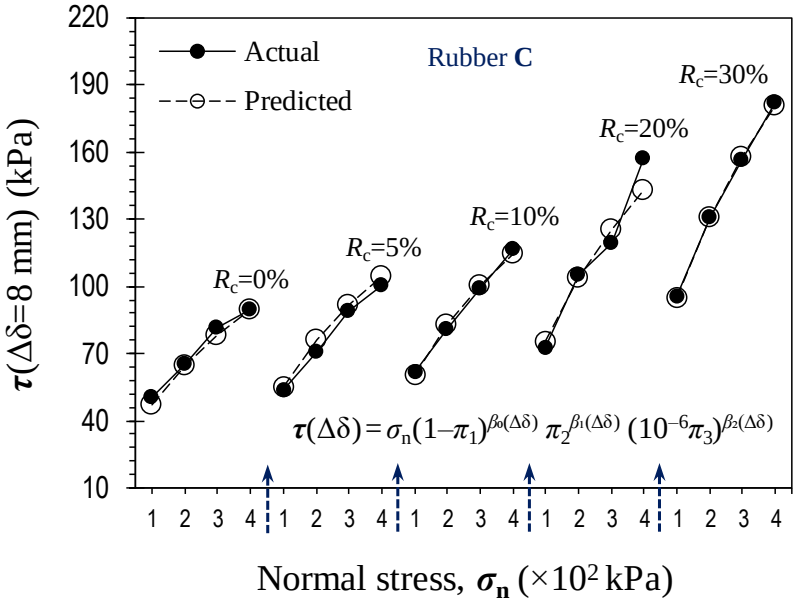

Rubber C: Δδ=8 mm

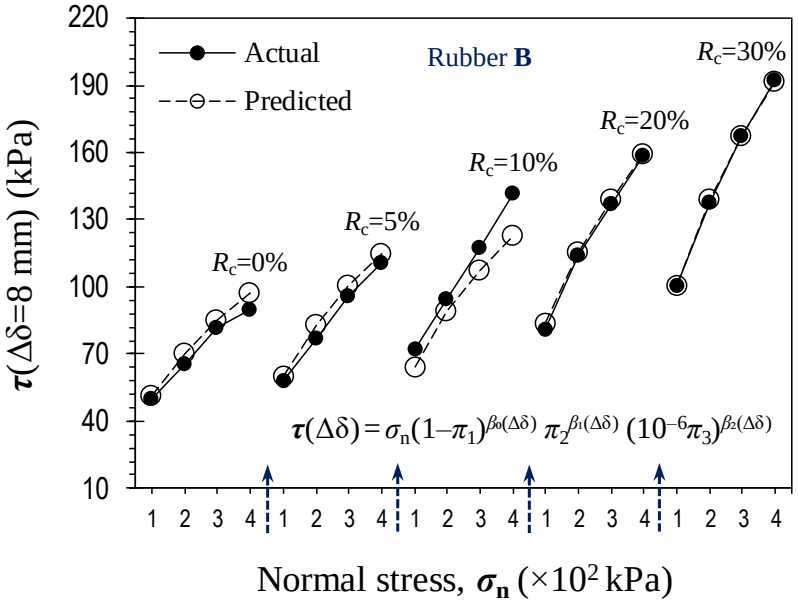

Rubber B: Δδ=8 mm

Figure 12. Typical experimental shear stress–horizontal displacement curves along with their respective simulations by means of the proposed dimensional model given in **Equation 22**.

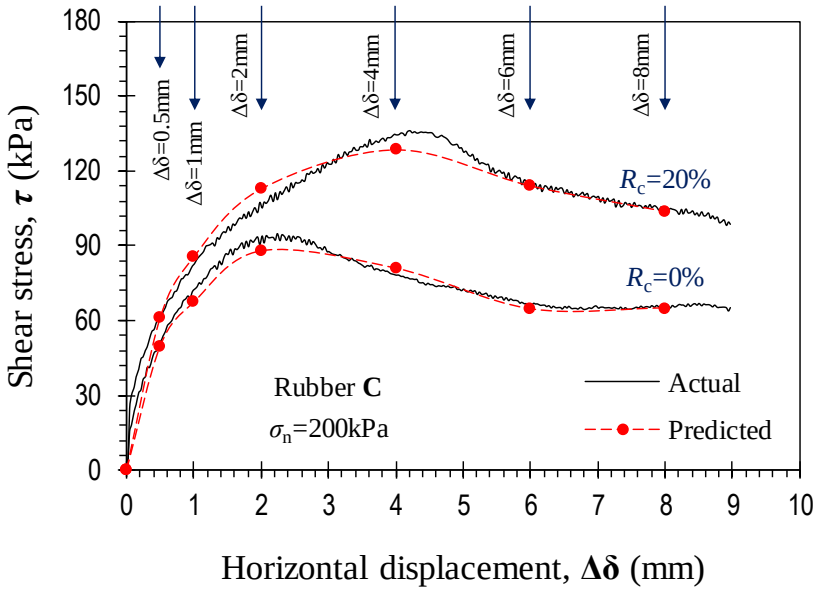

Rubber C: R_c=0% and 20%; and σ_n=200 kPa

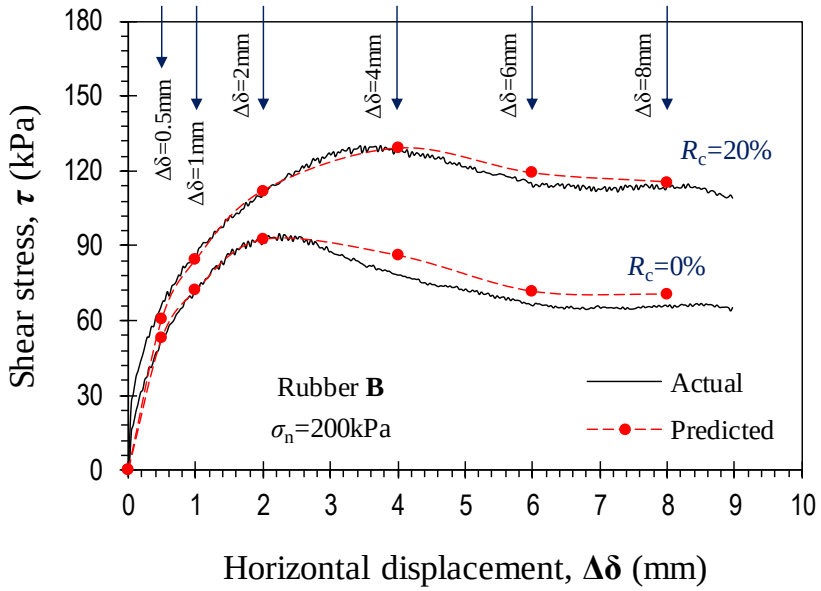

Rubber B: R_c=0% and 20%; and σ_n=200 kPa

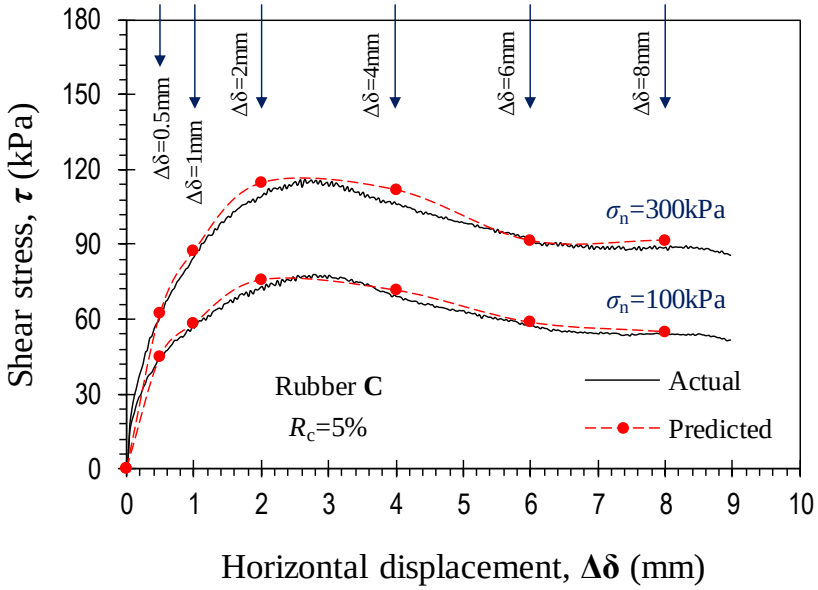

Rubber C: R_c=5%; and σ_n=100 kPa and 300 kPa

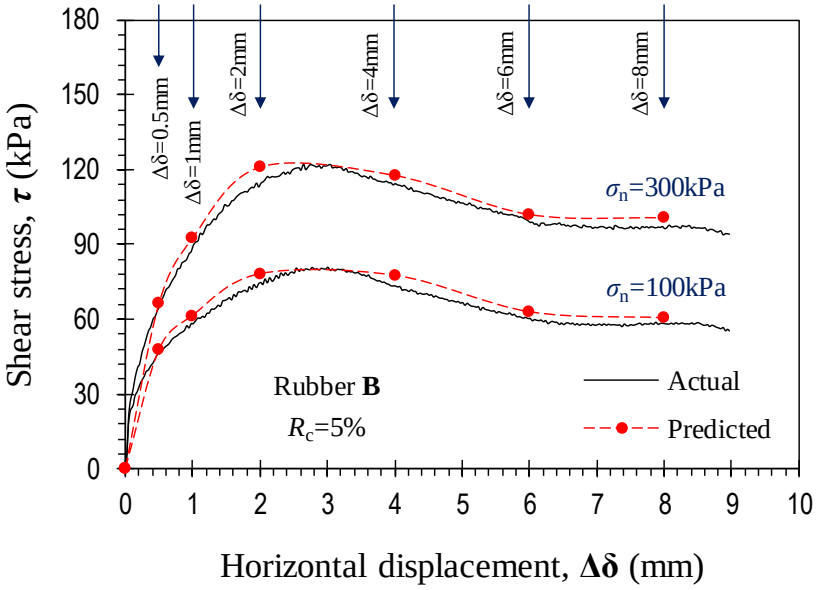

Rubber B: R_c=5%; and σ_n=100 kPa and 300 kPa

Appendix A

The experimental database used for the development of the dimensional models, i.e. Models M_1 (**Equation 14**), M_2 (**Equation 17**) and M_3 (**Equation 20**), is summarized in **Table A1**.

Table A1. Summary of the experimental database used for dimensional analysis.

Rubber	d_{50} (mm)	R_c (%)	w_L (%)	w_P (%)	I_P (%)	S_a (m^2/g)	w_o (%)	γ_{do} (kN/m^3)	σ_n (kPa)	τ_p (kPa)	τ_{cr} (kPa)
—	—	0	59.60	27.28	32.32	51.17	26.00	15.07	100	74.25	49.19
									200	94.65	64.24
									300	107.80	80.11
									400	126.45	89.36
Rubber C	0.461	5	57.03	27.02	30.01	47.87	24.77	14.63	100	77.59	53.06
									200	96.48	70.38
									300	116.19	87.53
									400	133.60	100.55
		10	55.04	25.54	29.50	47.14	23.87	14.35	100	88.60	55.54
									200	107.01	74.39
									300	129.72	90.80
									400	159.71	110.25
		20	51.51	23.46	28.05	45.07	21.85	13.87	100	102.61	68.49
									200	136.23	95.94
									300	156.45	110.39
									400	189.67	147.03
		30	49.58	22.70	26.88	43.40	20.07	13.52	100	130.42	82.44
									200	151.88	123.48
									300	193.08	148.79
									400	215.80	171.99
Rubber B	1.582	5	56.88	26.61	30.27	48.24	24.47	14.61	100	80.67	56.88
									200	100.54	76.18
									300	121.99	95.89
									400	138.15	110.03
		10	55.62	24.77	30.85	49.07	23.46	14.37	100	95.40	66.81
									200	116.08	88.96
									300	146.26	110.71
									400	164.35	138.23
		20	52.44	23.27	29.17	46.67	21.15	13.86	100	100.49	75.22
									200	130.11	106.71
									300	154.32	123.00
									400	178.96	149.22
		30	51.21	22.15	29.06	46.51	19.94	13.52	100	113.46	93.05
									200	139.48	129.39
									300	171.26	158.55
									400	194.02	185.54

Appendix B

The linear or semi–linear system of equations given in **Equations** 15, 18 and 21 can be rewritten in matrix form (i.e. A**X**=B; where **X**=the matrix representing the model parameters) by the following relationships, respectively:

$$\mathrm{M}_1:\begin{bmatrix}1 & \eta_1^{(R_c^o,\sigma_n^m)}\\ 1 & \eta_1^{(R_c^m,\sigma_n^m)}\end{bmatrix}\times\begin{bmatrix}\beta_o\\ \beta_1\end{bmatrix}=\begin{bmatrix}\dfrac{\tau_p^{(R_c^o,\sigma_n^m)}\vee\tau_{cr}^{(R_c^o,\sigma_n^m)}}{\sigma_n^m}\\ \dfrac{\tau_p^{(R_c^m,\sigma_n^m)}\vee\tau_{cr}^{(R_c^m,\sigma_n^m)}}{\sigma_n^m}\end{bmatrix} \tag{B1}$$

$$\mathrm{M}_2:\begin{bmatrix}1 & \mathrm{Ln}\left\langle\eta_2^{(R_c^o,\sigma_n^m)}\right\rangle\\ 1 & \mathrm{Ln}\left\langle\eta_2^{(R_c^m,\sigma_n^m)}\right\rangle\end{bmatrix}\times\begin{bmatrix}\mathrm{Ln}\left\langle\beta_o\right\rangle\\ \beta_1\end{bmatrix}=\begin{bmatrix}\mathrm{Ln}\left\langle\dfrac{\tau_p^{(R_c^o,\sigma_n^m)}\vee\tau_{cr}^{(R_c^o,\sigma_n^m)}}{\sigma_n^m}\right\rangle\\ \mathrm{Ln}\left\langle\dfrac{\tau_p^{(R_c^m,\sigma_n^m)}\vee\tau_{cr}^{(R_c^m,\sigma_n^m)}}{\sigma_n^m}\right\rangle\end{bmatrix} \tag{B2}$$

$$\mathrm{M}_3:\begin{bmatrix}\mathrm{Ln}\left\langle1-\pi_1^{(R_c^o,\sigma_n^o)}\right\rangle & \mathrm{Ln}\left\langle\pi_2^{(R_c^o,\sigma_n^o)}\right\rangle & \mathrm{Ln}\left\langle\dfrac{\pi_3^{(R_c^o,\sigma_n^o)}}{10^6}\right\rangle\\ \mathrm{Ln}\left\langle1-\pi_1^{(R_c^o,\sigma_n^\infty)}\right\rangle & \mathrm{Ln}\left\langle\pi_2^{(R_c^o,\sigma_n^\infty)}\right\rangle & \mathrm{Ln}\left\langle\dfrac{\pi_3^{(R_c^o,\sigma_n^\infty)}}{10^6}\right\rangle\\ \mathrm{Ln}\left\langle1-\pi_1^{(R_c^m,\sigma_n^m)}\right\rangle & \mathrm{Ln}\left\langle\pi_2^{(R_c^m,\sigma_n^m)}\right\rangle & \mathrm{Ln}\left\langle\dfrac{\pi_3^{(R_c^m,\sigma_n^m)}}{10^6}\right\rangle\end{bmatrix}\times\begin{bmatrix}\beta_o\\ \beta_1\\ \beta_2\end{bmatrix}=\begin{bmatrix}\mathrm{Ln}\left\langle\dfrac{\tau_p^{(R_c^o,\sigma_n^o)}\vee\tau_{cr}^{(R_c^o,\sigma_n^o)}}{\sigma_n^o}\right\rangle\\ \mathrm{Ln}\left\langle\dfrac{\tau_p^{(R_c^o,\sigma_n^\infty)}\vee\tau_{cr}^{(R_c^o,\sigma_n^\infty)}}{\sigma_n^\infty}\right\rangle\\ \mathrm{Ln}\left\langle\dfrac{\tau_p^{(R_c^m,\sigma_n^m)}\vee\tau_{cr}^{(R_c^m,\sigma_n^m)}}{\sigma_n^m}\right\rangle\end{bmatrix} \tag{B3}$$

For ease of presentation, consider the following designations:

- $T_1=\dfrac{\tau_p^{(R_c^o,\sigma_n^m)}\vee\tau_{cr}^{(R_c^o,\sigma_n^m)}}{\sigma_n^m}$; $T_2=\dfrac{\tau_p^{(R_c^m,\sigma_n^m)}\vee\tau_{cr}^{(R_c^m,\sigma_n^m)}}{\sigma_n^m}$; $D_{11}=\eta_1^{(R_c^o,\sigma_n^m)}$; and $D_{12}=\eta_1^{(R_c^m,\sigma_n^m)}$.
- $T_1'=\mathrm{Ln}\left\langle\dfrac{\tau_p^{(R_c^o,\sigma_n^m)}\vee\tau_{cr}^{(R_c^o,\sigma_n^m)}}{\sigma_n^m}\right\rangle$; $T_2'=\mathrm{Ln}\left\langle\dfrac{\tau_p^{(R_c^m,\sigma_n^m)}\vee\tau_{cr}^{(R_c^m,\sigma_n^m)}}{\sigma_n^m}\right\rangle$; $D_{21}=\mathrm{Ln}\left\langle\eta_2^{(R_c^o,\sigma_n^m)}\right\rangle$; and $D_{22}=\mathrm{Ln}\left\langle\eta_2^{(R_c^m,\sigma_n^m)}\right\rangle$.

- $T_1'' = \mathrm{Ln}\left\langle \dfrac{\tau_{\mathrm{p}}^{(R_{\mathrm{c}}^{\mathrm{o}},\sigma_{\mathrm{n}}^{\mathrm{o}})} \vee \tau_{\mathrm{cr}}^{(R_{\mathrm{c}}^{\mathrm{o}},\sigma_{\mathrm{n}}^{\mathrm{o}})}}{\sigma_{\mathrm{n}}^{\mathrm{o}}} \right\rangle$; $T_2'' = \mathrm{Ln}\left\langle \dfrac{\tau_{\mathrm{p}}^{(R_{\mathrm{c}}^{\mathrm{o}},\sigma_{\mathrm{n}}^{\infty})} \vee \tau_{\mathrm{cr}}^{(R_{\mathrm{c}}^{\mathrm{o}},\sigma_{\mathrm{n}}^{\infty})}}{\sigma_{\mathrm{n}}^{\infty}} \right\rangle$; $P_{11} = \mathrm{Ln}\left\langle 1-\pi_1^{(R_{\mathrm{c}}^{\mathrm{o}},\sigma_{\mathrm{n}}^{\mathrm{o}})} \right\rangle$;

  $P_{21} = \mathrm{Ln}\left\langle \pi_2^{(R_{\mathrm{c}}^{\mathrm{o}},\sigma_{\mathrm{n}}^{\mathrm{o}})} \right\rangle$; $P_{31} = \mathrm{Ln}\left\langle \dfrac{\pi_3^{(R_{\mathrm{c}}^{\mathrm{o}},\sigma_{\mathrm{n}}^{\mathrm{o}})}}{10^6} \right\rangle$; $P_{12} = \mathrm{Ln}\left\langle 1-\pi_1^{(R_{\mathrm{c}}^{\mathrm{o}},\sigma_{\mathrm{n}}^{\infty})} \right\rangle$; $P_{22} = \mathrm{Ln}\left\langle \pi_2^{(R_{\mathrm{c}}^{\mathrm{o}},\sigma_{\mathrm{n}}^{\infty})} \right\rangle$;

  $P_{32} = \mathrm{Ln}\left\langle \dfrac{\pi_3^{(R_{\mathrm{c}}^{\mathrm{o}},\sigma_{\mathrm{n}}^{\infty})}}{10^6} \right\rangle$; $P_{13} = \mathrm{Ln}\left\langle 1-\pi_1^{(R_{\mathrm{c}}^{\mathrm{m}},\sigma_{\mathrm{n}}^{\mathrm{m}})} \right\rangle$; $P_{23} = \mathrm{Ln}\left\langle \pi_2^{(R_{\mathrm{c}}^{\mathrm{m}},\sigma_{\mathrm{n}}^{\mathrm{m}})} \right\rangle$; and $P_{33} = \mathrm{Ln}\left\langle \dfrac{\pi_3^{(R_{\mathrm{c}}^{\mathrm{m}},\sigma_{\mathrm{n}}^{\mathrm{m}})}}{10^6} \right\rangle$.

Therefore, explicit solutions to **Equations B1**, **B2** and **B3**, defined as $\mathbf{X}=\mathrm{A}^{-1}\mathrm{B}$, can be derived as:

$$\mathrm{M}_1:\begin{cases}\beta_{\mathrm{o}} = \dfrac{T_1 D_{12} - T_2 D_{11}}{D_{12} - D_{11}} \\ \beta_1 = \dfrac{T_2 - T_1}{D_{12} - D_{11}}\end{cases} \tag{B4}$$

$$\mathrm{M}_2:\begin{cases}\beta_{\mathrm{o}} = \exp\left(\dfrac{T_1' D_{22} - T_2' D_{21}}{D_{22} - D_{21}}\right) \\ \beta_1 = \dfrac{T_2' - T_1'}{D_{22} - D_{21}}\end{cases} \tag{B5}$$

$$\mathrm{M}_3:\begin{cases}\beta_{\mathrm{o}} = \dfrac{P_{21}(T_2'P_{32} - T_2''P_{33}) + P_{22}(T_1''P_{33} - T_2'P_{31}) + P_{23}(T_2''P_{31} - T_1''P_{32})}{P_{11}(P_{22}P_{33} - P_{23}P_{32}) + P_{12}(P_{23}P_{31} - P_{21}P_{33}) + P_{13}(P_{21}P_{32} - P_{22}P_{31})} \\ \beta_1 = \dfrac{P_{11}(T_2''P_{33} - T_2'P_{32}) + P_{12}(T_2'P_{31} - T_1''P_{33}) + P_{13}(T_1''P_{32} - T_2''P_{31})}{P_{11}(P_{22}P_{33} - P_{23}P_{32}) + P_{12}(P_{23}P_{31} - P_{21}P_{33}) + P_{13}(P_{21}P_{32} - P_{22}P_{31})} \\ \beta_2 = \dfrac{P_{11}(T_2'P_{22} - T_2''P_{23}) + P_{12}(T_1''P_{23} - T_2'P_{21}) + P_{13}(T_2''P_{21} - T_1''P_{22})}{P_{11}(P_{22}P_{33} - P_{23}P_{32}) + P_{12}(P_{23}P_{31} - P_{21}P_{33}) + P_{13}(P_{21}P_{32} - P_{22}P_{31})}\end{cases} \tag{B6}$$

Statement of Authorship

Statement of Authorship

Title of Paper	Interfacial Shear Strength of Rubber–Reinforced Clays: A Dimensional Analysis Perspective
Publication Status	☐ Published ■ Submitted for Publication ☐ Accepted for Publication ☐ Unpublished and Unsubmitted work written in manuscript style
Publication Details	**Soltani A**, Deng A, Taheri A, Mirzababaei M and Nikraz H **(2018)** Interfacial Shear Strength of Rubber–Reinforced Clays: A Dimensional Analysis Perspective. ***Geosynthetics International*** **x(x): x–x**, http://doi.org/x. **Note:** Under Review [submitted in revised form on **13 July 2018**].

Principal Author

Name of Principal Author (Candidate)	Amin Soltani (**Email:** Amin.Soltani@adelaide.edu.au)		
Contribution to the Paper	Overall paper preparation		
Overall percentage (%)	85%		
Certification:	This paper reports on original research I conducted during the period of my Higher Degree by Research candidature and is not subject to any obligations or contractual agreements with a third party that would constrain its inclusion in this thesis. I am the primary author of this paper.		
Signature		Date	07/15/2018

Co-Author Contributions

By signing the Statement of Authorship, each author certifies that:

i. the candidate's stated contribution to the publication is accurate (as detailed above);
ii. permission is granted for the candidate in include the publication in the thesis; and
iii. the sum of all co-author contributions is equal to 100% less the candidate's stated contribution.

Name of Co-Author	An Deng **Senior Lecturer**, School of Civil, Environmental and Mining Engineering, The University of Adelaide, Adelaide, SA 5005, Australia (**Email:** An.Deng@adelaide.edu.au)		
Contribution to the Paper	Paper review and revision		
Signature		Date	07/23/2018

Name of Co-Author	Abbas Taheri **Senior Lecturer**, School of Civil, Environmental and Mining Engineering, The University of Adelaide, Adelaide, SA 5005, Australia (**Email:** Abbas.Taheri@adelaide.edu.au)		
Contribution to the Paper	Paper review and revision		
Signature		Date	07/16/2018

Name of Co-Author	Mehdi Mirzababaei **Lecturer**, School of Engineering and Technology, Central Queensland University (CQU), Melbourne, VIC 3000, Australia (**Email:** M.Mirzababaei@cqu.edu.au)		
Contribution to the Paper	Paper review and revision		
Signature		Date	07/23/2018

1

Name of Co-Author	Hamid Nikraz **Professor**, School of Civil and Mechanical Engineering, Curtin University, Perth, WA 6102, Australia (**Email:** H.Nikraz@curtin.edu.au)		
Contribution to the Paper	Paper review and revision		
Signature		Date	09/02/2018

Chapter 6

California Bearing Ratio of Tire Crumbles–Fly Ash Mixed with Clay: A Dimensional Analysis Perspective

Amin Soltani [a,†] and Mehdi Mirzababaei [b]

[a] **PhD Student** − School of Civil, Environmental and Mining Engineering, The University of Adelaide, Adelaide, SA 5005, Australia (**Email:** Amin.Soltani@adelaide.edu.au; **ORCID:** 0000-0002-0483-7487)

[b] **Lecturer** − School of Engineering and Technology, Central Queensland University, Melbourne, VIC 3000, Australia (**Email:** M.Mirzababaei@cqu.edu.au)

[†] **Correspondence:** Amin Soltani (**Email:** Amin.Soltani@adelaide.edu.au; **ORCID:** 0000-0002-0483-7487)

Publication Details: **Soltani A** and Mirzababaei M **(2018)** Comment on "Compaction and Strength Behavior of Tire Crumbles–Fly Ash Mixed with Clay" by A. Priyadarshee, A. Kumar, D. Gupta, and P. Pushkarna. ***Journal of Materials in Civil Engineering*** **x(x): x–x**, https://doi.org/x.[10]

1. Introduction

Recently, Priyadarshee et al. (2018) examined the combined capacity of tire crumbles inclusion and fly ash treatment as a sustainable solution towards ameliorating the inferior engineering characteristics of clayey soils. The work under discussion takes a strategic step towards improving the mechanical performance of construction materials while counteracting the adverse environmental impacts associated with human activities, and thus is gratefully acknowledged. The present discussion/comment aims at addressing some of the shortcomings associated with the aforementioned study, as well as complementing the original work by outlining a novel point of view.

[10]**In Press** [accepted on **11 May 2018**].

A portion of the original manuscript was devoted to the development of a regression model claimed to be capable of predicting the California Bearing Ratio (CBR) of clay–tire crumbles–fly ash mixtures under unsoaked and soaked conditions. In this case, the authors proposed the conventional multiple linear regression model (MLR) with two independent variables, which can be given as:

$$\mathrm{R}^{\mathrm{U}} \vee \mathrm{R}^{\mathrm{S}} = \frac{\mathrm{CBR}^{\mathrm{U}}_{\mathrm{mix}}}{\mathrm{CBR}^{\mathrm{U}}_{\mathrm{clay}}} \vee \frac{\mathrm{CBR}^{\mathrm{S}}_{\mathrm{mix}}}{\mathrm{CBR}^{\mathrm{S}}_{\mathrm{clay}}} = \rho_{\mathrm{o}} + \rho_1 T_{\mathrm{c}} + \rho_2 F_{\mathrm{c}} \tag{1}$$

where R^{U}=unsoaked CBR ratio (i.e. stabilized to unstabilized CBR ratio under unsoaked condition); R^{S}=soaked CBR ratio (i.e. stabilized to unstabilized CBR ratio under soaked condition); T_{c}=tire crumbles content; F_{c}=fly ash content; and ρ_{o} to ρ_2=fitting parameters or regression coefficients.

A suitable regression/empirical model can be characterized as one that maintains a perfect balance between simplicity (ease of application) and accuracy (low forecast error), thereby involving a limited number of conventional physical parameters (linked by a limited number of model/fitting parameters) capable of arriving at a reliable estimate of the problem in hand. Quite clearly, the MLR model given in **Equation 1** well satisfies the simplicity requirement. The same, however, cannot be concluded in terms of the accuracy. The authors report the coefficient of determination as R^2=0.83–0.84 (see **Equations 3** and **4** in the original manuscript), which basically implies that only 83%–84% of the variations in experimental observations are captured and further explained by the suggested MLR model. Furthermore, the authors fail to report any relevant error–related fit–measure index associated with MLR predictions. The root mean squares error RMSE and the normalized root mean squares error NRMSE (in %) are two well–accepted indices in this context, which can be given as (Estabragh et al. 2016; Soltani et al. 2018):

$$\mathrm{RMSE} = \sqrt{\frac{1}{N}\sum_{i=1}^{N}\left(y_i^{\mathrm{p}} - y_i^{\mathrm{a}}\right)^2} \tag{2}$$

$$\mathrm{NRMSE} = \frac{\mathrm{RMSE}}{y_{\mathrm{max}}^{\mathrm{a}} - y_{\mathrm{min}}^{\mathrm{a}}} \times 100 \tag{3}$$

where y^{p}=predicted value of the dependent variable y (e.g. $\mathrm{R}^{\mathrm{U}} \vee \mathrm{R}^{\mathrm{S}}$); y^{a}=actual value of the dependent variable y; N=number of data points used for model development (=30, as outlined

in **Table 5** of the original manuscript); i=index of summation; y^{a}_{max} =maximum value of y^{a} data; and y^{a}_{min} =minimum value of y^{a} data.

Making use of the data presented in **Figures 14** and **15** of the original manuscript, the NRMSE can be found as 18.47%–19.06%, which is approximately four times greater than the acceptable 5% reference margin. Given that the variations of both the unsoaked and soaked CBR with respect to T_c and/or F_c are strongly monotonic (see **Figure 13** in the original manuscript), along with the fact that the datasets used for model development are rather small in size (N=30 for each MLR model), high R^2 (> 0.95) and low NRMSE (< 5%) values should be simply accomplishable. Quite clearly, the CBR exhibits a non–linear increasing trend with increase in T_c and/or F_c (see **Figure 13** in the original manuscript), and thus cannot be adequately simulated by means of a planar regression surface such as the MLR. More importantly, the MLR in its current form fails to capture tire crumbles–fly ash interactions, as evident with the absence of a $T_c \times F_c$ term in **Equation 1**. Most strength–related soil stabilization problems involving two independent variables exhibit non–linearity or curvature (e.g. Mirzababaei et al. 2013; Olgun 2013; Soltani 2017), and thus can be efficiently represented by the multiple quadratic regression model (MQR). For the problem in hand, a suitable MQR model can be expressed as:

$$R^{U} \vee R^{S} = \frac{CBR^{U}_{mix}}{CBR^{U}_{clay}} \vee \frac{CBR^{S}_{mix}}{CBR^{S}_{clay}} = \rho_o + \rho_1 T_c + \rho_2 F_c + \rho_3 T_c^{\,2} + \rho_4 F_c^{\,2} + \rho_5 T_c F_c \quad (4)$$

where ρ_o to ρ_5=fitting parameters or regression coefficients.

Figures 1a and **1b** illustrate the MQR regression surface or **Equation 4** fitted to the experimental data, reported in the original manuscript, for the unsoaked and soaked CBR ratios, respectively. As opposed to the MLR, the MQR well captures the curvature exhibited in experimental observations. The MQR model given in **Equation 4** leads to higher R^2 and lower NRMSE values compared with that of the MLR suggested by the authors (i.e. R^2=0.980–0.981; and NRMSE=3.45%–3.55%). However, the MQR sacrifices simplicity in favor of higher accuracy. The MQR contains a total of six fitting parameters, which in turn could lead to long–lasting and potentially sophisticated calibration procedures. In addition, both the MQR and the MLR fail to consider the mixture's indigenous (or index) properties in describing the CBR. Quite clearly, the clay–tire crumbles–fly ash CBR problem is also dependent on the mixture's initial placement (or compaction) condition, specific surface area, grain–size distribution and curing time, which are not accounted for in **Equations 1** and **4**. As a result, both the MQR and

the MLR are limited to the current experimental design and hence cannot be further extended to other soil types and/or design schemes.

It has been the discussers' experience that the dimensional analysis technique (Buckingham 1914) well provides a feasible path towards the development of physically meaningful models capable of efficiently estimating strength–related parameters of stabilized soil mixtures as a function of the mixture's index properties. The present discussion aims at the development of a simple and practical dimensional model capable of simulating the CBR (at both unsoaked and soaked conditions) of clay–tire crumbles–fly ash mixtures with an acceptable degree of accuracy, thereby avoiding the hurdles of conducting time–consuming laboratory CBR tests.

2. Dimensional Analysis

2.1. Model Development

For a given type of clay soil blended with tire crumbles and/or treated with fly ash, the governing variables with respect to the clay–tire crumbles–fly ash CBR problem, as evident with the experimental results discussed by the authors in the original manuscript, can be categorized as: **i)** total weight of the mixture W_M (in kg); **ii)** weight of tire crumbles W_T (in kg); **iii)** weight of fly ash W_F (in kg); **iv)** weight of water W_W (in kg); **v)** initial dry unit weight of the mixture composite γ_{do} (in N/m^3); **vi)** specific surface area of the mixture S_a^{mix} (in m^2/kg); **vii)** mean particle size/diameter of the mixture D_{50}^{mix} (in m); and **viii)** curing time t (in s). Therefore, the clay–tire crumbles–fly ash CBR problem, for unsoaked or soaked condition $CBR^U \vee CBR^S$, can be expressed as:

$$CBR^U \vee CBR^S = f_1(W_M, W_T, W_F, W_W, \gamma_{do}, S_a^{mix}, D_{50}^{mix}, t) \quad (5)$$

where f_1=an unknown multi–variable functional expression.

The Buckingham Pi theorem provides a method for deriving sets of dimensionless variables (commonly referred to as Pi or π terms) from given physical parameters, even if the governing functional expression (i.e. f_1 in **Equation 5**) remains unknown (Buckingham 1914). The theorem states that any physical problem, such as the clay–tire crumbles–fly ash CBR problem expressed by **Equation 5**, involving N_1 number of physical parameters with N_2 number of basic physical dimensions (or units) can be further simplified to a new problem involving $K=N_1–N_2$ number of dimensionless variables (or Pi terms) capable of adequately describing the original

problem in hand. As such, the system of N_1=8 physical parameters (γ_{do} is related to W_M) and N_2=3 basic physical dimensions (i.e. mass [M], length [L] and time [T]) given in **Equation 5** can be simplified to a new system involving K=5 dimensionless Pi terms as:

$$\pi_o = \mathrm{CBR}^U \vee \mathrm{CBR}^S \tag{6}$$

$$\pi_1 = \frac{W_T}{W_M} = T_c \tag{7}$$

$$\pi_2 = \frac{W_F}{W_M} = F_c \tag{8}$$

$$\pi_3 = \frac{W_W}{W_M} = w_o \tag{9}$$

$$\pi_4 = \frac{g_o t}{D_{50}^{mix}\sqrt{\gamma_{do} S_a^{mix}}} \tag{10}$$

where π_o=dependent Pi term; π_1 to π_4=independent Pi terms; w_o=initial water content of the mixture composite; and g_o=standard gravitational acceleration (=9.81 m/s^2).

Therefore, the clay–tire crumbles–fly ash CBR problem (for unsoaked or soaked condition) can be represented by the following simplified expression:

$$\pi_o = \mathrm{CBR}^U \vee \mathrm{CBR}^S = f_2(\pi_1, \pi_2, \pi_3, \pi_4) \tag{11}$$

where f_2=an unknown multi–variable functional expression.

As outlined by the authors in the original manuscript, samples for the CBR tests were prepared at the corresponding optimum condition of each mixture (obtained via modified Proctor effort), thus implying that w_o=optimum water content and γ_{do}=maximum dry unit weight (values have been presented in **Figures 10** and **11** of the original manuscript). The specific surface area for the clay soil can be estimated by the following empirical relationship (Locat et al. 1984; Williamson and Cortes 2014):

$$S_a^C = \tfrac{10}{7} I_p + 5 \tag{12}$$

where S_a^C =specific surface area of the clay soil (in m^2/gr); and I_p=plasticity index of the clay soil (in %).

Based on **Table 1** in the original manuscript, the clay soil has a plasticity index of 18.8%, thus implying that S_a^C =31.86 m^2/gr. For mixtures involving either tire crumbles and/or fly ash, the following relationship can be used to estimate the mixture's specific surface area S_a^{mix} (Williamson and Cortes 2014; Zhao et al. 2016):

$$S_a^{mix} = \left(1 - \frac{W_T + W_F}{W_M}\right) S_a^C + \left(\frac{W_T}{W_M}\right) S_a^T + \left(\frac{W_F}{W_M}\right) S_a^F \tag{13}$$

where S_a^T =specific surface area of tire crumbles (taken as 0.050 m^2/gr, as reported by Thiele and Winkler (2005)); and S_a^F =specific surface area of fly ash (taken as 0.355 m^2/gr, as reported by Ramezanianpour (2014)).

Similarly, the mixture's mean particle size/diameter D_{50}^{mix} can be estimated by:

$$D_{50}^{mix} = \left(1 - \frac{W_T + W_F}{W_M}\right) D_{50}^C + \left(\frac{W_T}{W_M}\right) D_{50}^T + \left(\frac{W_F}{W_M}\right) D_{50}^F \tag{14}$$

where D_{50}^C =mean particle size of the clay soil (taken as 1.728×10^{-3} mm based on **Figure 1** in the original manuscript); D_{50}^T =mean particle size of tire crumbles (=0.73 mm, as reported in **Table 2** of the original manuscript); and D_{50}^F =mean particle size of fly ash (=0.01 mm, as reported in **Table 3** of the original manuscript).

In **Equation 11**, f_2 is an unknown multi–variable functional expression which is to be obtained through trial and error. To complement the derivation of a simple and practical dimensional model, it is essential that any suggested functional expression, while arriving at a reliable estimate of CBR^U and CBR^S, contains a limited number of model (or fitting) parameters which could be adequately calibrated by minimal experimental effort as well as simple explicit calculations. One of the more common yet simple solutions in this context includes the multi–variable power function (Simon et al. 2017), which for the four independent Pi terms problem given in **Equation 11** can be expressed as:

$$\pi_o = \mathrm{CBR}^U \vee \mathrm{CBR}^S = f_2(\pi_1, \pi_2, \pi_3, \pi_4) = \prod_{i=1}^{4} \pi_i^{\beta_{i-1}} \quad (15)$$

where and β_{i-1}=model parameter (dimensionless); and i=index of multiplication.

To avoid mathematical singularities and/or scaling effects associated with SI unit conversions, each of the independent Pi terms, while retaining their dimensionless nature, can be mathematically manipulated. Common manipulations, as suggested in the literature (e.g. Buzzi et al. 2011; Simon et al. 2017), include π+R, π×R and π^R (i.e. R=a constant real number). As outlined in **Table 5** of the original manuscript, the independent Pi terms $\pi_1=T_c$ and $\pi_2=F_c$ can also take values of zero for some mix designs (e.g. clay soil blended with no tire crumbles and treated with F_c=5% fly ash or clay soil blended with T_c=0.5% tire crumbles and treated with no fly ash). As such, π_1 and π_2 were changed to $(1-\pi_1)$ and $(1-\pi_2)$ to avoid mathematical singularities. In addition, π_4 was multiplied by 10^{-8} to avoid scaling effects and hence improve convergence in fitting of the experimental data. Taking into account the aforementioned considerations, **Equation 15** can now be expressed as:

$$\pi_o = (1-\pi_1)^{\beta_0}(1-\pi_2)^{\beta_1}(\pi_3)^{\beta_2}(10^{-8}\pi_4)^{\beta_3} \quad (16)$$

$$\mathrm{CBR}^U \vee \mathrm{CBR}^S = (1-T_c)^{\beta_0}(1-F_c)^{\beta_1}(w_o)^{\beta_2}\left(\frac{10^{-8} g_o t}{D_{50}^{\mathrm{mix}}\sqrt{\gamma_{do} S_a^{\mathrm{mix}}}}\right)^{\beta_3} \quad (17)$$

The only unknown in **Equation 17** is the curing time t. Given that this aspect was not mentioned in the original manuscript, it was perceived that immediate curing conditions prevail. An immediate curing condition can be represented by t=1 s, which was also adopted in this discussion for model calibration.

2.2. Model Performance

The dimensional model given in **Equation 17** was fitted to the experimental CBR^U and CBR^S datasets (presented in **Figure 13** of the original manuscript) by means of the non–linear least squares optimization technique (Soltani et al. 2018). Statistical fit–measure indices, i.e. R^2, RMSE (**Equation 2**) and NRMSE (**Equation 3**), were then obtained for model validation (and to compare the performance of the proposed dimensional model with the MLR model or **Equation 1** suggested in the original manuscript). The regression analysis outputs with respect

to the proposed dimensional model or **Equation 17** are summarized in **Table 1** for both unsoaked and soaked conditions. The dimensional model clearly outperforms the MLR suggested in the original manuscript, as evident with the higher R^2 and lower NRMSE values. The R^2 values were unanimously above the 0.98 margin (0.83–0.84 for the MLR model), indicating that leastwise 98% of the variations in experimental observations are captured and further explained by the dimensional model. The NRMSE values were found to be less than 4% for all cases (18.47%–19.06% for the MLR model), signifying a maximum offset of only 4% associated with the predictions. **Figures 2a** and **2b** illustrate predicted (by **Equation 17**) versus actual data, along with the corresponding 95% prediction bands/intervals, for various clay–tire crumbles–fly ash mix designs at unsoaked and soaked conditions, respectively. As opposed to the MLR model (see **Figures 14** and **15** in the original manuscript), minor scatter can be observed, as evident with the clustering/overlapping of data points with the line of equality. In addition, all data points firmly lie between the upper and lower 95% prediction intervals, thus indicating no major outliers associated with the predictions.

3. Summary and Conclusions

The dimensional analysis concept was successfully extended to the clay–tire crumbles–fly ash CBR problem, thereby leading to the development of a simple and practical dimensional model capable of predicting the CBR (at both unsoaked and soaked conditions) as a function of the mixture's basic index properties, i.e. stabilizer content, initial placement (or compaction) condition, specific surface area, grain–size distribution and curing time. The predictive capacity of the proposed dimensional model was examined and further validated by statistical techniques. The proposed dimensional model contains a total of four model (or fitting) parameters, which can be calibrated by little experimental effort and hence implemented for predictive purposes. The model parameters can be adequately estimated by a total of four unsoaked or soaked CBR tests. Four scenarios consisting of the clay soil with no additives, a desired clay–tire crumbles mixture (no fly ash), a desired clay–fly ash mixture (no tire crumbles), and a desired clay–tire crumbles–fly ash mixture are recommended for the calibration phase. The choice of tire crumbles and fly ash contents are arbitrary; however, from a statistical perspective, median contents are expected to yield a more reliable estimate of the model parameters (Mirzababaei et al. 2018).

Acknowledgements

Special thanks go to **Dr. An Deng** and **Dr. Abbas Taheri**, of the School of Civil, Environmental and Mining Engineering, The University of Adelaide, for their valuable suggestions to the authors.

References

Buckingham, E. **(1914)**. "On physically similar systems; illustrations of the use of dimensional equations." *Physical Review*, 4(4), 345–376. doi:10.1103/physrev.4.345.

Buzzi, O., Giacomini, A., and Fityus, S. **(2011)**. "Towards a dimensionless description of soil swelling behaviour." *Géotechnique*, 61(3), 271–277. doi:10.1680/geot.7.00194.

Estabragh, A. R., Soltani, A., and Javadi, A. A. **(2016)**. "Models for predicting the seepage velocity and seepage force in a fiber reinforced silty soil." *Computers and Geotechnics*, 75, 174–181. doi:10.1016/j.compgeo.2016.02.002.

Locat, J., Lefebvre, G., and Ballivy, G. **(1984)**. "Mineralogy, chemistry, and physical properties interrelationships of some sensitive clays from Eastern Canada." *Canadian Geotechnical Journal*, 21(3), 530–540. doi:10.1139/t84-055.

Mirzababaei, M., Miraftab, M., Mohamed, M., and McMahon, P. **(2013)**. "Unconfined compression strength of reinforced clays with carpet waste fibers." *Journal of Geotechnical and Geoenvironmental Engineering*, 139(3), 483–493. doi:10.1061/(asce)gt.1943-5606.0000792.

Mirzababaei, M., Mohamed, M., Arulrajah, A., Horpibulsuk, S., and Anggraini, V. **(2018)**. "Practical approach to predict the shear strength of fibre–reinforced clay." *Geosynthetics International*, 25(1), 50–66. doi:10.1680/jgein.17.00033.

Olgun, M. **(2013)**. "The effects and optimization of additives for expansive clays under freeze–thaw conditions." *Cold Regions Science and Technology*, 93, 36–46. doi:10.1016/j.coldregions.2013.06.001.

Priyadarshee, A., Kumar, A., Gupta, D., and Pushkarna, P. **(2018)**. "Compaction and strength behavior of tire crumbles–fly ash mixed with clay." *Journal of Materials in Civil Engineering*, 30(4), 04018033:1–04018033:9. doi:10.1061/(asce)mt.1943-5533.0002171.

Ramezanianpour, A. A. **(2014)**. "Fly ash." *Cement replacement materials: Properties, durability, sustainability*, 1st ed., Springer–Verlag Berlin Heidelberg, Germany, 47–156. doi:10.1007/978-3-642-36721-2_2, ISBN:9783642367212.

Simon, V., Weigand, B., and Gomaa, H. **(2017)**. *Dimensional analysis for engineers*, 1st ed., Springer International Publishing AG, Gewerbestrasse, Cham, Switzerland. doi:10.1007/978-3-319-52028-5, ISBN:9783319520285.

Soltani, A. **(2017)**. "Discussion of 'Optimization of carpet waste fibers and steel slag particles to reinforce expansive soil using response surface methodology' by M. Shahbazi, M. Rowshanzamir, S.M. Abtahi, S.M. Hejazi [Appl. Clay Sci., doi:10.1016/j.clay.2016.11.027]." *Applied Clay Science*, in press. doi:10.1016/j.clay.2017.07.020.

Soltani, A., Deng, A., Taheri, A., Sridharan, A., and Estabragh, A. R. **(2018)**. "A framework for interpretation of the compressibility behavior of soils." *Geotechnical Testing Journal*, 41(1), 1–16. doi:10.1520/gtj20170088.

Thiele, K., and Winkler, U. **(2005)**. “Incorporation of recyclate and its effect on bound rubber.” *International Polymer Science and Technology*, 32(5), T23–T28.

Williamson, S., and Cortes, D. D. **(2014)**. “Dimensional analysis of soil–cement mixture performance.” *Géotechnique Letters*, 4(1), 33–38. doi:10.1680/geolett.13.00082.

Zhao, Y., Gao, Y., Zhang, Y., and Wang, Y. **(2016)**. “Effect of fines on the mechanical properties of composite soil stabilizer–stabilized gravel soil.” *Construction and Building Materials*, 126, 701–710. doi:10.1016/j.conbuildmat.2016.09.082.

List of Tables

Table 1. Summary of the regression analysis outputs with respect to the proposed dimensional model or **Equation 17** for both unsoaked and soaked conditions.

Table 1. Summary of the regression analysis outputs with respect to the proposed dimensional model or **Equation 17** for both unsoaked and soaked conditions.

Variable	β_0	β_1	β_2	β_3	R^2	**RMSE**	**NRMSE (%)**
CBR^U (dimensionless)	4.633	0.250	4.551	–0.406	0.981	1.898×10^{-2}	3.44
CBR^S (dimensionless)	4.075	0.292	4.747	–0.390	0.980	1.168×10^{-2}	3.51

List of Figures

Figure 1. The multiple quadratic regression (MQR) surface or **Equation 4** fitted to the CBR data reported in the original manuscript: **(a)** unsoaked CBR ratio R^U; and **(b)** soaked CBR ratio R^S.

Figure 2. Predicted (by **Equation 17**) versus actual data, along with the corresponding 95% prediction bands, for various clay–tire crumbles–fly ash mix designs: **(a)** unsoaked CBR; and **(b)** soaked CBR.

Figure 1. The multiple quadratic regression (MQR) surface or **Equation 4** fitted to the CBR data reported in the original manuscript: **(a)** unsoaked CBR ratio R^U; and **(b)** soaked CBR ratio R^S.

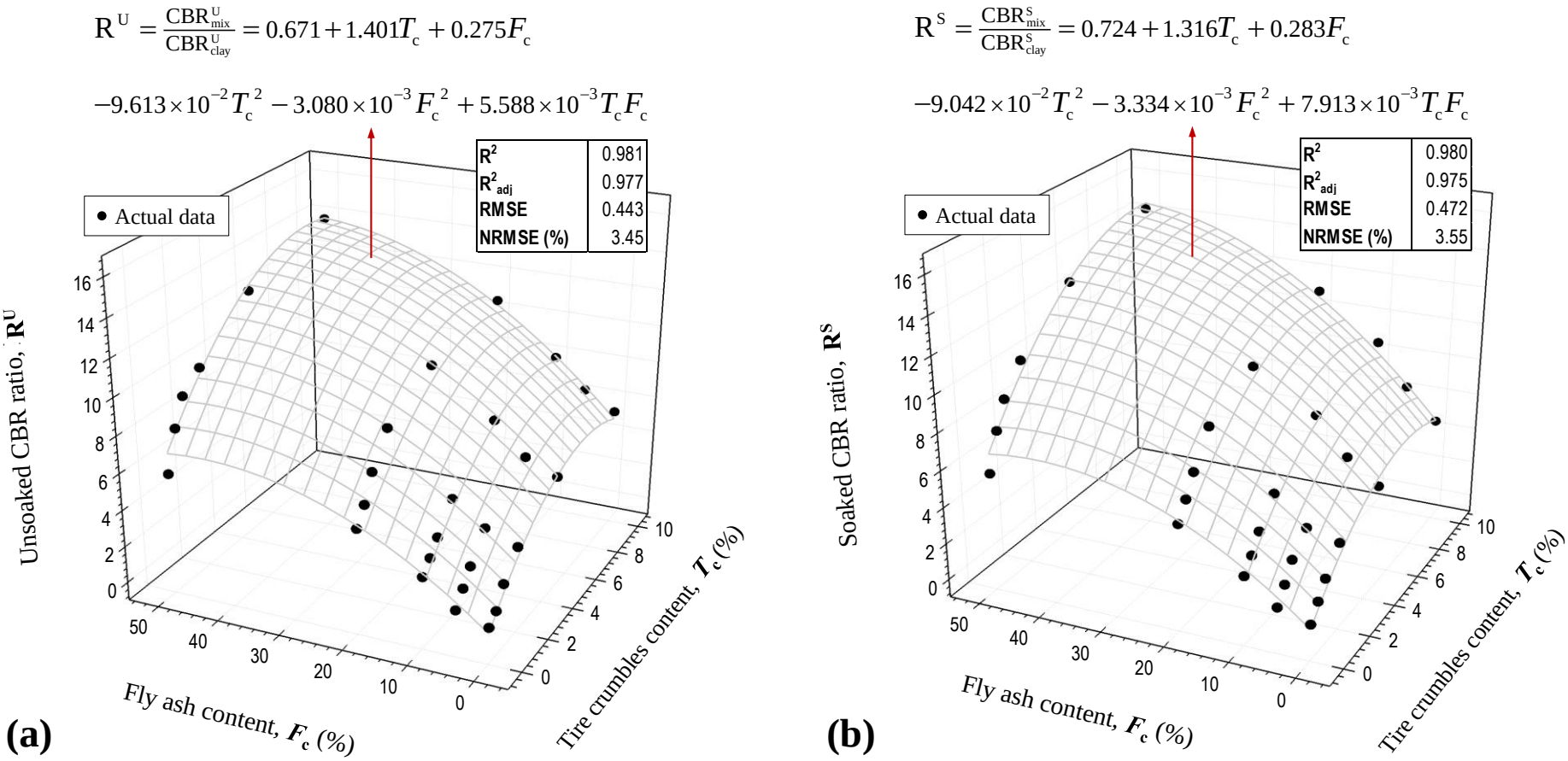

Figure 2. Predicted (by **Equation 17**) versus actual data, along with the corresponding 95% prediction bands, for various clay–tire crumbles–fly ash mix designs: **(a)** unsoaked CBR; and **(b)** soaked CBR.

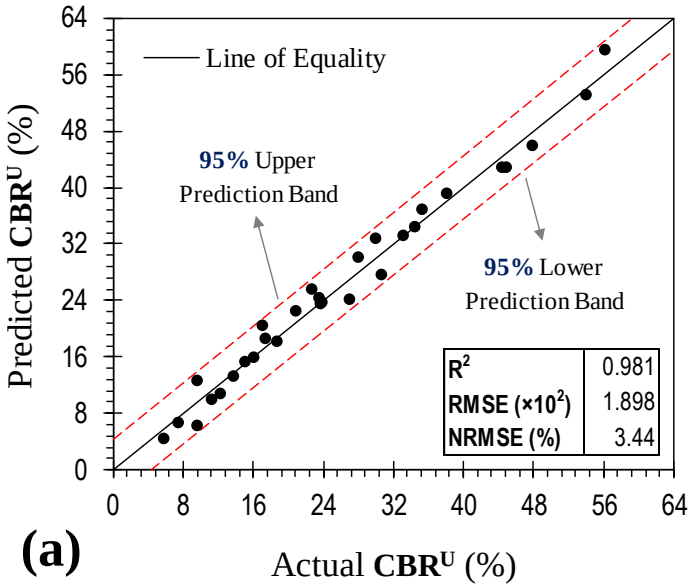

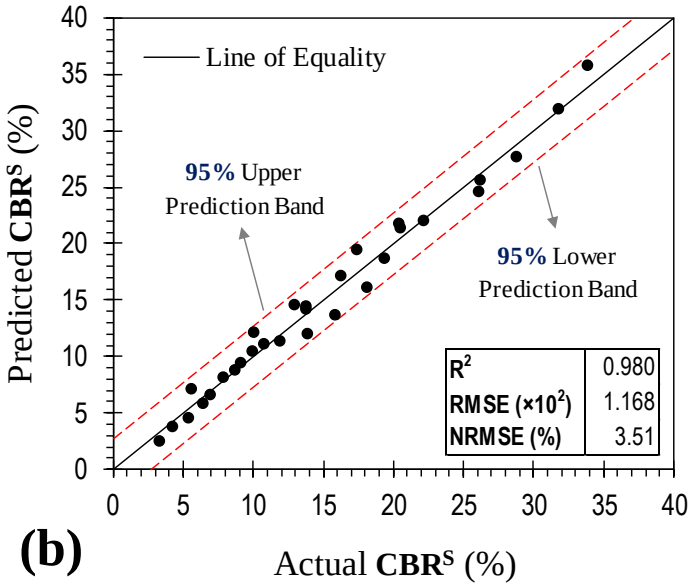

Statement of Authorship

Statement of Authorship

Title of Paper	Comment on "Compaction and Strength Behavior of Tire Crumbles–Fly Ash Mixed with Clay" by A. Priyadarshee, A. Kumar, D. Gupta, and P. Pushkarna
Publication Status	☐ Published ☐ Submitted for Publication ■ Accepted for Publication ☐ Unpublished and Unsubmitted work written in manuscript style
Publication Details	**Soltani A** and Mirzababaei M **(2018)** Comment on "Compaction and Strength Behavior of Tire Crumbles–Fly Ash Mixed with Clay" by A. Priyadarshee, A. Kumar, D. Gupta, and P. Pushkarna. ***Journal of Materials in Civil Engineering* x(x): x–x**, https://doi.org/x.

Principal Author

Name of Principal Author (Candidate)	Amin Soltani (**Email:** Amin.Soltani@adelaide.edu.au)		
Contribution to the Paper	Overall paper preparation		
Overall percentage (%)	85%		
Certification:	This paper reports on original research I conducted during the period of my Higher Degree by Research candidature and is not subject to any obligations or contractual agreements with a third party that would constrain its inclusion in this thesis. I am the primary author of this paper.		
Signature		Date	06/29/2018

Co-Author Contributions

By signing the Statement of Authorship, each author certifies that:

i. the candidate's stated contribution to the publication is accurate (as detailed above);
ii. permission is granted for the candidate in include the publication in the thesis; and
iii. the sum of all co-author contributions is equal to 100% less the candidate's stated contribution.

Name of Co-Author	Mehdi Mirzababaei **Lecturer**, School of Engineering and Technology, Central Queensland University (CQU), Melbourne, VIC 3000, Australia (**Email:** M.Mirzababaei@cqu.edu.au)		
Contribution to the Paper	Paper review and revision		
Signature		Date	07/23/2018

1

Chapter 7

Swell–Shrink Behavior of Rubberized Expansive Clays During Alternate Wetting and Drying

Amin Soltani [a,†], An Deng [b], Abbas Taheri [c], Mehdi Mirzababaei [d] and Sai K. Vanapalli [e]

[a] **PhD Student** − School of Civil, Environmental and Mining Engineering, The University of Adelaide, Adelaide, SA 5005, Australia (**Email:** Amin.Soltani@adelaide.edu.au; **ORCID:** 0000-0002-0483-7487)

[b] **Senior Lecturer** − School of Civil, Environmental and Mining Engineering, The University of Adelaide, Adelaide, SA 5005, Australia (**Email:** An.Deng@adelaide.edu.au)

[c] **Senior Lecturer** − School of Civil, Environmental and Mining Engineering, The University of Adelaide, Adelaide, SA 5005, Australia (**Email:** Abbas.Taheri@adelaide.edu.au)

[d] **Lecturer** − School of Engineering and Technology, Central Queensland University, Melbourne, VIC 3000, Australia (**Email:** M.Mirzababaei@cqu.edu.au)

[e] **Professor** – Department of Civil Engineering, University of Ottawa, Ottawa, ON K1N 6N5, Canada (**Email:** Sai.Vanapalli@uottawa.ca)

[†] **Correspondence:** Amin Soltani (**Email:** Amin.Soltani@adelaide.edu.au; **ORCID:** 0000-0002-0483-7487)

Publication Details: **Soltani A**, Deng A, Taheri A, Mirzababaei M and Vanapalli SK **(2018)** Swell–Shrink Behavior of Rubberized Expansive Clays During Alternate Wetting and Drying. ***x*** **x(x): x–x**, https://doi.org/x.[11]

Abstract

This study examines the rubber's capacity of ameliorating the swell–shrink potential of expansive clays. The test program consisted of standard Proctor compaction and cyclic wetting–drying tests. The scanning electron microscopy analysis was also performed to identify the soil–

[11]**Target Journals:** *Journal of Geotechnical and Geoenvironmental Engineering* [Link], *Geotechnical Testing Journal* [Link], *Geotextiles and Geomembranes* [Link], *Geosynthetics International* [Link], *Proceedings of the Institution of Civil Engineers–Ground Improvement* [Link]

rubber amending mechanisms, and to observe the evolution of fabric in response to alternate wetting and drying. Cyclic wetting–drying led to the reconstruction of the soil/soil–rubber micro–structure by way of inducing aggregation and cementation of the soil grains. The greater the number of applied cycles the lower the swell–shrink features, following a monotonic decreasing trend with the rubberized blends holding a notable advantage over the virgin soil. The tendency for reduction, however, was in favor of a larger rubber size and more importantly the rubber's elongated form factor, thus predicating a rubber size/shape–dependent amending mechanism. The soil–rubber amending mechanisms were discussed in three aspects, namely increase in non–expansive content, frictional resistance generated as a result of soil–rubber contact, and mechanical interlocking of rubber particles and soil grains. The swell–shrink patterns indicated an expansive accumulated deformation for the virgin soil, while the rubberized blends manifested a relatively neutral deformational state, thereby corroborating the rubber's capacity to counteract the heave and/or settlement incurred by alternate wetting and drying.

Keywords: Expansive clay; Rubber size/shape; Cyclic wetting–drying; Swell–shrink potential; Accumulated deformation; Frictional resistance; Mechanical interlocking.

1. Introduction

The design and implementation of geo–structures often necessitate incorporating expansive clays, with high moisture susceptibility and low bearing capacity, into the construction. A notable fraction of the expansive clay is constituted of active smectite minerals, such as montmorillonite, which exhibits significant swell–shrink volume changes (as well as desiccation–induced cracking) upon the addition or removal of water (Jones and Jefferson 2012). Such actions bring forth major instability concerns to the overlying structures, and thus demand engineering solutions to alleviate the associated socio–economic impacts on human life (Soltani et al. 2018[a]). Common solutions to counteract the adversities associated with expansive clays include soil replacement and/or soil stabilization. The former involves substituting a portion of the low–graded expansive clay with desired quarried materials (or aggregates) possessing minimal swell–shrink tendency. The latter refers to any chemical, mechanical or combined chemical–mechanical practice of altering the expansive clay fabric to meet the intended engineering criteria (Soltani et al. 2017[a]). The chemical stabilization scheme makes use of chemical binders, e.g. cement, lime, fly ash, polymers and sulfonated oils, which initiate a series of short– and long–term chemical reactions in the soil–binder medium, thereby amending the soil fabric into a coherent matrix of improved mechanical performance (e.g. Al-Rawas et al. 2005; Mirzababaei et al. 2009; Estabragh et al. 2014; Onyejekwe and Ghataora 2015; Alazigha et al. 2016; Soltani et al. 2017[b]; Mirzababaei et al. 2018[a]). Mechanical stabilization often involves the placement of random or systematically–engineered reinforcements in the soil regime, e.g. fibers and geogrids, thereby engendering a spatial three–dimensional reinforcement network in favor of weaving/interlocking the soil grains into a unitary mass of restricted swell–shrink movements (e.g. Al-Omari and Hamodi 1991; Cai et al. 2006; Al-Akhras et al. 2008; Viswanadham et al. 2009; Estabragh et al. 2014; Phanikumar and Singla 2016; Soltani et al. 2018[b]). Though proven effective, conventional stabilization agents often suffer from sustainability issues related to high manufacturing and/or transportation costs, and environmental concerns due to greenhouse gas emissions.

A sustainable stabilization scheme can be characterized as one that maintains a perfect balance between infrastructure performance and the social, economic and ecological processes required to maintain human equity, diversity, and the functionality of natural systems. The transition towards sustainable stabilization necessitates reusing solid wastes and/or industrial by–products as part of the infrastructure system, and more specifically as replacements for conventional stabilization agents. Promising replacements, as reported in the literature, consist of recycled

tire rubbers, waste textiles, demolition wastes and silicate/calcium geopolymers (e.g. Kim et al. 2008; Mirzababaei et al. 2013[a], 2013[b]; Arulrajah et al. 2017; Kua et al. 2017; Mirzababaei et al. 2018[b]; Phummiphan et al. 2018). Among others, discarded tires constitute for the largest volume of disposals throughout the world, and as such, demand further attention. The use of recycled tire rubbers in geotechnical practice dates back to the early 1990s, where theoretical concepts governing the performance of soil–rubber blends were put into perspective. It was noted that similar to fiber–reinforced soils, the rubber assemblage randomly distributes in the soil regime, and when optimized in content and geometry, alters the soil fabric by amending the bonding along the interface (or contact) between the soil and the reinforcement, thereby enhancing the integrity and stability of the low–graded host soil (Edil and Bosscher 1994; Foose et al. 1996; Al-Tabbaa et al. 1997; Lee et al. 1999; Zornberg et al. 2004). The literature from this era, however, was mainly focused on coarse–grained soils, and as such, the rubber's capacity in ameliorating the inferior characteristics of expansive clays remained rather vague. Recent contributions addressing the swelling behavior of rubber mixed expansive clays are summarized in **Table 1**. Based on these studies, the soil–rubber amending mechanisms can be primarily attributed to the rubber content, with higher rubber inclusions yielding a more pronounced reduction of the swelling capacity. Moreover, the rubber's geometrical features, mainly defined in terms of the rubber's mean particle size, may also portray an equally important role. The latter, however, still remains a rather limited area of study and hence requires further examination.

Seasonal fluctuations, defined as alternate periods of rainfall and drought (or cyclic wetting–drying), lead to the reconstruction of the soil micro–structure, which in turn alters the volume change behavior of the expansive clay (Zhang et al. 2006). Consequently, arriving at reliable solutions capable of counteracting the adversities associated with expansive clays demands a further examination of the introduced stabilization scheme under the cyclic wetting–drying action. The cyclic wetting–drying behavior of natural expansive clays has been well documented in the literature (e.g. Osipov et al. 1987; Dif and Bluemel 1991; Day 1994; Al-Homoud et al. 1995; Subba Rao 2000; Tripathy et al. 2002; Alonso et al. 2005; Tripathy and Subba Rao 2009; Estabragh et al. 2015; Rosenbalm and Zapata 2017; Zhao et al. 2017; Estabragh et al. 2018). In comparison, the number of documented studies addressing the cyclic wetting–drying behavior of stabilized expansive clays are limited, most of which have been carried out in the context of chemical stabilization by means of cementitious and polymeric agents (e.g. Guney et al. 2007; Yazdandoust and Yasrobi 2010; Kalkan 2011; Estabragh et al.

2013; Thyagaraj and Zodinsanga 2014; Alazigha et al. 2016; Soltani et al. 2017[b]). To the authors' knowledge, however, the cyclic wetting–drying behavior of rubber mixed expansive clays remains undetermined.

To complement a further step towards sustainability, the present study intends to examine the rubber's capacity (of both fine and coarse categories) in ameliorating the inferior characteristics of expansive clays. The experimental program consisted of standard Proctor compaction and cyclic wetting–drying tests. The scanning electron microscopy (SEM) analysis was also introduced to identify the soil–rubber amending mechanisms, and to observe the evolution of fabric in response to alternate wetting and drying.

2. Materials

2.1. Expansive Clay Soil

The soil used in this study was a mixture of 85% kaolinite and 15% sodium–activated bentonite (Soltani et al. 2018[c]). Mechanical properties of the soil, determined as per relevant ASTM and Australian standards, are summarized in **Table 2**. The conventional gradation analysis, carried out in accordance with ASTM D422–07, indicated a clay fraction (< 2 μm) of 52.80%, along with 46.16% silt (2–75 μm) and 1.04% fine sand (0.075–0.425 mm). The liquid limit and plasticity index were measured as w_L=59.60% and I_P=32.32%, from which the soil was characterized as *clay with high plasticity* (CH) in accordance with the Unified Soil Classification System (USCS). The free swell ratio was measured as FSR=2.91, from which the soil was graded as *highly expansive* (Sridharan and Prakash 2000[a]; Prakash and Sridharan 2004). Other soil properties, as supplied by the manufacturer, included a pH of 7.80, a specific surface area (SSA) of 42.75 m^2/g, and a cation exchange capacity (CEC) of 21.65 meq/100mL.

2.2. Recycled Tire Rubbers

Commercially available recycled tire rubbers of both fine (herein RA) and coarse (herein RB) gradations were used for swell–shrink mitigation (Soltani et al. 2018[c]). Physical properties and chemical composition of the rubbers, as supplied by the manufacturer, are tabulated in **Table 3**. The particles of RA were analogous in size to fine–medium sand (0.075–2 mm), whereas RB was graded into the medium–coarse sand category (0.425–4.75 mm). The coefficients of uniformity and curvature were measured as C_u=2.81 and C_c=1.20 for RA, and C_u=1.56 and C_c=1.04 for RB, from which both rubber types were characterized as *poorly–graded* (SP) in

accordance with the USCS criterion. The specific gravity (at 20 °C) for both rubber types was provided as G_{sr}=1.09, which is in compliance with that reported in the literature (see Yadav and Tiwari (2017[c]) for details). The scanning electron microscopy (SEM) technique was utilized to observe the rubber's surface features, and the results are provided in **Figure 1**. The rubber particles are non–spherical and highly irregular in shape, with some cavities and micro–cracks propagated along the rubber's surface, thus predicating a rough surface texture. Such surface features may potentially engender a spatial three–dimensional reinforcement network in favor of interlocking the soil grains into a coherent matrix of enhanced mechanical performance (Yadav and Tiwari 2017[b]; Soltani et al. 2018[a]).

3. Experimental Methodologies

Three mix designs, consisting of the virgin soil (herein C) and two rubberized blends (herein CRA and CRB), were considered for the experimental program. The choice of rubber content for the rubberized blends was taken as 10% (by weight of dry soil), which was deemed as optimum to satisfy desirable improvements in the swell–shrink–consolidation capacity (without cyclic wetting–drying action) as well as the strength–related features (see Soltani et al. (2018[c]) for details). The experimental program was carried out in two phases consisting of preliminary compaction studies and cyclic wetting–drying tests. The scanning electron microscopy (SEM) analysis was also introduced to complement the discussion on soil–rubber interactions during alternate wetting and drying.

3.1. Compaction Studies and Sample Preparations

The three mix designs, i.e. C, CRA and CRB, were tested for Standard Proctor compaction characteristics in accordance with ASTM D698–12, and the results are provided in **Figure 2**. The specific gravity of CRA and CRB was estimated by the weighted averaging technique (Trouzine et al. 2012; Soltani et al. 2018[d]), which resulted in G_{sm}=2.40 for both rubberized blends. As a result of rubber inclusion, the compaction locus experienced a downward–leftward translation over the γ_d:w space (γ_d=dry unit weight; and w=water content), indicating a notable reduction in both the maximum dry unit weight γ_{dmax} and the optimum water content w_{opt}. The effect of rubber size, however, was observed to be marginal. The virgin soil resulted in γ_{dmax}=15.07 kN/m^3 (w_{opt}=26.00%), while the inclusion of 10% RA and RB resulted in γ_{dmax}=14.35 kN/m^3 and 14.37 kN/m^3 (w_{opt}=23.87% and 23.46%), respectively. Such trends can be attributed to the lower specific gravity, larger specific surface area and lower water

adsorption capacity of the rubber particles compared with the soil grains (Cabalar et al. 2014; Signes et al. 2016; Soltani et al. 2018[d]).

Samples for the cyclic wetting–drying tests were prepared at their respective dry of optimum condition (defined as 5% less than optimum water content and its relative dry unit weight), i.e. point O for C, point A for CRA and point B for CRB (see **Figure 2**). The choice of dry of optimum placement was to accommodate delay in compaction under field conditions. The virgin soil and the two rubberized blends were each statically compacted to the desired placement condition in the oedometer mold (measuring 50 mm in diameter and 20 mm in height), and further subjected to cyclic wetting–drying tests (see **Section 3.2**). Supplementary details with regard to the sample preparations, including mixing and static compaction, can be found in Soltani et al. (2018[c]).

3.2. Cyclic Wetting–Drying Test

The desired sample, i.e. C, CRA or CRB, was inundated with water and allowed to freely swell in a conventional oedometer setup under a low nominal overburden stress of 1 kPa (ASTM D4546–14). The incurred axial swelling strain was recorded (by a digital displacement transducer) during predefined time intervals to a point at which the ultimate swelling strain, denoted as swelling potential, could be achieved. Upon completion of the wetting process, reservoir water was drained through a drainage valve embedded within the oedometer cell. The oedometer cell, which houses the swollen sample, was then transferred to an oven where drying of the sample was attempted at a constant temperature of 40 °C. The incurred axial shrinkage strain was regularly monitored (by a dial displacement transducer) to a point at which the ultimate shrinkage strain, denoted as shrinkage potential, could be achieved. The combination of one wetting and the subsequent drying stage is designated as one wetting–drying cycle. For any given cycle, the swelling/shrinkage potential can be obtained as:

$$S_{\mathrm{p}}(N) \vee SH_{\mathrm{p}}(N) = \frac{\Delta H_{\mathrm{u}}(N)}{H_{\mathrm{o}}(N-1)} \quad \ni \quad N \in \mathbb{N} \tag{1}$$

where $S_{\mathrm{P}}(N)$=swelling potential with respect to the N^{th} wetting cycle; $SH_{\mathrm{P}}(N)$=shrinkage potential with respect to the N^{th} drying cycle; $\Delta H_{\mathrm{u}}(N)$=ultimate change in the sample's thickness with respect to the N^{th} wetting or drying cycle; and $H_{\mathrm{o}}(N-1)$=sample's thickness prior commencement of the N^{th} wetting or drying cycle.

The swelling and shrinkage potentials may either decrease or increase with an increase in the number of applied cycles, and regardless of the observed trend, attain equilibrium upon the completion of several cycles (Subba Rao 2000). In the present study, the equilibrium condition was noted at the fourth cycle, and as such, only five wetting–drying cycles were implemented for the tested samples. The void ratio–water content relationship during shrinkage, denoted as the shrinkage curve, was also measured at the first and fifth drying cycles. For each mix design, a total of two duplicated samples were subjected to cyclic wetting–drying and dismantled upon completion of the first and fifth wetting stages. The swollen samples were then carefully removed from the oedometer cell and transferred to an oven where drying was attempted at a constant temperature of 40 ^{o}C. The samples were regularly tested for void ratio (ASTM D427–04) and water content (ASTM D2216–10) to a point at which shrinkage ceased.

3.3. Micro–Structure Analysis

Scanning electron microscopy (SEM) studies were carried out to observe the evolution of fabric in response to alternate wetting and drying. The Philips XL20 scanning electron microscope, with a resolution of 4 μm and a maximum magnification ratio of 50,000×, was employed for SEM imaging. Two cases (or samples) were tested for each mix design: **i)** prior wetting–drying (or as–compacted); and **ii)** after wetting–drying (or at the end of the fifth drying cycle). The samples were carefully fractured into small cubes, measuring approximately 1 cm^3 in volume (Tang et al. 2007; Yazdandoust and Yasrobi 2010; Soltani et al. 2018[a]), and further scanned over various magnification ratios ranging from 150x to 20,000x.

4. Results and Discussion

4.1. Swelling Characteristics

Swell–time curves for the samples C, CRA and CRB during alternate wetting cycles are provided in **Figures 3a**–**3c**, respectively. As a result of alternate wetting and drying, the swell–time locus encountered a major downward shift over the ε_{sw}:log$t$ space (ε_{sw}=axial swelling strain; and t=elapsed time of swelling), indicating a significant reduction in the magnitude of exhibited swelling strain during swell evolvement. At any given elapsed time of swelling, the greater the number of applied cycles N the lower the swelling tendency, with both rubberized blends holding a notable advantage over the virgin soil. At t=24 h, for instance, the virgin soil resulted in ε_{sw}=15.23%, 14.05%, 9.20%, 7.95% and 8.07% at N=1–5 (see **Figure 3a**), while the

inclusion of 10% RA resulted in lower values of 11.77%, 9.96%, 7.92%, 6.67% and 6.37%, respectively (see **Figure 3b**). The same 10% inclusion of RB demonstrated a more pronounced decreasing trend, as the aforementioned values dropped to ε_{sw}=11.44%, 8.43%, 6.51%, 4.59% and 4.69% (at N=1–5), respectively (see **Figure 3c**).

Figure 4 illustrates the variations of swelling potential S_P against the number of applied cycles for the tested samples. The greater the number of applied cycles the lower the swelling potential, following a monotonic decreasing trend with marginal variations beyond the equilibrium cycle (or N=4). For any given cycle, the swelling potential can be orderly ranked as C > CRA > CRB, thus predicating a rubber size/shape–dependent amending mechanism. The virgin soil resulted in S_P=18.35%, 15.34%, 10.43%, 9.04% and 9.20% at N=1–5, respectively. With the inclusion of 10% RA, the aforementioned values dropped to 13.01%, 11.21%, 8.64%, 7.21% and 7.13%, respectively. The rubber of coarser category (or RB) consistently outperformed the finer rubber (or RA) in terms of lower S_P values (particularly at $N \geq 2$), which were measured as 12.18%, 9.37%, 7.11%, 5.01% and 5.09% at N=1–5, respectively.

A typical swell–time path, plotted over the ε_{sw}:log$t$ space, develops into an S–shaped curve, thereby suggesting three phases during swell evolvement, i.e. initial, primary and secondary swelling (Sivapullaiah et al. 1996; Day 1999; Sridharan and Gurtug 2004; Soltani et al. 2017[a], 2018[a]). The initial swelling stage progresses at macro–structural level where swelling of active smectite minerals takes place within the inter–assemblage pore–spaces. This stage prolongs to a point at which the inter–assemblage pore–spaces become incapable of accommodating further expansion incurred by active clay minerals. Consequently, initial swelling accounts for minor inter–void volume changes often less than 10% of the total volume increase or swelling potential (e.g. see sample C at N=1 in **Figure 3a**). The primary swelling stage constitutes for up to 80% of the total volume increase, and is graphically represented by a steep–sloped linear relationship, indicating an escalated rate of swelling with respect to time (e.g. see sample C at N=1 in **Figure 3a**). The secondary swelling stage takes place as a result of double–layer repulsion, and thus accounts for small time–dependent volume changes often similar to that of the initial swelling phase (e.g. see sample C at N=1 in **Figure 3a**). As opposed to initial swelling, both the primary and secondary swelling phases evolve at micro–structural level. The time–dependency nature of the swelling phenomenon can be interpreted by means of the coefficients of primary and secondary swelling, i.e. χ_{psw} and χ_{ssw}, which can be defined as (Soltani et al. 2018[b]):

$$\chi_{psw} = \frac{\Delta\varepsilon_{sw}(t)}{\Delta \log t}\Bigg]_{t_{isw}}^{t_{psw}} = \frac{\varepsilon_{psw}}{\log\left[\frac{t_{psw}}{t_{isw}}\right]} \tag{2}$$

$$\chi_{ssw} = \frac{\Delta\varepsilon_{sw}(t)}{\Delta \log t}\Bigg]_{t_{psw}}^{t_{ssw}} = \frac{\varepsilon_{ssw}}{\log\left[\frac{t_{ssw}}{t_{psw}}\right]} \tag{3}$$

where t_{isw}, t_{psw} and t_{ssw}=completion time (from t=0) of the initial, primary and secondary swelling stages; and ε_{psw} and ε_{ssw}=axial swelling strain exhibited during the primary and secondary swelling regions.

Figures 5a and 5b illustrate the variations of χ_{psw} and χ_{ssw} against the number of applied cycles for the tested samples, respectively. Similar to the swelling potential (see **Figure** 4), the greater the number of applied cycles the lower the swelling coefficients, with both rubberized blends holding a notable advantage over the virgin soil, thereby corroborating the rubber's capacity to counteract the heave in both magnitude and time. The tendency for reduction, however, was found to be in favor of a larger rubber size, as evident with the lower swelling coefficients exhibited by CRB compared with that of CRA. The samples C, CRA and CRB resulted in χ_{psw}=8.38×10^{-2}, 5.92×10^{-2} and 5.58×10^{-2} (χ_{ssw}=2.56×10^{-2}, 1.46×10^{-2} and 1.19×10^{-2}) at N=1, respectively. As optimum cases, the aforementioned values dropped to χ_{psw}=4.14×10^{-2}, 3.27×10^{-2} and 2.27×10^{-2} (χ_{ssw}=1.15×10^{-2}, 0.77×10^{-2} and 0.50×10^{-2}) at the equilibrium cycle (or N=4), respectively.

4.2. Shrinkage Characteristics

Figure 6 illustrates the variations of shrinkage potential SH_P (obtained as per oedometer testing conditions) against the number of applied cycles N for the tested samples. The shrinkage potential demonstrated a trend similar to that observed for the swelling potential (compare **Figures** 4 and 6). In this case, the greater the number of applied cycles the lower the shrinkage potential, following a monotonic decreasing trend up to the equilibrium cycle (or N=3–4), beyond of which only marginal variations were noted. For any given cycle, the rubberized blends consistently outperformed the virgin soil in terms of lower SH_P values. The tendency for shrinkage reduction, however, was found to be in favor of a larger rubber size, as evident with the lower SH_P values (particularly at $N \geq 3$) exhibited by CRB compared with that of CRA (compare the trendlines CRA and CRB in **Figure** 4). The virgin soil resulted in SH_P=15.96%,

11.54%, 8.02%, 8.07% and 8.22% at N=1–5, while the inclusion of 10% RA resulted in lower values of 11.83%, 8.11%, 6.45%, 6.57% and 6.20%, respectively. The same 10% inclusion of RB demonstrated a more pronounced decreasing trend, as the aforementioned values dropped to SH_P=10.67%, 8.05%, 4.87%, 4.97% and 5.21% (at N=1–5), respectively.

Void ratio–water content shrinkage curves for the tested samples at N=1 and 5 are provided in **Figure 7**. Similar to the swell–time path (see **Figure 3**), the shrinkage curve also develops into an *S*–shaped curve, and thus suggests three phases during shrink evolvement, i.e. structural, primary and residual shrinkage (Haines 1923; Tripathy et al. 2002; Cornelis et al. 2006; Estabragh et al. 2015; Thyagaraj et al. 2017). The structural shrinkage phase progresses at macro–structural level where drainage of water takes place from the larger inter–assemblage pore–spaces. Consequently, this stage constitutes for minor (and often negligible) changes in the bulk soil volume (e.g. see sample C at N=1 in **Figure 7a**). The primary shrinkage stage is graphically represented by a steep–sloped linear relationship, indicating an escalated rate of shrinkage with respect to water loss. This portion of the shrinkage curve is theoretically parallel to the S_r=100% saturation line, and as such, the decrease in water volume brings forth an equal decrease in the bulk soil volume. Primary shrinkage extends up to the shrinkage limit where particles come into close contact and the contained water is just sufficient to fill the intra–assemblage pore–spaces (e.g. see sample C at N=1 in **Figure 7a**). The residual shrinkage phase marks the entrance of air into the intra–assemblage pore–spaces, thereby promoting air–filled porosity coupled with a dense particle configuration. At this stage, the volume of lost water exceeds the decrease in bulk soil volume (e.g. see sample C at N=1 in **Figure 7a**).

As a result of alternate wetting and drying, the shrinkage curve encountered a major vertical dilation over the e:w space (e=void ratio; and w=water content), indicating a reduced tendency for shrinkage. Furthermore, the primary shrinkage segment shifted away from its corresponding S_r=100% saturation line, thus signifying a tendency towards a more unsaturated character upon achieving equilibrium condition (compare N=1 with N=5 in **Figure 7**). As a typical case outlined in **Figure 7b** (see sample CRB at N=1), the shrinkage curve can be employed to obtain the volumetric shrinkage strain ε_{vsh} by means of basic volume–mass relations, i.e. $\varepsilon_{vsh}=\Delta e/1+e_o$ (Δe=change in void ratio; and e_o=initial void ratio). The virgin soil resulted in ε_{vsh}=26.97% and 14.28% at N=1 and 5, while the inclusion of 10% RA resulted in lower values of 20.33% and 10.73%, respectively. The same 10% inclusion of RB demonstrated a slightly more pronounced decreasing trend, as the aforementioned values dropped to ε_{vsh}=19.60% and 9.85% (at N=1 and 5), respectively. Cyclic wetting–drying and/or rubber inclusion led to a notable increase in the

shrinkage limit w_S. The effect of rubber size/shape, however, was found to be rather marginal. The samples C, CRA and CRB resulted in w_S=14.88%, 18.00% and 16.40% at N=1, while the aforementioned values increased to 17.47%, 20.87% and 19.92% at N=5, respectively. The shrinkage limit is adversely related to the packing capacity of particles during drying, which in turn is governed by the grain–size distribution. The more uniform/poor the grain–size distribution the lower the packing capacity and hence the higher the shrinkage limit (Sridharan and Prakash 1998, 2000[b]). The inclusion of poorly–graded rubber (see **Table 3**) offsets the well–graded distribution of the host soil, and as such, gives rise to higher shrinkage limits. Similarly, cyclic wetting–drying leads to a more uniform grain–size distribution by inducing aggregation and cementation of the soil grains (see **Section 4.4** for details), which in turn results in higher shrinkage limits.

4.3. Swell–Shrink Patterns

The swelling and shrinkage potentials, obtained as per **Equation 1** and illustrated in **Figures 4** and **6**, can be incorporated (in a cumulative manner) to arrive at the accumulated axial deformation during alternate wetting and drying (Soltani et al. 2017[b]; Zhao et al. 2017):

$$\varepsilon_c(N)=\begin{cases}\mathrm{W}:\sum_{N=1}^{\infty}\left[S_p(N)-SH_p(N-1)\right] \ \ni \ N\in\mathbb{N}\\ \mathrm{D}:\sum_{N=1}^{\infty}\left[S_p(N)-SH_p(N)\right] \ \ni \ N\in\mathbb{N}\end{cases} \tag{4}$$

where $\varepsilon_c(N)$=accumulated axial deformation at the N^{th} wetting (specified as W) or drying (specified as D) cycle with respect to the sample's initial (or as–compacted) placement condition.

The accumulated deformation plotted against the number of applied cycles, commonly referred to as the swell–shrink pattern/path, can be employed to perceive/predict free surface ground movements under field conditions. Swell–shrink paths for the samples C, CRA and CRB are provided in **Figure 8**. As a result of rubber inclusion, the swell–shrink path, while lingering above the reference deformation level (or ε_c=0), encountered a notable downward shift over the ε_c:N space, thereby corroborating the rubber's capacity to counteract the heave and/or settlement incurred by alternate wetting and drying. The nature and extent of the accumulated deformation can be interpreted by the slope of a two–parameter linear trendline fitted through

the desired ε_c–N dataset, i.e. $\eta=\Delta\varepsilon_c/\Delta N$. Depending on the sign (and magnitude) of η, three scenarios can be hypothesized (Soltani et al. 2017[b]):

- **$\eta>0$:** The magnitude of incurred swelling is greater than that of shrinkage, and as such, the accumulated deformation is *expansive*. Quite clearly, the greater the magnitude of η the higher the expansive tendency.

- **$\eta<0$:** The magnitude of incurred shrinkage is greater than that of swelling, and as such, the accumulated deformation is *contractive*. In this case, the greater the magnitude of η the higher the tendency for contraction.

- **$\eta=0$:** The magnitude of incurred swelling and shrinkage are on par with each other, and as such, the accumulated deformation is *neutral* and hence desirable for minimizing free surface ground movements.

In terms of η, the tested mix designs can be orderly ranked as C > CRA >> CRB. The virgin soil resulted in η=1.42%, thus signifying an *expansive* accumulated deformation as a result of alternate wetting and drying. With the inclusion of 10% RA, the aforementioned value dropped to 1.23%, which indicates an *expansive* condition with lower expansive tendency compared with that of the virgin soil. The same 10% inclusion of RB, however, manifested a relatively *neutral* value of η=0.52%, thereby suggesting a more effective resistance to alternate wetting and drying compared with that of RA.

4.4. Amending Mechanisms and Fabric Evolution

The swelling and shrinkage potentials both exhibited a notable decreasing trend with an increase in the number of applied cycles (see **Figures 4** and **6**). Such trends can be attributed to the reconstruction of the soil micro–structure upon completion of the first or second cycle (Subba Rao 2000; Zhang et al. 2006; Estabragh et al. 2015; Zhao et al. 2017; Soltani et al. 2018[a]). Capillary stresses generated as a consequence of drying facilitate the formation of strong van der Waals bonds capable of inducing aggregation and cementation of the soil grains. This is followed by a decrease in the expansive clay content, thereby leading to a reduced specific surface area and hence a lower water adsorption–retention capacity, which in turn bring forth a reduced tendency for swelling and shrinkage.

Scanning electron micrographs for the samples C, CRA and CRB, prior and after cyclic wetting–drying (or *N*=5), are provided in **Figure 9**. The micro–fabric of the as–compacted virgin soil sample (without wetting–drying action) exhibited a partly–dense matrix, along with a notable number of intra–assemblage pore–spaces which facilitate the entrance of water into the sample during wetting (see **Figure 9a**). As a result of alternate wetting and drying, the micro–fabric became more uniform in nature, indicating aggregation and cementation of the soil grains and hence the development of a matured dense matrix. Moreover, the intra–assemblage pore–spaces displayed a notable reduction in both number and size, thus leading to a decreased water intrusion capacity and hence a reduced tendency for swelling (see **Figure 9b**). Similar to the as–compacted virgin soil sample, the micro–fabric of the as–compacted rubberized blends, i.e. CRA and CRB, consisted of a partly–dense matrix, accompanied by a number of inter–assemblage pore–spaces mainly distributed along the soil–rubber connection interface. The rubber inclusions effectively limited the clay's available surface area for interaction with water, which in turn gave rise to a reduced swelling potential compared with that of the as–compacted virgin soil sample. In addition, the rubber particles acted as physical anchors within the fabric, thereby interlocking the neighboring clay aggregates and hence withstanding tensile stresses developed during desiccation (see **Figures 9c** and **9e**). Quite clearly, the larger particle size and elongated form factor of RB makes for a more pronounced interlocking and hence a higher resistance against swelling and shrinkage compared with that of RA (compare **Figures 9c** and **9e**). With the progression of cyclic wetting–drying, the connection interface between the rubber particles and the clay matrices was markedly improved, as evident with the reduced number of inter–assemblage pore–spaces as well as the presence of clothed rubber particles; this in turn resulted in a further reduction of the swelling and shrinkage potentials (see **Figures 9d** and **9f**).

Taking into account the above discussions, as well as those outlined in previous studies (e.g. Patil et al. 2011; Trouzine et al. 2012; Yadav and Tiwari et al. 2017[b]; Soltani et al. 2018[a]; 2018[c]), the soil–rubber amending mechanisms can be ascribed to the following three aspects:

- **Increase in non–expansive content:** The swell–shrink capacity is primarily a function of the soil's expansive clay content, implying that the lower the expansive clay content the lower the tendency for swelling and shrinkage. The rubber inclusions substitute a fraction of the expansive clay content with non–plastic hydrophobic rubber particles, thereby leading to a reduction of the swell–shrink capacity.

- **Frictional resistance generated as a result of soil–rubber contact:** The frictional resistance is a function of soil–rubber contact area, with greater contact levels offering a higher resistance to bear the swell–shrink forces. Consequently, this amending mechanism can be ascribed to the rubber content, and to some degree the rubber size. For any given rubber content, the coarser the rubber particles (or the lower the rubber's specific surface area) the greater the achieved contact level (or interface) between the rubber particles and the soil grains, and thus the higher the generated frictional resistance against swelling and shrinkage (compare CRB with CRA in **Figures 4** and **6**).

- **Mechanical interlocking of rubber particles and soil grains:** Mechanical interlocking is achieved during sample preparation (or compaction), and induces matrix adhesion by immobilizing the soil grains against swell–shrink movements. Quite clearly, the more effective the achieved mechanical interlocking the higher the resistance to swelling and shrinkage. Consequently, this amending mechanism is in line with the rubber content, and more importantly the rubber shape. As opposed to the granular form factor of RA, the particles of RB are rather fiber–shaped or elongated (see **Figure 1**), and thus favor a more pronounced mechanical interlocking by entwining within the matrix and immobilizing the soil grains against swell–shrink movements with increased efficiency (compare CRB with CRA in **Figures 4** and **6**).

5. Conclusions

The following conclusions can be drawn from this study:

- Alternate wetting and drying led to the reconstruction of the soil/soil–rubber micro–structure by way of inducing aggregation and cementation of the soil grains. The greater the number of applied cycles the lower the swelling and shrinkage potentials, following a monotonic decreasing trend with the rubberized blends holding a notable advantage over the virgin soil. The tendency for reduction, however, was found to be in favor of a larger rubber size, thus signifying a rubber size/shape–dependent amending mechanism.

- The axial swelling strain–time data (time in logarithmic scale) developed into an *S*–shaped curve, and thus suggested three phases during swell evolvement, i.e. initial, primary and secondary swelling. As a result of cyclic wetting–drying and/or rubber inclusion, the swell–

time locus encountered a major downward shift, thereby indicating a capacity to counteract the heave in both magnitude and time.

- The void ratio–water content shrinkage data also developed into an *S*–shaped curve, and thus suggested three phases during shrink evolvement, i.e. structural, primary and residual shrinkage. As a result of cyclic wetting–drying and/or rubber inclusion, the shrinkage curve encountered a major vertical dilation, thus indicating a reduced tendency for shrinkage. Furthermore, alternate wetting and drying and/or rubber inclusion led to a notable increase in the shrinkage limit, while the effect of rubber size/shape was found to be marginal.

- The rubber inclusions led to a notable decrease in the magnitude of the accumulated axial deformation during successive wetting–drying cycles. The swell–shrink patterns/paths indicated an *expansive* accumulated deformation for the virgin soil, while the rubberized blends, particularly the one blended with the rubber of coarser category, manifested a relatively *neutral* accumulated deformation, thereby corroborating the rubber's capacity to counteract the heave and/or settlement incurred by alternate wetting and drying.

Acknowledgments

Special thanks go to Prof. Asuri Sridharan of the Indian National Science Academy (INSA) for valuable suggestions to the authors. This research was funded by the Australian Research Council (ARC) by way of project No. **DP140103004**; this support is gratefully acknowledged.

References

Al-Akhras NM, Attom MF, Al-Akhras KM and Malkawi AIH (**2008**) Influence of fibers on swelling properties of clayey soil. *Geosynthetics International* **15**(**4**): 304–309, http://doi.org/10.1680/gein.2008.15.4.304.

Alazigha DP, Indraratna B, Vinod JS and Ezeajugh LE (**2016**) The swelling behaviour of lignosulfonate–treated expansive soil. *Proceedings of the Institution of Civil Engineers–Ground Improvement* **169**(**3**): 182–193, http://doi.org/10.1680/jgrim.15.00002.

Al-Homoud AS, Basma AA, Malkawi AIH and Al-Bashabsheh MA (**1995**) Cyclic swelling behaviour of clays. *Journal of Geotechnical Engineering* **121**(**7**): 562–565, http://doi.org/10.1061/(asce)0733-9410(1995)121:7(562).

Al-Omari RR and Hamodi FJ (**1991**) Swelling resistant geogrid–A new approach for the treatment of expansive soils. *Geotextiles and Geomembranes* **10**(**4**): 295–317, http://doi.org/10.1016/0266-1144(91)90008-k.

Alonso EE, Romero E, Hoffmann C and García-Escudero E (**2005**) Expansive bentonite–sand mixtures in cyclic controlled–suction drying and wetting. *Engineering Geology* **81**(**3**): 213–226, http://doi.org/10.1016/j.enggeo.2005.06.009.

Al-Rawas AA, Hago AW and Al-Sarmi H (**2005**) Effect of lime, cement and Sarooj (artificial pozzolan) on the swelling potential of an expansive soil from Oman. *Building and Environment* **40**(**5**): 681–687, http://doi.org/10.1016/j.buildenv.2004.08.028.

Al-Tabbaa A and Aravinthan T (**1998**) Natural clay–shredded tire mixtures as landfill barrier materials. *Waste Management* **18**(**1**): 9–16, http://doi.org/10.1016/s0956-053x(98)00002-6.

Al-Tabbaa A, Blackwell O and Porter SA (**1997**) An investigation into the geotechnical properties of soil–tyre mixtures. *Environmental Technology* **18**(**8**): 855–860, http://doi.org/10.1080/09593331808616605.

Arulrajah A, Mohammadinia A, D'Amico A and Horpibulsuk S (**2017**) Effect of lime kiln dust as an alternative binder in the stabilization of construction and demolition materials. *Construction and Building Materials* **152**(**999**–**1007**), http://doi.org/10.1016/j.conbuildmat.2017.07.070.

Cabalar AF, Karabash Z and Mustafa WS (**2014**) Stabilising a clay using tyre buffings and lime. *Road Materials and Pavement Design* **15**(**4**): 872–891, http://doi.org/10.1080/14680629.2014.939697.

Cai Y, Shi B, Ng CWW and Tang CS (**2006**) Effect of polypropylene fibre and lime admixture on engineering properties of clayey soil. *Engineering Geology* **87**(**3**–**4**): 230–240, http://doi.org/10.1016/j.enggeo.2006.07.007.

Cokca E and Yilmaz Z (**2004**) Use of rubber and bentonite added fly ash as a liner material. *Waste Management* **24**(**2**): 153–164, http://doi.org/10.1016/j.wasman.2003.10.004.

Cornelis WM, Corluy J, Medina H, Díaz J, Hartmann R, van Meirvenne M and Ruiz ME (**2006**) Measuring and modelling the soil shrinkage characteristic curve. *Geoderma* **137**(**1**–**2**): 179–191, http://doi.org/10.1016/j.geoderma.2006.08.022.

Day RW (**1994**) Swell–shrink behaviour of compacted clay. *Journal of Geotechnical Engineering* **120**(**3**): 618–623, http://doi.org/10.1061/(asce)0733-9410(1994)120:3(618).

Day RW (**1999**) *Geotechnical and Foundation Engineering: Design and Construction (1st ed)*. McGraw–Hill, New York, New York, USA, ISBN:9780071341387.

Dif A and Bluemel W (**1991**) Expansive soils under cyclic drying and wetting. *Geotechnical Testing Journal* **14**(**1**): 96–102, http://doi.org/10.1520/gtj10196j.

Edil T and Bosscher P (**1994**) Engineering properties of tire chips and soil mixtures. *Geotechnical Testing Journal* **17**(**4**): 453–464, http://doi.org/10.1520/gtj10306j.

Estabragh AR, Parsaei B and Javadi AA (**2015**) Laboratory investigation of the effect of cyclic wetting and drying on the behaviour of an expansive soil. *Soils and Foundations* **55**(**2**): 304–314, http://doi.org/10.1016/j.sandf.2015.02.007.

Estabragh AR, Pereshkafti MRS, Parsaei B and Javadi AA (**2013**) Stabilised expansive soil behaviour during wetting and drying. *International Journal of Pavement Engineering* **14**(**4**): 418–427, http://doi.org/10.1080/10298436.2012.746688.

Estabragh AR, Rafatjo H and Javadi AA (**2014**) Treatment of an expansive soil by mechanical and chemical techniques. *Geosynthetics International* **21**(**3**): 233–243, http://doi.org/10.1680/gein.14.00011.

Estabragh AR, Soltani A and Javadi AA (**2018**) Effect of pore water chemistry on the behaviour of a kaolin–bentonite mixture during drying and wetting cycles. *European Journal of Environmental and Civil Engineering* **in press**, http://doi.org/10.1080/19648189.2018.1428691.

Foose GJ, Benson CH and Bosscher PJ (**1996**) Sand reinforced with shredded waste tires. *Journal of Geotechnical Engineering* **122**(**9**): 760–767, http://doi.org/10.1061/(asce)0733-9410(1996)122:9(760).

Guney Y, Sari D, Cetin M and Tuncan M (**2007**) Impact of cyclic wetting–drying on swelling behavior of lime-stabilized soil. *Building and Environment* **42**(**2**): 681–688, http://doi.org/10.1016/j.buildenv.2005.10.035.

Haines WB (**1923**) The volume–changes associated with variations of water content in soil. *The Journal of Agricultural Science* **13**(**3**): 296–310, http://doi.org/10.1017/s0021859600003580.

Jones LD and Jefferson I (**2012**) Expansive soils. In *ICE Manual of Geotechnical Engineering: Volume I* (Burland J, Chapman T, Brown M and Skinner H (eds)). ICE Publishing, London, UK, pp. 413–441, http://doi.org/10.1680/moge.57074.0413.

Kalkan E (**2011**) Impact of wetting–drying cycles on swelling behavior of clayey soils modified by silica fume. *Applied Clay Science* **52**(**4**): 345–352, http://doi.org/10.1016/j.clay.2011.03.014.

Kalkan E (**2013**) Preparation of scrap tire rubber fiber–silica fume mixtures for modification of clayey soils. *Applied Clay Science* **80**–**81**: 117–125, http://doi.org/10.1016/j.clay.2013.06.014.

Kim YT, Kim HJ and Lee GH (**2008**) Mechanical behavior of lightweight soil reinforced with waste fishing net. *Geotextiles and Geomembranes* **26**(**6**): 512–518, http://doi.org/10.1016/j.geotexmem.2008.05.004.

Kua TA, Arulrajah A, Mohammadinia A, Horpibulsuk S and Mirzababaei M (**2017**) Stiffness and deformation properties of spent coffee grounds based geopolymers. *Construction and Building Materials* **138**: 79–87, http://doi.org/10.1016/j.conbuildmat.2017.01.082.

Lee JH, Salgado R, Bernal A and Lovell CW (**1999**) Shredded tires and rubber–sand as lightweight backfill. *Journal of Geotechnical and Geoenvironmental Engineering* **125**(**2**): 132–141, http://doi.org/10.1061/(asce)1090-0241(1999)125:2(132).

Mirzababaei M, Arulrajah A, Horpibulsuk S, Soltani A and Khayat N (**2018**[a]) Stabilization of soft clay using short fibers and poly vinyl alcohol. *Geotextiles and Geomembranes* **46**(**5**): 646–655, http://doi.org/10.1016/j.geotexmem.2018.05.001.

Mirzababaei M, Miraftab M, Mohamed M and McMahon P (**2013**[a]) Impact of carpet waste fibre addition on swelling properties of compacted clays. *Geotechnical and Geological Engineering* **31**(**1**): 173–182, http://doi.org/10.1007/s10706-012-9578-2.

Mirzababaei M, Miraftab M, Mohamed M and McMahon P (**2013**[b]) Unconfined compression strength of reinforced clays with carpet waste fibers. *Journal of Geotechnical and Geoenvironmental Engineering* **139**(**3**): 483–493, http://doi.org/10.1061/(asce)gt.1943-5606.0000792.

Mirzababaei M, Mohamed M, Arulrajah A, Horpibulsuk S and Anggraini V (**2018**[b]) Practical approach to predict the shear strength of fibre–reinforced clay. *Geosynthetics International* **25**(**1**): 50–66, http://doi.org/10.1680/jgein.17.00033.

Mirzababaei M, Yasrobi SS and Al-Rawas AA (**2009**) Effect of polymers on swelling potential of expansive soils. *Proceedings of the Institution of Civil Engineers–Ground Improvement* **162**(**3**): 111–119, http://doi.org/10.1680/grim.2009.162.3.111.

Mukherjee K and Mishra AK (**2017**) The impact of scrapped tyre chips on the mechanical properties of liner materials. *Environmental Processes* **4**(**1**): 219–233, http://doi.org/10.1007/s40710-017-0210-6.

Mukherjee K and Mishra AK (**2018**) Hydraulic and mechanical characteristics of compacted sand–bentonite: Tyre chips mix for its landfill application. *Environment, Development and Sustainability* **in press**, http://doi.org/10.1007/s10668-018-0094-2.

Onyejekwe S and Ghataora GS (**2015**) Soil stabilization using proprietary liquid chemical stabilizers: Sulphonated oil and a polymer. *Bulletin of Engineering Geology and the Environment* **74**(**2**): 651–665, http://doi.org/10.1007/s10064-014-0667-8.

Osipov VI, Bik NN and Rumjantseva NA (**1987**) Cyclic swelling of clays. *Applied Clay Science* **2**(**4**): 363–374, http://doi.org/10.1016/0169-1317(87)90042-1.

Patil U, Valdes JR and Evans TM (**2011**) Swell mitigation with granulated tire rubber. *Journal of Materials in Civil Engineering* **23**(**5**): 721–727, http://doi.org/10.1061/(asce)mt.1943-5533.0000229.

Phanikumar BR and Singla R (**2016**) Swell–consolidation characteristics of fibre–reinforced expansive soils. *Soils and Foundations* **56**(**1**): 138–143, http://doi.org/10.1016/j.sandf.2016.01.011.

Phummiphan I, Horpibulsuk S, Rachan R, Arulrajah A, Shen SL and Chindaprasirt P (**2018**) High calcium fly ash geopolymer stabilized lateritic soil and granulated blast furnace slag blends as a pavement base material. *Journal of Hazardous Materials* **341**: 257–267, http://doi.org/10.1016/j.jhazmat.2017.07.067.

Prakash K and Sridharan A (**2004**) Free swell ratio and clay mineralogy of fine–grained soils. *Geotechnical Testing Journal* **27**(**2**): 220–225, http://doi.org/10.1520/gtj10860.

Rosenbalm D and Zapata CE (**2017**) Effect of wetting and drying cycles on the behavior of compacted expansive soils. *Journal of Materials in Civil Engineering* **29**(**1**): 4016191:1–9, http://doi.org/10.1061/(asce)mt.1943-5533.0001689.

Seda JH, Lee JC and Carraro JAH (**2007**) Beneficial use of waste tire rubber for swelling potential mitigation in expansive soils. In *Geo–Denver 2007: Soil Improvement (GSP 172)* (Schaefer VR, Filz GM, Gallagher PM, Sehn AL and Wissmann KJ (eds)). ASCE, Denver, Colorado, USA, pp. 1–9, http://doi.org/10.1061/40916(235)5.

Signes CH, Garzón-Roca J, Fernández PM, Torre MEG and Franco RI (**2016**) Swelling potential reduction of Spanish argillaceous marlstone Facies Tap soil through the addition of crumb rubber particles from scrap tyres. *Applied Clay Science* **132**–**133**: 768–773, http://doi.org/10.1016/j.clay.2016.07.027.

Sivapullaiah P V., Sridharan A and Stalin VK (**1996**) Swelling behaviour of soil–bentonite mixtures. *Canadian Geotechnical Journal* **33**(**5**): 808–814, http://doi.org/10.1139/t96-106-326.

Soltani A, Deng A and Taheri A (**2018**[**b**]) Swell–compression characteristics of a fiber–reinforced expansive soil. *Geotextiles and Geomembranes* **46**(**2**): 183–189, http://doi.org/10.1016/j.geotexmem.2017.11.009.

Soltani A, Deng A, Taheri A and Mirzababaei M (**2017**[**b**]) A sulphonated oil for stabilisation of expansive soils. *International Journal of Pavement Engineering* **in press**, http://doi.org/10.1080/10298436.2017.1408270.

Soltani A, Deng A, Taheri A and Mirzababaei M (**2018**[**a**]) Rubber powder–polymer combined stabilization of South Australian expansive soils. *Geosynthetics International* **25**(**3**): 304–321, http://doi.org/10.1680/jgein.18.00009.

Soltani A, Deng A, Taheri A and Sridharan A (**2018**[**c**]) Swell–shrink–consolidation behavior of rubber–reinforced expansive soils. *Geotechnical Testing Journal* **in press**, http://doi.org/10.1520/gtj20170313.

Soltani A, Deng A, Taheri A and Sridharan A (**2018**[**d**]) Consistency limits and compaction characteristics of clay soils containing rubber waste. *Proceedings of the Institution of Civil Engineers–Geotechnical Engineering* **in press**, http://doi.org/10.1680/jgeen.18.00042.

Soltani A, Taheri A, Khatibi M and Estabragh AR (**2017**[a]) Swelling potential of a stabilized expansive soil: A comparative experimental study. *Geotechnical and Geological Engineering* **35**(**4**): 1717–1744, http://doi.org/10.1007/s10706-017-0204-1.

Sridharan A and Gurtug Y (**2004**) Swelling behaviour of compacted fine–grained soils. *Engineering Geology* **72**(**1**): 9–18, http://doi.org/10.1016/s0013-7952(03)00161-3.

Sridharan A and Nagaraj HB (**2000**) Compressibility behaviour of remoulded, fine–grained soils and correlation with index properties. *Canadian Geotechnical Journal* **37**(**3**): 712–722, http://doi.org/10.1139/t99-128.

Sridharan A and Prakash K (**1998**) Mechanism controlling the shrinkage limit of soils. *Geotechnical Testing Journal* **21**(**3**): 240–250, http://doi.org/10.1520/gtj10897j.

Sridharan A and Prakash K (**2000**[a]) Classification procedures for expansive soils. *Proceedings of the Institution of Civil Engineers–Geotechnical Engineering* **143**(**4**): 235–240, http://doi.org/10.1680/geng.2000.143.4.235.

Sridharan A and Prakash K (**2000**[b]) Shrinkage limit of soil mixtures. *Geotechnical Testing Journal* **23**(**1**): 3–8, http://doi.org/10.1520/gtj11118j.

Srivastava A, Pandey S and Rana J (**2014**) Use of shredded tyre waste in improving the geotechnical properties of expansive black cotton soil. *Geomechanics and Geoengineering* **9**(**4**): 303–311, http://doi.org/10.1080/17486025.2014.902121.

Subba Rao KS (**2000**) Swell–shrink behaviour of expansive soils – Geotechnical Challenges. *Indian Geotechnical Journal* **30**(**1**): 1–68.

Tang CS, Shi B, Gao W, Chen F and Cai Y (**2007**) Strength and mechanical behavior of short polypropylene fiber reinforced and cement stabilized clayey soil. *Geotextiles and Geomembranes* **25**(**3**): 194–202, http://doi.org/10.1016/j.geotexmem.2006.11.002.

Thyagaraj T and Zodinsanga S (**2014**) Swell–shrink behaviour of lime precipitation treated soil. *Proceedings of the Institution of Civil Engineers–Ground Improvement* **167**(**4**): 260–273, http://doi.org/10.1680/grim.12.00028.

Thyagaraj T, Thomas SR and Das AP (**2017**) Physico–chemical effects on shrinkage behavior of compacted expansive clay. *International Journal of Geomechanics* **17**(**2**): 06016013:1–11, http://doi.org/10.1061/(asce)gm.1943-5622.0000698.

Tripathy S and Subba Rao KS (**2009**) Cyclic swell–shrink behaviour of a compacted expansive soil. *Geotechnical and Geological Engineering* **27**(**1**): 89–103, http://doi.org/10.1007/s10706-008-9214-3.

Tripathy S, Subba Rao KS and Fredlund DG (**2002**) Water content–void ratio swell–shrink paths of compacted expansive soils. *Canadian Geotechnical Journal* **39**(**4**): 938–959, http://doi.org/10.1139/t02-022.

Trouzine H, Bekhiti M and Asroun A (**2012**) Effects of scrap tyre rubber fibre on swelling behaviour of two clayey soils in Algeria. *Geosynthetics International* **19**(**2**): 124–132, http://doi.org/10.1680/gein.2012.19.2.124.

Viswanadham BVS, Phanikumar BR and Mukherjee R V. (**2009**) Swelling behaviour of a geofiber–reinforced expansive soil. *Geotextiles and Geomembranes* **27**(**1**): 73–76, http://doi.org/10.1016/j.geotexmem.2008.06.002.

Yadav JS and Tiwari SK (**2017[a]**) A study on the potential utilization of crumb rubber in cement treated soft clay. *Journal of Building Engineering* **9**: 177–191, http://doi.org/10.1016/j.jobe.2017.01.001.

Yadav JS and Tiwari SK (**2017[b]**) Effect of waste rubber fibres on the geotechnical properties of clay stabilized with cement. *Applied Clay Science* **149**: 97–110, http://doi.org/10.1016/j.clay.2017.07.037.

Yadav JS and Tiwari SK (**2017[c]**) The impact of end–of–life tires on the mechanical properties of fine–grained soil: A Review. *Environment, Development and Sustainability* **in press**, http://doi.org/10.1007/s10668-017-0054-2.

Yazdandoust F and Yasrobi SS (**2010**) Effect of cyclic wetting and drying on swelling behavior of polymer–stabilized expansive clays. *Applied Clay Science* **50**(**4**): 461–468, http://doi.org/10.1016/j.clay.2010.09.006.

Zhang R, Yang H and Zheng J (**2006**) The effect of vertical pressure on the deformation and strength of expansive soil during cyclic wetting and drying. In *Unsaturated Soils 2006: Proceedings of the Fourth International Conference on Unsaturated Soils* (Miller GA, Zapata CE, Houston SL and Fredlund DG (eds)), ASCE, Carefree, Arizona, USA, pp. 894–905, http://doi.org/10.1061/40802(189)71.

Zhao NF, Ye WM, Chen YG, Chen B and Cui YJ (**2017**) Investigation on swelling–shrinkage behavior of unsaturated compacted GMZ bentonite on wetting–drying cycles. *Bulletin of Engineering Geology and the Environment* **in press**, http://doi.org/10.1007/s10064-017-1095-3.

Zornberg JG, Cabral AR and Viratjandr C (**2004**) Behaviour of tire shred–sand mixtures. *Canadian Geotechnical Journal* **41**(**2**): 227–241, http://doi.org/10.1139/t03-086.

List of Tables

Table 1. Recent contributions addressing the swelling behavior of rubber mixed expansive clays.

Table 2. Mechanical properties of the expansive clay soil.

Table 3. Physical properties and chemical composition of the recycled tire rubbers.

Table 1. Recent contributions addressing the swelling behavior of rubber mixed expansive clays.

Reference	Soil properties			Rubber properties			Other additives
	w_L (%)	I_P (%)	USCS	Type	Size (mm)	Content (%)	
Al-Tabbaa and Aravinthan (1998)	34	12	CL	Shreds	1–4 and 4–8	6–15 (w)	—
Cokca and Yilmaz (2004)	—	—	—	Crumbs	0.08–0.85	1–10 (w)	Bentonite
Seda et al. (2007)	52	34	CH	Shreds	2–6.7	30 (v)	—
Patil et al. (2011)	81	58	CH	Crumbs	0.075–0.85	20–36 (v)	—
Trouzine et al. (2012)	45	22	CI	Fibers	5–30 in length	10–50 (w)	—
	133	83	CH				
Kalkan (2013)	72	37	MH	Fibers	5–10 in length (0.25–1.25 in width)	1–4 (w)	Silica fume
Cabalar et al. (2014)	50	27	CI	Buffings	0.6–4.75	5–15 (w)	Lime
Srivastava et al. (2014)	61	32	CH	Shreds	0.075–2 and 2–4.75	5–50 (w)	—
Signes et al. (2016)	52	28	CH	Crumbs	0.08–2	2.5–25 (w)	—
Mukherjee and Mishra (2017)	32	—	—	Chips	2–4.75	5–15 (w)	—
Yadav and Tiwari (2017[a])	34	9	CI	Crumbs	0.8–2	2.5–10 (w)	Cement
Yadav and Tiwari (2017[b])	34	9	CI	Fibers	10–15 in length (2–3 in width)	2.5–10 (w)	Cement
Mukherjee and Mishra (2018)	—	—	—	Chips	2–4.75	5–15(w)	—
Soltani et al. (2018[a])	78	56	CH	Crumbs/Powder	0.075–1.18	10–30 (w)	Polyacrylamide
Soltani et al. (2018[c])	60	33	CH	Crumbs/Powder	0.075–1.18	5–30 (w)	—
				Buffings	1.18–4.75		

Note:
w_L=liquid limit; I_P=plasticity index; USCS=Unified Soil Classification System; CL=*clay with low plasticity*; CI=*clay with intermediate plasticity*; CH=*clay with high plasticity*; MH=*silt with high plasticity*; (w)=by weight; and (v)=by volume.

Table 2. Mechanical properties of the expansive clay soil.

Properties	Value	Standard designation
Specific gravity, G_{ss}	2.73	ASTM D854–14
Grain–size distribution		
Clay (< 2 μm) (%)	52.80	ASTM D422–07
Silt (2–75 μm) (%)	46.16	
Fine sand (0.075–0.425 mm) (%)	1.04	
Medium sand (0.425–2 mm) (%)	—	
Coarse sand (2–4.75 mm) (%)	—	
Consistency limits		
Liquid limit, w_L (%)	59.60	AS 1289.3.9.1–15
Plastic limit, w_P (%)	27.28	AS 1289.3.2.1–09
Plasticity index, $I_P=w_L–w_P$ (%)	32.32	
Linear shrinkage, L_S (%)	8.19	AS 1289.3.4.1–08
Shrinkage index, $I_S=w_L–L_S$ (%)	51.41	Sridharan and Nagaraj (2000)
Classifications		
USCS classification	CH	ASTM D2487–11
Free swell ratio, FSR†	2.91	Sridharan and Prakash (2000[a])/ Prakash and Sridharan (2004)
Degree of expansivity	High	
Compaction characteristics		
Optimum water content, w_{opt} (%)	26.00	ASTM D698–12
Maximum dry unit weight, γ_{dmax} (kN/m^3)	15.07	
Strength characteristics		
Unconfined compressive strength, q_u (kPa)‡	112.62	ASTM D2166–16
Splitting tensile strength, q_s (kPa)‡	13.57	ASTM C496–17

Note:
†ratio of equilibrium sediment volume of 10 g oven–dried soil passing sieve 425 μm in distilled water to that of kerosene; and ‡tested at Proctor optimum condition.

Table 3. Physical properties and chemical composition of the recycled tire rubbers.

Properties	Crumbs (RA)	Buffings (RB)
Grain–size distribution[†]		
D_{10} (mm)	0.182	1.077
D_{30} (mm)	0.334	1.370
D_{60} (mm)	0.513	1.682
D_{90} (mm)	0.864	2.105
Coefficient of uniformity, $C_u=D_{60}/D_{10}$	2.81	1.56
Coefficient of curvature, $C_c=D_{30}^2/D_{10}D_{60}$	1.20	1.04
USCS classification	SP	SP
Physical properties		
Solubility in water	Insoluble	
Water adsorption	Negligible (< 4%)	
Resistance to acid/alkaline	Excellent	
Softening point (^oC)	170	
Specific gravity, G_{sr} (at 20 ^oC)	1.09	
Chemical composition		
Styrene–Butadiene copolymer (%)	55	
Carbon black (%)	25–35	
Acetone extract (%)	5–20	
Zinc oxide (%)	2–3	
Sulphur (%)	1–3	

Note:
[†]ASTM D422–07 method.

List of Figures

Figure 1. Recycled tire rubbers at different magnification ratios: **(a)** RA (no magnification); **(b)** RA (150x magnification); **(c)** RA (500x magnification); **(d)** RB (no magnification); **(e)** RB (150x magnification); and **(f)** RB (250x magnification).

Figure 2. Standard Proctor compaction curves for the tested mix designs (ZAV=zero–air voids): **(a)** C/CRA; and **(b)** C/CRB.

Figure 3. Swell–time curves during alternate wetting cycles: **(a)** C; **(b)** CRA; and **(c)** CRB.

Figure 4. Variations of swelling potential against the number of applied cycles for the tested samples.

Figure 5. Rate of swelling for the tested samples during alternate wetting cycles: **(a)** primary swelling coefficient; and **(b)** secondary swelling coefficient.

Figure 6. Variations of shrinkage potential against the number of applied cycles for the tested samples.

Figure 7. Void ratio–water content shrinkage curves (at N=1 and 5) for the tested samples: **(a)** C/CRA; and **(b)** C/CRB.

Figure 8. Swell–shrink patterns for the tested samples.

Figure 9. Scanning electron micrographs for the tested samples.

Figure 1. Recycled tire rubbers at different magnification ratios: **(a)** RA (no magnification); **(b)** RA (150x magnification); **(c)** RA (500x magnification); **(d)** RB (no magnification); **(e)** RB (150x magnification); and **(f)** RB (250x magnification).

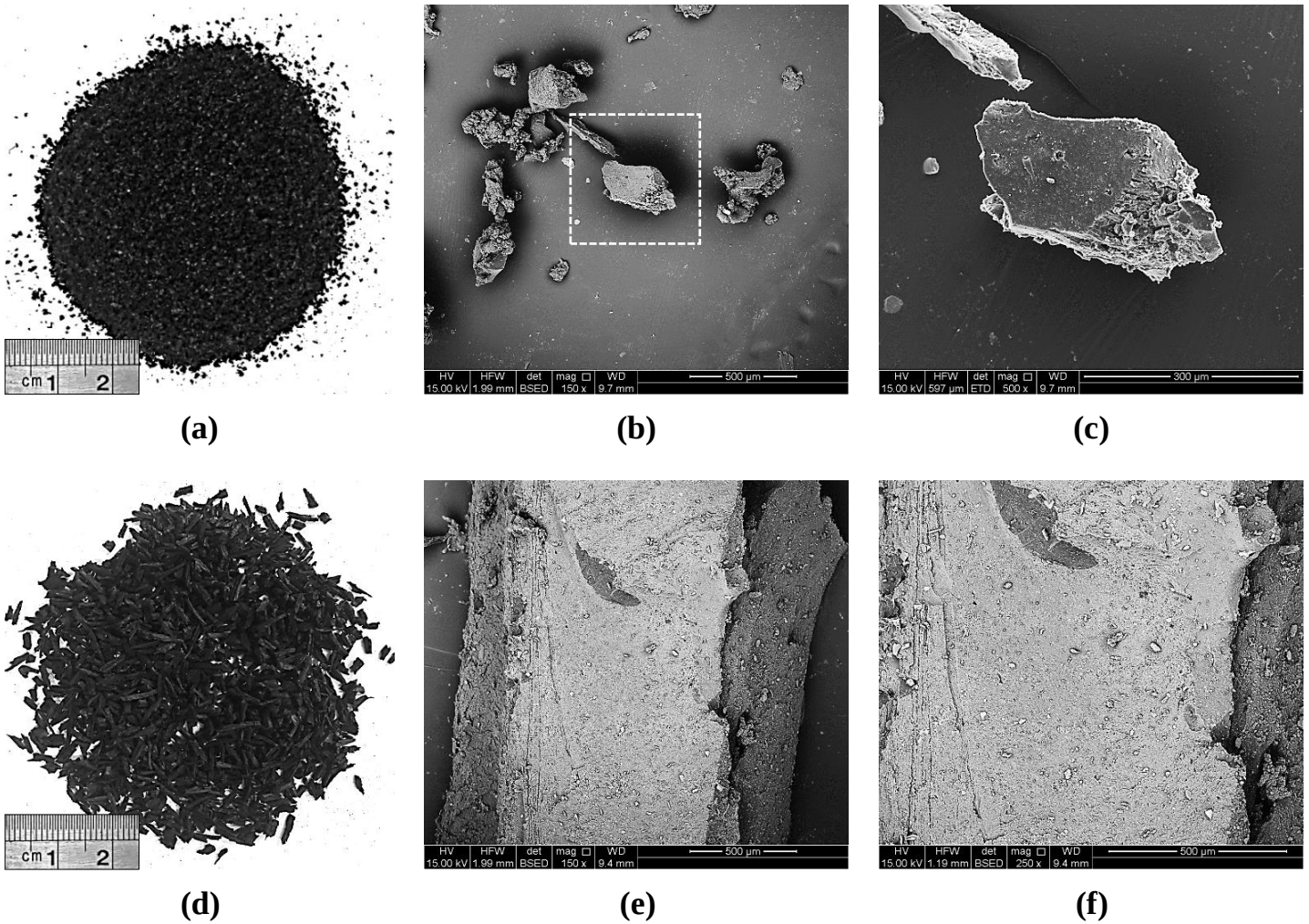

(a) **(b)** **(c)**

(d) **(e)** **(f)**

Figure 2. Standard Proctor compaction curves for the tested mix designs (ZAV=zero–air voids): **(a)** C/CRA; and **(b)** C/CRB.

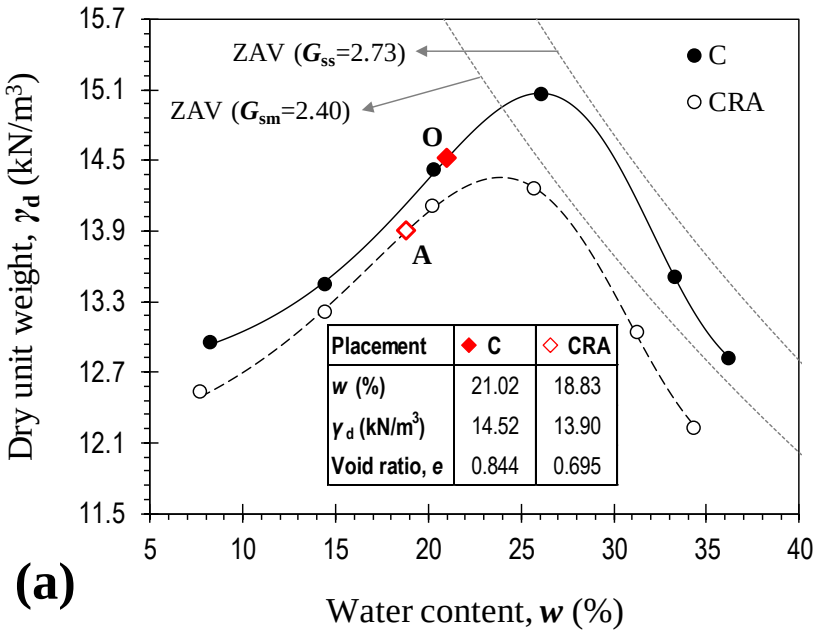

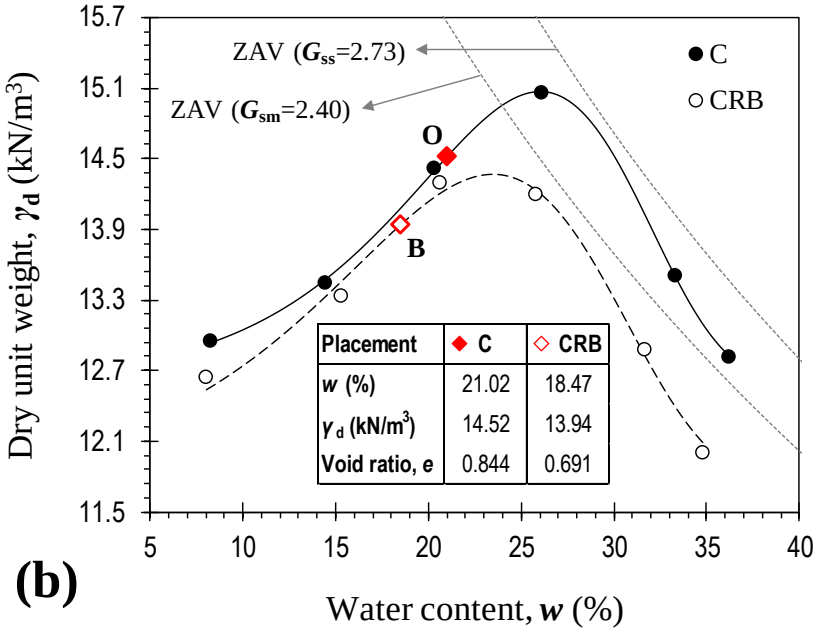

Figure 3. Swell–time curves during alternate wetting cycles: **(a)** C; **(b)** CRA; and **(c)** CRB.

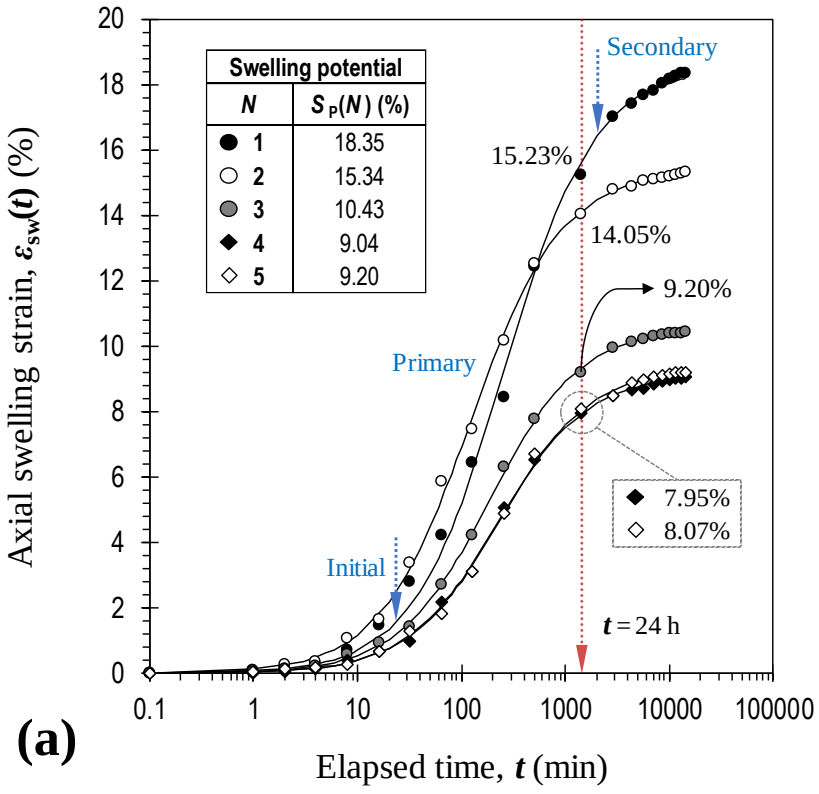

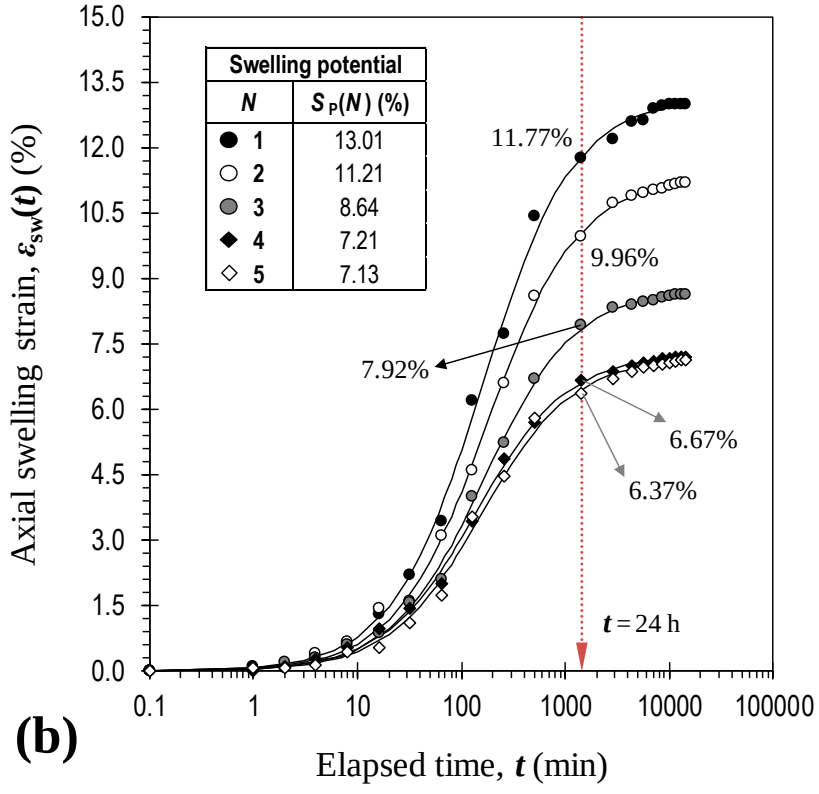

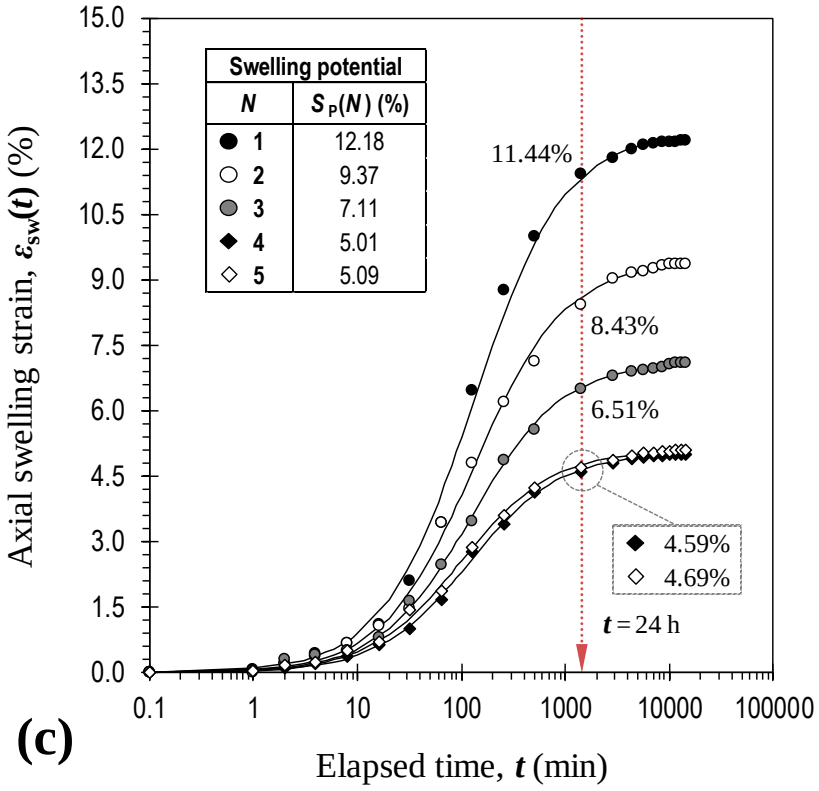
Swelling potential
N
$S_P(N)$ (%)
1 12.18
2 9.37
3 7.11
4 5.01
5 5.09
11.44%
8.43%
6.51%
4.59%
4.69%
t = 24 h
Axial swelling strain, $\varepsilon_{sw}(t)$ (%)
Elapsed time, t (min)
15.0
13.5
12.0
10.5
9.0
7.5
6.0
4.5
3.0
1.5
0.0
0.1
1
10
100
1000
10000
100000

(c)

Figure 4. Variations of swelling potential against the number of applied cycles for the tested samples.

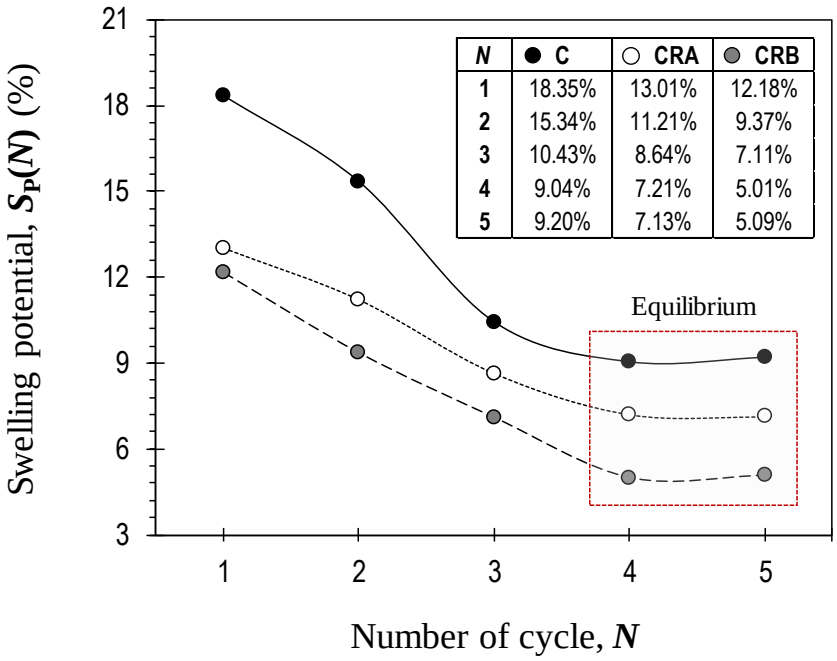

Figure 5. Rate of swelling for the tested samples during alternate wetting cycles: **(a)** primary swelling coefficient; and **(b)** secondary swelling coefficient.

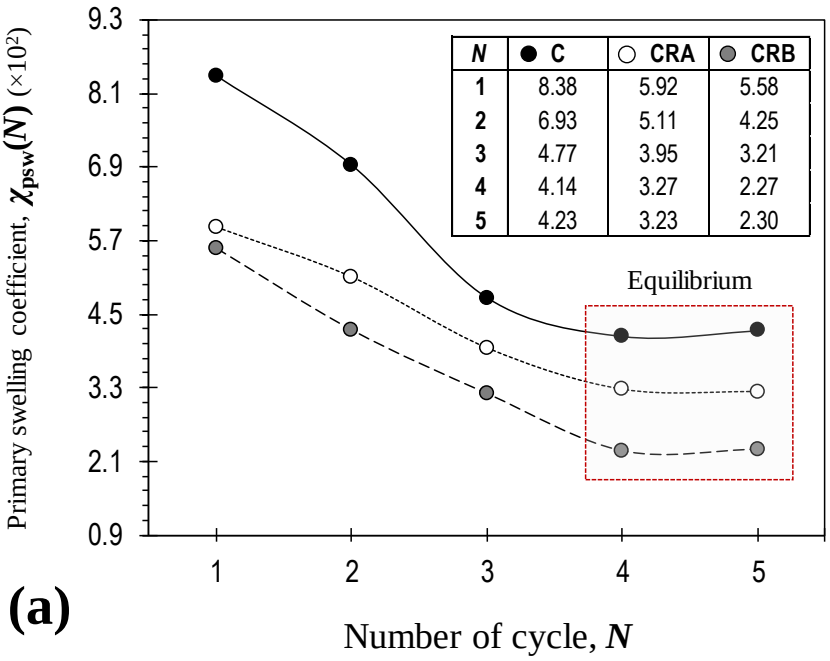

N	C	CRA	CRB
1	8.38	5.92	5.58
2	6.93	5.11	4.25
3	4.77	3.95	3.21
4	4.14	3.27	2.27
5	4.23	3.23	2.30

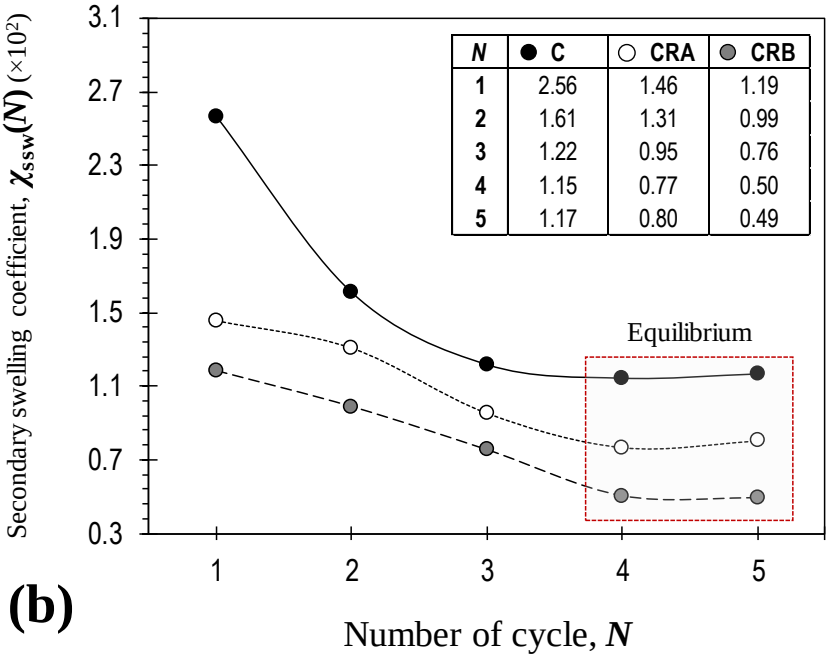

N	C	CRA	CRB
1	2.56	1.46	1.19
2	1.61	1.31	0.99
3	1.22	0.95	0.76
4	1.15	0.77	0.50
5	1.17	0.80	0.49

Figure 6. Variations of shrinkage potential against the number of applied cycles for the tested samples.

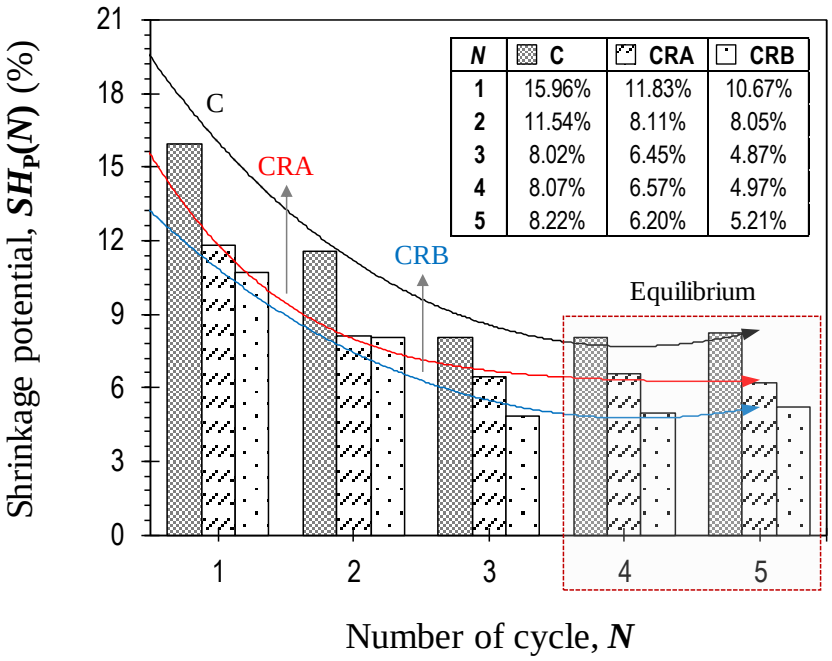

N	C	CRA	CRB
1	15.96%	11.83%	10.67%
2	11.54%	8.11%	8.05%
3	8.02%	6.45%	4.87%
4	8.07%	6.57%	4.97%
5	8.22%	6.20%	5.21%

Figure 7. Void ratio–water content shrinkage curves (at N=1 and 5) for the tested samples: **(a)** C/CRA; and **(b)** C/CRB.

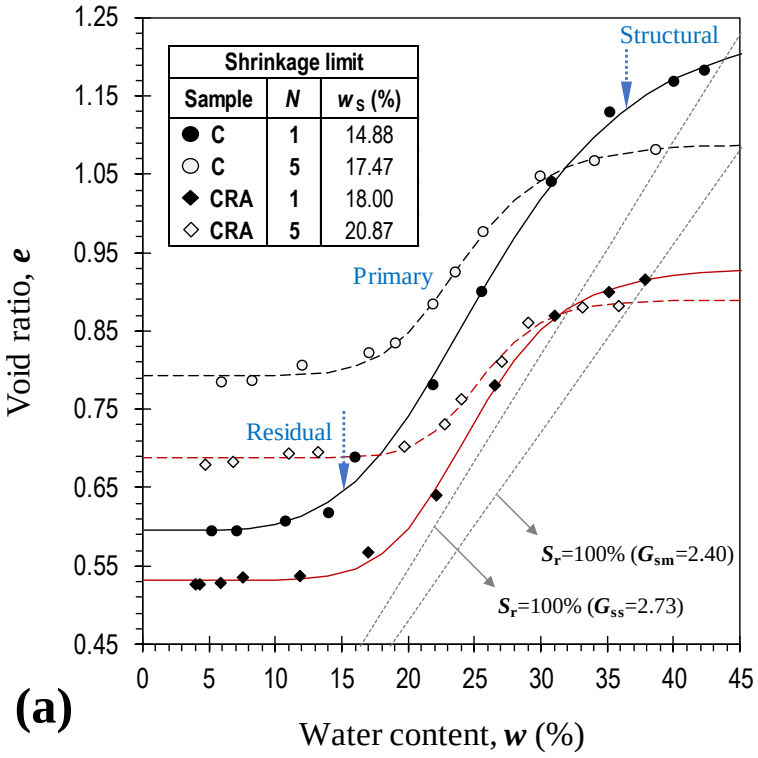

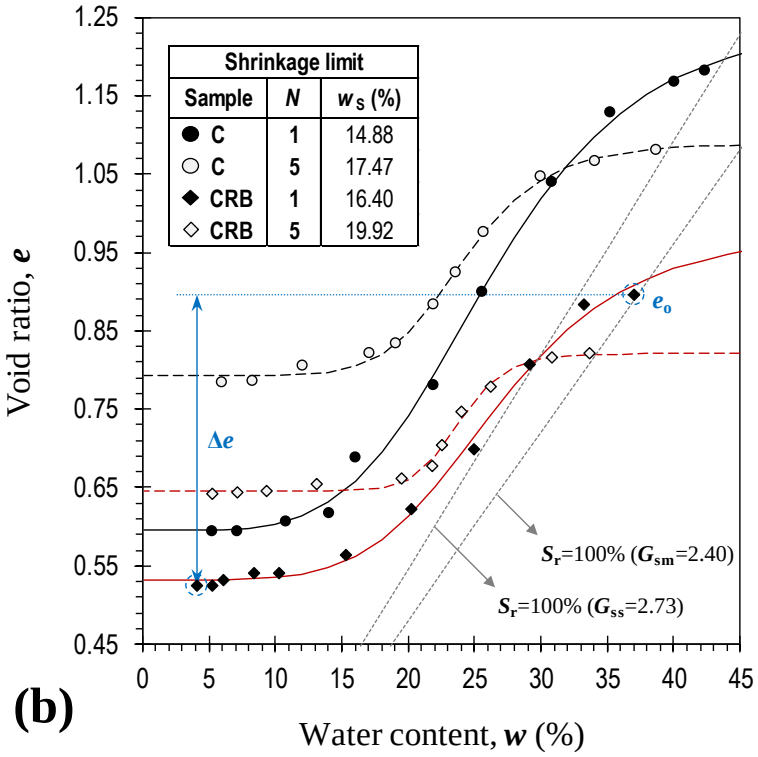

Figure 8. Swell–shrink patterns for the tested samples.

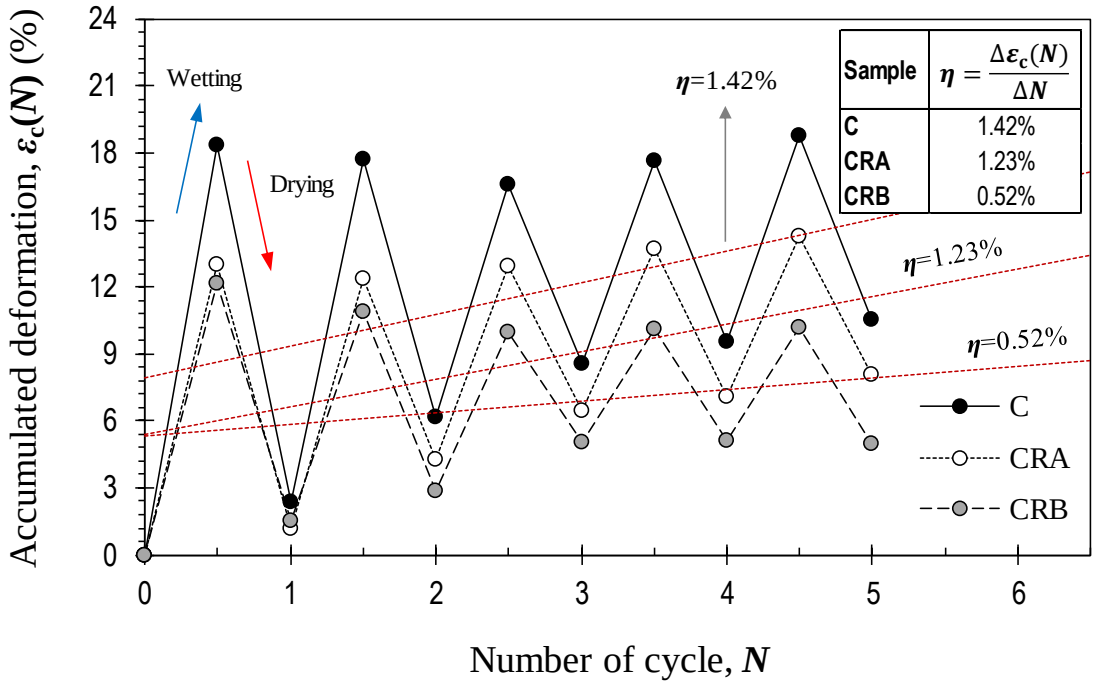

Figure 9. Scanning electron micrographs for the tested samples.

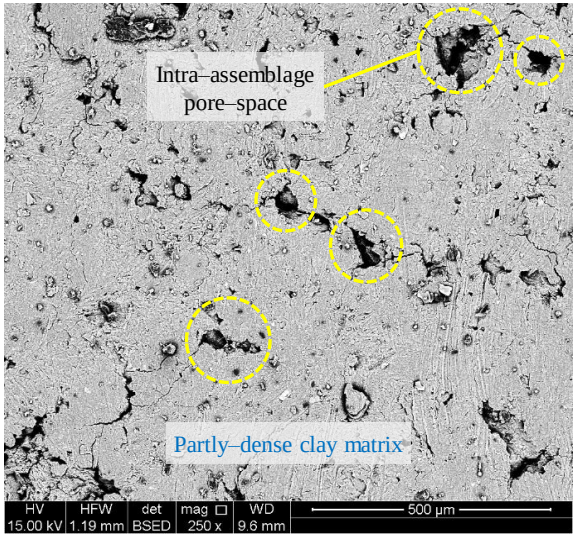

(a) Sample C (as–compacted)

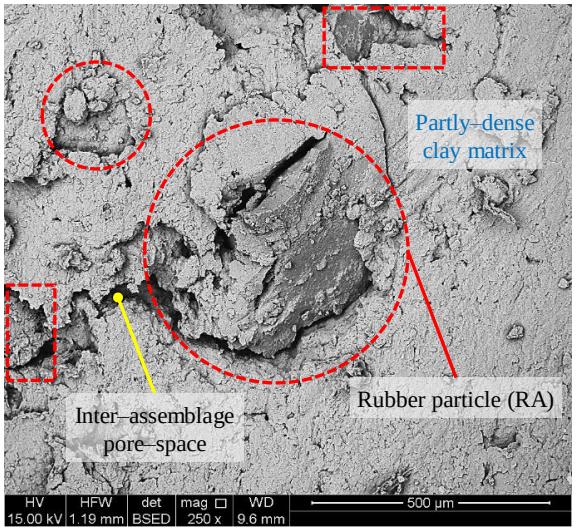

(c) Sample CRA (as–compacted)

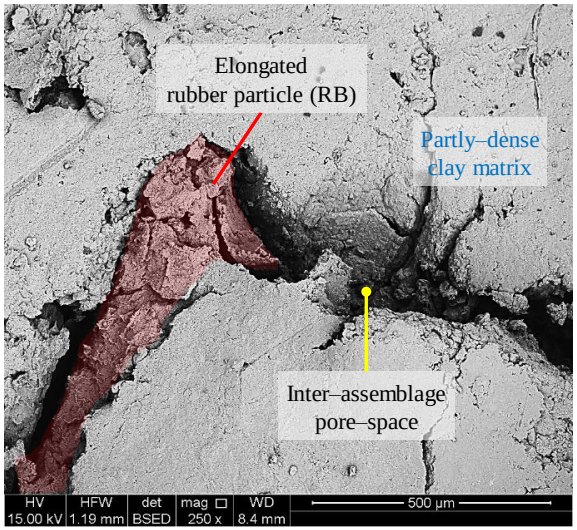

(e) Sample CRB (as–compacted)

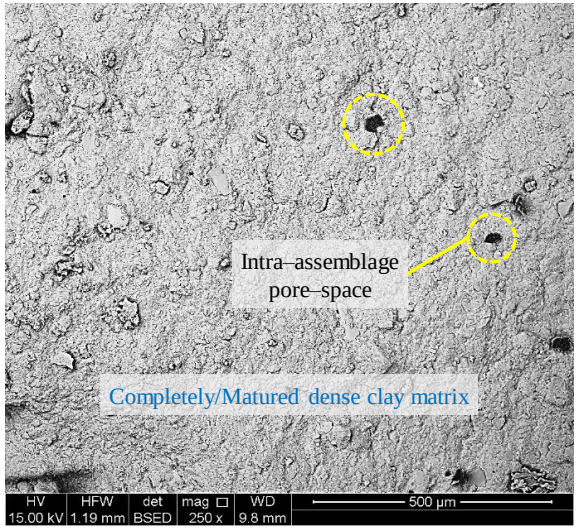

(b) Sample C (*N*=5)

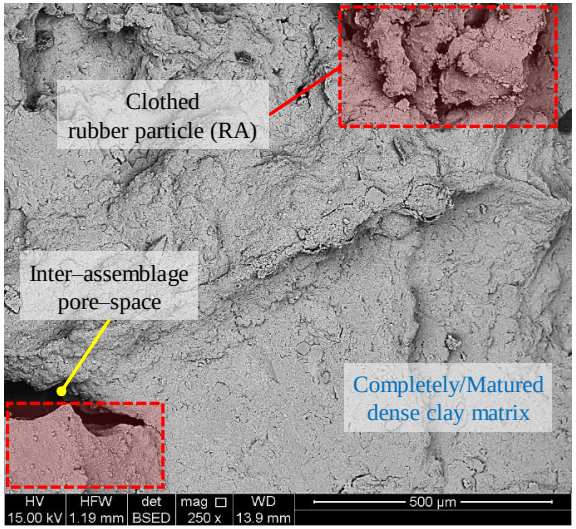

(d) Sample CRA (*N*=5)

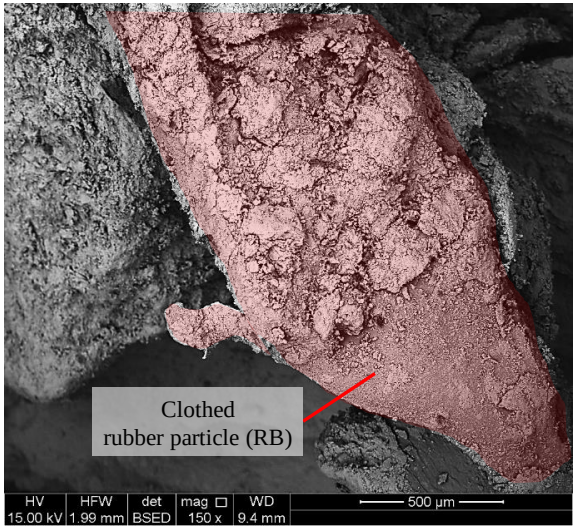

(f) Sample CRB (*N*=5)

Statement of Authorship

Statement of Authorship

Title of Paper	Swell–Shrink Behavior of Rubberized Expansive Clays During Alternate Wetting and Drying
Publication Status	☐ Published ☐ Accepted for Publication ☐ Submitted for Publication ■ Unpublished and Unsubmitted work written in manuscript style
Publication Details	**Soltani A**, Deng A, Taheri A and Mirzababaei M **(2018)** Swell–Shrink Behavior of Rubberized Expansive Clays During Alternate Wetting and Drying. ***x* x(x): x–x**, http://doi.org/x. **Note:** **Target Journals:** *Journal of Geotechnical and Geoenvironmental Engineering* [Link], *Geotechnical Testing Journal* [Link], *Geotextiles and Geomembranes* [Link], *Geosynthetics International* [Link], *Proceedings of the Institution of Civil Engineers–Ground Improvement* [Link]

Principal Author

Name of Principal Author (Candidate)	Amin Soltani (**Email:** Amin.Soltani@adelaide.edu.au)		
Contribution to the Paper	Overall paper preparation		
Overall percentage (%)	85%		
Certification:	This paper reports on original research I conducted during the period of my Higher Degree by Research candidature and is not subject to any obligations or contractual agreements with a third party that would constrain its inclusion in this thesis. I am the primary author of this paper.		
Signature		Date	08/10/2018

Co-Author Contributions

By signing the Statement of Authorship, each author certifies that:

i. the candidate's stated contribution to the publication is accurate (as detailed above);
ii. permission is granted for the candidate in include the publication in the thesis; and
iii. the sum of all co-author contributions is equal to 100% less the candidate's stated contribution.

Name of Co-Author	An Deng **Senior Lecturer**, School of Civil, Environmental and Mining Engineering, The University of Adelaide, Adelaide, SA 5005, Australia (**Email:** An.Deng@adelaide.edu.au)		
Contribution to the Paper	Paper review and revision		
Signature		Date	08/10/2018

Name of Co-Author	Abbas Taheri **Senior Lecturer**, School of Civil, Environmental and Mining Engineering, The University of Adelaide, Adelaide, SA 5005, Australia (**Email:** Abbas.Taheri@adelaide.edu.au)		
Contribution to the Paper	Paper review and revision		
Signature		Date	08/10/2018

Name of Co-Author	Mehdi Mirzababaei **Lecturer**, School of Engineering and Technology, Central Queensland University (CQU), Melbourne, VIC 3000, Australia (**Email:** M.Mirzababaei@cqu.edu.au)		
Contribution to the Paper	Paper review and revision		
Signature		Date	08/10/2018

1

Name of Co-Author	Sai K. Vanapalli **Professor**, Department of Civil Engineering, University of Ottawa, Ottawa, ON K1N 6N5, Canada (**Email:** Sai.Vanapalli@uottawa.ca)		
Contribution to the Paper	Paper review and revision		
Signature	**Note:** Sign–off by Principal Supervisor in place of this co–author who is based overseas. Co–author agreement in email is retained by Candidate.	Date	10/09/2018

Chapter 8

Rubber Powder–Polymer Combined Stabilization of South Australian Expansive Soils

Amin Soltani [a,†], An Deng [b], Abbas Taheri [c] and Mehdi Mirzababaei [d]

[a] **PhD Student** − School of Civil, Environmental and Mining Engineering, The University of Adelaide, Adelaide, SA 5005, Australia (**Email:** Amin.Soltani@adelaide.edu.au; **ORCID:** 0000-0002-0483-7487)

[b] **Senior Lecturer** − School of Civil, Environmental and Mining Engineering, The University of Adelaide, Adelaide, SA 5005, Australia (**Email:** An.Deng@adelaide.edu.au)

[c] **Senior Lecturer** − School of Civil, Environmental and Mining Engineering, The University of Adelaide, Adelaide, SA 5005, Australia (**Email:** Abbas.Taheri@adelaide.edu.au)

[d] **Lecturer** − School of Engineering and Technology, Central Queensland University, Melbourne, VIC 3000, Australia (**Email:** M.Mirzababaei@cqu.edu.au)

[†] **Correspondence:** Amin Soltani (**Email:** Amin.Soltani@adelaide.edu.au; **ORCID:** 0000-0002-0483-7487)

Publication Details: **Soltani A**, Deng A, Taheri A and Mirzababaei M **(2018)** Rubber Powder–Polymer Combined Stabilization of South Australian Expansive Soils. ***Geosynthetics International*** **25(3): 304–321**, http://doi.org/10.1680/jgein.18.00009.

Abstract

This study examines the combined capacity of rubber powder inclusion and polymer–treatment in solving the swelling problem of South Australian expansive soils. The rubber powder (1.18–0.075 mm) was incorporated into the soil at three different rubber contents (by weight) of 10%, 20% and 30%. The preliminary testing phase consisted of a series of consistency limits and free swell ratio tests, the results of which were analyzed to arrive at the optimum polymer concentration. The main test program included standard Proctor compaction, oedometer swell–compression, soil reactivity (shrink–swell index), cyclic wetting and drying, crack intensity,

and micro–structure analysis by means of the scanning electron microscopy (SEM) technique. The improvement in swelling potential and swelling pressure was dependent on the rubber content, with polymer–treated mixtures holding a notable advantage over similar untreated cases. A similar dependency was also observed for the crack intensity factor and the shrink–swell index. The beneficial effects of rubber inclusion were compromised under the cyclic wetting and drying condition. However, this influence was eliminated where the rubber powder was paired with the polymer agent. A rubber inclusion of 20%, preferably paired with 0.2 g/l polymer, was suggested to effectively stabilize South Australian expansive soils.

Keywords: Geosynthetics; Expansive soil; Rubber powder; Polymer; Swelling potential; Swelling pressure; Crack intensity; Cyclic wetting and drying.

Abbreviations

CH	clay with high plasticity
E^R	extremely reactive
H	highly expansive
H^R	highly reactive
L	lowly expansive
M	moderately expansive
M^R	moderately reactive
PC	polymer
pF	potential of free energy (a unit for soil suction)
SEM	scanning electron microscopy
S^R	slightly reactive
USCS	unified soil classification system
VH	very highly expansive

Notation[12]

C_c	coefficient of curvature (dimensionless)
CIF	crack intensity factor (%)
C_{ps}	primary swelling rate (dimensionless)
CRF	crack reduction factor (%)
C_{ss}	secondary swelling rate (dimensionless)
C_u	coefficient of uniformity (dimensionless)
d_{10}	particle diameter corresponding to 10% finer (m)
d_{30}	particle diameter corresponding to 30% finer (m)
d_{50}	particle diameter corresponding to 50% finer (m)
d_{60}	particle diameter corresponding to 60% finer (m)
d_{90}	particle diameter corresponding to 90% finer (m)
e_0	initial void ratio (dimensionless)
FSR	free swell ratio (dimensionless)
G_{sm}	specific gravity of soil–rubber mixture (dimensionless)
I_{ss}	shrink–swell index ($\%Pa^{-1}$)
LL	liquid limit (%)
LS	linear shrinkage (%)
n	number of wetting–drying cycle (dimensionless)
PI	plasticity index (%)
PL	plastic limit (%)

[12]Basic SI units are given in parentheses.

P_s	swelling pressure (Pa)
R_c	rubber content by dry weight of soil (%)
S_p	swelling potential (%)
$S_p(n)$	swelling potential with respect to the n^{th} wetting–drying cycle (%)
t	elapsed time of swelling (s)
t_{is}	completion time of the initial swelling phase (s)
t_{ps}	completion time of the primary swelling phase (s)
t_{ss}	completion time of the secondary swelling phase (s)
γ_{dmax}	maximum dry unit weight (N/m^3)
$\varepsilon_a(t)$	axial swelling strain with respect to elapsed time t (%)
ε_{ais}	initial swelling strain (%)
ε_{aps}	primary swelling strain (%)
ε_{ass}	secondary swelling strain (%)
ε_{sh}	ultimate shrinkage strain with respect to the shrink–swell index test (%)
ε_{sw}	ultimate swelling strain with respect to the shrink–swell index test (%)
ω_{opt}	optimum moisture content (%)

1. Introduction

Previous testing conducted in South Australia indicates that the majority of soils in the state are expansive clays. The predominant soils are Hindmarsh and Keswick clays, which are abundantly found in high–population commercial and residential areas. Where exposed to seasonal environments, such soils are prone to significant volume changes, i.e. heave and settlements, thereby bringing forth instability concerns to the overlying structures. These concerns have incurred a large amount of maintenance costs, and thus demand engineering solutions to alleviate the associated socio–economic impacts on human's life. Chemical stabilization by means of traditional cementitious agents such as cement and lime is often implemented as a common soil improvement technique (e.g. Al-Rawas et al. 2005; Estabragh et al. 2014; Soltani et al. 2017[a]). Though effective, the application of such agents is often limited by leaching problems, and in some cases, may result in adverse effects when treating soils containing large amounts of organic matter, sulfates and salts (Sivapullaiah et al. 2000; Puppala et al. 2004; Hoyos et al. 2006). Other disadvantages include their inherent time–dependency nature, reduction in material workability, low durability against local environmental conditions (e.g. acidic and alkaline flows), high transportation costs, and rising environmental concerns due to greenhouse gas emissions (Rao et al. 2001; Guney et al. 2007; Estabragh et al. 2013; Georgees et al. 2015; Alazigha et al. 2016). As the global community is shifting towards a more sustainable mindset, alternate stabilization techniques capable of replacing or minimizing the need for such traditional agents have been highly encouraged. Beneficial reuse of solid waste materials and industrial by–products, e.g. carpet waste fibers, kiln dusts, silicate/calcium chloride geopolymers and demolition wastes, can be regarded amongst the most well–received propositions in this context (e.g. Mirzababaei et al. 2013[a], 2013[b]; Arulrajah et al. 2017[a], 2017[b], 2017[c]; Kua et al. 2017; Mirzababaei et al. 2017[a], 2017[b]; Suksiripattanapong et al. 2017; Phummiphan et al. 2018).

In Australia, it is estimated that 48 million tires are disposed each year, meaning that there is a relative abundance of waste tires available for recycling and beneficial reuse (Hannam 2014). Similar to fiber–reinforced soils, the rubber assemblage randomly distributes in the soil regime, and where optimized in dosage and geometry, amends the expansive soil with respect to moisture insensitivity (i.e. swell–shrink related volume changes), strength increase, and ductility improvement (e.g. Cetin et al. 2006; Akbulut et al. 2007; Özkul and Baykal 2007; Seda et al. 2007; Patil et al. 2011; Trouzine et al. 2012; Kalkan 2013; Srivastava et al. 2014; Signes et al. 2016; Yadav and Tiwari 2017[a]). A literature survey indicates a rather common emphasis

on the application of coarse–graded tire rubber material, e.g. long tire rubber fibers. Such materials, however, would be associated with implementation difficulties when dealing with cohesive soils. On this basis, less regarded types of recycled tires such as tire rubber powder take the advantage of better workability, and thus add value if introduced to treat expansive soils.

Simple application procedures coupled with improved sustainability have promoted polymer–based additives as an attractive alternative to traditional cementitious agents. While commercially branded and readily accessible, such products have not yet received widespread acceptance among practicing engineers. This may be attributed to the lack of sufficient published data by independent establishments, and inadequate information provided by manufacturers regarding effective application rates or implementation procedures. A number of documented studies can be found which have assessed the efficiency of various polymer–based additives in treating expansive soils, thus mitigating the effect of swell–shrink related subsidence (e.g. Rauch et al. 2002; Inyang et al. 2007; Mirzababaei et al. 2009; Yazdandoust and Yasrobi 2010; Onyejekwe and Ghataora 2015; Alazigha et al. 2016; Ayeldeen and Kitazume 2017; Soltani et al. 2017[b]). Though promising, the reported results are not consistent on defining an ad hoc stabilization solution, and thus demands further examination.

The key to finding effective solutions to enhance the applications of expansive soils is to fundamentally understand their behavior in the face of changing moisture and temperature environments. For arid and semi–arid environments such as the Adelaide region of South Australia, this aspect is translated into alternate wetting and drying, incurred by changing periods of rainfall and drought. As such, prior promoting any stabilization technique as an effective scheme, its efficiency where exposed to periodic wetting and drying should be examined. A number of studies have assessed the volume change behavior of expansive soils treated with cementitious admixtures (e.g. Rao et al. 2001; Guney et al. 2007; Kalkan 2011; Estabragh et al. 2013) and polymer–based additives (e.g. Yazdandoust and Yasrobi 2010; Alazigha et al. 2016; De Camillis et al. 2017; Soltani et al. 2017[b]) during wetting and drying. However, the volume change behavior of expansive soil–rubber composites treated with polymer–based additives during wetting and drying has not yet been addressed in the literature.

The present study intends to examine the combined capacity of rubber powder inclusion and polymer–treatment in ameliorating the inferior engineering characteristics of a highly expansive soil found in Adelaide, South Australia. The experimental program was carried out

in two phases consisting of preliminary and main tests. The preliminary testing phase consisted of a series of consistency limits and free swell ratio tests. The main test program included standard Proctor compaction, oedometer swell–compression, soil reactivity (shrink–swell index), cyclic wetting and drying, desiccation–induced cracking, and micro–structure analysis by means of the scanning electron microscopy (SEM) technique.

2. Materials

2.1. Soil

A large quantity of expansive clay was sourced from a landfill site in Adelaide, South Australia and was used for this study. This soil was characterized as *clay with high plasticity* (CH) in accordance with the Unified Soil Classification System (USCS). Mechanical properties of the soil, determined as per relevant ASTM and Australian standards, are summarized in **Table 1**. The grain–size distribution curve, as illustrated in **Figure 1**, indicated a clay fraction (< 2 μm) of 44%, along with 36% silt (2–75 μm), 15% fine sand (0.075–0.425 mm), 4% medium sand (0.425–2 mm) and 1% coarse sand (2–4.75 mm). The swelling potential and free swell ratio (FSR) were, respectively, measured as 10.68% and 2.27, from which the soil was graded into *highly expansive* with respect to the classification criteria suggested by Seed et al. (1962) and Sridharan and Prakash (2000).

2.2. Tire Rubber Powder

Commercially available recycled tire rubber powder, supplied by a local distributor, was used to stabilize the expansive soil. **Figure 1** illustrates the grain–size distribution curve for the rubber particles, along with the used soil, determined as per the ASTM D422 (2007) standard. The rubber particles are similar in size to fine–medium sand, with particles ranging between 1.18 mm and 75 μm. The particle diameters corresponding to 10%, 30%, 50%, 60% and 90% finer (or passing) were measured as d_{10}=0.182 mm, d_{30}=0.334 mm, d_{50}=0.478 mm, d_{60}=0.513 mm and d_{90}=0.864 mm (see **Figure 1**). In addition, the uniformity (i.e. $C_u=d_{60}/d_{10}$) and curvature (i.e. $C_c=d_{30}^2/d_{10}d_{60}$) coefficients were determined as C_u=2.81 and C_c=1.20, from which the rubber particles were classified as *poorly–graded* in accordance with the USCS criterion. **Figure 2** illustrates microscopic micrographs of the rubber particles at different magnification ratios. The rubber particles are non–spherical and irregular in shape (see **Figure 2b** at 50x magnification), with some cavities and micro–cracks propagated along the rubber's

surface (see **Figure 2c** at 100x magnification), thus making for a rough surface texture. Such surface characteristics could potentially promote adhesion and/or induce interfacial friction between the rubber particles and the soil grains, thereby altering the soil fabric into a coherent matrix of restricted heave/settlement. Physical properties and chemical composition of the rubber particles, as supplied by the manufacturer, are provided in **Table 2**. The specific gravity (at 20 ^{o}C) was found to be 1.09, which is in compliance with that reported in the literature (see Yadav and Tiwari (2017[b]) for details).

2.3. Polymer

A commercially manufactured polymer agent, hereafter referred to as PC, was used as the binder. PC, chemically referred to as polyacrylamide or PAM (–$CH_2CHCONH_2$–), is a water–soluble anionic synthetic polymer formed from acrylamide subunits. The anionic polymerization is accomplished through substituting NH_2^- (amidogen) by OH^- (hydroxide) (Seybold 1994). PAM is often employed to increase the viscosity of water or to encourage flocculation of clay particles present in water (Seybold 1994; Lu et al. 2002; Graber et al. 2006). PC, in particular, has been successfully implemented in Australian roadway construction as a suitable binder for a variety of clays, shales and gravels (Andrews and Sharp 2010; Camarena 2013; Georgees et al. 2015). It is supplied in granular form, and often diluted with water (i.e. 200 g of PC into 1000 l of water, as recommended by the manufacturer) for application. Other properties include a specific gravity (at 25 ^{o}C) of 0.8 and a pH (at 25 ^{o}C) of 6.9.

3. Experimental Work

The rubber powder was incorporated into the soil at three different rubber contents (defined as rubber to dry soil weight ratio), i.e. R_c=10%, 20% and 30%. The experimental program was carried out in two phases consisting of preliminary and main tests. The preliminary testing phase included a series of consistency limits and free swell ratio tests. The intention of the preliminary testing phase was to identify a PC concentration rate capable of yielding an effective soil–rubber stabilization scheme. The natural soil and various soil–rubber mixtures were examined with three different PC concentrations (defined as weight of PC to volume of water ratio), i.e. 0.2 g/l (manufacturer–recommended), 0.4 g/l and 0.6 g/l. The consistency limits, i.e. liquid limit, plastic limit, plasticity index and linear shrinkage, were measured as per Australian standards (see relevant standard designations in **Table 1**). The free swell ratio is defined as the ratio of equilibrium sediment volume of 10 g oven–dried soil passing sieve 425

μm in water (or in the case of this study PC solution) to that of kerosene (Sridharan and Prakash 2000). As a consequence of rubber particles floating on water, only the natural soil was tested for the free swell ratio. Hereafter, the following coding system is adopted to designate the various mix designs:

$$NR_xP_y \quad (1)$$

where N=natural soil; R_x=x% rubber (x=0, 10%, 20% and 30%); and P_y=y g/l PC (y=0, 0.2 g/l, 0.4 g/l and 0.6 g/l). The natural with no additives is, therefore, denoted as NR_0P_0. As a typical example, $NR_{20}P_{0.4}$ represents the natural soil mixed with 20% rubber and treated with 0.4 g/l PC. A total of 16 mix designs were tested for consistency limits during the preliminary testing phase, whereas only four scenarios, i.e. NR_0P_0, $NR_0P_{0.2}$, $NR_0P_{0.4}$ and $NR_0P_{0.6}$., were considered for the free swell ratio test.

The main test program was carried out on the natural soil and various soil–rubber mixtures without and with the optimum PC concentration. Hereafter, the former will be referred to as untreated, while the latter will be denoted as treated. The optimum PC concertation was selected as 0.2 g/l based on the preliminary test results, which will be further discussed in **Section 4.1**. The main test program consisted of the following tests: **i)** standard Proctor compaction; **ii)** oedometer swell–compression; **iii)** soil reactivity (shrink–swell index); **iv)** cyclic wetting and drying; **v)** desiccation–induced cracking; and **vi)** micro–structure (SEM) analysis. The methodology associated with each component of the main test program will be further outlined in detail.

3.1. Compaction Studies and Sample Preparation

A series of standard Proctor compaction tests were carried out on the natural soil (NR_0P_0) and various soil–rubber mixtures, untreated and treated with 0.2 g/l PC, in accordance with the ASTM D698 (2012) standard. Samples for the oedometer swell–compression, soil reactivity (shrink–swell index), cyclic wetting and drying and SEM tests were prepared by the static compaction technique at the corresponding optimum moisture content and maximum dry unit weight of each mixture (see **Table 3**). The required amount of water or PC solution (with 0.2 g/l concentration) corresponding to the desired optimum moisture content was added to each mixture, and thoroughly mixed by hand. Extensive care was dedicated to pulverize the lumped particles, targeting homogeneity of the mixtures. Mixtures were then enclosed in plastic bags

and stored under room temperature conditions for 24 hours, ensuring even distribution of moisture throughout the soil mass. A special split mold, similar to that described in Soltani et al. (2017[a]), was designed and fabricated from stainless steel to accomplish static compaction. The mold consisted of three sections, i.e. the top collar, the middle oedometer ring, and the bottom collar. The oedometer ring measures 50 mm in diameter and 20 mm in height, and accommodates the sample for oedometer testing conditions. The moist mixtures were compressed in the mold at three layers by a constant displacement rate of 1.5 mm/min to a specific compaction load, each layer having attained the desired/target maximum dry unit weight. The surface of the first and second compacted layers were scarified to ensure a good bond between adjacent layers of the mixture. Samples for the simplified core shrinkage test (i.e. a component of the soil reactivity test, as further outlined in **Section 3.3**) were prepared in a similar fashion. In this case, however, a different mold with a middle section measuring 50 mm in diameter and 100 mm in height, along with five compaction layers, was adopted. As a consequence of rubber particles floating on water, standard procedures outlined in the ASTM D854 (2014) standard for measuring the specific gravity of particles were not applicable. Therefore, the average specific gravity of various soil–rubber mixtures was estimated by the following theoretical equation (Trouzine et al. 2012):

$$G_{sm} = \frac{G_{ss} G_{sr} (w_s + w_r)}{w_s G_{sr} + w_r G_{ss}} \tag{2}$$

where G_{sm}=specific gravity of soil–rubber mixture; w_{ss}=weight of dry soil; w_r=weight of rubber particles; G_{ss}=specific gravity of soil solids (=2.67); and G_{sr}=specific gravity of rubber particles (=1.09).

Basic mechanical properties of the prepared samples used for the main tests are summarized in **Table 3**. A total of eight mix designs, divided into two groups of untreated (designated as NR_0P_0, $NR_{10}P_0$, $NR_{20}P_0$ and $NR_{30}P_0$) and treated with 0.2 g/l PC (designated as $NR_0P_{0.2}$, $NR_{10}P_{0.2}$, $NR_{20}P_{0.2}$ and $NR_{30}P_{0.2}$), were considered for the main experimental program.

3.2. Oedometer Swell–Compression Test

The prepared samples were subjected to a series of oedometer swell–compression tests as specified in the ASTM D4546 (2014) standard. The test included two stages, i.e. swell and compression. In the first stage, the desired sample was allowed to freely swell under a low

nominal overburden stress of σ'_0=7 kPa. The incurred axial swelling strain or heave was recorded during various time intervals to a point in which swell–time equilibrium, a state corresponding to the sample's swelling potential (defined as the ultimate axial swelling strain), was achieved. During the compression stage, the swollen sample was gradually loaded to counteract the built–up axial swelling strain. The stress required to retain the sample's initial placement condition (or void ratio e_0, as outlined in **Table 3**) was taken as the swelling pressure (Sridharan et al. 1986).

The conventional oedometer swell test has been regarded as the most common technique to assess the soil's expansive potential or degree of expansivity (Sridharan and Keshavamurthy 2016). Some limitations, however, include its dependency to the sample's initial moisture condition and not accounting for suction variations. Some of the more common classification procedures for expansive soils, developed with respect to percent expansion in oedometer under σ'_0=7 kPa (Holtz and Gibbs 1956; Seed et al. 1962; Sridharan and Prakash 2000), are summarized in **Table 5**.

3.3. Soil Reactivity Test and the Shrink–Swell Index

The shrink–swell index, determined in accordance with the AS 1289.7.1.1 (2003) standard, can be characterized as a direct method of evaluating the soil's degree of expansivity (referred to as reactivity in Australian geotechnical practice). Other significant applications include its widespread use for predicting free surface ground movements (Cameron 1989; Fityus et al. 2005; Li et al. 2016). Despite its successful adoption in routine geotechnical practice in Australia, its existence and use within Australia have not been widely recognized by the international geotechnical community (Fityus et al. 2005). The shrink–swell index requires incorporating test results obtained from the simplified core shrinkage and the modified oedometer swell tests, which are further presented in detail:

- In the simplified core shrinkage test, the desired cylindrical sample, measuring 50 mm in diameter and 100 mm in height (see **Section 3.1**), is allowed to desiccate under room temperature conditions. The variations of axial shrinkage strain is monitored during various time intervals to a point in which shrinkage ceases. The sample is then oven–dried at 105 ^{o}C to remove any remaining moisture. Final height measurements are taken by a Vernier caliper, from which the sample's ultimate shrinkage strain, denoted as ε_{sh}, can be derived.

- The modified oedometer swell test is essentially similar to the first stage of the oedometer swell–compression test, as outlined in **Section 3.2**. In this case, however, a higher nominal overburden stress equal to σ'_0=25 kPa is adopted. The ultimate axial swelling strain upon achieving swell–time equilibrium is denoted as ε_{sw}.

Finally, the shrink–swell index I_{ss} is obtained by the following (AS 1289.7.1.1 2003):

$$I_{ss} = \frac{\varepsilon_{sh} + \frac{1}{2}\varepsilon_{sw}}{1.8} \quad (3)$$

The denominator in **Equation 3** is an empirical coefficient, which is defined as the range of total suction change with respect to the soil's volume increase from air–dry to near saturation condition. The range of total suction change is commonly taken as 1.8 pF (pF=potential of free energy, which is a unit for soil suction and is related to kilopascals through pF=1+log[kPa]) for the majority of reactive soils in Australia. This value was suggested based on collective experience of the AS 2870 (2011) code committee, and is supported by the observation that the majority of volume change takes place in a linear manner between the wilting point for trees and a moisture content close to saturation (Fityus et al. 2005). Previous studies have reported the wilting point suction to vary between 4.0 pF and 4.4 pF (Wray 1998; Cameron 2001). Furthermore, the variations of total suction at moisture contents near saturation state have been reported to fall in the range of 2.2 pF to 2.5 pF (Fityus et al. 2005). As such, the suggested value of 1.8 pF can be deemed as reasonable. The shrink–swell index represents percentage axial strain, either swelling or shrinkage, per change in unit suction of the soil (i.e. $\%pF^{-1}$). Thus, it is expected to address some limitations associated with other expansive soil classification criteria which are either dependent on the soil's initial moisture condition or do not account for suction variations (e.g. the conventional oedometer swell test, as outlined in **Table 5**). Classification procedures for expansive soils with respect to the shrink–swell index, as suggested by Seddon (1992), are summarized in **Table 6**.

3.4. Cyclic Wetting and Drying Test

Similar to the first step in the oedometer swell–compression test (see **Section 3.2**), the desired sample was allowed to freely swell under σ'_0=7 kPa resulting from a cylindrical load directly applied to the sample. Upon completion of the wetting process (i.e. achieving swell–time equilibrium), reservoir water was drained through a drainage valve embedded within the oedometer cell. The oedometer cell, along with the cylindrical load, were then transferred to an

oven set to a constant temperature of 40 °C for drying. The drying process was carried out for about five days to ensure shrinkage equalization. The combination of one wetting and the subsequent drying stage is designated as one wetting–drying cycle. Alternate wetting and drying of the sample was repeated in a similar fashion to a point in which the swelling potential subject to two successive cycles reached a nearly constant value. In this study, four mix designs, i.e. NR_0P_0, $NR_{30}P_0$, $NR_0P_{0.2}$ and $NR_{30}P_{0.2}$, were tested for cyclic wetting and drying.

The swelling potential may either decrease or increase with increase in number of applied wetting–drying cycles, and regardless of the observed trend, further converges to a nearly constant value upon the completion of several cycles (Soltani et al. 2017[b]). This state is defined as swell–shrink (or elastic) equilibrium, which signifies a transitional deformation state where the plastic (or irreversible) deformation incurred in the soil structure (during wetting and drying) largely fades out, and thus change to elastic (or reversible) in character (Tripathy et al. 2002; Alonso et al. 2005; Estabragh et al. 2015). In this study, the equilibrium condition was achieved at the fourth cycle, thus only five cycles were implemented for the tested samples.

3.5. Desiccation–Induced Crack Studies

Desiccation–induced cracking can adversely influence the performance of various soil structures (e.g. excavations, earth slopes, highway embankments and clay liners), and thus assumes a significant role in fulfilling design criteria when constructing on expansive soils. The intensity of cracks is commonly quantified by means of the crack intensity factor (CIF) and the crack reduction factor (CRF), which are defined as (Yesiller et al. 2000; Miller and Rifai 2004):

$$\mathrm{CIF} = \frac{A_c}{A_0} \times 100 \tag{4}$$

$$\mathrm{CRF} = \frac{\mathrm{CIF_n} - \mathrm{CIF_s}}{\mathrm{CIF_n}} \tag{5}$$

where A_c=area of cracks; A_0=initial area of the tested sample; CIF_n=crack intensity factor for the natural soil (NR_0P_0); and CIF_s=crack intensity factor for the stabilized sample.

Desiccation–induced crack tests were carried out on the natural soil and various soil–rubber mixtures (untreated and treated with 0.2 g/l PC) prepared by the slurry technique at their respective liquid limit, as commonly adopted in the literature (e.g. Tang et al. 2012; Costa et al.

2013; Chaduvula et al. 2017). The required amount of water or PC solution corresponding to the desired liquid limit (see **Table 3**) was added to each mixture, and thoroughly mixed to obtain slurries of uniform consistency. The resultant slurries were poured into petri dishes, measuring 100 mm in diameter and 15 mm in height, and gently tapped on a wooden platform to remove entrapped air. To simulate severe ambient conditions of the Adelaide region, samples were allowed to desiccate under a constant temperature of 40 ^{o}C. Upon the completion of drying (moisture equalization), still photographs were taken using a high resolution digital camera fixed at a vertical angle 50 cm above the desiccated samples. The ImageJ software package was then implemented to quantify the crack features.

3.6. Scanning Electron Microscopy (SEM)

Significant information on the micro–structure can be obtained by the scanning electron microscopy (SEM) technique. Typical mixtures including NR_0P_0, $NR_{20}P_0$, $NR_0P_{0.2}$ and $NR_{20}P_{0.2}$ were investigated. The desired samples, prepared as per **Section 3.1**, were allowed to air–dry for about 14 days. The samples were then carefully fractured into small cubic–shaped pieces corresponding to a volume of approximately 1 cm^3, as suggested in the literature (e.g. Tang et al. 2007; Mirzababaei et al. 2009; Yazdandoust and Yasrobi 2010), and further scanned over various magnification ratios ranging from 250x to 20,000x. In this study, the Philips XL20 SEM device, with a resolution of 4 μm and a maximum magnification ratio of 50,000x, was used for scanning electron microscopy imaging.

4. Results and Discussion

4.1. Consistency Limits and the Free Swell Ratio

Figures 3a, **3b** and **3c** illustrate the variations of liquid limit *LL*, plasticity index *PI* and linear shrinkage *LS* against PC concentration for the tested mix designs (i.e. NR_xP_y; where x=0, 10%, 20% and 30%, and y=0, 0.2 g/l, 0.4 g/l and 0.6 g/l), respectively. Untreated soil–rubber mixtures (NR_xP_0) exhibited lower consistency limits compared with that of the natural soil (NR_0P_0). In this case, the higher the rubber content the lower the consistency limits, following a monotonic decreasing trend. For instance, the natural soil resulted in *LL*=78.04%, while the inclusion of 10%, 20% and 30% rubber resulted in *LL*=73.32%, 68.59% and 65.58%, respectively. It is well–accepted that the consistency limits are primarily a function of the mixture's clay content. An increase in rubber content substitutes a larger portion of the clay content, and thus leads to

lower consistency limits. The lower specific surface area and water adsorption capacity of the rubber particles compared with the soil grains also contributes to lower consistency limits (Cetin et al. 2006; Trouzine et al. 2012; Srivastava et al. 2014). As a result of PC–treatment, the natural soil experienced a notable increase in the consistency limits. The magnitude of increase, however, was observed to be independent from the adopted PC concertation, as all three concentrations exhibited similar results with marginal differences (see NR_0P_y in **Figure 3**). As a typical case, *LL* increased from 78.04% for the natural soil (NR_0P_0) to 87.61%, 87.22% and 85.80% for $NR_0P_{0.2}$, $NR_0P_{0.4}$ and $NR_0P_{0.6}$, respectively. An increase in the consistency limits, the liquid limit in particular, implies that a flocculated fabric dominates the clay–rubber matrix (Mitchell and Soga 2005). As opposed to a face–to–face aggregated (or dispersed) fabric, an edge–to–face flocculated fabric offers more resistance to shear (or cone penetration), thereby leading to an increased liquid limit. PAM molecules are hydrophilic in nature, and thus provide additional adsorption sites for water molecules, which in turn contributes to higher consistency limits (Kim and Palomino 2009).

The location of the tested mix designs on Cassgrande's plasticity chart is illustrated in **Figure 4**. All mixtures lie within the CH region (*clay with high plasticity*) of the plasticity chart. The variations of *PI* against *LL* followed a linear path nearly parallel to the A–line of the plasticity chart, i.e. $PI=0.73(LL-20)$. In this case, a conventional regression analysis indicated the existence of a strong linear agreement in the form of $PI=0.77(LL-6.84)$ (with $R^2=0.989$) for the tested mixtures. For a given PC concentration, an increase in rubber content relocated the soil towards lower plasticity regions (e.g. see the typical linear trendline for NR_xP_0 in **Figure 4**). On the contrary, for a given soil–rubber mixture (constant rubber content), PC–treatment repositioned the soil towards higher plasticity regions (e.g. see the typical arrowed path linking NR_0P_0 to NR_0P_y in **Figure 4**). The magnitude of increase in *LL* and *PI*, however, was observed to be independent from the adopted PC concentration, as evident with the clustering of data points at constant rubber contents (compare $NR_xP_{0.2}$ with $NR_xP_{0.4}$ and $NR_xP_{0.6}$ in **Figure 4** at any arbitrary x value).

Results of the free swell ratio tests are summarized in **Table 4**. Suspension of the soil in distilled water (NR_0P_0) resulted in a free swell ratio of FSR=2.27. Where suspended in PC solutions of 0.2 g/l, 0.4 g/l and 0.6 g/l, FSR was measured as 1.67, 1.63 and 1.53, respectively. Classification procedures for expansive soils with respect to the FSR value, as suggested by Sridharan and Prakash (2000), are outlined in **Table 4**. The natural soil was classified as *highly expansive*, while PC–treated mixtures ($NR_0P_{0.2}$, $NR_0P_{0.4}$ and $NR_0P_{0.6}$) manifested a *moderate* degree of

expansivity. As evident with the FSR values and their corresponding classifications, excessive PC concentrations, i.e. 0.4 g/l and 0.6 g/l, seem not to provide additional improvements.

Basic geotechnical properties such as the consistency limits and the free swell ratio can be employed to infer the soil's fabric, and thus arrive at initial judgements on the performance of various polymer agents at different concentrations (Worth and Wood 1978; Prakash and Sridharan 2004; Mitchell and Soga 2005). Taking into account the discussed results, the three adopted PC concentrations were observed to yield similar results with marginal differences. Therefore, the manufacturer–recommended concentration of 0.2 g/l was deemed as satisfactory, and thus was used for the main tests the results of which will be further presented and discussed in detail.

4.2. Compaction Characteristics

Standard Proctor compaction curves, along with corresponding zero air void (ZAV) saturation lines, for the natural soil (NR_0P_0) and various soil–rubber mixtures untreated and treated with 0.2 g/l PC are provided in **Figures 5a** and **5b**, respectively. As a result of rubber inclusion, the natural soil exhibited a notable reduction in both the maximum dry unit weight γ_{dmax} and the optimum moisture content ω_{opt} (see the trendline in **Figure 5a**). As a result of PC–treatment, a marginal increase in both γ_{dmax} and ω_{opt} was noted for the natural soil (compare NR_0P_0 with $NR_0P_{0.2}$ in **Figure 5b**), while treated soil–rubber mixtures exhibited a trend similar to that observed for similar untreated cases (see the trendline in **Figure 5b**). Decrease in γ_{dmax} and ω_{opt} as a result of the rubber inclusions can be attributed to the lower specific gravity, specific surface area and water adsorption capacity of the rubber particles compared with the soil grains (Akbulut et al. 2007; Özkul and Baykal 2007; Seda et al. 2007; Kalkan 2013; Signes et al. 2016).

4.3. Swelling Characteristics

4.3.1. Swelling Potential and Swelling Pressure

Swell–time curves, represented by the two–parameter rectangular hyperbola function (e.g. Sivapullaiah et al. 1996; Sridharan and Gurtug 2004; Soltani et al. 2017[a]), for the natural soil (NR_0P_0) and various soil–rubber composites untreated and treated with 0.2 g/l PC are provided in **Figures 6a** and **6b**, respectively. As a result of rubber inclusion and/or PC–treatment, the swell–time locus experienced a major downward shift over the ε_a:log$t$ space (ε_a=axial swelling

strain; and t=time), indicating a significant reduction in the magnitude of exhibited swelling strain, and thus swelling potential (defined as the ultimate axial swelling strain) compared with the natural soil. At t=24 hr, for instance, the natural soil resulted in a swelling strain of $\varepsilon_a(t)$=9.65%, while the inclusion of 10%, 20% and 30% rubber resulted in $\varepsilon_a(t)$=7.55%, 6.35% and 4.85%, respectively (see **Figure 6a**). Similar treated samples exhibited a more pronounced decreasing trend, where the above given values dropped to $\varepsilon_a(t)$=6.45% ($NR_0P_{0.2}$), 5.25%, 3.25% and 2.43%, respectively (see **Figure 6b**). The natural soil and soil–rubber mixtures corresponding to R_c=10%, 20% and 30% resulted in swelling potential values of S_p=10.68%, 8.48%, 7.26% and 5.73%, respectively. As a result of PC–treatment, however, the aforementioned values further decreased to S_p=7.15%, 6.20%, 4.28% and 3.20%, respectively.

Figure 7 illustrates the variations of swelling pressure and swelling potential against rubber content for the tested samples. The variations of swelling pressure P_s followed a trend similar to that observed for swelling potential S_p, and indicated that, the higher the rubber content the greater the reduction in S_p and P_s, with treated samples holding a notable advantage over similar untreated cases (compare NR_xP_0 with $NR_xP_{0.2}$ in **Figure 7**). The natural soil (NR_0P_0) and soil–rubber mixtures corresponding to R_c=10%, 20% and 30% resulted in P_s=235 kPa, 131 kPa, 124 kPa and 93 kPa, respectively. Where treated with 0.2 g/l PC, these values dropped to P_s=165 kPa ($NR_0P_{0.2}$), 107 kPa, 86 kPa and 35 kPa, respectively. The classification criterion proposed by Seed et al. (1962) (see **Table 5**) was implemented to assess the expansive potential of the tested samples, and the results are depicted in **Figure 7**. The two mix designs containing 30% rubber inclusion ($NR_{30}P_0$ and $NR_{30}P_{0.2}$) were classified as *moderately expansive* (specified as 'M'), while other samples were graded into *highly expansive* (specified as 'H').

As demonstrated in **Figure 8**, the evolution of swelling with time, represented by an S–shaped curve over the ε_a:log$t$ space, takes place at three stages, i.e. the initial, primary and secondary swelling (Sivapullaiah et al. 1996; Sridharan and Gurtug 2004; Rao et al. 2006; Soltani et al. 2017[b], 2018). The initial swelling phase, also recognized to as inter–void swelling, occurs at macro–structural level, and results in small volume changes mainly less than 10% of the total volume increase (< 10%S_p). The primary swelling phase constitutes for up to 80% of the total volume increase (≈ 80%S_p), and is graphically represented by a steep–sloped linear portion bounded by the initial and primary swelling time margins. The secondary swelling phase takes place as a result of double–layer repulsion, and accounts for small time–dependent volume changes. As opposed to the initial swelling phase, both the primary and secondary swelling phases evolve at micro–structural level where swelling of active clay minerals takes place.

Critical variables obtained from the *S*–shaped curve, defined as swell–time characteristics, can be adopted to describe the time–dependency nature of the swelling phenomenon. These variables, as outlined in **Figure 8**, are characterized as: **i)** completion time of the initial and primary swelling phases (t_{is} and t_{ps}); **ii)** initial, primary and secondary swelling strains (ε_{ais}, ε_{aps} and ε_{ass}; $S_p=\varepsilon_{ais}+\varepsilon_{aps}+\varepsilon_{ass}$); and **iii)** primary and secondary swelling rates (C_{ps} and C_{ss}), which are defined as (Soltani et al. 2018):

$$C_{ps}=\frac{\Delta\varepsilon_a}{\Delta\log t}\Bigg]_{t=t_{is}}^{t=t_{ps}}=\frac{\varepsilon_{aps}}{\log\left(\frac{t_{ps}}{t_{is}}\right)} \tag{6}$$

$$C_{ss}=\frac{\Delta\varepsilon_a}{\Delta\log t}\Bigg]_{t=t_{ps}}^{t=t_{ss}}=\frac{\varepsilon_{ass}}{\log\left(\frac{t_{ss}}{t_{ps}}\right)} \tag{7}$$

where t_{ss}=completion time of the secondary swelling phase (=14,400 min).

Swell–time characteristics for the tested samples are summarized in **Table 7**. The primary and secondary swelling strains mainly demonstrated a trend similar to that observed for the swelling potential S_p, meaning that R_c=30% promoted the lowest ε_{aps} and ε_{ass} values for both untreated and treated soil–rubber mixtures (see $NR_{30}P_0$ and $NR_{30}P_{0.2}$ in **Table 7**). **Figures 9a** and **9b** illustrate the variations of C_{ps} and C_{ss} against rubber content for the tested samples, respectively. The rubber inclusions led to a noticeable reduction in both C_{ps} and C_{ss}, indicating a capacity of counteracting the heave in both magnitude and time. The higher the rubber content the lower the swelling rates, following a monotonic decreasing trend, with treated samples exhibiting more efficiency in reducing C_{ps} and C_{ss} compared with similar untreated cases (compare NR_xP_0 with $NR_xP_{0.2}$ in **Figure 9**). For the natural soil (NR_0P_0), C_{ps} and C_{ss} were measured as 4.85×10^{-2} and 1.07×10^{-2}, respectively. As optimal cases, these values, respectively, dropped to 2.63×10^{-2} and 7.06×10^{-3} for $NR_{30}P_0$, and 1.50×10^{-2} and 5.28×10^{-3} for $NR_{30}P_{0.2}$.

4.3.2. Shrink–Swell Index

Variations of the shrinkage and swelling strains, i.e. ε_{sh} and ε_{sw}, along with corresponding shrink–swell index values, are provided in **Figure 10**. Increase in rubber content led to a noticeable reduction in both ε_{sh} and ε_{sw}, and thus the shrink–swell index I_{ss}. For the treated

cases, however, a more pronounced decreasing trend can be observed (compare NR_xP_0 with $NR_xP_{0.2}$ in **Figure 10**). The degree of expansivity, in this case referred to as reactivity, was characterized in accordance with the Seddon (1992) classification criterion (see **Table 6**), and the results are depicted in **Figure 10**. The natural soil (NR_0P_0) was graded into *highly reactive* (H^R) corresponding to I_{ss}=4.21 $\%pF^{-1}$. For untreated cases, R_c=10%, 20% and 30% resulted in I_{ss}=3.30 $\%pF^{-1}$, 2.12 $\%pF^{-1}$ and 1.49 $\%pF^{-1}$, and thus classified as *moderately*/*highly reactive* (M^R/H^R), *moderately reactive* (M^R) and *slightly reactive* (S^R), respectively. Where treated with 0.2 g/l PC, the aforementioned values dropped to I_{ss}=2.51 $\%pF^{-1}$ (M^R), 1.88 $\%pF^{-1}$ (M^R), 1.80 $\%pF^{-1}$ (M^R) and 1.04 $\%pF^{-1}$ (S^R), respectively.

4.3.3. Amending Mechanisms

Similar to fiber–reinforced soils, the rubber inclusions are able to amend the soil fabric through improvements achieved in three aspects: **i)** increase in non–expansive fraction, which is a function of rubber content; **ii)** interlocking of rubber particles and soil grains; and **iii)** interfacial frictional resistance generated as a result of soil–rubber contact (Tang et al. 2007; Al-Akhras et al. 2008; Viswanadham et al. 2009[a], 2009[b]; Tang et al. 2010; Patil et al. 2011; Trouzine et al. 2012; Kalkan 2013; Estabragh et al. 2014; Phanikumar and Singla 2016; Soltani et al. 2018; Yadav and Tiwari 2017[a]). The randomly distributed rubber particles resemble a spatial three–dimensional network in favor of weaving (or interlocking) the soil grains into a coherent matrix of restricted heave. The greater the number of included rubber particles (i.e. increase in rubber content) the more effective the interlocking effect. Frictional resistance grows as a consequence of rubber particles experiencing tensile stress in the presence of strong swelling forces. This interfacial resistance is a function of soil–rubber contact area, with greater contact levels offering a higher resistance to swelling. Consequently, this amending mechanism is in line with rubber content. The greater the number of included rubber particles the greater the soil–rubber contact level, which in turn promotes an induced interfacial frictional resistance capable of counteracting swelling with more efficiency.

The type of polymer charge, i.e. cationic, non–ionic or anionic, strongly influences the degree of polymer adsorption/attraction to clay particles. Positively charged polymers are electrostatically attracted to the negatively charged clay surface, while non–ionic polymers accomplish adsorption through van der Waals and/or hydrogen bonding (Theng 1982; Wallace et al. 1986; Miller et al. 1998). Even though anionic polymers, such as the one used in this study, tend to be repelled by clay particles (owing to charge repulsion), adsorption can still take

place through the presence of cations acting as bridges. The degree of attraction in this case is dependent on the amount and type of exchangeable cations, clay content, pH and polymer molecular size (Theng 1982; Lu et al. 2002; Rabiee et al. 2013). Polyvalent cations such as Ca^{2+} and Mg^{2+}, for instance, offer greater efficiency in attracting the carboxylate groups on the polymer chains compared with univalent cations such as Na^{+} (Letey 1994; Laird 1997). As such, the role of PC in controlling the effect of swelling can be attributed to its ability to form ionic bonds holding clay particles together through the cationic bridging mechanism, thereby shrinking the electrical double layer. This in turn induces flocculation of clay particles by forming coarse aggregates, which is further accompanied by a reduction in the clay content size, and thus a reduction in the swelling behavior. Where paired with rubber, PC–treatment may further enhance the interlocking of rubber particles and soil grains, thus promoting a greater reduction in swelling compared with similar untreated cases.

4.3.4. Cyclic Wetting and Drying

Figure 11 illustrates the variations of swelling potential S_p against number of applied wetting–drying cycles n for the samples NR_0P_0, $NR_{30}P_0$, $NR_0P_{0.2}$ and $NR_{30}P_{0.2}$. With regard to untreated cases (NR_0P_0 and $NR_{30}P_0$), S_p exhibited a rise–fall behavior, peaking at the second cycle and then decreasing to an equilibrium value upon the completion of five cycles. The treated samples ($NR_0P_{0.2}$ and $NR_{30}P_{0.2}$), however, demonstrated a monotonic decreasing trend with lower S_p values compared with similar untreated cases. At the first cycle (n=1), the samples were allowed to swell from their respective optimum moisture content, thus the Seed et al. (1962) classification criterion, which complies with the initial placement condition (see **Table 5**), was implemented to assess the expansive potential of the tested samples. With regard to other cycles ($n \geq 2$), where the samples undergo swelling from an initially dry condition (due to the previous drying cycle), the two classification criteria suggested by Holtz and Gibbs (1956) and Sridharan and Prakash (2000) (see **Table 5**) were adopted. The classification results are summarized in **Table 8**. The classifications were either maintained or improved as a result of rubber inclusion and/or PC–treatment, thus indicating that the beneficial effects of both stabilization agents in counteracting the swell–shrink related volume changes were fairly preserved under the influence of alternate wetting and drying. Upon the completion of five cycles, a slight increase in S_p was noted for the untreated sample containing 30% rubber inclusion (see $NR_{30}P_0$ in **Figure 11**), i.e. $S_p(1)$=5.73% against $S_p(5)$=6.20%. This implies that the blending of rubber particles and soil grains, obtained by compaction, could potentially be compromised under the influence

of alternate wetting and drying. As a result of PC–treatment, however, the interlocking of rubber particles and soil grains, enhanced by the polymer binder, remains intact during successive cycles (compare $NR_{30}P_0$ with $NR_{30}P_{0.2}$ in **Figure 11**).

Reduction in swelling potential as a result of alternate wetting and drying can be attributed to the reconstruction of the clay micro–structure upon completion of the first or second cycle (Dif and Bluemel 1991; Zhang et al. 2006; Kalkan 2011; Estabragh et al. 2015). Capillary stresses generated as a consequence of drying facilitate the formation of strong van der Waals bonds, promoting cementation and aggregation of clay particles. This is followed by the development of some relatively large inter–pores among the aggregated soil lumps, which decreases the available surface for interaction with water, thereby reducing the specific surface area and plasticity of the clay content accompanied by a decreased tendency for swelling (Basma et al. 1996; Zhang et al. 2006; Estabragh et al. 2013; Soltani et al. 2017[b]).

4.4. Crack Intensity

Variations of the crack intensity factor (CIF), along with corresponding crack reduction factors (CRF), are provided in **Figure 12**. In addition, crack patterns observed for the tested samples are illustrated in **Figure 13**. The rubber inclusions were able to amend desiccation–induced cracking. In this case, the higher the rubber content the greater the improvement, with PC–treated mixtures holding a notable advantage over similar untreated cases (compare NR_xP_0 with $NR_xP_{0.2}$ in **Figure 12**). A typical hierarchical cracking pattern can be observed for the natural soil, which divides the soil mass into a series of rather small cells with wide crack openings. On the contrary, soil–rubber mixtures manifested larger cells with relatively smaller crack openings (e.g. compare NR_0P_0 with $NR_{20}P_0$ and $NR_{20}P_{0.2}$). The natural soil (NR_0P_0) and soil–rubber mixtures corresponding to R_c=10%, 20% and 30% resulted in CIF=23.67%, 16.79%, 9.03% and 4.73% (i.e. CRF=29.06%, 61.86% and 80.01%), respectively. Similar mixtures treated with 0.2 g/l PC resulted in lower CIF and higher CRF values. In this case, the aforementioned values dropped to CIF=15.57%, 11.90%, 7.74% and 2.47% (i.e. CRF=34.21%, 49.73%, 67.32% and 89.56%), respectively.

As a consequence of internal restrains (e.g. non–uniform drying) and/or external restrains (e.g. boundary friction/adhesion) acting on the soil during drying, tensile stresses developed within the soil can exceed the soil's tensile strength, thus resulting in the development and propagation of cracks (Konrad and Ayad 1997; Kodikara and Chakrabarti 2005; Nahlawi and Kodikara

2006; Tang et al. 2012; Costa et al. 2013). The development and propagation of cracks are primarily a function of clay content, meaning that the higher the clay content the greater the intensity of cracks (Mitchell and Soga 2005). As such, the rubber inclusions are able to amend the soil fabric through clay–substitution. Consequently, this amending mechanism is a function of rubber content, with higher rubber inclusions substituting a larger portion of the clay content, and thus ameliorating the effect of cracking with increased efficiency. The ductile character of the rubber particles can complement a notable improvement in the soil's tensile strength, thus restricting the propagation of cracks. Increase in the soil's tensile strength may also be achieved through interlocking of rubber particles and soil grains. As previously discussed (see **Section 4.3.3**), the interlocking effect can be considered as a direct function of rubber content, and it is further enhanced in the presence of the polymer binder.

4.5. Micro–Structure (SEM) Analysis

Figures 14a–14d illustrate SEM micrographs for the samples NR_0P_0, $NR_{20}P_0$, $NR_0P_{0.2}$ and $NR_{20}P_{0.2}$, respectively. The micro–fabric of the natural soil (NR_0P_0) included a number of large inter– and intra–assemblage pore–spaces formed between and within the clay aggregates, respectively (see **Figure 14a**). The inter–assemblage pore–spaces are formed during sample preparation (or compaction), and thus are directly proportional to the sample's initial void ratio. The shape and extension of the pore–spaces, however, may change during the drying process of SEM sample fabrication (see **Section 3.6**), owing to the development of tensile stresses within the soil fabric during desiccation. As a result of rubber inclusion ($NR_{20}P_0$), the extent of the inter–assemblage pore–spaces were slightly reduced, which can be attributed to the role of rubber particles acting as physical anchors within the soil fabric, thus interlocking neighboring aggregates and withstanding tensile stresses developed during desiccation. However, as long as the rubber particles are relatively larger in size compared with the clay particles, the micro–fabric of the compacted soil–rubber mixture still includes a number of intra–assemblage pore–spaces, owing to the inconsistency in arrangement of the soil–rubber mixture's constituents (see **Figure 14b**). Treating the natural soil with PC ($NR_0P_{0.2}$) resulted in the formation of large uniform aggregates with relatively small intra–assemblage pore–spaces, indicating that the polymer solution could effectively sip into the soil's micro–fabric, and thus bond the clay aggregates together. The larger clay aggregates with less number of intra–assemblage pore–spaces are less prone to water infiltration, which in turn mitigates the swelling behavior of the soil (see **Figure 14c**). Once the soil is included with rubber particles and treated with PC

($NR_{20}P_{0.2}$), the connection interface between the rubber particles and the clay matrices is markedly improved. In micro view, the addition of polymer contributes to the formation of composite aggregates, with rubber particles embedded within the clay aggregates (see the clothed rubber particles in **Figure 14d**). This improves the stability of the compacted soil–rubber mixture against wetting and drying cycles, as the rubber particles contribute to the shear strength of the mixture by providing tensile strength between the clay aggregates and the polymer solution improves the bonding quality of the rubber particles with the clay aggregates; therefore, harnessing the swelling potential of the soil subjected to desiccation cycles (see **Figure 14d**).

5. Conclusions

The following conclusions can be drawn from this study:

- As a result of rubber inclusion and/or PC–treatment, the swell–time locus experienced a major downward shift over the semi–log space, indicating a capacity of counteracting the heave in both magnitude and time. The variations of swelling pressure followed a trend similar to that observed for swelling potential, meaning that the higher the rubber content the greater the reduction in swelling potential and swelling pressure, with PC–treated mixtures holding a notable advantage over similar untreated cases.

- Based on common expansive soil classification criteria, i.e. the conventional oedometer swell test and the shrink–swell index, a rubber inclusion of 20% by dry weight of soil (preferably paired with 0.2 g/l PC) would be required to mitigate the swelling problem of South Australian expansive soils.

- The beneficial effects of rubber inclusion and PC–treatment in counteracting the swell–shrink related volume changes were fairly preserved under the influence of alternate wetting and drying. The blending of rubber particles and soil grains, obtained by compaction, could potentially be compromised during wetting and drying. As a result of PC–treatment, however, the interlocking of rubber particles and soil grains, enhanced by the polymer binder, remained intact during successive cycles.

- The rubber inclusions were able to amend desiccation–induced cracking. In this case, the higher the rubber content the greater the improvement in cracking intensity, with PC–treated mixtures holding a slight advantage over similar untreated cases.

Acknowledgements

Funding support provided by the Australian Research Council (ARC) via project No. **DP140103004** is gratefully acknowledged.

References

Akbulut, S., Arasan, S. & Kalkan, E. (**2007**). Modification of clayey soils using scrap tire rubber and synthetic fibers. *Applied Clay Science*, **38**, No. 1–2, 23–32, http://dx.doi.org/10.1016/j.clay.2007.02.001.

Al-Akhras, N. M., Attom, M. F., Al-Akhras, K. M. & Malkawi, A. I. H. (**2008**). Influence of fibers on swelling properties of clayey soil. *Geosynthetics International*, **15**, No. 4, 304–309, http://dx.doi.org/10.1680/gein.2008.15.4.304.

Alazigha, D. P., Indraratna, B., Vinod, J. S. & Ezeajugh, L. E. (**2016**). The swelling behaviour of lignosulfonate–treated expansive soil. *Proceedings of the Institution of Civil Engineers–Ground Improvement*, **169**, No.3, 182–193, http://dx.doi.org/10.1680/jgrim.15.00002.

Alonso, E. E., Romero, E., Hoffmann, C. & García-Escudero, E. (**2005**). Expansive bentonite–sand mixtures in cyclic controlled–suction drying and wetting. *Engineering Geology*, **81**, No.3, 213–226, http://dx.doi.org/10.1016/j.enggeo.2005.06.009.

Al-Rawas, A. A., Hago, A. W. & Al-Sarmi, H. (**2005**). Effect of lime, cement and Sarooj (artificial pozzolan) on the swelling potential of an expansive soil from Oman. *Building and Environment*, **40**, No.5, 681–687, http://dx.doi.org/10.1016/j.buildenv.2004.08.028.

Andrews, R. & Sharp, K. (**2010**). A protocol for conducting field trials for best value management of unsealed roads. *Proceedings of the 24th ARRB Conference–Building on 50 Years of Road and Transport Research*, ARRB, Melbourne, Victoria, Australia, October 2010, pp. 1–14.

Arulrajah, A., Kua, T. A., Horpibulsuk, S., Mirzababaei, M. & Chinkulkijniwat, A. (**2017b**). Recycled glass as a supplementary filler material in spent coffee grounds geopolymers. *Construction and Building Materials*, **151**, 18–27, http://dx.doi.org/10.1016/j.conbuildmat.2017.06.050.

Arulrajah, A., Kua, T. A., Suksiripattanapong, C., Horpibulsuk, S. & Shen, J. S. (**2017a**). Compressive strength and microstructural properties of spent coffee grounds–bagasse ash based geopolymers with slag supplements. *Journal of Cleaner Production*, **162**, 1491–1501, http://dx.doi.org/10.1016/j.jclepro.2017.06.171.

Arulrajah, A., Mohammadinia, A., D'Amico, A. & Horpibulsuk, S. (**2017c**). Effect of lime kiln dust as an alternative binder in the stabilization of construction and demolition materials. *Construction and Building Materials*, **152**, 999–1007, http://dx.doi.org/10.1016/j.conbuildmat.2017.07.070.

AS 1289.3.2.1:09 (**2009**). Methods of testing soils for engineering purposes: Soil classification tests – Determination of the plastic limit of a soil. *Standards Australia*, Sydney, New South Wales, Australia.

AS 1289.3.3.1:09 (**2009**). Methods of testing soils for engineering purposes: Soil classification tests – Calculation of the plasticity index of a soil. *Standards Australia*, Sydney, New South Wales, Australia.

AS 1289.3.4.1:08 (**2008**). Methods of testing soils for engineering purposes: Soil classification tests – Determination of the linear shrinkage of a soil. *Standards Australia*, Sydney, New South Wales, Australia.

AS 1289.3.9.1:15 (**2015**). Methods of testing soils for engineering purposes: Soil classification tests – Determination of the cone liquid limit of a soil. *Standards Australia*, Sydney, New South Wales, Australia.

AS 1289.7.1.1:03 (**2003**). Methods of testing soils for engineering purposes: Soil reactivity tests – Determination of the shrinkage index of a soil – Shrink–swell index. *Standards Australia*, Sydney, New South Wales, Australia.

AS 2870:11 (**2011**). Residential slabs and footings. *Standards Australia*, Sydney, New South Wales, Australia.

ASTM D2487-11 (**2011**). Standard practice for classification of soils for engineering purposes (Unified Soil Classification System). *ASTM International*, West Conshohocken, Pennsylvania, USA, http://dx.doi.org/10.1520/d2487-11.

ASTM D422-63(2007)e2 (**2007**). Standard test method for particle–size analysis of soils. *ASTM International*, West Conshohocken, Pennsylvania, USA, http://dx.doi.org/10.1520/d0422-63r07e02.

ASTM D4546-14 (**2014**). Standard test methods for one–dimensional swell or collapse of soils. *ASTM International*, West Conshohocken, Pennsylvania, USA, http://dx.doi.org/10.1520/d4546.

ASTM D698-12e2 (**2012**). Standard test methods for laboratory compaction characteristics of soil using standard effort (12,400 ft–lbf/ft^3 (600 kN–m/m^3)). *ASTM International*, West Conshohocken, Pennsylvania, USA, http://dx.doi.org/10.1520/d0698-12e02.

ASTM D854-14 (**2014**). Standard test methods for specific gravity of soil solids by water pycnometer. *ASTM International*, West Conshohocken, Pennsylvania, USA, http://dx.doi.org/10.1520/d0854-14.

Ayeldeen, M. & Kitazume, M. (**2017**). Using fiber and liquid polymer to improve the behaviour of cement–stabilized soft clay. *Geotextiles and Geomembranes*, **45**, No.6, 592–602, http://dx.doi.org/10.1016/j.geotexmem.2017.05.005.

Basma, A. A., Al-Homoud, A. S., Malkawi, A. I. H. & Al-Bashabsheh, M. A. (**1996**). Swelling–shrinkage behavior of natural expansive clays. *Applied Clay Science*, **11**, No. 2–4, 211–227, http://dx.doi.org/10.1016/s0169-1317(96)00009-9.

Camarena, S. (**2013**). Sustainable road maintenance and construction utilising new technologies. *Proceedings of the IPWEA International Public Works Conference*, IPWEA, Darwin, Northern Territory, Australia, August 2013, pp. 1–11.

Cameron, D. A. (**1989**). Tests for reactivity and prediction of ground movement. *Civil Engineering Transactions/The Institution of Engineers, Australia*, **31**, No. 3, 121–132.

Cameron, D. A. (**2001**). The extent of soil desiccation near trees in a semi–arid environment. *Geotechnical and Geological Engineering*, **19**, No.3–4, 357–370, http://dx.doi.org/10.1023/a:1013168708654.

Cetin, H., Fener, M. & Gunaydin, O. (**2006**). Geotechnical properties of tire–cohesive clayey soil mixtures as a fill material. *Engineering Geology*, **88**, No. 1–2, 110–120, http://dx.doi.org/10.1016/j.enggeo.2006.09.002.

Chaduvula, U., Viswanadham, B. V. S. & Kodikara, J. (**2017**). A study on desiccation cracking behavior of polyester fiber–reinforced expansive clay. *Applied Clay Science*, **142**, 163–172, http://dx.doi.org/10.1016/j.clay.2017.02.008.

Costa, S., Kodikara, J. & Shannon, B. (**2013**). Salient factors controlling desiccation cracking of clay in laboratory experiments. *Géotechnique*, **63**, No. 1, 18–29, http://dx.doi.org/10.1680/geot.9.p.105.

De Camillis, M., Di Emidio, G., Bezuijen, A., Flores, D. V., Stappen, J. V. & Cnudde, V. (**2017**). Effect of wet–dry cycles on polymer treated bentonite in seawater: Swelling ability, hydraulic conductivity and crack analysis. *Applied Clay Science*, **142**, 52–59, http://dx.doi.org/10.1016/j.clay.2016.11.011.

Dif, A. & Bluemel, W. (**1991**). Expansive soils under cyclic drying and wetting. *Geotechnical Testing Journal*, **14**, No. 1, 96–102, http://dx.doi.org/10.1520/gtj10196j.

Estabragh, A. R., Parsaei, B. & Javadi, A. A. (**2015**). Laboratory investigation of the effect of cyclic wetting and drying on the behaviour of an expansive soil. *Soils and Foundations*, **55**, No. 2, 304–314, http://dx.doi.org/10.1016/j.sandf.2015.02.007.

Estabragh, A. R., Pereshkafti, M. R. S., Parsaei, B. & Javadi, A. A. (**2013**). Stabilised expansive soil behaviour during wetting and drying. *International Journal of Pavement Engineering*, **14**, No. 4, 418–427, http://dx.doi.org/10.1080/10298436.2012.746688.

Estabragh, A. R., Rafatjo, H. & Javadi, A. A. (**2014**). Treatment of an expansive soil by mechanical and chemical techniques. *Geosynthetics International*, **21**, No. 3, 233–243, http://dx.doi.org/10.1680/gein.14.00011.

Fityus, S. G., Cameron, D. A. & Walsh, P. F. (**2005**). The shrink swell test. *Geotechnical Testing Journal*, **28**, No. 1, 92–101, http://dx.doi.org/10.1520/gtj12327.

Georgees, R. N., Hassan, R. A., Evans, R. P. & Jegatheesan, P. (**2015**). Effect of the use of a polymeric stabilizing additive on unconfined compressive strength of soils. *Transportation Research Record: Journal of the Transportation Research Board*, **2473**, 200–208, http://dx.doi.org/10.3141/2473-23.

Graber, E. R., Fine, P. & Levy, G. J. (**2006**). Soil stabilization in semiarid and arid land agriculture. *Journal of Materials in Civil Engineering*, **18**, No. 2, 190–205, http://dx.doi.org/10.1061/(asce)0899-1561(2006)18:2(190).

Guney, Y., Sari, D., Cetin, M. & Tuncan, M. (**2007**). Impact of cyclic wetting–drying on swelling behavior of lime–stabilized soil. *Building and Environment*, **42**, No. 2, 681–688, http://dx.doi.org/10.1016/j.buildenv.2005.10.035.

Hannam, P. (**2014**). Tyre industry divided over how to handle toxic waste. *The Sydney Morning Herald*, Sydney, New South Wales, Australia. See http://www.smh.com.au/environment/tyre-industry-divided-over-how-to-handle-toxic-waste-20140120-314ic.html (accessed 12/12/2017)

Holtz, W. G. & Gibbs, H. J. (**1956**). Engineering properties of expansive clays. *Transactions of the American Society of Civil Engineers*, **121**, No. 1, 641–663.

Hoyos, L. R., Chainuwat, P. & Puppala, A. J. (**2006**). Dynamic characterization of chemically modified expansive soil. In: *Expansive Soils: Recent Advances in Characterization and Treatment*, Al-Rawas, A. A. & Goosen, M. F. A., Eds., Taylor & Francis Group, London, UK, pp. 465–481, http://dx.doi.org/10.1201/9780203968079.ch32.

Inyang, H. I., Bae, S., Mbamalu, G. & Park, S. (**2007**). Aqueous polymer effects on volumetric swelling of Na–Montmorillonite. *Journal of Materials in Civil Engineering*, **19**, No. 1, 84–90, http://dx.doi.org/10.1061/(asce)0899-1561(2007)19:1(84).

Kalkan, E. (**2011**). Impact of wetting–drying cycles on swelling behavior of clayey soils modified by silica fume. *Applied Clay Science*, **52**, No. 4, 345–352, http://dx.doi.org/10.1016/j.clay.2011.03.014.

Kalkan, E. (**2013**). Preparation of scrap tire rubber fiber–silica fume mixtures for modification of clayey soils. *Applied Clay Science*, **80**–**81**, 117–125, http://dx.doi.org/10.1016/j.clay.2013.06.014.

Kim, S. & Palomino, A. M. (**2009**). Polyacrylamide–treated kaolin: A fabric study. *Applied Clay Science*, **45**, No.4, 270–279, http://dx.doi.org/10.1016/j.clay.2009.06.009.

Kodikara, J. & Chakrabarti, S. (**2005**). Modeling of moisture loss in cementitiously stabilized pavement materials. *International Journal of Geomechanics*, **5**, No. 4, 295–303, http://dx.doi.org/10.1061/(asce)1532-3641(2005)5:4(295).

Konrad, J. M. & Ayad, R. (**1997**). A idealized framework for the analysis of cohesive soils undergoing desiccation. *Canadian Geotechnical Journal*, **34**, No. 4, 477–488, http://dx.doi.org/10.1139/t97-015.

Kua, T. A., Arulrajah, A., Mohammadinia, A., Horpibulsuk, S. & Mirzababaei, M. (**2017**). Stiffness and deformation properties of spent coffee grounds based geopolymers. *Construction and Building Materials*, **138**, 79–87, http://dx.doi.org/10.1016/j.conbuildmat.2017.01.082.

Laird, D. A. (**1997**). Bonding between polyacrylamide and clay mineral surfaces. *Soil Science*, **162**, No. 11, 826–832, http://dx.doi.org/10.1097/00010694-199711000-00006.

Letey, J. (**1994**). Adsorption and desorption of polymers on soil. *Soil Science*, **158**, No. 4, 244–248, http://dx.doi.org/10.1097/00010694-199410000-00003.

Li, J., Zou, J., Bayetto, P. & Barker, N. (**2016**) Shrink–swell index database for Melbourne. *Australian Geomechanics*, **51**, No. 3, 61–76.

Lu, J. H., Wu, L. & Letey, J. (**2002**). Effects of soil and water properties on anionic polyacrylamide sorption. *Soil Science Society of America Journal*, **66**, No. 2, 578–584, http://dx.doi.org/10.2136/sssaj2002.5780.

Miller, C. J. & Rifai, S. (**2004**). Fiber reinforcement for waste containment soil liners. *Journal of Environmental Engineering*, **130**, No. 8, 891–895, http://dx.doi.org/10.1061/(asce)0733-9372(2004)130:8(891).

Miller, W. P., Willis, R. L. & Levy, G. J. (**1998**). Aggregate stabilization in kaolinitic soils by low rates of anionic polyacrylamide. *Soil Use and Management*, **14**, No. 2, 101–105, http://dx.doi.org/10.1111/j.1475-2743.1998.tb00623.x.

Mirzababaei, M., Miraftab, M., Mohamed, M. & McMahon, P. (**2013[a]**). Impact of carpet waste fibre addition on swelling properties of compacted clays. *Geotechnical and Geological Engineering*, **31**, No. 1, 173–182, http://dx.doi.org/10.1007/s10706-012-9578-2.

Mirzababaei, M., Miraftab, M., Mohamed, M. & McMahon, P. (**2013[b]**). Unconfined compression strength of reinforced clays with carpet waste fibers. *Journal of Geotechnical and Geoenvironmental Engineering*, **139**, No. 3, 483–493, http://dx.doi.org/10.1061/(asce)gt.1943-5606.0000792.

Mirzababaei, M., Mohamed, M. & Miraftab, M. (**2017[b]**). Analysis of strip footings on fiber–reinforced slopes with the aid of particle image velocimetry. *Journal of Materials in Civil Engineering*, **29**, No. 4, 04016243:1–04016243:14. http://dx.doi.org/10.1061/(asce)mt.1943-5533.0001758.

Mirzababaei, M., Mohamed, M., Arulrajah, A., Horpibulsuk, S. & Anggraini, V. (**2017[a]**). Practical approach to predict the shear strength of fibre–reinforced clay. *Geosynthetics International*, **in press**, http://dx.doi.org/10.1680/jgein.17.00033.

Mirzababaei, M., Yasrobi, S. S. & Al-Rawas, A. A. (**2009**). Effect of polymers on swelling potential of expansive soils. *Proceedings of the Institution of Civil Engineers–Ground Improvement*, **162**, No. 3, 111–119, http://dx.doi.org/10.1680/grim.2009.162.3.111.

Mitchell, J. K. & Soga, K. (**2005**). Fundamentals of soil behavior (3rd Ed.). John Wiley & Sons, Hoboken, New Jersey, USA, 592 pp.

Nahlawi, H. & Kodikara, J. K. (**2006**). Laboratory experiments on desiccation cracking of thin soil layers. *Geotechnical and Geological Engineering*, **24**, No. 6, 1641–1664, http://dx.doi.org/10.1007/s10706-005-4894-4.

Onyejekwe, S. & Ghataora, G. S. (**2015**). Soil stabilization using proprietary liquid chemical stabilizers: Sulphonated oil and a polymer. *Bulletin of Engineering Geology and the Environment*, **74**, No. 2, 651–665, http://dx.doi.org/10.1007/s10064-014-0667-8.

Özkul, Z. H. & Baykal, G. (**2007**). Shear behavior of compacted rubber fiber–clay composite in drained and undrained loading. *Journal of Geotechnical and Geoenvironmental Engineering*, **133**, No. 7, 767–781, http://dx.doi.org/10.1061/(asce)1090-0241(2007)133:7(767).

Patil, U., Valdes, J. R. & Evans, T. M. (**2011**). Swell mitigation with granulated tire rubber. *Journal of Materials in Civil Engineering*, **23**, No. 5, 721–727, http://dx.doi.org/10.1061/(asce)mt.1943-5533.0000229.

Phanikumar, B. R. & Singla, R. (**2016**). Swell–consolidation characteristics of fibre–reinforced expansive soils. *Soils and Foundations*, **56**, No. 1, 138–143, http://dx.doi.org/10.1016/j.sandf.2016.01.011.

Phummiphan, I., Horpibulsuk, S., Rachan, R., Arulrajah, A., Shen, S. L. & Chindaprasirt, P. (**2018**). High calcium fly ash geopolymer stabilized lateritic soil and granulated blast furnace slag blends as

a pavement base material. *Journal of Hazardous Materials*, **341**, 257–267, http://dx.doi.org/10.1016/j.jhazmat.2017.07.067.

Prakash, K. & Sridharan, A. (**2004**). Free swell ratio and clay mineralogy of fine–grained soils. *Geotechnical Testing Journal*, **27**, No.2, 220–225, http://dx.doi.org/10.1520/gtj10860.

Puppala, A. J., Griffin, J. A., Hoyos, L. R. & Chomtid, S. (**2004**). Studies on sulfate–resistant cement stabilization methods to address sulfate–induced soil heave. *Journal of Geotechnical and Geoenvironmental Engineering*, **130**, No. 4, 391–402, http://dx.doi.org/10.1061/(asce)1090-0241(2004)130:4(391).

Rabiee, A., Gilani, M., Jamshidi, H. & Baharvand, H. (**2013**). Synthesis and characterization of a calcium– and sodium–containing acrylamide–based polymer and its effect on soil strength. *Journal of Vinyl and Additive Technology*, **19**, No. 2, 140–146, http://dx.doi.org/10.1002/vnl.21310.

Rao, S. M., Reddy, B. V. V. & Muttharam, M. (**2001**). The impact of cyclic wetting and drying on the swelling behavior of stabilized expansive soils. *Engineering Geology*, **60**, No. 1–4, 223–233, http://dx.doi.org/10.1016/s0013-7952(00)00103-4.

Rao, S. M., Thyagaraj, T. & Thomas, H. R. (**2006**). Swelling of compacted clay under osmotic gradients. *Géotechnique*, **56**, No. 10, 707–713, http://dx.doi.org/10.1680/geot.2006.56.10.707.

Rauch, A., Harmon, J., Katz, L. & Liljestrand, H. (**2002**). Measured effects of liquid soil stabilizers on engineering properties of clay. *Transportation Research Record: Journal of the Transportation Research Board*, **1787**, 33–41, http://dx.doi.org/10.3141/1787-04.

Seda, J. H., Lee, J. C. & Carraro, J. A. H. (**2007**). Beneficial use of waste tire rubber for swelling potential mitigation in expansive soils. In: *Geo-Denver 2007: Soil Improvement (GSP 172)*, Schaefer, V. R., Filz, G. M., Gallagher, P. M., Sehn, A. L. & Wissmann, K. J., Eds., ASCE, Denver, Colorado, USA, pp. 1–9, http://dx.doi.org/10.1061/40916(235)5.

Seddon, K. D. (**1992**). Reactive soils. In: *Engineering Geology of Melbourne*, Peck, W. A., Neilson, J. L., Olds, R. J. & Seddon, K. D. Eds., A.A. Balkema, Melbourne, Victoria, Australia, pp. 33–37.

Seed, H. B., Woodward, J. & Lundgren, R. (**1962**). Prediction of swelling potential for compacted clays. *Journal of the Soil Mechanics and Foundations Division*, **88**, No. 3, 53–88.

Seybold, C. A. (**1994**). Polyacrylamide review: Soil conditioning and environmental fate. *Communications in Soil Science and Plant Analysis*, **25**, No. 11–12, 2171–2185, http://dx.doi.org/10.1080/00103629409369180.

Signes, C. H., Garzón-Roca, J., Fernández, P. M., Torre, M. E. G. & Franco, R. I. (**2016**). Swelling potential reduction of Spanish argillaceous marlstone Facies Tap soil through the addition of crumb rubber particles from scrap tyres. *Applied Clay Science*, **132**–**133**, 768–773, http://dx.doi.org/10.1016/j.clay.2016.07.027.

Sivapullaiah, P. V., Sridharan, A. & Ramesh, H. N. (**2000**). Strength behaviour of lime–treated soils in the presence of sulphate. *Canadian Geotechnical Journal*, **37**, No. 6, 1358–1367, http://dx.doi.org/10.1139/t00-052.

Sivapullaiah, P. V., Sridharan, A. & Stalin, V. K. (**1996**). Swelling behaviour of soil–bentonite mixtures. *Canadian Geotechnical Journal*, **33**, No. 5, 808–814, http://dx.doi.org/10.1139/t96-106-326.

Soltani, A., Deng, A. & Taheri, A. (**2018**). Swell–compression characteristics of a fiber–reinforced expansive soil. *Geotextiles and Geomembranes*, **46**, No. 2, 183–189, http://dx.doi.org/10.1016/j.geotexmem.2017.11.009.

Soltani, A., Deng, A., Taheri, A. & Mirzababaei, M. (**2017**[b]). A sulphonated oil for stabilisation of expansive soils. *International Journal of Pavement Engineering*, **in press**, http://dx.doi.org/10.1080/10298436.2017.1408270.

Soltani, A., Taheri, A., Khatibi, M. & Estabragh, A. R. (**2017**[a]). Swelling potential of a stabilized expansive soil: A comparative experimental study. *Geotechnical and Geological Engineering*, **35**, No. 4, 1717–1744, http://dx.doi.org/10.1007/s10706-017-0204-1.

Sridharan, A. & Gurtug, Y. (**2004**). Swelling behaviour of compacted fine–grained soils. *Engineering Geology*, **72**, No. 1, 9–18, http://dx.doi.org/10.1016/s0013-7952(03)00161-3.

Sridharan, A. & Keshavamurthy, P. (**2016**). Expansive soil characterisation: An appraisal. *INAE Letters*, **1**, No. 1, 29–33, http://dx.doi.org/10.1007/s41403-016-0001-9.

Sridharan, A. & Prakash, K. (**2000**). Classification procedures for expansive soils. *Proceedings of the Institution of Civil Engineers–Geotechnical Engineering*, **143**, No. 4, 235–240, http://dx.doi.org/10.1680/geng.2000.143.4.235.

Sridharan, A., Rao, A. & Sivapullaiah, P. (**1986**). Swelling pressure of clays. *Geotechnical Testing Journal*, **9**, No. 1, 24–33, http://dx.doi.org/10.1520/gtj10608j.

Srivastava, A., Pandey, S. & Rana, J. (**2014**). Use of shredded tyre waste in improving the geotechnical properties of expansive black cotton soil. *Geomechanics and Geoengineering*, **9**, No.4, 303–311, http://dx.doi.org/10.1080/17486025.2014.902121.

Suksiripattanapong, C., Kua, T. A., Arulrajah, A., Maghool, F. & Horpibulsuk, S. (**2017**). Strength and microstructure properties of spent coffee grounds stabilized with rice husk ash and slag geopolymers. *Construction and Building Materials*, **146**, 312–320, http://dx.doi.org/10.1016/j.conbuildmat.2017.04.103.

Tang, C. S., Shi, B. & Zhao, L. Z. (**2010**). Interfacial shear strength of fiber reinforced soil. *Geotextiles and Geomembranes*, **28**, No. 1, 54–62, http://dx.doi.org/10.1016/j.geotexmem.2009.10.001.

Tang, C. S., Shi, B., Cui., Y. J., Liu, C. & Gua, K. (**2012**). Desiccation cracking behavior of polypropylene fiber–reinforced clayey soil. *Canadian Geotechnical Journal*, **49**, No. 9, 1088–1101, http://dx.doi.org/10.1139/t2012-067.

Tang, C. S., Shi, B., Gao, W., Chen, F. & Cai, Y. (**2007**). Strength and mechanical behavior of short polypropylene fiber reinforced and cement stabilized clayey soil. *Geotextiles and Geomembranes*, **25**, No. 3, 194–202, http://dx.doi.org/10.1016/j.geotexmem.2006.11.002.

Theng, B. K. G. (**1982**). Clay–polymer interactions: Summary and perspectives. *Clays and Clay Minerals*, **30**, No. 1, 1–10, http://dx.doi.org/10.1346/ccmn.1982.0300101.

Tripathy, S., Subba Rao, K. S. & Fredlund, D. G. (**2002**). Water content–void ratio swell–shrink paths of compacted expansive soils. *Canadian Geotechnical Journal*, **39**, No.4, 938–959, http://dx.doi.org/10.1139/t02-022.

Trouzine, H., Bekhiti, M. & Asroun, A. (**2012**). Effects of scrap tyre rubber fibre on swelling behaviour of two clayey soils in Algeria. *Geosynthetics International*, **19**, No. 2, 124–132, http://dx.doi.org/10.1680/gein.2012.19.2.124.

Viswanadham, B. V. S., Phanikumar, B. R. & Mukherjee, R. V. (**2009[b]**). Effect of polypropylene tape fibre reinforcement on swelling behaviour of an expansive soil. *Geosynthetics International*, **16**, No. 5, 393–401, http://dx.doi.org/10.1680/gein.2009.16.5.393.

Viswanadham, B. V. S., Phanikumar, B. R. & Mukherjee, R. V. (**2009[a]**). Swelling behaviour of a geofiber–reinforced expansive soil. *Geotextiles and Geomembranes*, **27**, No. 1, 73–76, http://dx.doi.org/10.1016/j.geotexmem.2008.06.002.

Wallace, A., Wallace, G. A. & Cha, W. J. (**1986**). Mechanisms involved in soil conditioning by polymers. *Soil Science*, **141**, No. 5, 381–386, http://dx.doi.org/10.1097/00010694-198605000-00017.

Wray, W. K. (**1998**). Mass transfer in unsaturated soils: A review of theory and practices. *Proceedings of the 2nd International Conference on Unsaturated Soils (Unsat 98)*, International Academic Publishing House, Beijing, China, August 1998, pp. 99–155.

Wroth, C. P. & Wood, D. M. (**1978**). The correlation of index properties with some basic engineering properties of soils. *Canadian Geotechnical Journal*, **15**, No.2, 137–145, http://dx.doi.org/10.1139/t78-014.

Yadav, J. S. & Tiwari, S. K. (**2017[a]**). Effect of waste rubber fibres on the geotechnical properties of clay stabilized with cement. *Applied Clay Science*, **149**, 97–110, http://dx.doi.org/10.1016/j.clay.2017.07.037.

Yadav, J. S. & Tiwari, S. K. (**2017[b]**). The impact of end–of–life tires on the mechanical properties of fine–grained soil: A Review. *Environment, Development and Sustainability*, **in press**, http://dx.doi.org/10.1007/s10668-017-0054-2.

Yazdandoust, F. & Yasrobi, S. S. (**2010**). Effect of cyclic wetting and drying on swelling behavior of polymer–stabilized expansive clays. *Applied Clay Science*, **50**, No. 4, 461–468, http://dx.doi.org/10.1016/j.clay.2010.09.006.

Yesiller, N., Miller, C. J., Inci, G. & Yaldo, K. (**2000**). Desiccation and cracking behavior of three compacted landfill liner soils. *Engineering Geology*, **57**, No. 1–2, 105–121, http://dx.doi.org/10.1016/s0013-7952(00)00022-3.

Zhang, R., Yang, H. & Zheng, J. (**2006**). The effect of vertical pressure on the deformation and strength of expansive soil during cyclic wetting and drying. In: *Unsaturated Soils 2006*, Miller, G. A., Zapata, C. E., Houston, S. L. & Fredlund, D. G., Eds., ASCE, Carefree, Arizona, USA, pp. 894–905, http://dx.doi.org/10.1061/40802(189)71.

List of Tables

Table 1. Physical and mechanical properties of the soil.

Table 2. Physical properties and chemical composition of tire rubber powder (as supplied by the manufacturer).

Table 3. Mix designs and their properties used for the main experimental program.

Table 4. Free swell ratio (FSR) for the natural soil treated with various PC concentrations.

Table 5. Classification procedures for expansive soils with respect to the oedometer swell test.

Table 6. Classification procedures for expansive soils with respect to the shrink–swell index (Seddon 1992).

Table 7. Summary of the swell–time characteristics for the tested samples.

Table 8. Degree of expansivity for the tested samples during wetting and drying cycles.

Table 1. Physical and mechanical properties of the soil.

Properties	Value	Standard designation
Specific gravity, G_s	2.76	ASTM D854 (2014)
Grain–size distribution		
Clay (< 2 μm) (%)	44	ASTM D422 (2007)
Silt (2–75 μm) (%)	36	
Fine sand (0.075–0.425 mm)	15	
Medium sand (0.425–2 mm)	4	
Coarse sand (2–4.75 mm)	1	
Consistency limits		
Liquid limit, *LL* (%)	78.04	AS 1289.3.9.1 (2015)
Plastic limit, *PL* (%)	22.41	AS 1289.3.2.1 (2009)
Plasticity index, *PI* (%)	55.63	AS 1289.3.3.1 (2009)
Linear shrinkage, *LS* (%)	15.78	AS 1289.3.4.1 (2008)
USCS soil classification	CH	ASTM D2487 (2011)
Swelling properties		
Swelling potential, S_p (%)†	10.68	ASTM D4546 (2014)
Swelling pressure, P_s (kPa)	235	
Free swell ratio, FSR‡	2.27	Sridharan and Prakash (2000)
Compaction characteristics		
Maximum dry unit weight, γ_{dmax} (kN/m^3)	15.9	ASTM D698 (2012)
Optimum moisture content, ω_{opt} (%)	21.0	

Note:
†% expansion in oedometer from optimum moisture content to saturated condition under σ'_0=7 kPa; and ‡ratio of equilibrium sediment volume of 10 g oven–dried soil passing sieve 425 μm in distilled water to that of kerosene.

Table 2. Physical properties and chemical composition of tire rubber powder (as supplied by the manufacturer).

Properties	Value/Description
Physical properties	
Physical appearance	Fine black powder
Solubility in water	Insoluble
Water adsorption	Negligible
Resistance to acid and alkaline	Excellent
Specific gravity (at 20 ^{o}C), G_s	1.09
Softening point (^{o}C)	170
Chemical composition	
Styrene–Butadiene copolymer (%)	55
Acetone extract (%)	5–20
Carbon black (%)	25–35
Zinc oxide (%)	2.5
Sulphur (%)	1–3

Table 3. Mix designs and their properties used for the main experimental program.

Soil (%)	R_c (%)	PC (g/l)	Designation	LL (%)†	ω_{opt} (%)‡	γ_{dmax} (kN/m^3)‡	G_{sm}*	e_0‡
100	0	0	NR_0P_0	78.04	21.0	15.9	2.76	0.706
90	10		$NR_{10}P_0$	73.32	18.1	15.4	2.42	0.538
80	20		$NR_{20}P_0$	68.59	16.5	15.2	2.20	0.422
70	30		$NR_{30}P_0$	65.58	15.0	14.7	2.04	0.359
100	0	0.2	$NR_0P_{0.2}$	87.61	22.0	16.2	2.76	0.668
90	10		$NR_{10}P_{0.2}$	83.67	18.9	15.6	2.42	0.524
80	20		$NR_{20}P_{0.2}$	77.73	17.0	15.1	2.20	0.424
70	30		$NR_{30}P_{0.2}$	72.14	15.5	14.9	2.04	0.344

Note:
†initial placement condition for desiccation–induced crack tests; ‡initial placement condition for oedometer swell–compression, soil reactivity (shrink–swell index), cyclic wetting and drying and SEM tests; and *specific gravity of mixtures obtained as per **Equation 2**.

Table 4. Free swell ratio (FSR) for the natural soil treated with various PC concentrations.

Mixture	V_k (cm^3)	V_d (cm^3)	V_p (cm^3)	FSR	Degree of expansivity	Classification procedures with respect to FSR (Sridharan and Prakash 2000)				
NR_0P_0	15.0	34.0	—	2.27	High	≤ 1	1–1.5	1.5–2	2–4	> 4
$NR_0P_{0.2}$†	15.0	—	25.0	1.67	Moderate	Negligible	Low	Moderate	High	Very High
$NR_0P_{0.4}$	15.0	—	24.5	1.63	Moderate					
$NR_0P_{0.6}$	15.0	—	23.0	1.53	Moderate					

Note:
†manufacturer–recommended concentration; FSR=V_d/V_k or V_p/V_k; and V_k, V_d and V_p=equilibrium sediment volume of 10 g oven–dried soil passing sieve 425 μm in kerosene, distilled water and PC solution, respectively.

Table 5. Classification procedures for expansive soils with respect to the oedometer swell test.

Degree of expansivity	Holtz and Gibbs (1956)†	Seed et al. (1962)‡	Sridharan and Prakash (2000)†
Low (L)	< 10	0–1.5	1–5
Moderate (M)	10–20	1.5–5	5–15
High (H)	20–30	5–25	15–25
Very High (VH)	> 30	> 25	> 25

Note:
†% expansion in oedometer from air–dry to saturated condition under σ'_0=7 kPa; and ‡% expansion in oedometer from optimum moisture content to saturated condition under σ'_0=7 kPa.

Table 6. Classification procedures for expansive soils with respect to the shrink–swell index (Seddon 1992).

Degree of expansivity/reactivity	**Shrink–Swell index, I_{ss} (%pF^{-1})**
Slightly reactive (S^R)	0.8–1.7
Moderately reactive (M^R)	1.7–3.3
Highly reactive (H^R)	3.3–5.8
Extremely reactive (E^R)	> 5.8

Table 7. Summary of the swell–time characteristics for the tested samples.

Mixture	t_{is} (min)	t_{ps} (min)	ε_{ais} (%)	ε_{aps} (%)	ε_{ass} (%)	S_p (%)	C_{ps} ($\times 10^2$)	C_{ss} ($\times 10^3$)
NR_0P_0	21	939	1.40	8.00	1.27	10.68	4.85	10.71
$NR_{10}P_0$	26	1161	1.11	6.46	1.03	8.60	3.92	9.38
$NR_{20}P_0$	28	1167	0.95	5.38	0.93	7.26	3.32	8.53
$NR_{30}P_0$	34	1441	0.74	4.28	0.71	5.73	2.63	7.06
$NR_0P_{0.2}$	18	753	0.94	5.33	0.88	7.15	3.28	6.84
$NR_{10}P_{0.2}$	29	1343	0.79	4.71	0.70	6.20	2.83	6.79
$NR_{20}P_{0.2}$	35	1412	0.54	3.20	0.53	4.28	1.99	5.30
$NR_{30}P_{0.2}$	62	2387	0.41	2.38	0.41	3.20	1.50	5.28

Table 8. Degree of expansivity for the tested samples during wetting and drying cycles.

Mixture	*n*	$S_p(n)$ (%)	Degree of expansivity	Degree of expansivity
NR_0P_0	1	10.68	High[†]	High[†]
	2	13.28	Moderate[‡]	Moderate[*]
	3	9.23	Low[‡]	Moderate[*]
	4	7.45	Low[‡]	Moderate[*]
	5	7.55	Low[‡]	Moderate[*]
$NR_{30}P_0$	1	5.73	High[†]	High[†]
	2	7.03	Low[‡]	Moderate[*]
	3	6.63	Low[‡]	Moderate[*]
	4	6.35	Low[‡]	Moderate[*]
	5	6.20	Low[‡]	Moderate[*]
$NR_0P_{0.2}$	1	7.15	High[†]	High[†]
	2	5.10	Low[‡]	Moderate[*]
	3	4.10	Low[‡]	Low[*]
	4	3.70	Low[‡]	Low[*]
	5	3.80	Low[‡]	Low[*]
$NR_{30}P_{0.2}$	1	3.20	Moderate[†]	Moderate[†]
	2	2.75	Low[‡]	Low[*]
	3	2.00	Low[‡]	Low[*]
	4	1.80	Low[‡]	Low[*]
	5	1.70	Low[‡]	Low[*]

Note:
[†]classified as per Seed et al. (1962) (see **Table 5**); [‡]classified as per Holtz and Gibbs (1956) (see **Table 5**); and [*]classified as per Sridharan and Prakash (2000) (see **Table 5**).

List of Figures

Figure 1. Grain–size distribution curves for the soil and tire rubber powder.

Figure 2. Tire rubber powder at different magnifications: **(a)** without magnification; **(b)** 50x magnification; and **(c)** 100x magnification.

Figure 3. Consistency limits for the natural soil (NR_0P_0) and various soil–rubber mixtures treated with different PC concentrations: **(a)** liquid limit; **(b)** plasticity index; and **(c)** linear shrinkage.

Figure 4. Location of various soil–rubber–PC mix designs on Casagrande's plasticity chart.

Figure 5. Standard Proctor compaction curves for the natural soil (NR_0P_0) and various soil–rubber mixtures: **(a)** untreated; and **(b)** treated with 0.2 g/l PC.

Figure 6. Swell–time curves for the natural soil (NR_0P_0) and various soil–rubber mixtures: **(a)** untreated; and **(b)** treated with 0.2 g/l PC.

Figure 7. Variations of swelling pressure and swelling potential against rubber content for the tested samples (**H**=*highly expansive*; and **M**=*moderately expansive*).

Figure 8. Swell–time characteristics with respect to the oedometer swell test (modified from Soltani et al. (2017[b] and 2018)).

Figure 9. Variations of the **(a)** primary and **(b)** secondary swelling rates against rubber content for the tested samples.

Figure 10. Variations of the shrinkage and swelling strains, along with corresponding shrink–swell index values, against rubber content for the tested samples ($\mathbf{H^R}$=*highly reactive*; $\mathbf{M^R}$=*moderately reactive*; and $\mathbf{S^R}$=*slightly reactive*).

Figure 11. Variations of swelling potential against number of applied wetting–drying cycles for the samples NR_0P_0, $NR_{30}P_0$, $NR_0P_{0.2}$ and $NR_{30}P_{0.2}$.

Figure 12. Variations of the crack intensity factor, along with corresponding crack reduction factors, against rubber content for the tested samples.

Figure 13. Observed crack patterns for the tested samples.

Figure 14. Scanning electron micrographs (SEM): **(a)** NR_0P_0; **(b)** $NR_{20}P_0$; **(c)** $NR_0P_{0.2}$; and **(d)** $NR_{20}P_{0.2}$.

Figure 1. Grain–size distribution curves for the soil and tire rubber powder.

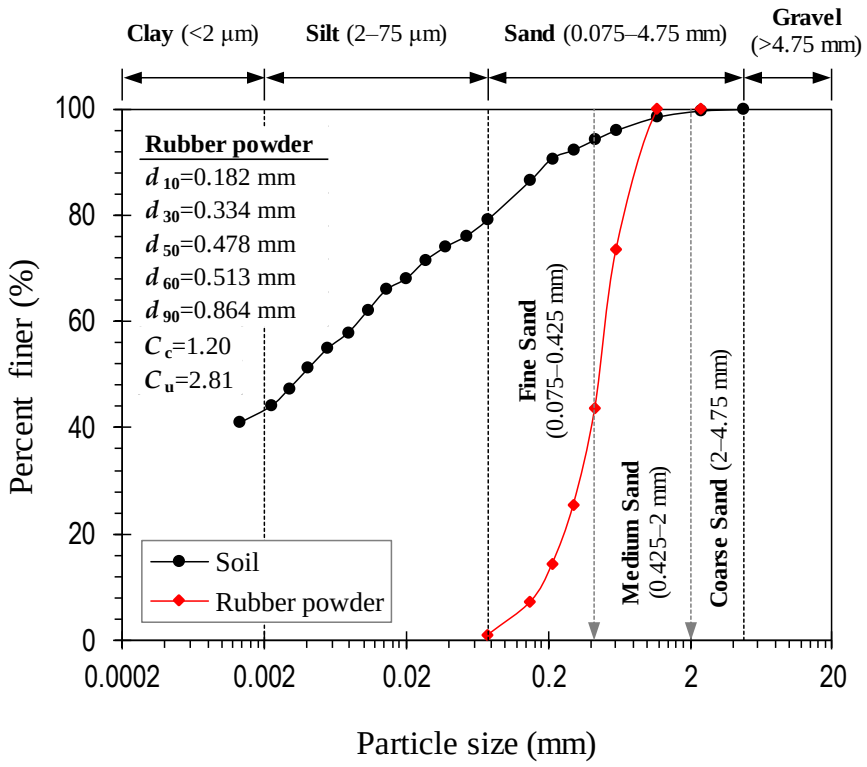

Figure 2. Tire rubber powder at different magnifications: **(a)** without magnification; **(b)** 50x magnification; and **(c)** 100x magnification.

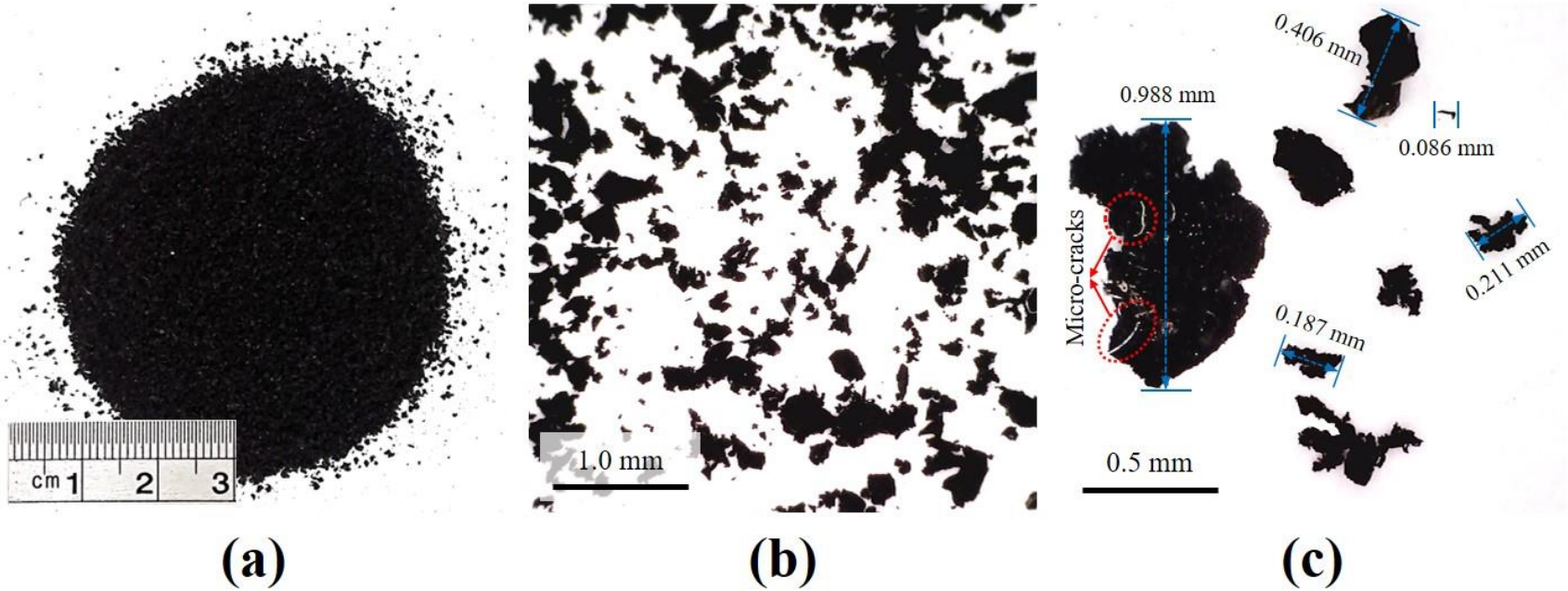

Figure 3. Consistency limits for the natural soil (NR_0P_0) and various soil–rubber mixtures treated with different PC concentrations: **(a)** liquid limit; **(b)** plasticity index; and **(c)** linear shrinkage.

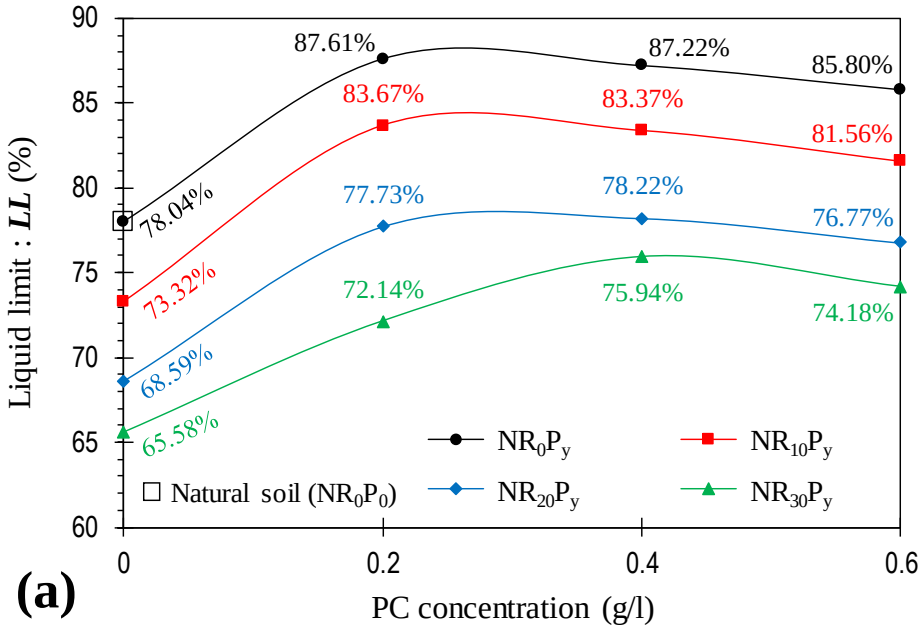

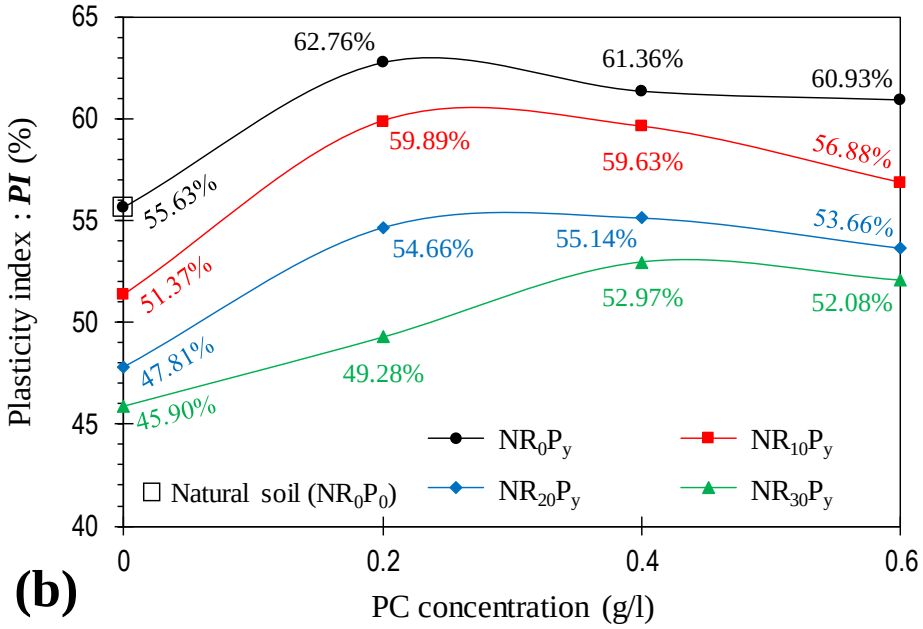

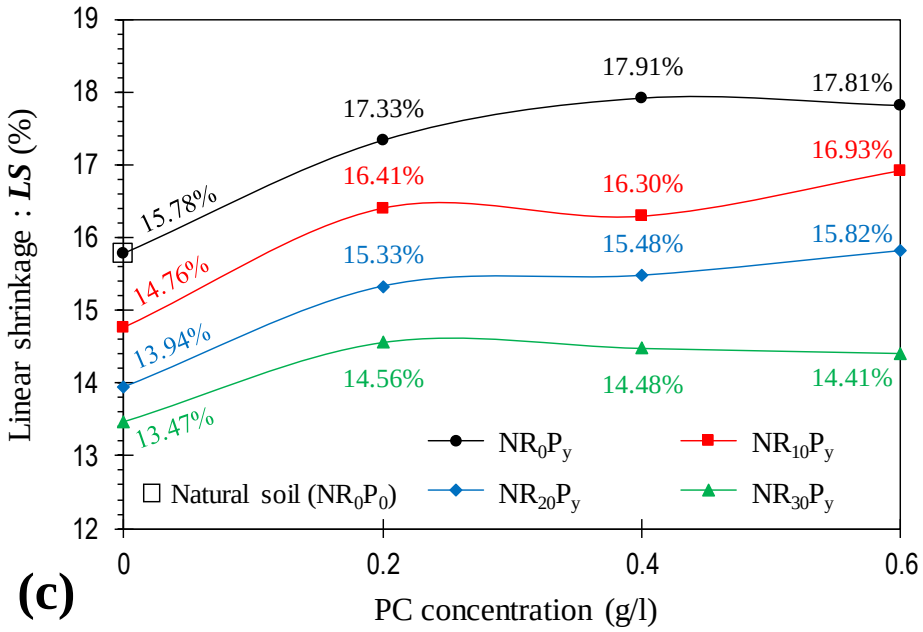
Linear shrinkage : LS (%)
PC concentration (g/l)
19
18
17
16
15
14
13
12
0
0.2
0.4
0.6
17.33%
17.91%
17.81%
16.41%
16.30%
16.93%
15.33%
15.48%
15.82%
14.56%
14.48%
14.41%
15.78%
14.76%
13.94%
13.47%
Natural soil (NR0P0)
NR0Py
NR10Py
NR20Py
NR30Py

(c)

Figure 4. Location of various soil–rubber–PC mix designs on Casagrande's plasticity chart.

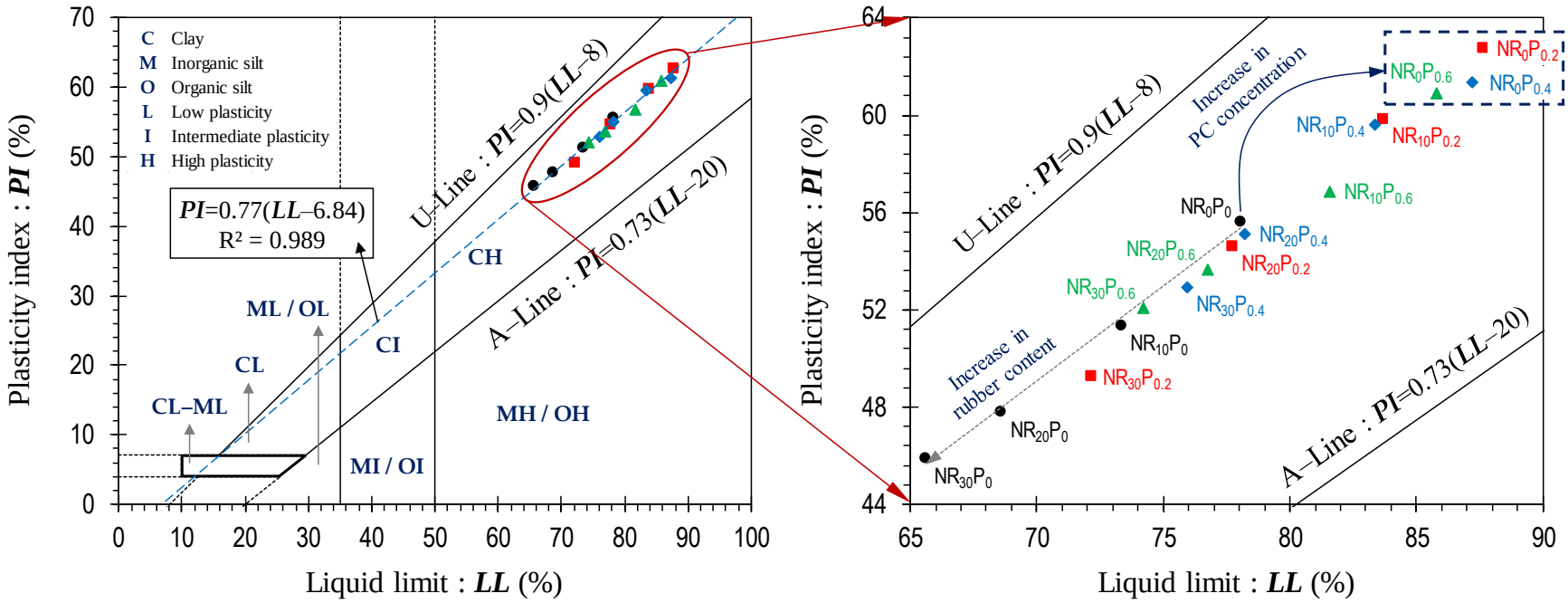

Figure 5. Standard Proctor compaction curves for the natural soil (NR_0P_0) and various soil–rubber mixtures: **(a)** untreated; and **(b)** treated with 0.2 g/l PC.

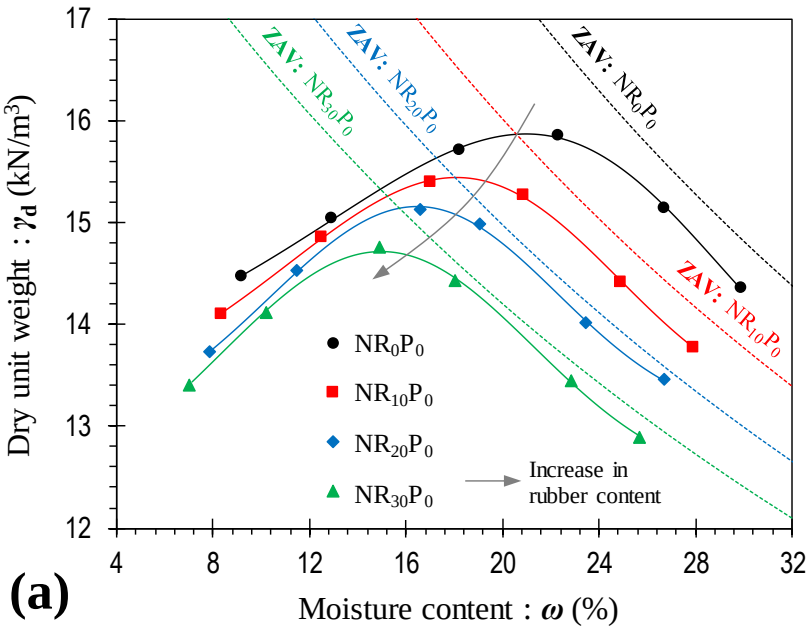

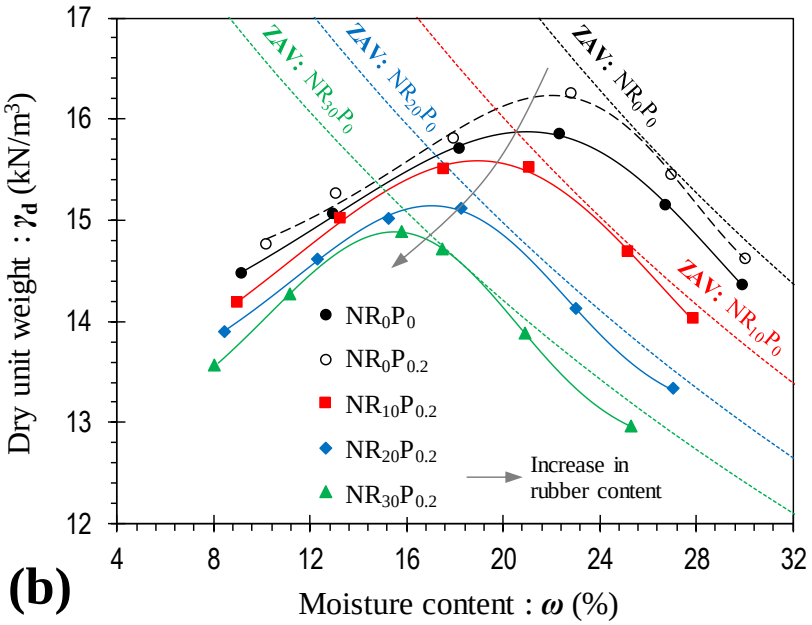

Figure 6. Swell–time curves for the natural soil (NR_0P_0) and various soil–rubber mixtures: **(a)** untreated; and **(b)** treated with 0.2 g/l PC.

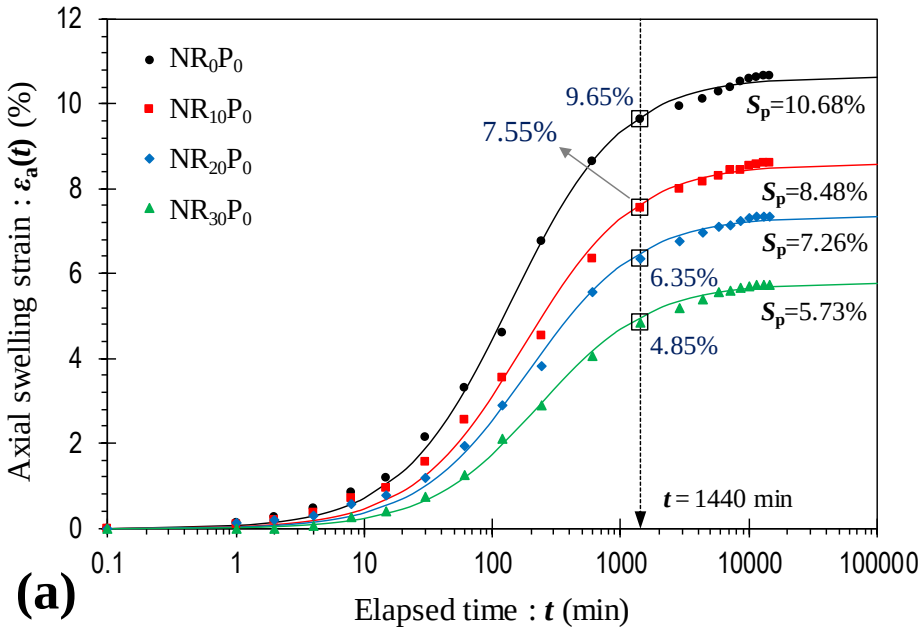

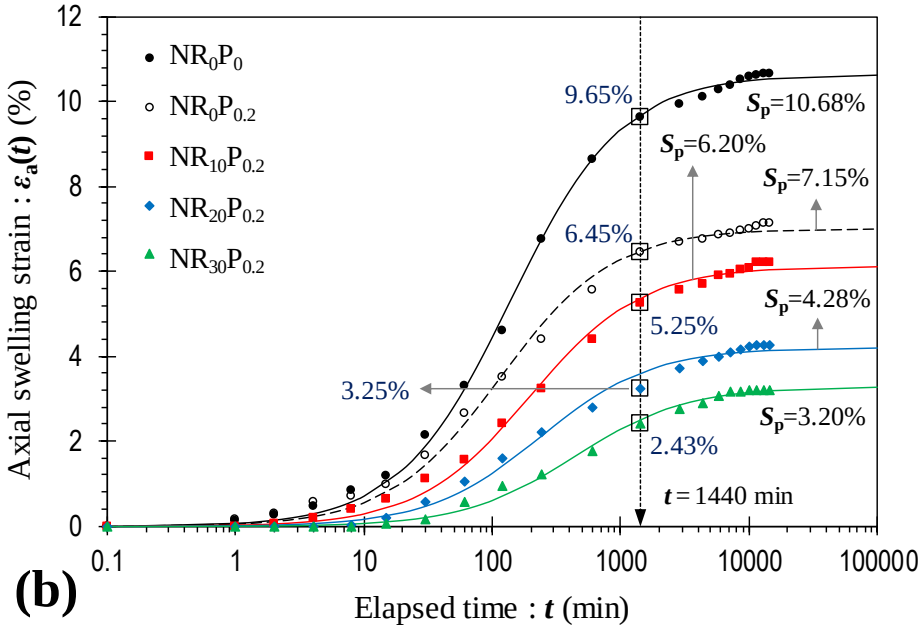

Figure 7. Variations of swelling pressure and swelling potential against rubber content for the tested samples (**H**=*highly expansive*; and **M**=*moderately expansive*).

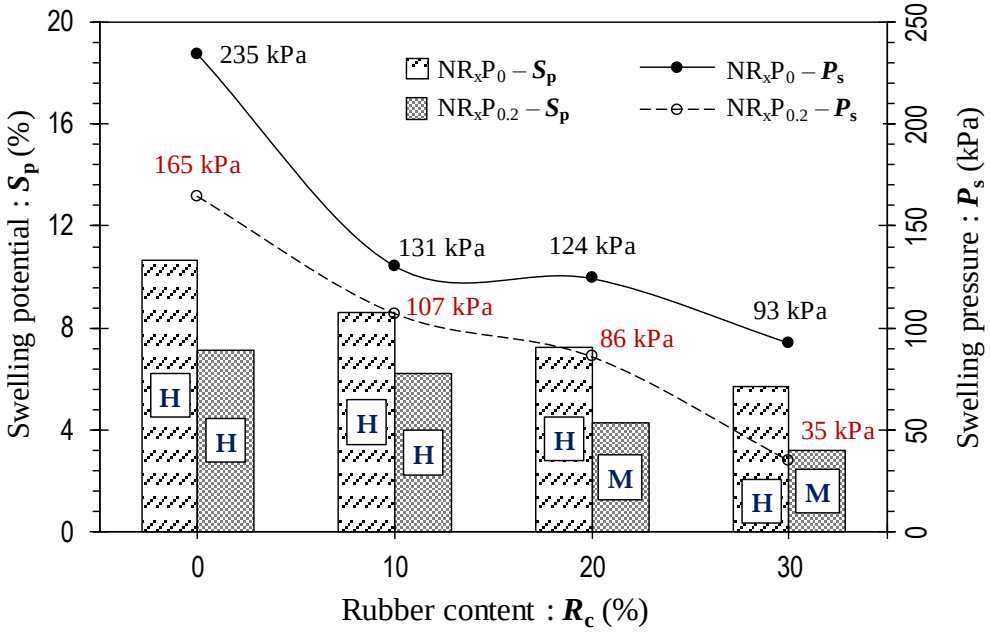

Figure 8. Swell–time characteristics with respect to the oedometer swell test (modified from Soltani et al. (2017[b] and 2018)).

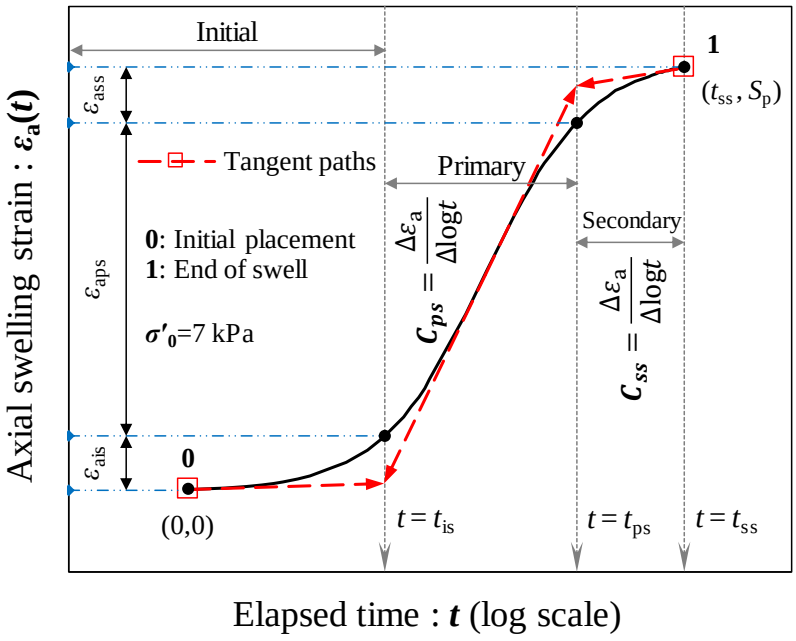

Figure 9. Variations of the **(a)** primary and **(b)** secondary swelling rates against rubber content for the tested samples.

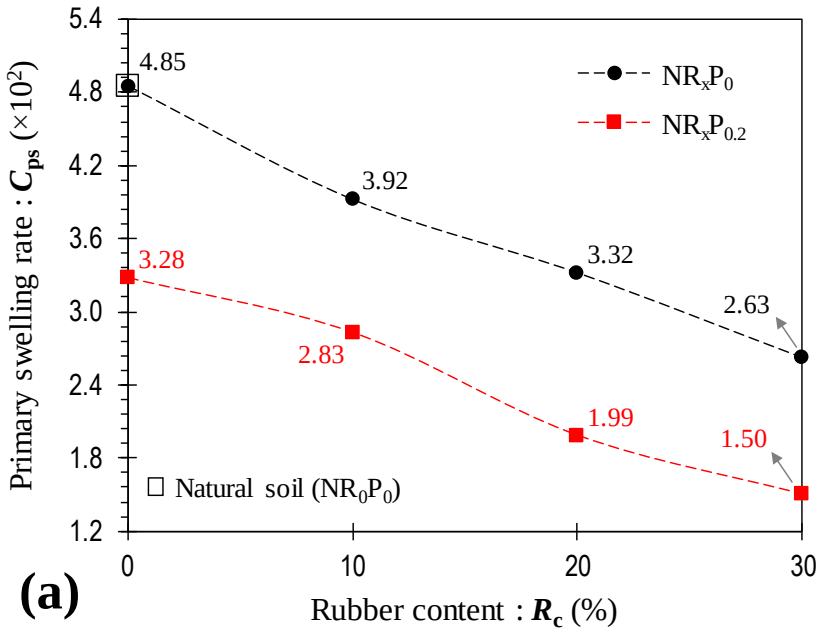

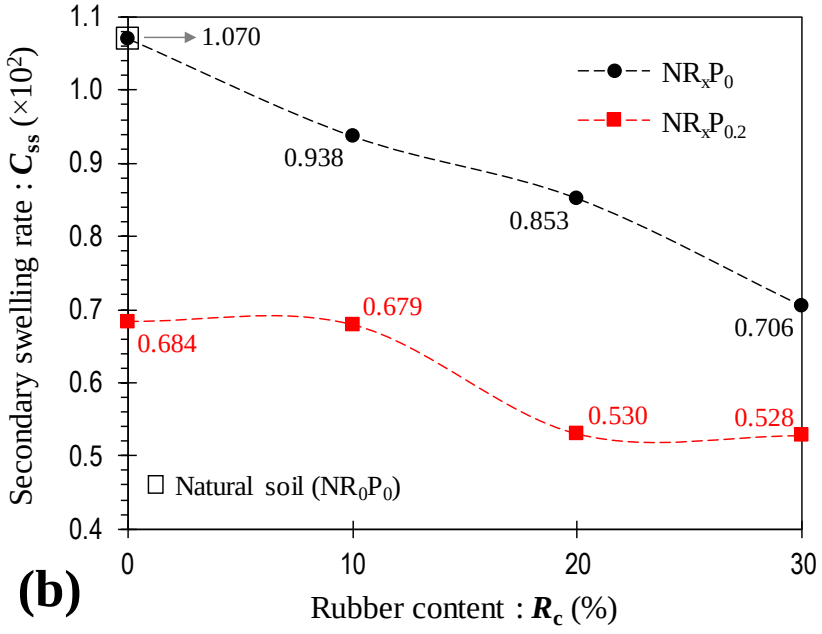

Figure 10. Variations of the shrinkage and swelling strains, along with corresponding shrink–swell index values, against rubber content for the tested samples ($\mathbf{H^R}$=*highly reactive*; $\mathbf{M^R}$=*moderately reactive*; and $\mathbf{S^R}$=*slightly reactive*).

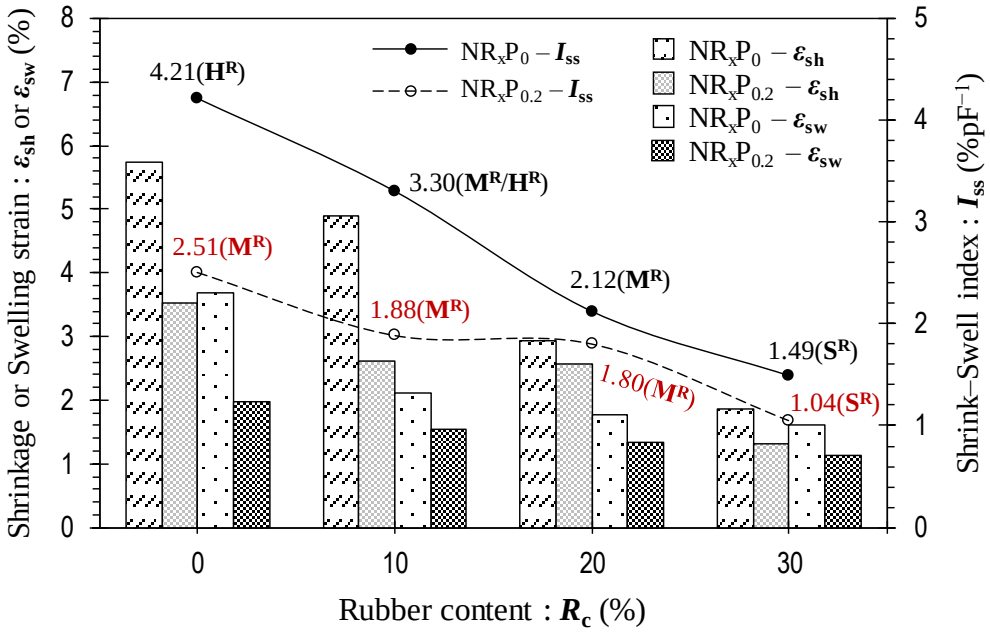

Figure 11. Variations of swelling potential against number of applied wetting–drying cycles for the samples NR_0P_0, $NR_{30}P_0$, $NR_0P_{0.2}$ and $NR_{30}P_{0.2}$.

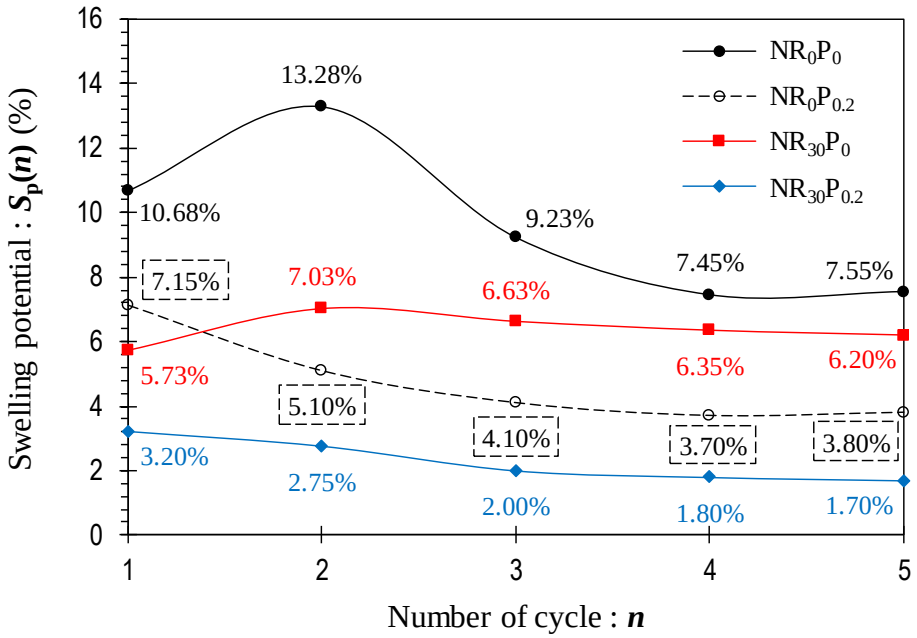

Figure 12. Variations of the crack intensity factor, along with corresponding crack reduction factors, against rubber content for the tested samples.

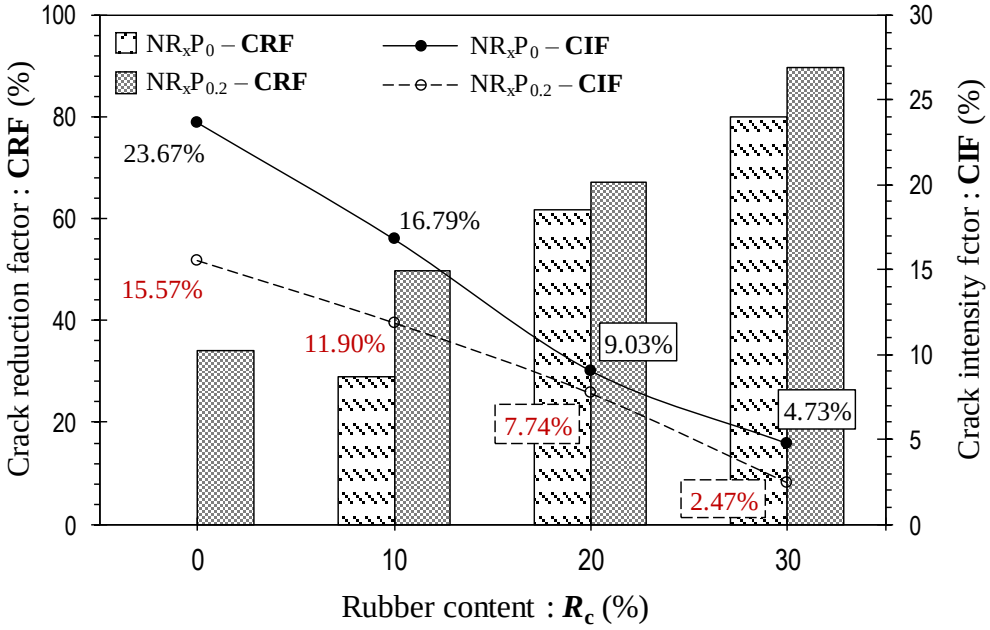

Figure 13. Observed crack patterns for the tested samples.

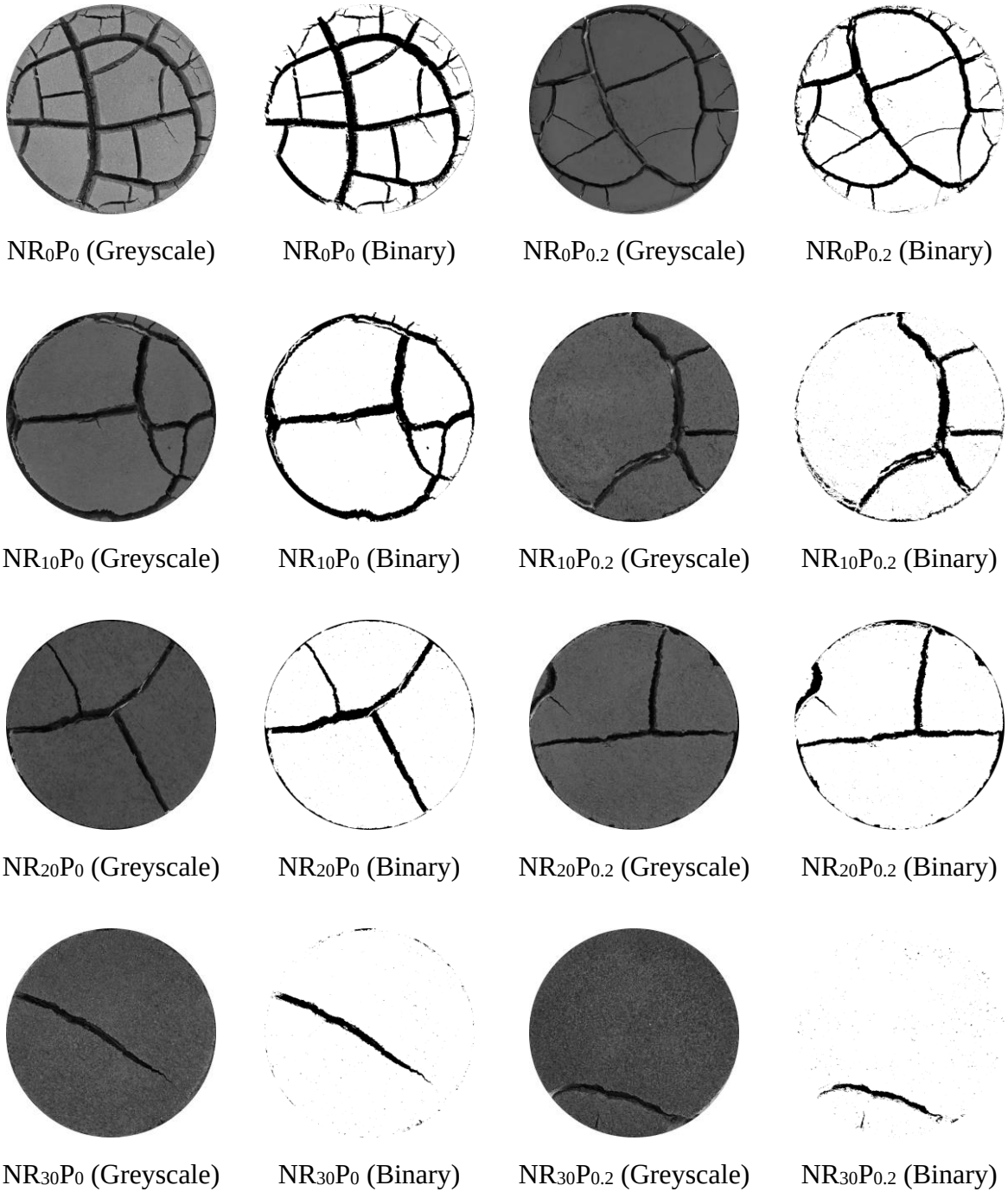

Figure 14. Scanning electron micrographs (SEM): **(a)** NR_0P_0; **(b)** $NR_{20}P_0$; **(c)** $NR_0P_{0.2}$; and **(d)** $NR_{20}P_{0.2}$.

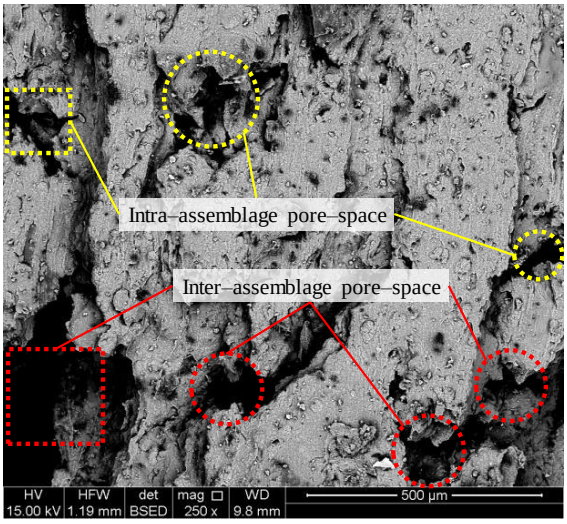

(a)

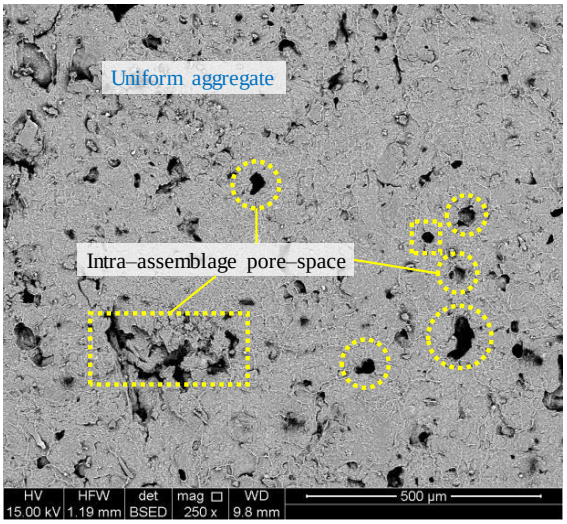

(c)

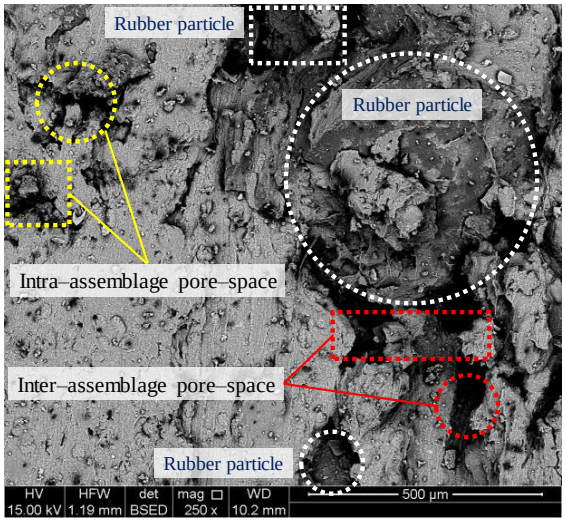

(b)

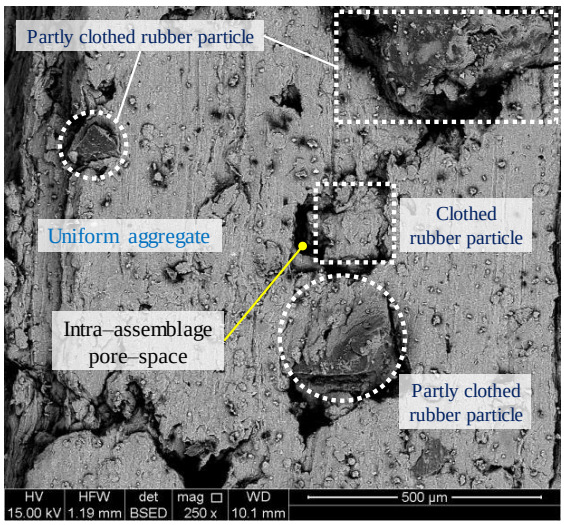

(d)

Statement of Authorship

Statement of Authorship

Title of Paper	Rubber Powder–Polymer Combined Stabilization of South Australian Expansive Soils
Publication Status	■ Published ☐ Accepted for Publication ☐ Submitted for Publication ☐ Unpublished and Unsubmitted work written in manuscript style
Publication Details	**Soltani A**, Deng A, Taheri A and Mirzababaei M **(2018)** Rubber Powder–Polymer Combined Stabilization of South Australian Expansive Soils. ***Geosynthetics International* 25(3): 304–321**, http://doi.org/10.1680/jgein.18.00009.

Principal Author

Name of Principal Author (Candidate)	Amin Soltani (**Email:** Amin.Soltani@adelaide.edu.au)		
Contribution to the Paper	Overall paper preparation		
Overall percentage (%)	85%		
Certification:	This paper reports on original research I conducted during the period of my Higher Degree by Research candidature and is not subject to any obligations or contractual agreements with a third party that would constrain its inclusion in this thesis. I am the primary author of this paper.		
Signature		Date	06/29/2018

Co-Author Contributions

By signing the Statement of Authorship, each author certifies that:

i. the candidate's stated contribution to the publication is accurate (as detailed above);
ii. permission is granted for the candidate in include the publication in the thesis; and
iii. the sum of all co-author contributions is equal to 100% less the candidate's stated contribution.

Name of Co-Author	An Deng **Senior Lecturer**, School of Civil, Environmental and Mining Engineering, The University of Adelaide, Adelaide, SA 5005, Australia (**Email:** An.Deng@adelaide.edu.au)		
Contribution to the Paper	Paper review and revision		
Signature		Date	07/23/2018

Name of Co-Author	Abbas Taheri **Senior Lecturer**, School of Civil, Environmental and Mining Engineering, The University of Adelaide, Adelaide, SA 5005, Australia (**Email:** Abbas.Taheri@adelaide.edu.au)		
Contribution to the Paper	Paper review and revision		
Signature		Date	07/16/2018

Name of Co-Author	Mehdi Mirzababaei **Lecturer**, School of Engineering and Technology, Central Queensland University (CQU), Melbourne, VIC 3000, Australia (**Email:** M.Mirzababaei@cqu.edu.au)		
Contribution to the Paper	Paper review and revision		
Signature		Date	07/23/2018

1

Published Copy [Link]

Geosynthetics International, 2018, **25**, No. 3

Rubber powder–polymer combined stabilization of South Australian expansive soils

A. Soltani[1], A. Deng[2], A. Taheri[3] and M. Mirzababaei[4]

[1] *PhD Student, School of Civil, Environmental and Mining Engineering, The University of Adelaide, Adelaide, SA 5005, Australia, E-mail: amin.soltani@adelaide.edu.au (corresponding author) (Orcid:0000-0002-0483-7487)*
[2] *Senior Lecturer, School of Civil, Environmental and Mining Engineering, The University of Adelaide, Adelaide, SA 5005, Australia, E-mail: an.deng@adelaide.edu.au*
[3] *Senior Lecturer, School of Civil, Environmental and Mining Engineering, The University of Adelaide, Adelaide, SA 5005, Australia, E-mail: abbas.taheri@adelaide.edu.au*
[4] *Lecturer, School of Engineering and Technology, Central Queensland University, Melbourne, VIC 3000, Australia, E-mail: m.mirzababaei@cqu.edu.au*

Received 28 June 2017, revised 19 December 2017, accepted 19 January 2018, published 25 May 2018

ABSTRACT: This study examines the combined capacity of rubber powder inclusion and polymer treatment in solving the swelling problem of South Australian expansive soils. The rubber powder was incorporated into the soil at three different rubber contents (by weight) of 10%, 20% and 30%. The preliminary testing phase consisted of a series of consistency limits and free swell ratio tests, the results of which were analyzed to arrive at the optimum polymer concentration. The main test program included standard Proctor compaction, oedometer swell–compression, soil reactivity (shrink–swell index), cyclic wetting and drying, crack intensity, and micro-structure analysis by means of the scanning electron microscopy (SEM) technique. The improvement in swelling potential and swelling pressure was dependent on the rubber content, with polymer–treated mixtures holding a notable advantage over similar untreated cases. A similar dependency was also observed for the crack intensity factor and the shrink–swell index. The beneficial effects of rubber inclusion were compromised under the cyclic wetting and drying condition. However, this influence was eliminated where the rubber powder was paired with the polymer agent. A rubber inclusion of 20%, preferably paired with 0.2 g/l polymer, was suggested to effectively stabilize South Australian expansive soils.

KEYWORDS: Geosynthetics, Expansive soil, Rubber powder, Polymer, Swelling potential, Swelling pressure, Crack intensity, Cyclic wetting and drying

REFERENCE: Soltani, A., Deng, A., Taheri, A. and Mirzababaei, M. (2018). Rubber powder–polymer combined stabilization of South Australian expansive soils. *Geosynthetics International*, **25**, No. 3, 304–321. [https://doi.org/10.1680/jgein.18.00009]

1. INTRODUCTION

Previous testing conducted in South Australia indicates that the majority of soils in the state are expansive clays. The predominant soils are Hindmarsh and Keswick clays, which are abundantly found in high-population commercial and residential areas. Where exposed to seasonal environments, such soils are prone to significant volume changes, that is, heave and settlements, thereby bringing forth instability concerns to the overlying structures. These concerns have incurred significant maintenance costs, and thus demand engineering solutions to alleviate the associated socio-economic impacts on human life. Chemical stabilization by means of traditional cementitious agents such as cement and lime is often implemented as a common soil improvement technique (e.g. Al-Rawas *et al.* 2005; Estabragh *et al.* 2014; Soltani *et al.* 2017a). Though effective, the application of such agents is often limited by leaching problems, and in some cases, may result in adverse effects when treating soils containing large amounts of organic matter, sulfates and salts (Sivapullaiah *et al.* 2000; Puppala *et al.* 2004; Hoyos *et al.* 2006). Other disadvantages include their inherent time-dependent nature, reduction in material workability, low durability against local environmental conditions (e.g. acidic and alkaline flows), high transportation costs, and rising environmental concerns due to greenhouse gas emissions (Rao *et al.* 2001; Guney *et al.* 2007; Estabragh *et al.* 2013; Georgees *et al.* 2015; Alazigha *et al.* 2016). As the global community is shifting towards a more sustainable

Offprint provided courtesy of www.icevirtuallibrary.com
Author copy for personal use, not for distribution

mindset, alternate stabilization techniques capable of replacing or minimizing the need for such traditional agents have been highly encouraged. Beneficial reuse of solid waste materials and industrial byproducts, for example carpet waste fibers, kiln dusts, silicate/calcium chloride geopolymers and demolition wastes, can be regarded amongst the most well-received propositions in this context (e.g. Mirzababaei *et al.* 2013a, 2013b, 2017, 2018; Kua *et al.* 2017; Suksiripattanapong *et al.* 2017; Arulrajah *et al.* 2017a, 2017b, 2017c; Phummiphan *et al.* 2018).

In Australia, it is estimated that 48 million tires are disposed of each year, meaning that there is a relative abundance of waste tires available for recycling and beneficial reuse (Hannam 2014). Similar to fiber–reinforced soils, the rubber assemblage randomly distributes in the soil regime, and where optimized in dosage and geometry, amends the expansive soil with respect to moisture insensitivity (i.e. swell–shrink related volume changes), strength increase, and ductility improvement (e.g. Cetin *et al.* 2006; Akbulut *et al.* 2007; Özkul and Baykal 2007; Seda *et al.* 2007; Patil *et al.* 2011; Trouzine *et al.* 2012; Kalkan 2013; Srivastava *et al.* 2014; Signes *et al.* 2016; Yadav and Tiwari 2017a). A literature survey indicates a rather common emphasis on the application of coarse-graded tire rubber material, for example long tire rubber fibers. Such materials, however, would be associated with implementation difficulties when dealing with cohesive soils. On this basis, less regarded types of recycled tires such as tire rubber powder have the advantage of better workability, and thus add value if introduced to treat expansive soils.

Simple application procedures coupled with improved sustainability have promoted polymer-based additives as an attractive alternative to traditional cementitious agents. While commercially branded and readily accessible, such products have not yet received widespread acceptance among practicing engineers. This may be attributed to the lack of sufficient published data from independent establishments, and inadequate information provided by manufacturers regarding effective application rates or implementation procedures. A number of documented studies can be found which have assessed the efficiency of various polymer-based additives in treating expansive soils, thus mitigating the effect of swell–shrink related subsidence (e.g. Rauch *et al.* 2002; Inyang *et al.* 2007; Mirzababaei *et al.* 2009; Yazdandoust and Yasrobi 2010; Onyejekwe and Ghataora 2015; Alazigha *et al.* 2016; Ayeldeen and Kitazume 2017; Soltani *et al.* 2017b). Though promising, the reported results are not consistent in defining an ad hoc stabilization solution, and thus demand further examination.

The key to finding effective solutions to enhance the applications of expansive soils is to fundamentally understand their behavior in the face of changing moisture and temperature environments. For arid and semi-arid environments such as the Adelaide region of South Australia, this aspect is translated into alternate wetting and drying, incurred by varying periods of rainfall and drought. As such, before promoting any stabilization technique as an effective scheme, its efficiency where exposed to periodic wetting and drying should be examined. A number of studies have assessed the volume change behavior of expansive soils treated with cementitious admixtures (e.g. Rao *et al.* 2001; Guney *et al.* 2007; Kalkan 2011; Estabragh *et al.* 2013) and polymer-based additives (e.g. Yazdandoust and Yasrobi 2010; Alazigha *et al.* 2016; De Camillis *et al.* 2017; Soltani *et al.* 2017b) during wetting and drying. However, the volume change behavior of expansive soil–rubber composites treated with polymer-based additives during wetting and drying has not yet been addressed in the literature.

The present study intends to examine the combined capacity of rubber powder inclusion and polymer treatment in ameliorating the inferior engineering characteristics of a highly expansive soil found in Adelaide, South Australia. The experimental program was carried out in two phases consisting of preliminary and main tests. The preliminary testing phase consisted of a series of consistency limits and free swell ratio tests. The main test program included standard Proctor compaction, oedometer swell–compression, soil reactivity (shrink–swell index), cyclic wetting and drying, desiccation-induced cracking, and micro-structure analysis by means of the scanning electron microscopy (SEM) technique.

2. MATERIALS

2.1. Soil

A large quantity of expansive clay was sourced from a landfill site in Adelaide, South Australia, and was used for this study. This soil was characterized as clay with high plasticity (CH) in accordance with the Unified Soil Classification System (USCS). Mechanical properties of the soil, determined as per the relevant ASTM and Australian standards, are summarized in Table 1. The grain-size distribution curve, as illustrated in Figure 1, indicated a clay fraction (<2 μm) of 44%, along with 36% silt (2–75 μm), 15% fine sand (0.075–0.425 mm), 4% medium sand (0.425–2 mm) and 1% coarse sand (2–4.75 mm). The swelling potential and free swell ratio (FSR) were, respectively, measured as 10.68% and 2.27, from which the soil was graded into highly expansive with respect to the classification criteria suggested by Seed *et al.* (1962) and Sridharan and Prakash (2000).

2.2. Tire rubber powder

Commercially available recycled tire rubber powder, supplied by a local distributor, was used to stabilize the expansive soil. Figure 1 illustrates the grain-size distribution curve for the rubber particles, along with the used soil, determined as per the ASTM D422 standard. The rubber particles are similar in size to fine–medium sand, with particles ranging between 1.18 mm and 75 μm. The particle diameters corresponding to 10%, 30%, 50%, 60% and 90% finer (or passing) were measured as $d_{10} = 0.182$ mm, $d_{30} = 0.334$ mm, $d_{50} = 0.478$ mm, $d_{60} = 0.513$ mm and $d_{90} = 0.864$ mm (see Figure 1). In addition, the uniformity (i.e. $C_u = d_{60}/d_{10}$) and curvature (i.e. $C_c = d_{30}^2/d_{10}d_{60}$) coefficients were determined as

Offprint provided courtesy of www.icevirtuallibrary.com
Author copy for personal use, not for distribution

Table 1. Physical and mechanical properties of the soil

Properties	Value	Standard designation
Specific gravity, G_s	2.76	ASTM D854
Grain-size distribution		
Clay (<2 μm) (%)	44	ASTM D422
Silt (2 75 μm) (%)	36	
Fine sand (0.075 0.425 mm)	15	
Medium sand (0.425 2 mm)	4	
Coarse sand (2 4.75 mm)	1	
Consistency limits		
Liquid limit, LL (%)	78.04	AS 1289.3.9.1
Plastic limit, PL (%)	22.41	AS 1289.3.2.1
Plasticity index, PI (%)	55.63	AS 1289.3.3.1
Linear shrinkage, LS (%)	15.78	AS 1289.3.4.1
USCS soil classification	CH	ASTM D2487
Swelling properties		
Swelling potential, S_p (%)[a]	10.68	ASTM D4546
Swelling pressure, P_s (kPa)	235	
Free swell ratio, FSR[b]	2.27	Sridharan and Prakash (2000)
Compaction characteristics		
Maximum dry unit weight, γ_{dmax} (kN/m^3)	15.9	ASTM D698
Optimum moisture content, ω_{opt} (%)	21.0	

[a]Percentage expansion in oedometer from optimum moisture content to saturated condition under $\sigma'_0 = 7$ kPa; and
[b]Ratio of equilibrium sediment volume of 10 g oven-dried soil passing sieve 425 μm in distilled water to that of kerosene.

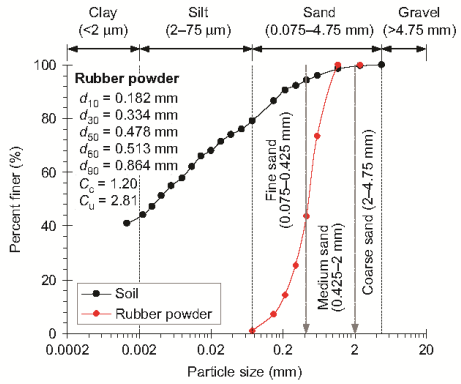

Figure 1. Grain-size distribution curves for the soil and tire rubber powder

$C_u = 2.81$ and $C_c = 1.20$, from which the rubber particles were classified as poorly-graded in accordance with the USCS criteria. Figure 2 illustrates microscopic micrographs of the rubber particles at different magnification ratios. The rubber particles are non-spherical and irregular in shape (see Figure 2b at 50 × magnification), with some cavities and micro-cracks propagated along the rubber's surface (see Figure 2c at 100 × magnification), thus making for a rough surface texture. Such surface characteristics could potentially promote adhesion and/or induce interfacial friction between the rubber particles and the soil grains, thereby altering the soil fabric into a coherent matrix of restricted heave/settlement. Physical properties and chemical composition of the rubber particles, as supplied by the manufacturer, are provided in Table 2. The specific gravity (at 20°C) was found to be 1.09, which is in compliance with that reported in the literature (see Yadav and Tiwari (2017b) for details).

2.3. Polymer

A commercially manufactured polymer agent, hereafter referred to as PC, was used as the binder. PC, chemically referred to as polyacrylamide or PAM ($–CH_2CHCONH_2–$), is a water-soluble anionic synthetic polymer formed from acrylamide subunits. The anionic polymerization is accomplished through substituting NH_2^- (amidogen) by OH^- (hydroxide) (Seybold 1994). PAM is often employed to increase the viscosity of water or to encourage flocculation of clay particles present in water (Seybold 1994; Lu *et al.* 2002; Graber *et al.* 2006). PC, in particular, has been successfully implemented in Australian roadway construction as a suitable binder for a variety of clays, shales and gravels (Andrews and Sharp 2010; Camarena 2013; Georgees *et al.* 2015). It is supplied in granular form, and often diluted with water (i.e. 200 g of PC into 1000 litres of water, as recommended by the manufacturer) for application. Other properties include a specific gravity (at 25°C) of 0.8 and a pH (at 25°C) of 6.9.

3. EXPERIMENTAL WORK

The rubber powder was incorporated into the soil at three different rubber contents (defined as rubber to dry soil weight ratio), that is $R_c = 10\%$, 20% and 30%. The experimental program was carried out in two phases consisting of preliminary and main tests. The preliminary testing phase included a series of consistency limits and free swell ratio tests. The intention of the preliminary testing phase was to identify a PC concentration rate capable of yielding an effective soil–rubber stabilization scheme. The natural soil and various soil–rubber mixtures were examined with three different PC concentrations (defined as weight of PC to volume of water ratio), that is 0.2 g/l (manufacturer-recommended), 0.4 g/l and 0.6 g/l. The consistency limits, that is, the liquid limit, plastic limit, plasticity index and linear shrinkage, were measured as per Australian standards (see relevant standard designations in Table 1). The free swell ratio is defined as the ratio of equilibrium sediment volume of 10 g oven-dried soil passing a 425 μm sieve in water (or in the case of this study, PC solution) to that of kerosene (Sridharan and Prakash 2000). As a consequence of rubber particles floating on water, only the natural soil was tested for the free swell ratio. Hereafter, the following coding system is adopted to designate the various mix designs

$$NR_xP_y \quad (1)$$

Offprint provided courtesy of www.icevirtuallibrary.com
Author copy for personal use, not for distribution

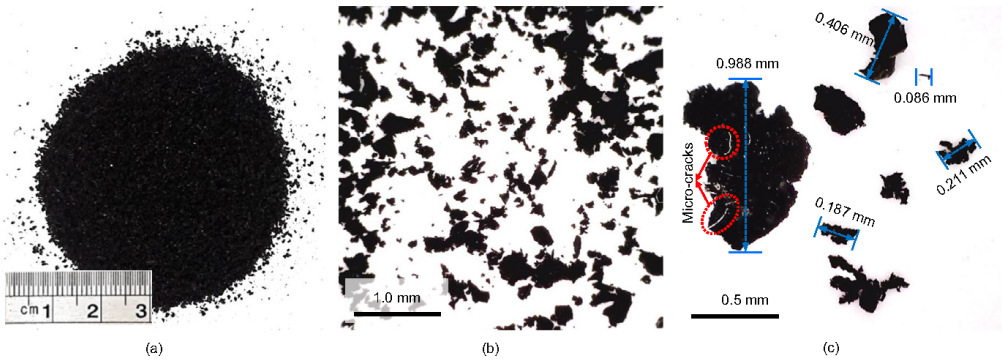

Figure 2. Tire rubber powder at different magnifications: (a) without magnification; (b) 50 × magnification; (c) 100 × magnification

Table 2. Physical properties and chemical composition of tire rubber powder (as supplied by the manufacturer)

Properties	Value/Description
Physical properties	
Physical appearance	Fine black powder
Solubility in water	Insoluble
Water adsorption	Negligible
Resistance to acid and alkaline	Excellent
Specific gravity (at 20°C), G_s	1.09
Softening point (°C)	170
Chemical composition	
Styrene Butadiene copolymer (%)	55
Acetone extract (%)	5 20
Carbon black (%)	25 35
Zinc oxide (%)	2.5
Sulphur (%)	1 3

where N = natural soil; R_x = x% rubber (x = 0, 10%, 20% and 30%); and P_y = y g/l PC (y = 0, 0.2 g/l, 0.4 g/l and 0.6 g/l). The natural soil with no additives is, therefore, denoted as NR_0P_0. As a typical example, $NR_{20}P_{0.4}$ represents the natural soil mixed with 20% rubber and treated with 0.4 g/l PC. A total of 16 mix designs were tested for consistency limits during the preliminary testing phase, whereas only four scenarios, that is, NR_0P_0, $NR_0P_{0.2}$, $NR_0P_{0.4}$ and $NR_0P_{0.6}$, were considered for the free swell ratio test.

The main test program was carried out on the natural soil and various soil–rubber mixtures without and with the optimum PC concentration. Hereafter, the former will be referred to as untreated, while the latter will be denoted as treated. The optimum PC concentration was selected as 0.2 g/l based on the preliminary test results, which will be further discussed in Section 4.1. The main test program consisted of the following tests: (i) standard Proctor compaction; (ii) oedometer swell–compression; (iii) soil reactivity (shrink–swell index); (iv) cyclic wetting and drying; (v) desiccation-induced cracking; and (vi) microstructure (SEM) analysis. The methodology associated with each component of the main test program will be further outlined in detail.

3.1. Compaction studies and sample preparation

A series of standard Proctor compaction tests were carried out on the natural soil (NR_0P_0) and various soil–rubber mixtures, untreated and treated with 0.2 g/l PC, in accordance with the ASTM D698 standard. Samples for the oedometer swell–compression, soil reactivity (shrink–swell index), cyclic wetting and drying and SEM tests were prepared by the static compaction technique at the corresponding optimum moisture content and maximum dry unit weight of each mixture (see Table 3). The required amount of water or PC solution (with 0.2 g/l concentration) corresponding to the desired optimum moisture content was added to each mixture, and thoroughly mixed by hand. Extensive care was dedicated to pulverizing the clumped particles, targeting homogeneity of the mixtures. Mixtures were then enclosed in plastic bags and stored under room temperature conditions for 24 h, ensuring even distribution of moisture throughout the soil mass. A special split mold, similar to that described in Soltani *et al.* (2017a), was designed and fabricated from stainless steel to accomplish static compaction. The mold consisted of three sections, that is, the top collar, the middle oedometer ring, and the bottom collar. The oedometer ring measures 50 mm in diameter and 20 mm in height, and accommodates the sample for oedometer testing conditions. The moist mixtures were compressed in the mold in three layers at a constant displacement rate of 1.5 mm/min to a specific compaction load, each layer having attained the desired/target maximum dry unit weight. The surfaces of the first and second compacted layers were scarified to ensure a good bond between adjacent layers of the mixture. Samples for the simplified core shrinkage test (i.e. a component of the soil reactivity test, as further outlined in Section 3.3) were prepared in a similar fashion. In this case, however, a different mold with a middle section measuring 50 mm in diameter and 100 mm in height, along with five compaction layers, was adopted. As a consequence of rubber particles floating on water, standard procedures outlined in the ASTM D854 standard for measuring the specific gravity of particles were

Offprint provided courtesy of www.icevirtuallibrary.com
Author copy for personal use, not for distribution

Table 3. Mix designs and their properties used for the main experimental program

Soil (%)	R_c (%)	PC (g/l)	Designation	LL (%)[a]	ω_{opt} (%)[b]	γ_{dmax} (kN/m^3)[b]	G_{sm}[c]	e_0[b]
100	0	0	NR_0P_0	78.04	21.0	15.9	2.76	0.706
90	10		$NR_{10}P_0$	73.32	18.1	15.4	2.42	0.538
80	20		$NR_{20}P_0$	68.59	16.5	15.2	2.20	0.422
70	30		$NR_{30}P_0$	65.58	15.0	14.7	2.04	0.359
100	0	0.2	$NR_0P_{0.2}$	87.61	22.0	16.2	2.76	0.668
90	10		$NR_{10}P_{0.2}$	83.67	18.9	15.6	2.42	0.524
80	20		$NR_{20}P_{0.2}$	77.73	17.0	15.1	2.20	0.424
70	30		$NR_{30}P_{0.2}$	72.14	15.5	14.9	2.04	0.344

[a]Initial placement condition for desiccation-induced crack tests;
[b]Initial placement condition for oedometer swell compression, soil reactivity (shrink swell index), cyclic wetting and drying and SEM tests; and
[c]Specific gravity of mixtures obtained as per Equation 2.

not applicable. Therefore, the average specific gravity of various soil–rubber mixtures was estimated by the following theoretical equation (Trouzine *et al.* 2012)

$$G_{sm} = \frac{G_{ss}G_{sr}(w_s + w_r)}{w_s G_{sr} + w_r G_{ss}} \quad (2)$$

where G_{sm} = specific gravity of soil–rubber mixture; w_{ss} = weight of dry soil; w_r = weight of rubber particles; G_{ss} = specific gravity of soil solids (=2.67); and G_{sr} = specific gravity of rubber particles (=1.09).

Basic mechanical properties of the prepared samples used for the main tests are summarized in Table 3. A total of eight mix designs, divided into two groups of untreated (designated as NR_0P_0, $NR_{10}P_0$, $NR_{20}P_0$ and $NR_{30}P_0$) and treated with 0.2 g/l PC (designated as $NR_0P_{0.2}$, $NR_{10}P_{0.2}$, $NR_{20}P_{0.2}$ and $NR_{30}P_{0.2}$), were considered for the main experimental program.

3.2. Oedometer swell–compression test

The prepared samples were subjected to a series of oedometer swell–compression tests as specified in the ASTM D4546 standard. The test included two stages, that is swell and compression. In the first stage, the desired sample was allowed to freely swell under a low nominal overburden stress of $\sigma_0' = 7$ kPa. The incurred axial swelling strain or heave was recorded during various time intervals to a point in which swell–time equilibrium, a state corresponding to the sample's swelling potential (defined as the ultimate axial swelling strain), was achieved. During the compression stage, the swollen sample was gradually loaded to counteract the built-up axial swelling strain. The stress required to retain the sample's initial placement condition (or void ratio e_0, as outlined in Table 3) was taken as the swelling pressure (Sridharan *et al.* 1986).

The conventional oedometer swell test has been regarded as the most common technique to assess the soil's expansive potential or degree of expansivity (Sridharan and Keshavamurthy 2016). Some limitations, however, include its dependency to the sample's initial moisture condition and not accounting for suction variations. Some of the more common classification procedures for expansive soils, developed with respect to percent expansion in the oedometer under $\sigma_0' = 7$ kPa (Holtz and Gibbs 1956; Seed *et al.* 1962; Sridharan and Prakash 2000), are summarized in Table 5.

3.3. Soil reactivity test and the shrink–swell index

The shrink–swell index, determined in accordance with the AS 1289.7.1.1 standard, can be characterized as a direct method of evaluating the soil's degree of expansivity (referred to as reactivity in Australian geotechnical practice). Other significant applications include its widespread use for predicting free surface ground movements (Cameron 1989; Fityus *et al.* 2005). Despite its successful adoption in routine geotechnical practice in Australia, its existence and use within Australia have not been widely recognized by the international geotechnical community (Fityus *et al.* 2005). The shrink–swell index requires incorporating test results obtained from the simplified core shrinkage and the modified oedometer swell tests, which are further presented in detail.

- In the simplified core shrinkage test, the desired cylindrical sample, measuring 50 mm in diameter and 100 mm in height (see Section 3.1), is allowed to desiccate under room temperature conditions. The variations of axial shrinkage strain are monitored during various time intervals to a point at which shrinkage ceases. The sample is then oven-dried at 105°C to remove any remaining moisture. Final height measurements are taken by a Vernier caliper, from which the sample's ultimate shrinkage strain, denoted as ε_{sh}, can be derived.
- The modified oedometer swell test is essentially similar to the first stage of the oedometer swell–compression test, as outlined in Section 3.2. In this case, however, a higher nominal overburden stress equal to $\sigma_0' = 25$ kPa is adopted. The ultimate axial swelling strain upon achieving swell–time equilibrium is denoted as ε_{sw}.

Finally, the shrink–swell index I_{ss} is obtained by the following (AS 1289.7.1.1)

$$I_{ss} = \frac{\varepsilon_{sh} + \frac{1}{2}\varepsilon_{sw}}{1.8} \quad (3)$$

Offprint provided courtesy of www.icevirtuallibrary.com
Author copy for personal use, not for distribution

The denominator in Equation 3 is an empirical coefficient, which is defined as the range of total suction change with respect to the soil's volume increase from air-dry to near saturation condition. The range of total suction change is commonly taken as 1.8 pF (pF = potential of free energy, which is a unit for soil suction and is related to kilopascals through pF = 1 + log [kPa]) for the majority of reactive soils in Australia. This value was suggested based on collective experience of the AS 2870 code committee, and is supported by the observation that the majority of volume change takes place in a linear manner between the wilting point for trees and a moisture content close to saturation (Fityus *et al.* 2005). Previous studies have reported the wilting point suction to vary between 4.0 pF and 4.4 pF (Wray 1998; Cameron 2001). Furthermore, the variations of total suction at moisture contents near saturation state have been reported to fall in the range of 2.2 pF to 2.5 pF (Fityus *et al.* 2005). As such, the suggested value of 1.8 pF can be deemed as reasonable. The shrink–swell index represents percentage axial strain, either swelling or shrinkage, per change in unit suction of the soil (i.e. $\%pF^{-1}$). Thus, it is expected to address some limitations associated with other expansive soil classification criteria, which are either dependent on the soil's initial moisture condition or do not account for suction variations (e.g. the conventional oedometer swell test, as outlined in Table 5). Classification procedures for expansive soils with respect to the shrink–swell index, as suggested by Seddon (1992), are summarized in Table 6.

3.4. Cyclic wetting and drying test

Similar to the first step in the oedometer swell–compression test (see Section 3.2), the desired sample was allowed to freely swell under $\sigma'_0 = 7$ kPa resulting from a cylindrical load directly applied to the sample. Upon completion of the wetting process (i.e. achieving swell–time equilibrium), reservoir water was drained through a drainage valve embedded within the oedometer cell. The oedometer cell, along with the cylindrical load, were then transferred to an oven set to a constant temperature of 40°C for drying. The drying process was carried out for about five days to ensure shrinkage equalization. The combination of one wetting and the subsequent drying stage is designated as one wetting–drying cycle. Alternate wetting and drying of the sample was repeated in a similar fashion to a point at which the swelling potential subject to two successive cycles reached a nearly constant value. In this study, four mix designs, that is, NR_0P_0, $NR_{30}P_0$, $NR_0P_{0.2}$ and $NR_{30}P_{0.2}$, were tested for cyclic wetting and drying.

The swelling potential may either decrease or increase with an increase in the number of applied wetting–drying cycles, and regardless of the observed trend, further converges to a nearly constant value upon the completion of several cycles (Soltani *et al.* 2017b). This state is defined as swell–shrink (or elastic) equilibrium, which signifies a transitional deformation state where the plastic (or irreversible) deformation incurred in the soil structure (during wetting and drying) largely fades out, and thus change to elastic (or reversible) in character (Tripathy *et al.* 2002; Alonso *et al.* 2005; Estabragh *et al.* 2015). In this study, the equilibrium condition was achieved at the fourth cycle, thus only five cycles were implemented for the tested samples.

3.5. Desiccation-induced crack studies

Desiccation-induced cracking can adversely influence the performance of various soil structures (e.g. excavations, earth slopes, highway embankments and clay liners), and thus assumes a significant role in fulfilling design criteria when constructing on expansive soils. The intensity of cracks is commonly quantified by means of the crack intensity factor (CIF) and the crack reduction factor (CRF), which are defined as (Yesiller *et al.* 2000; Miller and Rifai 2004)

$$\mathrm{CIF} = \frac{A_c}{A_0} \times 100 \tag{4}$$

$$\mathrm{CRF} = \frac{\mathrm{CIF_n} - \mathrm{CIF_s}}{\mathrm{CIF_n}} \tag{5}$$

where A_c = area of cracks; A_0 = initial area of the tested sample; $\mathrm{CIF_n}$ = crack intensity factor for the natural soil (NR_0P_0); and $\mathrm{CIF_s}$ = crack intensity factor for the stabilized sample.

Desiccation-induced crack tests were carried out on the natural soil and various soil–rubber mixtures (untreated and treated with 0.2 g/l PC) prepared by the slurry technique at their respective liquid limit, as commonly adopted in the literature (e.g. Tang *et al.* 2012; Costa *et al.* 2013; Chaduvula *et al.* 2017). The required amount of water or PC solution corresponding to the desired liquid limit (see Table 3) was added to each mixture, and thoroughly mixed to obtain slurries of uniform consistency. The resultant slurries were poured into petri dishes, measuring 100 mm in diameter and 15 mm in height, and gently tapped on a wooden platform to remove entrapped air. To simulate the severe ambient conditions of the Adelaide region, samples were allowed to desiccate under a constant temperature of 40°C. Upon the completion of drying (moisture equalization), still photographs were taken using a high resolution digital camera fixed at a vertical angle 50 cm above the desiccated samples. The ImageJ software package was then implemented to quantify the crack features.

3.6. Scanning electron microscopy (SEM)

Significant information on the micro-structure can be obtained by the scanning electron microscopy (SEM) technique. Typical mixtures including NR_0P_0, $NR_{20}P_0$, $NR_0P_{0.2}$ and $NR_{20}P_{0.2}$ were investigated. The desired samples, prepared as per Section 3.1, were allowed to air dry for about 14 days. The samples were then carefully fractured into small cube-shaped pieces corresponding to a volume of approximately 1 cm^3, as suggested in the literature (e.g. Tang *et al.* 2007; Mirzababaei *et al.* 2009; Yazdandoust and Yasrobi 2010), and further scanned over

Offprint provided courtesy of www.icevirtuallibrary.com
Author copy for personal use, not for distribution

various magnification ratios ranging from 250× to 20 000×. In this study, the Philips XL20 SEM device, with a resolution of 4 μm and a maximum magnification ratio of 50 000×, was used for scanning electron microscopy imaging.

4. RESULTS AND DISCUSSION

4.1. Consistency limits and the free swell ratio

Figures 3a–3c illustrate the variations of liquid limit LL, plasticity index PI and linear shrinkage LS against PC concentration for the tested mix designs (i.e. NR_xP_y; where x = 0, 10%, 20% and 30%, and y = 0, 0.2 g/l, 0.4 g/l and 0.6 g/l), respectively. Untreated soil–rubber mixtures (NR_xP_0) exhibited lower consistency limits compared with that of the natural soil (NR_0P_0). In this case, the higher the rubber content the lower the consistency limits, following a monotonic decreasing trend. For instance, the natural soil resulted in LL = 78.04%, while the inclusion of 10%, 20% and 30% rubber resulted in LL = 73.32%, 68.59% and 65.58%, respectively. It is well-accepted that the consistency limits are primarily a function of the mixture's clay content. An increase in rubber content substitutes a larger portion of the clay content, and thus leads to lower consistency limits. The lower specific surface area and water adsorption capacity of the rubber particles compared with the soil grains also contributes to lower consistency limits (Cetin *et al.* 2006; Trouzine *et al.* 2012; Srivastava *et al.* 2014). As a result of PC treatment, the natural soil experienced a notable increase in the consistency limits. The magnitude of increase, however, was observed to be independent from the adopted PC concentration, as all three concentrations exhibited similar results with marginal differences (see NR_0P_y in Figure 3). As a typical case, LL increased from 78.04% for the natural soil (NR_0P_0) to 87.61%, 87.22% and 85.80% for $NR_0P_{0.2}$, $NR_0P_{0.4}$ and $NR_0P_{0.6}$, respectively. An increase in the consistency limits, the liquid limit in particular, implies that a flocculated fabric dominates the clay–rubber matrix (Mitchell and Soga 2005). As opposed to a face–to–face aggregated (or dispersed) fabric, an edge–to–face flocculated fabric offers more resistance to shear (or cone penetration), thereby leading to an increased liquid limit. PAM molecules are hydrophilic in nature, and thus provide additional adsorption sites for water molecules, which in turn contribute to higher consistency limits (Kim and Palomino 2009).

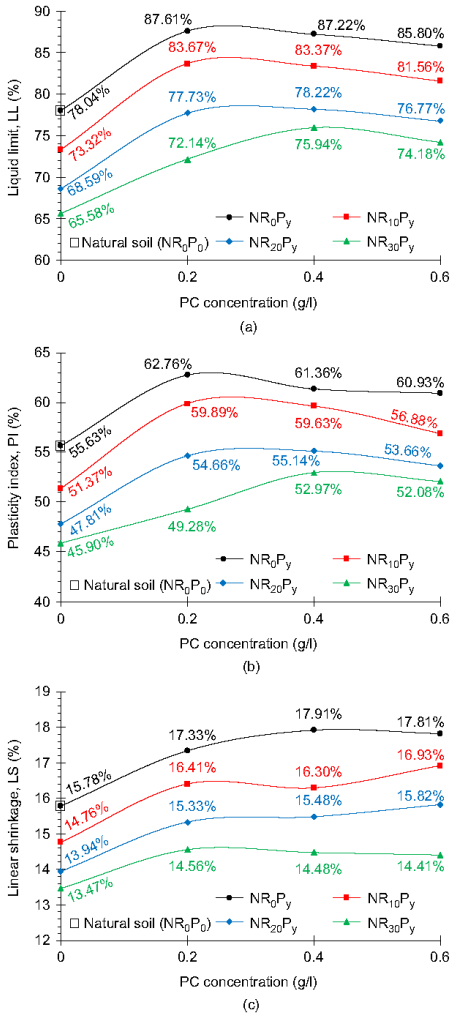

Figure 3. Consistency limits for the natural soil (NR_0P_0) and various soil–rubber mixtures treated with different PC concentrations: (a) liquid limit; (b) plasticity index; (c) linear shrinkage

The location of the tested mix designs on Casagrande's plasticity chart is illustrated in Figure 4. All mixtures lie within the CH region (clay with high plasticity) of the plasticity chart. The variations of PI against LL followed a linear path nearly parallel to the A line of the plasticity chart, that is, PI = 0.73(LL–20). In this case, a conventional regression analysis indicated the existence of a strong linear agreement in the form of PI = 0.77(LL–6.84) (with $R^2 = 0.989$) for the tested mixtures. For a given PC concentration, an increase in rubber content relocated the soil towards lower plasticity regions (e.g. see the typical linear trendline for NR_xP_0 in Figure 4). On the contrary, for a given soil–rubber mixture (constant rubber content), PC treatment repositioned the soil towards higher plasticity regions (e.g. see the typical arrowed path linking NR_0P_0 to NR_0P_y in Figure 4). The magnitude of increase in LL and PI, however, was observed to be independent from the adopted PC concentration, as evident with the clustering of data points at constant rubber contents (compare $NR_xP_{0.2}$ with $NR_xP_{0.4}$ and $NR_xP_{0.6}$ in Figure 4 at any arbitrary x value).

Results of the free swell ratio tests are summarized in Table 4. Suspension of the soil in distilled water (NR_0P_0) resulted in a free swell ratio of FSR = 2.27. Where suspended in PC solutions of 0.2 g/l, 0.4 g/l and 0.6 g/l,

Offprint provided courtesy of www.icevirtuallibrary.com
Author copy for personal use, not for distribution

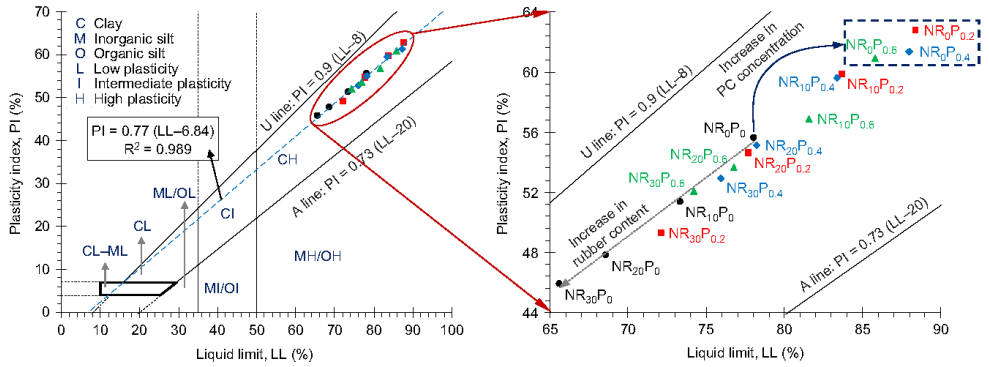

Figure 4. Location of various soil–rubber–PC mix designs on Casagrande's plasticity chart

FSR was measured as 1.67, 1.63 and 1.53, respectively. Classification procedures for expansive soils with respect to the FSR value, as suggested by Sridharan and Prakash (2000), are outlined in Table 4. The natural soil was classified as highly expansive, while PC–treated mixtures ($NR_0P_{0.2}$, $NR_0P_{0.4}$ and $NR_0P_{0.6}$) manifested a moderate degree of expansivity. As evident with the FSR values and their corresponding classifications, excessive PC concentrations, that is 0.4 g/l and 0.6 g/l, seem not to provide additional improvements.

Basic geotechnical properties such as the consistency limits and the free swell ratio can be employed to infer the soil's fabric, and thus arrive at initial judgements on the performance of various polymer agents at different concentrations (Wroth and Wood 1978; Prakash and Sridharan 2004; Mitchell and Soga 2005). Taking into account the discussed results, the three adopted PC concentrations were observed to yield similar results with marginal differences. Therefore, the manufacturer-recommended concentration of 0.2 g/l was deemed as satisfactory, and thus was used for the main tests, the results of which will be further presented and discussed in detail.

4.2. Compaction characteristics

Standard Proctor compaction curves, along with corresponding zero air void (ZAV) saturation lines, for the natural soil (NR_0P_0) and various soil–rubber mixtures untreated and treated with 0.2 g/l PC are provided in Figures 5a and 5b, respectively. As a result of rubber inclusion, the natural soil exhibited a notable reduction in both the maximum dry unit weight γ_{dmax} and the optimum moisture content ω_{opt} (see the trendline in Figure 5a). As a result of PC treatment, a marginal increase in both γ_{dmax} and ω_{opt} was noted for the natural soil (compare NR_0P_0 with $NR_0P_{0.2}$ in Figure 5b), while treated soil–rubber mixtures exhibited a trend similar to that observed for similar untreated cases (see the trendline in Figure 5b). Decrease in γ_{dmax} and ω_{opt} as a result of the rubber inclusions can be attributed to the lower specific gravity, specific surface area and water adsorption capacity of the rubber particles compared with the soil grains (Akbulut *et al.* 2007; Özkul and Baykal 2007; Seda *et al.* 2007; Kalkan 2013; Signes *et al.* 2016).

4.3. Swelling characteristics

4.3.1. *Swelling potential and swelling pressure*

Swell–time curves, represented by the two-parameter rectangular hyperbola function (e.g. Sivapullaiah *et al.* 1996; Sridharan and Gurtug 2004; Soltani *et al.* 2017a), for the natural soil (NR_0P_0) and various soil–rubber composites untreated and treated with 0.2 g/l PC are provided in Figures 6a and 6b, respectively. As a result of rubber inclusion and/or PC treatment, the swell–time locus experienced a major downward shift over the ε_a:log$t$ space (ε_a = axial swelling strain; and t = time), indicating a significant reduction in the magnitude of exhibited swelling strain, and thus swelling potential (defined as

Table 4. Free swell ratio (FSR) for the natural soil treated with various PC concentrations

Mixture	V_k (cm^3)	V_d (cm^3)	V_p (cm^3)	FSR	Degree of expansivity	Classification procedures with respect to FSR (Sridharan and Prakash 2000)				
NR_0P_0	15.0	34.0		2.27	High					
$NR_0P_{0.2}$[a]	15.0		25.0	1.67	Moderate	≤1	1 1.5	1.5 2	2 4	>4
$NR_0P_{0.4}$	15.0		24.5	1.63	Moderate	Negligible	Low	Moderate	High	Very High
$NR_0P_{0.6}$	15.0		23.0	1.53	Moderate					

[a]Manufacturer-recommended concentration; FSR = V_d/V_k or V_p/V_k; and V_k, V_d and V_p = Equilibrium sediment volume of 10 g oven-dried soil passing sieve 425 μm in kerosene, distilled water and PC solution, respectively.

Offprint provided courtesy of www.icevirtuallibrary.com
Author copy for personal use, not for distribution

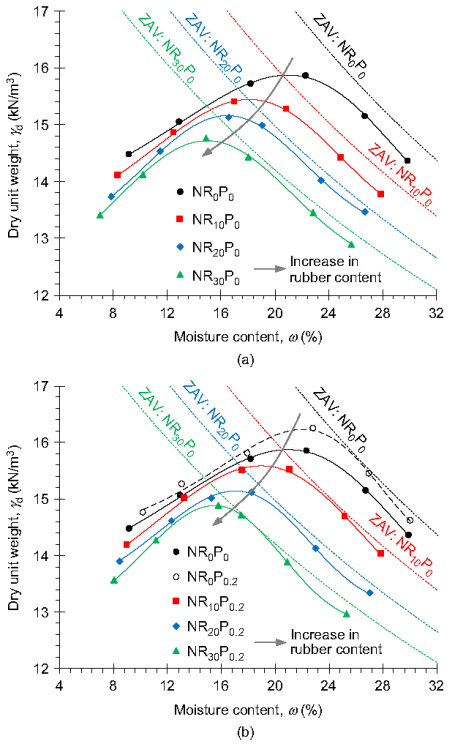

Figure 5. Standard Proctor compaction curves for the natural soil (NR_0P_0) and various soil–rubber mixtures: (a) untreated; (b) treated with 0.2 g/l PC

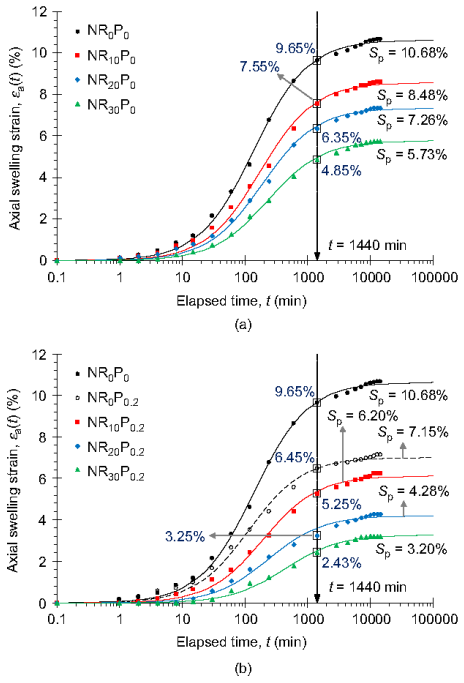

Figure 6. Swell–time curves for the natural soil (NR_0P_0) and various soil–rubber mixtures: (a) untreated; (b) treated with 0.2 g/l PC

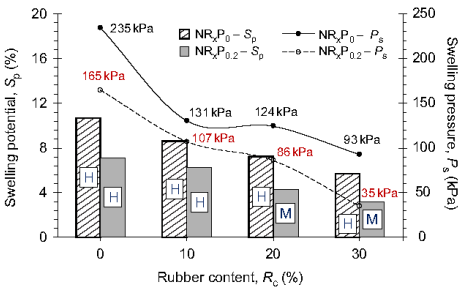

Figure 7. Variations of swelling pressure and swelling potential against rubber content for the tested samples (H = highly expansive; M = moderately expansive)

the ultimate axial swelling strain) compared with the natural soil. At $t = 24$ h, for instance, the natural soil resulted in a swelling strain of $\varepsilon_a(t) = 9.65\%$, while the inclusion of 10%, 20% and 30% rubber resulted in $\varepsilon_a(t) = 7.55\%$, 6.35% and 4.85%, respectively (see Figure 6a). Similar treated samples exhibited a more pronounced decreasing trend, where the above given values dropped to $\varepsilon_a(t) = 6.45\%$ ($NR_0P_{0.2}$), 5.25%, 3.25% and 2.43%, respectively (see Figure 6b). The natural soil and soil–rubber mixtures corresponding to $R_c = 10\%$, 20% and 30% resulted in swelling potential values of $S_p = 10.68\%$, 8.48%, 7.26% and 5.73%, respectively. As a result of PC treatment, however, the aforementioned values further decreased to $S_p = 7.15\%$, 6.20%, 4.28% and 3.20%, respectively.

Figure 7 illustrates the variations of swelling pressure and swelling potential against rubber content for the tested samples. The variations of swelling pressure P_s followed a trend similar to that observed for swelling potential S_p, and indicated that the higher the rubber content the greater the reduction in S_p and P_s, with treated samples having a notable advantage over similar untreated cases (compare NR_xP_0 with $NR_xP_{0.2}$ in Figure 7). The natural soil (NR_0P_0) and soil–rubber mixtures corresponding to $R_c = 10\%$, 20% and 30% resulted in $P_s = 235$ kPa, 131 kPa, 124 kPa and 93 kPa, respectively. Where treated with 0.2 g/l PC, these values dropped to $P_s = 165$ kPa ($NR_0P_{0.2}$), 107 kPa, 86 kPa and 35 kPa, respectively. The classification criterion proposed by Seed *et al.* (1962) (see Table 5) was implemented to assess the expansive potential of the tested samples, and the results are depicted in Figure 7. The two mix designs containing 30% rubber inclusion ($NR_{30}P_0$ and $NR_{30}P_{0.2}$) were classified as moderately expansive (specified as 'M'),

Offprint provided courtesy of www.icevirtuallibrary.com
Author copy for personal use, not for distribution

while other samples were graded into highly expansive (specified as 'H').

As demonstrated in Figure 8, the evolution of swelling with time, represented by an *S*–shaped curve over the ε_a:log*t* space, takes place in three stages, that is, the initial, primary and secondary swelling (Sivapullaiah *et al.* 1996; Sridharan and Gurtug 2004; Rao *et al.* 2006; Soltani *et al.* 2017b, 2018). The initial swelling phase, also recognized as inter-void swelling, occurs at the macro-structural level, and results in small volume changes mainly less than 10% of the total volume increase (<10%S_p). The primary swelling phase constitutes up to 80% of the total volume increase (≈80%S_p), and is graphically represented by a steep-sloped linear portion bounded by the initial and primary swelling time margins. The secondary swelling phase takes place as a result of double-layer repulsion, and accounts for small time-dependent volume changes. As opposed to the initial swelling phase, both the primary and secondary swelling phases evolve at micro-structural level where swelling of active clay minerals takes place. Critical variables obtained from the *S*–shaped curve, defined as swell–time characteristics, can be adopted to describe the time-dependency nature of the swelling phenomenon. These variables, as outlined in Figure 8, are characterized as: (i) completion time of the initial and primary swelling phases (t_{is} and t_{ps}); (ii) initial, primary and secondary swelling strains (ε_{ais}, ε_{aps} and ε_{ass}; $S_p = \varepsilon_{ais} + \varepsilon_{aps} + \varepsilon_{ass}$); and (iii) primary and secondary swelling rates (C_{ps} and C_{ss}), which are defined as (Soltani *et al.* 2018)

$$C_{ps} = \frac{\Delta\varepsilon_a}{\Delta \log t}\Bigg]_{t-t_{is}}^{t-t_{ps}} = \frac{\varepsilon_{aps}}{\log\left(t_{ps}/t_{is}\right)} \tag{6}$$

$$C_{ss} = \frac{\Delta\varepsilon_a}{\Delta \log t}\Bigg]_{t-t_{ps}}^{t-t_{ss}} = \frac{\varepsilon_{ass}}{\log\left(t_{ss}/t_{ps}\right)} \tag{7}$$

where t_{ss} = completion time of the secondary swelling phase (=14 400 min).

Swell–time characteristics for the tested samples are summarized in Table 7. The primary and secondary swelling strains mainly demonstrated a trend similar to that observed for the swelling potential S_p, meaning that R_c = 30% promoted the lowest ε_{aps} and ε_{ass} values for both untreated and treated soil–rubber mixtures (see $NR_{30}P_0$ and $NR_{30}P_{0.2}$ in Table 7). Figures 9a and 9b illustrate the variations of C_{ps} and C_{ss} against rubber content for the tested samples, respectively. The rubber inclusions led to a noticeable reduction in both C_{ps} and C_{ss}, indicating a capacity of counteracting the heave in both magnitude and time. The higher the rubber content the lower the

Table 5. Classification procedures for expansive soils with respect to the oedometer swell test

Degree of expansivity	Holtz and Gibbs (1956)[a]	Seed *et al.* (1962)[b]	Sridharan and Prakash (2000)[a]
Low (L)	<10	0 1.5	1 5
Moderate (M)	10 20	1.5 5	5 15
High (H)	20 30	5 25	15 25
Very high (VH)	>30	>25	>25

[a] % expansion in oedometer from air-dry to saturated condition under σ_0' = 7 kPa; and
[b] % expansion in oedometer from optimum moisture content to saturated condition under σ_0' = 7 kPa.

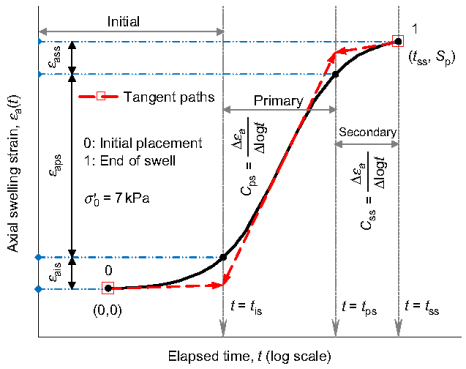

Figure 8. Swell–time characteristics with respect to the oedometer swell test (modified from Soltani *et al.* (2017b, 2018))

Table 6. Classification procedures for expansive soils with respect to the shrink–swell index (Seddon 1992)

Degree of expansivity/reactivity	Shrink swell index, I_{ss} (%pF^{-1})
Slightly reactive (S^R)	0.8 1.7
Moderately reactive (M^R)	1.7 3.3
Highly reactive (H^R)	3.3 5.8
Extremely reactive (E^R)	>5.8

Table 7. Summary of the swell–time characteristics for the tested samples

Mixture	t_{is} (min)	t_{ps} (min)	ε_{ais} (%)	ε_{aps} (%)	ε_{ass} (%)	S_p (%)	C_{ps} (×10^2)	C_{ss} (×10^3)
NR_0P_0	21	939	1.40	8.00	1.27	10.68	4.85	10.71
$NR_{10}P_0$	26	1161	1.11	6.46	1.03	8.60	3.92	9.38
$NR_{20}P_0$	28	1167	0.95	5.38	0.93	7.26	3.32	8.53
$NR_{30}P_0$	34	1441	0.74	4.28	0.71	5.73	2.63	7.06
$NR_0P_{0.2}$	18	753	0.94	5.33	0.88	7.15	3.28	6.84
$NR_{10}P_{0.2}$	29	1343	0.79	4.71	0.70	6.20	2.83	6.79
$NR_{20}P_{0.2}$	35	1412	0.54	3.20	0.53	4.28	1.99	5.30
$NR_{30}P_{0.2}$	62	2387	0.41	2.38	0.41	3.20	1.50	5.28

Offprint provided courtesy of www.icevirtuallibrary.com
Author copy for personal use, not for distribution

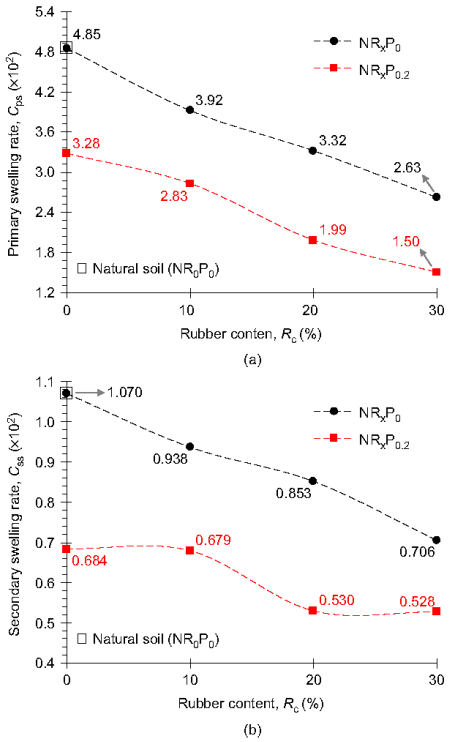

Figure 9. Variations of the (a) primary and (b) secondary swelling rates against rubber content for the tested samples

swelling rates, following a monotonic decreasing trend, with treated samples exhibiting more efficiency in reducing C_{ps} and C_{ss} compared with similar untreated cases (compare NR_xP_0 with $NR_xP_{0.2}$ in Figure 9). For the natural soil (NR_0P_0), C_{ps} and C_{ss} were measured as 4.85×10^{-2} and 1.07×10^{-2}, respectively. As optimal cases, these values, respectively, dropped to 2.63×10^{-2} and 7.06×10^{-3} for $NR_{30}P_0$, and 1.50×10^{-2} and 5.28×10^{-3} for $NR_{30}P_{0.2}$.

4.3.2. *Shrink–swell index*

Variations of the shrinkage and swelling strains, that is, ε_{sh} and ε_{sw}, along with corresponding shrink–swell index values, are provided in Figure 10. Increase in rubber content led to a noticeable reduction in both ε_{sh} and ε_{sw}, and thus the shrink–swell index I_{ss}. For the treated cases, however, a more pronounced decreasing trend can be observed (compare NR_xP_0 with $NR_xP_{0.2}$ in Figure 10). The degree of expansivity, in this case referred to as reactivity, was characterized in accordance with the Seddon (1992) classification criterion (see Table 6), and the results are depicted in Figure 10. The natural soil (NR_0P_0) was graded into highly reactive (H^R) corresponding to $I_{ss} = 4.21\%pF^{-1}$. For untreated cases, $R_c = 10\%$, 20% and 30% resulted in $I_{ss} = 3.30\%pF^{-1}$,

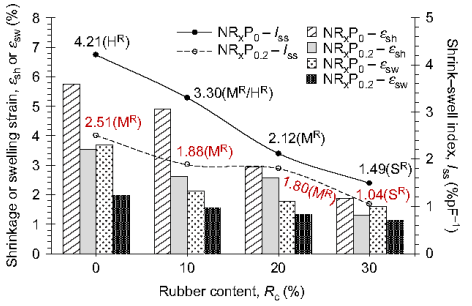

Figure 10. Variations of the shrinkage and swelling strains, along with corresponding shrink–swell index values, against rubber content for the tested samples (H^R = highly reactive; M^R = moderately reactive; S^R = slightly reactive)

$2.12\%pF^{-1}$ and $1.49\%pF^{-1}$, and thus classified as moderately/highly reactive (M^R/H^R), moderately reactive (M^R) and slightly reactive (S^R), respectively. Where treated with 0.2 g/l PC, the aforementioned values dropped to $I_{ss} = 2.51\%pF^{-1}$ (M^R), $1.88\%pF^{-1}$ (M^R), $1.80\%pF^{-1}$ (M^R) and $1.04\%pF^{-1}$ (S^R), respectively.

4.3.3. *Amending mechanisms*

Similar to fiber–reinforced soils, the rubber inclusions are able to amend the soil fabric through improvements achieved in three aspects: (i) increase in the non-expansive fraction, which is a function of rubber content; (ii) interlocking of rubber particles and soil grains; and (iii) interfacial frictional resistance generated as a result of soil–rubber contact (Tang *et al.* 2007, 2010; Al-Akhras *et al.* 2008; Viswanadham *et al.* 2009a, 2009b; Patil *et al.* 2011; Trouzine *et al.* 2012; Kalkan 2013; Estabragh *et al.* 2014; Phanikumar and Singla 2016; Yadav and Tiwari 2017a; Soltani *et al.* 2018). The randomly distributed rubber particles resemble a spatial three-dimensional network in favor of weaving (or interlocking) the soil grains into a coherent matrix of restricted heave. The greater the number of included rubber particles (i.e. increase in rubber content) the more effective the interlocking effect. Frictional resistance grows as a consequence of rubber particles experiencing tensile stress in the presence of strong swelling forces. This interfacial resistance is a function of soil–rubber contact area, with greater contact levels offering a higher resistance to swelling. Consequently, this amending mechanism is in line with rubber content. The greater the number of included rubber particles, the greater the soil–rubber contact level, which in turn promotes an induced interfacial frictional resistance capable of counteracting swelling with more efficiency.

The type of polymer charge, that is cationic, non-ionic or anionic, strongly influences the degree of polymer adsorption/attraction to clay particles. Positively charged polymers are electrostatically attracted to the negatively charged clay surface, while non-ionic polymers

Offprint provided courtesy of www.icevirtuallibrary.com
Author copy for personal use, not for distribution

accomplish adsorption through van der Waals forces and/or hydrogen bonding (Theng 1982; Wallace *et al.* 1986; Miller *et al.* 1998). Even though anionic polymers, such as the one used in this study, tend to be repelled by clay particles (owing to charge repulsion), adsorption can still take place through the presence of cations acting as bridges. The degree of attraction in this case is dependent on the amount and type of exchangeable cations, clay content, pH and polymer molecular size (Theng 1982; Lu *et al.* 2002; Rabiee *et al.* 2013). Polyvalent cations such as Ca^{2+} and Mg^{2+}, for instance, offer greater efficiency in attracting the carboxylate groups on the polymer chains compared with univalent cations such as Na^{+} (Letey 1994; Laird 1997). As such, the role of PC in controlling the effect of swelling can be attributed to its ability to form ionic bonds holding clay particles together through the cationic bridging mechanism, thereby shrinking the electrical double layer. This in turn induces flocculation of clay particles by forming coarse aggregates, which is further accompanied by a reduction in the clay content size, and thus a reduction in the swelling behavior. Where paired with rubber, PC treatment may further enhance the interlocking of rubber particles and soil grains, thus promoting a greater reduction in swelling compared with similar untreated cases.

4.3.4. *Cyclic wetting and drying*

Figure 11 illustrates the variations of swelling potential S_p against number of applied wetting–drying cycles n for the samples NR_0P_0, $NR_{30}P_0$, $NR_0P_{0.2}$ and $NR_{30}P_{0.2}$. With regard to untreated cases (NR_0P_0 and $NR_{30}P_0$), S_p exhibited a rise–fall behavior, peaking at the second cycle and then decreasing to an equilibrium value upon the completion of five cycles. The treated samples ($NR_0P_{0.2}$ and $NR_{30}P_{0.2}$), however, demonstrated a monotonic decreasing trend with lower S_p values compared with similar untreated cases. At the first cycle ($n = 1$), the samples were allowed to swell from their respective optimum moisture content, thus the Seed *et al.* (1962) classification criterion, which complies with the initial placement condition (see Table 5), was implemented to assess the expansive potential of the tested samples. With regard to other cycles ($n \geq 2$), where the samples undergo swelling from an initially dry condition (due to the previous drying cycle), the two classification criteria suggested by Holtz and Gibbs (1956) and Sridharan and Prakash (2000) (see Table 5) were adopted. The classification results are summarized in Table 8. The classifications were either maintained or improved as a result of rubber inclusion and/or PC treatment, thus indicating that the beneficial effects of both stabilization agents in counteracting the swell–shrink related volume changes were fairly preserved under the influence of alternate wetting and drying. Upon the completion of five cycles, a slight increase in S_p was noted for the untreated sample containing 30% rubber inclusion (see $NR_{30}P_0$ in Figure 11), that is, $S_p(1) = 5.73\%$ against $S_p(5) = 6.20\%$. This implies that the blending of rubber particles and soil grains, obtained by compaction, could potentially be compromised under the influence of alternate wetting and drying. As a result of PC treatment, however, the interlocking of rubber particles and soil grains, enhanced by the polymer binder, remains intact during successive cycles (compare $NR_{30}P_0$ with $NR_{30}P_{0.2}$ in Figure 11).

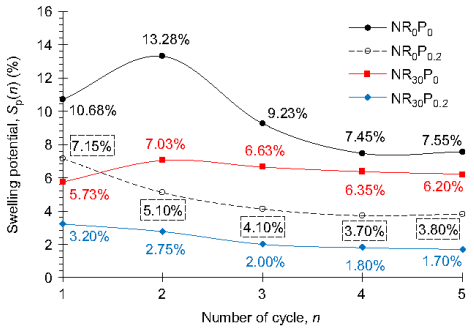

Figure 11. Variations of swelling potential against number of applied wetting–drying cycles for the samples NR_0P_0, $NR_{30}P_0$, $NR_0P_{0.2}$ and $NR_{30}P_{0.2}$

Reduction in swelling potential as a result of alternate wetting and drying can be attributed to the reconstruction of the clay micro-structure upon completion of the first or second cycle (Dif and Bluemel 1991; Zhang *et al.* 2006; Kalkan 2011; Estabragh *et al.* 2015). Capillary stresses generated as a consequence of drying facilitate the formation of strong van der Waals bonds, promoting cementation and aggregation of clay particles. This is followed by the development of some relatively large

Table 8. Degree of expansivity for the tested samples during wetting and drying cycles

Mixture	n	$S_p(n)$ (%)	Degree of expansivity	Degree of expansivity
NR_0P_0	1	10.68	High[a]	High[a]
	2	13.28	Moderate[b]	Moderate[c]
	3	9.23	Low[b]	Moderate[c]
	4	7.45	Low[b]	Moderate[c]
	5	7.55	Low[b]	Moderate[c]
$NR_{30}P_0$	1	5.73	High[a]	High[a]
	2	7.03	Low[b]	Moderate[c]
	3	6.63	Low[b]	Moderate[c]
	4	6.35	Low[b]	Moderate[c]
	5	6.20	Low[b]	Moderate[c]
$NR_0P_{0.2}$	1	7.15	High[a]	High[a]
	2	5.10	Low[b]	Moderate[c]
	3	4.10	Low[b]	Low[c]
	4	3.70	Low[b]	Low[c]
	5	3.80	Low[b]	Low[c]
$NR_{30}P_{0.2}$	1	3.20	Moderate[a]	Moderate[a]
	2	2.75	Low[b]	Low[c]
	3	2.00	Low[b]	Low[c]
	4	1.80	Low[b]	Low[c]
	5	1.70	Low[b]	Low[c]

[a]Classified as per Seed *et al.* (1962) (see Table 5);
[b]Classified as per Holtz and Gibbs (1956) (see Table 5); and
[c]Classified as per Sridharan and Prakash (2000) (see Table 5).

Offprint provided courtesy of www.icevirtuallibrary.com
Author copy for personal use, not for distribution

inter-pores among the aggregated soil clumps, which decreases the available surface for interaction with water, thereby reducing the specific surface area and plasticity of the clay content accompanied by a decreased tendency for swelling (Basma *et al.* 1996; Zhang *et al.* 2006; Estabragh *et al.* 2013; Soltani *et al.* 2017b).

4.4. Crack intensity

Variations of the crack intensity factor (CIF), along with corresponding crack reduction factors (CRF), are provided in Figure 12. In addition, crack patterns observed for the tested samples are illustrated in Figure 13. The rubber inclusions were able to amend desiccation-induced cracking. In this case, the higher the rubber content, the greater the improvement, with PC–treated mixtures holding a notable advantage over similar untreated cases (compare NR_xP_0 with $NR_xP_{0.2}$ in Figure 12). A typical hierarchical cracking pattern can be observed for the natural soil, which divides the soil mass into a series of rather small cells with wide crack openings. On the contrary, soil–rubber mixtures manifested larger cells with relatively smaller crack openings (e.g. compare NR_0P_0 with $NR_{20}P_0$ and $NR_{20}P_{0.2}$). The natural soil (NR_0P_0) and soil–rubber mixtures corresponding to $R_c = 10\%$, 20% and 30% resulted in CIF = 23.67%, 16.79%, 9.03% and 4.73% (i.e. CRF = 29.06%, 61.86% and 80.01%), respectively. Similar mixtures treated with 0.2 g/l PC resulted in lower CIF and higher CRF values. In this case, the aforementioned values dropped to CIF = 15.57%, 11.90%, 7.74% and 2.47% (i.e. CRF = 34.21%, 49.73%, 67.32% and 89.56%), respectively.

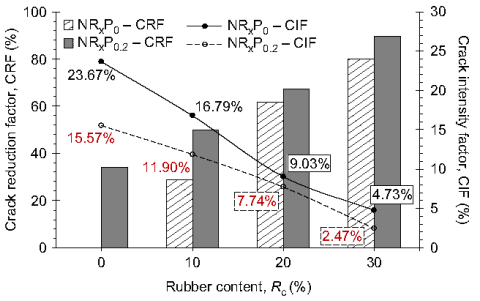

Figure 12. Variations of the crack intensity factor, along with corresponding crack reduction factors, against rubber content for the tested samples

As a consequence of internal restraints (e.g. non-uniform drying) and/or external restraints (e.g. boundary friction/adhesion) acting on the soil during drying, tensile stresses developed within the soil can exceed the soil's tensile strength, thus resulting in the development and propagation of cracks (Konrad and Ayad 1997; Kodikara and Chakrabarti 2005; Nahlawi and Kodikara 2006; Tang *et al.* 2012; Costa *et al.* 2013). The development and propagation of cracks are primarily a function of clay content, meaning that the higher the clay content, the

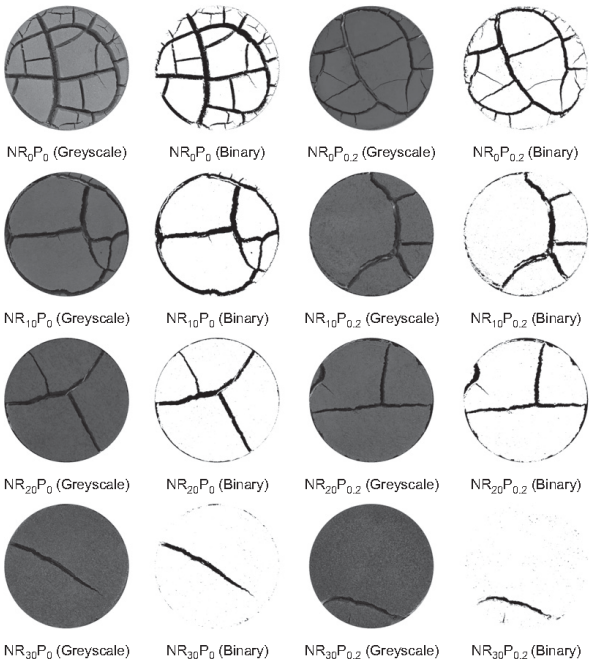

Figure 13. Observed crack patterns for the tested samples

Offprint provided courtesy of www.icevirtuallibrary.com
Author copy for personal use, not for distribution

greater the intensity of cracks (Mitchell and Soga 2005). As such, the rubber inclusions are able to amend the soil fabric through clay substitution. Consequently, this amending mechanism is a function of rubber content, with higher rubber inclusions substituting a larger portion of the clay content, and thus ameliorating the effect of cracking with increased efficiency. The ductile character of the rubber particles can complement a notable improvement in the soil's tensile strength, thus restricting the propagation of cracks. Increase in the soil's tensile strength may also be achieved through interlocking of rubber particles and soil grains. As previously discussed (see Section 4.3.3), the interlocking effect can be considered as a direct function of rubber content, and it is further enhanced in the presence of the polymer binder.

4.5. Micro-structure (SEM) analysis

Figures 14a–14d illustrate SEM micrographs for the samples NR_0P_0, $NR_{20}P_0$, $NR_0P_{0.2}$ and $NR_{20}P_{0.2}$, respectively. The micro-fabric of the natural soil (NR_0P_0) included a number of large inter- and intra-assemblage pore spaces formed between and within the clay aggregates, respectively (see Figure 14a). The inter-assemblage pore spaces are formed during sample preparation (or compaction), and thus are directly proportional to the sample's initial void ratio. The shape and extent of the pore spaces, however, may change during the drying process of SEM sample fabrication (see Section 3.6), owing to the development of tensile stresses within the soil fabric during desiccation. As a result of rubber inclusion ($NR_{20}P_0$), the extent of the inter-assemblage pore spaces was slightly reduced, which can be attributed to the role of rubber particles acting as physical anchors within the soil fabric, thus interlocking neighboring aggregates and withstanding tensile stresses developed during desiccation. However, as long as the rubber particles are relatively larger in size compared with the clay particles, the micro-fabric of the compacted soil–rubber mixture still includes a number of intra-assemblage pore spaces, owing to the inconsistency in arrangement of the soi–rubber mixture's constituents (see Figure 14b). Treating the natural soil with PC ($NR_0P_{0.2}$) resulted in the formation of large uniform aggregates with relatively small intra-assemblage pore spaces, indicating that the polymer solution could effectively slip into the soil's micro-fabric, and thus bond the clay aggregates together.

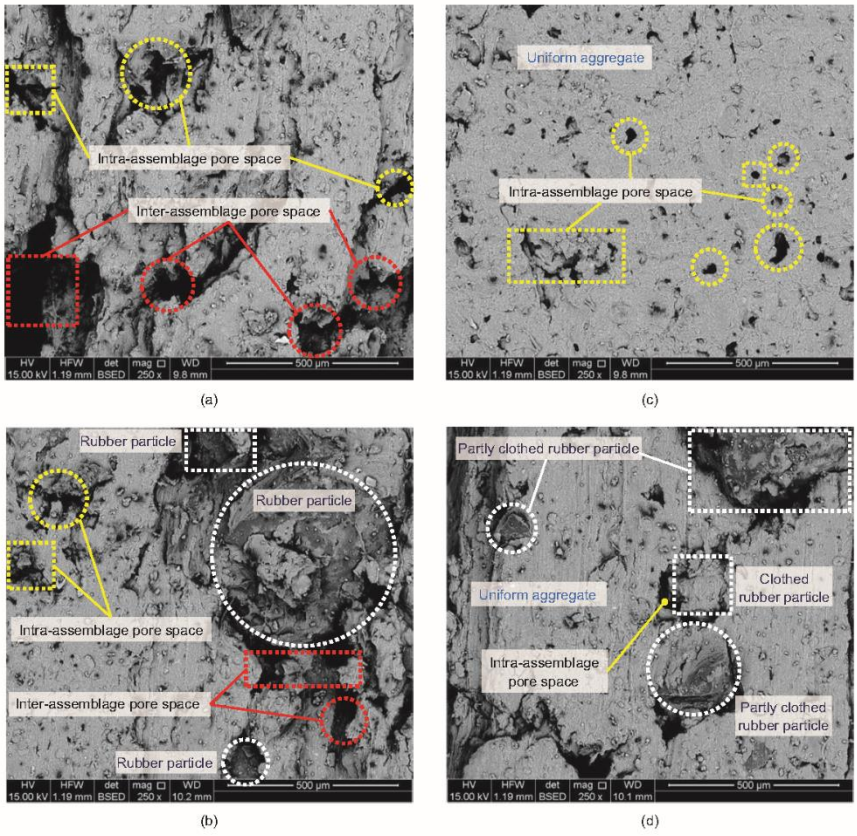

Figure 14. Scanning electron micrographs (SEM): (a) NR_0P_0; (b) $NR_{20}P_0$; (c) $NR_0P_{0.2}$; (d) $NR_{20}P_{0.2}$

Offprint provided courtesy of www.icevirtuallibrary.com
Author copy for personal use, not for distribution

The larger clay aggregates with less number of intra-assemblage pore spaces are less prone to water infiltration, which in turn mitigates the swelling behavior of the soil (see Figure 14c). Once the soil is included with rubber particles and treated with PC ($NR_{20}P_{0.2}$), the connection interface between the rubber particles and the clay matrices is markedly improved. In micro view, the addition of polymer contributes to the formation of composite aggregates, with rubber particles embedded within the clay aggregates (see the clothed rubber particles in Figure 14d). This improves the stability of the compacted soil–rubber mixture against wetting and drying cycles, as the rubber particles contribute to the shear strength of the mixture by providing tensile strength between the clay aggregates, and the polymer solution improves the bonding quality of the rubber particles with the clay aggregates; therefore, harnessing the swelling potential of the soil subjected to desiccation cycles (see Figure 14d).

5. CONCLUSIONS

The following conclusions can be drawn from this study.

- As a result of rubber inclusion and/or PC treatment, the swell–time locus experienced a major downward shift over the semi-log space, indicating a capacity of counteracting the heave in both magnitude and time. The variations of swelling pressure followed a trend similar to that observed for swelling potential, meaning that the higher the rubber content the greater the reduction in swelling potential and swelling pressure, with PC treated mixtures holding a notable advantage over similar untreated cases.
- Based on common expansive soil classification criteria, that is, the conventional oedometer swell test and the shrink–swell index, a rubber inclusion of 20% by dry weight of soil (preferably paired with 0.2 g/l PC) would be required to mitigate the swelling problem of South Australian expansive soils.
- The beneficial effects of rubber inclusion and PC treatment in counteracting the swell–shrink related volume changes were fairly preserved under the influence of alternate wetting and drying. The blending of rubber particles and soil grains, obtained by compaction, could potentially be compromised during wetting and drying. As a result of PC treatment, however, the interlocking of rubber particles and soil grains, enhanced by the polymer binder, remained intact during successive cycles.
- The rubber inclusions were able to amend desiccation-induced cracking. In this case, the higher the rubber content the greater the improvement in cracking intensity, with PC–treated mixtures holding a slight advantage over similar untreated cases.

ACKNOWLEDGEMENTS

Funding support provided by the Australian Research Council (ARC) via project No. DP140103004 is gratefully acknowledged.

NOTATION

Basic SI units are given in parentheses.

A_0	initial area of the sample tested for cracking (m^2)
A_c	area of cracks (m^2)
C_c	coefficient of curvature (dimensionless)
CIF	crack intensity factor (dimensionless)
CIF_n	crack intensity factor for the natural soil (dimensionless)
CIFs	crack intensity factor for the stabilized sample (dimensionless)
C_{ps}	primary swelling rate (dimensionless)
CRF	crack reduction factor (dimensionless)
C_{ss}	secondary swelling rate (dimensionless)
C_u	coefficient of uniformity (dimensionless)
d_{10}	particle diameter corresponding to 10% finer (m)
d_{30}	particle diameter corresponding to 30% finer (m)
d_{50}	particle diameter corresponding to 50% finer (m)
d_{60}	particle diameter corresponding to 60% finer (m)
d_{90}	particle diameter corresponding to 90% finer (m)
e_0	initial void ratio (dimensionless)
FSR	free swell ratio (dimensionless)
G_{sm}	specific gravity of soil–rubber mixture (dimensionless)
G_{sr}	specific gravity of rubber particles (dimensionless)
G_{ss}	specific gravity of soil solids (dimensionless)
I_{ss}	shrink–swell index ($\%Pa^{-1}$)
LL	liquid limit (dimensionless)
LS	linear shrinkage (dimensionless)
n	number of wetting–drying cycles (dimensionless)
PI	plasticity index (dimensionless)
PL	plastic limit (dimensionless)
P_s	swelling pressure (Pa)
R_c	rubber content by dry weight of soil (dimensionless)
S_p	swelling potential (dimensionless)
$S_p(n)$	swelling potential with respect to the nth wetting–drying cycle (dimensionless)
t	elapsed time of swelling (s)
t_{is}	completion time of the initial swelling phase (s)
t_{ps}	completion time of the primary swelling phase (s)
t_{ss}	completion time of the secondary swelling phase (s)
w_r	weight of rubber particles (kg)
w_{ss}	weight of dry soil (kg)
γ_{dmax}	maximum dry unit weight (N/m^3)
$\varepsilon_a(t)$	axial swelling strain with respect to elapsed time t (dimensionless)
ε_{ais}	initial swelling strain (dimensionless)
ε_{aps}	primary swelling strain (dimensionless)
ε_{ass}	secondary swelling strain (dimensionless)

Offprint provided courtesy of www.icevirtuallibrary.com
Author copy for personal use, not for distribution

ε_{sh} ultimate shrinkage strain with respect to the shrink–swell index test (dimensionless)
ε_{sw} ultimate swelling strain with respect to the shrink–swell index test (dimensionless)
σ'_0 nominal overburden stress (Pa)
ω_{opt} optimum moisture content (dimensionless)

ABBREVIATIONS

CH clay with high plasticity
E^R extremely reactive
H highly expansive
H^R highly reactive
L lowly expansive
M moderately expansive
M^R moderately reactive
PC polymer
pF potential of free energy (a unit for soil suction)
SEM scanning electron microscopy
S^R slightly reactive
USCS unified soil classification system
VH very highly expansive

REFERENCES

Akbulut, S., Arasan, S. & Kalkan, E. (2007). Modification of clayey soils using scrap tire rubber and synthetic fibers. *Applied Clay Science*, **38**, No. 1 2, 23 32, https://doi.org/10.1016/j.clay.2007.02.001.

Al-Akhras, N. M., Attom, M. F., Al-Akhras, K. M. & Malkawi, A. I. H. (2008). Influence of fibers on swelling properties of clayey soil. *Geosynthetics International*, **15**, No. 4, 304 309, https://doi.org/10.1680/gein.2008.15.4.304.

Alazigha, D. P., Indraratna, B., Vinod, J. S. & Ezeajugh, L. E. (2016). The swelling behaviour of lignosulfonate-treated expansive soil. *Proceedings of the Institution of Civil Engineers Ground Improvement*, **169**, No. 3, 182 193, https://doi.org/10.1680/jgrim.15.00002.

Alonso, E. E., Romero, E., Hoffmann, C. & García-Escudero, E. (2005). Expansive bentonite-sand mixtures in cyclic controlled-suction drying and wetting. *Engineering Geology*, **81**, No. 3, 213 226, https://doi.org/10.1016/j.enggeo.2005.06.009.

Al-Rawas, A. A., Hago, A. W. & Al-Sarmi, H. (2005). Effect of lime, cement and Sarooj (artificial pozzolan) on the swelling potential of an expansive soil from Oman. *Building and Environment*, **40**, No. 5, 681 687, https://doi.org/10.1016/j.buildenv.2004.08.028.

Andrews, R. & Sharp, K. (2010). A protocol for conducting field trials for best value management of unsealed roads. *Proceedings of the 24th ARRB Conference Building on 50 Years of Road and Transport Research*, ARRB, Melbourne, VIC, Australia, pp. 1 14.

Arulrajah, A., Kua, T. A., Suksiripattanapong, C., Horpibulsuk, S. & Shen, J. S. (2017a). Compressive strength and microstructural properties of spent coffee grounds bagasse ash based geopolymers with slag supplements. *Journal of Cleaner Production*, **162**, 1491 1501, https://doi.org/10.1016/j.jclepro.2017.06.171.

Arulrajah, A., Kua, T. A., Horpibulsuk, S., Mirzababaei, M. & Chinkulkijniwat, A. (2017b). Recycled glass as a supplementary filler material in spent coffee grounds geopolymers. *Construction and Building Materials*, **151**, 18 27, https://doi.org/10.1016/j.conbuildmat.2017.06.050.

Arulrajah, A., Mohammadinia, A., D'Amico, A. & Horpibulsuk, S. (2017c). Effect of lime kiln dust as an alternative binder in the stabilization of construction and demolition materials. *Construction and Building Materials*, **152**, 999 1007, https://doi.org/10.1016/j.conbuildmat.2017.07.070.

AS 1289.3.2.1 *Methods of Testing Soils for Engineering Purposes: Soil Classification Tests Determination of the Plastic Limit of a Soil.* Standards Australia, Sydney, NSW, Australia.

AS 1289.3.3.1 *Methods of Testing Soils for Engineering Purposes: Soil Classification Tests Calculation of the Plasticity Index of a Soil.* Standards Australia, Sydney, NSW, Australia.

AS 1289.3.4.1 *Methods of Testing Soils for Engineering Purposes: Soil Classification Tests Determination of the Linear Shrinkage of a Soil.* Standards Australia, Sydney, NSW, Australia.

AS 1289.3.9.1 *Methods of Testing Soils for Engineering Purposes: Soil Classification Tests Determination of the Cone Liquid Limit of a Soil.* Standards Australia, Sydney, NSW, Australia.

AS 1289.7.1.1 *Methods of Testing Soils for Engineering Purposes: Soil Reactivity Tests Determination of the Shrinkage Index of a Soil Shrink Swell Index.* Standards Australia, Sydney, NSW, Australia.

AS 2870 *Residential Slabs and Footings.* Standards Australia, Sydney, NSW, Australia.

ASTM D2487 *Standard Practice for Classification of Soils for Engineering Purposes (Unified Soil Classification System).* ASTM International, West Conshohocken, PA, USA.

ASTM D422 *Standard Test Method for Particle Size Analysis of Soils.* ASTM International, West Conshohocken, PA, USA.

ASTM D4546 *Standard Test Methods for One Dimensional Swell or Collapse of Soils.* ASTM International, West Conshohocken, PA, USA.

ASTM D698 *Standard Test Methods for Laboratory Compaction Characteristics of Soil using Standard Effort (12,400 ft lbf/ft^3 (600 kN m/m^3)).* ASTM International, West Conshohocken, PA, USA.

ASTM D854 *Standard Test Methods for Specific Gravity of Soil Solids by Water Pycnometer.* ASTM International, West Conshohocken, PA, USA.

Ayeldeen, M. & Kitazume, M. (2017). Using fiber and liquid polymer to improve the behaviour of cement stabilized soft clay. *Geotextiles and Geomembranes*, **45**, No. 6, 592 602, https://doi.org/10.1016/j.geotexmem.2017.05.005.

Basma, A. A., Al-Homoud, A. S., Malkawi, A. I. H. & Al-Bashabsheh, M. A. (1996). Swelling-shrinkage behavior of natural expansive clays. *Applied Clay Science*, **11**, No. 2 4, 211 227, https://doi.org/10.1016/s0169-1317(96)00009-9.

Camarena, S. (2013). Sustainable road maintenance and construction utilising new technologies. *Proceedings of the IPWEA International Public Works Conference*, IPWEA, Darwin, NT, Australia, pp. 1 11.

Cameron, D. A. (1989). Tests for reactivity and prediction of ground movement. *Civil Engineering Transactions/The Institution of Engineers, Australia*, **31**, No. 3, 121 132.

Cameron, D. A. (2001). The extent of soil desiccation near trees in a semi arid environment. *Geotechnical and Geological Engineering*, **19**, No. 3 4, 357 370, https://doi.org/10.1023/a:1013168708654.

Cetin, H., Fener, M. & Gunaydin, O. (2006). Geotechnical properties of tire cohesive clayey soil mixtures as a fill material. *Engineering Geology*, **88**, No. 1 2, 110 120, https://doi.org/10.1016/j.enggeo.2006.09.002.

Chaduvula, U., Viswanadham, B. V. S. & Kodikara, J. (2017). A study on desiccation cracking behavior of polyester fiber reinforced expansive clay. *Applied Clay Science*, **142**, 163 172, https://doi.org/10.1016/j.clay.2017.02.008.

Costa, S., Kodikara, J. & Shannon, B. (2013). Salient factors controlling desiccation cracking of clay in laboratory experiments. *Géotechnique*, **63**, No. 1, 18 29, https://doi.org/10.1680/geot.9.p.105.

De Camillis, M., Di Emidio, G., Bezuijen, A., Flores, D. V., Stappen, J. V. & Cnudde, V. (2017). Effect of wet dry cycles on polymer treated bentonite in seawater: swelling ability, hydraulic conductivity and crack analysis. *Applied Clay Science*, **142**, 52 59, https://doi.org/10.1016/j.clay.2016.11.011.

Dif, A. & Bluemel, W. (1991). Expansive soils under cyclic drying and wetting. *Geotechnical Testing Journal*, **14**, No. 1, 96 102, https://doi.org/10.1520/gtj10196j.

Offprint provided courtesy of www.icevirtuallibrary.com
Author copy for personal use, not for distribution

Estabragh, A. R., Pereshkafti, M. R. S., Parsaei, B. & Javadi, A. A. (2013). Stabilised expansive soil behaviour during wetting and drying. *International Journal of Pavement Engineering*, **14**, No. 4, 418 427, https://doi.org/10.1080/10298436.2012.746688.

Estabragh, A. R., Rafatjo, H. & Javadi, A. A. (2014). Treatment of an expansive soil by mechanical and chemical techniques. *Geosynthetics International*, **21**, No. 3, 233 243, https://doi.org/10.1680/gein.14.00011.

Estabragh, A. R., Parsaei, B. & Javadi, A. A. (2015). Laboratory investigation of the effect of cyclic wetting and drying on the behaviour of an expansive soil. *Soils and Foundations*, **55**, No. 2, 304 314, https://doi.org/10.1016/j.sandf.2015.02.007.

Fityus, S. G., Cameron, D. A. & Walsh, P. F. (2005). The shrink swell test. *Geotechnical Testing Journal*, **28**, No. 1, 92 101, https://doi.org/10.1520/gtj12327.

Georgees, R. N., Hassan, R. A., Evans, R. P. & Jegatheesan, P. (2015). Effect of the use of a polymeric stabilizing additive on unconfined compressive strength of soils. *Transportation Research Record*, **2473**, 200 208, https://doi.org/10.3141/2473-23.

Graber, E. R., Fine, P. & Levy, G. J. (2006). Soil stabilization in semiarid and arid land agriculture. *Journal of Materials in Civil Engineering*, **18**, No. 2, 190 205, https://doi.org/10.1061/(asce)0899-1561(2006)18:2(190).

Guney, Y., Sari, D., Cetin, M. & Tuncan, M. (2007). Impact of cyclic wetting-drying on swelling behavior of lime stabilized soil. *Building and Environment*, **42**, No. 2, 681 688, https://doi.org/10.1016/j.buildenv.2005.10.035.

Hannam, P. (2014). *Tyre Industry Divided Over How to Handle Toxic Waste*, The Sydney Morning Herald, Sydney, NSW, Australia. See http://www.smh.com.au/environment/tyre-industry-divided-over-how-to-handle-toxic-waste-20140120-314ic.html (accessed 12/12/2017).

Holtz, W. G. & Gibbs, H. J. (1956). Engineering properties of expansive clays. *Transactions of the American Society of Civil Engineers*, **121**, No. 1, 641 663.

Hoyos, L. R., Chainuwat, P. & Puppala, A. J. (2006). Dynamic characterization of chemically modified expansive soil. In *Expansive Soils: Recent Advances in Characterization and Treatment*, Al-Rawas, A. A. & Goosen, M. F. A., Editors, Taylor & Francis Group, London, UK, pp. 465 481.

Inyang, H. I., Bae, S., Mbamalu, G. & Park, S. (2007). Aqueous polymer effects on volumetric swelling of Na Montmorillonite. *Journal of Materials in Civil Engineering*, **19**, No. 1, 84 90, https://doi.org/10.1061/(asce)0899-1561(2007)19:1(84).

Kalkan, E. (2011). Impact of wetting drying cycles on swelling behavior of clayey soils modified by silica fume. *Applied Clay Science*, **52**, No. 4, 345 352, https://doi.org/10.1016/j.clay.2011.03.014.

Kalkan, E. (2013). Preparation of scrap tire rubber fiber silica fume mixtures for modification of clayey soils. *Applied Clay Science*, **80–81**, 117 125, https://doi.org/10.1016/j.clay.2013.06.014.

Kim, S. & Palomino, A. M. (2009). Polyacrylamide-treated kaolin: a fabric study. *Applied Clay Science*, **45**, No. 4, 270 279, https://doi.org/10.1016/j.clay.2009.06.009.

Kodikara, J. & Chakrabarti, S. (2005). Modeling of moisture loss in cementitiously stabilized pavement materials. *International Journal of Geomechanics*, **5**, No. 4, 295 303, https://doi.org/10.1061/(asce)1532-3641(2005)5:4(295).

Konrad, J. M. & Ayad, R. (1997). An idealized framework for the analysis of cohesive soils undergoing desiccation. *Canadian Geotechnical Journal*, **34**, No. 4, 477 488, https://doi.org/10.1139/t97-015.

Kua, T. A., Arulrajah, A., Mohammadinia, A., Horpibulsuk, S. & Mirzababaei, M. (2017). Stiffness and deformation properties of spent coffee grounds based geopolymers. *Construction and Building Materials*, **138**, 79 87, https://doi.org/10.1016/j.conbuildmat.2017.01.082.

Laird, D. A. (1997). Bonding between polyacrylamide and clay mineral surfaces. *Soil Science*, **162**, No. 11, 826 832, https://doi.org/10.1097/00010694-199711000-00006.

Letey, J. (1994). Adsorption and desorption of polymers on soil. *Soil Science*, **158**, No. 4, 244 248, https://doi.org/10.1097/00010694-199410000-00003.

Lu, J. H., Wu, L. & Letey, J. (2002). Effects of soil and water properties on anionic polyacrylamide sorption. *Soil Science Society of America Journal*, **66**, No. 2, 578 584, https://doi.org/10.2136/sssaj2002.5780.

Miller, C. J. & Rifai, S. (2004). Fiber reinforcement for waste containment soil liners. *Journal of Environmental Engineering*, **130**, No. 8, 891 895, https://doi.org/10.1061/(asce)0733-9372(2004)130:8(891).

Miller, W. P., Willis, R. L. & Levy, G. J. (1998). Aggregate stabilization in kaolinitic soils by low rates of anionic polyacrylamide. *Soil Use and Management*, **14**, No. 2, 101 105, https://doi.org/10.1111/j.1475-2743.1998.tb00623.x.

Mirzababaei, M., Yasrobi, S. S. & Al-Rawas, A. A. (2009). Effect of polymers on swelling potential of expansive soils. *Proceedings of the Institution of Civil Engineers Ground Improvement*, **162**, No. 3, 111 119, https://doi.org/10.1680/grim.2009.162.3.111.

Mirzababaei, M., Miraftab, M., Mohamed, M. & McMahon, P. (2013a). Impact of carpet waste fibre addition on swelling properties of compacted clays. *Geotechnical and Geological Engineering*, **31**, No. 1, 173 182, https://doi.org/10.1007/s10706-012-9578-2.

Mirzababaei, M., Miraftab, M., Mohamed, M. & McMahon, P. (2013b). Unconfined compression strength of reinforced clays with carpet waste fibers. *Journal of Geotechnical and Geoenvironmental Engineering*, **139**, No. 3, 483 493, https://doi.org/10.1061/(asce)gt.1943-5606.0000792.

Mirzababaei, M., Mohamed, M., Arulrajah, A., Horpibulsuk, S. & Anggraini, V. (2018). Practical approach to predict the shear strength of fibre reinforced clay. *Geosynthetics International*, **25**, No. 1, 50 66, https://doi.org/10.1680/jgein.17.00033.

Mirzababaei, M., Mohamed, M. & Miraftab, M. (2017). Analysis of strip footings on fiber reinforced slopes with the aid of particle image velocimetry. *Journal of Materials in Civil Engineering*, **29**, No. 4, 04016243:1 04016243:14, https://doi.org/10.1061/(asce)mt.1943-5533.0001758.

Mitchell, J. K. & Soga, K. (2005). *Fundamentals of Soil Behavior*, 3rd edn. John Wiley & Sons, Hoboken, NJ, USA.

Nahlawi, H. & Kodikara, J. K. (2006). Laboratory experiments on desiccation cracking of thin soil layers. *Geotechnical and Geological Engineering*, **24**, No. 6, 1641 1664, https://doi.org/10.1007/s10706-005-4894-4.

Onyejekwe, S. & Ghataora, G. S. (2015). Soil stabilization using proprietary liquid chemical stabilizers: sulphonated oil and a polymer. *Bulletin of Engineering Geology and the Environment*, **74**, No. 2, 651 665, https://doi.org/10.1007/s10064-014-0667-8.

Özkul, Z. H. & Baykal, G. (2007). Shear behavior of compacted rubber fiber clay composite in drained and undrained loading. *Journal of Geotechnical and Geoenvironmental Engineering*, **133**, No. 7, 767 781, https://doi.org/10.1061/(asce)1090-0241(2007)133:7(767).

Patil, U., Valdes, J. R. & Evans, T. M. (2011). Swell mitigation with granulated tire rubber. *Journal of Materials in Civil Engineering*, **23**, No. 5, 721 727, https://doi.org/10.1061/(asce)mt.1943-5533.0000229.

Phanikumar, B. R. & Singla, R. (2016). Swell-consolidation characteristics of fibre-reinforced expansive soils. *Soils and Foundations*, **56**, No. 1, 138 143, https://doi.org/10.1016/j.sandf.2016.01.011.

Phummiphan, I., Horpibulsuk, S., Rachan, R., Arulrajah, A., Shen, S. L. & Chindaprasirt, P. (2018). High calcium fly ash geopolymer stabilized lateritic soil and granulated blast furnace slag blends as a pavement base material. *Journal of Hazardous Materials*, **341**, 257 267, https://doi.org/10.1016/j.jhazmat.2017.07.067.

Prakash, K. & Sridharan, A. (2004). Free swell ratio and clay mineralogy of fine grained soils. *Geotechnical Testing Journal*, **27**, No. 2, 220 225, https://doi.org/10.1520/gtj10860.

Puppala, A. J., Griffin, J. A., Hoyos, L. R. & Chomtid, S. (2004). Studies on sulfate resistant cement stabilization methods to address sulfate-induced soil heave. *Journal of Geotechnical and Geoenvironmental Engineering*, **130**, No. 4, 391 402, https://doi.org/10.1061/(asce)1090-0241(2004)130:4(391).

Rabiee, A., Gilani, M., Jamshidi, H. & Baharvand, H. (2013). Synthesis and characterization of a calcium and sodium containing acrylamide-based polymer and its effect on soil strength. *Journal*

Offprint provided courtesy of www.icevirtuallibrary.com
Author copy for personal use, not for distribution

of Vinyl and Additive Technology, **19**, No. 2, 140 146, https://doi.org/10.1002/vnl.21310.

Rao, S. M., Reddy, B. V. V. & Muttharam, M. (2001). The impact of cyclic wetting and drying on the swelling behavior of stabilized expansive soils. *Engineering Geology*, **60**, No. 1 4, 223 233, https://doi.org/10.1016/s0013-7952(00)00103-4.

Rao, S. M., Thyagaraj, T. & Thomas, H. R. (2006). Swelling of compacted clay under osmotic gradients. *Géotechnique*, **56**, No. 10, 707 713, https://doi.org/10.1680/geot.2006.56.10.707.

Rauch, A., Harmon, J., Katz, L. & Liljestrand, H. (2002). Measured effects of liquid soil stabilizers on engineering properties of clay. *Transportation Research Record*, **1787**, 33 41, https://doi.org/10.3141/1787-04.

Seda, J. H., Lee, J. C. & Carraro, J. A. H. (2007). Beneficial use of waste tire rubber for swelling potential mitigation in expansive soils. In *Geo-Denver 2007: Soil Improvement (GSP 172)*, Schaefer, V. R., Filz, G. M., Gallagher, P. M., Sehn, A. L. & Wissmann, K. J., Editors, ASCE, Denver, CO, USA, pp. 1 9.

Seddon, K. D. (1992). Reactive soils. In *Engineering Geology of Melbourne*, Peck, W. A., Neilson, J. L., Olds, R. J. & Seddon, K. D., Editors, A.A. Balkema, Melbourne, VIC, Australia, pp. 33 37.

Seed, H. B., Woodward, J. & Lundgren, R. (1962). Prediction of swelling potential for compacted clays. *Journal of the Soil Mechanics and Foundations Division*, **88**, No. 3, 53 88.

Seybold, C. A. (1994). Polyacrylamide review: soil conditioning and environmental fate. *Communications in Soil Science and Plant Analysis*, **25**, No. 11 1, No. 2, 2171 2185, https://doi.org/10.1080/00103629409369180.

Signes, C. H., Garzón-Roca, J., Fernández, P. M., Torre, M. E. G. & Franco, R. I. (2016). Swelling potential reduction of Spanish argillaceous marlstone Facies Tap soil through the addition of crumb rubber particles from scrap tyres. *Applied Clay Science*, **132–133**, 768 773, https://doi.org/10.1016/j.clay.2016.07.027.

Sivapullaiah, P. V., Sridharan, A. & Stalin, V. K. (1996). Swelling behaviour of soil-bentonite mixtures. *Canadian Geotechnical Journal*, **33**, No. 5, 808 814, https://doi.org/10.1139/t96-106-326.

Sivapullaiah, P. V., Sridharan, A. & Ramesh, H. N. (2000). Strength behaviour of lime-treated soils in the presence of sulphate. *Canadian Geotechnical Journal*, **37**, No. 6, 1358 1367, https://doi.org/10.1139/t00-052.

Soltani, A., Taheri, A., Khatibi, M. & Estabragh, A. R. (2017a). Swelling potential of a stabilized expansive soil: a comparative experimental study. *Geotechnical and Geological Engineering*, **35**, No. 4, 1717 1744, https://doi.org/10.1007/s10706-017-0204-1.

Soltani, A., Deng, A., Taheri, A. & Mirzababaei, M. (2017b). A sulphonated oil for stabilisation of expansive soils. *International Journal of Pavement Engineering*, (in press), https://doi.org/10.1080/10298436.2017.1408270.

Soltani, A., Deng, A. & Taheri, A. (2018). Swell-compression characteristics of a fiber-reinforced expansive soil. *Geotextiles and Geomembranes*, **46**, No. 2, 183 189, https://doi.org/10.1016/j.geotexmem.2017.11.009.

Sridharan, A. & Gurtug, Y. (2004). Swelling behaviour of compacted fine-grained soils. *Engineering Geology*, **72**, No. 1, 9 18, https://doi.org/10.1016/s0013-7952(03)00161-3.

Sridharan, A. & Keshavamurthy, P. (2016). Expansive soil characterisation: an appraisal. *INAE Letters*, **1**, No. 1, 29 33, https://doi.org/10.1007/s41403-016-0001-9.

Sridharan, A. & Prakash, K. (2000). Classification procedures for expansive soils. *Proceedings of the Institution of Civil Engineers Geotechnical Engineering*, **143**, No. 4, 235 240, https://doi.org/10.1680/geng.2000.143.4.235.

Sridharan, A., Rao, A. & Sivapullaiah, P. (1986). Swelling pressure of clays. *Geotechnical Testing Journal*, **9**, No. 1, 24 33, https://doi.org/10.1520/gtj10608j.

Srivastava, A., Pandey, S. & Rana, J. (2014). Use of shredded tyre waste in improving the geotechnical properties of expansive black cotton soil. *Geomechanics and Geoengineering*, **9**, No. 4, 303 311, https://doi.org/10.1080/17486025.2014.902121.

Suksiripattanapong, C., Kua, T. A., Arulrajah, A., Maghool, F. & Horpibulsuk, S. (2017). Strength and microstructure properties of spent coffee grounds stabilized with rice husk ash and slag geopolymers. *Construction and Building Materials*, **146**, 312 320, https://doi.org/10.1016/j.conbuildmat.2017.04.103.

Tang, C. S., Shi, B., Gao, W., Chen, F. & Cai, Y. (2007). Strength and mechanical behavior of short polypropylene fiber reinforced and cement stabilized clayey soil. *Geotextiles and Geomembranes*, **25**, No. 3, 194 202, https://doi.org/10.1016/j.geotexmem.2006.11.002.

Tang, C. S., Shi, B. & Zhao, L. Z. (2010). Interfacial shear strength of fiber reinforced soil. *Geotextiles and Geomembranes*, **28**, No. 1, 54 62, https://doi.org/10.1016/j.geotexmem.2009.10.001.

Tang, C. S., Shi, B., Cui, Y. J., Liu, C. & Gua, K. (2012). Desiccation cracking behavior of polypropylene fiber reinforced clayey soil. *Canadian Geotechnical Journal*, **49**, No. 9, 1088 1101, https://doi.org/10.1139/t2012-067.

Theng, B. K. G. (1982). Clay polymer interactions: summary and perspectives. *Clays and Clay Minerals*, **30**, No. 1, 1 10, https://doi.org/10.1346/ccmn.1982.0300101.

Tripathy, S., Subba Rao, K. S. & Fredlund, D. G. (2002). Water content-void ratio swell-shrink paths of compacted expansive soils. *Canadian Geotechnical Journal*, **39**, No. 4, 938 959, https://doi.org/10.1139/t02-022.

Trouzine, H., Bekhiti, M. & Asroun, A. (2012). Effects of scrap tyre rubber fibre on swelling behaviour of two clayey soils in Algeria. *Geosynthetics International*, **19**, No. 2, 124 132, https://doi.org/10.1680/gein.2012.19.2.124.

Viswanadham, B. V. S., Phanikumar, B. R. & Mukherjee, R. V. (2009a). Swelling behaviour of a geofiber reinforced expansive soil. *Geotextiles and Geomembranes*, **27**, No. 1, 73 76, https://doi.org/10.1016/j.geotexmem.2008.06.002.

Viswanadham, B. V. S., Phanikumar, B. R. & Mukherjee, R. V. (2009b). Effect of polypropylene tape fibre reinforcement on swelling behaviour of an expansive soil. *Geosynthetics International*, **16**, No. 5, 393 401, https://doi.org/10.1680/gein.2009.16.5.393.

Wallace, A., Wallace, G. A. & Cha, W. J. (1986). Mechanisms involved in soil conditioning by polymers. *Soil Science*, **141**, No. 5, 381 386, https://doi.org/10.1097/00010694-198605000-00017.

Wray, W. K. (1998). Mass transfer in unsaturated soils: a review of theory and practices. *Proceedings of the 2nd International Conference on Unsaturated Soils (Unsat 98)*, International Academic Publishing House, Beijing, China, pp. 99 155.

Wroth, C. P. & Wood, D. M. (1978). The correlation of index properties with some basic engineering properties of soils. *Canadian Geotechnical Journal*, **15**, No. 2, 137 145, https://doi.org/10.1139/t78-014.

Yadav, J. S. & Tiwari, S. K. (2017a). Effect of waste rubber fibres on the geotechnical properties of clay stabilized with cement. *Applied Clay Science*, **149**, 97 110, https://doi.org/10.1016/j.clay.2017.07.037.

Yadav, J. S. & Tiwari, S. K. (2017b). The impact of end-of-life tires on the mechanical properties of fine-grained soil: a review. *Environment, Development and Sustainability*, (in press), https://doi.org/10.1007/s10668-017-0054-2.

Yazdandoust, F. & Yasrobi, S. S. (2010). Effect of cyclic wetting and drying on swelling behavior of polymer stabilized expansive clays. *Applied Clay Science*, **50**, No. 4, 461 468, https://doi.org/10.1016/j.clay.2010.09.006.

Yesiller, N., Miller, C. J., Inci, G. & Yaldo, K. (2000). Desiccation and cracking behavior of three compacted landfill liner soils. *Engineering Geology*, **57**, No. 1 2, 105 121, https://doi.org/10.1016/s0013-7952(00)00022-3.

Zhang, R., Yang, H. & Zheng, J. (2006). The effect of vertical pressure on the deformation and strength of expansive soil during cyclic wetting and drying. In *Unsaturated Soils 2006*, Miller, G. A., Zapata, C. E., Houston, S. L. & Fredlund, D. G., Editors, ASCE, Carefree, AZ, USA, pp. 894 905, https://doi.org/10.1061/40802(189)71.

The Editor welcomes discussion on all papers published in Geosynthetics International. Please email your contribution to discussion@geosynthetics-international.com by 15 December 2018.

Offprint provided courtesy of www.icevirtuallibrary.com
Author copy for personal use, not for distribution